Northumbria Research Link

Recyclable Thermosets Based on Modified Epoxy-amine Network Polymers

L Anderson

PhD

2023

Recyclable Thermosets Based on Modified Epoxy-amine Network Polymers

Lynn Anderson (MChem)

A thesis submitted in partial fulfilment of the requirements of the

University of Northumbria at Newcastle for the degree of Doctor

of Philosophy

Research undertaken in the Department of Applied Sciences

May 2023

Dedicated to the best lab partner - Whom thankfully did not eat my homework.

Acknowledgements

Declaration

The research described in this thesis was carried out in the Department of Health and Life Sciences, at the University of Northumbria at Newcastle, between October 2019 and May 2023. I declare that the work contained in this thesis has not been submitted for any other award and that it is all my own work. I also confirm that this work fully acknowledges opinions, ideas, and contributions from the work of others.

The work presented in sections 3-6 has been published, prior to submitting, in a peer-reviewed journal:

L. Anderson, E. W. Sanders and M. G. Unthank, *Mater. Horizons*, 2023, **10**, 889-898 DOI:10.1039/D2MH01211A.

I declare that the Word Count of this Thesis is 57916 words.

Name: Lynn Anderson

Signature:

Date: 8th May 2023

Abstract

With growing interest in recyclable polymer materials, due to environmental concerns, attention has been aimed towards substantially reducing waste generation through prevention, reduction, recycling and reuse. In response to recycling polymer waste, the emerging field of covalent adaptable networks (CANs) has provided solutions to the reduction of thermoset polymer waste by utilising dynamic bonds to form three dimensional architectures. In particular, boronic esters provide a desirable associative CAN mechanism, for high-performance applications, plus a reversible route by hydrolysis or boronic esterification mechanisms. This offers routes to recycling in materials of this class.

This research investigates a novel dioxazaborocane crosslinking mechanism in epoxy-amine thermoset polymers for use as a CAN, creating an opportunity to form high performance, recyclable materials from established molecular building blocks, common to the plastics, composites, coatings and adhesive industries. This work establishes a practical methodology of fabricating polymer networks of this class as well as the subsequent analysis and characterisation of their thermal and material properties, through T_g analysis and procurement of ultimate tensile strengths, to assess the suitability as a high-performance material for aerospace and wind turbine applications. Most notably, an efficient and low-cost process for the chemical recycling (disassembly and dissolution) of the thermoset material is demonstrated via two complementary synthetic processes, using either pinacol (diol) or mono-functional phenylboronic esters. Mechanical recycling has also been realised due to the facile topological rearrangement due to dynamic boronic ester bond exchange mechanisms.

This research demonstrates the value of designing chemical recyclability into the molecular architecture for a sustainable outlook on future thermosets.

List of Abbreviations

ATRP	Atom transfer radical polymerisation
CAN	Covalent adaptable network
CEM	Cysteine methyl ester
CGM	Continuous Glucose Monitoring
CHA	Cyclohexylamine
d	Tan Delta
DA	Diels-Alder
DBU	1,8-Diazabicyclo[5.4.0]undec-7-ene
DCB	Dynamic Covalent Bond
DEM	Diethylmalonate
DGEBA	Bisphenol diglycidyl ether
DGEBF	Diglycidyl bisphenol F
DHPM	N-(2,3-dihydroxypropyl)maleimide
DMA	Dynamic mechanical analysis
DMA	Dynamic mechanical analysis
DMAc	Dimethylacetamide
DOAB	Dioxazaborocane
DPBM	1,1′-(methylenedi-4,1-phenylene)bismaleimide
DSC	Dynamic scanning calorimetry
DTBD	Di-tertbutyl disulfide
ECH	Epichlorohydrin
EDG	Electron donating group
EWG	Electron withdrawing group
FA	Furfurylamine
FHF	1,6-hexamethylene-bis(2-furanylmethylcarbamate)

FRPC	Fibre reinforced polymer composite
FTIR	Fourier Transform Infrared
GSH	Glutathione
HA	n-Hexylamine
HOMO	Highest occupied molecular orbital
ILSS	Interlaminar shear strength tests
LUMO	Lowest unoccupied molecular orbital
MHHPA	Methylhexahydrophthalic anhydride
P(MMA-co-AEMA))	poly(methylmethacrylate-co-(2-acetoacetoxy)ethylmethacrylate)
PAN	Polyacrylonitrile
PBD	Poly-butadiene
PDMS	Polydimethylsiloxanes
RAFT	Reversible addition fragmentation chain transfer
SCNP	Single chain nano particle
SEC	Size exclusion chromatography
TBD	1,5,7-triazabicyclo [4.4.0] dec-5-ene
TCEP	Tris(2-carboxyethyl)phosphine
TE	Transesterification
UTS	Ultimate Tensile Strength
VU	Vinylogous Urethane
WLF	William-Landel-Ferry
YM	Youngs Modulus

Contents

Chapter 1

Introduction

1 Chapter 1 - Introduction

This introductory section aims to provide the reader with an understanding of important discussion topics related directly to the scope of this PhD project. This includes some basic polymer nomenclature and polymer properties, recycling characteristics and an in-depth review of reversible covalent bonds, previously employed for incorporation into network polymers, to create adaptable networks suitable for recycling. The dynamic bonding section includes a brief introduction to the area, regarding polymers, and is then organised into subsections by bond type, which includes a chemical overview, to familiarise those with a non-organic chemistry background with the reversible mechanisms. These subsections further define the network adaptable mechanisms (associative or dissociative), before covering the scope of the current literature and assessing the mechanical properties to aid in the evaluation of the work presented in this thesis.

1.1 Thermoset Polymers

Polymers are classified and sorted into three groups, shown in Figure 1, which differ based on their chemical structure: Thermoplastics, elastomers and thermosets. Thermoplastics typically have a linear polymer structure, which may include a degree of branching (green - Figure 1) and these polymers can continuously be reprocessed by heat due to the ability to flow. They find many practical applications in extrusion-based processes. Amorphous (purple - Figure 1 and semi-crystalline (blue -Figure 1) describes the chain ordering within the polymer. Regarding, amorphous polymers, they have no formal order and a higher degree of chain entanglement. Crystalline polymers are referred to as semi-crystalline because, although the chains are ordered, there are still some degree of amorphous areas within the material, as highlighted in Figure 1.[1]

Network polymers (black - Figure 1) are three-dimensional polymeric structures, grouped into thermosets and elastomers. Both contain crosslinks between polymer chains within the material structure, and these are further grouped according to the resultant material properties depending how rubbery or rigid the networks are, which is often influenced by the crosslinking density. Crosslinking can be observed, as the polymerisation reaction progresses, by the formation of an insoluble gel and an exponential increase in the material viscosity, which corresponds to the formation of an 'infinite' molecular weight polymer network structure, that cannot flow. The critical extent of reaction required to form a polymer gel in known as the gel point or p_{gel}.[2] Upon heating, the material will not flow, like thermoplastics, and will eventually combust on excess heating, rather than melting. A network polymer can be formed by reacting a multi-functional molecule or polymer, with another multi-functional molecule (or polymer) containing a complementary chemical functionality. Traditional network polymers/thermosets are not recyclable or reprocessable by currently employed means.
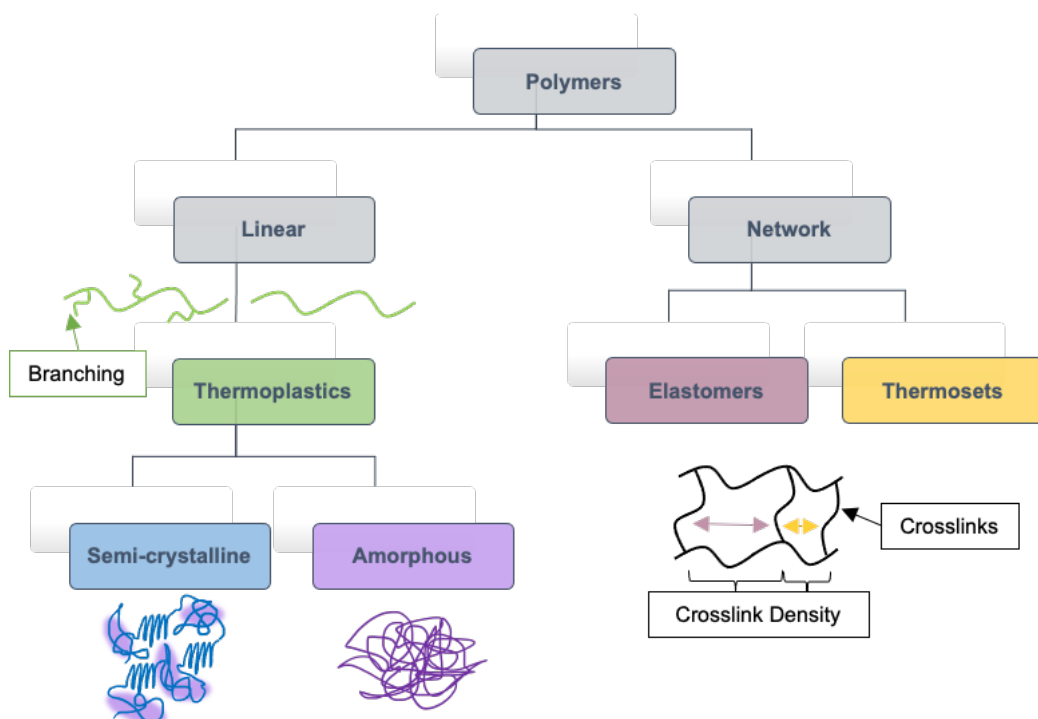
Figure 1: Polymer classification hierarchy and chain visualisations.

The network visualisation in Figure 1 is a simplified representation between two polymer chain segments, when in reality the crosslinking occurs between several different polymer chain segments, forming three-dimensional networks. Hence, forming a molecule with an 'infinite' molecular weight. The degree of crosslinking is represented by the distance between crosslinks in the molecule, with elastomers having a larger distance between crosslinks per unit volume of polymer (low crosslink density) and vice versa for thermosets. Elastomers are rubbery networks, which means they can stretch and return to their original shape, to a degree, but cannot flow like thermoplastics due to the presence of permanent crosslinks. Thermosets are rigid structures which have restricted segmental motion due to having densely crosslinked structures. Controlling the extent of the crosslinking reactions provide the user with control over the material properties of the final polymer. Two theories are accepted for relating the gelation to the composition of the polymer: The Carothers theory and the Flory-Stockmayer theory.[2–4]

The Carothers theory is based on the average functionality (f_{avg}), where two functionalities are present in equivalent amounts. The f_{avg} is defined by Equation 1:

$$f_{avg} = \frac{\sum N_i f_i}{\sum N_i} \tag{1}$$

where N_i is the number of molecules of monomer i and f_i is functionality of the monomer i. This theory requires equivalent stoichiometry of functional groups and the assumption that the reactivity of the same type of functional group is equivalent, regardless of size of the molecule or the positions of the functional groups, with regards to other

substituents in the molecule. Equation 1 can be further derived to give the critical extent of the reaction (p_c), which is defined by Equation 2:

$$p_c = \frac{2}{f_{avg}}$$

(2)

The Carothers theory is not representative of non-stoichiometric ratios of monomers of multiple functional groups. Therefore, the Flory-Stockmayer theory was developed. The first theory, conceptualised by Paul Flory in 1941, was in regards to branched systems of the same monomer.[5] This was further derived, for step-growth polymerisations between two different types of monomers, by Walter Stockmayer in 1944.[6] The p_c, otherwise known as the gel point (P_{gel}), is defined as Equation 3:

$$p_{gel} = \frac{1}{\sqrt{r(f_a - 1)(f_b - 1)}}$$

(3)

where f_a or f_b is the functionalities of the respective monomers and r is the stoichiometric balance of the monomers *a* or *b*. The theory relies on three assumptions:

    i.   All functional groups of the same type have the same reactivity.

    ii.   Reactions are selective between A and B.

    iii.   There are no intramolecular reactions.

Applying the Flory-Stockmayer equation in the formulation of a crosslinked network can allow the user to determine the amount of reaction required to achieve gelation or the minimum functionality required to achieve gelation with a crosslinking molecule. The

reaction will achieve gelation when p_{gel} is less than 1. Realistically, gelation is observed at slightly higher conversions due to the idealised assumptions in the model.

The segmental motion of the polymer chains is severely restricted above the gel point and affects the thermal phase transition properties of polymers, which are more complex than standard small molecules. They show distinctive transitions between phases such as the glass transitions (T_g). The glass transition of a polymer is the temperature at which the network transitions from a hard "glassy" state (frozen segmental motion) to the softer rubbery state (chain segments can flow). These are conventionally measured by dynamic scanning calorimetry (DSC) where the sample is heated over a large temperature range at a specified heating rate producing a thermogram. The T_g is usually taken from the midpoint of the temperature range. It can also be found by dynamic mechanical analysis as the peak of the tan δ curve. The T_g can be an indicative factor for the upper service temperature of polymers utilised in commercial applications.

1.2 Epoxy-Amine Thermosets

The scope behind the work conducted throughout this PhD project involves epoxy-amine thermoset polymers. These types of polymers are highly regarded as high-performing polymers due to their high mechanical, thermal and chemical resistant properties. The simplest route to an epoxy-amine polymer involves the reaction between a diepoxy and an amine via a step growth polymerisation mechanism. This results in the formation of a linear, thermoplastic polymer. For the formation of a three-dimensional network polymer or thermoset, one of the reactants must contain >2 reactive sites on average. Typically, a diamine is employed, which has 4 reactive sites for epoxy ring opening reactions. Figure 2 shows the nucleophilic addition reaction mechanism between the nucleophilic primary amine and electrophilic epoxy groups, where the resulting molecule is a secondary amine, which can further react with another equivalent of epoxide to form a

tertiary amine.[3] The reaction results in the formation of a β-aminodiol group, referred to as diethanolamine (DEA) groups during this work, which is an important reactive site in the context of this thesis. Various catalysts can be employed to increase the reaction rate of reaction, between amine and epoxide groups, which includes tertiary amines, Lewis acids, H-bonding species and Bronsted acids.[7,8] Epoxy resins react relatively slowly with tertiary amines at room temperature therefore they are commonly employed as catalysts at elevated temperatures to increase the reaction rate. Hydroxyls are another known class of catalysts for the epoxy-amine mechanism, resulting in an auto-acceleration effect. This means that the DEA group produced in the stepwise reaction is can also act as a catalyst as the reaction progresses. The molecular building blocks that make up the epoxy resin/polymer and the nature of the R_2 group on the primary amine, can all contribute to the final thermal and mechanical properties of the epoxy-amine polymer, including important properties such as T_g, tensile strength, Young's modulus and thermal stability.
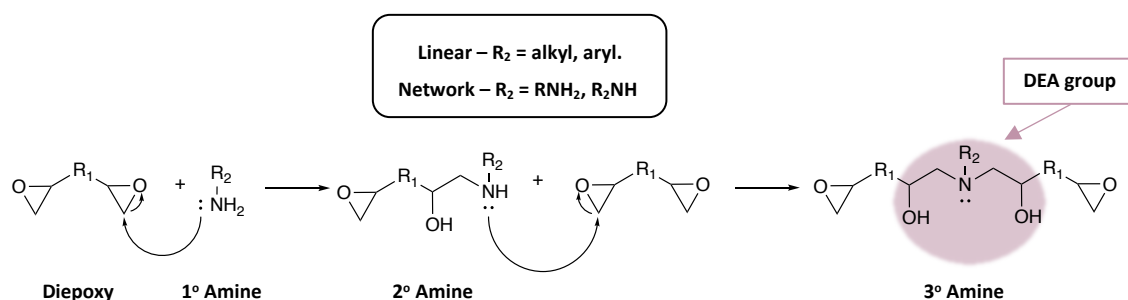
Figure 2: Epoxy-amine polymerisation curing mechanism.

A widely employed, diepoxy utilised in epoxy thermosets, as depicted in Figure 2, is derived from the reaction of bisphenol A and epichlorohydrin (ECH) as shown in Figure 3. This reacts in the presence of a base, such as NaOH, forming prepolymers known as epoxy resins, which is commonly referred to as diglycidyl ether of bisphenol A (DGEBA).[3,9] Secondary reactions can occur in small amounts and hence, the prepolymer

resins are formed in various purities. Other secondary reactions can occur in the manufacture of these pre-polymeric resins, which include hydrolysis of epoxy groups to form low concentrations of diols, and the formation of bound chlorine due to inefficient ring closure after reaction with epichlorohydrin.[9]
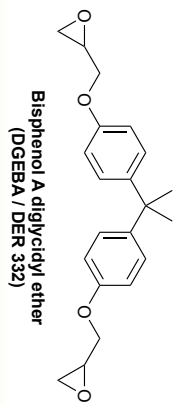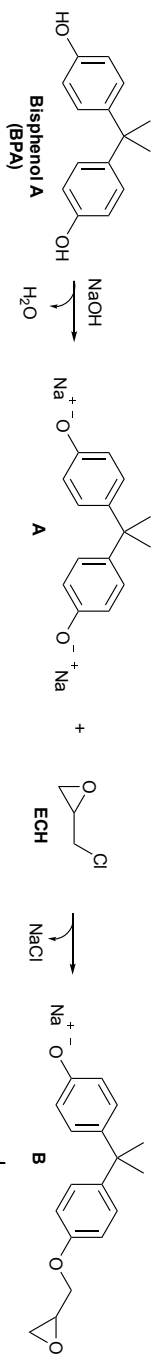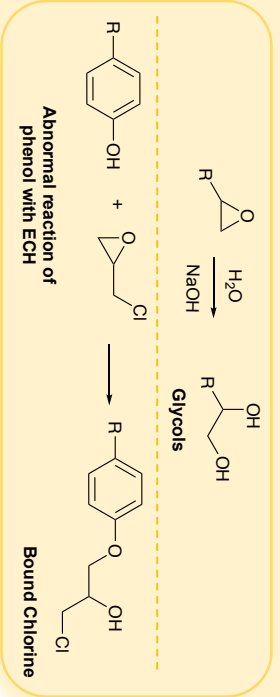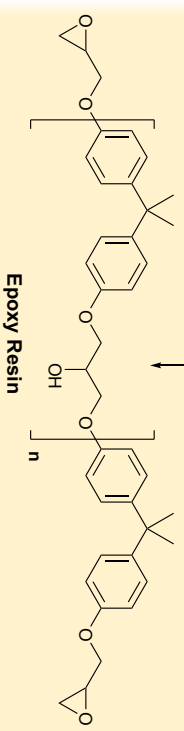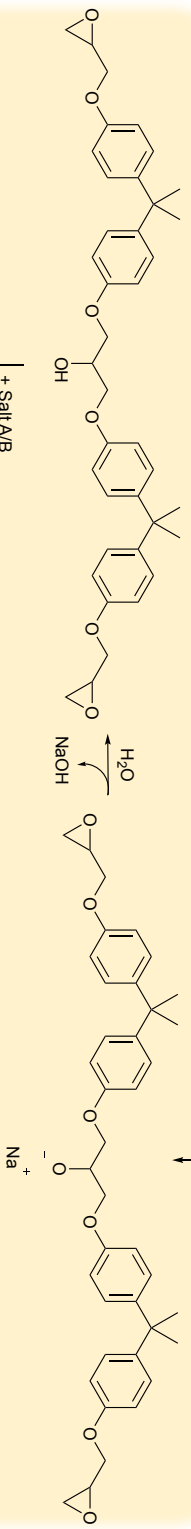
Figure 3: Epoxy resin pre-polymer synthesis showing the secondary reactions.

1.3 Recyclability in Polymers

Recycling of polymer waste is of pressing concern due to the profuse pollution in the environment. The UN recently released a sustainable development agenda in 2015, which set out a 15-year plan that all member states agreed to achieve by 2030. Rule number 12 is to "ensure sustainable consumption and production patterns", with one of the main goals of rule number 12 being "by 2030, to substantially reduce waste generation through prevention, reduction, recycling and reuse".[10] This means that fabrication of future consumer and commercially relevant polymers must have a planned route to be sustainable at the end of their service life.

Thermoplastics can be melted and recycled into repurposed items but thermosets cannot; they will only burn upon heat processing.[11] However, thermoset polymers are a vital class of materials utilised in areas such as medical, aerospace, energy and sports goods because of the lightweight and strong mechanical performances provided due to the high degree of crosslinking. In commercial, applications these can be applied as protective coatings or as composite materials, which are commonly impregnated with carbon or glass fibre to increase material strength, whilst maintaining light-weight material properties. This property is often referred to as a strength:weight ratio and is an indicator of good composite performance when striving to achieve light-weight materials for aviation or renewable energy infrastructure, such as wind turbines.

In aviation, thermoset composite materials are estimated to give up to a 25% reduction in industrial CO_2 emissions.[12] For wind turbines, the longer the rotor blades, the more efficient at collecting energy and converting to power (Figure 4). Therefore, lighter materials with the same mechanical strengths as traditionally employed composites can afford more efficiency. Consequently, it is unlikely that consumption of thermoset polymers will cease due to the advantages and excellent performance that such

materials present. Specific to wind turbines, the UK governments department for business, energy and industrial strategy released an interactive database that shows current and future wind farm plans.[13]

Year	Diameter (d) / m	Output / kW
1980-1990	17	75
1990-1995	30	300
1995-2000	50	750
2000-2005	70	1500
2005-2010	80	1800
2010	100	3000
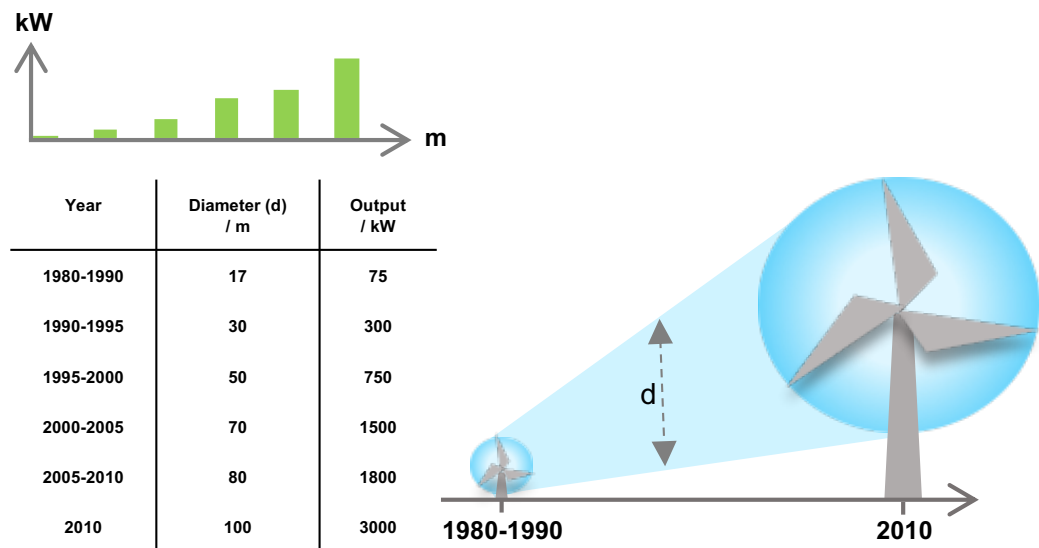
Figure 4: Wind turbine rotor blade development reported by the epoxy resin committee. Figure reproduced from reference 12.[14]

Figure 5 shows the geographical spread of the all the UK wind energy projects deemed to be operational, under construction, awaiting construction and with applications currently submitted without a decision. This does not include the decommissioned sites, of which there are only 8. The pie chart shows that more than 25% of all projects are still planned for the future construction, therefore there is a pressing demand for high-performance thermosets, and at present such materials are not currently recyclable.
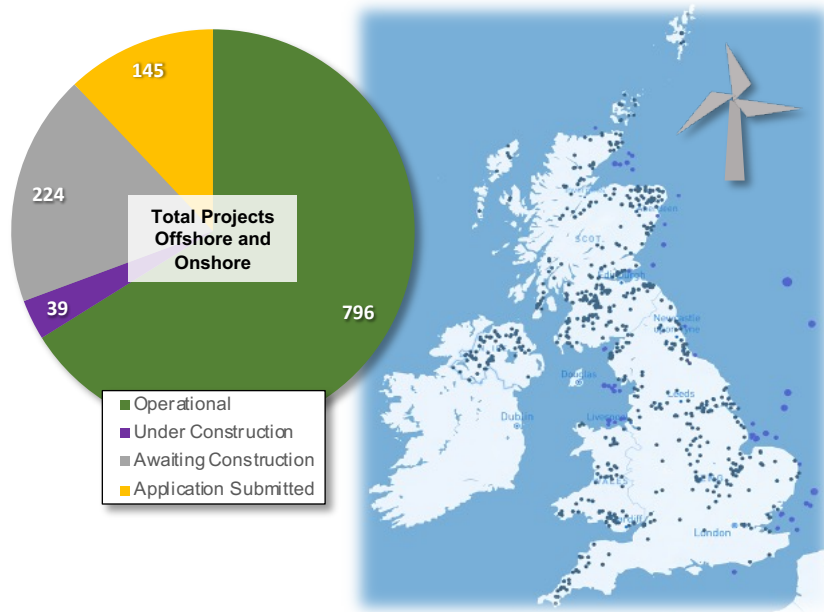
Figure 5: UK wind infrastructure and future projects

Although glass fibre is typically employed in wind turbine rotor blades[11], carbon fibre is the another attractive composite material to embed in a polymer matrix, for high-performance applications, owing to its low density, high strength, resistance to chemicals and strong heat resistance.[15] To the consumer, it typically comes in aesthetically pleasing, pre-fabricated sheets of interwoven carbon fibres, which are visible in a commercially available carbon fibre hockey stick shown in Figure 6, or as cheaper laminated sheets, both for less than £100 per m^2 depending on the quality.[16]

Figure 6: Visible woven carbon fibre (Black) in a 35% carbon composite hockey stick.

These sheets are then embedded in a polymer resin, usually via a vacuum infusion process or lamination. However, the development process is also one of the most

expensive due to demanding energy costs and specialized procedures. Hence, for less mechanically demanding uses they are often combined with cheaper glass fibres for reinforcement. Therefore, full recycling of this material is appealing, from a financial perspective. Another driving factor for recycling is the prevention of landfill disposal, as this poses environmental concerns.

The majority of carbon fiber is produced from poly-acrylonitrile (PAN) precursors, as a result of less voids in the material, compared to other precursors such as pitch (carbon-based i.e. crude oil) and rayon (plant-based i.e. cellulose).[15,17] Carbon fibres are produced in a multi-step process (Figure 7) involving: fibre spinning of PAN, subsequent stabilisation at 200-300 °C in an oxidative environment in which a radical cyclisation of PAN occurs. The next step of the process is carbonization in the absence of oxygen, between 1000 °C-1700 °C, with a higher temperature heat treatment up to 3000ºC, which provides the fibres with an increased tensile modulus.[15,17,18]
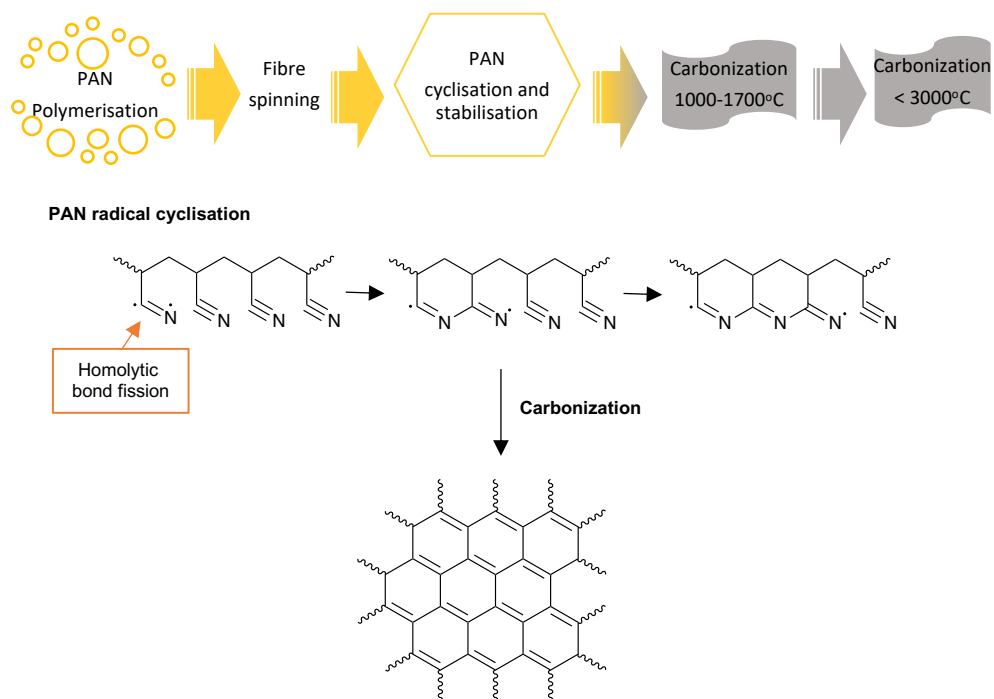
Figure 7: Visualisation of a generalised carbon fibre process from PAN polymers adapted from references.[15,17]

Epoxy composites, which generally comprise from epoxy-amines reactions described in Section 1.2, are widely employed as the polymer matrix for high-performance applications. As a result of being a lightweight replacement for traditionally metal parts, they enable industries such as automotive and aerospace to become more fuel efficient, hence reducing their environmental impact through reduced CO_2 emissions.[19] However, these types of composites are usually derived from petroleum-based bisphenols with the main resin of choice being derived from bisphenol A (Figure 8), which adds further issues towards sustainability because petroleum-based feedstocks are a finite resource that cannot be regenerated. For example, wind turbines are a renewable energy principally derived from non-renewable petroleum sources. As of 2015, up to 50% of European wind turbine rotor blade manufacturers employ epoxy resins in their process.[20] With the blades containing two thirds of the total epoxy resin consumption over the whole wind turbine manufacturing process and the other applied in coatings for the steel and concrete towers.[14,20] Therefore, recycling routes are critical to the thermoset industry. Current waste routes for the end-of-life wind turbine blades are landfill or incineration.[11]
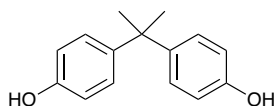
Figure 8: Structure of bisphenol A.

Processes to recycle of thermoset materials can be split into three methods: Thermal recycling, mechanical recycling and chemical recycling. Thermal recycling of composites is most widely employed for returning carbon fibres from epoxy matrixes. However, pyrolysis temperatures of 500-550 °C is a highly energy intensive process and destroys the polymer material via combustion but can allow recovery of carbon fibre. However, the resultant carbon fibre material can be of lower quality than pristine carbon fibres.[21] Mechanical recycling is where the thermoset composites are ground into fine particles

and can be reused as low-grade filler for other materials. However, this method offers the least return of the original material investment with a low return of material quality and value. In addition, future recycling cycles of the "filled" materials will add difficulties sorting the polymer waste in the future due to contamination and use of mixed materials. Chemical recycling focuses on depolymerisation or recovery of composite fibres by dissolution of the polymer matrix in solvents. Three main types of chemical recycling are prominent and they are: hydrolysis, glycolysis and acid digestion.[11] The first two methods are more environmentally friendly as the solvents can be recovered by distillation, but ultimately require high temperatures and pressures during the process which is energy intensive. The latter does not require high pressures but is a much slower process and can also lead to solvent waste. Chemical recycling is only suitable for certain polymer types and is a high energy consumption process.

Overall, recycling of thermoset polymers is extremely limited with repurposing as fillers for new materials one of the only methods of recycling. This is due to the crosslinked network structure, which imparts the materials strength and other useful properties, rendering thermosets insoluble and difficult to breakdown or reform by chemical methods or thermal methods. Therefore, manipulation at the chemical level is required to install recyclable mechanisms into the material. Dynamic bonds present an opportunity to insert a reversible or 'de-polymerisation' mechanism directly to the thermoset polymer network offering new potential routes to an unlockable polymer network structure, with whole system recycling, including recovery of polymer and fibre, ready for re-use.

1.4 Dynamic Polymers

1.4.1 Dynamic Bonding

Responsive materials are renowned for utilising the breaking and reformation of dynamic bonds, either autonomously or in response to an external stimulus.[22] The stimuli that are responsible for activating a response typically come from environments such as solvent, pH, light, temperature or mechanical stresses. The type of dynamic bonds can be categorised into two areas dependent on the bond type: dynamic covalent bonds (DCB's) or non-covalent dynamic interactions known as supramolecular interactions, in the case of polymers, and these involve interactions such as hydrogen bonding, metal-ligand coordination or $\pi-\pi$ Stacking.[23] The former is the chemistry behind the main focus of this thesis and the latter also subject to extensive research outside the current scope of this work.[24–28] Figure 9 shows two types of non-covalent interactions that are likely to be present in polymers containing aromatic groups or polymers containing hydrogen bonding functional capabilities. Therefore, it is worth noting that these intermolecular interactions can also affect the resultant material properties. For example, hydrogen bonding can increase a materials stiffness and also its stretchability, delaying fracture.[29]
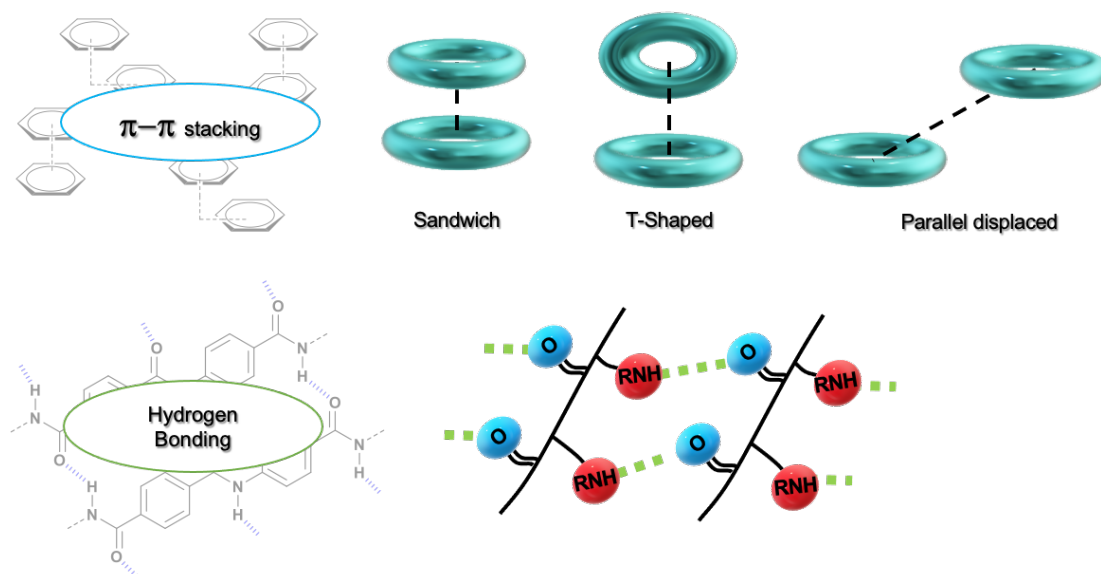
Figure 9: Visual representations of supramolecular interactions where the blue rings represent delocalised pi electrons on an aromatic benzene ring and the green dashed lines represent H-bonding intermolecular interactions.

Covalent bonds are ubiquitous throughout chemistry and the theory of the shared pair of electrons can be dated as far back as 1916 when Gilbert Newton Lewis proposed his cubical atoms.[30] DCB chemistry involves reversible covalent bonds and, when compared to traditional covalent bonds that are permanent in a molecules' structure, DCB's, when triggered by a specific stimulus, undergo reversible exchange reactions as a response to meet the thermodynamic equilibrium minima as depicted in Figure 10.[31] However, when the stimulus is removed, the dynamic bonds can return to their original product offering the reversibility in both reaction directions.[23,32] The thermodynamic vs kinetic control theory is of particular importance when the DCB of choice may form multiple products such as a mixture of isomers which are possible in commonly used dynamic Diels-Alder (DA) reactions that will be discussed further on in Section 1.4.2.1.1.
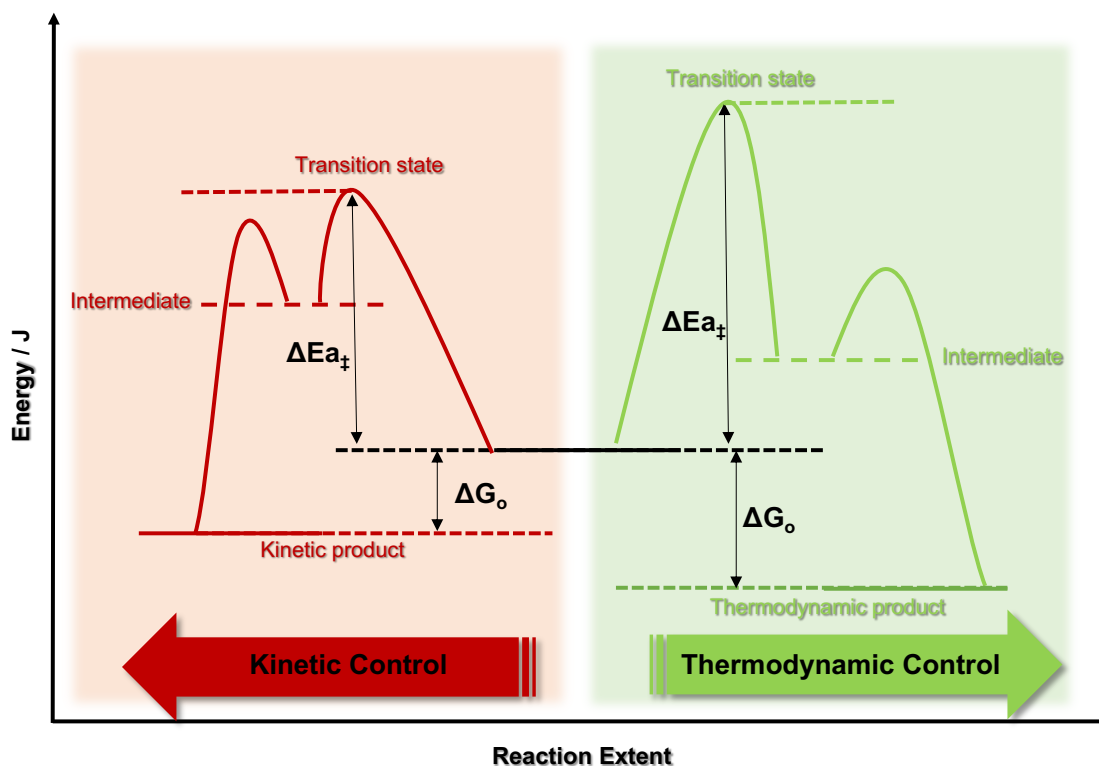
Figure 10: Kinetic vs thermodynamic reaction pathways in general terms where $\Delta Ea_{\ddagger}$ is the activation energy of the transition state and G_0 is the Gibbs free energy of the reaction.

1.4.2 Dynamic Covalent Bonds in Polymers

This sub-section aims to cover the chemical mechanisms and review the integration of DCB's in polymers and the resultant niche uses reported in the literature.

In recent times, much attention has been focused on the addition of dynamic bonding in polymers structure to either improve their properties or, from an ever-evolving requirement environmentally, to provide a route for reprocessability where this was previously unattainable. This is especially prevalent in the case of thermosets as discussed earlier in Section 1.1. Thermoset plastics and composites are irrefutably vital to society, the environment due to their outstanding mechanical performance, chemical resistance and light-weight properties, which increase longevity and service efficiency. Consequently, this comes at a price of limited recyclability due to the crosslinked, three-

dimensional polymer network structures, which prevents thermal reprocessing or dissolution in solvents. Thus, reprocessability should be, at the very least, a minimum requirement when designing novel polymers and, in an ideal scenario, full recyclability and recovery of materials should be considered when designing new polymer technologies.

The dynamic nature of the DCB's provide a fundamental basis for recyclable[33–35], self-healing[31,36–40], and smart/responsive polymer materials[32,41,42]. Several recent reviews cover DCB incorporation as a mechanism of molecular manipulation, within the polymer structure, to improve the reprocessability or the overall properties of the final polymers.[23,32,43–49] Polymers possessing DCB's are often broadly termed dynamers and networks are often specifically termed covalent adaptable networks (CANs).[44,46,50–53] CANs provide a promising route to high performing and recyclable thermoset polymer materials in which the reprocessability behaviour can be designed at the molecular level for specific end-use requirements.

Although "dynamic polymers" vastly populate the literature with 146,313 reports on Web of Science, these reports ultimately include non-covalent interactions and non-network polymers.[54] Within the specific field of "covalent adaptable networks (CANs)", which is relevant to the scope of this research, the first research publications emerge from around 2010, and were defined as such by the Bowman research group. This area has received significant attention in recent years.[55] The term CAN was coined after a previous publication in 2008 that utilised Diels-Alder dynamic bonds to crosslink network polymers.[56] Around a similar time (2011), Leibler and co-workers pioneered a CAN polymer that undergoes associative dynamic exchange based on transesterification,[57] which they referred to as vitrimers (2012),[58] as have several others since. Thus, care should be taken to include both terms when exploring the literature.
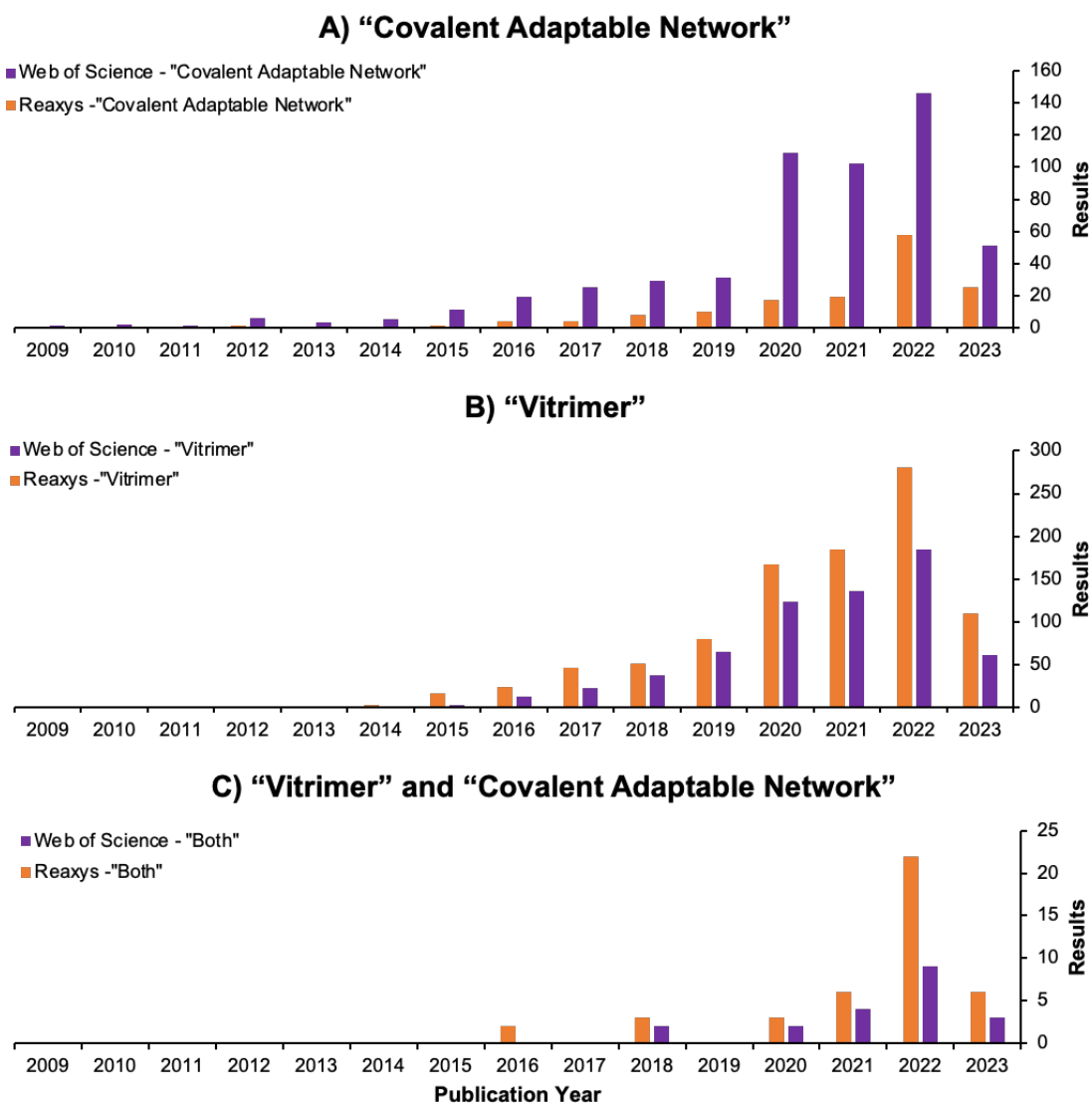
Figure 11: Literature results from common research search engines i) Web of Science (WoS) and ii) Reaxys, for the search terms A) "covalent adaptable network", B) "Vitrimers" and C) when a combination of both terms are searched (Reaxys) and/or refined (WoS). Date accessed: 5/5/2023.

As evidenced in Figure 11, there is a lack of both terms appearing in the same publication. In the last 3 years, since the beginning of this PhD project in 2019, there has been a substantial increase in the number of research publications in the literature quoting "covalent adaptable network" or "vitrimer" compared to preceding years. Thus, the explosion of new research in this area solidifies the contribution of the project to an exciting, emerging field of polymers. In addition, it was noted that there were no hits

covering the term appeared before 2009 on Web of Science or Reaxys prior to Bowmans group. However, there is an abundance of relevant literature for DCB usage in thermoplastic polymers prior to the CAN concept which will be referenced where relevant during the forthcoming sections in this introductory review.

CANs are macromolecular networks that can rearrange their topology due to dynamic bond exchange reactions, under various stimulus. CANs fall into two general categories based on the dynamic exchange mechanism of the DCB utilised as the crosslinker and are described as either i) associative or ii) dissociative. Vitrimers, first reported by Leibler and co-workers describe the similarity to vitreous silica, are included in the class of associative dynamic materials, with regards to thermally activated DCB bond exchange mechanisms.[57,58] Du Prez and co-workers later defined vitrimers based on three factors; covalent bonding, has an associative exchange mechanism and is thermally triggered.[59]

Figure 12 shows the generalised difference between reversible covalent bonding mechanisms in network polymers. For an associative exchange mechanism, the net number of covalent bonds in the system remain constant due to the dynamic bonds forming and breaking simultaneously, resulting in permanent network integrity. Whereas, for dissociative mechanisms, the integrity of the network can be lost upon being triggered by the stimulus due to the covalent bond must becoming broken before being reformed. Thus, resulting in a temporary reduction in crosslink density within the network polymer.

Associative
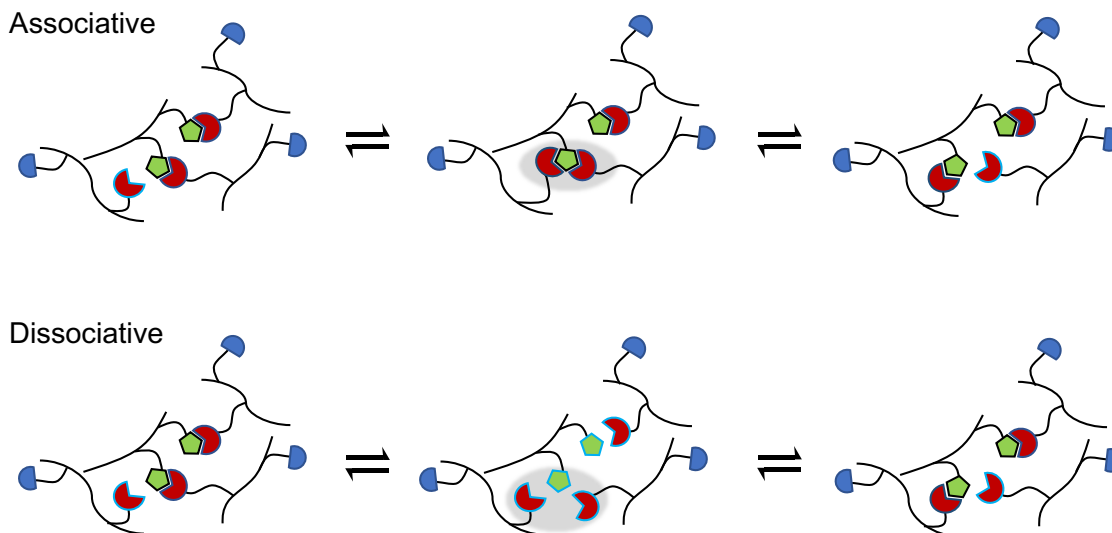
Dissociative

Figure 12: Visual representation of associative and dissociative exchange mechanisms where the shapes represent functional groups along a linear polymer chain (black). A light blue outline represents a free to exchange dynamic bond and the highlighted grey area focusses on differing integrity of the covalent bonds within the network, between exchange mechanism type.

Both groups (Leibler and Du Prez) appear to agree that there is another theoretical temperature dependency, relative to the rearrangement of the dynamic bonds present in the polymer, which is known as a topology freezing temperature (T_v). This is defined as the temperature at which dynamic exchange is assumed to be frozen, when below the T_v, or active when above T_g. Leibler et al. proposed that the network is frozen when the viscosity reaches 10^{12} Pa, indicating when the material is likely to behave as a thermoset (below T_v) or behave as viscoelastic fluid (above T_v).[57] This is regarded as hypothetical because although a value can be obtained from stress relaxation data, the physical transitions are ultimately dominated by segmental motion and hence controlled by T_g.[59] Therefore, T_v is more of an estimation of the importance of the dynamic exchange for controlling the material properties.[60] Vitrimers can display two characteristic behaviours regarding T_v, which are visualised in Figure 13.[22,59,61]
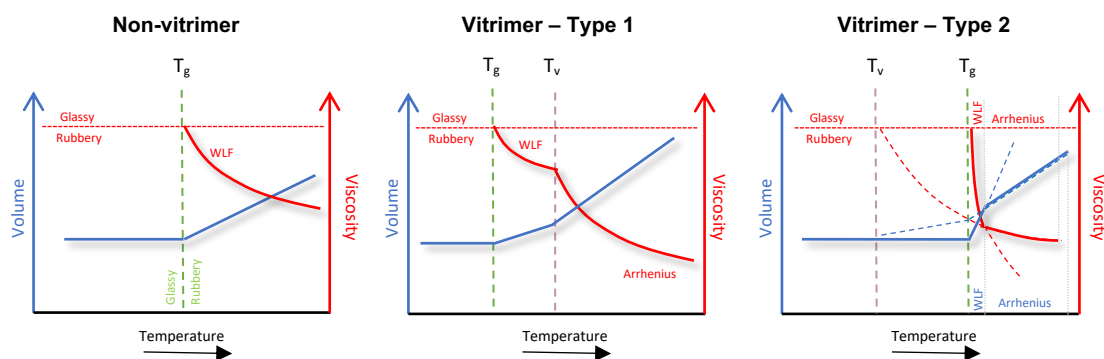
Figure 13: Theoretical effect of T_v material behaviour depending on the temperature relative to T_g. Figure adapted from references. [22,59,61]

Type 1 shown in Figure 13, represents a material with a $T_v > T_g$, which behaves like a normal polymer, controlled by diffusion and segmental motions by a William-Landels-Ferry model (WLF), until the T_v is passed, which then brings the exchange reactions into control and the polymer behaves Arrheniusly. Type 2 is where the $T_g > T_v$ and this presents unusual behaviour where the diffusion control below the T_g has limited the segmental motion of chains whilst the dynamic exchange is active, and with the rates of exchange also being controlled by temperature, upon passing T_g there is an uncontrolled fast bond exchange following WLF behaviour, which causes a sudden decrease in viscosity, before following a predictable Arrhenius behaviour.[61] Overall, prior knowledge of the T_v of the dynamic exchange reactions will provide useful insights into how the vitrimer will perform, which is crucial for high-performance applications where the service use is expected to be over a wide range of temperatures such as in aviation.

The reactions that associative and dissociative CAN mechanisms follow are related to three main types: addition, condensation, and exchange/substitution reactions. Addition and condensation reactions typically fall under dissociative pathways, whereas exchange/substitution typically fall under associative pathways. As displayed in Figure 14, the reversal process of the addition and condensation reactions would produce two separate products A and B that are not covalently bonded. Therefore, the net number of

covalent bonds present would decrease overall for the reverse process. Whereas an exchange reaction would have a constant number of covalent bonds through both the forward and backward reaction directions, therefore, the net overall would remain the same throughout the exchange process. Due to the difference in network density of the two mechanisms upon activation of the dynamic bond, one can expect significant differences in viscosity changes from glassy to viscous in dissociative mechanisms as well as solubility in common organic solvents, when the network ceases. Conversely, for associative mechanisms, one can expect less significant changes in viscosities over a temperature range whilst remaining insoluble in organic solvents at any temperature due to the fact the network remains intact. The importance of these associative and dissociative mechanisms are highlighted in a review focussed on improving a material's resistance to creep, at room temperature, whilst allowing self-healing/reprocessability at high temperatures.[62]

$$A + B \xrightarrow{\text{Addition}} AB$$

$$A + B \xrightarrow{\text{Condensation}} AB + C$$

$$AB + CB' \xrightarrow{\text{Exchange}} AB' + CB$$
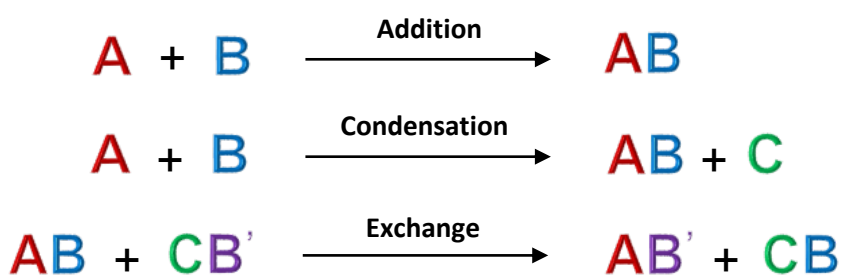
Figure 14: Reaction types that contribute to CANs mechanism type.

Materials made from polymers are prone to damage from external forces over their service life. In high performance applications, such as aerospace and transportation, failures in the material can lead to disastrous consequences. Therefore, extending the service life of these materials not only make for safer materials but can also prevent them prematurely needing replacing, or ending up in landfill or recycling plants. Therefore, research into self-healing materials is rising. Self-healing is the ability of a material to

recover from physical damage such as cracks, scratches, and full breakage, as visualised in Figure 15. Not only does self-healing recover its external shape but recovery of mechanical properties are also expected.[63] With regards to CANs, exploiting dynamic bonds as the mechanism for repair is categorised as intrinsic self-healing as the material can independently repair after external damage.[64]

The phenomenon of self-healing is usually achieved by applying the external stimulus, such as heat, to enable segmental motion in the materials, and with some degree of mechanical pressure to ensure there is also full contact between separated interfaces that will bring reacting groups in a close enough proximity. Other methods include use of solvent containing a compatibly reactive crosslinker to induce dynamic covalent chemical reactions and repairability.
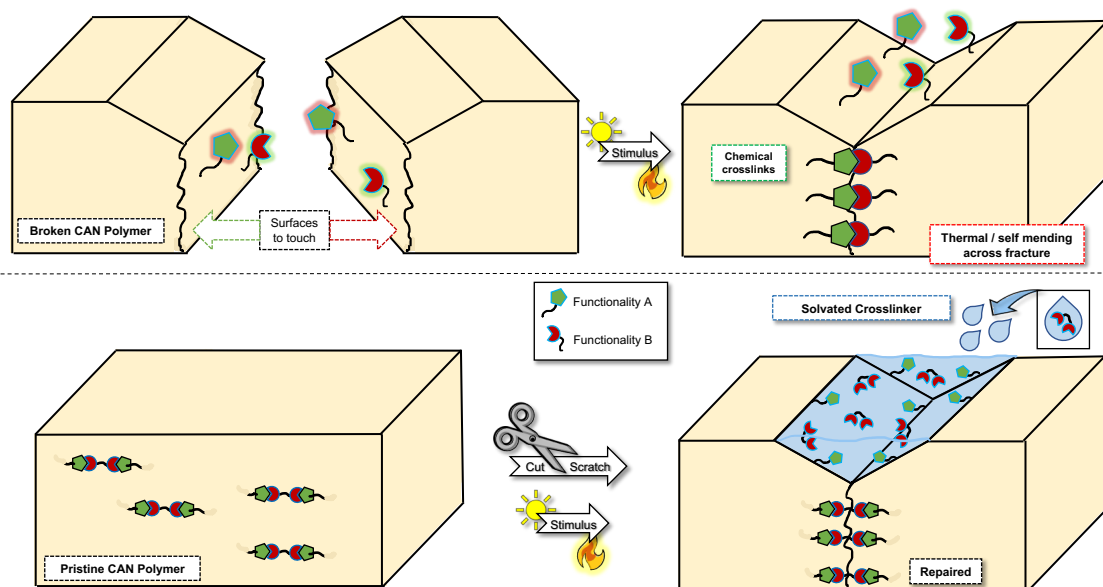
Figure 15: Visual representations of polymer healing over time in CAN polymers where the functionalities are representative of compatible dynamic bonds, which will be discussed throughout the remainder of this section.

25

Furthermore, with compatible functional groups present (represented by the green and red shapes in Figure 15) for dynamic bonding, polymer networks differing by their chemical make-up, have the ability to be adhered/welded to each other covalently at their surfaces. For example, a methacrylate polymer with functionality A (e.g., a carboxylic acid) may covalently link at the interface with another polymer such as an epoxy polymer with a compatible functionality B and will be covalently linked to one another. This is referred to as welding and has been visualised in Figure 16 with polymer A being covalently bonded at the interface with polymer B (AB welded). This means that substrates notoriously known to have difficulties adhering to one another, can be covalently linked by dynamic groups, thus exposure to the right stimulus may also enable self-healing between polymers.
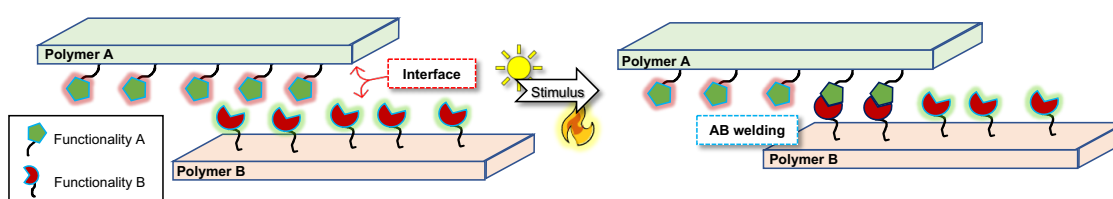
Figure 16: Welding at polymer interfaces.

One benefit of incompatible materials being covalently linked is the potential reduction of the number of layers needed for coatings, which can save time and money whilst affording the same resistance to corrosion of the substrate being coated. Self-healing materials applied to coatings would delay the inevitable onset of corrosion by reducing cracks/damage, reducing sites for water penetration and subsequent initiation of corrosion. The incorporation of dynamic bonds can also afford a mechanism in which to de-crosslink materials as a response to a specific stimulus, which in-turn will afford a route to full recyclability and reprocessing and hence the opportunity to reuse coatings materials, reducing the number of products destined for landfill.

The following subsections 1.4.2.1 to1.4.2.7 discuss the common chemistries, of the three reaction types listed in Figure 14, involved in CANs and review applications to traditional polymers used in thermoset networks to advance reprocessability or recycling pathways. They aim to cover various dynamic reactions that are at the forefront of CAN chemistry and intend on providing the reader with some basic mechanistic and conceptual understanding of the chemistry, behind the dynamic nature of the networks, as well as detailed review of current literature, with regards to polymers. This is to provide knowledge to a wider audience outside of organic chemistry and more orientated towards materials chemistry. Thus, material properties and recyclability opportunities are discussed, that may be useful for fields such as engineering.

1.4.2.1 Dynamic Reactions Employed in CANs for C-C Bond Formation

1.4.2.1.1 Diels-Alder Addition Reactions
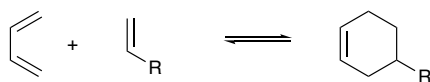
Figure 17: Diels-Alder reaction

Diels-Alder cycloaddition reactions are a widely used dynamic chemistry for the formation of C-C bonds via a 4 + 2 cycloaddition. This is a type of concerted reaction, that is thermally allowed under the 4n+2 Woodward-Hoffman rules for pericyclic cycloadditions.[65]

Diels-Alder reactions specifically involves a conjugated diene, in the s-cis orientation, where s refers to the single bond. This diene reacting with a substituted alkene (often termed as the dienophile or electron deficient diene) is a stereospecific, convenient route to forming a six membered ring as shown in Figure 17. As shown in Figure 18, the formation of new C-C bonds, via a Diels-Alder reaction, occurs so by simultaneously

breaking three π-bonds and forming two σ-bonds and one new π-bond in a six membered ring. For new bond formation to proceed the reacting orbitals must be in phase with bonding overlap. The orbitals that react have the smallest energy gap between them and are the highest occupied molecular orbital (HOMO) of one reactant and the lowest unoccupied molecular orbital (LUMO) of the other. In Diels-Alder reactions it is most commonly the HOMO of the diene and the LUMO of the dienophile that react.[65]
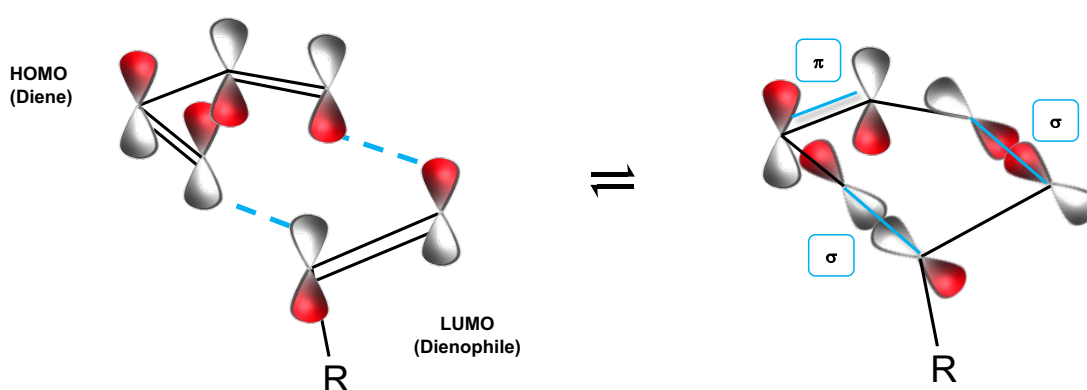
Figure 18: HOMO-LUMO visualisation of the simplest form (generalized scheme shown in Figure 7) of a Diels-Alder interaction where the stereochemistry of R is preserved through the reaction. The blue solid line represents the new C-C bonds formed.

The substituents on the reactants do not affect how the ring forms but they do influence the rate of the Diels-Alder reaction. For example, if the R group in Figure 18 is an electron withdrawing group (EWG), this will make the pi-bond electron deficient and more ready to react with the diene. An electron donating group (EDG) on the diene will help push electrons through to the dienophile. This type of Diels-Alder is known as a 'normal electron-demand' reaction and the opposite situation known as 'inverse electron-demand' is also possible but less frequent for an electron rich dienophile and electron deficient diene. The reason behind the increased reaction rate when the EWG is on the dienophile is that the energy gap between the HOMO of the diene and the LUMO of the

dienophile is reduced due to the lower energy of the LUMO. The same effect is seen when having an EDG on the diene increases the energy of the HOMO thus, bringing the energy gap closer to the LUMO. Furthermore, the reverse reaction (termed retro-Diels-Alder) proceeds when the temperature is high enough to become thermodynamically favourable. Retro-Diels-Alder reactions are unlikely to occur spontaneously at room temperature thus, heat is required to proceed the reverse reaction which allows greater control over the resultant products. Diels-Alder reactions also preserve the stereochemistry of the dienophile upon addition thus, provides an additional method to control the reaction depending on the desired configuration of the product.[65]

The Diels-Alder mechanism is an extensively studied topic in organic chemistry with 38,001 results on Web of Science when searching the term "Diels-Alder and further refining to "polymer" then "network" returned only 387 results indicating that this area is an emerging field of network polymer chemistry for adaptable networks.[66] Recently, attention has been paid towards applying the Diels-Alder mechanism in polymer synthesis as a covalent reversible crosslinking mechanism in CANs and numerous reviews outline the reactions utilized for recent advances to reversible thermoset chemistry.[22,23,47,67,68] The appeal of the Diels-Alder mechanism is that there are no by-products released during the reaction and the thermal reversal mechanism can be achieved at relatively low temperatures compared to traditional thermoset recycling temperatures. However, there are just a handful of Diels-Alder functionalities that have enabled recycling at temperatures below that of the polymer's degradation temperature.[69]

Common in the literature for a Diels-Alder adaptive network are the furan and maleimide functionalities, as shown in Figure 19, which depend greatly on temperature. These

moieties are known to be triggered in the reverse retro-Diels-Alder reaction at a temperature of ~110°C.[70]
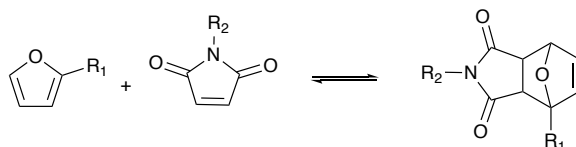
Figure 19: General Diels-Alder reaction between furan and maleimide derivatives

Prior to materialisation of the CAN concept, Wudl et al. were the first to develop a Diels-Alder network exploiting furan and maleimide Diels-Alder adducts as the crosslinks.[71] Their network boasted a tensile strength of 68 MPa which was in good accordance with commercial epoxy resins. Reversibility analysis by dynamic scanning calorimetry (DSC) and solid state ^{13}C NMR showed that the retro-Diels-Alder reaction did not occur below 120°C.

In 2008, Bowman's group synthesised a network polymer containing Diels-Alder compatible furan and maleimide functionalities and analysed the "reverse gelation", or in other words depolymerisation, over a series of temperatures and found a substantial equilibrium conversion to the Diels-Alder product from 74% at 85 °C to 24% at 155 °C.[56] This was achieved using 1,1′-methylenedi-4,1-phenylene as the R_2 group of the maleimide to form a bismaleimide curing agent (DPBM) and pentaerythritol-propoxylatetris(3-(furfurylthiol)-propionate) (PPTF) as the furan shown in Figure 19. This was also reported to be visibly liquid at 110 °C in line with the reported retro-Diels-Alder temperature for furan/maleimide reactions. Reported stress relaxation data found that the activation energy (E_a) for the dynamic furan/maleimide Diels-Alder reaction of this molecular combination was 88 ± 2 kJ mol^{-1}.

More recently, Xie et al. also employed DPBM as a bismaleimide, to act as the crosslinker, for application to epoxy-amine systems.[70] In their work, they synthesised epoxy-amine polymer chains with pendant furan functionalities by reacting the widely used aromatic epoxy resin bisphenol diglycidyl ether (DGEBA) with furfurylamine (FA), where R_1 is CH_2NH_2. Their effort achieved networks that showed excellent shape memory with a shape fixity (R_f) of 99.0% and a shape recovery (R_r) of 87.5%. These were calculated from Equation 4 and 5, from tests conducted using dynamic mechanical analysis (DMA) strain cycles, where ε_d is the fixed strain after removal of restrictions, ε_{load} is the maximum strain under load, and ε_{rec} is the recovered strain. The resultant dynamic polymer networks fitted ideal requirements for the application of complex engineering shape memory devices, such as biomedical devices that need to be inserted through keyhole and unfold to different shape in the body for its function.[72] The polymers also showed good reprocessability potential by accomplishing solution casting after dissolving in DMF at 110 °C.

$$R_f = \frac{\varepsilon_d}{\varepsilon_{load}} \qquad (4)$$

$$R_r = \frac{\varepsilon_d - \varepsilon_{rec}}{\varepsilon_d} \qquad (5)$$

Moreover, Sun et al. developed furan/maleimide Diels-Alder networks with polyurethane polymers enabling dynamic covalent networks with simultaneous dynamic non-covalent hydrogen bonding within the network, which was previously depicted in Figure 9.[73] Their approach focused on incorporating pendant *N*-(2,3-dihydroxypropyl)maleimide (DHPM) groups on the polyurethane polymer and crosslinking with a difuran, 1,6-hexamethylene-bis(2-furanylmethylcarbamate) (FHF). Monitoring the strength of the material with

differing ratios of furan to maleimide, from 0-1, showed significant increases in Youngs

modulus values as seen from their reported stress-strain curves, shown in Figure 20.
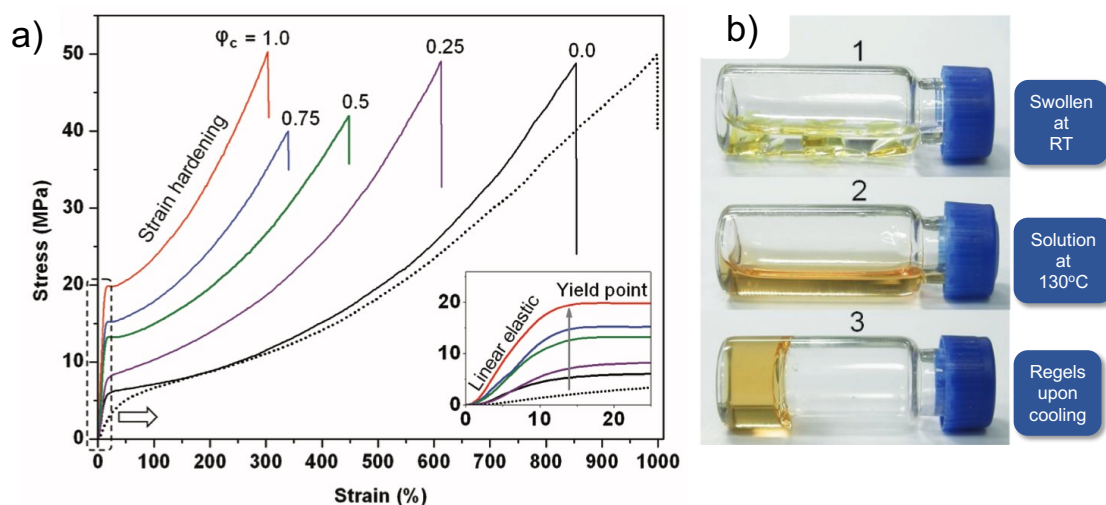
Figure 20: a) Tensile data reported by Sun et al. for polyurethane Diels-Alder networks and b) reprocessability demonstrated by thermal control in dimethylacetamide as a solvent also reported by Sun et al.[73] Figure adapted from S. Yu, R. Zhang, Q. Wu, T. Chen and P. Sun, Adv. Mater., 2013, 25, 4912–4917. Copyright © 2013 WILEY-VCH Verlag GmbH & Co. KGaA, Weinheim.

In 2019, Summerlin et al. reported furan/maleimide Diels-Alder crosslinked polymethacrylate polymers.[74] These were proved to be fully reversible in DMF at 153 °C with the aid of a maleimide scavenging diene.
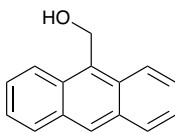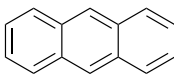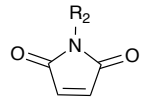
Figure 21: Maleimide scavenger used by Summerlin et al. for complete retro- Diels-Alder reaction in poly methacrylic polymer networks.

Further dynamic combinations of diene and dienophiles have been reported in the literature for polymer applications and have been summarised in a book review by Kuhl et al.[75] Important Diels-Alder reactions of note are; anthracene and maleimide and

cyclopentadiene dimerization (structures shown in Table 1). Sumerlin's work exploited

pair 1 in Table 1 by using the anthracene analogue, shown in Figure 21, as the maleimide

scavenger. Other, anthracene/maleimide work was conducted by Yoshie et al.[76] They

utilized a di-functional polyester (poly-ethylene adipate) with anthracene as the reactive

functional group and reacted that with a trifunctional maleimide. The resulting polymer

was found to be reversible by inducing mechanical stress, advancing self-healing ability

with a stimulus other than heat.

Table 1: Other types of Diels-Alder pairs

Pair	Diene	Dienophile
1	Anthracene	Maleimide
2	Cyclopentadiene	Cyclopentadiene

Cyclopentadiene dimerization has been explored by Wudl's group.[77] As shown in Figure

22, they prepared a dicyclopentene monomer which opens via the retro-Diels-Alder

mechanism producing a monomer with two cyclopentene functional groups and

subsequently reacts in the forward Diels-Alder reaction upon cooling, which results in a

linear polymer that still contains a C=C double bond able to react as a dienophile. Thus, enabling crosslinking to occur with unreacted monomer.
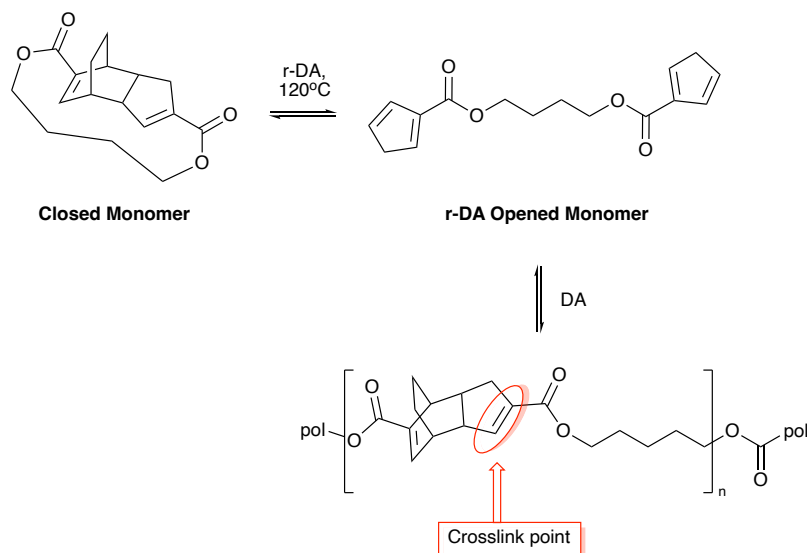
Figure 22: Polymerisation process by Wudl et al. for dicyclopentene monomers via a retro-Diels-Alder (r-DA) reversible mechanism. The red, circled double bond represents an available dienophile for the forward Diels-Alder reaction with unreacted opened monomer.[77] Adapted with permission from E. B. Murphy, E. Bolanos, C. Schaffner-Hamann, F. Wudl, S. R. Nutt and M. L. Auad, Macromolecules, 2008, 41, 5203–5209. Copyright 2008 American Chemical Society.

1.4.2.1.2 Olefin and Alkyne Metathesis
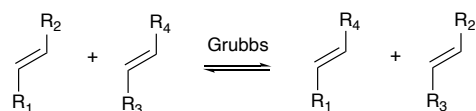
Figure 23: Olefin Metathesis exchange reaction

Olefin metathesis is an important tool for the formation of C=C bonds in organic chemistry and was the theme behind the Nobel prize in 2015. It involves the exchange of terminal alkene groups with an organometallic catalyst as the driving stimulus, such as the widely employed, ruthenium-based, Grubbs' catalyst, shown in Figure 24.[78] The Grubbs catalyst

is an ideal catalyst due to its high functional group tolerance, less bulky alkene and stability in air and moisture, compared to other organometallic catalysts used for olefin metathesis.[23] The first generation ruthenium catalyst was reported by Grubbs et al. in 1995, and was subsequently named after him.[79] The first generation catalyst is a precursor in the synthesis of the second generation of catalyst; the structures of which are shown in Figure 24. The second generation catalyst is was reported by Grubbs et al. and proposed to have less carbene stabilisation due to the lack of $\pi-$ interactions making it more basic than unsaturated imidazole alternatives.[80] Thus, any saturated imidazole derivatives for use as ligands in Grubbs' catalysts are recognised as second generation catalysts and generally have a higher activity in olefin metathesis.
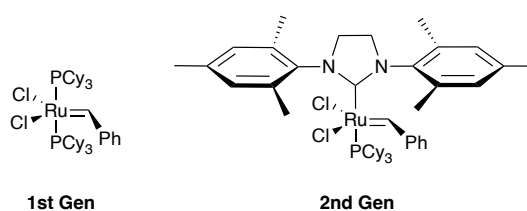
Figure 24: Common commercially available Grubbs' catalysts

The mechanism of olefin metathesis is catalysed by the Grubbs' catalyst via continuous formation and reversal of [2+2] cycloaddition four membered ring structures, which is shown in Figure 25. Hence, due to the exchange mechanism, affords an associative pathway to dynamic CANs.
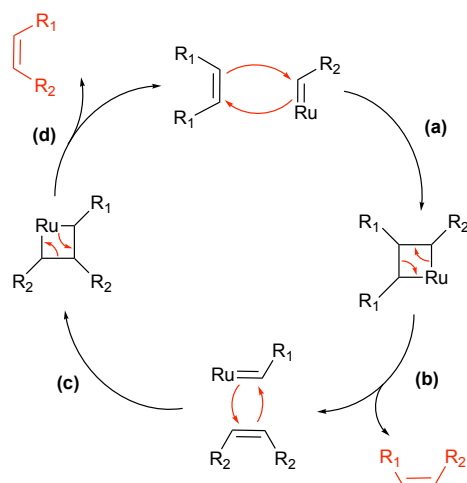
Figure 25: Olefin metathesis catalytic cycle showing regeneration of a simplified Grubbs catalyst.

With regards to polymers, olefin metathesis has become a key dynamic chemistry for development of CANs, where an alkene is present in the polymer chain, such as poly-butadiene (PBD) polymers. Leibler's group investigated olefin metathesis in PBD's as a route to make insoluble materials malleable at room temperature.[81] They compared the mechanical performance of their dynamic olefin CAN to an identical catalyst free control and found that the control had no malleability. Thus, confirming network rearrangement due to the Grubbs catalyst content enabling metathesis. Further work by Lu and Guan showed the self-healing effectiveness of PBD polymers loaded with small amounts of ruthenium catalyst.[47,82] They proposed that a PBD polymer containing the ruthenium catalyst could heal across the interface with an untreated control PBD sample. They found that venture successful reporting an 80% recovery of its maximum strain after just 3 hours at room temperature under 20 kPa of pressure.

Earlier attempts in olefin chemistry have been explored by Griffith in 1979 for exploitation of olefinic bonds in epoxy resins, as a means to input a cleavable weakness into a crosslinked material, for applications in flooring coatings that could be removed easily.[83] He proposed olefinic bonds can be cleaved in the network by strong oxidising agents such as acidic permanganate, which is shown in Figure 26.[43] Although this reaction is

36

not reversible, and is not technically olefin metathesis, it is worth noting as a potential route to recycling polymers of this class. The cleavage of the olefin bond could potentially be employed as part of a methodology in the future of dynamic polymers due to the loss of the alkene by oxidation and subsequent generation of carboxylic acids that could then be transesterified with alcohol functional groups, (see Section 1.4.2.3.1), which is something that has the potential to be explored for recycling purposes as well as smart complementary functionalisation attempts.
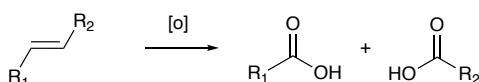
Figure 26: Oxidised olefinic bond [43,83]

The advantages of mild reaction conditions and wide variety of available catalysts, for olefin metathesis, are an attractive feature of this dynamic chemistry. However, lack of control over the alkene stereochemistry may be an issue. In addition, alkenes in the polymer chain may are likely be significantly less reactive than if they were terminal alkenes.[23]

1.4.2.2 Dynamic Reactions Employed in CANs for C-N Bond Formation

1.4.2.2.1 Imine Condensation and Exchange Reactions
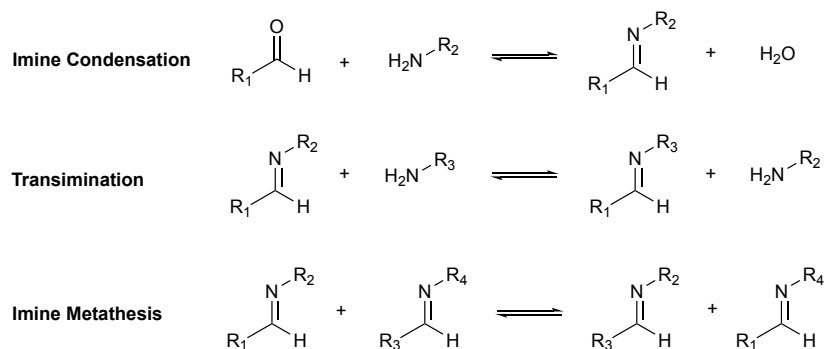
Figure 27: Dynamic imine reactions.

An imine is the nitrogen-containing analogue of an aldehyde or ketone, and are often referred to as Schiff's bases after Hugo Schiff initially discovered the reaction between a carbonyl and amine in 1864.[65,84] Formation of an imine is a popular "click" type reaction between an aldehyde or ketone with a primary amine.[85] Three reactions involving imines are commonly found in the literature for CAN polymers.[22,86]

The first reaction is a dissociative imine condensation reaction, as shown in Figure 27, of an aldehyde and a primary amine to form an imine. During this reaction a hemiaminal intermediate, shown in Figure 28 (a), is formed, which subsequently decomposes to the imine. This reaction is also reversible by hydrolysis and therefore the equilibrium can be shifted to the imine product by removal of water, and vice versa by the addition of water to favour the starting materials, according to Le Chatalier's principle. In addition, if the R_1 group is aliphatic on the carbonyl, the imine condensation will favour the reverse reaction, unless water is removed. However, if the R_1 group is aromatic, the forward reaction is favoured and simply mixing the reactants can produce the desired product in high yields.[87]

The second imine reaction, shown in Figure 27, is an associative CAN mechanism for the transamination exchange reaction, which involves an imine reacting with an amine via an aminal intermediate, shown in Figure 28 (b). The third imine reaction, shown in Figure 27, is imine metathesis and follows an associative CAN formation pathway. This reaction does not occur spontaneously but is catalysed by the presence of amines, acid, or transition metals. It has been proposed to metathesise via a cyclic 4 membered transition state, by means of $[2\pi + 2\pi]$ cycloaddition.[86,88]
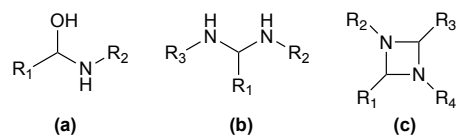
Figure 28: Imine reaction intermediates/transition states where the intermediates are a) hemiaminal b) aminal and c) 4 membered ring proposed for metathesis.

Imines have garnered considerable attention in recent years for their self-sorting dynamic nature.[28,67,89] The imine condensation reaction has been utilized as a dynamic clipping mechanism for the development of rotaxanes and catenates,[90] which was recognised as part of the Nobel prize in 2016 for the development of molecular machines.[91]
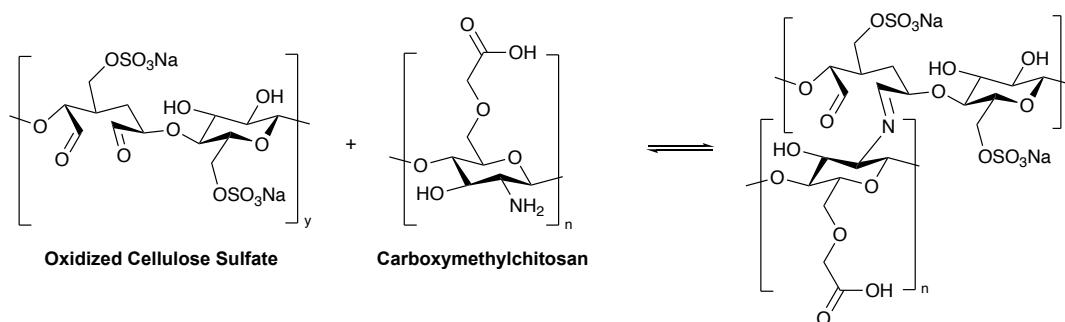
Figure 29: Crosslinking of oxidized cellulose sulfate and carboxymethylchitosan via imine bond formation. Scheme reproduced from Strätz et al.[92]

With regards to CANs, imine chemistry has been a common topic in several reviews.[46,47,60,61] Polyimines are notably affected by lowering the pH of the environment. Thus, providing a convenient stimulus for the recyclability of crosslinked networks that can be manipulated by triggering the reverse reaction with acidic solvents. Imines have been utilized as a crosslinking mechanism by Strätz et al. for applications in biopolymers.[92] Their work involved crosslinking carboxymethyl chitosan with oxidized cellulose sulphate, as shown in Figure 29, to produce hydrogels and subsequent hydrolytic stability testing was conducted which found that increasing the aldehyde content also increased the stability to hydrolytic cleavage.

Polyimines have also been reported by Taynton et al. and showed malleability with exposure to heat or water,[93] and full recyclability based on the dynamic imine bonds.[94] Polymer networks were formed by reacting the di-functional benzene-1,4-dicarboxaldehyde with a tri-functional amine and various di-functional amine incorporated to tune mechanical properties of the network. These networks were made into carbon-fibre composites and, upon immersion in a solution of neat diamine, the network was disrupted and allowed solubilisation. They reported that it was likely due to increased end groups shortening the chains and resulting in disassembly of the polymer network by reducing average functionality of the amine component.[2,5] An equilibrium shift favours the diamine over the triamine since there is such a large excess in neat solution. This would lead to loss of triamine in the polymer chain due to transamination reactions, hence linear polymers would dominate allowing dissolution of the polymer. Solubilisation of the polymer therefore occurs due to de-crosslinking, allowing subsequent recovery of the carbon-fibre.

Fulton and Jackson exploited imine bonds as crosslinkers between acrylamide based co-polymers for nanoparticles.[95] These materials also contained disulfide linkages to enable nanoparticle formation. A visualisation of the reaction pathways can be seen in Figure 30, which shows the general route to crosslink and then de-crosslink via dynamic bonds. They sought to demonstrate that two separate triggering environments initiate the full disassembly of the nanoparticle due to orthogonal relationship between the two different dynamic bonds. Low pH triggers imine reversal and a reductive environment triggers disulfide reversal. At a pH of 8.0 imine bond formation occurs, between the polymer chains and subsequent reactions for disulfide linkages do not affect the imine crosslinks, which keeps the nanoparticle intact and is represented by N1 and N2 in Figure 30. Two routes are then shown to de-crosslink to linear polymer chains (N4), differing only by the initial dynamic bonding reversal. Lowering the pH will break the imine bonds first leaving the disulfide bonds intact (N3), or the reductive environment is applied

first leaving the imine bonds intact (N5). A more detailed introduction to disulfide dynamic bonding can be found in Section 1.4.2.4.3.
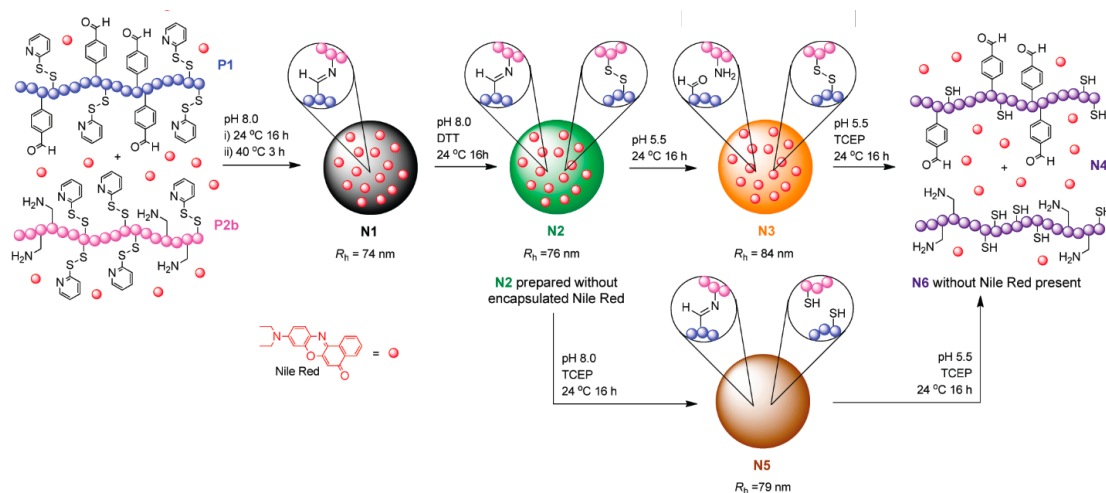
Figure 30: Route to imine/disulfide nanoparticles. Image reproduced from Fulton and Jackson's work for clarity.[95] Reprinted with permission from A. W. Jackson and D. A. Fulton, Macromolecules, 2012, 45, 2699–2708. Copyright © 2012, American Chemical Society.

More recently, imines have been applied to epoxy polymers when Liu et al. prepared epoxy based vitrimer using a novel amino-capped imine as the crosslinker, shown in Figure 31. Their epoxy of choice was the diglycidylbisphenol F (DGEBF) based epoxy resin and was crosslinked with their imine based crosslinker in a one-pot synthesis.[96] For a 1:1 (epoxy:NH group) polymer, based on the crosslinker shown in Figure 31, they reported excellent thermal and mechanical properties with a T_g of 150.3 °C from the tan delta peak of DMA analysis, a tensile strength of 119.5 MPa and a Youngs' modulus of 3636.5 MPa (at a 1 mm/min rate). However, the healing efficiency of the material after reprocessing, via a welding method then by further tensile analysis was only 13.1%. Good healing efficiencies of 87.8% when welded and 74.6% when remoulded were also reported for polymers that had a higher ratio of 1.75 epoxy groups per NH group. As a result of the excessive NH loading, the tensile strengths of the virgin material were reduced due to reduction of crosslink density. The lower T_g of 100.2 °C, which is

associated with lower crosslink densities, likely allows for more segmental motion at the healing temperature, hence, increasing the efficiency. The stress relaxation data reported an E_a of 61.94 kJ mol^{-1}, which aligns with the reported data in other literature for imine vitrimers (33.5-129 kJ mol^{-1}).[94,97]
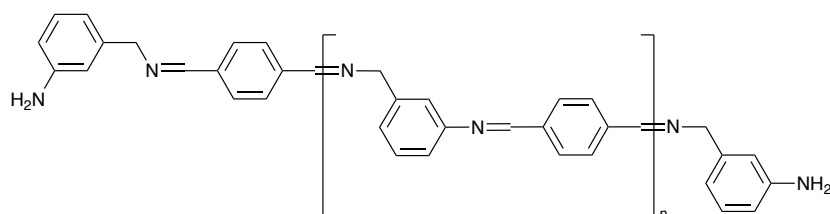
Figure 31: Novel amino-capped crosslinker reported by Liu et al.[96]

Bio-based feedstocks have also been utilised in epoxy-based imine vitrimers by Memon et al. in 2020.[98] They reported materials with excellent T_g's, between 121-127 °C, and good mechanical properties. For the DGEBA epoxy polymers crosslinked with the vanillin derived crosslinker, shown in Figure 32, a tensile strength of 60.1 ± 1.5 MPa and a Young's modulus of 2565 MPa. After three reprocessing cycles, the tensile strength decreased over each cycle to 44.8 ± 1.0 MPa whereas the Youngs modulus increased to 2832 ± 43 MPa. Thus, indicating some degradation of the material likely due to the thermal degradation of the material after hot press reprocessing at 170 °C. Conversely, when the material was chemically recycled in the presence of excess amine and the reprocessed vitrimers displayed similar results, with a tensile strength and Youngs modulus of 60.9 ± 1.0 MPa and 2608 ± 42 MPa respectively. In addition, stress relaxation data was obtained on the networks. For the network containing the crosslinker displayed in Figure 32, an activation energy (E_a) of 66 kJ mol^{-1} was reported, which is in line with current imine vitrimers in the literature (33.5-129 kJ mol^{-1}).[94,97]
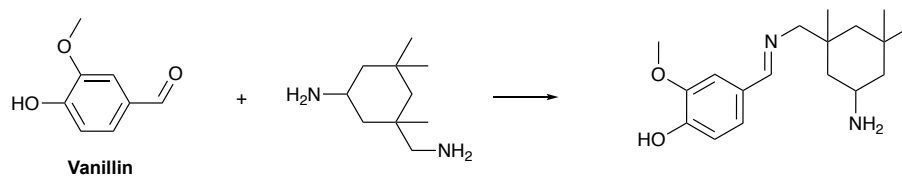
Figure 32: Novel vanillin-based amine crosslinker prepared by Memon et al.

Overall, imines prove to be a powerful tool in the endeavour for dynamic materials. However, a disadvantage of the use of imine bonds in CANs is that they are very susceptible to hydrolysis, which can reduce the scope of practical uses.[22] Thus, a route to overcome this is to replace imines with hydrazones or oximes, which are known to be less susceptible to hydrolysis.

1.4.2.2.2 Hydrazones and Oxime Condensation and Exchange Reactions (Imine Analogues)
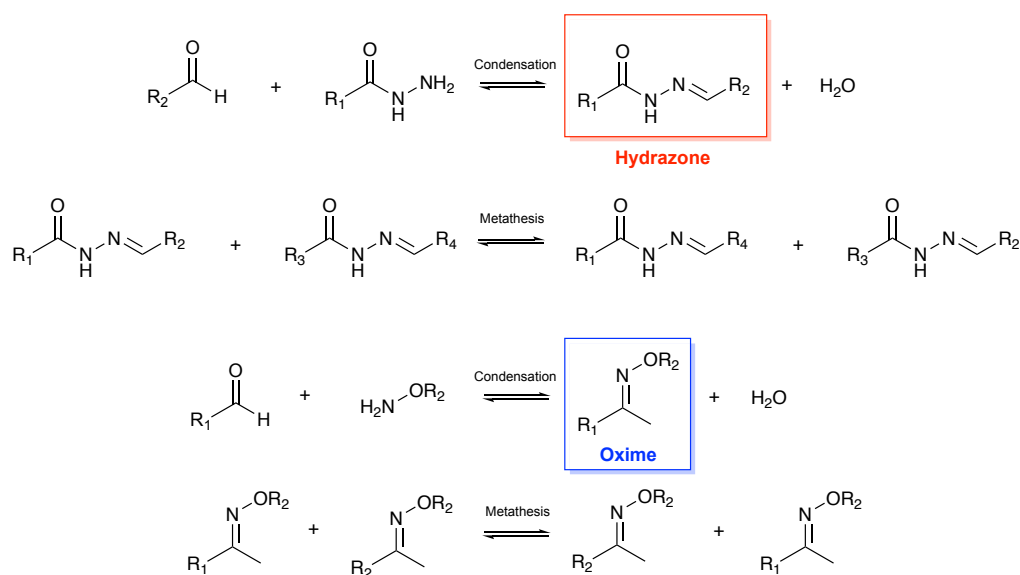
Figure 33: Hydrazone and oxime formations by condensation with aldehydes and dynamic exchange via metathesis.

Hydrazones form from the reaction of aldehydes or ketones with hydrazides, and oximes form by reacting carbonyls with hydroxylamines. Both are "click" type reactions and, therefore, can provide selective and efficient formation of crosslinks in CANs, which can then undergo associative metathesis mechanisms in response to stimulus.

Much attention has focused on hydrazones or oximes as they are generally more stable to hydrolysis than imines.[85,99–101] They are formed from the reaction of an aldehyde with a hydrazide or a hydroxylamine respectively (Figure 33). Both generally undergo the similar reactions to that of imines.[89] However, hydrazones require an acid catalyst in order to facilitate rapid bond exchange. It has also been reported that aniline acts as a nucleophilic base to catalyse the hydrazone exchange mechanism.[102] Another important benefit of using hydrazones, as the dynamic bond exchange mechanism in a polymer,

44

is that the reaction yields amide groups that are also available for hydrogen bonding. Thus, adding a second supramolecular assembly capability to the polymeric material.[103]

Deng et al. were the first to crosslink using hydrazone chemistry.[104] They achieved their network by utilizing a poly-ethyleneoxide linear polymer with hydrazide end groups as a di-functionality able to polymerize with a tri-functional aldehyde crosslinker. Subsequent reversal back to monomers were achieved by pH control. Furthermore, Kuhl et al. synthesised methacrylate polymers crosslinked by acylhydrazones for self-healing studies.[50] They demonstrated that polymers with 10 mol% of hydrazone crosslinker achieved sufficient self-healing at 125 °C. The self-healing behaviour was attributed to hydrazone metathesis rather than hydrolytic cleavage due to solid state NMR and FTIR not detecting free aldehydes or hydrazides. The work by He et al. incorporated oxime dynamic bonds in their polyester vitrimer, which is crosslinked by thiol-ene dynamic bonds.[100] The oximes added another degree of reversibility to the network and aided in reprocessability at high temperatures.

Sumerlin et al. recently developed vinylic hyperbranched polymers, with dynamic hydrazones as a crosslinker, by RAFT polymerisation with the aim to evaluate the tunability of the degradation of the polymer by the reverse hydrazone reaction compared to more hydrolytically stable oximes.[105] They found that the degradation rate increased as more labile imines such as the hydrazone were incorporated into the polymer over the more hydrolytically stable oximes and semicarbazones. A semicarbazones is formed from the reaction of a ketone or aldehyde with a semicarbazide, as shown by the general scheme in Figure 34.
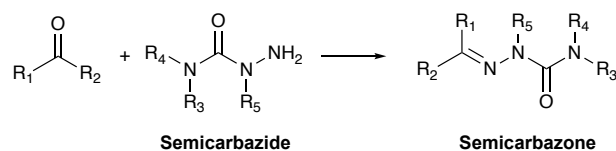
Figure 34: Semicarbazone formation from ketone and a semicarbazide.

Other work by Sumerlin et al. explored the use of oximes as a method of forming core crosslinked star polymers.[106] In their work, shown in Figure 35, a RAFT polymerisation yielded block co-polymers with an amide functional A-block and a block B being a ketone functional block. The ketone was crosslinked in a core by an alkoxyamine resulting in dynamic oxime crosslinked star polymers that were able to be disassembled via addition of monofunctional alkoxyamines or ketones under acidic conditions.
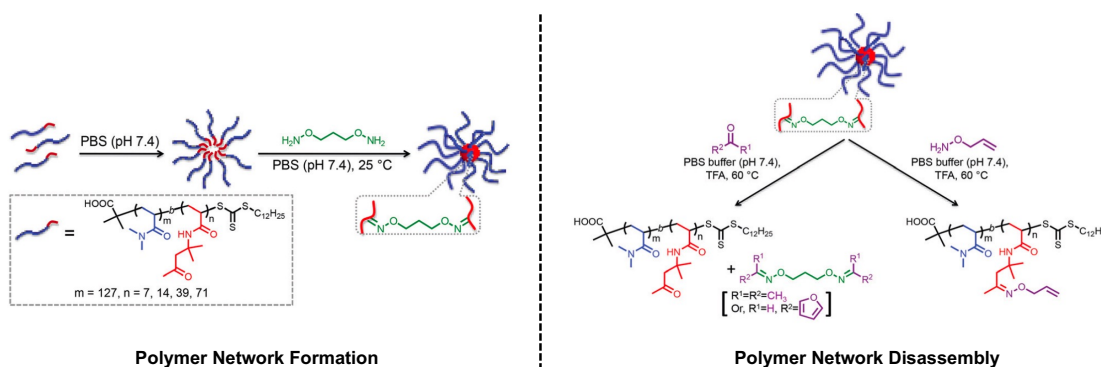
Figure 35: Star formation and disassembly by Sumerlin et al. by means of oxime reversibility. Figure reproduced and adapted from reference S. Mukherjee, A. P. Bapat, M. R. Hill and B. S. Sumerlin, Polym. Chem., 2014, 5, 6923–6931 with permission from the Royal Society of Chemistry. Copyright © 2014, The Royal Society of Chemistry.[106]

In addition, Maynard et al. also tuned the degradability and mechanical properties of poly-ethyleneglycol (PEG) polymers, by concomitant use of the more hydrolytically stable oxime and the lesser hydrolytically stable hydrazone dynamic bonds for crosslinks to make hydrogels.[107] They found that the stability of the hydrogel could be tuned from 24 hours to more than 7 days.

1.4.2.2.3 Transamination of Vinylogous Urethane (VU) Exchange
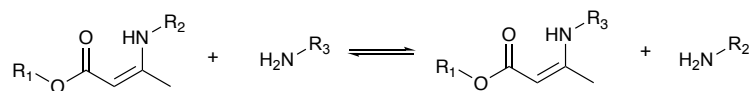
Figure 36: Vinylogous urethane exchange

Vinylogous urethanes (VU) are formed from the condensation reaction between acetoacetates and primary amines and can further exchange with free amines, as shown in Figure 36. This facile exchange is due to the Michael acceptor activity of the VU, which is a typical α, β–unsaturated carbonyl compounds, and allows nucleophilic addition of the amine through the vinylic double bond.[59,65] Moreover, the stabilisation of the VU molecule arises from the conjugation of the vinylic bond through the ester group and the intramolecular hydrogen bonding, which results in a thermodynamically stable bond.[108,109] Aliphatic acetoacetates selectively react with primary amines to form vinylogous urethanes whereas aromatic acetoacetates can react with the primary amine at both the ketone carbonyl or the ester carbonyl producing a vinylogous urea, as shown in Figure 37.[108] The extra reactive site is most likely due to delocalised electrons in the aromatic ring making phenol a better leaving group, and thus, the ester carbonyl more electrophilic and open to nucleophilic attack by the primary amine, which results in an amide that is not exchangeable.
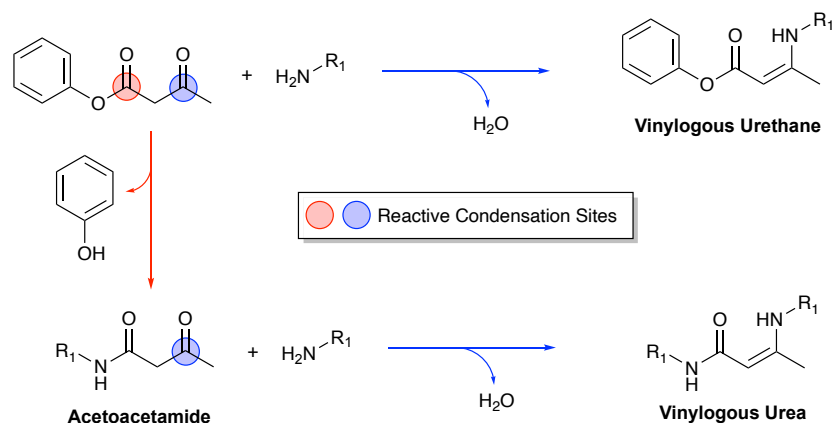
Figure 37: Synthesis of vinylogous urethane or vinylogous urea from an aromatic acetoacetate via condensation with an amine.

VU exchange occurs after heating at around 100-120 °C and poses as an effective associative exchange mechanism for CANs because of the catalyst free nature.[110] Current research focus in this area is prominent and a topic in several CAN review papers.[59,61,63,111] VU exchange was first applied to vitrimers in 2015 by Du Prez, Leibler and co-worker's and work on dynamic enamines, also known as VU's, for pH responsive polymers conducted by Sanchez-Sanchez et al. in the year prior.[110,112] The enamine work by Sanchez-Sanchez et al., shown in Figure 38, focused on developing single chain nanoparticles (SCNP's) from poly-(methyl methacrylate-co-(2-acetoacetoxy) ethyl methacrylate) (P(MMA-co-AEMA)) copolymers crosslinked with a diamine forming dynamic vinylogous urethane moieties that could be reversed by pH control. Analysis by size exclusion chromatography (SEC) showed that the nanoparticles eluted faster after treatment with phosphoric acid (H_3PO_4), which suggested that the hydrodynamic size of the polymers had increased, thus, indicating disassembly of the cross-linked SCNP, liberating the polymer to the solution. The disassembled copolymer was retreated with diamine crosslinker and the subsequent SCNP was reformed and confirmed by SEC. Therefore, demonstrating a proof of concept for dynamic pH responsive polymers utilising enamine/vinylogous urethane bonds.
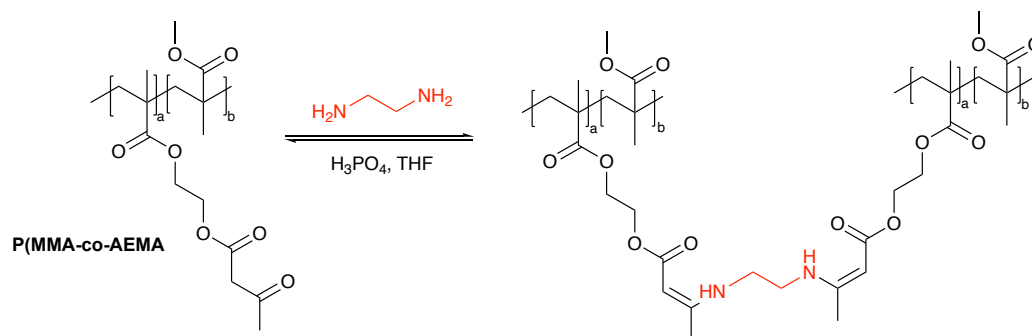
Figure 38: Block co-polymer SCNP synthesised by Sanchez-Sanchez et al. and resulting dynamic conditions to disassembly.[112]

Du Prez's pioneering work focused on using catalyst free VU functional vitrimers as an alternative mechanism to Leibler's groups original transesterification (TE) vitrimers, of which the reaction is reviewed in Section 1.4.2.3.1. They initially sought to utilise vinylogous amides, the structure of which differs at the ester oxygen in alpha position to the ketone in vinylogous urethanes, which is replaced by a CH_2 group in the vinylogous amide structure. However, the lack of low-cost and commercially available starting materials limited their capabilities, so the focus of their attention was towards VU's because the starting materials can easily be synthesised from low-cost reagents. Their network formation was based on the VU reaction to form polymeric chains from difunctional monomers whereas the work by Sanchez-Sanchez et al. utilised a traditional methacrylate polymer backbone, which cannot be returned to starting materials, with the VU as a crosslinking point to form the network. Ultimately, from a recyclability point of view it is preferred to regain all the starting reagents hence, Du Prez's method of dynamic network formation proves a more promising route to full recyclability whereas Sanchez-Sanchez's work would be more suited to a reprocessing method.

In 2017, further work on VU's by Du Prez's group attempted to chemically control the viscoelastic properties. This study found that vinylogous urea's exhibit faster exchange kinetics, although displaying similar activation energies.[113] This work was followed by

applying vinylogous urea's into fibre reinforced composites producing materials with good mechanical properties.[114] A high T_g of 110 °C was reported as well as a tensile strength of around 70 MPa and a young's modulus of around 2.2 GPa. They prove promising as an alternative to traditional epoxy composites as the mechanical properties were comparable to the traditional control epoxy.

In 2020, Du Prez's Group introduced a method to synthesise epoxy-VU vitrimers.[115] Continuing on from this work, Du Prez, Smulders and co-workers recently reported epoxy based VU coatings suitable for industrial applications, such as corrosion resistance, of which the chemical structures are shown in Figure 39.[116] Epoxy to amine ratio was 0.95 to leave an excess of free pendant amines which are known to catalyse the VU mechanism. They synthesised 4 VU-vitrimers (1.1, 1.2, 1.3 and 1.4 of which the numbers refer to the ratio of VU-amine groups/acetoacetate functionalities). They found that a used epoxy-VU vitrimer coating could be successfully re-applied to an aluminium substrate at 160 °C without delamination occurring, as well as some interesting insights for stress relaxation results which showed that an Arrhenius plot was not linear over the temperature range. Thus, diffusion controlled WLF model type behaviour of the segmental motion dominated at lower temperatures and Arrhenian behaviour dominated when the vitrimer was viscous, which is consistent with the T_v-T_g theory proposed by Du Prez for glassy vitrimers.[59] Interestingly, at a high temperature of 150 °C, the reported relaxation times were similar for all the VU vitrimers (1.1-1.4) with a range of 6000-14000s, and the group hypothesised that this was likely due to the rate determining step of the bond rearrangement being reliant on the availability of VU dynamic reactive functional groups, which is limited by segmental motion at lower temperatures.
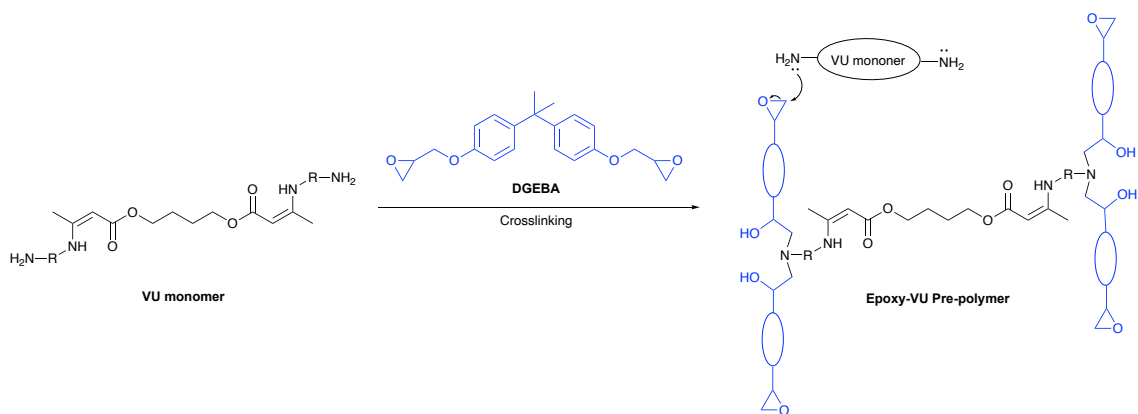
Figure 39: Epoxy-VU vitrimers designed by Du Prez and Smulders' group.[116]

Sumerlin's group sought to apply catalyst free VU vitrimers to methacrylate polymers (Figure 40).[117] The CAN was achieved by with a trifunctional amine as a crosslinker after reaction with a RAFT co-polymerised methacrylate pre-polymer, which contained reactive β-keto ester functionalities suitable for VU formation with primary amines. Thus, affording covalently crosslinked methacrylate polymers capable of VU exchange. The reported E_a was 102 ± 8 kJ mol^{-1}, which is higher than other VU materials without catalyst but, due to high T_g of the materials (110 ± 12 °C), diffusion was limiting the dynamic reaction kinetics. Reprocessing was achieved by compression moulding at 160 °C over multiple cycles. Also, addition of excess mono-functional amine enabled chemical recycling.
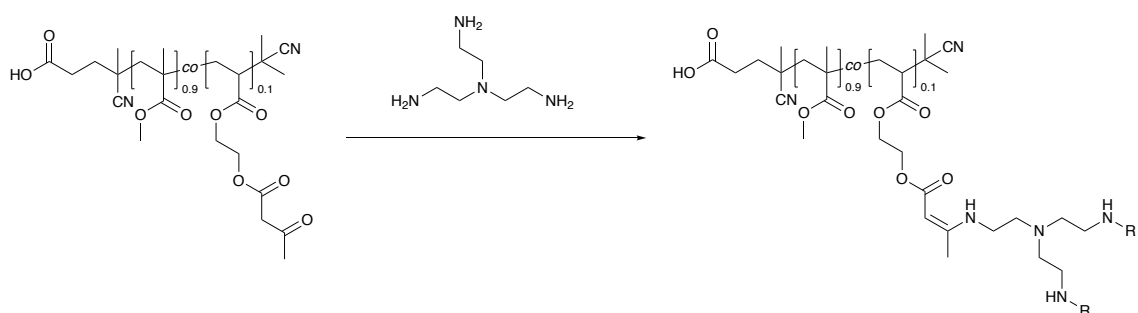
Figure 40: Methacrylate VU polymers reported by Sumerlin's group, where R = H or other polymer chain.

Furthermore, In other work by Du Prez's group in 2020, it was found that, when catalysed, VU vitrimers exhibit a dual temperature response with differing activation energies.[118] These are attributed to transimination (E_a I, Figure 41) at lower temperatures, due to the protic iminium pathway, and transamination (E_a II, Figure 41) with the relaxation response producing higher activation energies at higher temperatures. This is evident by the stress relaxation results of the non-acidic vitrimer, which is denoted by blue dots in Figure 41. It is clear that the response tends towards the iminium pathway as more acid is added to the vitrimer formulation by the similar relaxation response producing a lower E_a, which is calculated from the gradient of the tangent.
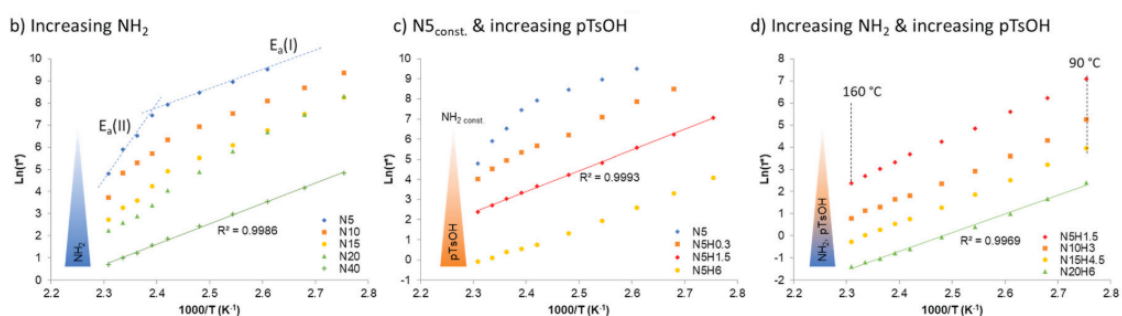
Figure 41: Dual temperature response reported by Du Prez's group. Figure reproduced under a creative commons licence from M. Guerre, C. Taplan, J. M. Winne and F. E. Du Prez, Chem. Sci., 2020, 11, 4855. Copyright © 2020, The Royal Society of Chemistry .[118]
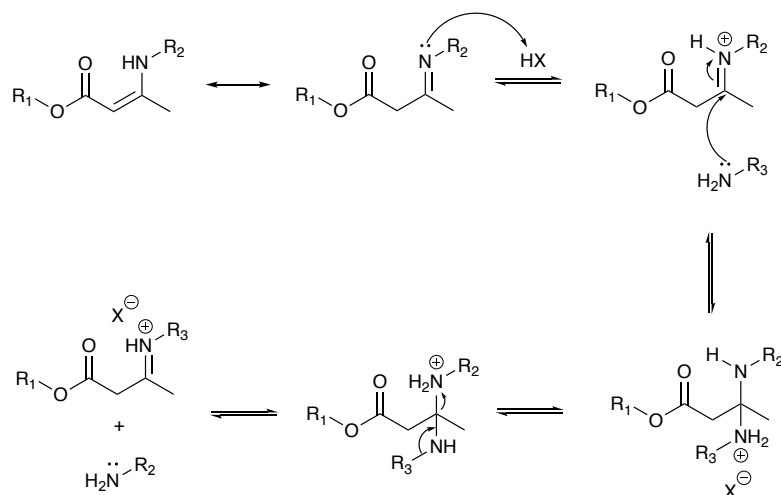
Figure 42: Iminium pathway proposed by Du Prez's group.

Haida and Abetz initially investigated the stress relaxation effects of VU vitrimers via a Bronsted acid catalysed (iminium ion pathway, Figure 42) and an autocatalysed pathway (excess amines).[109] They found, at 110 °C, vitrimers with excess free amines (V-Am) had much shorter relaxation times than vitrimers with excess acetates (V-Ac) in the formulation, reporting 29 seconds and over 15 hours respectively. And those with excess amines that were also Bronsted acid catalysed (V-Am^{H+}), with 0.05 wt% PTSA, had a relaxation time of 0.3 seconds at 110 °C. Calculated E_a's were in good accordance with literature results (60-102 kJ mol^{-1}),[110] reporting 60.3 kJ mol^{-1} for V-Am^{H+} and 75.9 kJ mol^{-1} for V-Am. An E_a for V-Ac could not be extrapolated due to long relaxation times and cracking in the material. These results supported the iminium pathway hypothesis as proposed by Du Prez's group. Following this work, Haida et al. sought to derive VU vitrimers from aromatic starting alcohols, in 2022, as this had not been reported in the literature for vitrimers.[108] They proposed a more efficient route for acetoacetylation of aromatic alcohols which is more attractive for scale up to industrial processes, by making use of phenolic based raw materials. They exploited the dual reactivity of aromatic acetoacetates to make blended vitrimers, with both vinylogous urethanes and vinylogous urea dynamic bonds, producing tensile strengths of up to 62.8 MPa and stress relaxation activation energies of 43.8–54.8 kJ mol^{-1}, which is in accordance with previous literature

for uncatalyzed VU type vitrimers.[110,115] Notably, when in the presence of acetic acid catalyst, increases in activation energies are observed up to 141 kJ mol^{-1}, which is expected as the acid shifts the ratio of vinylogous urethanes and vinylogous urea bonds towards vinylogous urethane's that show higher activation energies than vinylogous urea's.

Further work towards industrially practical VU vitrimers were explored by Tellers et al. and prepared poly-ethylene based VU vitrimers, depicted in Figure 43, via extrusion and injection moulding processes.[119]
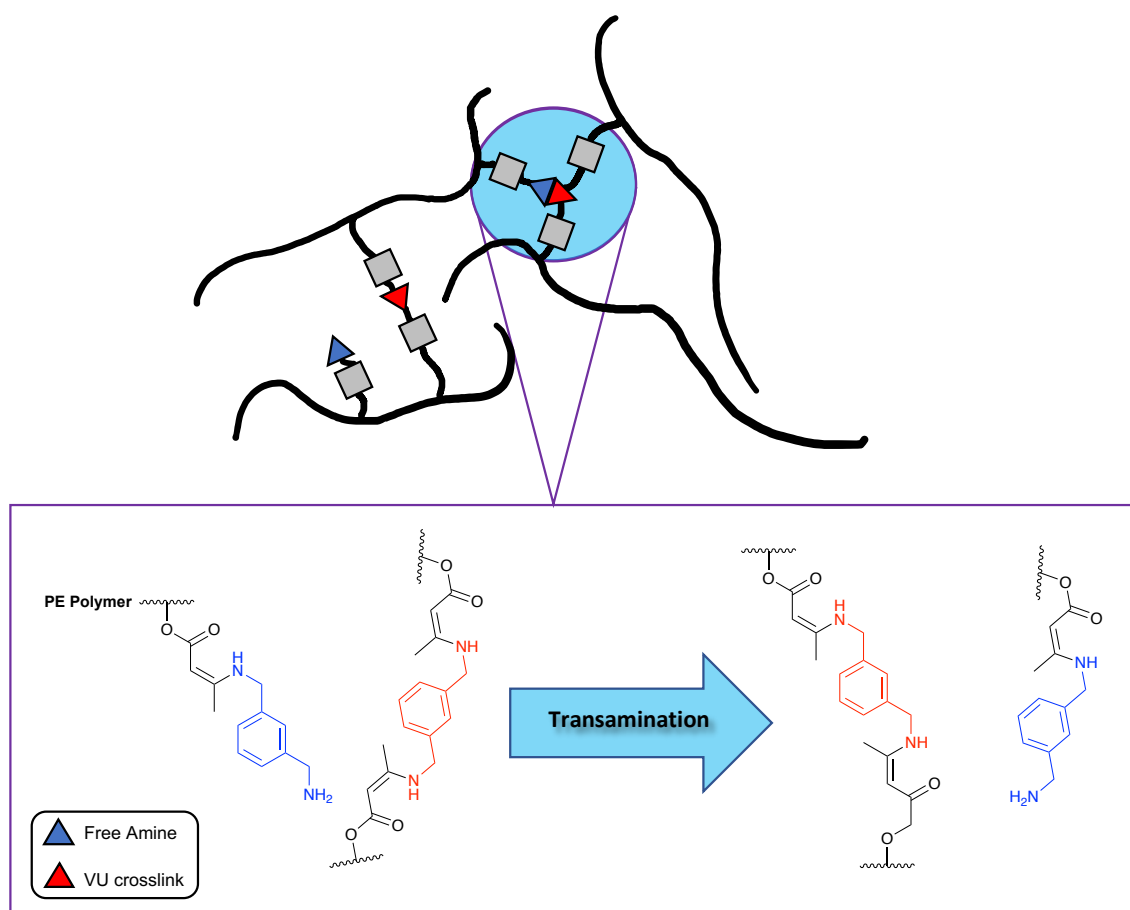
Figure 43: Structures of vitrimers designed by Tellers et al. and a visual representation transamination, highlighted in blue, indicating an associative exchange occurring.[119]

For their polymers, stress relaxation behaviour was observed noting higher activation energies than comparative literature results (from 59 ± 6 kJ mol^{-1} up to 81 ± 3 kJ mol^{-1}).[110,113] In the work by Tellers et al., polymers with 1.9 crosslinks per chain had an average activation energy of 75 ± 4 kJ mol^{-1}, whereas, with 2.6 links per chain it was 108 ± 4 kJ mol^{-1}. Thus, theorised to be a result of the segmental motion control over T_v due to significant retardation of diffusion for functional groups within the polymer. In addition, tensile results reported showed that increasing crosslink density to 2.6 links per chain from zero crosslinking increased the tensile strength from 10 ± 0.3 MPa to 17.2 ± 0.3 MPa. The increase in crosslink density also reduced the Young's modulus from 158 ± 9.8 MPa down to 62.2 ± 1.9 MPa. This was due to significant strain hardening observed in materials with more VU crosslinks.

Overall, VU network materials can serve as commercially viable CANs with good mechanical properties due to the associative nature. The hydrolytic stability is also better when compared to other DCB's in CANs such as imine exchange as they can be formed in water as a solvent. Recyclability of such CAN is promising for full recovery due to efficient which disassembly under pH triggers, as well as good thermal reprocessability at reasonable temperatures via facile exchange reactions.

1.4.2.3 Dynamic Reactions Employed in CANs for C-O Bond Formation.

1.4.2.3.1 Transesterification (TE)
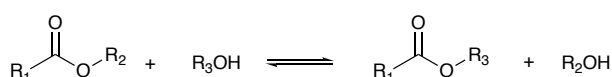
Figure 44: TE reaction.

The equilibrating transesterification (TE) reaction (Figure 44) occurs between an ester and an alcohol, forming a tetrahedral intermediate en-route to the new product and

alcohol after exchange, or also reverting to the starting ester and alcohol. In small

molecule synthesis or polymerisation reactions, the equilibrium can be driven towards

the new transesterified product by the removal of the alcohol produced in the exchange,

which is a relatively straightforward synthetic approach via distillation or via a large

excess of the alcohol intended to exchange by use as a solvent. The TE exchange

reaction can be triggered by heat and zinc catalysts, as well as acid or base.[120] In the

case of covalent adaptive networks, the catalysed TE reaction, excess OH or ester

moieties can trigger topological rearrangements required for dynamic covalent bond

exchange.[121]
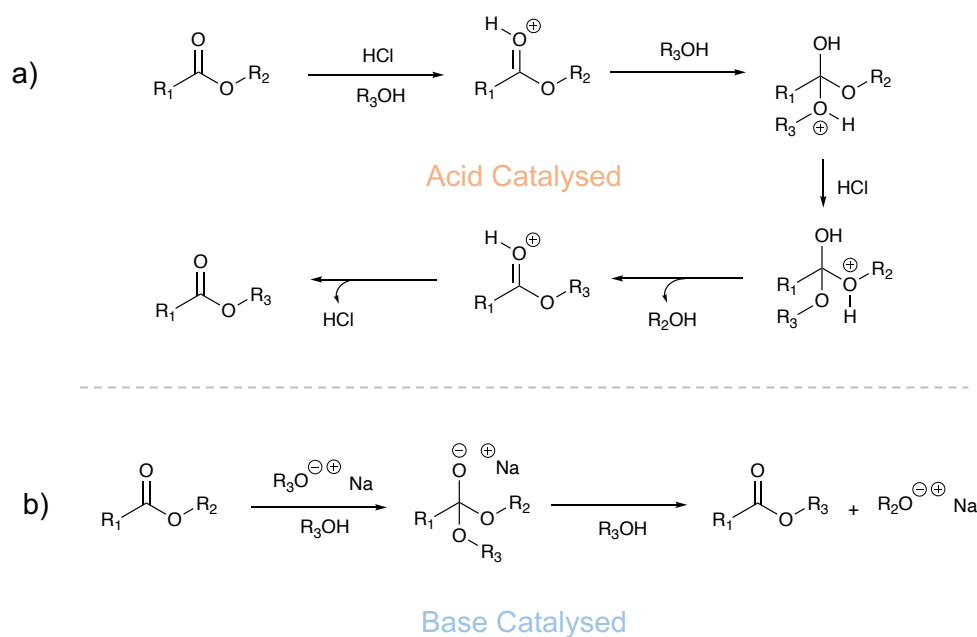
Figure 45: Forward reactions of transesterification via a) HCl as an acidic route or b) alkoxide as a basic route.

Figure 45 shows the acid and base catalysed routes of TE. When in the presence of an

acid the carbonyl group is protonated. However, in the presence of a base the alcohol

group is deprotonated. Therefore, under either sets of conditions, the reaction is either

catalysed because either i) the carbonyl is either more electrophilic, or ii) the alcohol is

more nucleophilic. For the acid catalysed mechanism, the first step is protonation of the

carbonyl, followed by a nucleophilic attack by the alcohol group, which forms a tetrahedral (associative) intermediate before deprotonation. Subsequently, protonation of the other oxygen (R_2), by the acid still present in the reaction, followed by elimination of the R_2 alcohol occurs before a final deprotonation step to form the transesterified product. For the basic system, an alkoxide ion will attack the carbonyl of the ester (associative) subsequently eliminating the leaving alkoxide group.

Catalysts Used in Epoxy-Carboxylic Acid Polymers.

Epoxy-carboxylic acid reactions can also be accelerated through the use of heat or a catalyst, such as a Lewis acid, nucleophilic (Lewis base) catalysts. One example of nucleophilic catalysis is using 2-methylimidazole (2-MI), shown in Figure 46, to prioritize epoxy ring opening over secondary homo-polymerisation of the epoxy groups.[122,123] The reaction of epoxy and carboxylic acid moieties are important to consider in the development of polymer networks for transesterification as they yield strong materials with free OH functionalities suitable for TE reactions.

2-MI
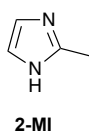
Figure 46: Structure of 2-methylimidazole

Zinc catalysts are found to also catalyse epoxy-carboxylic acid reactions.[124] This proved interesting for vitrimer developments by Leibler et al. because it facilitated the use of only one type of catalyst in vitrimer network formulation, as zinc acetate [Zn(OAc)$_2$] and zinc acetyl acetonate [Zn(acac)$_2$] are also well-known TE catalysts.[121,125] Investigations into the epoxy-acid network polymerisation were also investigated by Demongeot et al. and they found that 2-MI promoted epoxy-carboxylic acid chain extension reactions, resulting in no gelation, whereas [Zn(acac)$_2$] efficiently catalysed crosslinking.[125] Therefore, zinc

salts are better overall candidates for CAN development with dynamic transesterification. Catalysts in the formulation can also alter the thermal and mechanical properties of the final polymer, such as the T_g values, because of the faster curing in the presence of catalyst leading to lower crosslink density.[121]

Carboxylic ligands of zinc salts are nucleophilic in nature and can promote opening of epoxide rings, via coordination of the epoxy-oxygen lone pair to the zinc ion (Zn^{2+}), which then allows subsequent attack by the carboxylate counterion or alternatively, via coordination and reaction of carboxylic acid groups from polymers or other molecules in the reaction mixture. The resulting epoxy ring-opening reaction generates OH functional groups that can further polymerise with carboxylic acid (esterification) or react with further epoxy groups (homopolymerisation) present in the reaction mixture. This is likely to occur via a similar route via Zn^{2+} ion coordination promoting reaction. This theory is supported by Demongeot et al. where they investigated the coordination mechanism of Zn^{2+} in epoxy based vitrimers, by use of infrared and extended x-ray absorption fine structure (EXAFS) spectroscopy methods.[126] EXAFS confirmed that the Zn^{2+} is coordinated to two negatively charged and two neutral oxygen atoms with the Zn-O bond lengths in vitrimers similar to those of anhydrous zinc acetate.[126] This observation was also supported by IR analysis that revealed lengthening of the ester carbonyl. Thus, supporting a mechanism that the carbonyl coordinates to the Zn^{2+} making a more electrophilic carbon atom as well as supporting the theory that coordination brings the reactive moieties in close enough proximity to react. Notably, due to the high curing temperature, the counterion ligands are able to undergo evaporation from the reaction mixture (alongside any coordinated water) leaving the Zn^{2+} ion in the cured polymer.[121] Due to this and supported by Demongeot et al. the Zn^{2+} is understood to remain coordinated to the reactive groups of the cured TE vitrimers. Although, catalysis is not part of the scope of this thesis, a general understanding of the mechanism in which the crosslinks become dynamic is useful for future development of novel CANs.

The TE exchange is one of the prominently reported dynamic mechanisms that are utilised in polymers and follows an associative CAN mechanism. Several CAN reviews discuss the topic.[22,61,63,75,111,127,128] Because of the associative nature of TE resulting in a constant concentration of crosslinks, it is a favourable dynamic mechanism that has been employed in the development of mechanically robust and shape-stable dynamic networks, due to the ability to reprocess the polymer whilst retaining the network integrity. This is an ideal concept for developing high performing materials that must always retain mechanical properties and shape stability. Owing to the thermal responsiveness nature of this class of CAN, one can achieve control over the reprocessability. Because of this, TE was the dynamic mechanism of choice by Leibler et al. when they discovered thermally responsive TE networks, which they termed vitrimers.[57] As a result, countless reports of vitrimers utilise TE as a dynamic approach to network polymers, following the work by Leibler et al., to input self-healing mechanisms or to develop the mechanical properties of their polymers. For polymers with OH functionalities and esters, TE is easily incorporated into the network design, resulting in the majority of the relevant literature being devoted to epoxy-anhydride, epoxy-acid and alcohol-acid CAN polymers.

Catalysed TE

In the earlier work on vitrimers by Liebler et al., high-performance epoxy-acid networks are formed from the reaction of DGEBA with reacted with glutaric anhydride in in the presence of [Zn(acac)$_2$] catalyst.[57] The networks showed a good tensile strength of 55 MPa and an activation energy of 88 kJ mol^{-1}. Reprocessing was conducted via compression moulding at a relatively high temperature of 240 °C, close to the decomposition limit of many organic polymers. The group then focused attention on investigating the catalytic control that could be achieved with [Zn(OAc)$_2$].[122] They found that higher catalyst loading lead to faster stress relaxation times. They also found that they could control the topology freezing temperature (T_v) of the polymers, with smaller

amounts of catalyst having a higher T_v whilst the E_a remained the same at 90 kJ mol^{-1} for all amounts of catalyst (1, 5 and 10 mol %). Thus, proposing a method of controlling the temperature at which the materials can flow by addition of catalyst. Model reactions by the research group showed that uncatalyzed TE was slow to achieve equilibrium, taking up to 15 hours at 150 °C, whereas, adding 5 mol % of a Zn^{2+} metal salt resulted in an achieved equilibrium within in 2 hours.[58] This meant that for efficient exchange reactions to occur a metal catalyst is required.
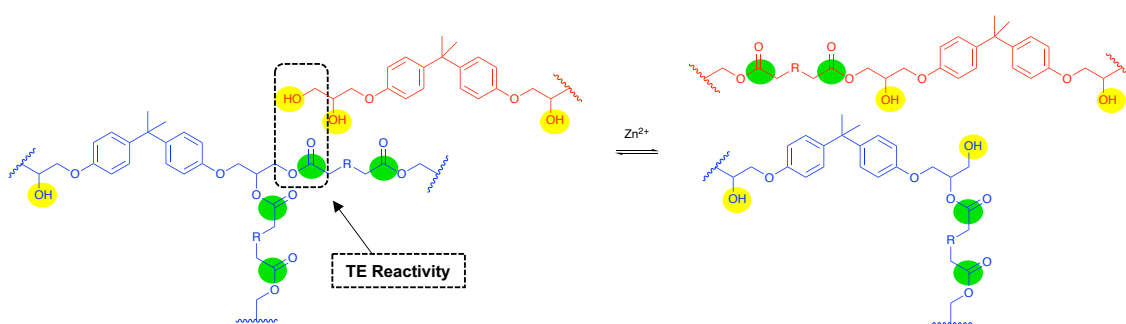
Figure 47: TE equilibrium of an epoxy-acid networks reported by Leibler et al. with complimentary reactive TE functionalities (highlighted in yellow and green) and where R is representative of various chain length di-acids as crosslinkers that could be used.

Giebler et al. recently investigated the effect of catalyst on epoxy anhydride vitrimers.[121] They envisioned that adding a tertiary amine (structures shown in Figure 48) into the structure of the monomers would catalyse the polymerisation and further catalyse the TE reaction with the goal to produce high T_g polymers with efficient stress relaxation. This resulted in polymers with T_g's from 125-140 °C for those with an absence of Zn^{2+} catalyst and E_a's of 154-161 kJ mol^{-1}. These are much higher than those of typical Zn^{2+} catalysed TE reactions (~88 kJ mol^{-1}) but showed that excess amine in the polymer could catalyse TE, less efficiently.
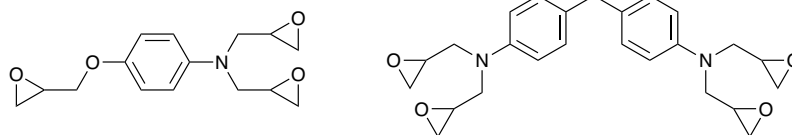
Efforts to make bio-based polymers are always of academic interest, as their use are seen to help address environmental concerns of using petrochemical derived feedstocks. For example, bisphenol A (BPA) based DGEBA epoxies are traditionally used for high-performance TE based CANs to enable materials with superior T_g's to be produced, however, BPA is derived from petroleum-based phenols, and hence is non-renewable.[129] Unreacted BPA (a known endocrine disruptor) is an inevitable concern and can also leach out of the final polymer, which is known to be a factor in various health concerns of the masses, due to the ubiquitous use of epoxy networks in everyday life.[130] Thus, a push towards replacing these with bio-derived epoxy monomers is attractive.

Liu et al. recently explored a bio-based epoxy-acid vitrimer with vanillin as a feedstock, which has previously been explored in Section 1.4.2.2.1, with regards crosslinkers for transimination vitrimers.[131] In this work, Liu et al. prepared a triepoxy from the reaction of vanillin and guaiacol (another bio-based aromatic compound) shown in Figure 49. The triepoxy is then crosslinked with an anhydride in the presence of a [Zn(acac)$_2$] catalyst. In polymers with a 1:1 equivalent stoichiometry of epoxy to anhydride group, a T_g of 187 °C was reported from the tan delta peak of the DMTA (see Section 5.1.2 for an introduction to this method), which was 30 °C more than the BPA epoxy equivalent (157 °C). The tensile strength of the bio-based vitrimer was 69.2 ± 2.1 MPa, which was on par with the traditional system. However, due to the high T_g, stress relaxation was only conducted at a temperature of 220 °C to prevent degradation of the material, and hence,

an activation energy could not be reported. In addition, healability studies were also conducted at this temperature due to the limited segmental motion of the material below this. They found that scratches were healed after 5 minutes at this temperature. Presence of catalyst were found to be required to exhibit obvious stress relaxation.
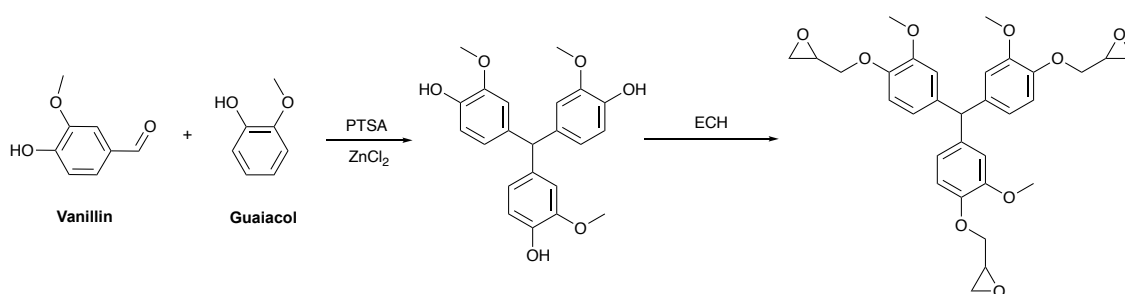
Figure 49: Triepoxy synthesised by Liu et al.[131]

Catalyst-free TE

More recently, research towards catalyst free systems has been a focus of many groups towards vitrimers. Due to the inevitable drawbacks associated with using metal catalysts, which include catalyst leaching or spent catalyst not available to drive the TE reaction.[22,132]

Recently, Debnath et al. reported catalyst-free TE based vitrimers (Figure 50) for poly-methacrylates with a bio-based β,β'-diester, diethylmalonate (DEM) as the crosslinker, which is typically derived from fruit juices.[133] The basis of this work was prompted from evidence that β-keto esters can react readily with primary alcohols at 110 °C, without catalysts.[134,135] The networks synthesised by Debnath et al. could be reprocessed at 150 °C and exhibited an E_a of 112 kJ mol^{-1} for the uncatalysed network, with a reported control, catalysed network being lower at 82.5 kJ mol^{-1}. This suggested addition of catalysts in the network allows re-processing at lower temperatures, which is in line with

the findings by Leibler's group. In addition, good mechanical strength was observed for their uncatalysed material with tensile strengths between 11.3-33 MPa.
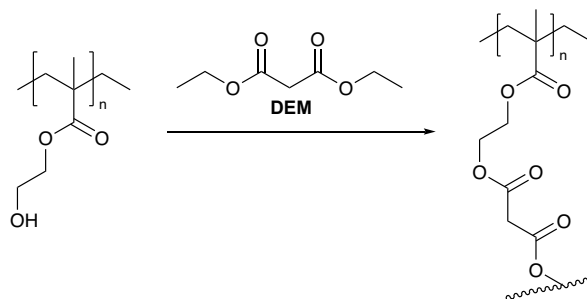
Figure 50: Methacrylate based catalyst-free TE vitrimers explored by Debnath et al.

High re-processing temperatures and the requirement for metal catalysts has sparked exploration of niche transesterification reactions that have lower activation energies for the dynamic mechanisms and can proceed to exchange efficiently without the need for catalysts.

Utilising oxime bonds, which was previously discussed in Section 1.4.2.2.2, rather than traditional alkyl esters for transesterification, He et al. constructed poly-oxime associative vitrimers by concomitant use of the recognised thiol-ene click chemistry, as shown in Figure 51.[100] This exploited the fact that the known pKa of an oxime is lower than that of the traditionally used alcohol moieties and hence, more reactive than most ester moieties. Model studies indicated an E_a of 63.5 ± 7.8 kJ mol^{-1},which was in accordance with their reported polymer networks but the specific polymer E_a was not mentioned in the report itself. This showed that it was lower than conventionally catalysed TE systems, which were around 88 kJ mol^{-1} as reported by Leibler et al.[122] Notably the films produced had low T_g and tensile properties of 14 °C and 2.8 ± 0.54 MPa respectively. This is most likely due to the longer, more flexible chains incorporated in the polymer chains rather than as a consequence of utilising the oxime mechanism. However, the reprocessability

of the polymer networks were excellent. Broken pieces could be reprocessed at 120 °C in 30 minutes by heat pressing. The network could also be chemically recycled upon addition of excess mono-functional oxime (acetophenone oxime), by altering the equilibrium of the reaction.
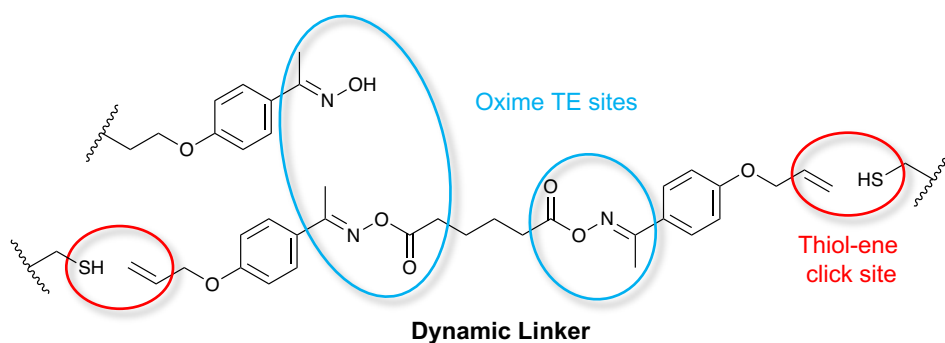
Figure 51: Thiol-ene based polymer networks crosslinked with via oxime dynamic bonds capable of oxime transesterification constructed by He et al.[100]

Overall, TE is a well-studied CAN chemistry and has found many uses in a broad set of polymer networks and is well suited for high temperature service due to the high activation temperature and associative nature of the reaction.

1.4.2.4   Dynamic Sulfur Reactions Employed in CANs for Various S-X bonds

1.4.2.4.1   Thiol-Michael Reactions for S-C Bond Formation
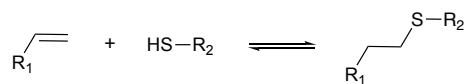
Figure 52: Reversible thiol-Michael based click reaction, where R_2 is an electron withdrawing group (EWG) or is α,β-conjugated.

The overall reaction that defines thiol-ene and thiol-Michael chemistry is the "click" type reaction of a thiol group with an alkene group. The former typically proceeds via photo-initiated radical addition and is not reversible. The latter is usually achieved in the presence of a catalytic amount of base or in the presence of nucleophiles and is reversible upon thermal or pH stimuli.[22] Two rules have been observed to govern the conversion rate of thiol-ene reactions which are; the electron density of the alkene and the stability of the carbon radicals.[136,137] Although analogous to each other, thiol-ene reactions proceed faster with more electron rich alkenes, whereas thiol-Michael reactions proceed faster with electron deficient Michael acceptors, due to the differing mechanisms of action.[136,138] The initiation of the thiol-Michael reaction involves catalysis by a base or nucleophile. Figure 53 a) shows a base catalysed initiation where the basic anion directly abstracts a proton from the thiol and Figure 53 b) shows the thiol-Michael reaction being catalysed by a nucleophile, where the nucleophile first attacks the Michael acceptor on the β-carbon forming a zwitterionic enolate that will abstract the hydrogen off the thiol to generate the thiolate anion to react with further Michael acceptors.[139]

Initiation

a)

b)

Zwitterionic
Enolate
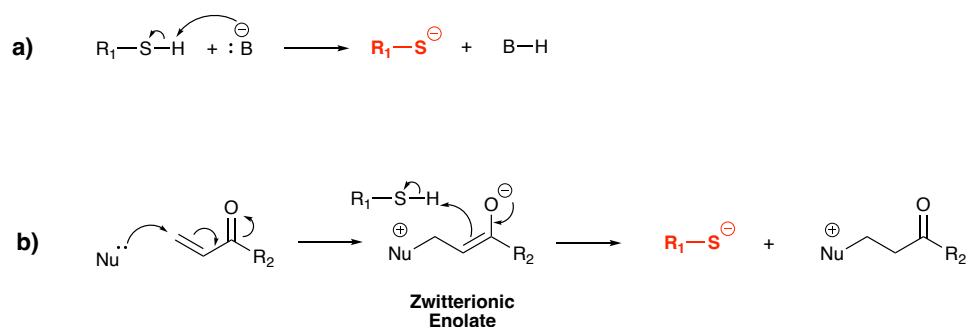
Figure 53: Thiol-Michael initiation via base (a) or Nucleophile (b) to generate thiolate anion.

The mechanism in which the thiolate anion propagates the in the thiol-Michael reaction is shown in Figure 54.[139,140] The cycle shows the thiolate anion behaving as a Michael-donor in a similar fashion to the nucleophilic initiation mechanism. The subsequent steps form the enolate, although not zwitterionic in contrast to the nucleophilic catalysed initiation. This enolate then abstracts the hydrogen of another free thiol, which regenerates a new thiolate anion to react via thiol-Michael addition.
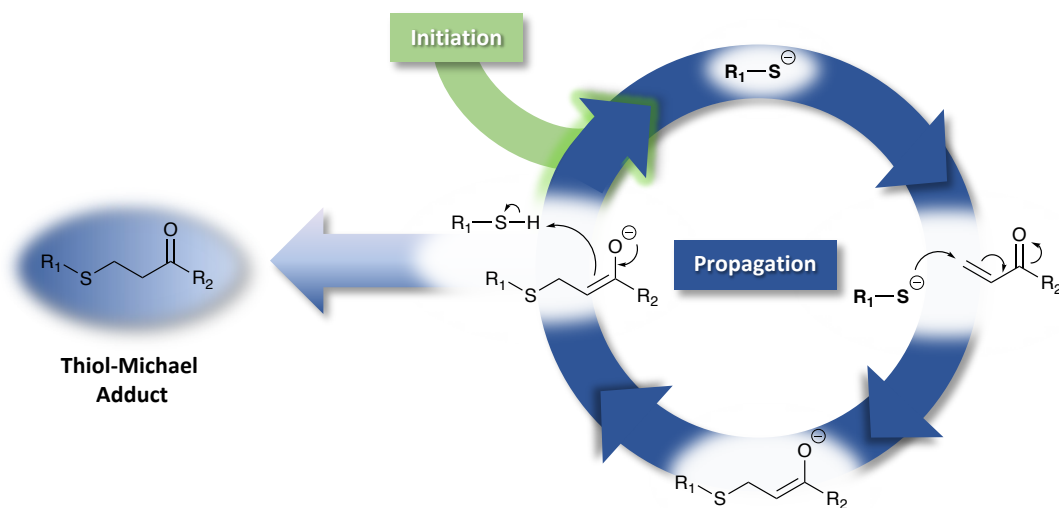
Figure 54: Thiolate anion mechanism of propagation.

Thiol-click reactions have proved to be a versatile tool in polymer synthesis due to the highly efficient and high yielding reactions.[141] However, much of the literature utilises thiol-ene chemistry for the construction of core polymer backbones because of good compatibility with common classes of polymer such as acrylates and methacrylates or for the efficiency of "clicking" monomers together. The resultant polymers will often contain a different, dynamically active, functional group in its monomer, for mechanisms such as transesterification, to enable CAN properties.[100] With regards to vitrimer chemistry, thiol-ene's are often included as a route to provide photocurable networks together with transesterification as the main thermal dynamic mechanism. For example, Lyon et al. developed thiol-ene vitrimers, utilising transesterification as the dynamic CAN mechanism, by thiol-ene click reactions to enable re-mouldable materials for nano-imprint lithography.[142] However, the thiol-ene was only part of the polymer construction and was not the primary mechanism for dynamic behaviour. Drawbacks of utilising thiol-ene's is the radical process as they can also generate undesirable side products from termination reactions.

Thiol-Michael addition is a focus of literature regarding reversible chemistry for CAN development as this has been known as a reversible process since as early as 1964.[143] Like thiol-ene's, thiol-Michael bonds also exhibit "click" efficiency. The appeal of thiol-Michael reactions is that they are easily formed at room temperature and dynamic at elevated temperatures or pH. Thiol-Michael CANs have been employed in self healable and degradable polymer networks and the widely accepted reversible mechanism, at elevated temperatures or pH, is thiol-Michael exchange.[144,145] . This has been reported to follow an associative CAN mechanism in response to stimuli.[47] However, multiple proposed mechanisms suggest the thiol-Michael adducts dissociate at elevated temperatures, via retro-Michael addition, into free thiol and Michael acceptor, followed by rapid formation of a new thiol-Michael adduct.[146,147] In addition, Winne et al. reviewed dynamic bonds and reviewed this dynamic chemistry in their dissociative group review,

just as McBride et al. have done in their review.[46,148] Although, there is some speculation as to whether this exchange mechanism is actually associative or dissociative, for the purpose of this discussion, a dissociative mechanism is presumed. The mechanism of thiol-Michael exchange proposed by Zhang et al. is shown in Figure 55.[147]
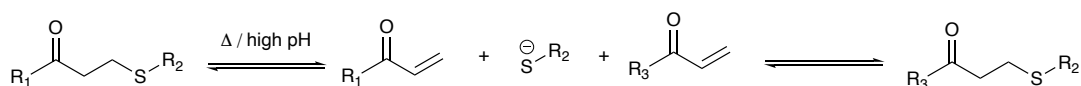
Figure 55: Thiol-Michael exchange (dissociative) mechanism.

In 2016 Kuhl et al. developed a thermally reversible thiol-Michael network from a tri-thiol monomer and a novel (bis)α,β-unsaturated alkene. This showed that excellent healing of scratches occurred at 60 °C within 30 minutes. However, at a higher temperature (150 °C) thermal degradation was observed by FT-Raman spectroscopy showing the release of H_2S. This was due to the increase in signals of C=C double bond signals at 1590 cm^{-1}, suggesting alkene formation, combined with a loss of S-H signals at 2573 cm^{-1}, confirming the release of H_2S.[145] This proves problematic in materials due to release of odorous and toxic sulfur compounds as well as removing network crosslinks from the material. Free thiols of this type are thermally unstable above 100 °C producing H_2S above this temperature.[149] This observation is also supported by Daymon and Miller, who developed polyester networks with thiol-Michael adducts and conducted experiments to prove H_2S release was the case at higher temperatures by collecting the gas produced at 120 °C in a silver nitrate ($AgNO_3$) solution producing silver sulfide (Ag_2S) as a black precipitate, confirming H_2S in the produced gas.[150] Noticeably, there was no precipitate at 100 °C, therefore, cure temperatures regarding thiol-Michael materials should be capped at 100 °C to prevent material degradation.

Zhang et al. recently reported thiol-Michael based vitrimers, with a T_g ranging from 9 °C to 16 °C with increasing crosslinker amount in the formulation. They could be healed at

90 °C and also recovered up to 90% of its original tensile strength (0.37 MPa), after 16 hours at healing temperature.[147] The material was stable to applied stress (creep) and strain (stress relaxation) at room temperature suggesting the dynamics of the material are not active until elevated temperatures. In 2017, the same research group lead by Dominik Konkolewicz utilised a maleimide adduct as a Michael acceptor group to synthesis acrylate crosslinkers with the respective thiol-Michael group in the structure, which is shown in Figure 56.[146] These materials also showed mechanical stability at room temperature supporting the findings of the previous work.
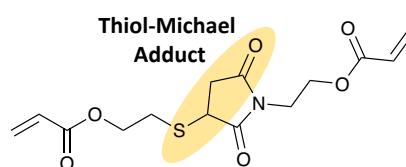
Figure 56: Maleimide based thiol-Michael crosslinker prepared by Konkolewicz group.[146]

Recently, Stubbs et al. prepared thiol-ene based polymers from L-carvone (structure shown in Figure 57), an inexpensive and bio-based reagent that contains an alkene moiety for thiol-ene reactions and a Michael accepting moiety to allow thiol-Michael dynamic reactions at elevated temperatures.[144] The networks were prepared by reacting a trifunctional thiol with the 2 functional L-carvone, one of which was a Michael accepting group. Model studies showed that addition of 5 mol% of base dissociated the thiol-Michael adduct at room temperature and was monitored by reappearing enone peaks in ^{1}H-NMR and the subsequent calculation of activation energy from a Van't-Hoff plot was revealed to be 49.3 kJ mol^{-1}. Depolymerisation could be achieved at 140 °C in the presence of base into soluble thiol-ene oligomers by regeneration of the free thiol and Michael acceptor. However, there was some solid particulates reported that were not dissolvable and were attributed to areas of high crosslink density. In comparison with the previous research by Kuhl et al., who noted degradation associated with thiol-Michael

polymers producing H_2S above 100 °C, this work utilized a similar tri-thiol monomer which also contains an ester moiety in the structure that can form an acrylate upon release of *HS* from the chain. Therefore, there is a small possibility that the insoluble network particles may have arisen from subsequent non-reversible acrylate polymerisation reactions, after retro-thiol-Michael reactions occur and H_2S is liberated, upon thermal degradation, at the high temperature used, but this was not explored in the work.
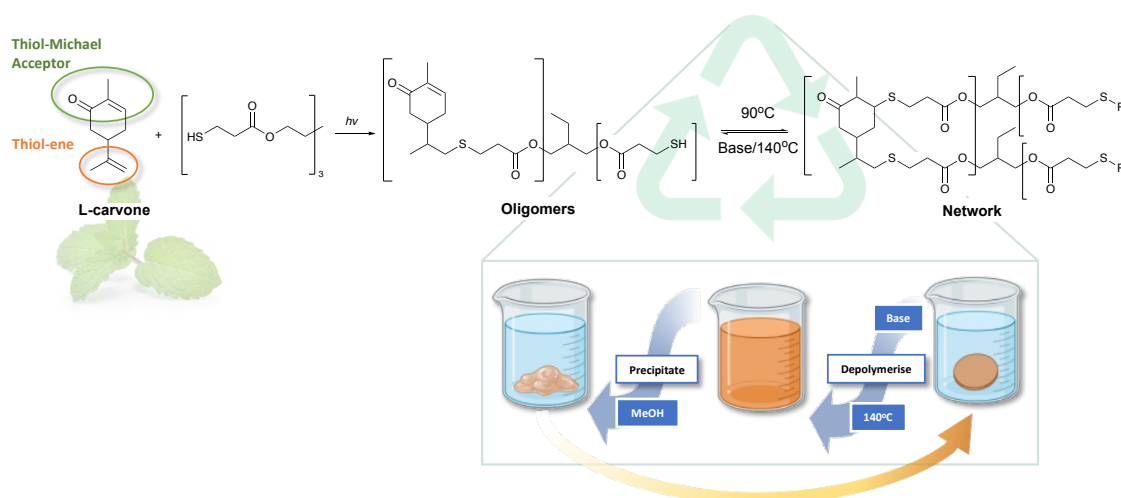
Figure 57: Bio-based thiol-Michael recycling scheme and visual depiction as reported by Stubbs et al.

Overall, although the literature regarding the thiol-Michael reaction is extensive and extremely efficient in general organic chemistry, it has not been thoroughly explored with regards to being the primary dynamic chemistry in CANs. Low thermal stability resulting in material degradation as well as odorous H_2S production as a result are undesirable in many material applications. In addition to this, complex synthesis methods for thiol-Michael crosslinkers can limit the commercial viability. Thus, research focused on developing simpler monomer synthesis and thermally stable thiol-Michael controlled CANs is attractive for future research.

1.4.2.4.2 Transthioesterification Reaction for C-SR Exchange
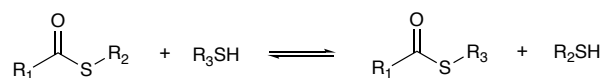
Figure 58: Transthioesterification reaction.

Thiol-thioester exchange is an associative dynamic mechanism between a thiol-ester and a free thiol, which can occur under ambient conditions and catalysed in the presence of a base or nucleophile.[22] Increased temperature also increases reaction rates. With respect to CANs, this dynamic exchange has received attention due to its low activation energy (30 kJ mol^{-1}) and also the simplicity of synthesising thioester-based monomers for polymer synthesis.[151] Like thiol-Michael based polymers, thiol-esters are well suited for incorporation into various alkene-based radically controlled polymers allowing construction of low polydispersity polymers via RAFT polymerisation or atom transfer radical polymerisation (ATRP).[152,153]
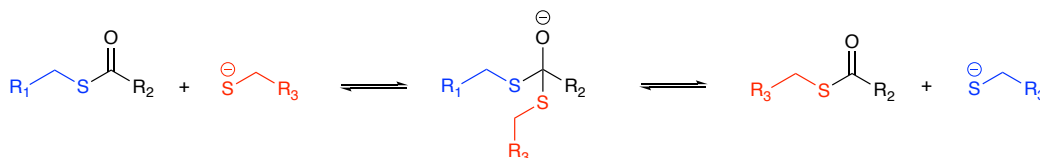
Figure 59: Transthioesterification equilibrium in the presence of base.

Bowman's group recently developed and patented a method of constructing networks via combination of thiol-ene radical polymerisation (Figure 60), for the network forming reactions, with thiol-ester groups, capable of transthioesterification, which are readily available in the crosslinkers structure.[154,155]
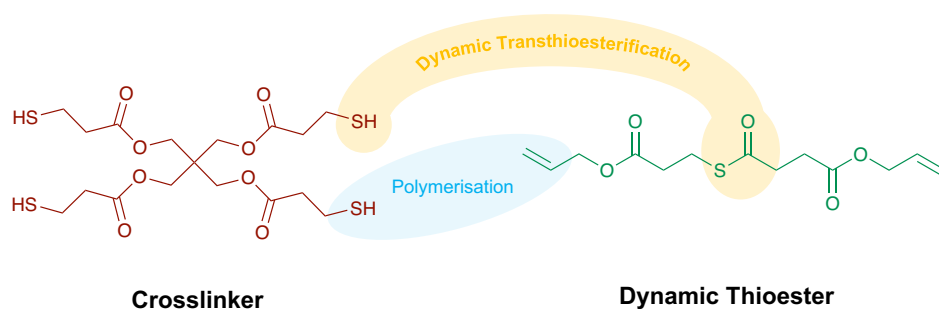
Figure 60: Monomers used by Bowman's group for transthioesterification CAN.

In their work, thiol-ene polymerisation is photoinitiated with use of 2,2- dimethoxy-1,2-diphenylethan-1-one (DMPA), which can readily form R-S radicals on the four-functional thiol-containing crosslinker, which is shown by the mechanisms in Figure 61.[156] The thiol radical subsequently reacts with the terminal alkenes of the thiol-ester containing monomer to form networks. Notably, there is likely to be a small presence of cross termination products and non-thiol promoted alkene propagation impurities in the network polymer, arising from the benzyl and the tertiary carbon radicals. However, due to the catalytic amounts added these impurities are not likely to inhibit the bulk material performance.
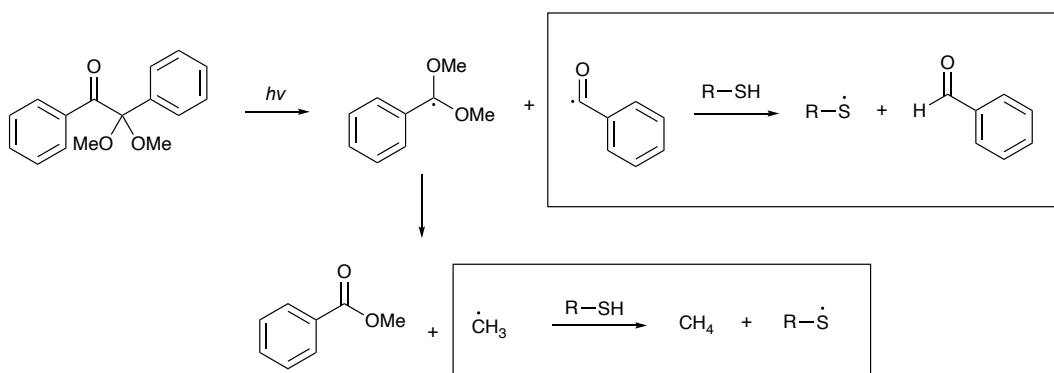
Figure 61: Generation of Thiol radicals by photoinitiation of DMPA.

Degradation of the networks by Bowman et al. was achieved via addition of a stoichiometric excesses of crosslinker and in the presence of a mild base, which was

subsequently reformed by addition of a stoichiometric amount of the alkene-thioester to make 1:1 equivalents of thiol:alkene. This method allowed dissolution of oligomer products within 3 hours, after the equilibrating degradation of the network by increasing the stoichiometry for the gel point to be greater than 1 with excess thiols. It also regenerated the network via reformation of thiol-ene bonds once the stoichiometry balance was restored and thermal and mechanical properties remained similar through 3 cycles, as shown in Figure 62. Properties of the material are tuneable by adapting the thiol-monomer functionality or the rigidity of the monomer structure, by means of a cyclic core, which was assessed by the T_g results. The T_g results were below room temperature indicating soft materials but ranged from -4 °C to 7 °C for tri, tetra and hexa-functional thiols. Utilising a cyclic core structure in the thiol monomer, increased the T_g from -2 °C to 6 °C. Thus, demonstrating appeal for the development of higher performing materials.
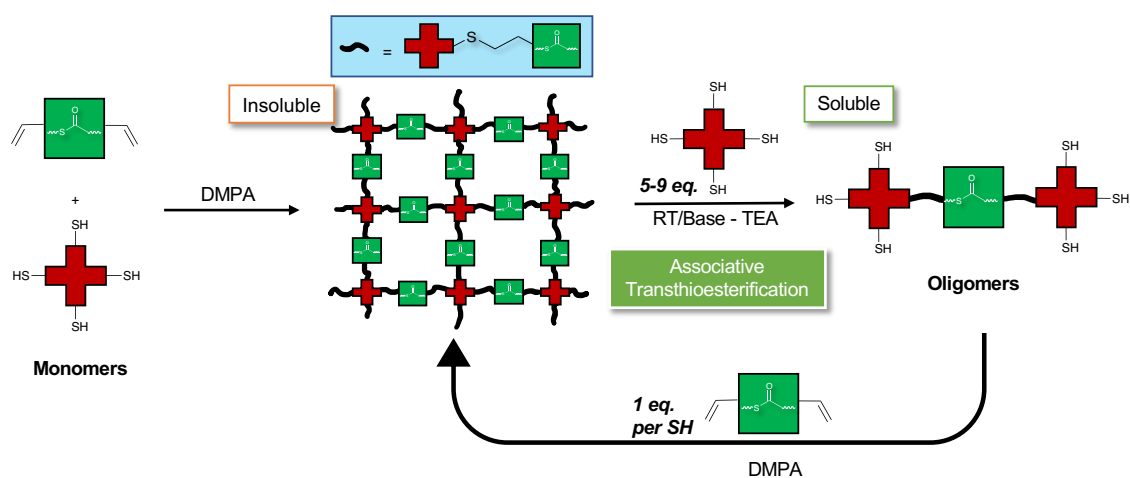
Figure 62: Bowman's groups thioester recycling method.

However, whilst this method proves the equilibrium of the thioester bond can be manipulated by controlling stoichiometry and allows a novel and repeatable reprocessing route for network polymers, it ultimately would require the consumption of increasingly more monomer per degradation cycle. Which may eventually lead to exhaustion of the monomer resources since the full recovery of monomers has not been achieved.

Other work by Bowmans research group investigated the effects of the thiol substitution within thioester reactions.[151] Primary and secondary thiols were investigated with regards to thiol-ene based thioester exchange networks, and it was found that secondary thiol networks showed slower dynamics based on stress relaxation experiments. Primary and secondary networks had activation energies of 36 and 53 kJ mol^{-1} respectively.

For the application of wound dressings, Grinstaff's group developed thiol-based dendrimer hydrogels that crosslinked via thiol-esterification and could be dissolved in excess thiolate solution, whilst also tuning the dissolution times with concentration of excess thiolates in solution.[157] Following this work the group sought to optimise their hydrogels by slowing the hydrogel formation and enabling faster dissolution.[158] They achieved this via utilisation of polyethylene glycol (PEG)-lysine-based dendrimers that form hydrogels when reacted with a crosslinker already containing thiol ester moieties (as shown in Figure 63), rather than forming the thioester in the crosslinking reaction. The optimised hydrogel can also undergo transthioesterification reactions in the presence of a mono-functional cysteine methyl ester (CME) solution, which the transthioesterification product is subsequently cleaved by native chemical ligation of the amine, allowing the dissolution of the hydrogel.[158]
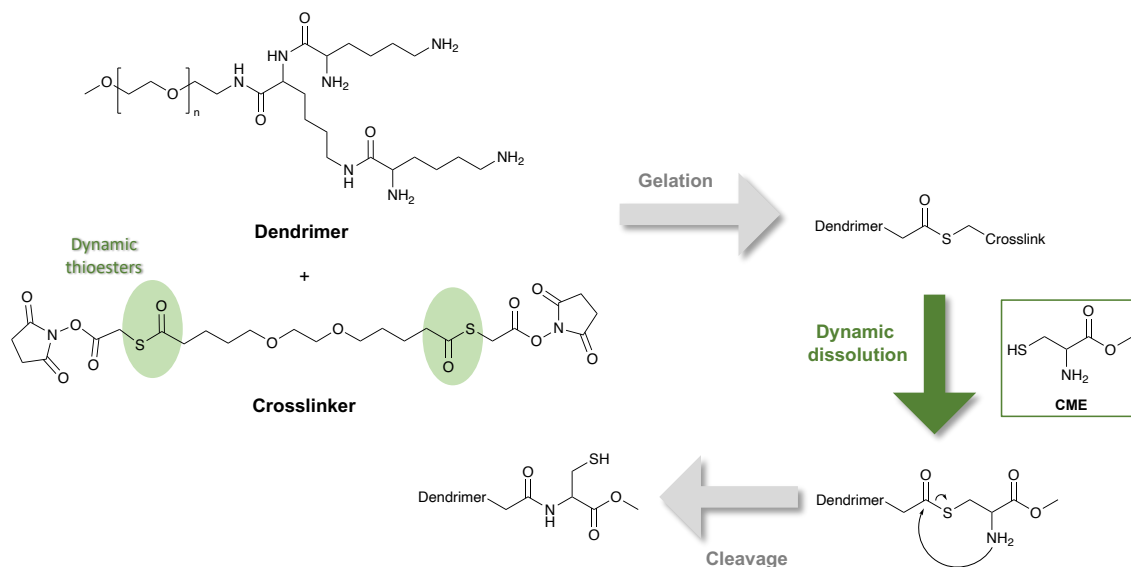
Figure 63: Route to dissolution scheme adapted with permission from M. D. Konieczynska, J. C. Villa-Camacho, C. Ghobril, M. Perez-Viloria, K. M. Tevis, W. A. Blessing, A. Nazarian, E. K. Rodriguez and M. W. Grinstaff, Angew. Chemie - Int. Ed., 2016, 55, 9984–9987. Copyright © 2016, WILEY-VCH Verlag GmbH & Co. KGaA, Weinheim.[158]

1.4.2.4.3 Disulfide Exchange for S-S Bond Formation
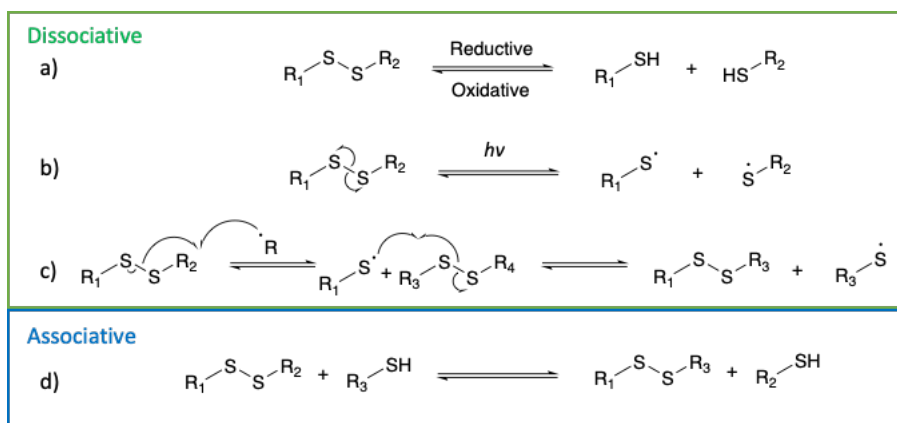
Figure 64: Reversible disulfide mechanisms.

One of the most popular reversible bonds to be incorporated into CAN networks due the versatility of the reversible reaction pathways, which are shown in Figure 64, is disulfide exchange. This has received significant attention previously as crosslinkers for in

vulcanised rubbers.[59] Vulcanisation is another term used to describe crosslinking but with respect to rubbers, which are used for industrial purposes such as tyres. This includes natural rubbers such as poly-isoprene and is traditionally vulcanised with disulfides reacting at allylic active sites in the elastomers.[159] The dynamic nature of disulfides affords flexibility in response to stresses as well as adding some rigidity from the crosslinked network.[160] Therefore, due to the ubiquitous use in the environment and owing to the response to various stimuli, degradable networks utilising disulfides has been a significant focus in CAN research.[161,162]

Disulfides can exchange via a dissociative mechanism, upon exposure to various stimuli such as redox control (Figure 64a) or homolytic cleavage (Figure 64b) via UV, heat or stress. They can also undergo cleavage via a radical initiator (Figure 64c).[111,163,164] Alternatively, they can also be associative in nature via the reaction with free thiols in excess, which can undergo addition-elimination reactions (Figure 64d).[59]

The disulfide bond has been previously mentioned so far in Section 1.4.2.2.1, when the work by Fulton and Jackson was discussed.[95] Reversal of the disulfide bond to thiols was achieved in a reductive environment, utilising tris(2-carboxyethyl)phosphine (TCEP) as the reducing agent (as depicted in Figure 65), and could be achieved both solitary or concomitantly with the simultaneous reversal of the imine bonds present in the network. Utilisation of the stimulated dynamic bonds allowed the network to keep structural integrity upon dissociation of each crosslinking bond type independently.
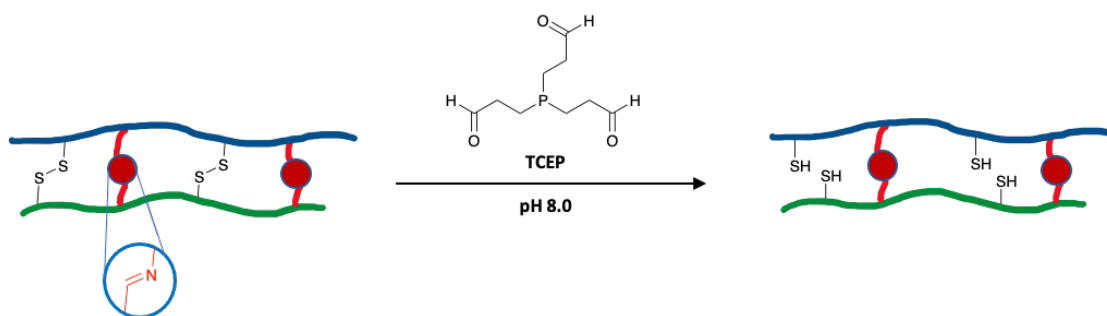
Figure 65: Disulfide reduction with TCEP utilised by Fulton and Jackson.[95]

Klumperman's group utilised disulfides in low T_g (-35 °C) epoxy networks to introduce self-healing to the material.[165] The resultant materials could be healed in 1 hour at 60 °C with minimal change to tensile properties over repeated self-healing cycles, as shown in Figure 66, where A shows the initial tensile repeats, B represents the different healing times and C shows the repeated cycles of self-healing. The authors only reported elongation values in their text, therefore, the graphs in Figure 66 are reproduced from the original article to give the reader insights into the strength of the material.
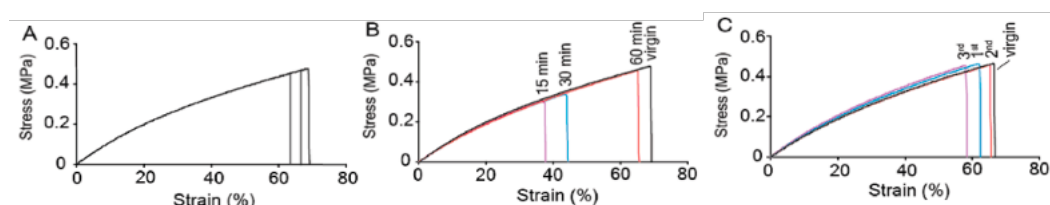
Figure 66: Tensile graphs reproduced with permission from J. Canadell, H. Goossens and B. Klumperman, Macromolecules, 2011, 44, 2536–2541. Copyright © 2011, American Chemical Society.

In 2018, Zhang et al. developed epoxy-anhydride based disulfide networks to incorporate self-healing and recyclability into their network for application to small electronics.[166] Their best performing network contained 22.7 wt% disulfide monomer (1,4,5-oxadithiepane-2,7-dione (DSSA)) with DGEBA and methylhexahydrophthalic anhydride (MHHPA) as a co-curing agent, to afford the 3D network shown in Figure 67. T_g's, observed from tan delta (δ) plots, ranged from 73-13 °C, for 45.6 – 0 wt% of disulfide monomer polymers. The increase in T_g results from a decrease in disulfide content. The best performing network had a T_g of 113 °C and a self-healing efficiency of 96% at 160 °C for 1 hour. The tensile strength was 69.10 ± 2.17 MPa for the pristine polymer which afforded 92% efficiency after remoulding with a tensile strength of 63.45 ± 2.01 MPa.
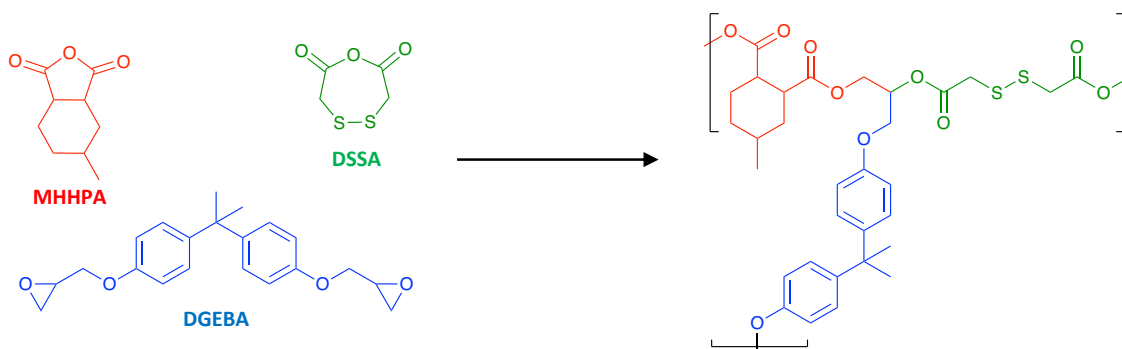
Figure 67: Epoxy-anhydride-disulfide networks synthesised by Zhang et al.[166]

This network was also chemically recycled via the process depicted in Figure 68. The polymer was utilised as an encasing medium for a general electronic induction coil (Figure 68a) before immersion in a di-tertbutyl disulfide (DTBD)/dimethylformamide (DMF) solution which swelled the polymer (Figure 68b) before addition of a catalytic amount of 4-dimethylaminopyridine (DMAP) and triphenyl phosphine (TPP) which catalysed disulfide exchange[167] between DTBD and the network forming soluble oligomers (Figure 68c) allowing retrieval of the original electrical component (Figure 68d).
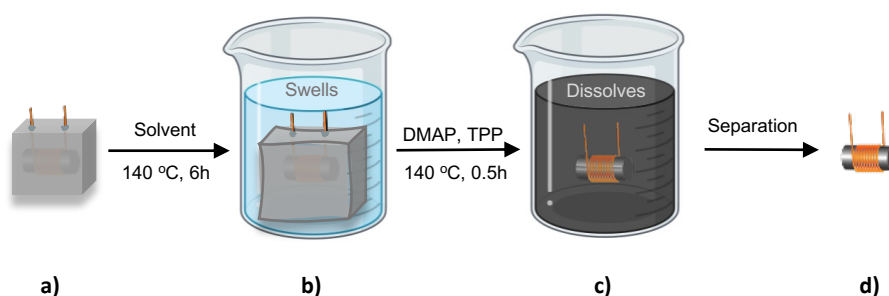
Figure 68: Recycling process of epoxy-anhydride disulfide networks demonstrated by Zhang et al.[166]

Odriozola's group prepared DGEBA-based epoxy-disulfide networks to achieve high T_g, reprocessable networks by utilisation of an aromatic diamine crosslinker containing a disulfide bridge in the structure (Figure 69).[168] It is known that aromatic disulfides can undergo exchange in the presence of tertiary amine catalysts at room

temperature compared to alkyl equivalents that require stimulus.[169] The T_g of the dynamic network was comparable to a traditionally cured reference network, which were 130 and 127 °C respectively. Both also showed similar tensile strengths of 88 and 81 MPa with respect to the dynamic and reference network. The dynamic materials were mechanically recycled via hot-pressing at 200 °C for 5 minutes. These materials were then applied to fibre reinforced polymer composites (FRPC's). The reinforcement fibre was recovered after dissolving the network in the presence of excess thiols (2-mercaptoethanol), thus, introducing chemical recycling to the system. Stress relaxation experiments gave a calculated activation energy of 55 kJ mol^{-1} which is lower than other reported systems due to the aromatic disulfide not requiring heat as aromatic disulfides are known to exchange at ambient temperatures. This is supported by Otsuka et al. who reported that aryl disulfides had a lower bond dissociation energy because the aryl radical is more stable than the alkyl radicals.[170] Otsuka et al. also reported that alkyl disulfides would not exchange without a stimulus, which was photoirradiation in their work.[171] Aromatic disulfides have been shown in a separate computational study, which was also reviewed by Azcune and Odriozola,[164] to exchange via a radical controlled mechanism rather than a metathesis reaction.[163]
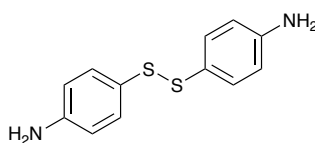
Figure 69: Aromatic disulfide crosslinker utilised by Odriozola's group.

Recent attention has been paid towards reprocessable bio-derived disulfide polymers and have been applied to areas such as 3D printing[172] as well as therapeutic anti-cancer drug delivery systems.[173] The work by Xu et al. exploits the reversible mechanism of a linear amphiphilic disulfide polymer (poly-ethylene glycol-

co-carbonate) with excess glutathione (GSH - a small mono functional thiol), which is present in high concentrations in a cancer cell environment, thus allowing the release of the intended drug at the cancer cell, upon depolymerisation of the disulfides (Figure 70). This method of polymer degradation may also be applied to disulfide networks.
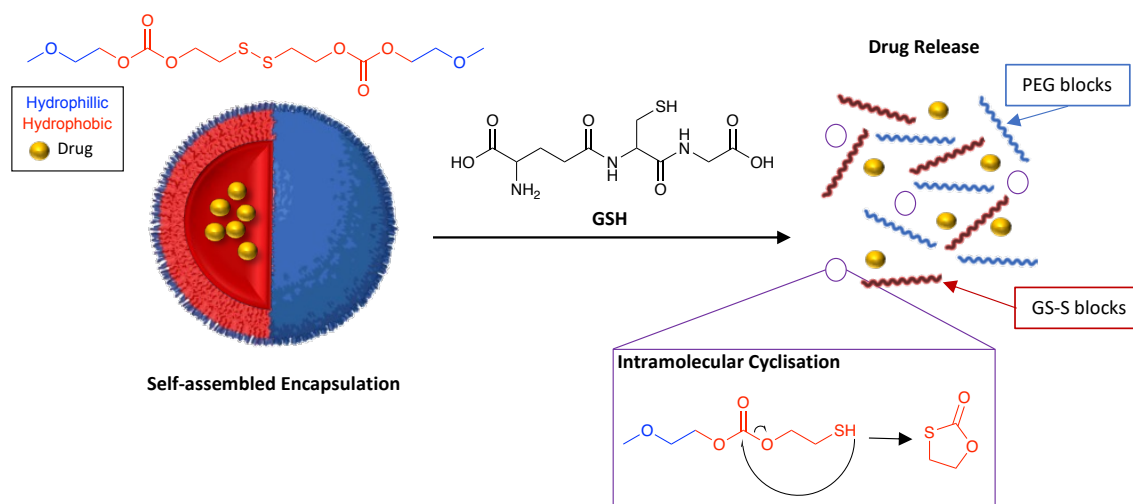
Figure 70: Visual depiction of the work by Xu et al. on drug delivery systems utilising reversible disulfide polymers, which are broken down in the presence of glutathione (GSH).[173]

In 2021, the Dove group constructed bio-based ester disulfide CANs from crosslinking disulfide-containing lipoic acid difunctional monomers with trithiol monomers.[174] The resultant networks had a T_g of 1.9 MPa and could be chemically dissolved in the presence of a base catalyst. Although, mechanical heat press recycling was inefficient leaving a tacky polymer, likely due to degradation of the DBU catalyst.

Tratnik et al. developed bio-derived epoxidized-starch based materials (Figure 71) with disulfide crosslinks that had a stress relaxation activation energy of 77 kJ mol^{-1} and showed self-strengthening upon self-healing.[175] Self-healing was achieved via

hot-pressing ground material at 150 °C for 1.25 hours. The T_g of the original material was 7 °C and showed a gradually increasing trend up to 25 °C for 5 healing cycles, which was also observed with the tensile strength. These values increased from 1.9 MPa to 18.5 MPa over 5 heating cycles. The material was also chemically recycled via excess small molecule thiol in DMF solvent at 50 °C for 24 hours.
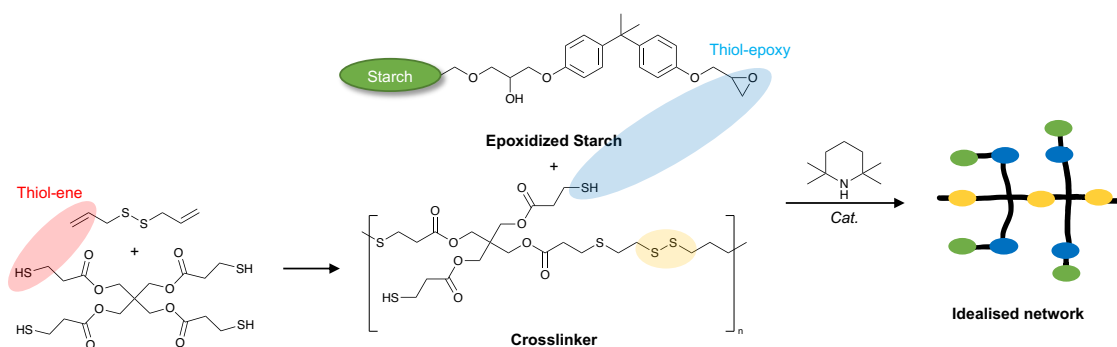
Figure 71: Disulfide networks prepared by Tratnik et al.[175]

The development of materials containing multiple dynamic systems is a reoccurring theme with disulfides. Guo et al. recently developed vanillin-based di-functional aldehyde monomers to react with tri-functional alkyl amines, which results in the formation of reversible imine networks.[176] The formulations contained a di-functional aromatic amine that had a disulfide bridge at the core. The T_g of the poly-imine control network was 35 °C and had a tensile strength of 7.24 MPa, which increased to 43 °C and 16.68 MPa for 10% ratio of disulfides in the network, which is likely due to the presence of aromatic rings in the disulfide containing amine. The material could be mechanically hot pressed at 60 °C for 20 minutes. And stress relaxation tests found an activation energy of 65.77 kJ mol^{-1} for the dynamic network which seems in good accordance with other disulfide literature. The network could also be chemically recycled in acidic solution with a pH of 2, which hydrolyses the imine bonds, hence breaking the network. This affords the precipitation of the vanillin-based aldehyde for reprocessing.

Another group investigated the concomitant use of disulfides with vinylogous urethanes (previously discussed in Section 1.4.2.2.3) in the network, which achieved networks with tri-functional and tetra-functional acetates and di-functional cystamines.[177] The respective tetra-functional dynamic material's T_g was 25 °C, which was similar to the equivalent poly-VU without disulfides (22 °C) as well as both showing similar tensile strengths of 5.20 MPa and 8.67 MPa for the dynamic and non-dynamic respectively. Interestingly, they also found that the introduction of disulfides lowered the dynamic activation energy from 94 kJ mol^{-1} to 72 kJ mol^{-1} for tri-functional, and 61 kJ mol^{-1} to 51 kJ mol^{-1} for tetra-functional equivalent networks. The materials could also be self-healed at 100 °C with an efficiency of 86.92% after 24 hours.

1.4.2.5 Analogous Variations of Transesterification Employed in CANs.

1.4.2.5.1 Phosphate Transesterification for P-O Formation
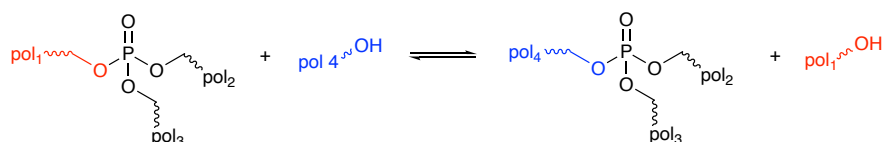
Figure 72: Phosphate transesterification.

An alternative version of transesterification involving phosphate esters are emerging in the field of CANs, which was first reported by Majumadar et al. in 2020.[178] They follow an associative mechanism and can be thermally reprocessed. CANs incorporating organophosphates for transesterification have potential applications biological field due to the ubiquitous presence of organophosphates in biological functions, such as genetic material (i.e. DNA) or biochemical energy production by the hydrolysis of adenosinetriphosphate (ATP).[179] Moreover, phosphate esters have found use in flame retardant applications in the effort to remove toxic halogenated based flame retardants.[97,180]

Majumdar et al. produced networks from triphenylphosphate and poly-ether based polymers reporting an activation energy of 104 kJ mol^{-1} from their stress relaxation experiments, which is similar to those of vinylogous urethanes reported in Section 1.4.2.2.3. and are commonly employed as an alternative to TE CANs. They reported recycling temperatures above 160 °C and low mechanical strength with a tensile strength of only 0.35 MPa.

In addition, catalyst free phosphate ester exchange has been employed for application to fireproof vitrimers by Feng and Li in 2021.[180] Their polymers were based on DGEBA epoxy resins polymerised by a commercially available phosphate ester, which can subsequently exchange with the β-hydroxy group that becomes available after opening of the epoxy. They reported a material with a T_g of 67 °C and a tensile strength of 43.2 ± 0.4 MPa, which is a significant improvement to the materials previously reported by Majumdar et al. An E_a of 56.2 kJ mol^{-1} was extrapolated from their stress relaxation results, which is significantly lower than the work by Majumadar et al. This is likely because of better reactivity of the phosphate group becoming more nucleophilic due to the aryl groups present in the DGEBA chains.

1.4.2.5.2 Siloxane Exchange
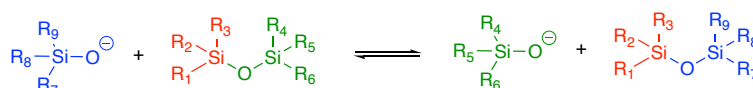
Figure 73: Siloxane exchange.

Similar to transesterification reactions, siloxane exchange occurs in the presence of heat and catalyst, anionic or basic with regards to siloxanes. The exchange mechanism with regards to siloxane CANs is associative because of the SN$_2$ type substitution reaction of the anionic species.[22,181,182] The substitution occurs from nucleophilic attack by the

catalysed anion on the silicon subsequently cleaving the original bond to oxygen, generating a new anionic Si-O chain end capable of further siloxane exchange. Thus, catalysed siloxane networks have living character due to reactive end groups.[22,183] The amount of basic catalyst used dictates the activation of siloxane bonds, and can lower the E_a respectively, which in theory will enable faster exchange at lower temperatures.[184]

Zheng and McCarthy were the first to appreciate the dynamic potential of poly-dimethylsiloxanes (PDMS), and conducted the research of exchange dynamics that was previously hypothesised in 1954.[183,185] Their networks had a low T_g of -129.5 °C, and therefore is in a rubbery state at room temperature. These could be cut and healed at 90 °C over 24 hours with new cracks appearing in separate sites to the healed site in response to applied stress.
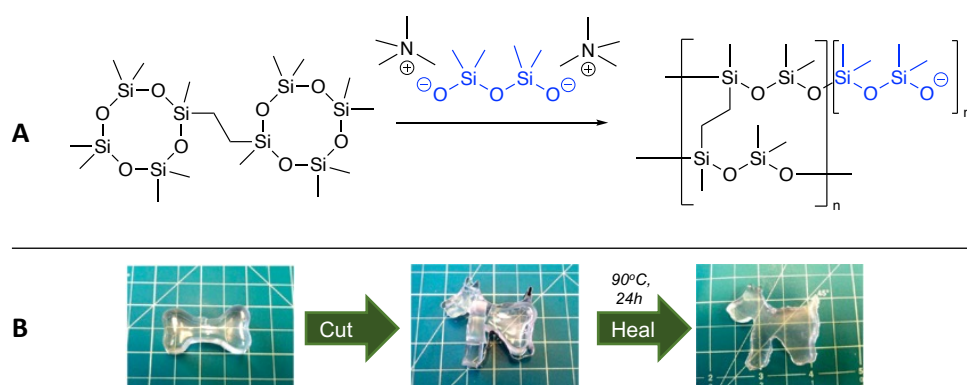
Figure 74: A) Zheng and McCarthy's PDMS network with living character from the anionic polymerisation initiator (blue). B) Their self-healing process of the PDMS network. Figures of self-healing reproduced from P. Zheng and T. J. McCarthy, J. Am. Chem. Soc., 2012, 134, 2024–2027. Copyright © 2012, American Chemical Society.[183]

Recently, Du Prez's group fabricated epoxy-amine-siloxane vitrimers using commercially available starting materials (Figure 75), which can exchange in the temperature range of 160-220 °C when in the presence of catalyst.[182] Their dynamic material exhibited a high T_g of 85 °C, which is suitable for fibre reinforced composites in applications such as wind

turbine blades. Their goal was to investigate faster exchange dynamics in the presence of 1,5,7-triazabicyclo [4.4.0] dec-5-ene (TBD), as a catalyst involving hydroxyls, which was previously found to increase dynamic exchange rates and have a relatively low E_a of 83 kJ mol^{-1} by Saed et al.[184] Du Prez's group found that their material had an E_a of 87.15 kJ mol^{-1} which remained similar through subsequent recycling processes (83 and 86 kJ mol^{-1} over the next two cycles respectively).
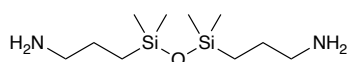
Figure 75: Commercially available siloxane crosslinker utilised by Du Prez's group in the network synthesis with DGEBA epoxy.

1.4.2.6   Dynamic Boron Bonds Employed in CANs for B-O Bond formation

1.4.2.6.1   Boronic Transesterification
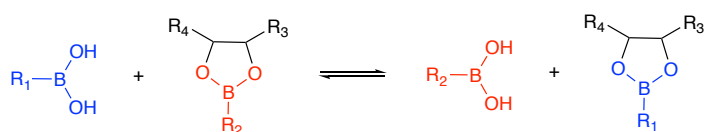
Figure 76: General boronic transesterification reaction.

Not found in nature, boronic acids must be synthesised from other sources of boron such as boric acid or boranes (structures of several boron derivatives are shown in Figure 77). Boronic acids were first synthesised and isolated over a century ago by Frankland et al. via the reaction of a borane with an alkyl zinc compound.[186] They have since become favourable in synthetic chemistry due to their stability and ease of handling, as well as having low toxicity properties.[187] They have also found fame in Suzuki–Miyaura cross coupling reactions, which is a core topic in undergraduate chemistry degrees. Boronic acids are typically white solids and tend to exist in an equilibrium between the acid and its anhydride trimer (boroxine - Figure 77), which occur due to dehydration.[188] Ester derivatives are typically derived from the esterification reaction between the boronic

acids (Figure 77) and alcohols.[187] Similar to transesterification reactions, boronic transesterification is a well-known reversible exchange between boronic esters (and other boron-type esters shown in Figure 77) with other alcohol functional molecules. This reaction has had a recent emergence in research of CANs due to the ease of hydrolysis, similar to imine reversible chemistries, and mild conditions required for both synthesis and recyclability prospects. In addition, manipulation of the boronic ester stability provides opportunity for tuning reactivity and material properties.
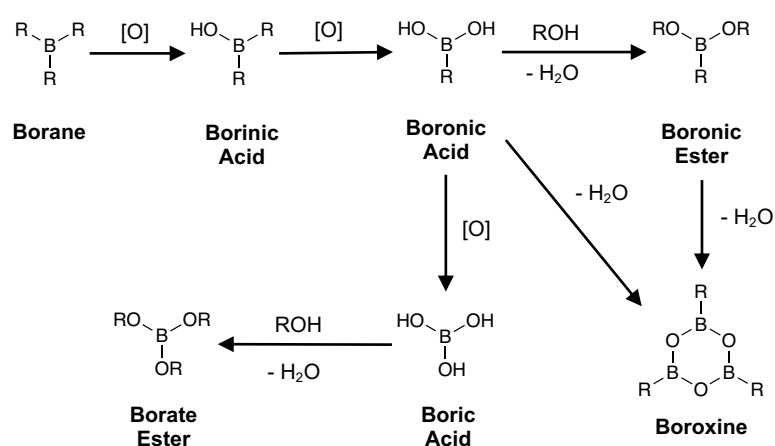
Figure 77: Route to boronic acid derivatives.

For instance, the reversible exchange is fundamental to the non-Newtonian behaviour of slime in a simple experiment using PVA glue and boric acid.[189] The reversibility has been exploited in more medically significant applications, such as diabetes monitoring through the glucose responsivity.[41,45,190–192]
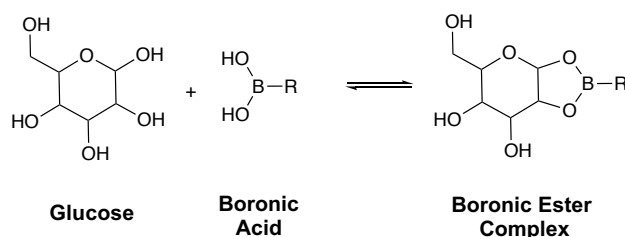
Figure 78: General reaction of glucose with boronic acid, where R is generic alkyl or aryl group.

Such applications have been introduced to society in continuous glucose monitoring (CGM) systems, which enable the user to see glucose levels on their smartphones in real-time over prolonged periods of time, thus enabling less invasive therapies for type-1 diabetes (Figure 79). Mortellaro and DeHennis developed a CGM for a private company in 2014.[193] Their device utilises a fluorescent anthracene derivative of boronic acid that monitors the intensity of the fluorescence upon binding with glucose due to increased Lewis acidity of boron forming weak bonds with nitrogen through its lone pair. Thus, preventing quenching by electron transfer from unpaired electrons.
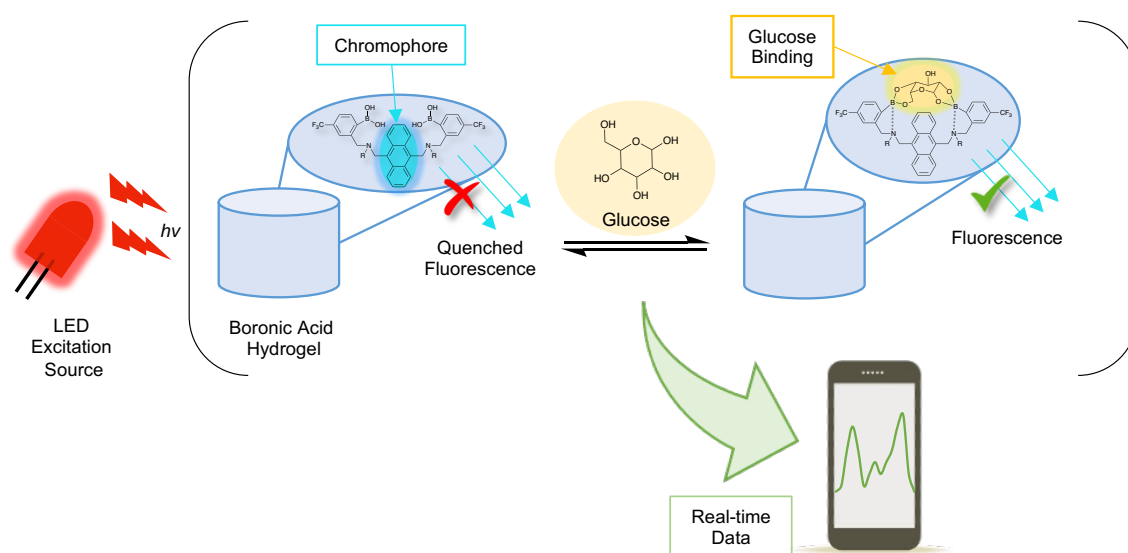
Figure 79: Visualisation of the glucose monitoring system, by boronic ester exchange, in the device reported by Mortellaro and Dehennis.[193]

With regards to CANs, boronic esterification reactions provide a convenient associative exchange mechanism.[194–196] When the pH of a solution containing boronic acids and alcohols is higher than the pKa of the boronic acids (~8-10 – phenylboronic acids),[197] the ester is favoured and when the pH is below the pKa of the acid the boronic acid is favoured.[22,198] The pKa of a boronic acid is the pH when 50% of the acid exists as the hydroxy anion.[199] Thus, pH control of networks utilising boronic acid as well as hydrolysis

routes provides a method of dissociation and subsequent recovery of polymers, molecules or other materials used in the formation of boronic acid based CANs..

Dioxaborolanes and Boroxines

Boronic acids have been utilised by Ogden and Guan to create boroxine crosslinked networks by dehydration to provide strong and recyclable materials.[195] Their materials had a T_g above room temperature (47 °C) and exhibited brittle tensile properties with a tensile strength of 32.9 MPa and a 5.6% strain at break. The reported materials could also be reprocessed by heat pressing at 80 °C or recycled back to monomers in boiling water. The E_a of the networks dynamic exchange was reported to be 79.5 kJ mol^{-1}, which is higher than reported materials that use the boronic ester exchange reaction.
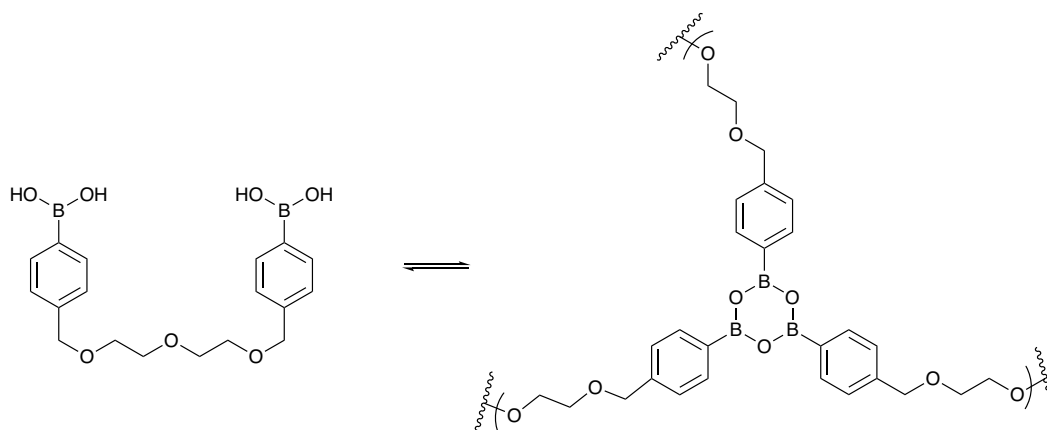
Figure 80: Boroxine CAN by Ogden and Guan.[195]

Wang et al. employed a phenyl monoboronic ester as a crosslinker between OH functional Novolac polymer resins.[200] The resultant network shown in Figure 81 could be dissolved in ethanol, via alcoholysis, which resulted in applications to achieve closed loop recycling of carbon fibre reinforced plastics. The materials with 30 wt% of boronic acid crosslinking had a T_g of 135 °C by DSC. 94% of the strength of the material was retained over the 3 recycling cycles tested however this was conducted by interlaminar

shear strength tests (ILSS) and not typical tensile tests and therefore should not be directly compared to other vitrimer tensile strengths discussed so far.
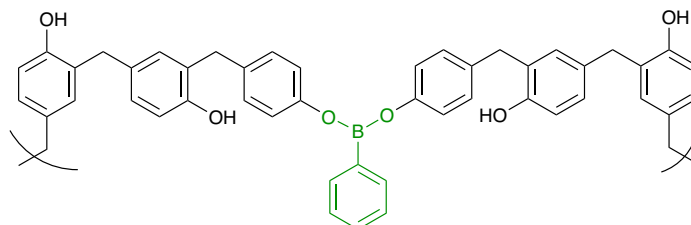
Figure 81: Boronic acid crosslinked novolac resin prepared by Wang et al.[200]

A further classification of boronic ester include the cyclic dioxaborolane series, which are boronic esters derived from diols. Leibler's group, one of the pioneers of vitrimer chemistry (Section 1.4.2.3.1), more recently expanded into boronic ester CANs.[194] They prepared materials from two methods that are visualised in Figure 82: 1) forming linear vinyl polymers (MMA and styrene) with a methacrylate containing a pendant monoboronic ester (denoted as PMMA-V or PS-V when styrene is incorporated) or 2) via reactive processing of HDPE, by extrusion, with maleimide functional boronic esters, which provides a route to dynamically crosslinked commercial thermoplastics (denoted as HDPE-V).[194]
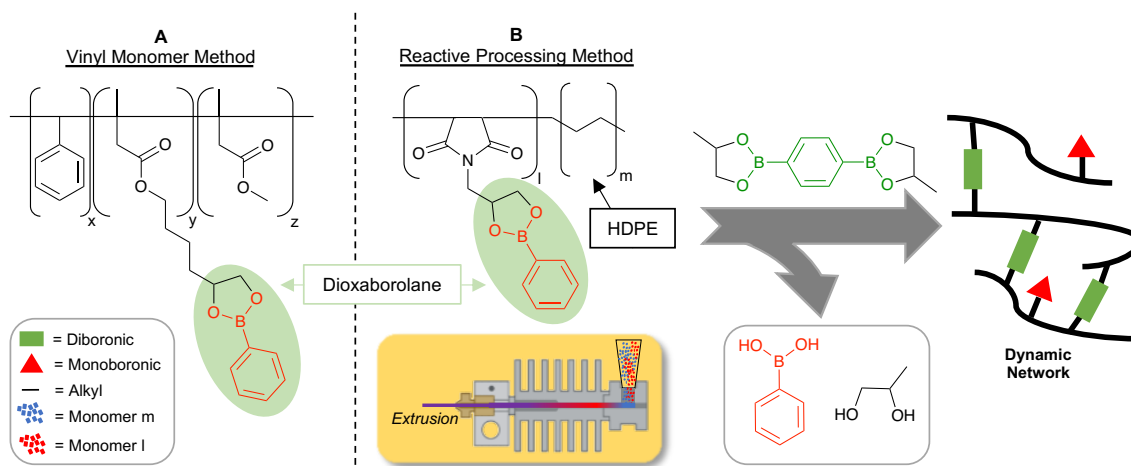
Figure 82: Methods of linear polymer synthesis by Leibler's group.[194] *PMMA-V in the main text denotes method A containing only x and y monomers and PS-V denotes x, y and z containing polymers form method A. HDPE-V denotes the vitrimers derived from method B.*

Both polymers were subsequently crosslinked by bis-dioxaborolanes, separately, to obtain a crosslinked CAN. A small molecule kinetic study, utilising gas chromatography, indicated an activation energy of 15.9 kJ mol^{-1} for boronic esterification. However, the E_a reported in the stress relaxation data, which is more conventionally reported for CANs, was 43.2 kJ mol^{-1} for a PMMA-vitrimer. This difference from the model study may be due to Restricted diffusion within the material or due to the different method of obtaining E_a. The vitrimer materials had high T_g consistent with traditional methacrylate networks. HDPE-V had a T_g of 128 °C by DSC and PMMA-vitrimers and PS-vitrimers had T_g's in the range of 80-100 °C. Tensile stress at breaking was between 20-30 MPa for PS-vitrimers, 30-40 MPa for PMMA-vitrimers and ~20 MPa for HDPE extruded vitrimers.

Chen et al. recently prepared 1,2-diol diboronic ester crosslinkers with a thiol moieties (Figure 83) for crosslinking via thiol-ene click-type reactions that were previously discussed in Section 1.4.2.4.1.[196] They observed the stress relaxation properties of the material and found E_a's between 7.7 and 13.8 kJ mol^{-1}, which is similar for other small molecule boronic transesterification reactions reported by Leibler's group (15.9 kJ mol^{-}

^{1}).[194] The activation energies are lower in comparison to other transesterification reactions as well as the other popular CAN chemistries, which is an attractive attribute for consideration when designing novel CANs. Their materials could be remoulded at 80 °C and had mechanical properties ranging from 1.70 MPa to 2.68 MPa for ultimate tensile strength and from 1.86 MPa to 2.43 MPa for Young's modulus, depending on increasing boronic ester content and this remained similar after reprocessing cycles, retaining more than 80% the original tensile strength. The healing efficiency was found to be better with prolonged healing times at 80 °C, ranging from 30% efficiency after 1 hour to 90% after 24 hours.
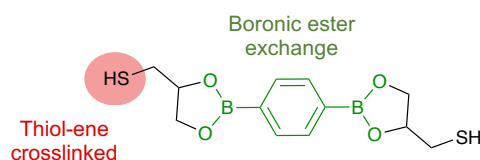
Figure 83: Thiol-boronic exchangeable crosslinker employed by Chen et al.

Sumerlin's group have extensively studied boronic acids in polymer systems over recent years. Most of the research conducted involves pendant monoboronic acids in a linear polymer chain for reactive functionalities. In 2009, they synthesised acrylamide co-polymers with a vinyl analogue of a phenyl monoboronic acid, via RAFT polymerisation, for glucose responsivity applications.[198] The resultant polymers formed micelles in aqueous media due to hydrophilic acrylamides and hydrophobic phenyl boronic acids. Changes to pH or addition of excess diols dissociated the micelles. High pH made the boronic acid aggregates water soluble due to the anionic state. Addition of glucose formed boronic esters which are also known to decrease hydrophobicity of the boronic moiety. In 2011, they synthesised the same acrylamide based monoboronic pendant polymers as in 2009.[201] However, in this work they crosslinked the boronic acid centres with various multifunctional diols to form star polymers and could subsequently

dissociate the boronic-diol network by addition of an excess of a mono-functional diol, which is shown in Figure 84.
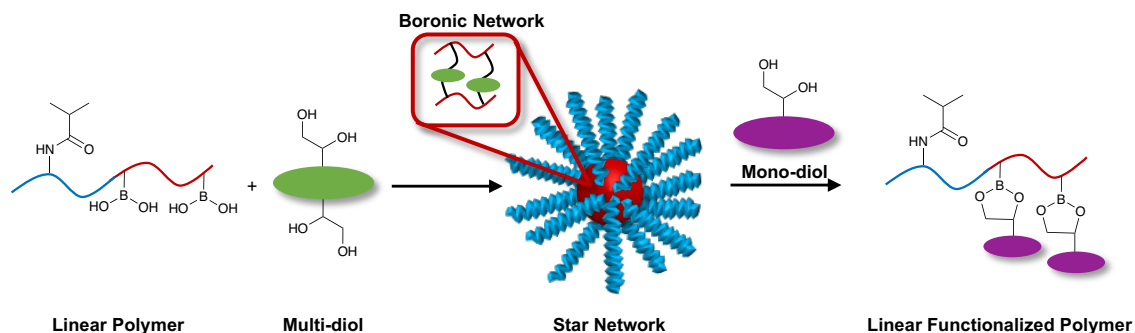
Figure 84: Boronic star network dissociation pathway reported by Sumerlin's group.[201]

In 2015, the group expanded into thiol-ene polymers crosslinked with a boronic ester with difunctional vinyl complementary reactive functional group to the thiols.[39] This enabled room-temperature self-healing when exposed to water at the surface, which is visualised in Figure 85. The T_g of the boronic crosslinked material was -3.5 °C and is in good accordance with the control material which was -3.9 °C. These T_g's are below room temperature which will aid the room temperature self-healing due to the materials ability to flow at ambient temperatures. The stress-strain profile after the cut and heal were similar to the original uncut profile, however the ultimate tensile stress was slightly lower (4.3 MPa for uncut and 4.1 MPa for the same material after healing). Notably, the visualisation in Figure 85 does not account for any boroxine formation that may also occur at the interface of the cut as boroxines are known to form between boronic acid groups. However, this is unlikely in the presence of water.
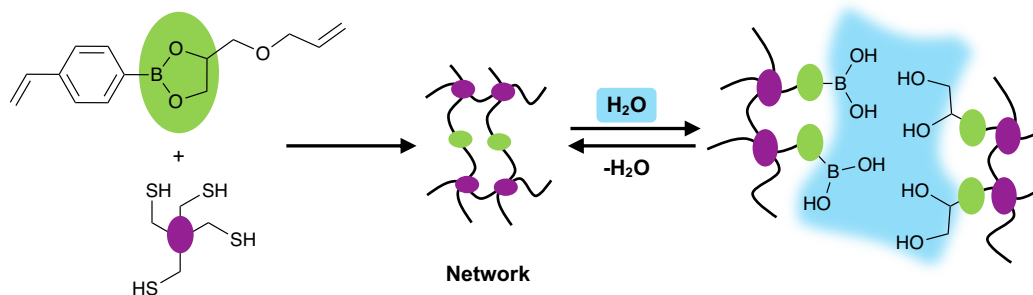
Figure 85: Room-temperature self-healing materials prepared by Sumerlins group and a visualisation of the exchange.[39]

In order to manipulate the design of their previous material to gain increased structural stability, 2018 saw the group incorporate irreversible covalent bonds symbiotically with the boronic acids and additional excess diols, for reversible boronic esterification crosslinking reactions, to negate the effects of creep from rapid exchange.[40] The resultant network materials could either heal by a dissociative hydrolysis mechanism or associative boronic transesterification. Furthermore, at low humidity levels (23%), increased free diol concentrations, shown in purple in Figure 86A and B, in the material or humidity in the environment afforded faster relaxation times, from 107 seconds (for a 99:1 boronic ester:diol ratio) down to 7 seconds (for a 95:5 ratio). This is consistent with free diol catalysis in traditional transesterification reactions that has been reported by Snyder et al. for polycarbonate transesterification vitrimers.[202] However, at high humidity levels (85%) the hydrolysis reactions dominated the exchange as all relaxation times were 1-2 seconds over all concentrations of diols. Incorporation of varying amounts of irreversible bonds, shown in Figure 86C, resulted in less efficient healing, when an increased number of irreversible bonds were present. Combining both irreversible and free diols (Figure 86B) provided faster stress relaxation compared to those without free diols (Figure 86C).
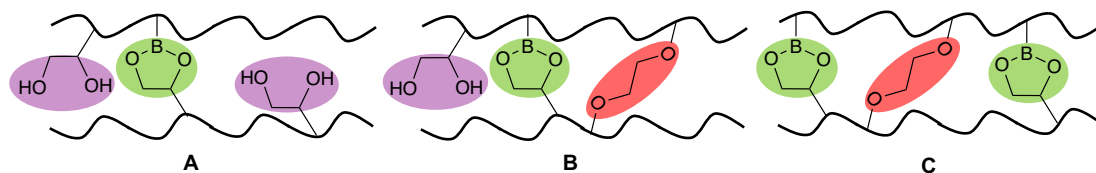
Figure 86: Networks reported by Sumerlin's group incorporating A) free diols (purple) only, B) free diols and irreversible bonds (red) and C) irreversible bonds only, which all three types contain boronic ester crosslinks (green).[40]

Dioxazaborocanes

Trivalent boronic acids and the corresponding esters are usually neutral triganol planar molecules and behave as mild Lewis acids due to readiness to accept lone pairs from Lewis bases in the vacant p-orbital.[187,188] Because boron has a deficient octet and can accept a lone pair from basic molecules, diethanolamine molecules (β-aminodiols) are known to form more stable boronic esters than simpler alcohols lacking an *N*-atom.[203] These complexes are known as dioxazaborocanes and are boronic esters that also contain an intramolecular boron-nitrogen bond. These adopt a tetrahedral shape, rather than planar, when the dative B-N bond is formed.[187] The B-N bond is known to be dative from computational studies of the bond lengths of dioxazaborocanes, with a longer bond length of ~1.67 Å in comparison to ~1.46 Å for a covalent B-N bond.[204] Dioxazaborocanes are readily synthesised via condensation with a diethanolamine functionalities at room temperature (Figure 87) and the resulting complexes have excellent stability towards heat and moisture. Most N-alkyl alcohol derivatives will react with boronic esters in this way. However, N-aryl alcohol derivatives do not readily form dioxazaborocanes due to the poor availability of the N-lone pair.[205]
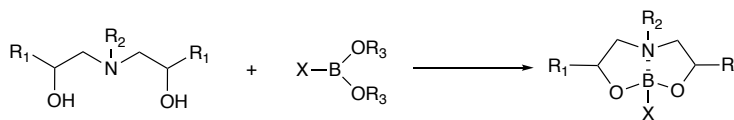
The first report of dioxazaborocane complexation in an epoxy-amine network polymer was in 2015 in an AkzoNobel patent by Wright, Unthank and Cameron for uses in coatings applications on metal or concrete substrates to enable better chemical resistance.[206] However, the action of the monoboronic esters, and one diboronic ester, were not elaborated on until a later patent filed by the same group in 2017.[207] The general structure of the boronic ester is shown in Figure 88. The latter patent introduced the theory of the boronic ester reacting with amino-diol functional groups, where the hydroxyl groups are in a β position to the nitrogen atom, and which are generated during the epoxy-amine curing mechanism. This was the invention that was expected to aid in the chemical resistance properties of the resulting coating material, via modification of the polymer polarity.

Figure 88: General boronic ester patented by The AkzoNobel group, where X is alkyl or aryl derivatives and Y is separated by at least 2 carbons.[207]

The invention was later investigated in depth, in 2019, by Unthank et al. with regards to the mechanistic overview of dioxazaborocane (DOAB) reactions in Novolac-epoxy based epoxy-amine polymer systems.[208] The resulting structure was proven by x-ray crystallography, which confirmed the epoxy-amine-boron (EAB) complex shown in Figure 89. Their work resulted in high T_g materials (110 °C) with improved chemical

resistance in comparison to traditional Novolac-amine coating materials, which was attributed to a lack of interaction from the nitrogen in hydrogen bonding, both within the material (intrinsically) and with external penetrant solvents, which is attributed to the interaction of the nitrogen with the boron. In addition, a model reaction study showed that the borate ester only reacted with the tertiary β-aminodiol and not the secondary β-aminoalcohol groups under mild conditions. Hence, in epoxy-amine polymer synthesis, the borate complexation was deemed a latent and selective mechanism with regards to tertiary β-aminodiols. Contrastingly, an earlier study in 2012, by Ortiz-Marciales' group showed that borate esters could react with secondary β-aminol groups.[209] However, the secondary β-aminoalcohols were significantly less sterically hindered than the ones used by Unthank et al.
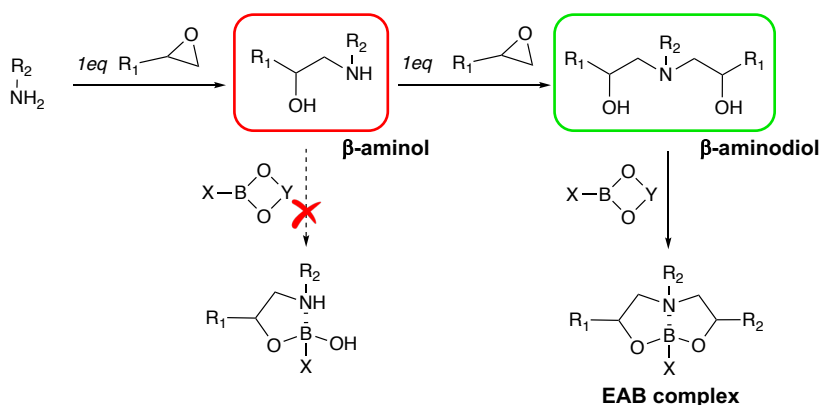
Figure 89: Epoxy-amine reaction followed generating amino alcohols and subsequent reactions with boronic acids or esters. Scheme reproduced and adapted, under a creative commons licence, from M. G. Unthank, C. Cameron, A. Wright, D. Hughes, M. A. Alam and M. R. Probert, Polym. Chem., 2019, 10, 4920. Copyright 2019, © The Royal Society of Chemistry. [208]

In 2018, Otsuka et al. exploited the reactivity of the intrinsic diethanolamine (DEA) group, formed in epoxy-amine polymerisations, towards boronic acids.[210] They modified a cured epoxy-amine polymer by introducing a crosslinkable reaction with diboronic acid. By dissolving the linear polymer in solvent and adding the diboronic acid in another step.

Upon gelling, the material exhibited higher T_g's, from 48.5 °C when linear to 67 °C when gelled, which is to be expected. However, when the amine cured control was modified with diboronic acid no noticeable change to T_g was observed (44.5 °C and 45.5 °C respectively), suggesting little significant changes to the network structure. The amine cured network and boronic acid modified version were compared by tensile tests. The boronic modified network showed improved mechanical properties compared to the amine control network, indicating successful network formation, with a maximum tensile strength of 1.8 MPa compared to the control material, which was 0.94 MPa. The group still did not study any recyclable aspects of their boronic acid modified linear polymer.

Further work by the group employed the boronic acid reactivity with DEA functionalities for adhesion purposes, as depicted in Figure 90.[211] They developed co-polymers by reacting butyl methacrylate monomers with vinyl-monoboronic acid and ester via radical polymerisation. This could improve the adhesion strength to an epoxy-amine polymer. This study showed that the surface of cured epoxy resins could be functionalised by boronic esterification. The adhesion strength after the adhesion of the boronic acid polymer to the methacrylate polymer was 0.173 MPa and the same DEA polymer adhered to the boronic ester containing polymer was 0.238 MPa, which was attributed less available boronic acids due to the formation of boroxines between some boronic acid groups. The reference material using styrene instead of boronic acid did not adhere and could be pulled off with minimal force. The reversibility of the boronic ester reaction with an epoxy-amine polymer was not studied by this group.
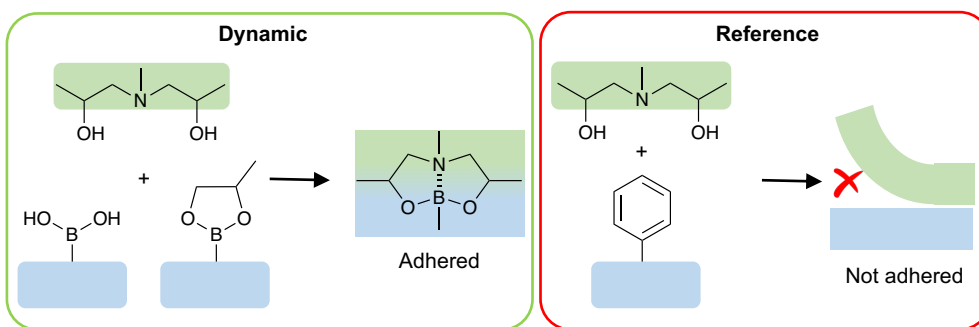
Figure 90: Dynamic adherence versus the non-adhering, non-dynamic styrene reference polymer reported by Otsuka et al.[211]

1.4.2.7 Summary of DCBs in CANs

Over the previous section, several dynamic bonds have been reviewed, with respect to CANs, highlighting reversible mechanisms, application of DCBs in traditional thermosetting polymers, as well as the thermal and mechanical properties of resulting polymers in current literature. This summative sub-section aims to provide the reader with a brief conclusive discussion of the dynamic covalent chemistry discussed thus far.

Selection of the type of dynamic bond used depends on the desired properties of the resultant material. Differences in a materials behaviour can arise between the associative and dissociative CAN mechanisms. Both mechanisms have clear benefits to recycling or reprocessing, but only associative will remain as a constant covalent network throughout processing and will follow typical Arrhenius behaviour, which is where the temperature-viscosity dependence is controlled by the chemical exchange reactions rather than diffusion controlled William-Landel-Ferry (WLF) behaviour.[59,61,149] However, depending on the end use, or goal method of recycling, selection of the dynamic chemistry should be carefully chosen in the design of new CAN.

For example, if the desired use of the network is for 3D printing, via a common extrusion method, a thermally activated mechanism (most likely a dissociative mechanism) may prove beneficial, as these will be thermoset at room temperature with the ability to deliver a lower melt viscosity at temperatures above a) the temperature at which the exchange proceeds or b) the T_g of the material if the former is lower (see T_v -Section 1.4.2). Furthermore, if reprocessing is the sustainable driving force of the research, a temperature dependent dynamic exchange mechanism is likely to prove advantageous as heat-pressing broken pieces into re-moulded, homogenous materials is proven to be successful for these CAN types. However, these temperature dependent materials can be highly susceptible to creep due to the exchange reactions often occurring at room temperature.

If the overall structural integrity of the material is a crucial factor, as is usually required in aerospace and wind turbine applications, associative mechanisms may be considered. This is due to the fact that associative dynamic exchange mechanisms maintain crosslink density throughout. Therefore, the materials high T_g and upper service temperatures are preserved. In addition, for smart responsive materials, where the intended application does not require robustness of the network, pH responsive mechanisms, which are predominantly dissociative in nature, such as the imine and hydrazone condensations, are beneficial as the "switch" can be controlled by the environment. This proves valuable for many applications, from drug delivery to full monomer recycling.

Dynamic reaction conditions and vulnerabilities also cause concerns when designing new CANs. In transesterification (TE) reactions, high temperatures and catalysts are required. The requirement for metal catalysts poses a concern for long term stability as any deactivated catalyst will no longer drive the reaction. Furthermore, leaching of the catalyst from the material can pose as a risk to the environment or cause health concerns, as well as reducing the materials ability to self-heal or recycle. In addition to

these drawbacks, TE reactions are susceptible to hydrolysis which may also affect the long-term stability of the material. As a result, there has been an ever-increasing surge towards the development of VU vitrimers, as an alternative to TE vitrimers, because of the catalyst free nature whilst maintaining comparable properties to TE vitrimers. Boronic esterification is also a catalyst free alternative to TE which also proceeds at lower temperatures.

Combinations of orthogonal dynamic CAN chemistries have been utilised synergistically in thermoset polymers, such as those by Fulton and Jackson.[95] For a successful CAN with multi-dynamic links, requirement of the dynamic chemistries to coexist in the material with no cross reactivity is essential.[60] Careful consideration of the activation pathway is also necessary. Considering the characteristic Ea's of the DCBs in contention, where DCBs with lower Ea's would proceed first (as discovered by Du Prez's group), or the differing activating stimuli of the DCBs together with the activated mechanism type (associative or dissociative) are all important deciding factors.
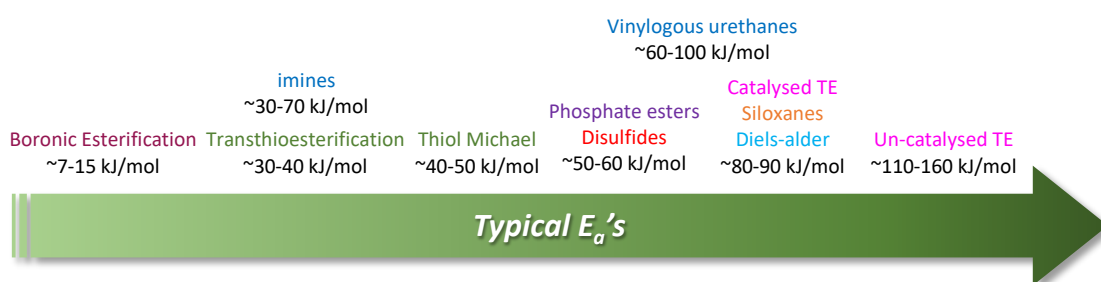
Figure 91: Lowest reported dynamic activation energies discussed in this thesis for dynamically crosslinked thermoset polymers.
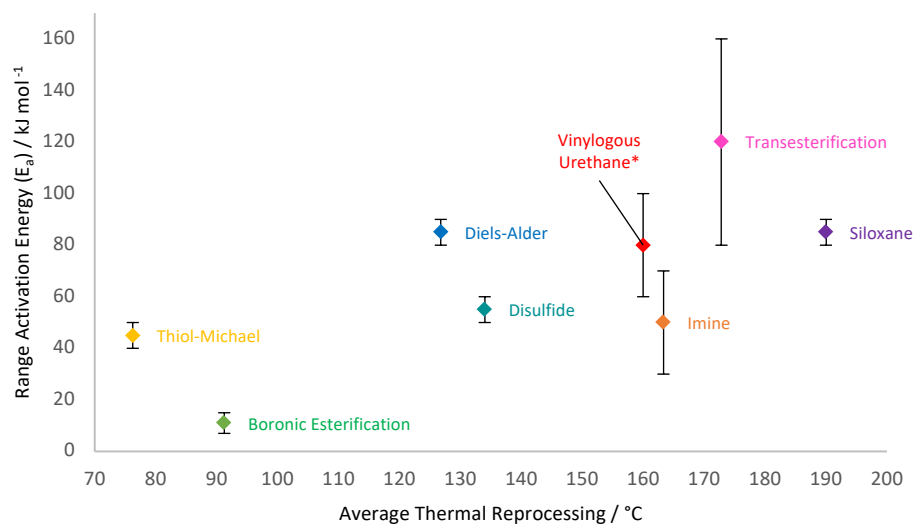
Figure 92: Reported DCB types with ranges of reported activation energies versus average temperatures of reprocessing.* Indicates where only one thermal processing temperature was reported (with an activation energy in the same publication) across the publications reviewed for this research area.

Overall, CANs prove to be an exciting and rapidly emerging area of polymer chemistry to combat the prevailing recycling concern with thermoset networks, with regards to single use and high-performance plastic polluting the natural environment.

Table 2: Summary of common dynamic CAN reactions

Dynamic Chemistry	CAN Type	Bond Type	Stimuli
Diels-Alder	D	C-C	Temperature (90-150 °C)[47]
Imine condensation	D	C-N	pH[22]
Transimination	A	C-N	pH[95], temperature[93], hydrolosis[93]
Hydrazone Condensation	D	C-N	pH, catalyst[89], Nu⁻ base[102]
Hydrazone metathesis/TE	A	C-N	Temperature[47]
Oxime metathesis / TE	A	C-N	Heat[100], pH[101]
Vinylogous urethanes	A	C-N	pH, temperature (80-100 °C)[119,212]
Transesterification (TE)	A	C-O	Temperature, catalyst[22,57]
Disulfide Exchange	D/A	S-S	pH, catalyst, temperature, shear[59], excess thiol[173]
Thiol-Michael Exchange	D	S-C	pH, temperature[22,47,146]
Transthioesterification	A	S-C	Temperature[47]
Boronic esterification	A	B-O	pH, temperature
Si-O Exchange	A	Si-O	Catalyst[22], temperature[182] hydrolysis

Table 3: Thermal and mechanical properties of thermally responsive CANs without performance increasing additives.

Dynamic Chemistry	Polymer type description (Polymer chain / crosslinking)	Tensile Strength (MPa)	T_g (°C)	Thermal Reprocessing (°C)	Ref
Diels-Alder	[c] Epoxy / [d]FM	*2.84	35	100	[70]
	Methacrylate / [g]AM	-	-5 < 105	[f]135-152	[74]
	Poly-ester / [d]FM	68	-	>120	[71]
	Epoxy-amine / [d]FM	-	97	[f]127	[213]
Imines	[h]PDMS / transimination	2.8	-105.2	180	[214]
	[c]Aromatic – epoxy / vanilin imine	60.6	127	170	[98]
	epoxy/ transimination	119.5	[i]150.3	140	[96]
Hydrazones / Oximes	Multifuntional Thiol-oxime	2.8	14	120	[100]
Vinylogous Urethanes	Methacrylate / VU	-	110	160	[117]
Transesterification	[a]EVO / COOH	8.5, 22	17, 25	170	[215], [216]
	[c]Aromatic – epoxy / COOH	94, 9	135, -	190, -	[217], [57]
	[c]Aromatic – epoxy / anhydride	55, 41.2	80, 98	[b]250, 180	[57], [34]
	Alkyl – epoxy / carbonate	36	34	100	[202]
	Poly-ester / methacrylate	11.3-33.0	[i]120-130	150	[133]
Disulfide Exchange	[c] Epoxy-anhydride	69.1	[i]113	160	[166]
	[c] Epoxy-(Aryl disulfide)	88	130	200	[168]
	[c] Epoxidized-starch	1.9 [k](20.0)	7 [k](26)	150	[175]
	Biobased-ester	1.8	-37	-	[174]
	Vanillin / amine	16.68	[i] 43	60	[176]
	VU / cystamine	5.2	25	100	[177
Thiol-Michael Exchange	Polyester / thiol-Michael	1.35	[i] 4.8, -14.5	RT-100	[150]
	Acrylate / thiol-maleimide	0.30	20	90	[146]
	Acrylate / thiol-Michael	0.37	16	90	[147]
Transthioesterification	Thiol-ene/ thiol-ester	- ([j]8)	[i]7	-	[154]
Boronic Esterification	Boroxine	32.9	47	80	[195]
	Novolac / boronic acid	-	153	180	[200]
	Thiol-ene / boronic ester	2.68	[i]~0	80	[196]
		4.3	-3.5	25	[39]
Siloxane Exchange	Epoxy-amine	-	85	160-220	[182]

[a]*Epoxidized Vegetable oil, COOH = carboxylic acid,* [b]*Injection moulding temperature,* [c]*Bisphenol derived,* [d]*Furan/maleimide reversibility,* * at 60 °C, [f] *By observation of network loss by DSC,* [g] *AM = anthracene/Maleimide reversibility,* [h] *PDMS = poly-dimethylsiloxane,* [i] *Tg by DMA tan delta peak,* [j] *Youngs modulus data*

1.5 Aims and Goals

The purpose of this PhD research is to establish a novel method of fabricating, analysing and recycling a thermoset polymer, for high performance applications, based on dynamic dioxazaborocane crosslinking. To the best of my knowledge, this is the first of its kind. The primary goal of the research is to obtain dioxazaborocane based CANs, that can compete mechanically with epoxy-amine thermoset network polymers that are currently utilised for high-performance applications, which can also be reprocessed indefinitely or can be chemically recycled with the prospect of preventing end-of-life disposal in conventional waste streams.

Chapter 3 explores the small molecule synthesis and model reactions behind the boronic acid crosslinking reaction. The goal behind this research was to determine the most practically suitable solution for a single-step thermoset polymer reaction crosslinked by multi-functional boronic acids/esters. The factors that have been considered in this research were: Miscibility in the epoxy resin, storage stability, reactivity with the diethanolamine (DEA) group, ease and cost of synthetic procedure to maximise suitability for a scalable process for commercial viability.

The research in Chapter 4 utilised molecular-level material design, controlling factors critical to material performance including (i) polymer molecular weight (ii) average polymer functionality and (iii) cross-link density, for developing strong materials in a suitable state to test mechanically and be suitable for an end-use product. This enabled the assessment of high-performance attributes such as tensile strength and Young's modulus.

Chapter 5 probes the mechanical properties of the dioxazaborocane networks presented in this research. This provided a means to compare the performance of the

dioxazaborocane crosslinked materials with commonly utilised epoxy-amine thermoset materials for aerospace and wind turbine applications. In addition, thermal and molecular weight characterisation was undertaken to investigate the material behaviour in response to temperature as this is known to be a stimulus for this class of CAN.

Chapter 6 develops reprocessability and chemical recycling methods to recycle the dioxazaborocane crosslinked polymer networks. This was the main motivation behind this research and delivered a means to recycle a thermoset epoxy-amine polymer which is the first of its kind. The results of the work conducted throughout Chapters 3 through 6 and have been published in L. Anderson, E. W. Sanders and M. G. Unthank, Mater. Horizons, 2023,10, 889-898.

Chapter 7 develops the recyclable polymer formulations investigated previously. The linear chain epoxy-amine dioxazaborocane crosslinked polymer networks were developed to contain an aromatic epoxy with the expectations of exceeding the current material performance for the class of CAN reported in Chapter 5, and to match the performance of commodity epoxy-amine thermosets. The work in this chapter forms a foundation for future work in the scope of this research.

Chapter 2

Experimental

2 Chapter 2 - Experimental

2.1 Materials

All materials were purchased from commercial vendors listed in Table 4 and used as received without further purification for synthesis unless specifically stated.

Table 4: List of chemicals used as reagents or solvents and grouped by use.

Chemical	CAS	Supplier	Purity
Model Ligands			
Phenyl Glycidyl ether (PGE)	122-60-1	Acros Organics	99%
Cyclohexylamine (CHA)	108-91-8	Acros Organics	99%
Hexylamine (HA)	111-26-2	Acros Organics	99%
Monoboronic Acids/ Esters			
Phenyl boronic acid hydrate (PhBac)	98-80-6	Fluorochem	95%
(4,4,5,5-Tetramethy-1,3,2-dioxaborolan-2-yl)benzene (Phenylboronic acid pinacol ester)	24388-23-6	Fluorochem	98%
Diboronic Acids/ Esters			
1,4-phenylene diboronic acid	4612-26-4	Fluorochem	97%
1,4-Bis(4,4,5,5-tetramethyl-1,3,2-dioxaborolan-2-yl)benzene (1,4-phenylene diboronic acid dipinacol ester)	99770-93-1	Fluorochem	97%
Epoxy Resins			
1,4-butanediol glycidyl ether (BGE)	2425-79-8	Alfa Aesar	96%
DER 332 (Bisphenol A epoxy resin)	25068-38-6	Olin	>99%
Aliphatic Amines			
4,4'-diamino dicyclohexylmethane (4,4'-MDH)	1761-71-3	Alfa Aesar	98%
1,6-hexane diamine	124-09-4	Acros Organics	99.5%

General Solvents/Reagents			
Tetrahydrofuran	109-99-9	Fischer	99.5% / Lab grade
Deuterated chloroform (CDCl$_3$)	865-49-6	Cambridge Isotope Laboratories	99.8% + 0.05% w/v TMS
Deuterated dimethyl sulfoxide (DMSO-6)	2206-27-1	Cambridge Isotope Laboratories	99.9% + 0.05% w/v TMS
Acetonitrile	75-05-8	Fischer	99.9% / HPLC grade
Butan-1-ol	71-36-3	Fischer	99%
n-Butyllithium, 2.5M solution in hexanes (n-BuLi)	109-72-8	Acros Organics	N/A
Triisopropyl borate	5419-55-6	Acros Organics	98%
Bromobenzene	108-86-1	Acros Organics	99%
2,3-Dimethyl-2,3-butanediol (pinacol)	76-09-5	Alfa Aesar	99%
Ethylene glycol (1,2-diol)	107-21-1	Acros Organics	99%

2.2 Instrumentation and Analysis

2.2.1 Nuclear Magnetic Resonance (NMR)

NMR analyses were acquired at 25 °C using a JEOL ECS400 Delta spectrometer at frequencies of 399.78 MHz for ^{1}H-NMR, 100.53 MHz for ^{13}C-NMR and 128.28 MHz for ^{11}B-NMR. All chemical shifts are quoted as parts per million (ppm) relative to tetramethylsilane (TMS, δ = 0 ppm) as an internal standard in either deuterated chloroform (CDCl$_3$) or deuterated dimethyl sulfoxide (DMSO-d^6). Hydroxy (OH) group analyses were confirmed by doping samples with a drop of deuterated water (D$_2$O). ^{13}C-NMR assignment was confirmed by DEPT analysis. The spectral data is recorded as chemical shift (δ), relative integral, multiplicity (s=singlet, br=broad, d=doublet, t=triplet, q=quartet, quin=quintet, sext=sextet, dd=doublet of doublets, m=multiplet) and coupling constant (J = Hz).

2.2.2 Fourier Transform Infrared Spectroscopy (FTIR)

Infrared spectroscopy was performed on a Bruker alpha Platinum-ATR with a diamond crystal and the outputs analysed in OPUS software. Absorption maxima are expressed in wavenumbers (cm^{-1}). All spectra shown are the result of 16 scans.

2.2.3 Mass Spectrometry (MS)

Samples were acquired using a Thermo RSLC coupled to an ABSciex 6600 QTof. The equivalent of 1-5 µM (1-5 pmol/µl) was injected onto the system per run. The loading pump was used at high flow to run linear chromatography gradients. All samples were acquired in positive mode. The buffer system comprised of Buffer A 0.1% (v/v) Formic Acid and Buffer B 99.9% Acetonitrile, 0.1% (v/v) Formic Acid. Chromatographic separations were achieved using a Fortis C8 column, 100 mm x 2.1 mm, 3 µM particle size, 45 °C at a flow rate of 250 µl/min. Samples were loaded onto the column and desalted online for 1 minute, with eluent diverted to waste. A valve switch directed flow

to the mass spectrometer. Samples were then eluted from the column using a linear gradient from 3-70% Buffer B over 12 min. Total run time was 17 min. The eluent was directed into an ABSciex 6600 QTof, operated in positive mode. Source conditions were; temperature 180°C, GS1 25, GS2 15, ISFV 4500v. Data was acquired in MS scan mode between 100-1000 m/z. Resolution of the instrument was 45,000 at m/z 829.54.

2.2.4 Gel Permeation Chromatography (GPC)

Polymer samples were dissolved in THF (2 mg/mL) and filtered through 0.2 µm nylon filters. Samples were analysed using an Agilent 1260 infinity II system equipped with a RI and viscometry detector, fitted with PLgel MiniMIX-E and PLgel MiniMIX-D columns in sequence, using a THF mobile phase and a flow rate of 0.6 mL/min or 0.4 mL/min. Analysis was performed against a calibration curve of polystyrene standards (EasiVial PS-M supplied by Agilent).

2.2.5 Thermogravimetric Analysis (TGA)

TGA analysis was conducted using a Perkin-Elmer Pyris 6 TGA thermal analyser and results analysed in Pyris software (version 11.1.1.0492). Polymer samples of between 16-20 mg weight were heated in ceramic crucibles from 30 °C to 650 °C at a constant ramp rate of 20 °C per minute, under a flow of N_2 (40 mL/min). The residual mass was recorded as a percentage weight, of the original mass, that remained at 600 °C (within the range where mass remained constant after the degradation of organic material).

2.2.6 Differential Scanning Calorimetry (DSC)

Glass transition (T_g) analyses were conducted on all polymeric materials using a Perkin-Elmer Pyris DSC 8500 and analysed on Pyris software (version 11.1.1.0492). Samples had previously been thermally cured in an oven at 170 °C. Sample masses of 3-6 mg were weighed into standard aluminium DSC pans with perforated lids and were heated

from -50 °C to 200 °C at a constant rate of 20 °C per minute (unless otherwise stated) and the T_g reported as the midpoint of the endothermic step in the heat flow signal output (T_g onset and endpoint was also recorded). Melting point analysis was conducted using a Perkin-Elmer Pyris DSC 8500 with an intercooler II and analysed on Pyris software (version 11.1.1.0492). Solid samples between 3-6 mg were weighed into standard aluminium DSC pans and heated from -50 °C to 300 °C at a constant rate of 20 °C per minute and the melting point taken from the peak of the endothermic event that corresponds to the melting transition on the heat flow signal output.

2.2.7 Dynamic Mechanical Thermal Analysis (DMTA)

DMTA analyses were conducted for network polymers on a Perkin-Elmer DMA 8000 and analysed in Pyris software (version 11.1.1.0492). Temperature scans were performed on 30 mm x 5 mm x 0.3 mm samples and were analysed in tension geometry in a dual cantilever mode with a fixed length of 11.52 mm, a frequency of 1 Hz and a constant temperature ramp of 3 °C/min from -80 °C to 200 °C. Storage modulus (E'), loss modulus (E'') and tan delta (Tan δ) signals were recorded.

2.2.8 Laser Cutting

Samples were prepared for mechanical testing using a Glowforge™ Basic equipped laser cutter with a 40W CO_2 laser tube.

2.2.9 Tensile Testing

Thin film polymer samples were laser cut to a modified ASTM standard 638-14-type V and experiments were conducted on either an Instron 5969 or Instron 3343 with a displacement ramp rate of 10 mm/min.

2.2.10 Hot Press (Mechanical) Recycling

Mechanical recycling was conducted using a 2 " x 3 " Mini Manual Hot Press Machine (TTLIFE) with LCD Controller at 700-1000 lbs pressure. Ground polymer samples were place between PTFE sheets before pressing at 170 °C for 30 minutes, before allowing to cool to 25 °C overnight. Samples were then removed from the press and prepared for testing.

2.3 Experimental Synthesis and Procedures

2.3.1 Boronic Ester Synthesis (1a-d)

2.3.1.1 Phenylboronic Acid 1,2-ethanediol ester (1a)

1a
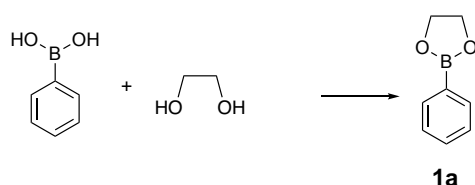
A mixture of phenylboronic acid (0.97 g, 0.007 mol), ethylene glycol (0.86 g, 0.014 mol, 2 equivs) and DCM (20 mL) were charged to a round bottom flask under nitrogen gas and stirred with excess $MgSO_4$ at room temperature for 18 hours. The mixture was filtered to remove the $MgSO_4$ and the filtrate concentrated under reduced pressure to give the crude product as a pale-yellow liquid. The crude product was then purified by vacuum distillation affording the purified product as a pale-yellow oil (87% yield). δH (400 MHz; $CDCl_3$; Me_4Si) δ 7.82 (d, J = 6.9 Hz, 2H), 7.48 (t, J = 7.3 Hz, 1H), 7.38 (t, J = 7.3 Hz, 2H), 4.37 (s, 4H). δC (101 MHz; $CDCl_3$; Me_4Si) δ 134.9 (C-Ar), 131.6 (C-Ar), 128.0 (C-Ar), 66.1 (CH_2O). δB (128.28 MHz; $CDCl_3$ Me_4Si) δ 31 (s, br, Ph-B(OR)$_2$). v^{max}/cm^{-1} 3053 (ar-CH stretch) 2979 (CH stretch), 2908 (CH_2 Stretch), 1602 (C=C ring stretch), 1499 (C=C ring stretch), 1480 (C=C ring stretch), 1440 (CH_2 Bend – scissor), 1395 (B-O stretch), 1371, (B-O stretch), 1332 (B-O stretch), 1213 (C-O stretch), 1091 (B-C stretch), 696-638 (aromatic CH bend), 639 (B-O Bend out of plane).

2.3.1.2 Phenylboronic acid pinacol ester (1b)

1b
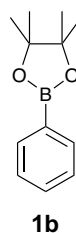
Phenylboronic acid pinacol ester was purchased from Fluorochem and used as received.

δH (400 MHz; CDCl$_3$; Me$_4$Si) δ 7.80 (m, 2H), 7.45 (m, 1H), 7.34-7.38 (m, 2H), 1.34 (s, 12H). δC (101 MHz; CDCl$_3$; Me$_4$Si) δ 134.8 (C-Ar), 131.4 (C-Ar), 127.8 (C-Ar), 83.9 ((CH$_3$)$_2$C-), 24.9 (CH$_3$). δB (128.28 MHz; CDCl$_3$ Me$_4$Si) δ 28 (s, br, Ph-B(OR)$_2$). vmax/cm^{-1} 2979-2944 (CH stretch), 1600 (C=C ring stretch), 1437 (CH$_2$ Bend – scissor), 1356 (B-O stretch), 1138 (C-O stretch), 1091 (B-C stretch).

2.3.1.3 bis(propan-2-yl)phenylboronate (1c)[218]

1c
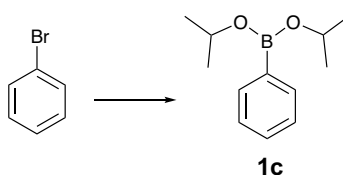
The isopropyl monoboronic ester **(1c)** was synthesised in accordance with the method developed by Wesela-Bauman et al.[218] Bromobenzene (6.3 mL, 0.060 mol) was added dropwise to a sealed vessel under an inert nitrogen atmosphere, at -78 °C, containing a mixture of anhydrous THF (30 mL) and n-BuLi (25.2 mL, 0.063 mol). The mixture was left to stir at -78 °C for 30 minutes. Triisopropyl borate (14.5 mL 0.063 mol) was added dropwise to the reaction vessel at -78 °C and stirred for a further 30 minutes. The reaction vessel was warmed to room temperature and quenched with 2M HCl in diethyl ether (37.5 mL, 0.075 mol). The solvents were removed from the mixture under reduced pressure and the resulting pale-yellow residue was subjected to fractional distillation producing a colourless liquid (78% yield, 9.67 g). (Bpt = 65-75 °C, 6 mmHg). δH (400 MHz; CDCl$_3$; Me$_4$Si) δ 7.56-7.54 (m, 2H), 7.34-7.33 (m, 3H), 4.62-4.60 (q, J = 6.0 Hz,

2H), 1.23-1.21 (d, J= 6.0 Hz, 12H). δC (101 MHz; CDCl$_3$; Me$_4$Si) δ 133.0 (C-Ar), 129.4 (C-Ar), 127.9 (C-Ar), 66.3 (CH$_3$CHO), 24.9 (CH$_3$). δB (128.28 MHz; CDCl$_3$ Me$_4$Si) δ 28 (s, br, Ph-B(OR)$_2$). v^{max}/cm^{-1} 3054 (Ar-CH stretch), 2971-2927 (CH stretch), 1599-1434 (C=C ring stretch), 1375 (B-O stretch), 1308 (B-O stretch), 1117 (C-O stretch) 948 (B-C stretch) 699-651 (aromatic CH bend), 651 (B-O bend - wag).

2.3.1.4 Bis(butyl)phenylboronate (1d)
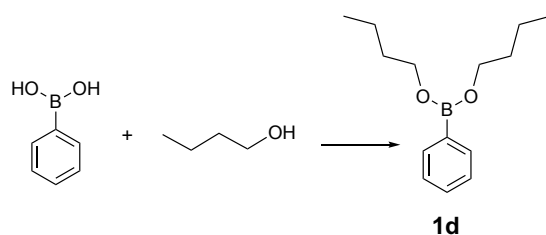
A mixture of phenylboronic acid (46.7 g, 0.334 mol) and butanol (98.93 g, 1.335 mol, 4 equivs) was stirred at 110 °C using Dean-Stark apparatus under nitrogen for 4 hours then left to stir at room temperature for 18 hours under nitrogen. The crude product was evaporated under reduced pressure affording a straw liquid (yield = 92%, Purity 98%). δH (400 MHz; CDCl$_3$; Me$_4$Si) δ 7.66 (d, J = 7.3 Hz, 2H), 7.46-7.38 (m, 3H), 4.07 (t, J = 6.4 Hz, 4H), 1.69-1.62 (quin, 4H), 1.46 (sext, J = 14.9, 7.3 Hz, 4H), 0.98 (t, J = 7.6 Hz, 6H). δC (101 MHz; CDCl$_3$; Me$_4$Si) δ 133.4 (C-Ar), 129.5 (C-Ar), 127.7 (C-Ar), 64.4 (CH$_2$-O), 34.0 (CH$_2$), 19.0 (CH$_2$), 14.0 (CH$_3$). δB (128.28 MHz; CDCl$_3$ Me$_4$Si) 28 (s, br, Ph-B(OR)$_2$). v^{max}/cm^{-1} 3054 (Ar-CH stretch) 2958-2873 (CH stretch), 1600 (C=C ring stretch), 1437 (CH$_2$ Bend – scissor), 1407 (CH$_3$ deformation), 1317 (B-O stretch), 1127 (C-O stretch), 1073 (B-C stretch), 1025-967 (C=C-H in plane bend), 758-699 (aromatic CH bend), 649 (B-O wag).

2.3.2 Model ligand Synthesis of Tertiary β-amino Diols

2.3.2.1 *N*-(Cyclohexylamino)-3-phenoxypropan-2-ol (2)[208]
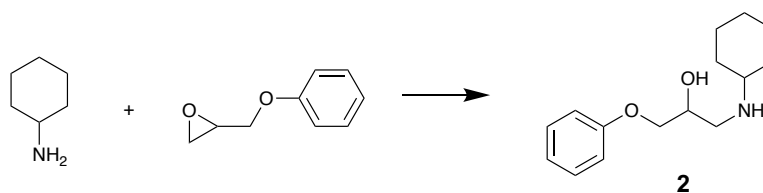
Cyclohexylamine (33.20 g, 0.335 moles, 5 equivs.) and phenylglycidyl ether (10.00 g, 0.067 moles, 1 equivs.) were combined in a round bottomed flask under an inert atmosphere of nitrogen gas with stirring. The reaction mixture was heated to 50 °C for a period of 4 hours before the excess cyclohexylamine was removed under reduced pressure using a rotary evaporator, resulting in the isolation of the crude product as a white solid (17.24 g). The crude product was recrystallized from toluene (25 mL) to produce a pure white solid (14.236 g, 85.9%, mp = 105 °C). δ_H (400 MHz; CDCl$_3$; Me$_4$Si) δ 7.25-7.30 (m, 2H, CH-Ar), 6.93 (dd, J = 18.1, 7.6 Hz, 3H, CH-Ar), 3.95-4.01 (m, 3H, CH$_2$CH-OH), 2.90-2.93 (m, 1H, CH$_2$-NH), 2.74 (dd, J = 11.9, 7.3 Hz, 1H, CH$_2$-NH), 2.42 (tt, J = 10.3, 3.7 Hz, 1H, CH-N-cyclohexyl), 1.90 (d, J = 12.4 Hz, 2H, CH$_2$-cyclohexyl), 1.72 (q, J = 4.3 Hz, 2H, CH$_2$-cyclohexyl), 1.58-1.62 (m, 1H, CH$_2$-cyclohexyl), 1.00-1.31 (m, 5H, CH$_2$-cyclohexyl). δ_C (101 MHz; CDCl$_3$; Me$_4$Si) δ 158.7 (C-Ar), 129.5 (CH-Ar), 120.9 (CH-Ar), 114.5 (CH-Ar), 70.4 (CH$_2$-O), 68.4 (CH-OH), 56.7 (CH-NH), 48.8 (CH$_2$-NH), 34.0 (CH$_2$), 26.1 (CH$_2$), 25.0 (CH$_2$). v^{max}/cm^{-1} 3275 (N-H stretch, 2° -amine), 3100 br. (O-H stretch, 2° alcohol), 3040 (C-H stretch, aromatic), 2928 and 2850 (C-H and C-H$_2$ stretch), 1597 and 1495 (C=C ring stretch, aromatic), 1458 (N-H bend, 2° amine), 1244 (C-N stretch) 1033 (C-O stretch). *m/z* 250.2164 (MH$^+$, 100% calc. for C$_{15}$H$_{24}$NO$_2$ = 250.1806).

2.3.2.2 N,N-bis(2-hydroxy-3-phenoxy-propyl)-cyclohexanamine (β-amino diol (3))[208]

3
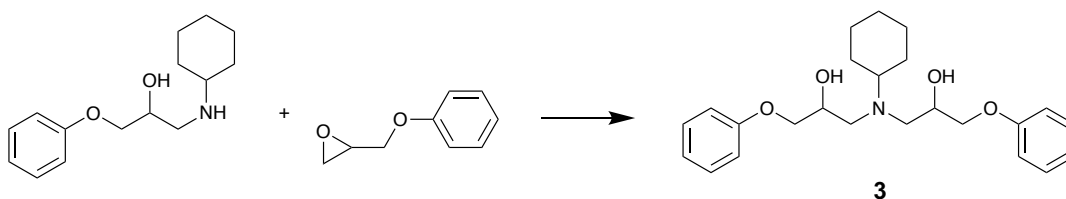
1-(cyclohexylamino)-3-phenoxypropan-2-ol (8.124 g, 0.032 mol, 1 equiv) and phenylglycidyl ether (5.137 g, 0.033 moles, 1.05 equivs.) were combined in a round bottomed flask under an inert atmosphere of nitrogen gas with stirring. The reaction mixture was heated to 90 °C for 1 hour, followed by a further 4 hours at 100 °C before allowing to cool overnight producing the product as a pale-yellow viscous liquid which was used without further purification (8.95 g, 0.022 mol, 67%). δH (400 MHz; CDCl$_3$; Me$_4$Si) δ 7.27 (t, J = 7.6 Hz, 4H), 6.90-6.97 (m, 6H), 3.95-4.05 (m, 6H), 3.50 (br.s, 2H), 2.82 (dt, J = 22.90, 9.16 Hz, 2H), 2.66 (ddd, J = 28.5, 13.6, 8.6 Hz, 2H), 2.47-2.53 (m, 1H), 1.72-1.88 (m, 4H), 1.62 (d, J = 11.9 Hz, 1H), 1.04-1.39 (m, 5H). δC(101 MHz; CDCl$_3$; Me$_4$Si) δ 158.7 (C-Ar), 129.6 (CH-Ar), 121.1 (CH- Ar), 121.1 (CH- Ar), 114.6 (CH-Ar) , 70.2 (CH$_2$-O), 70.2 (CH$_2$-O), 68.6 (CH-OH), 68.0 (CH-OH), 61.6 (CH-N), 61.4 (CH-N), 54.6 (CH$_2$-N), 54.0 (CH$_2$-N), 30.6 (CH$_2$), 29.2 (CH$_2$), 27.8 (CH$_2$), 26.2 (CH$_2$), 26.2 (CH$_2$). v^{max}/cm^{-1} 3589 (Free OH-stretch), 3311 (br. OH stretch), 3040 (CH stretch Aromatic), 2930-2836 (CH$_2$, CH stretch), 1600-1495 (C=C ring stretch Aromatic), 1242 (C-N stretch) 1086 (C-O stretch), 751-687 (CH bend mono substituted Aromatic). *m/z* 400.3061 (MH$^+$, 100% calc. for C$_{24}$H$_{34}$NO$_4$ = 400.2488)

2.3.2.3 Model Reaction 1
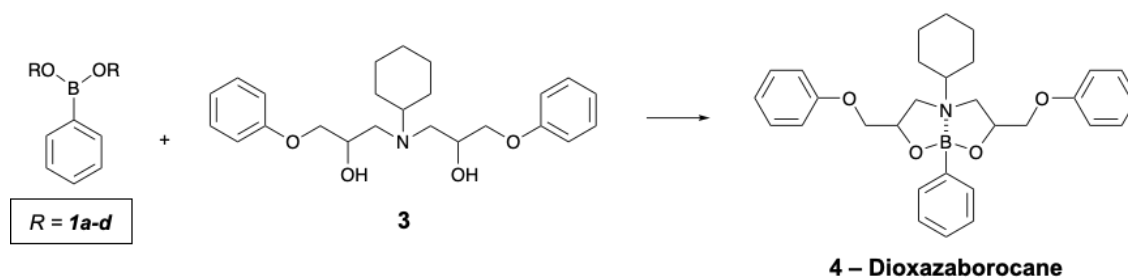
The method for the reaction of β-amino diol **1** with monoboronic ester (**1a**-**1d**) was as follows. A stock solution of β-amino diol **3** in deuterated chloroform was prepared (0.4 M). The β-amino diol **3** stock solution (5 mL, 0.4 M, 0.002 mol) and an equal molar equivalent (0.002 mol) of the selected monoboronic ester (**1a**-**1d**) were mixed and analysed by ^{1}H-NMR at a predetermined time period. The ratio of unreacted boronic ester (**1a**-**1d**) to model dioxazaborocane product **4** was determined by integration of aromatic signals of boronic ester (**H$_{(1)}$**, **1a**-**1d** - Figure 104), at 7.81 ppm for cyclic esters or 7.54-7.60 ppm for linear esters, to the more electron rich aromatic signals of dioxazaborocane **4** at 7.7 ppm (**H$_{(2)}$** - Figure 106).

2.3.2.4 Model reaction 2
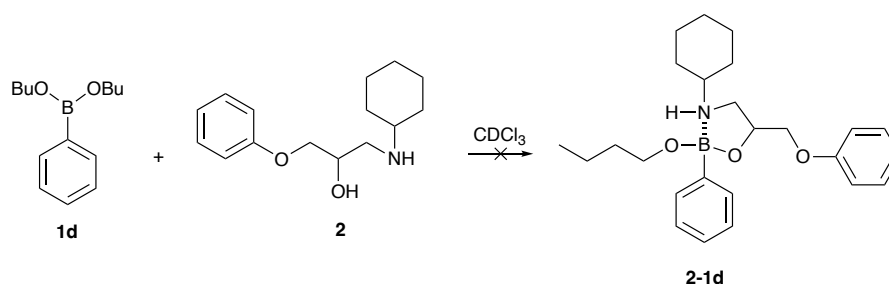
The method for the reaction of β-aminol **2** with monoboronic ester (**1d**) was as follows. **2** (1.02 g, 0.004 mol, 1 equiv.) was dissolved in 6 mL of CDCl$_3$ (0.682 mol L^{-1}). **1d** (0.96 g, 0.004 mol, 1 equiv.) was added to the solution and stirred for 10 minutes before

decanting a sample for 1H NMR. The reaction did not produce a clear spectra and was unsuccessful.

2.3.2.5 Model reaction 3
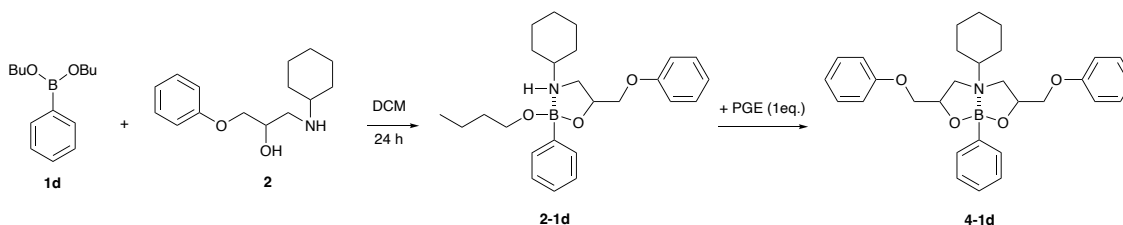
The method for the reaction of β-aminol **2** with monoboronic ester (**1d**) and subsequent reaction with PGE to form the dioxazaborocane **4-1d** was as follows. For step 1, **2** (0.510 g, 0.002 mol, 1 equiv.) was dissolved in 5 mL DCM then **1d** (0.478 g, 0.002 mol, 1 equiv.) was added to the solution and stirred for 1 hour at 40 °C. The solution was then subjected to reduced pressure at 50 °C in a vacuum oven for 18 hours, to remove solvent, prior to ^{1}H NMR and step 2. For step 2, the phenyl glycidyl ether – PGE (0.307 g, 0.002 mol^{-1}, 1 equiv.) was mixed with 5 mL DCM then added to the reaction vessel of step 1 and stirred at room temperature for 16 hours. The solution was subjected to reduced pressure at 50 °C for 5 ours, by a rotary evaporator, affording a white solid. The product was dried in a vacuum oven, under reduced pressure, at 50 °C for a further 18 hours, affording a white solid.

2.3.3 Diboronic Esters

2.3.3.1 1,4-Phenylenediboronic bis(1,2-diol) Ester (5)[187]
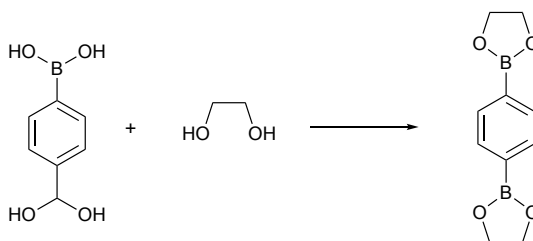
1,4-phenylenediboronic acid (10.0 g, 0.060 mol) was suspended in toluene (250 mL) and ethylene glycol (11.2 g, 0.180 mol, 3 equivs.) then was refluxed for 3 hours under nitrogen and water removed by azeotropic distillation using Dean-Stark apparatus. Solvent was then removed under reduced pressure affording the crude product as a white solid. The crude product was recrystalised from toluene and washed in cold toluene before drying in a vacuum oven at 100 °C for 30 minutes. The product was isolated as a white solid (yield = 10.95 g, 84%, Mpt = 238 °C). δH (400 MHz; CDCl$_3$; Me$_4$Si) δ 7.82 (s, 4H, CH-Ar) 4.39 (s, 8H, CH$_2$). δC (101 MHz; CDCl$_3$; Me$_4$Si) δ 134.2 (C-Ar), 66.2 (CH$_2$-O). δB (128.28 MHz; CDCl$_3$ Me$_4$Si) δ 29 (s, br, Ph-B(OR)$_2$). v^{max}/cm^{-1} 3033 (Ar-CH stretch), 2982-2908 (CH stretch), 1519-1478 (C=C ring stretch), 1406-1327 (B-O stretch), 1212-1104 (C-O stretch), 986 (B-C stretch), 842 (para-aromatic CH bend), 645 (B-O bend - wag).

2.3.3.2 1,4-Phenylenediboronic Acid Tetrabutyl Ester (6)
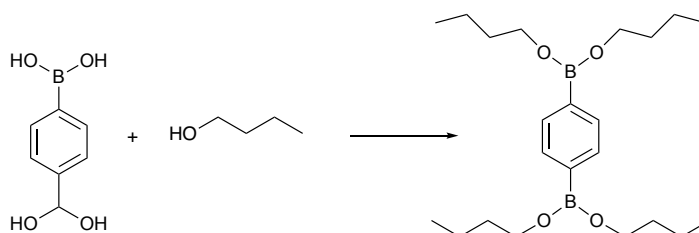
1,4-phenylenediboronic acid (3.00 g, 0.018 mol) and excess n-butanol (170 g, 2.29 mol, 127 equivs) were combined in a round bottom flask and stirred at room temperature for 24 hours under nitrogen. The reaction mixture was then evaporated slowly under reduced pressure at 40 °C affording the product as a colourless liquid, which was used without further purification (yield = 76%, Purity 98%). δH (400 MHz; CDCl$_3$; Me$_4$Si) 7.58 (s, 4H), 4.00 (t, J = 6.4 Hz, 8H), 1.55-1.62 (p, J = 7.3 Hz, 8H), 1.40 (sx, J = 7.3Hz, 8H), 0.92 (t, J = 7.3 Hz, 12H). δC (101 MHz; CDCl$_3$; Me$_4$Si) 14.1 (CH$_3$), 19.1 (CH$_2$), 34.0 (CH$_2$), 64.3 (CH$_2$-O), 132.5 (C-Ar), 134.8 (br. C-Ar). δB (128.28 MHz; CDCl$_3$ Me$_4$Si) δ 30 (s, br, Ph-B(OR)$_2$). v^{max}/cm^{-1} 3064 (Ar-CH stretch), 2955-2874 (CH stretch), 1508-1464 (C=C ring stretch), 1410-1308 (B-O stretch), 1117 (C-O stretch), 1067-1023 (B-C stretch), 825 (para-aromatic CH bend), 659 (B-O bend - wag).

2.3.3.3 1,4-Phenylenediboronic Acid Pinacol Ester (7)
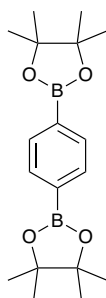
1,4-phenylene diboronic acid dipinacol ester was purchased from Fluorochem and used as received. δH (400 MHz; CDCl$_3$; Me$_4$Si) δ 7.80 (s, 4H, CH-Ar) 1.35 (s, 12H, 4 x CH$_3$). δC (101 MHz; CDCl$_3$; Me$_4$Si) δ 134.0 (C-Ar), 84.0 (C-O), 25.0 (CH$_3$). δB (128.28 MHz;

CDCl$_3$ Me$_4$Si) δ 29 (s, br, Ph-B(OR)$_2$). ν^{max}/cm^{-1} 2983-2930 (CH stretch), 1519 (C=C ring

stretch), 1340 (B-O stretch), 1139-1096 (C-O stretch).

2.3.4 Network Polymer Development

2.3.4.1 Aromatic Epoxy Polymers

2.3.4.1.1 CHA/HA-based DER332 Epoxy Linear Control Polymers and Polymer Networks (CHA-E1 and HA-E1)
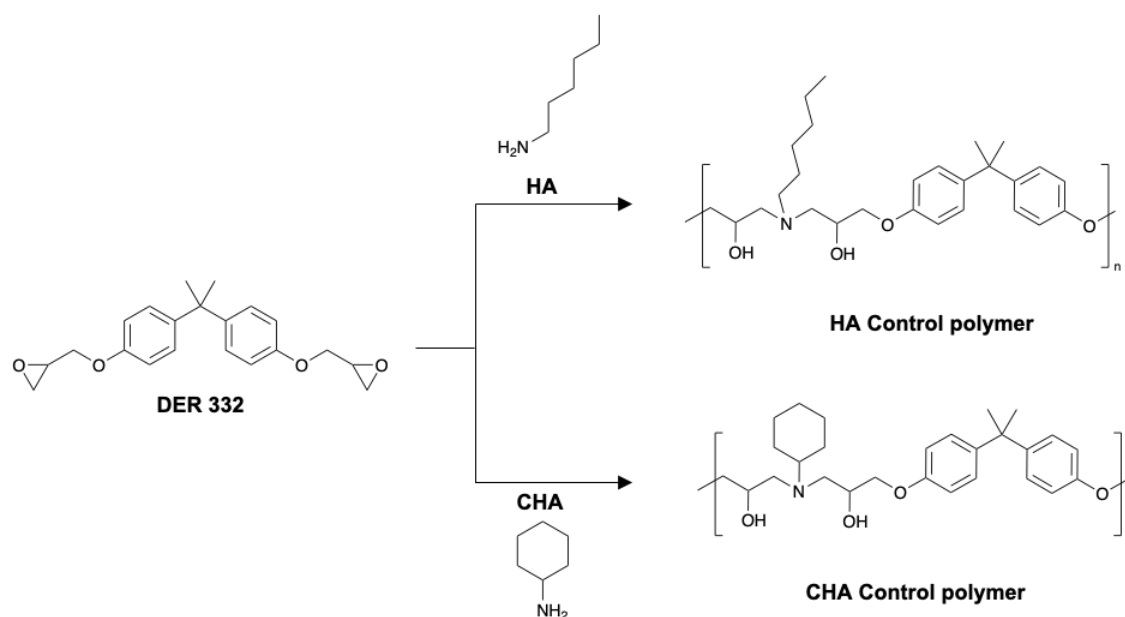
Figure 93: Routes to polymers in this work using BPA based epoxy resin DER 332.

The polymers in Figure 93 were prepared according to the following general methods:

Control polymers contained a monofunctional amine (cyclohexylamine or hexylamine, 0.003 mol) and epoxy resin (DER332, 1.02 g, 0.003 mol) in 1:1 equivalent moles to form the linear polymer. DMP-30 (tertiary amine catalyst, 1 wt%) was added to some samples to catalyse the epoxy amine reaction. The synthetic procedure was to stir all the desired monomers and catalyst in a vial until homogenous and then drawn-down onto glass microscope slides with a 400 μm draw-down bar to control film thickness. Films were

subjected to three curing schedules: A) room temperature for 24 hours, B) room temperature for 24 hours then 80 °C, or C) 80 °C immediately after drawn down.

Dynamic polymers were prepared as above with the inclusion of diboronic ester **6** in the formulation (0.0015 moles for 100% crosslinking in theory), varying amount dependant on the desired amount of crosslinking.
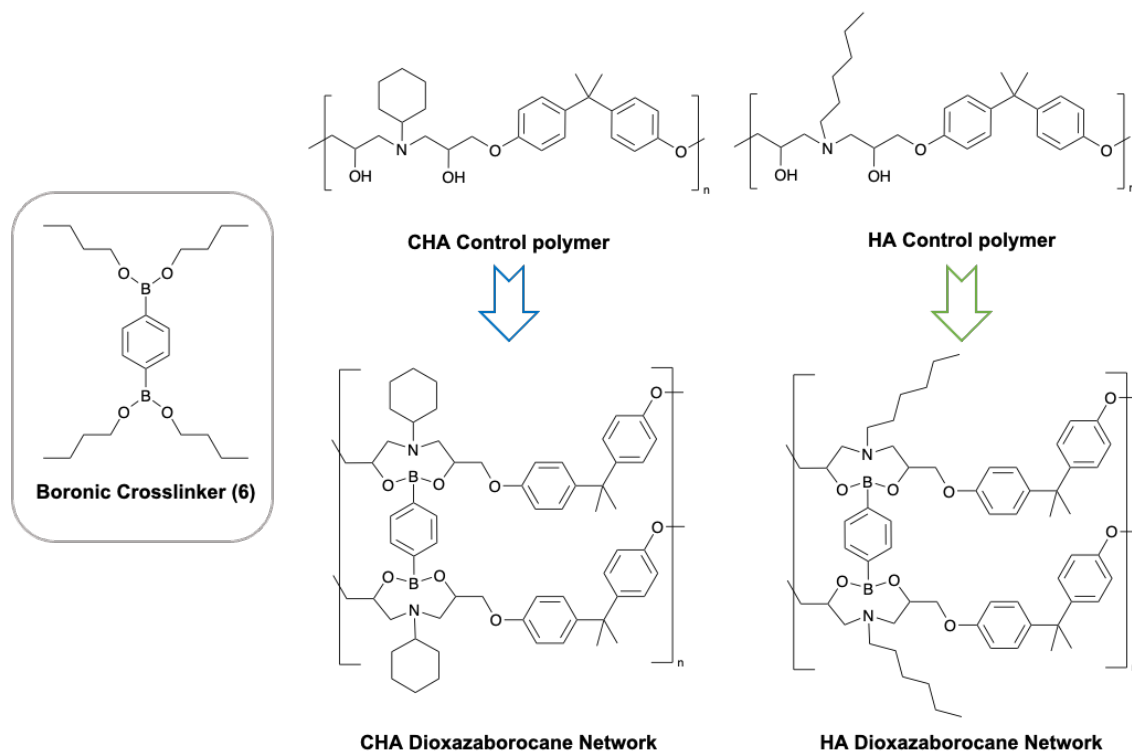
Figure 94: Routes to crosslinking in DER polymers in this work.

Table 5: Formulations for DER 332 polymers in this work.

Monomer	CHA	HA	CHA	HA
	Mass / g		Moles / mol	
CHA / HA	0.2987	0.2973	0.0030	0.0029
DER 332	1.0250	1.0000	0.0030	0.0029
Diboronic ester (6)	0.5876	0.5733	0.0015	0.00147
DMP-30 catalyst (1 wt%)	0.0191	0.0187	-	-

2.3.4.1.2 End capped HA-based DER332 epoxy polymer networks (HA-E1(DEA-5))

The linear control polymer was prepared according to the following procedures:
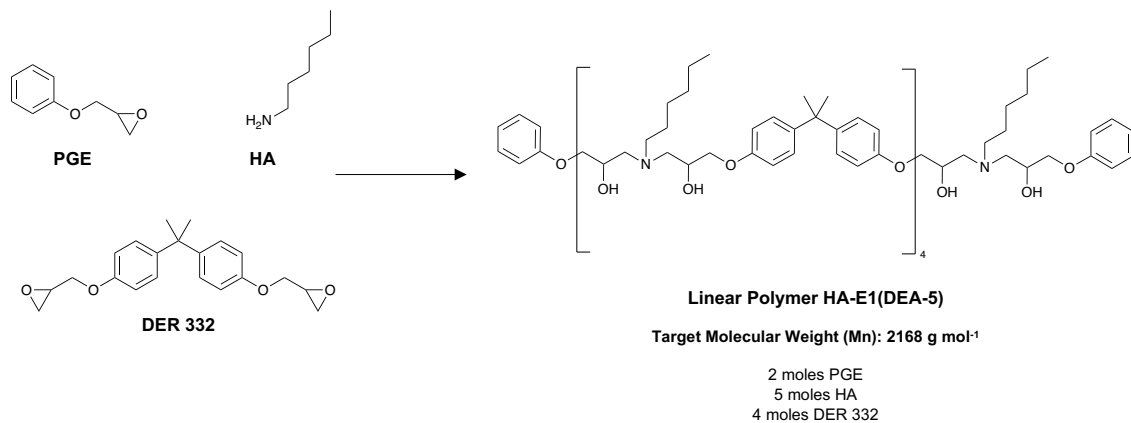
Figure 95: Route to linear polymer backbone of end-capped polymers in this work

The control aromatic epoxy-amine polymer structure that contains 5 DEA functionalities (HA-E1(DEA-5)), represented above, was prepared by mixing DER 332 (2.00 g, 0.0058 moles), phenyl glycidyl ether (0.44 g, 0.0029 moles) were combined in a glass vial with stirring. To the reaction mixture, n-hexylamine (HA) (0.74g, 0.0073 moles) was added and stirred until homogenous before being drawn-down onto a glass microscope slide with a 400 μm draw-down bar to control film thickness. The resulting film was allowed to cure at room temperature for 24 hours, followed by a thermal post cure at 80 °C.
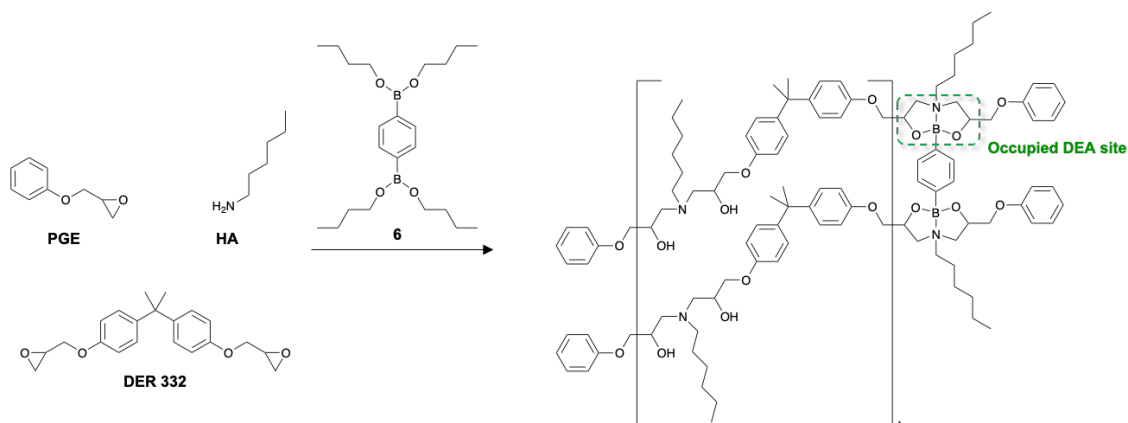
Figure 96: Route of crosslinking in BPA based polymers in this work.

Dynamic polymers were prepared via the same method as the control polymer above but with the inclusion of diboronic ester **6** in the formulation (0.72 g, 0.0018 moles - for 50% stoichiometric occupation of DEA functional functionalities).

2.3.4.2 Linear Epoxy Modified HA Network Polymers.

The polymers were prepared according to the following methods:

The preparation for all polymers and crosslinked (thermoset) polymeric materials was conducted by a simple one pot synthesis. Linear polymers were formulated to have a number average functionality of 5 amino-diol groups and a series of 0-100 mol% crosslinked thermoset (per moles of amino diol) polymers were prepared with either butyl diboronic ester **6** (dioxazaborocane crosslinked D-series) or diamine crosslinker, selected from either 1,6-hexandiamine or 4,4'-diaminodicyclohexylmethane (4,4'-MDH) (amine control materials = A series).

Dioxazaborocane crosslinked D-series polymers (D0-D100) were prepared according to the procedure below:

1,4-butanediol glycidyl ether (BGE, 4.00 g, 0.020 moles), phenyl glycidyl ether (PGE, 1.49 g, 0.010 moles) and n-hexylamine (HA, 2.50 g, 0.025 moles) were combined in a round bottom flask under nitrogen with stirring. To the reaction mixture the appropriate mass of 1,4-phenylenediboronic acid tetrabutyl ester (**6**) was added according to Table 6. The reaction mixture was stirred at 55 °C for 1 hour and 45 minutes under nitrogen whilst viscosity slowly increased, before drawing down onto a non-stick PTFE sheet using a 400 μm draw-down bar to control film thickness. The resulting films were allowed to cure at room temperature for 16 hours under nitrogen, followed by a post cure schedule ramp at 80 (1 hour), 120 (1 hour) then 170 °C (1 hour, total 3 hours thermal

cure). After cooling to room temperature, the resulting polymeric films were removed from the PTFE sheet to give dioxazaborocane crosslinked epoxy-amine polymers (D0-D100) or viscous liquid films (D0-D40).

Table 6: Dioxazaborocane polymers (D0-D100 series) where the desired crosslinking percentage comes from calculation of the percentage from the total equivalent amine moles in the formulation.

Crosslinker stoichiometry (mol%)	Dibutyl boronic ester content (g, mol)
100	4.82, 0.012
80	3.86, 0.010
60	2.89, 0.007
40	1.92, 0.005
20	0.96, 0.002
0	0.0, 0.0

Epoxy-amine control materials, A series (A20-A100) were prepared according to the procedure below.

1,4-butanediol glycidyl ether (4.00 g, 0.020 moles), phenyl glycidyl ether (1.49 g, 0.010 moles) were combined in a round bottom flask under nitrogen with stirring. To the reaction mixture, the appropriate mass of n-hexylamine (HA) and 1,6-hexanediamine was added according to Table 7 (below). The reaction mixture was stirred at 55°C for 1 hour and 45 minutes under nitrogen whilst viscosity slowly increased, before drawing down onto a non-stick PTFE sheet using a 400 μm draw-down bar to control film thickness. The resulting film was allowed to cure at room temperature for 16 hours under nitrogen, followed by a post cure schedule ramp at 80 (1 hour), 120 (1 hour) then 170 °C (1 hour, total 3 hours thermal cure). After cooling to room temperature, the resulting

polymeric films were removed from the PTFE sheet to give solid sheets of epoxy-amine polymer (A60-A100) or viscous liquid films (A0-A40).

Table 7: Epoxy-amine polymers (A0-100 series) where the desired crosslinking percentage comes from the calculation of the percentage from the total equivalent epoxy moles in the formulation and the remaining non-crosslinking amine content arises from the difference of the total epoxy moles less the crosslinking equivalent moles.

	Amine Crosslinker	**Non-crosslinking amine**
Crosslinking / mol%	1,6-hexane diamine content (g, mol)	n-Hexylamine Content (g, mol)
100	1.44, 0.012	0.00, 0.000
80	1.15, 0.010	0.50, 0.005
60	0.86, 0.007	1.00, 0.010
40	0.57, 0.005	1.50, 0.015
20	0.29, 0.002	2.00, 0.021
0	-	2.50, 0.025

All A^2 series polymers ($A^2$20-$A^2$100) were prepared according to the procedure below. 1,4-butanediol glycidyl ether (BGE, 4.00 g, 0.020 moles), phenyl glycidyl ether (PGE, 1.49 g, 0.010 moles) were combined in a round bottoms flask under nitrogen with stirring. To the reaction mixture, the appropriate mass of n-hexylamine (HA) and 4,4'-MDH was added according to Table 8 (below). The reaction mixture was stirred at 55 °C for 1 hour and 45 minutes under nitrogen whilst viscosity slowly increase, before drawing down onto a non-stick PTFE sheet using a 400 µm draw-down bar to control film thickness. The resulting film was allowed to cure at room temperature for 16 hours under nitrogen, followed by a post cure schedule ramp at 80 (1 hour), 120 (1 hour) then 170 °C (1 hour, total 3 hours thermal cure). After cooling to room temperature, the resulting polymeric

films were removed from the PTFE sheet to give sheets of epoxy-amine polymer (A60-A100) or viscous liquid films (A0-A40).

Table 8: Epoxy- amine polymer ($A^2$0-100 series) crosslinking content where the desired crosslinking percentage comes from the calculation of the percentage from the total equivalent epoxy moles in the formulation and the remaining non-crosslinking amine content arises from the difference of the total epoxy moles less the crosslinking equivalent moles.

	Amine Crosslinker	**Non-crosslinking amine**
Crosslinking / mol%	4,4'-MDH Content (g, mol)	n-Hexylamine Content (g, mol)
100	2.60, 0.012	0.00, 0.000
80	2.08, 0.010	0.50, 0.005
60	1.56, 0.007	1.00, 0.010
40	0.57, 0.005	1.50, 0.015
20	0.29, 0.002	2.00, 0.021
0	-	2.50, 0.025

All A^3 series polymers ($A^3$20-$A^3$100) were prepared according to the procedure below. Bisphenol A epoxy resin (DGBE, 4.00 g, 0.012 moles), phenyl glycidyl ether (PGE, 0.88 g, 0.006 moles) were combined in a round bottom flask under nitrogen with stirring. To the reaction mixture the appropriate mass of cyclohexylamine (CHA) and 4,4'-MDH was added according to Table 9 (below). The reaction mixture was stirred at 55 °C for 45 minutes under nitrogen whilst viscosity slowly increase, before drawing down onto a non-stick PTFE sheet using a 400 um draw-down bar to control film thickness. The resulting film was allowed to cure at room temperature for 16 hours under nitrogen, followed by a post cure schedule ramp at 80 (1 hour), 120 (1 hour) then 170 °C (1 hour, total 3 hours thermal cure). After cooling to room temperature, the resulting polymeric films were removed from the PTFE sheet to give sheets of epoxy-amine polymer ($A^3$60-$A^3$100).

Table 9: Epoxy-amine polymer (A^320-100 series) crosslinking content where the desired crosslinking percentage comes from the calculation of the percentage from the total equivalent epoxy moles in the formulation and the remaining non-crosslinking amine content arises from the difference of the total epoxy moles less the crosslinking equivalent moles.

	Amine Crosslinker	**Non-crosslinking amine**
Crosslinking / mol%	4,4'-MDH Content (g, mol)	Cyclohexylamine Content (g, mol)
100	1.55, 0.007	0.00, 0.000
80	1.23, 0.006	0.29, 0.003
60	0.93, 0.004	0.58, 0.006

Representative structure of linear (non-crosslinked) epoxy-amine polymer (D0) is shown below.
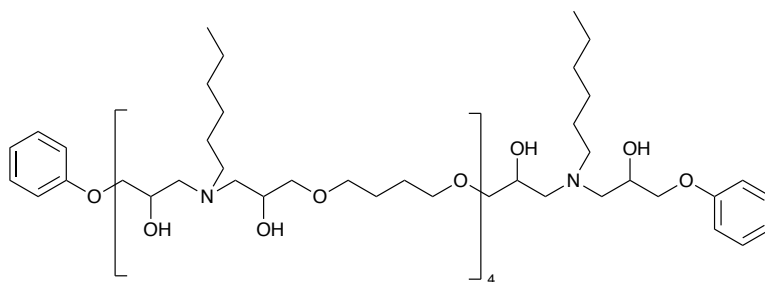
Figure 97: Representative structure of linear low T_g polymers used throughout this work with a target number average molecular weight (Mn) = 1615.32 g mol^{-1}.

The representative structures of epoxy-amine-dioxazaborocane polymers (D20-D100) are shown below, where degree of occupied vs unoccupied crosslinking sites depends on the mole% of 1,4-phenylenediboronic acid tetrabutyl ester (**6**) according to Table 6.
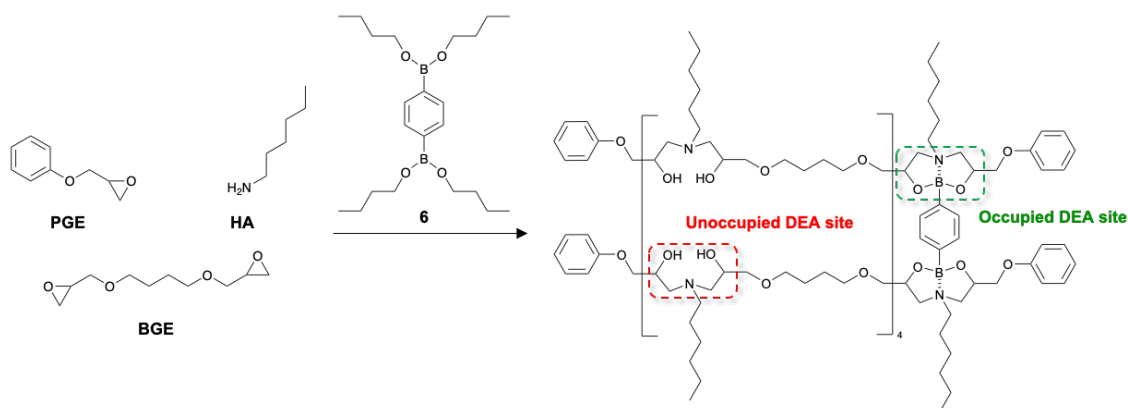
Figure 98: Route to dynamic crosslinking in non-aromatic based polymers in this work.

Representative structures of A-series and A^2-series epoxy-amine (control, A20-A100 and $A^2$20-$A^2$100) network polymers, where degree of occupied vs unoccupied crosslinking sites depends on the mole% of 1,6-hexanediamine according to Table 7 and the mole% of 14,4'-MDH according to Table 8.
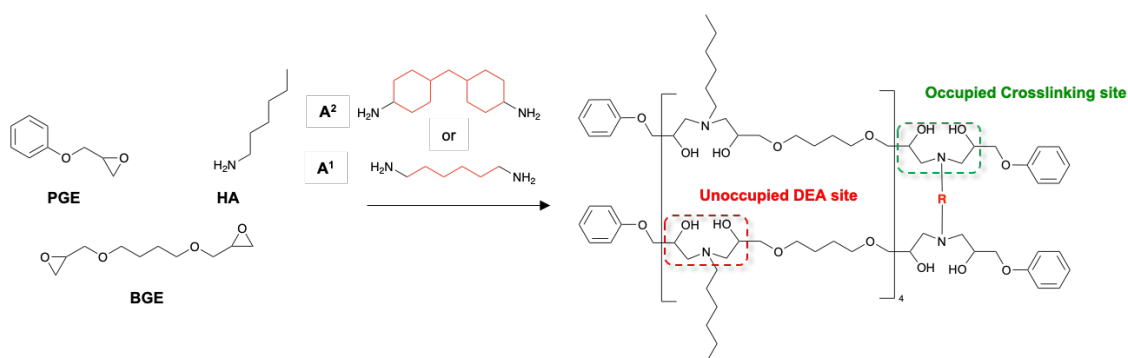
Figure 99: Route to traditional amine crosslinking in non-aromatic based polymers in this work.

Representative structure of A^3-series epoxy-amine (control, A^{3}20-A^{3}100) network polymers, where degree of occupied vs unoccupied crosslinking sites depends on the mole% of 4,4'-MDH according to Table 9.
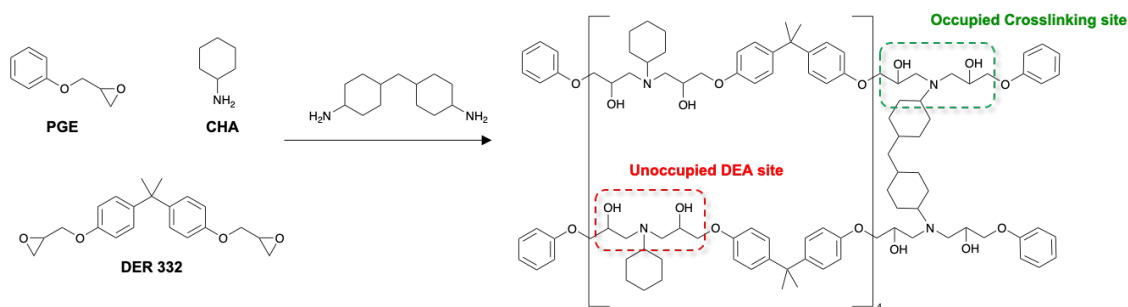
Figure 100: Route to traditional amine crosslinking in aromatic based polymers in this work.

2.3.4.3 Polymers Fabricated for Chapter 7

The formulation of the D0/A^2 linear polymers were adapted to reduce PGE gradually according to Table 10 below based on the molar ratio of 1,4-butyl diglycidyl ether (BGE) to mono-functional phenyl glycidyl ether (PGE), which equals the total sum of n-hexylamine in the polymer (i.e. 2.50 g , 0.0494 equivalent moles of mono-functional amine would require the stoichiometry of epoxy monomers below).

Table 10: ratios of PGE moles to BGE moles in the linear polymer backbones investigated in Chapter 7.

PGE content / % of D0/A2	Moles of di-functional epoxy (BGE) / mol%	Moles of mono-functional epoxy (PGE) / mol%	Mass epoxy / g (BGE,PGE)	Equivalent Moles epoxy / mol (BGE,PGE)
100 (*Avg* DEA-5 chain length)	80	20	4.00, 1.49	0.0396, 0.0099
50%	90	10	4.49, 0.74	0.0445, 0.0049
25%	95	5	4.75, 0.37	0.0469, 0.0025
12.5	97.5	2.5	4.87, 0.19	0.0482, 0.0012
0	100	0	4.99, 0.00	0.0494, 0.0000

Shown on the next page in Figure 101 are representative structures of the 'traditional' and 'dynamic dioxazaborocane' - 0% PGE content - network polymers with 80% crosslink density. (HA-E1(DEA-infinite)A[4]-80 and HA-E1(DEA-infinite)D-80), where degree of occupied vs unoccupied crosslinking sites depends on the 20:80 mol% stoichiometry of 4,4'-MDH compared to n-hexylamine in the control formulation. (i.e. 20% of 0.0494 equivalent moles of epoxy) in the diamine crosslinked system and where the stoichiometry of boronic ester is 80% of the mono-functional amine content, which makes up the full amine content in D-series materials.
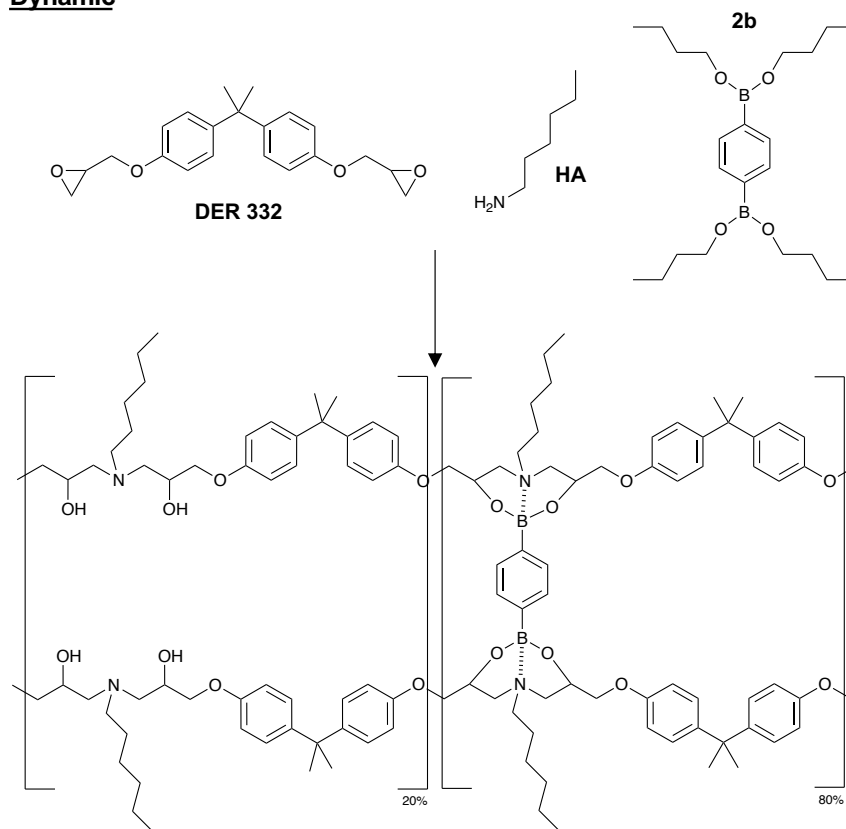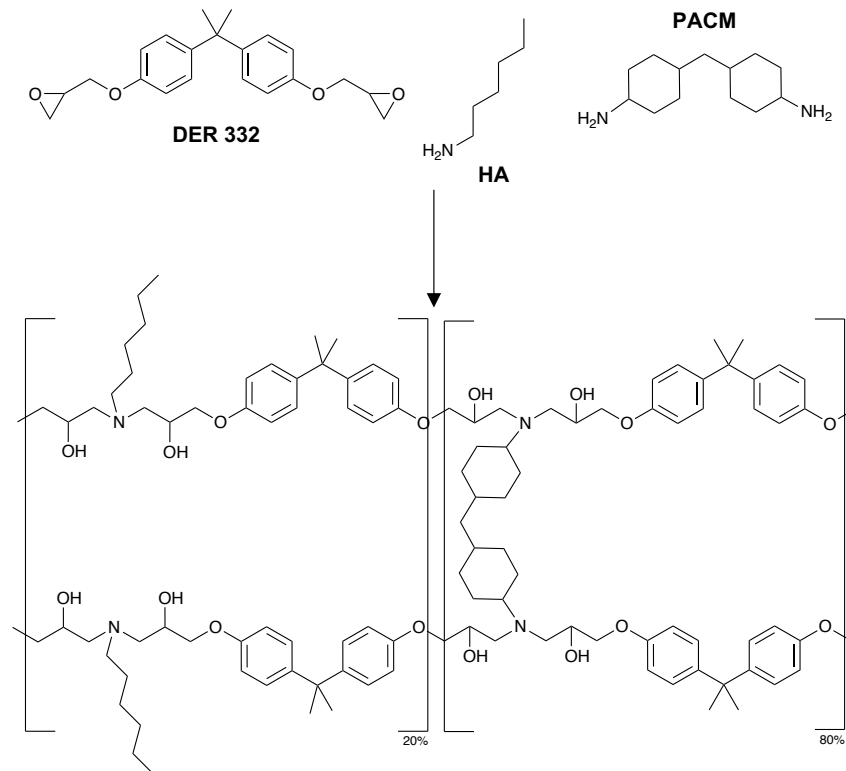
Figure 101: Infinite chain networks (HA-E1(DEA-infinite)A⁴-80 (traditional)) and HA-E1(DEA-infinite)D-80)(dynamic) used in this work.

2.3.4.4 Recycling

2.3.4.4.1 Mechanical Recycling

Mechanical recycling of D80 polymer where steps a-d are as follows: a) broken virgin D80 material is added to the mould and pressed at 170 °C for 30 mins then annealed overnight, b) recycled polymer is removed from the mould as a new polymer sheet, c) recycled sheet can be cut to dimensions for mechanical testing and d) broken recycled polymer can be reprocessed again.
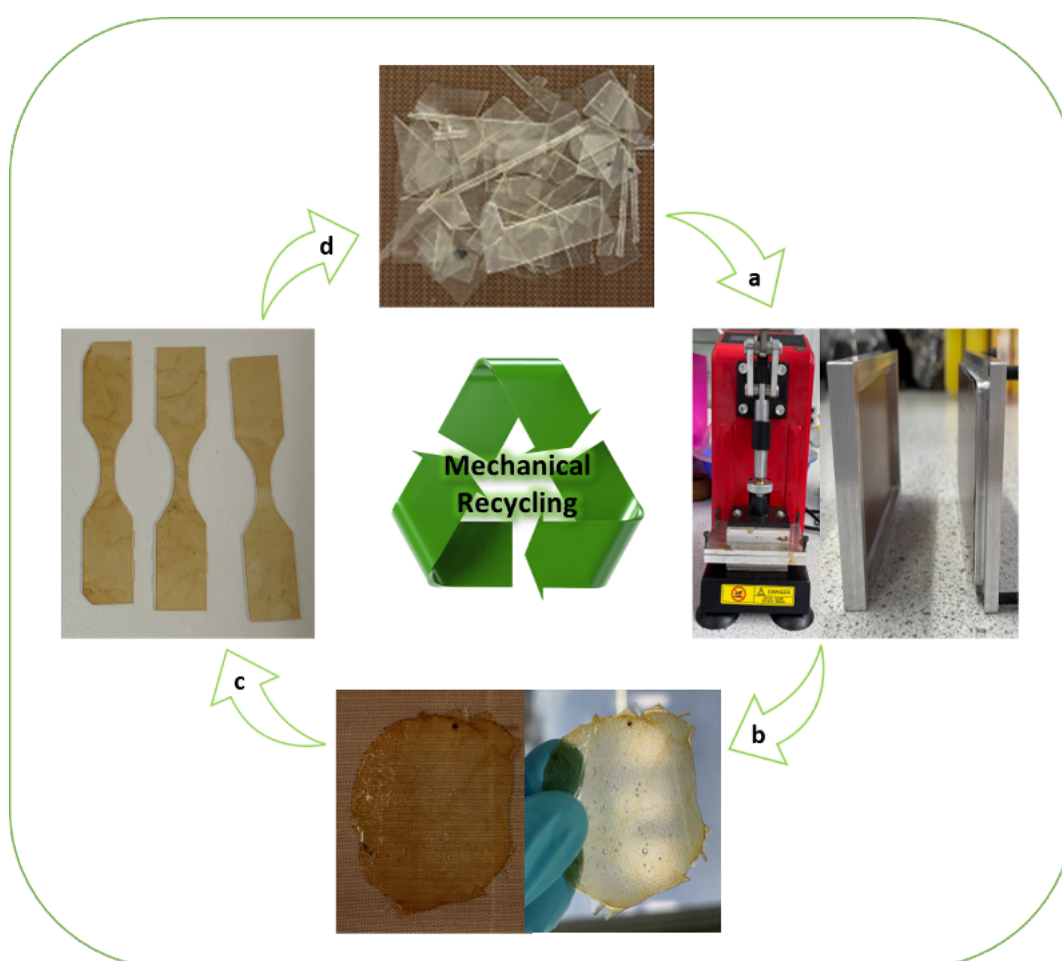
2.3.4.4.2 Chemical Recycling

GPC samples for analysis of chemically recycled (disassembled) network polymers were prepared as follows. A sample of D100 (0.1 g) was immersed in THF (10 mL) and treated with either bis(butyl)phenylboronate, 0.2257 g, 0.000964 mol, 5 equiv. based on

calculated moles of dioxazaborocane groups in D100) or pinacol (0.1139 g, 0.000964 mol, 5 equiv. based on calculated moles of dioxazaborocane groups in D100). The solutions were held for 5 days at room temperature to promote dissolution. The samples were then diluted to a concentration of 2 mg/mL (based on original D100 mass), filtered through a 0.2 µm nylon filter and analysed by GPC.

Chapter 3

Model Reactions

---

3 Chapter 3 - Model Reactions

3.1 Introduction

As introduced in Chapter 1, epoxy-based network polymers are the main polymeric component in several high-performance applications, including in wind turbine production, aerospace composites and high-performance coatings and adhesives. During the reaction where epoxy resins are cured by amines, the reagents transition from the liquid state to a hard, glassy thermoset polymer network, which cannot typically be reprocessed or remoulded. Therefore, it is favourable for the network formation to be completed in the formed shape intended for use, through moulding techniques, prior to network formation. A single-stage process is an attractive attribute for industrially scaled processes. As discussed in Chapter 1, carbon-fibre polymer composites are commonly employed for high-performance uses, due to the increased mechanical properties delivered by the carbon fibre, for the demanding requirements the application must sustain throughout its service. Such applications are typically manufactured via manual lay-up or resin infusion processes. For example, wind turbine blades are typically formed by resin infusion. Overall requirements of the reaction for practicality in infusion processes is that curing is delayed or is thermally triggered, to allow time for the polymer resin to infuse through the mould, into the required shape before the networking forming reaction results in vitrification or gelation.

Also discussed in Chapter 1, was the exploitation of the diethanolamine (DEA) functionality, produced by the epoxy-amine reaction, by Unthank et al.[206–208] and Otsuka et al.[210,211]. They demonstrated that the DEA functionality was reactive towards boronic acids or esters, producing dioxazaborocane functional groups, and hence, this provides an opportunity to cross-link epoxy-amines reversibly. This would present an important prospect to recycle network polymers though removal or exchange of cross-linking groups in the thermoset material, which could represent a significant contribution to

136

sustainable plastics, vital to mitigate environment concerns in the current climate. Unthank et al. showed that the boronic ester was selective towards the DEA functionality, under mild conditions typically employed during an epoxy-amine curing reaction.[208] Under the various conditions, they observed no reaction of the boronic ester with either epoxy or amine, or any evidence of complexation with the initial β-amino alcohol produced by the epoxy and the primary amine reaction. Thus, presenting a clear opportunity for the design of a highly desirable, latent cure mechanism in epoxy-amine stepwise network polymerisations. Otsuka et al. demonstrated a crosslinking reaction between diboronic acid and epoxy amine polymers, which displayed an obvious gelation.[210] However, this was a post-cure modification to an already formed epoxy-amine polymer, which would be impractical in currently employed industrial coating, composite or adhesive application processes.

Herein, it is envisioned that a latent cure mechanism combined with recyclability designed into the molecular structure of low-cost high-performing polymer networks will provide cheap, efficient and environmentally friendly materials, that can replace materials that are currently unrecyclable. It is hypothesised that the dioxazaborocane complex can provide a novel class of associative CAN polymers for a wide range of applications.
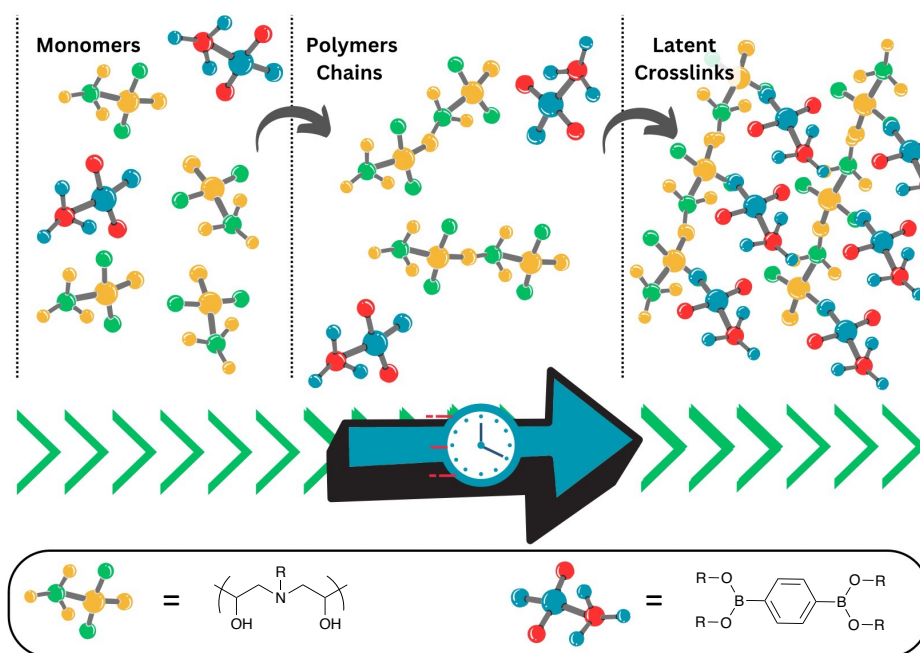
Figure 102: Visualisation of desired latent crosslinking.

3.2 Monoboronic Ester and Model Ligand Synthesis

In order to assess the latent cure mechanism, a model reaction was chosen to be the best representation to conventional reactions in traditional epoxy-amine thermosets. In particular DGEBA is a low-cost, high purity bisphenol A (BPA) based liquid epoxy resin, that is utilised in numerous high performing applications, due to the excellent mechanical properties the resultant networks possess. This is due in part to the structure of the aromatic phenyl groups and the presence of polar groups which all restrict rotation of the main polymer chains. The aromatic phenyl rings greatly restrict rotation, compared to their aliphatic analogues. In addition, epoxy-amines have various polar groups that can support hydrogen bonding and dipole-dipole interactions between polymer chains, which will also affect the free movement of polymer chains. This combined can allow the formation of strong glassy polymers with high T_g's and high tensile strength which are suitable for high-performance applications. The structure of the amine is also considered to affect the materials mechanical and thermal performance, as they add an additional

junction for branching, which is known to affect the packing of chains and thus, affect the non-covalent interactions between chains. Like the epoxy, the structure of the amine affects the properties of the polymer in a similar order: aliphatic < cycloaliphatic < aromatic, with regards to the T_g of the resultant polymer.

Considering the scope of the PhD project to develop new recyclable materials for high-performance applications, the model studies of the dioxazaborocane formation were designed to imitate a traditional aromatic epoxy-amine polymer structure that is to be utilised as the network polymer throughout this research project. Furthermore, it is well-known from the literature that the type of boronic ester can affect the stability of the transesterification equilibrium[203] and the rate of hydrolysis.[219,220] The stability of the boronic ester is controlled by: entropy, steric bulk, size of the heterocycle and chelation conformation.[219] Therefore, to attempt to control the degree of latency and rate of the crosslinking reaction, a series of mono-phenylboronic esters (**1a-d**) were synthesised (or purchased) to study the reaction with (**3**), shown in Figure 103.
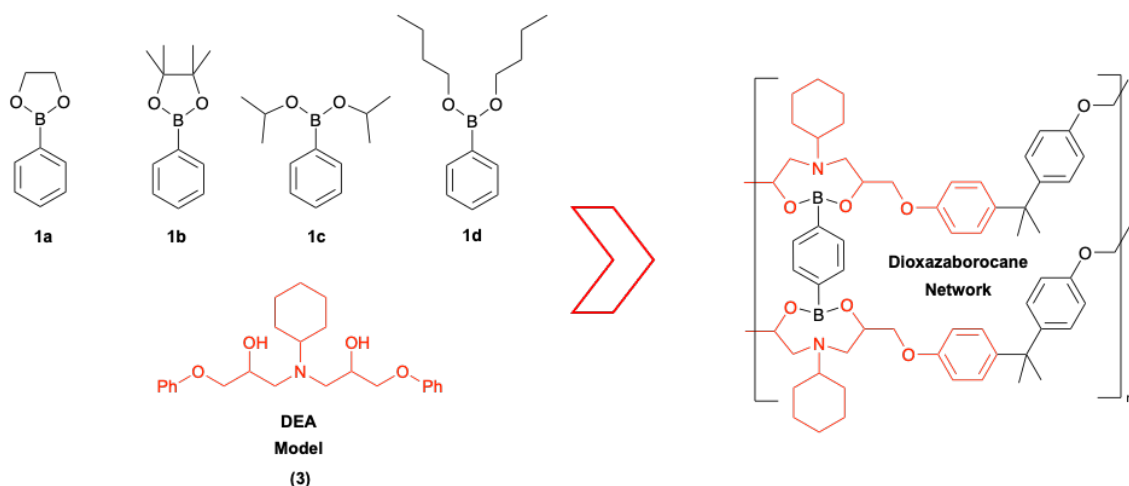
Figure 103: Structures of the boronic esters (1a-d) and the model ligand (3) to represent the envisioned dioxazaborocane network polymer in this research.

These were selected on a varying degree of entropic favourability and steric hindrance. The cycloaliphatic 1,2-diol esters were chosen due to their prominence as the dynamic boronic ester transesterification mechanism of choice in several CANs, which was previously discussed in Chapter 1 – Section 1.4.2.6.1. It was anticipated for the order of stability to be **1d** < **1c** < **1a** < **1b**. The synthesis of the ester **1d** involved a simple dehydration using a Dean-Stark apparatus under an inert atmosphere, to remove the water from the reactions and drive equilibrium to the right. **1a** was expected to be more stable towards hydrolysis than acyclic boronic esters,[187] and therefore a simpler dehydration in the presence of magnesium sulfate, followed by filtration and subsequent distillation was feasible and afforded a pure compound with an good yield. **1c** required a more challenging synthetic procedure (Scheme 1) to synthesise, where bromobenzene was subject to a lithium-halogen exchange reaction with n-butyllithium, followed by subsequent reaction with tri-isopropyl borate.
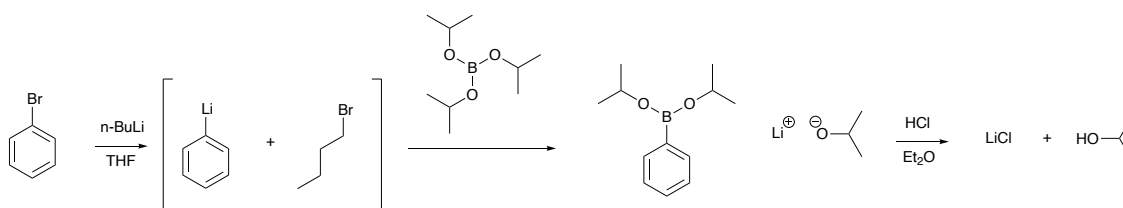
Scheme 1: Synthetic steps to boronic ester 1c.

Dean-Stark attempts were ineffective which is likely to be due to the boiling point of the isopropanol (82 °C) is lower than the boiling point of the azeotrope of toluene and water (84 °C). The dehydrating agent method utilised for **1a** would also be ineffective due to the subsequent filtrations and steps risking exposure to atmospheric air. Therefore, these methods were not attempted for **1c**. **1b** was purchased from a commercial vendor listed in Table 4 - Section 2.1. Furthermore, the vulnerability of boronic acids to form boroxines upon dehydration is a concern for the polymer networks proposed in this work. A major advantage of employing boronic esters in our hypothesis is that they cannot be

dehydrated and form boroxines (in the absence of water).[204] If boroxines were to form this would decrease the amount of boronic esters available for reacting with DEA functionalities in the final polymers, which presents a disadvantage to the desired crosslinking degree within the polymer network and can affect the resultant thermal and mechanical properties of the final material. This would also reduce the control over the structure of the network polymer.

The ^{1}H NMR spectra of monoboronic esters **1a-d** are shown in Figure 104, and the environments, highlighted in green (H_1), represent the hydrogens in ortho-position to the boron on the phenyl ring, which is indicated on the chemical structure. These regions appear as apparent doublets between 7.80-7.82 ppm for cyclic analogues and between 7.58-7.62 ppm for linear analogues. The differing chemical shifts become significant upon complexation to model ligand **3**, because all the equivalent signals for each monoboronic ester appears to shift to a doublet at 7.69-7.70 ppm when coordinated to the nitrogen of the model ligand. Therefore, integration of these peaks on the ^{1}H NMR spectra can be directly compared to their corresponding peak in the spectra for the model complex **4**, without interference from unreacted starting materials or alcohol liberated as the model reaction progresses. This presents a convenient way to study the relative reactivities of the different boronic esters **1a**-**1d** with the β-amino diol model ligand **3**.
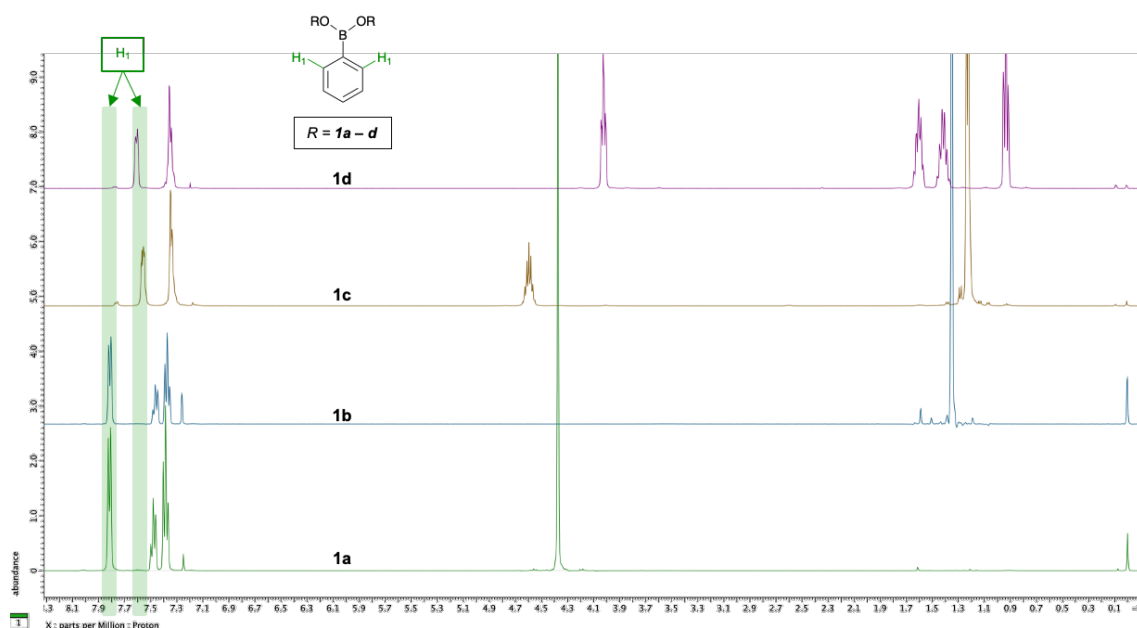
Figure 104: ^1H NMR of the boronic esters (1a-d) synthesised in this work, highlighting hydrogen environments of interest.

The chemical shift appearing downfield for cyclic esters, compared to the linear boronic ester analogues, suggests less shielding around the indicated hydrogen environment. Further exploration as to why is not necessary for the overall scope of this project but it is likely that the geometry of the oxygen lone pairs in the cyclic ester are restricted and may result in poor overlap with the p-orbital on the boron atom. The linear ester are less restricted in their geometry and have increased donation into the boron p-orbital, increasing electron density on the boron and reducing the relative shift of the ortho-aromatic protons (ppm).

Structure **3**, shown in Scheme 2, was selected to be a representative DEA functionality as a model epoxy-amine ligand. The exact model ligand used in this work was previously investigated by Unthank et al. for the reactions with trialkyl borate esters.[208] However, the work in this thesis utilises different low-cost phenylboronic acid to further enhance commercial viability of the research conducted, and hence, further insights into the reaction were required. Otsuka et al. also employed a similar model ligand system,

varying amines by their aromatic and aliphatic chains, to assess the reactivity of the nitrogen lone pair towards the boron atom, which was monitored by successful complexation. As expected from other reports in the literature, the aromatic amine did not yield a dioxazaborocane complex due to the likely delocalisation of the *N*-lone pair in the aromatic ring rather than participating in an interaction with the vacant p-orbital of the boron atom.[204,205,221] This meant that, for the research being conducted here, the highest performing polymer, based on strength and rigidity, would likely include an cycloaliphatic/aliphatic amine and aromatic epoxy. Therefore, molecule **3** (Scheme 1) was chosen for further study.
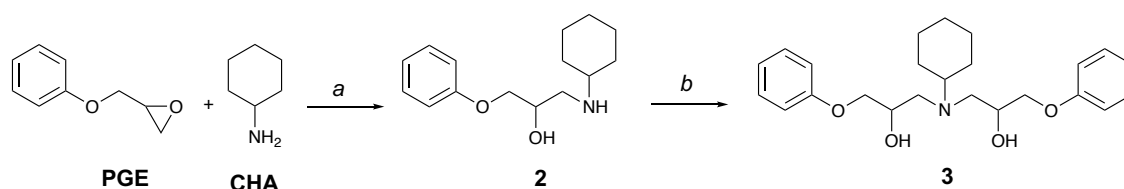
Scheme 2: Route to model ligand.

To the best of my knowledge the model ligand reaction with the boronic esters investigated in this project have not been explored before, although, similar DEA molecules have been transesterified with various types of boronic esters.[203] However, these did not have the aromatic end-groups consistent with a typical BPA epoxy-amine polymer.

The synthetic procedure for the model ligand (**3**) was developed by Unthank et al., in 2019, and was followed precisely in this work, as reported in Section 2.3.2.[208] This route contained two synthetically simple steps (*a* and *b* shown in Scheme 2) to obtain the final product. The synthesis of molecule **2** involved the reaction of phenylglycidyl ether (PGE) in an excess of cyclohexylamine (CHA) in toluene at 50°C for 4 hours before evaporation to yield a crude solid, which was isolated as pure white crystals, by recrystallisation in toluene. Part b of the reaction required addition of another equivalent of PGE under

elevated temperatures, delivering the crude product as a viscous liquid, in 67% yield from compound **2**. The modest yield was a result of material being lost during transfer between glassware due to the sticky viscous nature of the product. The viscosity of the model ligand (**3**) can be seen in Figure 105 as the air bubbles are visible for long periods of time after pouring. In addition, the ligand solidifies over time due to crystallisation.
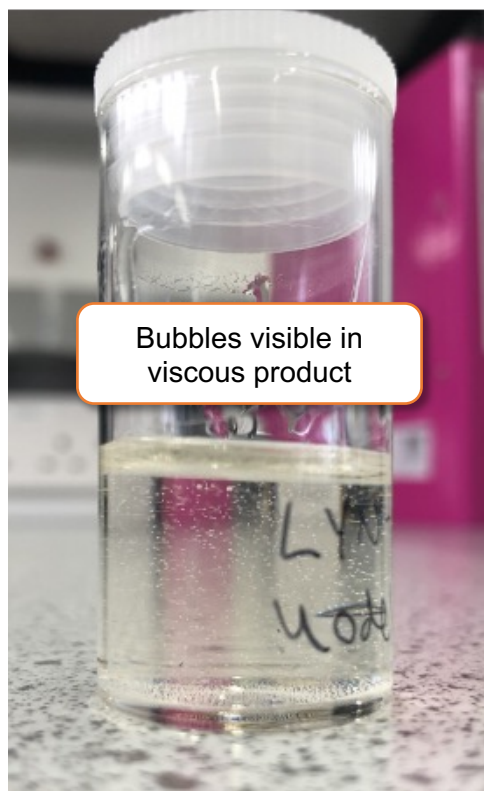
Figure 105: Picture of model ligand product (3).

3.3 Dioxazaborocane Model Reaction

The model reaction depicted in Scheme 3, was conducted in CDCl$_3$ for 5 minutes at 25 °C in 1:1 molar ratios of **1a-d** with **3** and investigated by ^{1}H NMR. The aim of this study was to decipher whether the different boronic ester analogues would alter the position of the equilibrium or relative rate of reaction with the model ligand to form the dioxazaborocane product **4**.
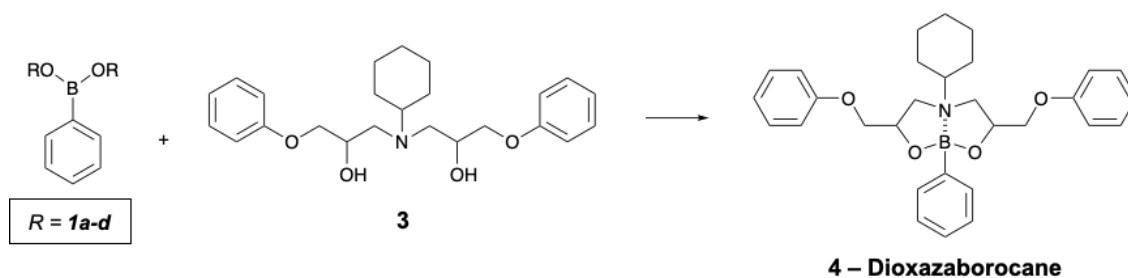
Scheme 3: Dioxazaborocane model reaction.

Each boronic ester **1a-d** produced the ^{1}H NMR spectra, shown in Figure 106, which shows the appearance of the dioxazaborocane molecule (**4**) and is recognised as such by the emergence of a characteristic peak at 7.69-7.71 ppm, which is indicated by H$_2$ (blue). Diastereomeric peaks at 4.49, 4.61 and 4.75 ppm, indicated by H$_3$ (red), are also characteristic of the dioxazaborocane molecule and appear in a 1:1:2 ratio, which integrate for 2H overall. The peak indicated by H$_2$ is attributed to the aromatic protons in ortho position to the boron substituted carbon. The peaks at H$_3$ are attributed to the chiral environment in a β-position relative to the nitrogen.
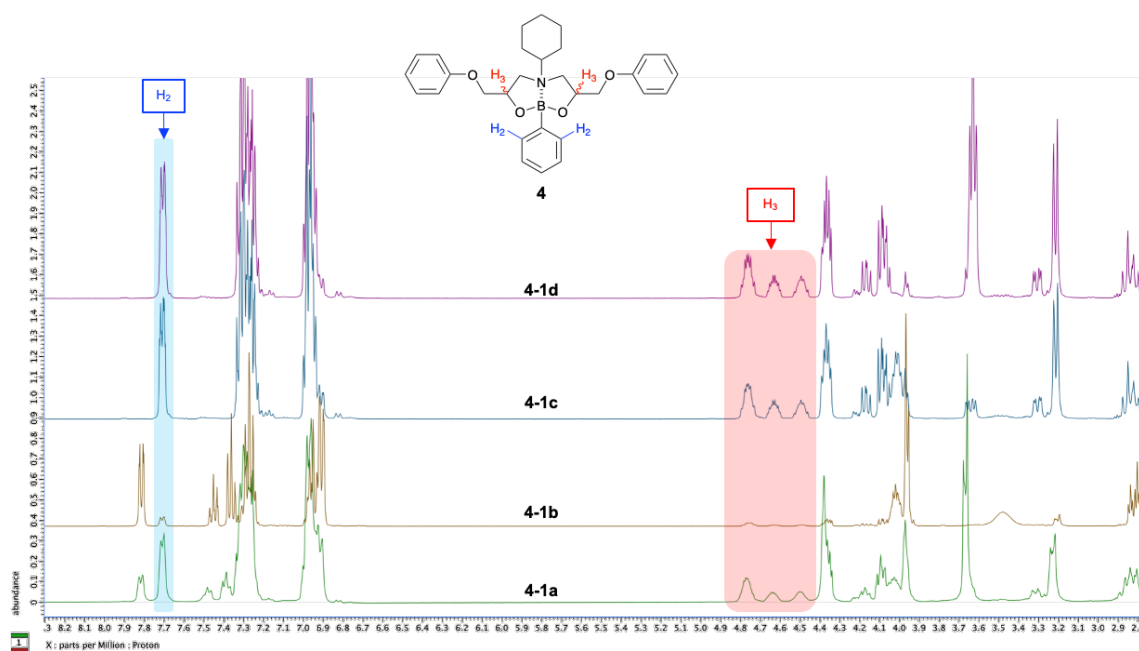
Figure 106: ^{1}H NMR overlay of dioxazaborocane **4** produced from the reaction between boronic esters **1a-d** and model ligand **3** after a maximum of 3.5 hours. Labels **4-1a – 4-1d** are indicative of the boronic ester that the dioxazaborocane originated from.

An important conclusion drawn from Figure 106 was that for the linear boronic esters (**1c** and **1d)**, the reaction goes to full completion quickly (in the time it takes to run an NMR sample), indicating the equilibrium favours the dioxazaborocane (**4**) whereas the cyclic boronic esters have only undergo partial reaction, which is proven by the presence of the boronic ester starting material in the spectra. This is likely a result of the entropic effects of the forward reaction, as the forward reaction will be favoured, in the case of positive entropies, according to Le Chatalier's principle.[219] In the case of the linear esters, the reaction liberates 2 moles of alcohol for 1 mol of ester hence going from 2 moles of reactants to 3 moles of products overall. In comparison, there is no net change in the number of moles of molecules in the system with the cyclic esters. In the case of the cyclic esters the forward reaction generates 2 moles of products for every 2 moles of reactants.

The Integral of the peaks at H_2 could be compared to the boronic ester reactant peaks, at the chemical shifts previously indicated by H_1 in Figure 104. Thus, enabling a percentage conversion to the dioxazaborocane **4**, since there is no interference in these regions of the NMR spectra. Table 11 shows the calculated percentage reaction completion of the model reaction described previously. These were calculated by the normalising the dioxazaborocane peak H_2 for 2H and calculating the percentage from the relative amount of starting boronic ester at peaks arising from the chemical shifts indicated by H_1. For both **1c** and **1d**, the reaction achieved were 100% conversion and for **1a** and **1b** they were 64.7% and 15.5% respectively. One may desire to use the diastereomeric peaks observed in the chemical shift region indicated by H_3, which is discussed in detail later (Section 3.6), as the dioxazaborocane reference point, but the isopropyl starting ester (**1c**) displays a multiplet in this region, which could obscure the results, especially if the reaction did not go to completion. Therefore, the method utilised here, provides the most accuracy, without the addition of an external reference.

Table 11: Dioxazaborocane model reaction yields within 24 hours.

Monoboronic Ester	$H_{(1)}$	$H_{(2)}$	Yield of dioxazaborocane product 4 (%)
1a	0.74	2.00	64.72 (45 mins)
1b	13.99	2.00	15.54 (3.5 hours)
1c	0.00	2.00	100.0
1d	0.00	2.00	100.0

Overall, the yields associated with the initial dioxazaborocane formation suggest that the product is thermodynamically more stable than the linear boronic esters but is closer in thermodynamic stability to the cyclic esters and specifically the more hindered pinacol boronic esters are even more stable than the dioxazaborocane, with the equilibrium favouring the left (starting materials) in this hindered cyclic ester system.

3.4 Boronic Ester Selection

From the results of the percentage conversion to dioxazaborocane complex (**4**) shown in Table 11, it is conclusive that the cyclic esters do not fully react with the DEA functionality. This means that if pinacol or 1,2-ethandiol esters were selected for use in network formation/crosslinking reactions, they would not result in a high yield of cross-linking based on this study. This would result in polymers, that are formulated to have a certain degree of crosslinking/crosslink density required to deliver the critical extent of reaction required for gelation (p_{gel}),[2] would actually fall short of the point of gelation, compromising the resulting network structure and related material properties. In addition, any unreacted product would remain within the polymer as the ester. An excess of boronic ester in the polymer matrix means it would not be part of the network and would leach out or be extracted out overtime. Concerning the dioxazaborocane crosslinks, free excess esters in the polymer matrix may facilitate the dynamic exchange mechanism.[40]

With regards to the extent of the forward reaction, the pinacol boronic ester (**1b**) barely reacts with the DEA model ligand (**3**) in the first few hours, only reaching an equilibrium at around 15.5% towards the product, in comparison to the same reaction with **1a**, which reached 64.7% reaction product at equilibrium. The stability of the pinacol ester is due to the steric bulk of the resultant 5-membered ring and is a consequence of the Thorpe-Ingold effect induced by the geminal dimethyl substituted carbons in the pinacol chain, favouring the cyclisation. After 96 hours, there was no substantial change in the equilibrium ratio of **1a:4**, concluding this system had achieved its thermodynamic equilibrium. However, for the pinacol ester **1b** the equilibrium slowly favoured the dioxazaborocane over time, resulting in 92.59 % completion after 96 hours. The overlays of the ^{1}H NMR spectra over time can be seen in the appendix (Section 10.1.1.7 to 10.1.1.9), along with the percentage conversions calculated from the integrals of the starting ester and dioxazaborocane product peaks.

In addition to requiring full conversion to dioxazaborocane complex, it is essential the selected boronic esters are fully soluble in epoxy resins. The cyclic <u>di</u>boronic ester (1,2-diol - **5**), which is a structural requirement to allow crosslinking between the epoxy amine polymer chains, afforded a stable, solid crystalline product with a high melting point, and limited solubility in epoxy resin. This product was also insoluble in most organic solvents listed in Table 12 and those that did eventually solubilise the ester required warming for a short time ($CDCl_3$) or required sustaining at the elevated temperature (THF). Thus, concluding that the cyclic diboronic esters would not provide a practically efficient route to network polymers, for the target application of this research.

Table 12: 1,4-phenylenediboronic bis(1,2-diol) ester solubility.

Solvent	Solubility of molecule 5
$CDCl_3$	Yes
THF	Yes – hot only
Acetone	No
PET 60:40	No
TEA	No
MeOH	No
Butanol	No
^{t}Bu-Methyl ether	No
Butyl acetate	No
Hexane	No

Therefore, the final choice of ester was limited to the linear analogues **1c** and **1d**, which both fully react with the DEA ligand and were both liquids that were fully miscible with the epoxy resins and amines required for network polymerisation. So, the final decision to choose the boronic ester for further study was based on the practicality of the polymer

synthesis, which would be most suitable for a scaled up industrial process. The simplicity to synthesise the butyl ester (**1d),** by means of a one-step dehydration reaction, was discussed previously in Section 3.2. In comparison to the synthesis of the isopropyl ester **1c**, the number of steps and risks posed by each step as well as the by-products of the reactions in each step were assessed and proved to be more favourable for the butyl ester. As a result, the butyl ester was selected for further investigation. Although less stable to moisture, appropriate cold storage under inert gases, preserved the linear esters for future use.

3.5 Thermodynamic Stability

The model reaction appeared to reach an equilibrium, according to the initial ^{1}H NMR results shown in Figure 106, for the esters **1a-d**. Consequently, raising uncertainties as to whether the resultant dioxazaborocane **4** is a kinetic or thermodynamic product, and if the equilibrium may change. In response, each reaction sample was subject to repeat ^{1}H NMR scans, periodically over 24 hours, to see if there was any changes to the product initially produced.

The ^{1}H NMR spectra, shown in Figure 107, shows the progress of the model reaction between monoboronic ester **1d** and model ligand (**3**) over a 24-hour time period. The mixtures were mixed in CDCl$_3$ for 5 minutes prior to direct transfer to an NMR tube for analysis. The highlighted areas H$_1$-H$_3$, were previously assigned in Figure 104 and Figure 106, and are also indicated in the ^{1}H NMR spectra below. Upon complexation, the apparent doublet at 7.58-7.61 ppm for **1d** had shifted downfield to 7.69-7.71 ppm, with no residual butyl ester peaks, supporting the conclusion that the linear esters are less thermodynamically stable than the dioxazaborocane, and will remain completely as the product. This is attractive for future polymerisation reactions.
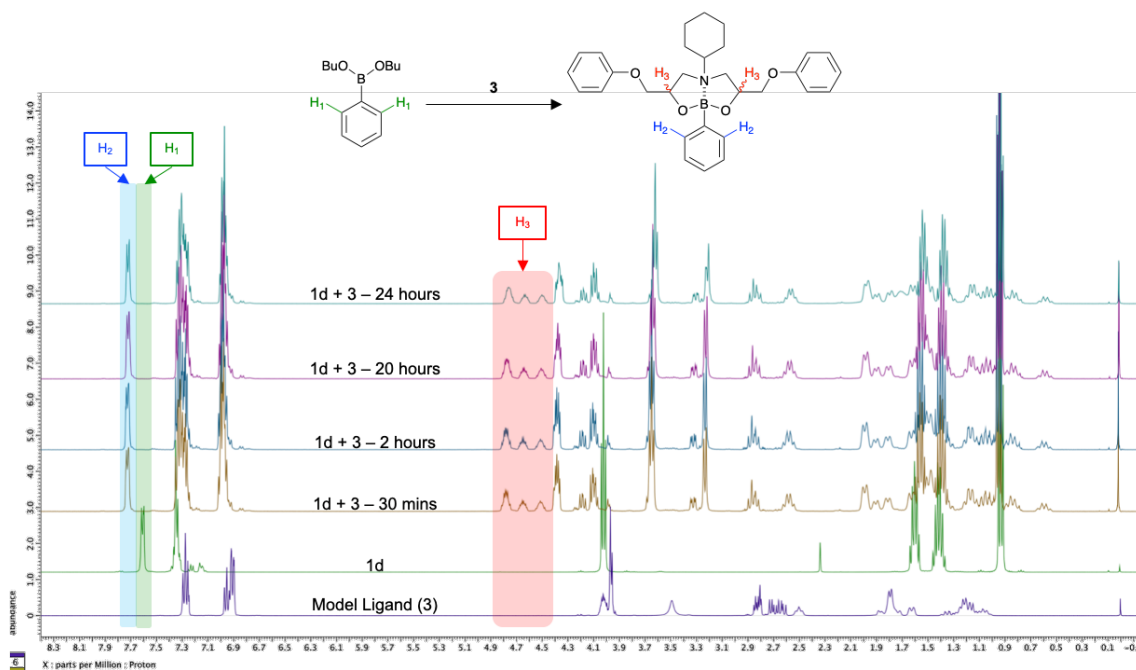
Figure 107: The 1H NMR spectra of the reaction of model ligand (3) with 1d over 24 hours at room temperature with areas of interest highlighted in colours matching the hydrogen environments depicted in the structures above the spectra.

All of the other esters (**1a-c**) revealed that after the initial NMR sample was run there was no further change to the equilibrium over time, which meant it had been reached shortly after mixing for all esters. The overlays of the ^{1}H NMR spectra over various times for **4-1a** to **4-1c** can be found in the appendix section 10.1.1.7 to 10.1.1.9. This was significant concerning the hypothesis that proposed the substituent effect of the boronic ester could delay the onset of gelation. It is proven here that linear boronic esters show little latency towards the proposed crosslinking reaction, which means that any effect, that may be governed by the bulkier substituents of the boronic ester in the case of the isopropyl ester (**1c**), towards the rates of the reaction, is unobserved in a reasonable timeframe. This is supported by the fast transesterification times observed in the literature especially with unhindered and linear boronic esters.[203,219,220] Furthermore, the pinacol ester (**1b**) slowly reaches a thermodynamic equilibrium showing a latent mechanism in comparison to the 1,2-diol ester (**1c**), which reaches its thermodynamic

equilibrium in the first 10 minutes if not quicker. However, both do not reach full conversion to the dioxazaborocane (**4**) which renders this unsuitable for the proposed polymerisations regardless of the latency envisioned. Therefore, shifting the scope of the project to focus solely on the reversible aspect and not on a delayed stepwise polymerisation. Although, future endeavours may focus on manipulating the time to gelation with a broader range of more soluble and more stable boronic esters for easier handling during the process.

3.6 Diastereomers of Dioxazaborocanes

Another interesting area of Figure 107 is highlighted in red (H_3) and is attributed to the chiral hydrogen environment indicated on the complexed structure in red. It was found that the 3 peaks highlighted integrated for a total of 2 when combined, suggesting that they are likely due a combination of diastereomers, as a result of the chirality, which is shown in Figure 108. Diastereomeric protons can be distinguished by ^{1}H NMR because these have differing chemical shift environments to one another. The dioxazaborocane complex (**4**) has 2 chiral centres. These arise from the stereochemistry in the initial PGE molecule and this is retained in the resultant model ligand and subsequent complex. The dioxazaborocane complex (**4**), which has a [5,5] fused bicyclic ring system with a N-B dative covalent bond at the bridgehead, is expected to behave similar to a more well-known carbon bicyclic equivalents, due to the tetrahedral geometry of the boron and nitrogen adopted upon N-B bond formation. Therefore, the stereoisomers of these systems are commonly found as the more stable cis-isomers at the bridgehead, indicated by the wedged bonds on structure for in Figure 108.[222–224]
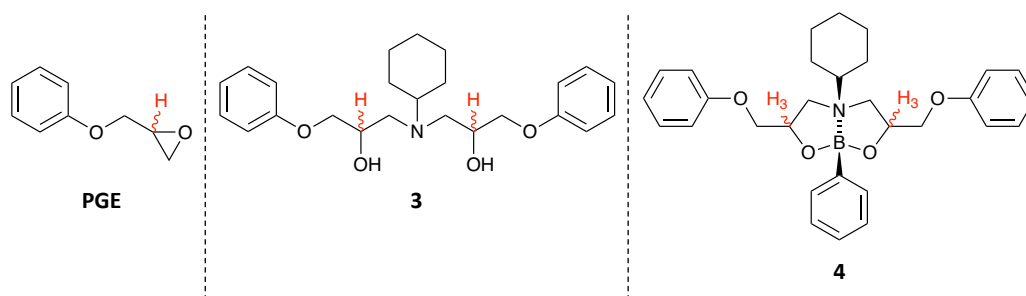
Figure 108: Stereogenic environments on molecules throughout the dioxazaborocane model synthesis.

This hydrogen environment for the model ligand (**3**) appears as a multiplet at 4.02 ppm and, notably, the corresponding environment in the dioxazaborocane complex (**4**) has also shifted downfield to 4.49, 4.61 and 4.75 ppm attributed to the three diastereomers present when in the favourable cis-isomer at the bridgehead. The structures of the possible cis-isomers are shown in Figure 109, where the structural mirror images are labelled with an apostrophe. 1 and 1', 2 and 2' are mesomers, which renders the structures 1 and 2 the only diastereomers signals for molecules with R_3 on the same face, and therefore, appear at different chemical shifts. 3 and 3' are enantiomers, as are 4 and 4'. 3 and 4 are also enantiomers, but 3' is the same molecule as 4 and 4' is the same molecule as 3. Hence, resulting in only 2 equivalent signals that are diastereotopic to 1 and 2, and therefore appear at a separate chemical shift, but the enantiomers 3 and 4 cannot be differentiated between by ^{1}H NMR and so appear at the same chemical shift. Without a more focused investigation dedicated to solving the absolute stereochemistry, it is difficult to assign the chemical shifts to a specific structure. Nonetheless, it is reasonable to suggest the enantiomeric pair are the cause of the signal at 4.7 ppm because of the integral ratio being double compared to each of the other two peaks. The environments at 4.5 ppm and 4.6 ppm cannot be assigned for certain but may be reasonable to hypothesise that structure 2 will have a lower chemical shift, further upfield.
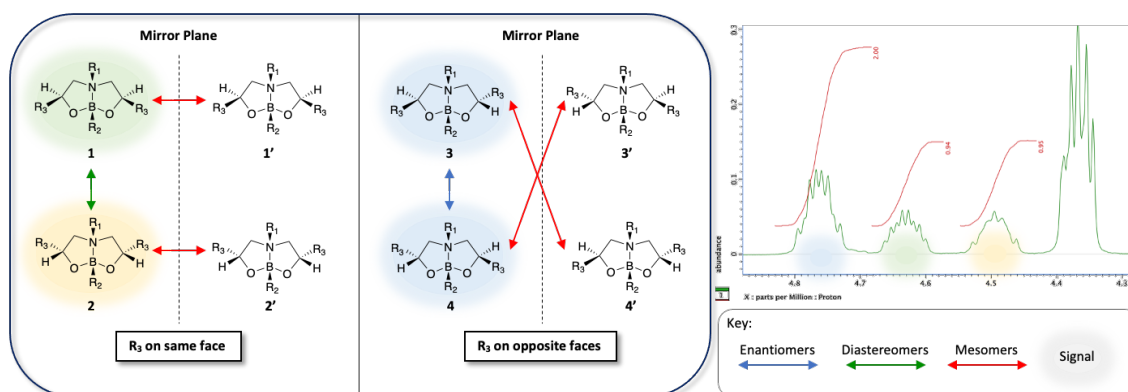
Figure 109: Structures of the stereoisomers of dioxazaborocane (4) and reasonable assumptions of the chemical shifts where the corresponding signals appear. The signals on opposite faces are also diastereomers of structures on the same face.

The downfield shift for all diastereomers, compared to the model ligand (**3**), suggests de-shielding of this environment in the complexed structure for similar reasons discussed for the aromatic environments. The C-H groups in the starting material contains an OH (alcohol) group which is converted to a boronic ester C-O-B group in the dioxazaborocane product, resulting in a de-shielding effect. Recent literature has reported a similar downfield chemical shift going from a DEA molecule to a dioxazaborocane complex, for similar chemical environments, in a β-position to the nitrogen. They reported a chemical shift moving from 3.57 ppm to 4.21 ppm, for the DEA to dioxazaborocane respectively.[225] However, the structure of their molecule was not chiral and represents a CH_2 environment, which is in accordance with the slightly lower reported chemical shift compared to the work presented here.

3.7   Half Complexes – The Reaction of Secondary Amine (2) with Monoboronic Ester (1d)

For the proposed application of this project, it is required that the presence of a boronic ester in the reaction mixture does not inhibit or prevent the 'primary' polymerisation reaction between the epoxy resin and the amine. This includes the secondary amines

(β-amino alcohol) produced after the first epoxy ring opening reaction with the amine, which has been reported previously by Unthank et al.[208] Therefore, the crosslinking is not likely to have any adverse effects towards the epoxy amine polymerisation. Initial tests following the same procedure as the previous models (reaction of **1a-d** + **3**) in CDCl$_3$ for 5 minutes suggest no significant reaction between the β-amino alcohol and the mono-boronic esters **1a-d**, as shown in Figure 110, as indicated by the lack of new peaks in the ^{1}H NMR. However, there is a noticeable disappearance of the sharp peaks a-d for the half ligand (**2**), and a slight broadening of peak a, for **1d**. This suggests it is not a simple mixture of reactant 1 + reactant 2, and that there may be some other interactions occurring that could potentially affect the polymerisation reaction.
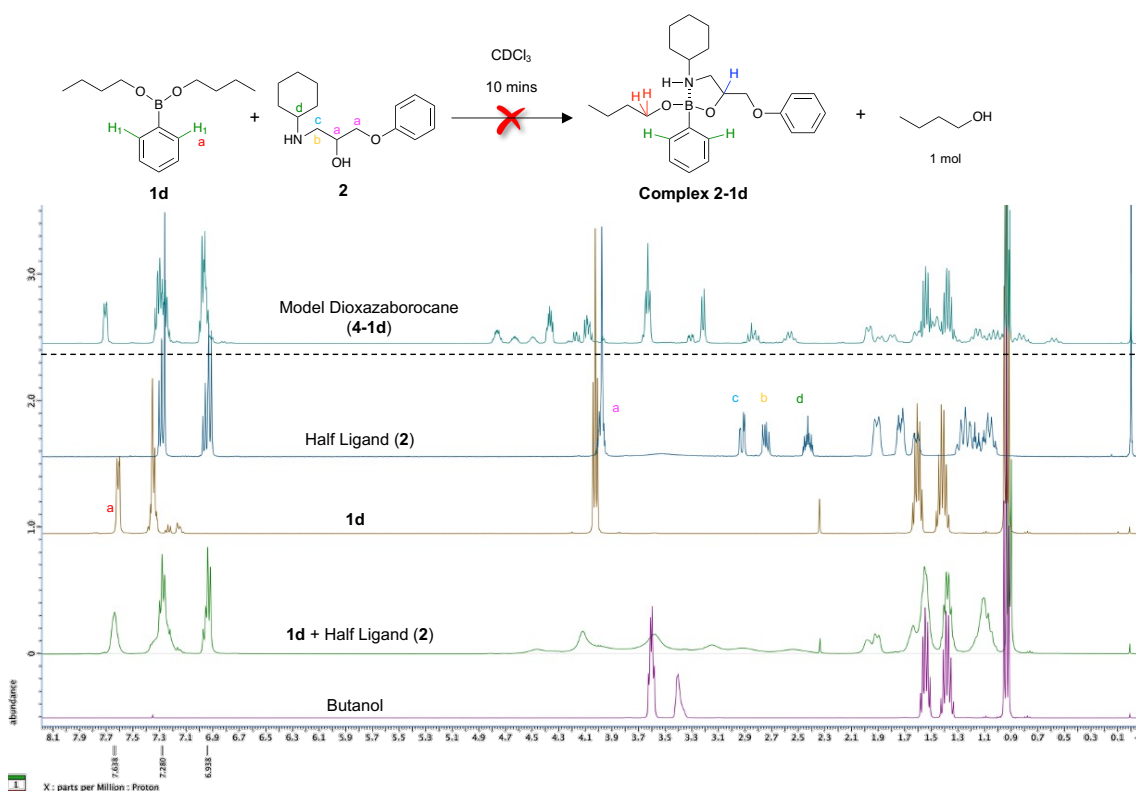
*Figure 110: ^{1}H NMR spectra (green) and relevant overlays of model reaction of **1d** with the secondary amino diol ligand (**2**).*

Figure 111 shows the ^{1}H NMR spectra overlay of the reaction between molecule **2** (half ligand) and boronic ester **1d** after mixing in DCM at 40 °C for 1 hour before drying at 50 °C in a vacuum oven overnight to remove DCM solvent and the liberated butanol. Again, with the secondary β-amino alcohol (**2**), the reaction did not show conclusive evidence of consumption of starting materials but did indicate a potential interaction or mixture of products. The weak, broad noise appearing after 4 ppm may be a small amount of an anticipated product but cannot be definitively concluded as such.
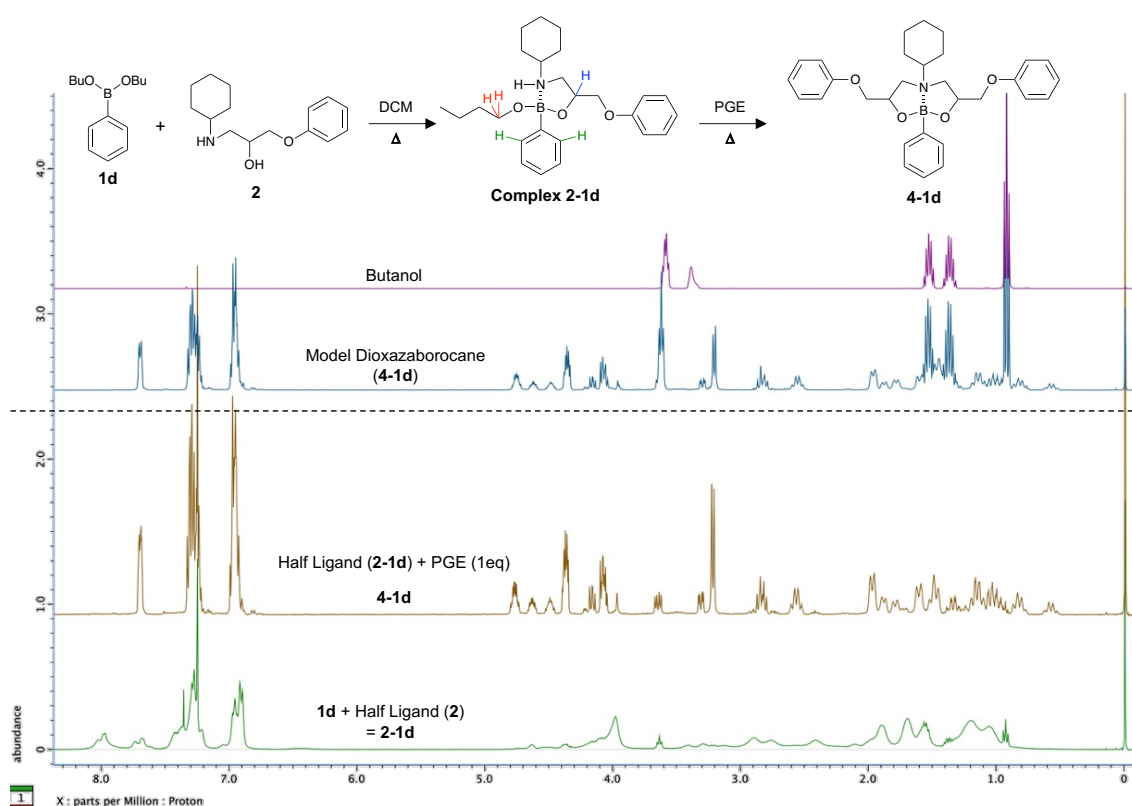
*Figure 111: ^{1}H NMR spectra (green) and relevant overlays of model reaction of **1d** with the secondary amino diol ligand (**2**) in the presence of DCM, including the spectra of the subsequent addition of 1 equivalent of PGE (brown).*

Furthermore, the appearance of a signal at around 8 ppm is indicative of boronic acid (B-OH) bonds, which is likely a result of some residual water in the DCM solvent that hydrolyses the boronic ester. Important conclusions to note are 1) the starting material

is not consumed, 2) there is no clear evidence of signal product 3) resulting reaction mixture readily reacts with another equivalent of PGE, so the crosslinking reaction, with regards to epoxy-amine-dioxazaborocane materials envisioned, is clearly not inhibited by any boronic complexes with the β-amino alcohol groups. The most important observation from this experiment is that the addition of a further equivalent of PGE, to form the desired tertiary β-amino diol complex **4-1d,** is successful (brown - Figure 111). The addition of PGE produces an identical spectrum to the original model tests (blue - Figure 111) utilising the tertiary β-amino diol (**3)**, with the exception being that the butanol is still present in the earlier models because these were not dried prior to ^{1}H NMR sampling. As a result, it can be concluded that any interaction as the half complex (**2-1d**) does not impact the reaction of the secondary amine with another equivalent of epoxy and thus, is unlikely to significantly affect the desired polymerisation mechanism.

3.8 Conclusions

The model reactions show that the nature of the boronic ester has a significant effect on the reaction yield to form dioxazaborocane complexes, with different boronic esters reacting to dioxazaborocane product (**4**) to different extents. In this research, liquid linear chain boronic esters (**1c**-isopropyl and **1d**-butyl) reacted to give a 100% yield of product. The cyclic esters did not give 100% yields and remained in an equilibrium. Furthermore, half complex reactivity did not inhibit subsequent amine reactivity with another equivalent of PGE, which means that it will not likely inhibit the step-wise polymerisation mechanism. The butyl ester (**1d**) was selected based on the factors described and additionally on the basis that the synthetic procedure was simple and offers good scale up opportunities as well as good miscibility in the epoxy resins when the diboronic analogue is utilised for crosslinking.

Chapter 4

Polymer Development

4   Chapter 4 – Polymer Development

4.1   Introduction

Building on the conclusions arrived at in the model study of Chapter 3, this chapter focusses on applying the dioxazaborocane reaction, with a butyl diboronic ester, into network forming polymerisation reactions via a single-stage synthesis, which are ideally suitable for scalable practices. To the best of my knowledge this has not been achieved so far in thermoset polymers. The most relevant literature regarding a crosslinking boronic acid was reported by Ito et al. in 2018.[210] This method included solubilising a pre-made linear epoxy amine polymer and dropping in a solution of diboronic acid, which gelled instantly. Thus, providing no control over the materials final form. The groups work around for this was to soak a preformed epoxy-amine dog-bone in a solution of diboronic acid in THF. However, this method provides no control over the boronic acid crosslinking degree, and the resulting material properties arising due to the boronic links cannot be easily studied.

Therefore, the scope behind this PhD project involves the development of a novel method of crosslinking epoxy-amine polymers with diboronic ester analogues and this chapter deals with overcoming the problems arising with incorporating diboronic esters into traditional epoxy-amine polymer synthesis techniques to make useable polymer samples for mechanical performance testing. The focus was to achieve a CAN polymer in a single-stage process.

4.2   Synthesis of Diboronic Ester Curing Agent

1,4-phenylenediboronic acid tetrabutyl ester (**6**) was selected for further development due to the ideal dioxazaborocane equilibrium, with 100% product formation, as seen in the polymer model of Chapter 3. The synthetic procedure was just as simple as the 1,2-diol ester (**5**), via distillation of water under reduced pressure in the presence of a large

excess of butanol. This method also offers an attractive route to scalability due to the practicable recovery of excess materials (butanol and water), which helps to afford a greener synthetic procedure, compared to the 1,2-diol diboronic ester (**5**). The diboronic butyl ester (**6**) was also found to be miscible with the polymer resin, which is one of the most important factors for achieving a single stage network forming process. Therefore, the diboronic butyl crosslinker was selected for a "one-pot" network development throughout the rest of this work.

4.3 Network Development

The objective behind the work in this section was to develop a process for the creation of thermoset, uniform, transparent polymeric material sample, as free films that are suitable for various material analysis techniques, in order that the structure-property relationships of this new material type could be studied.

4.3.1 Aromatic Epoxy-based Polymers (E1)

As aromatic types of epoxides, such as epoxides of bisphenol A, are renowned for their high strengths and are ubiquitous in high performance applications, which is discussed in Chapter 1.3, the objective here was to apply the novel boronic ester crosslinking reaction to this class of epoxy-amine polymers in the anticipation that this would crosslink the linear polymers.

4.3.1.1 Cyclohexylamine with DER332 (CHA-E1)

The general strategy for the polymer synthesis in this section was to develop a process by which all the monomers could be combined in a single reaction vessel until homogenous and then draw down as thin films onto glass microscope slides. Initial formulations contained a 1:1 stoichiometry of the moles of DER332 epoxy resin to moles of cyclohexylamine (CHA), which should form a linear polymer chain containing

diethanolamine functionalities as a control reference. Diboronic ester (**6**) was then added in various stoichiometric equivalents to make up 100% or 50% crosslinks per polymer. The catalyst 2,4,6-tris-(dimethylaminomethyl)phenol (DMP-30) was incorporated to catalyse the polymerisation process. This meant, in theory, that either 100% or 50% of the available diethanolamine functional groups were crosslinked with boronic ester assuming 100% conversion of the epoxy and amine groups in the polymerisation process. The full experimental method can be found in Section 2.3.4. and the idealised structures of the polymers and catalyst are shown in Figure 112, where n represents the degree of polymerisation and the amount of consumed DEA is proportional to the moles of boronic ester functional groups as a percentage of either 100%, 75% or 50%. The control polymer is the linear polymer backbone that will be present in the network polymers.
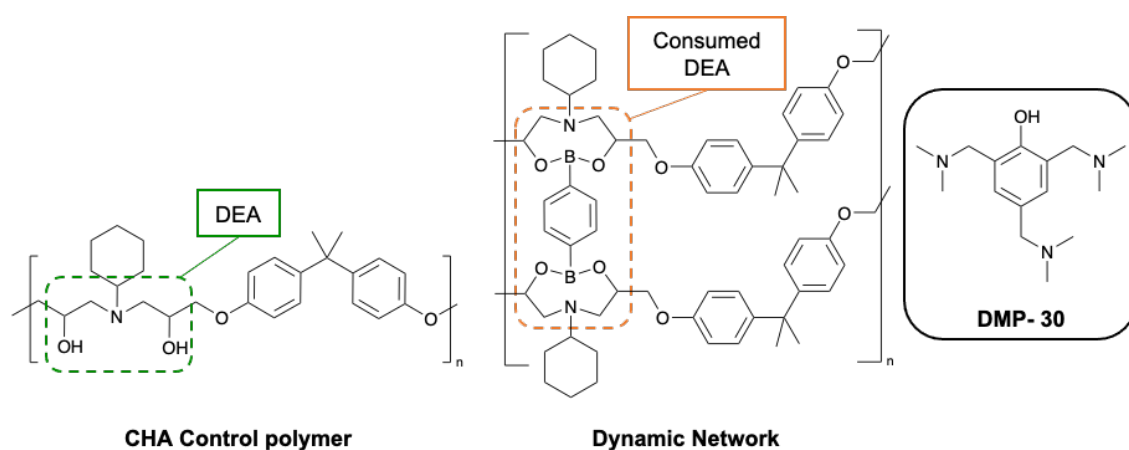
Figure 112: Structures of polymers prepared by a CHA amine and DER332 (CHA-E1) and the structure of DMP-30 catalyst.

The mechanism by which DMP-30 catalyses the epoxy-amine reaction is not fully understood but it is known to accelerate the cure of epoxy-amine coatings and as such is commonly used for such applications. A recent paper has speculated mechanisms regarding epoxy-anhydride reactions in the presence of DMP-30.[226] It is believed the Lewis base behaviour of the catalyst can catalyse the main curing mechanism promoted

by either the phenol group, the tertiary amine group or a combination of both. The generally accepted mechanism for epoxy-amine ring opening reactions in the presence of DMP-30 are suggested in Figure 113. Mechanism 1 and 2 involves hydrogen bonding between the epoxide lone pair and the phenol hydroxyl group of DMP-30, which increases the partial positive charge on the adjacent carbon allowing the tertiary amine to open the ring or the primary amine designed for the main polymerisation reaction to react faster.
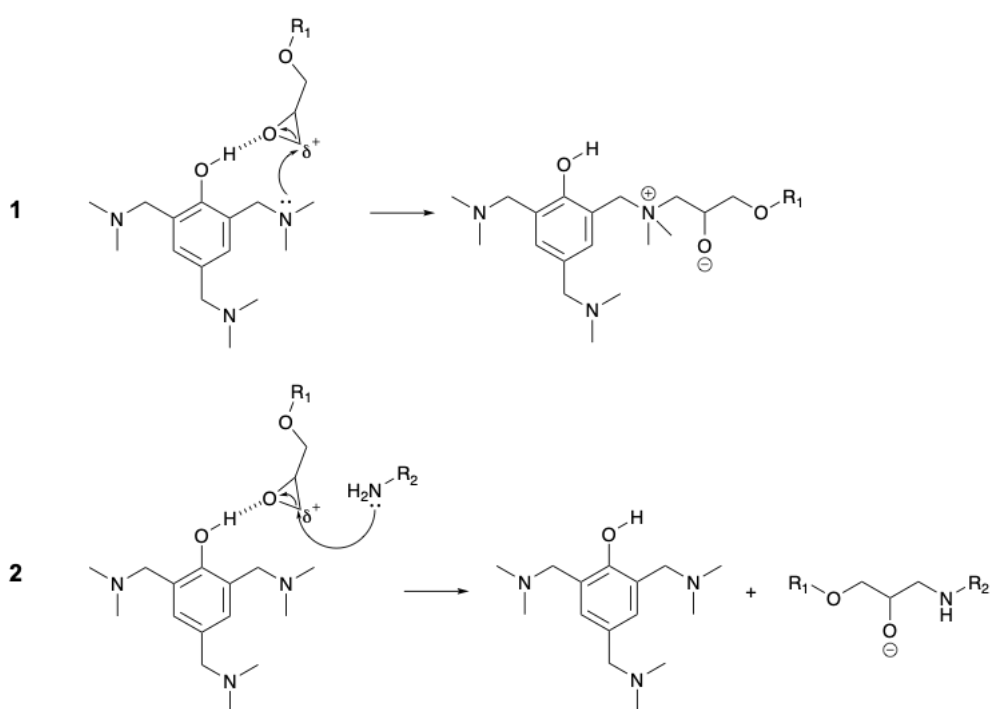
Figure 113: Speculated mechanisms of DMP-30 catalysation in epoxy-amine polymers .

Preliminary experiments involved testing the cure schedule to investigate if the cure time or temperature changed the material at all. Table 13 shows the various conditions and general formulations of polymer to be described in this section and form the basis for further polymer development. The purpose behind these initial studies were purely observational in the endeavour to achieve samples of polymeric material suitable for material testing and analysis. Therefore, any characterisation of materials was not explored until acceptable polymer samples were synthesised.

	1	2	3	4	5	6
Cure schedule	Control	Control + catalyst	Covalent Adaptable network (CAN) 100%	CAN + catalyst 100%	CAN + catalyst 75%	CAN + catalyst 50%
A RTP only	A1	A2	A3	A4	A5	A6
B RTP + heat combined	B1	B2	B3	B4	B5	B6
C Heat only	C1	C2	C3	C4	C5	C6

All of the CHA based polymers were colourless, and those without boronic ester were clear. The various polymer film observations have been visualised in Figure 114 will be described as such in the text.
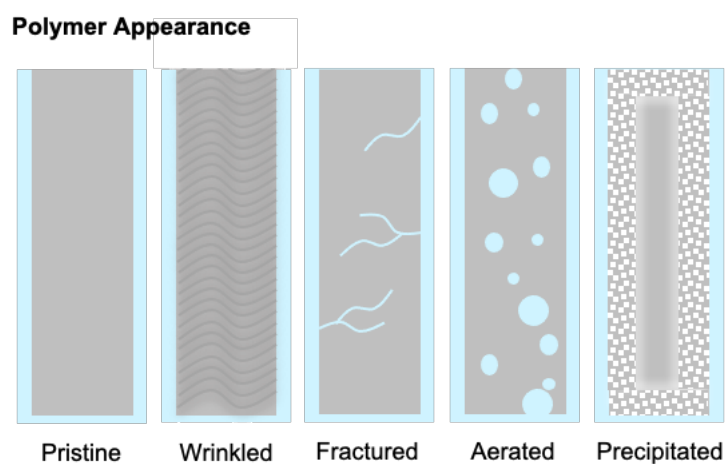
Figure 114: Visualisation of polymer observations.

To understand if the diboronic ester (**6**) could be used in the proposed way to induce crosslinking of linear epoxy-amine polymers, the linear (thermoplastic) epoxy-amine control polymer was prepared as a comparison. It was expected that the crosslinking reaction would produce hard, polymers whereas the control would likely be a viscous liquid.

The control polymer without the addition of catalyst (A1) was a tacky, viscous liquid after 24 hours at room temperature, which was expected as there is no crosslinking intended in this polymer. The same polymer did not incur any apparent changes in physical state upon heat cure at 80 °C for a further 16 hours (B1). In direct comparison to polymer A1, polymer A2 that contained 1 wt% DMP-30 catalyst in the formulation, was a smooth, soft solid after the same conditions, which also did not have any obvious change in physical state after a further heat cure (B2). The final state of the polymer B2 is shown in Figure 115. It is likely that the addition of catalyst to the system increases the rate of polymerisation reaction resulting in high molecular weight polymer chains, which solidify/vitrify during the reaction. In addition, the DMP-30 catalyst is known to promote homopolymerisation in epoxy polymerisation reactions which may cause branching and even potentially gelation.

Figure 115: Photo of polymer film B2 after room temperature cure for 24 hours followed by a thermal cure at 80 °C for 16 hours.

In addition, another conclusion that can be drawn here is that the polymerisation was likely finished after 24 hours at room temperature, because there was no apparent change upon a heat cure which is known to increase the polymerisation reaction rate. However, because the T_g of BPA-type epoxy polymers are usually very high, it is common for industrial processes to include a thermal cure at temperatures above T_g to ensure the polymer can fully polymerise and not be limited by diffusion, when they vitrify/solidify into the glassy state. Furthermore, cure schedule C had no clear effect on the materials. Therefore, the best curing schedule for future investigations was deduced to be room temperature followed by a final thermal cure to allow any residual reaction to take place.

The addition of diboronic ester **6** to the formulation resulted in hard, but extremely brittle polymers, which indicated that crosslinking had likely occurred. This was also significant because any attempt to remove from the slide resulted in broken pieces of polymer, due to the highly brittle nature. Further development was required to alleviate this brittle property.

Moreover, the appearance of a white precipitate (Figure 116) became apparent in the crosslinked films, which seemed more pronounced when higher quantities of diboronic ester were present (100% boronic crosslinks). Although, films did not consistently have precipitate, it was attributed to hydrolysis of the boronic ester to boronic acid, which was then insoluble in the polymer matrix. The hydrolysis is expected to occur due to the presence of water in air, which was not eliminated from the reaction conditions at this point of the study or controlled. This may explain the more varied occurrence in the films because the humidity of the environment will to be different from day to day. As the environment at this stage was not controlled to mitigate hydrolysis from air moisture. It is difficult to prove that the precipitate was solely due to hydrolysis, therefore, a study looking at reduction in the boronic ester content of the reactive formulations was the next

logical step to employ to observe if the precipitate reduced in the resulting polymer films. Practical efforts to prevent the hydrolysis phenomenon through further method development will be discussed in Section 4.4.
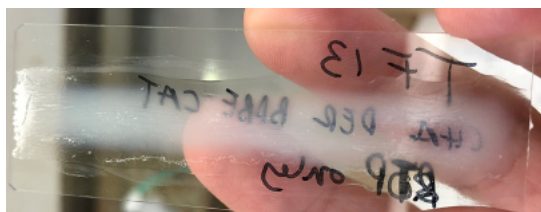
Figure 116: Picture showing white precipitate in film of A4 after a room temperature cure for 24 hours.

Figure 117: Picture of fractured and aerated film B3 film with 100% equivalence of diboronic crosslinks.

In addition to the white precipitate in the polymer film, the appearance of bubbles occurred in the films with diboronic ester **6** (Figure 117), with the number of bubbles appearing to be proportional to higher amounts of boronic ester in the formulation, which is represented by an aerated diagram in Figure 114. This was credited to the evaporation, especially at elevated temperatures, of the butanol liberated from diboronic ester **6,** upon transesterification with the DEA groups on the epoxy-amine polymer. Another possibility is that they arise from trapped gasses unable to diffuse through the polymer matrix. The result of this is a detrimental effect on the mechanical properties of the resulting polymeric sample, as it contains defects in the final material, rendering it inadequate for performance testing. As a result, combined with the precipitate hypothesis, further investigation was focused on reducing the diboronic ester content.

To study the impact of degree of crosslinking on the properties of the resulting material, as well as understanding whether controlling humidity could eliminate the precipitation issue, two further samples were prepared. These were formulated to have either 50% or 75% of all possible DEA functional groups (formed from epoxy-amine polymerisation) crosslinked with diboronic esters. These were allowed to undergo a room temperature cure in a desiccator for 24 hours. However, as evident in Figure 118, the appearance of white areas in the film still prevailed.

Figure 118: CHA films with 75% diboronic ester content (yellow) and 50% boronic ester content (red) after a room temperature cure in a desiccator.

When 50% of the DEA functional groups were consumed, there was a dramatic reduction in the bubbles present in the films compared to films with 100% DEA consumption, after a thermal cure (Figure 119). This evidence suggested that bubbles were proportional to the amount of butanol liberated from the boronic ester reaction of **1d** with the DEA groups. Furthermore, less crosslinking may result in less shrinkage and cracking.
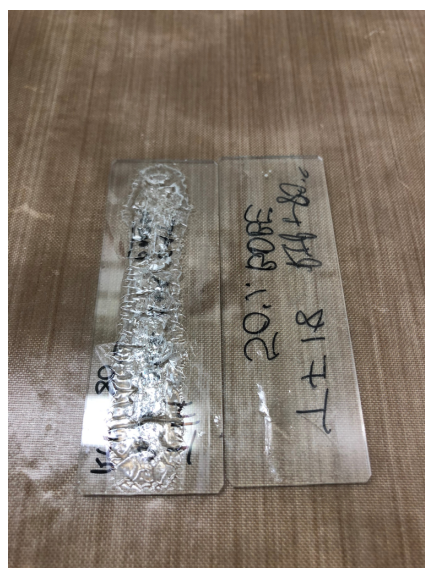
Figure 119: Picture of polymer films B4 (left) and B6 (right) showing a reduction of fractures, bubbles and white areas in the 50% boronic crosslinked polymer.

However, even with the lower amount of boronic crosslinks, the polymers containing CHA remained extremely brittle and unable to remove from the glass substrate as free films. Thus, replacing CHA with a linear analogue (hexylamine – HA) in the polymer formulation was investigated as a route to plasticise the films and reduce the brittleness.

4.3.1.2   n-Hexylamine (HA) with DER332 (HA-E1)

The general synthetic procedure for the HA-based polymers was kept the same as with CHA based polymers with addition of 1 wt% DMP-30 and the structure is shown in Figure 120. The retained method for curing was cure schedule A and B, which was room temperature for 24 hours followed by 16 hours at 80 °C. Table 14 shows the polymer groups that were prepared, with N/A representing the previous groups that were excluded from further study.
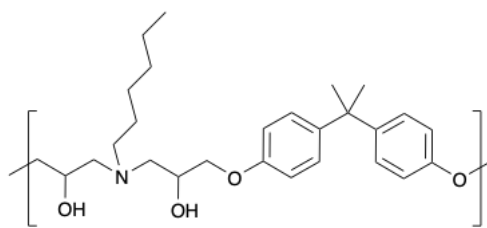
HA Control polymer

Figure 120: HA-based polymer structure (HA-E1).

Table 14: HA based preliminary trial polymers.

	1	2	3	4	5	6
Cure schedule	Control	Control + catalyst	Covalent Adaptable Network (CAN) 100%	CAN + catalyst 100%	CAN + catalyst 75%	CAN + catalyst 50%
A RTP only	N/A	**A2**	N/A	**A4**	N/A	**A6**
B RTP + heat combined	N/A	**B2**	N/A	**B4**	N/A	**B6**

The groups in Table 14 were selected to compare the observable effect of including diboronic ester to the formulation, based on previous observations seen in the CHA section.

Drawdowns of the control polymer revealed that the polymer had low viscosity, under the same conditions as CHA. This resulted in the control polymers not making uniform films and coagulating on the microscope slide, which is noticeable in Figure 121, even after the thermal cure stage. This evidence suggests that the T_g of the control materials with HA in the formulation is likely to be lower those previously prepared with CHA in the formulation, which may help to reduce the brittleness faced in these polymers.
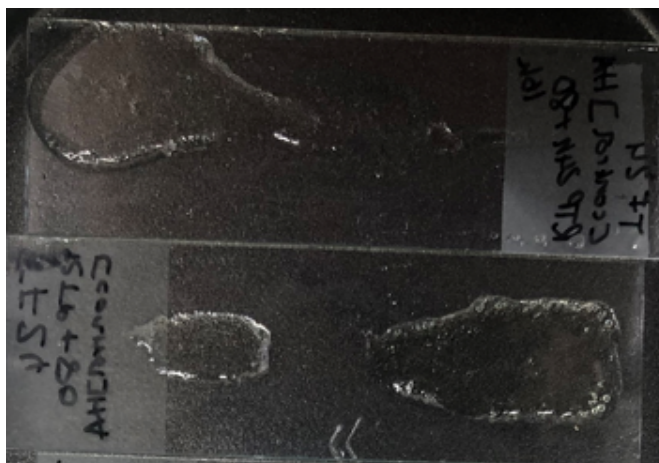
Figure 121: picture of control HA-based polymers B2 after drawdown and full cure.

Polymers A4 and B4 appeared to have a smooth drawdown, but after a room temp cure in schedule B, the white precipitate was abundant throughout the polymer, as shown in Figure 122, which wasn't as apparent in the B4 system of CHA-based polymers (Figure 119). Furthermore, there was less bubbles present in the HA comparison, presumably as a result of the lower polymer viscosity. Again, the presence of the white precipitate suggests hydrolysis of the boronic ester before reaction with the DEA functionalities, resulting in formation of the insoluble diboronic acid. Due to the amount of visible white precipitate, it is expected that the films with 100% diboronic ester content have not achieved the anticipated crosslinking extent because the diboronic ester could not stay miscible in the polymer mixture after hydrolysis.

The drawdowns provided more resistance as the polymers incorporating diboronic ester appeared more viscous during the drawdown step. This evidence suggests that the boronic esters are reacting with the polymer linear epoxy-amine more rapidly than in CHA-based polymers, due to the faster increase in viscosity witnessed, which is likely because of the increase rate in the formation of DEA functionalities. The faster reaction rate of the epoxy-amine when using the less hindered n-hexylamine may result in a gelation in a shorter reaction time. A welcome observation of the HA-based B4 polymer

170

was that it appeared to be far less brittle than the equivalent CHA polymer, which was evident from a visual observation of the polymer containing less fractures throughout and requiring more effort to force a fracture through external forces. This is likely due to a degree of flexibility introduced into the polymer chains through the linear n-hexyl amine compared to the sterically hindered cyclohexylamine.
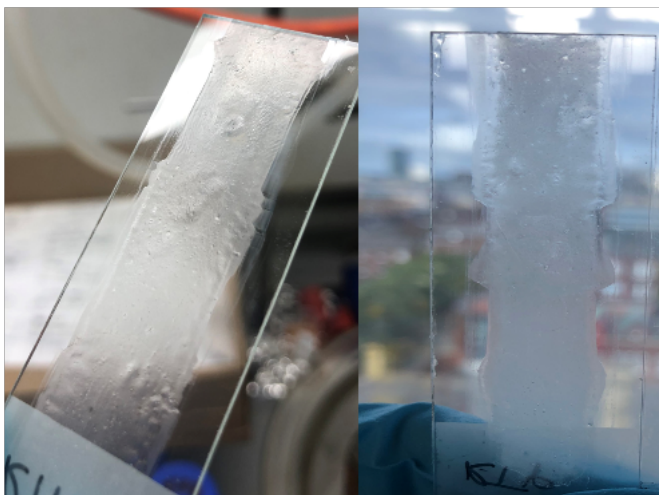
Figure 122: HA-based polymer with 100% boronic content A4 after initial drawdown (left) and after curing at room temperature (right).

The 50% boronic crosslinked material drastically reduced the amount of white precipitate, which is only noticeable around the polymer edge rather than throughout, as is evident in Figure 123. This supported the hypothesis that boronic ester (**6**) was hydrolysing to form insoluble diboronic acid and phase separating/precipitating from the polymeric mixture, during the course of the reaction. Development of the solution to this problem will be discussed further in Section 4.4. It is noted that there was no apparent visual changes to the materials after a thermal cure at 80 °C for 16 hours.

Figure 123: Visual comparison of HA-based polymer A4 (left) and A6 (right).

In addition, excess mixture from A6/B6 formulations was poured into a silicon mould to observe if this would be an ideal method for producing dog-bones for tensile testing. This enabled a free film to be removed after curing, as shown in Figure 124. However, the presence of bubbling in the polymer was observed and this would render materials unsuitable for tensile testing, as these voids throughout the film would create weaknesses and impact reproducibility of tensile or mechanical testing. It is believed that the expelled butanol, evaporating from the film as it hardens, is responsible for the voids forming and thus, thin films are necessary to limit this effect and and allow butanol transport and evaporation from the surface.
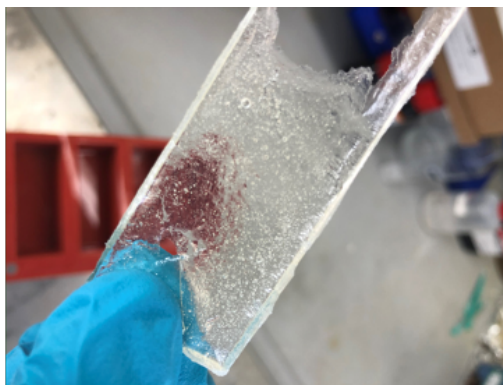
Figure 124: Excess HA-E1-A6/B6 mixture cured in a silicone mould.

It is also evident from Figure 124 that the wrinkling has not been observed, for the same mixture (A6/B6) that was drawn down onto the glass substrate, when cured on a non-stick silicone substrate. Hence, this supports the conclusion that wrinkling is likely to be due to internal stress relief of the polymer.[227] Further substrate development will be discussed in Section 4.5.

Furthermore, although the brittleness of the film has been reduced, by use of a more flexible linear amine, the issue of brittle films persisted, and difficulties associated with this arose when removing the polymer from the silicone substrate, as cracking occurred around challenging areas for the device employed to lift the polymer from the substrate. To address this issue, further adaption of the polymer's chemical building blocks was required. Utilisation of a more flexible diepoxy was employed in anticipation that this will add more flexibility into the polymer film and overcome the brittleness associated with the currently employed DER332™ based polymers. Moreover, an additional method of polymer manipulation, at the molecular level, is applied to add a controllable variable to the polymer by limiting the functionality of the polymer chains.

4.3.1.2.1 End-capped HA-DER 332 (HA-E1(DEA-5)) Polymers
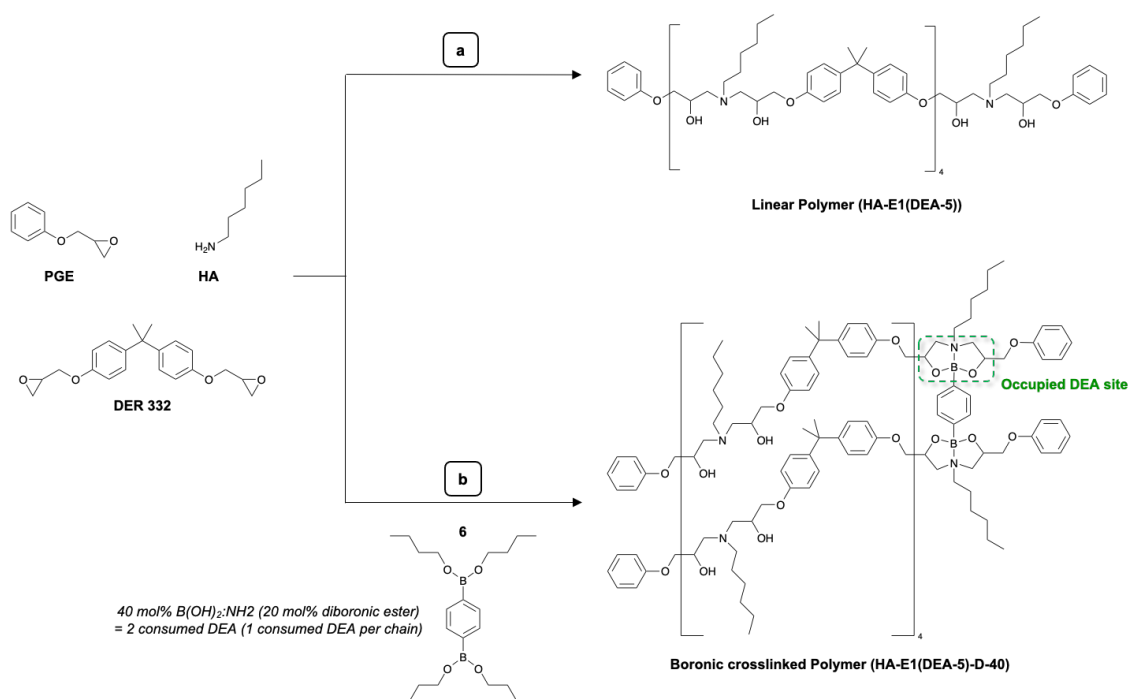
Figure 125: Route to PGE capped polymers with an average functionality of 5 DEA units per chain.

Phenyl glycidyl ether (PGE) was introduced in the polymer formulation as shown in Figure 125. The purpose for the inclusion of a monofunctional epoxy was to limit the epoxy-amine polymer chain growth and provide a variable that can control the average molecular weight of the chains. The effective control of the molecular weight transpires due to the fact the monofunctional epoxy molecule cannot undergo another reaction with an amine in a stepwise approach. Thus, delivering an unreactive end-group to the polymer chain, which prevents further chain growth. As a result, linear epoxy-amine polymers of a targeted molecular weight can be designed and synthesised, thus allowing exploration of this variable and its impact on material properties.

The resulting polymer, which was formulated to have 40% of the DEA functionalities consumed by a the boronic ester crosslinker, was extremely wrinkled on the glass substrate, as shown in Figure 126. This evidence suggested that a different substrate,

174

that induced less stress on the curing polymer, was required to progress the project further to complete meaningful property analysis, by producing free-films to achieve this.

Figure 126: Polymer HA-E1(DEA-5) with 40% diboronic ester (D40) consumed DEA groups after draw-down onto glass slide and cured at room temperature for 24 hours followed by a thermal cure at 80 ℃.

In an attempt, to acquire dog-bone test specimens for tensile testing, the polymer HA-E1(DEA-5)-D40 was casted into silicone moulds pre-formed to the required dimensions, of which the method is depicted in Figure 127. Furthermore, the same polymer formulated with cyclohexylamine (CHA) instead of HA was also cast as a comparison. The resulting dogbones from these tests are shown in Figure 128. It was immediately apparent that the CHA-based polymer was more brittle than the HA-based equivalent, as it fractured on attempts to release it from the silicone mould. This suggested that a method to make the polymer more flexible was required to fabricate samples suitable for mechanical and material testing.
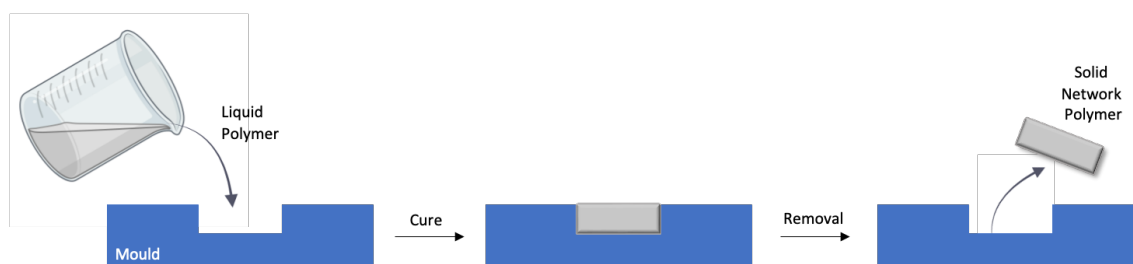
Figure 127: Visualisation of polymers casted in a silicone mould.

Figure 128: Initial dogbones produced from both CHA and HA-based DER 332 polymer formulations crosslinked with 40% DEA consumption by diboronic ester 6.

In addition, both polymers exhibited extensive formation of entrapped bubbles, shown in Figure 129, which would be detrimental to any tensile analysis of material performance. This evidence again supported the hypothesis that thin polymer films, where the expelled solvent can easily evaporate out of the bulk material, are required. Another observation from the mould casting was that the polymers appeared to solidify at the polymer-air interface resulting in a capsule-like film after the initial room temperature cure, which is shown in Figure 130. This film production at the air interface is most likely a result boronic ester hydrolysis at the air interface causing a skinning effect. Another method to attempt to fix the bubbling issue was to introduce a vacuum as the polymer cured. However, this appeared to exacerbate the problem further, by forcing movement through a glassy network material, as shown in Figure 131, which seemed to expand the material and increase the size of the bubbles within the final material. The solution to this problem is discussed in Section 4.4.
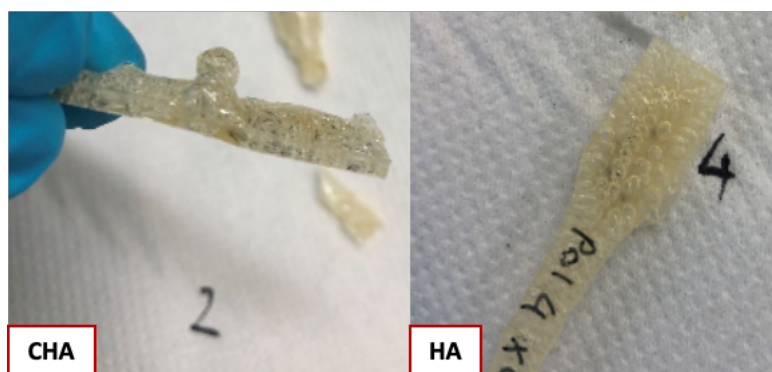
Figure 129: Pictures of bubbles present in thermally treated DER 332-based polymer networks with 40% consumed DEA by diboronic acids.
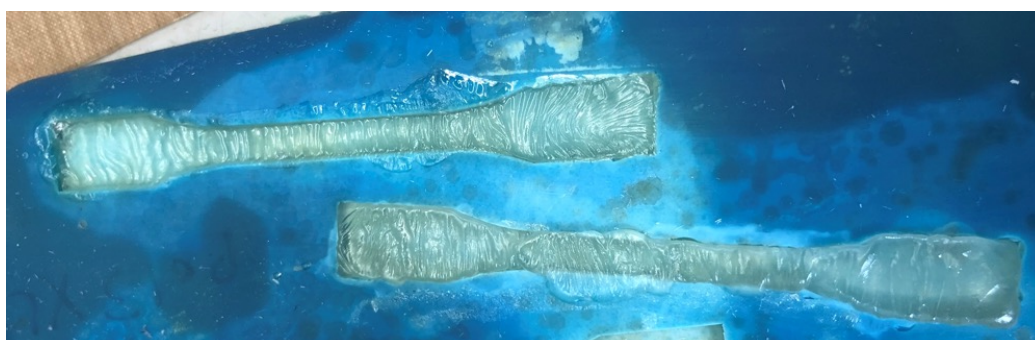
Film Formation
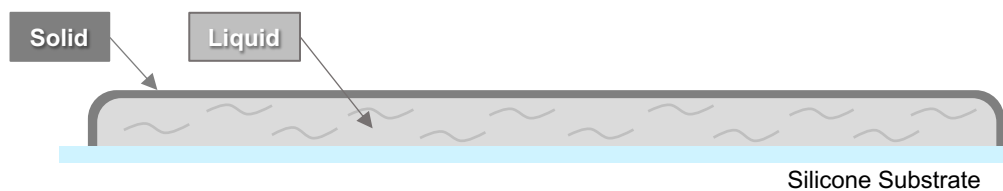
Figure 130: HA-E1(DEA-5)-D40 polymers cast into silicone moulds after a room temperature cure for 24 hours and a visual depiction of the film observed.

177

Figure 131: post-thermal cure, under vacuum, HA-E1(DEA-5)-D40 polymer.

However, a more encouraging prospect was that the crosslinked network could be released from silicone with ease and proved to be a promising substrate to persevere with, which will be discussed further in Section 4.5.

4.4 Hydrolysis Prevention

Prior to developing the polymer structure to overcome the brittle polymer issue, which is discussed in 4.6, it was clear that better measures were required to control the exposure to the moisture present in air, as this would fluctuate day to day. To limit the air exposure during mixing, the epoxy and amine functional monomers were charged to a round bottom flask and flushed with a constant flow of an inert gas, such as nitrogen, whilst initial mixing occurred. This was followed by addition of the pre-weighed mass of boronic ester (**6**), which had previously been stored under argon to limit any degradation back to boronic acid, before using a syringe to transfer to the reaction vessel. This was employed as a preventative measure, to ensure there was minimal boronic acid precipitating out of the mixture whilst the reaction proceeded, to ensure the desired number of crosslinks were able to form to create the network.

The highest risk of boronic ester hydrolysis in the polymer preparation methods arises from the prolonged curing times after draw-down, as they are left at room temperature

for 24 hours. Due to the extenuating circumstances presented by the covid-19 restrictions, there was no access to a glovebox available. Initial tests of an inert atmosphere, on polymer HA-E1(DEA-5)-D-40, seen in Figure 132, revealed that there was no wrinkling evident after 24 hours at room temperature. This supports the hypothesis that the exposure to air contributed to the wrinkling phenomenon, which may arise due to the skinning effect observed.
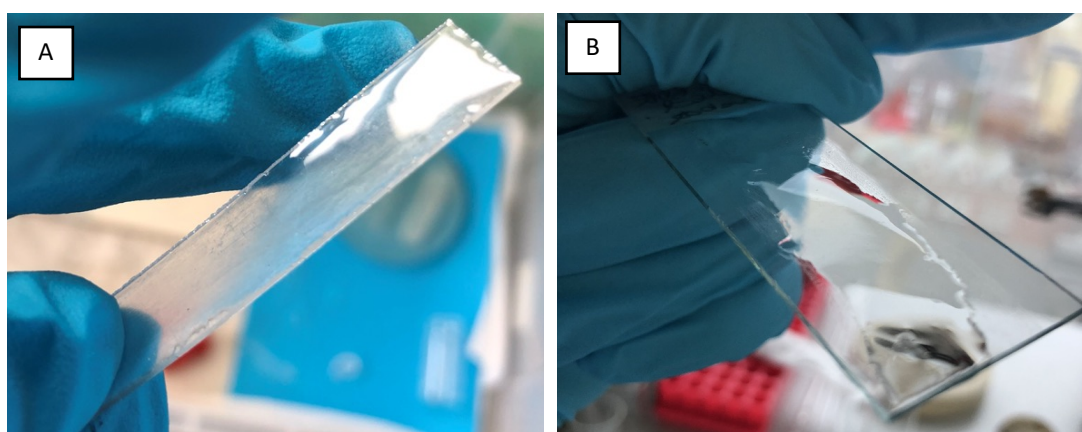
Figure 132: Polymer HA-E1(DEA-5)-D-40 after a room temperature cure for 24 hours under an argon filled AtmosBag when A) cast into a 1 mm thick silicone mould and B) drawn onto a glass substrate at 400 µm.

Although the room temperature cure provided smooth polymers without bubbles, the thermal cure did produce some bubbling in the free polymers from the thicker mould method, which is shown in whilst the thinner draw-down on glass remained defect free. Therefore, it was concluded that 400 µm would be the best thickness to overcome the bubbling moving forward.
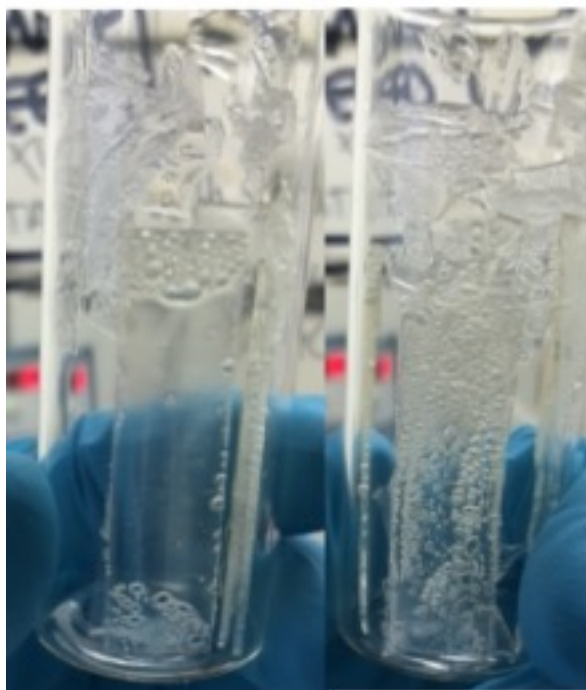
Figure 133: Polymer HA-E1(DEA5)-D-40 free from its substrate after a thermal cure at 80 °C.

As the AtmosBag method was impractical for preparing multiple different polymers at the same time, another method of inert curing was required. A new method was developed alongside preparation of the less brittle polymers (HA-E2), which are discussed in Section 4.6. This method was constructed to provide a constant flow of N_2 over the curing polymers, whilst maintaining the freedom of drawing-down without practical hindrances. This was achieved by means of directing the flowing gas through a funnel that was positioned directly above the polymers, as depicted in Figure 134. This method proved to be useful for preventing the hydrolysis and precipitation of the boronic acid throughout the remainder of the research program.
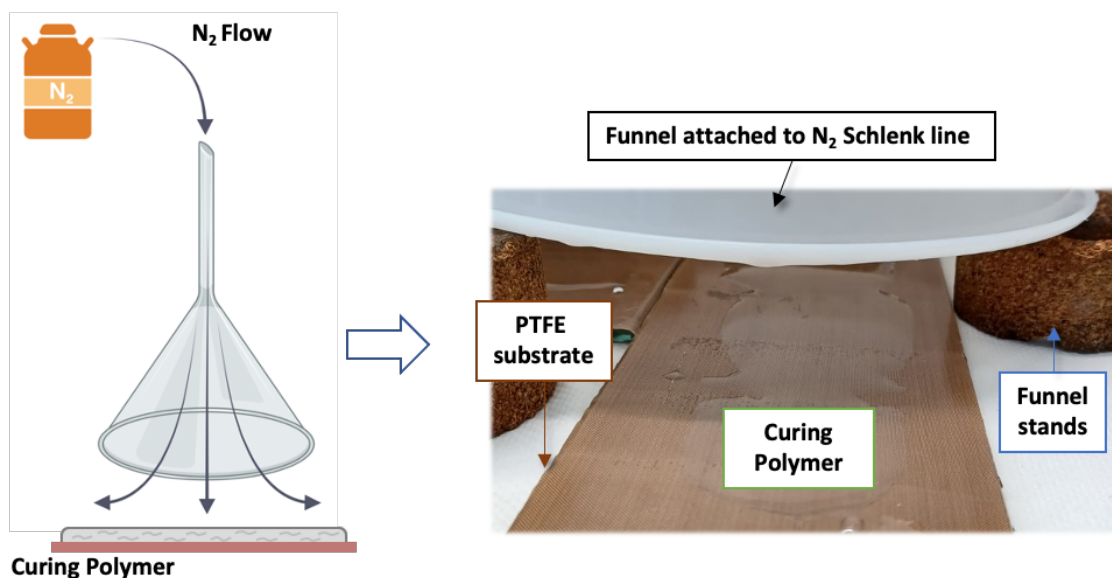
Figure 134: Nitrogen funnel curing visualisation and practical incorporation.

4.5 Substrate Development

The glass microscope slides were not ideal substrates for achieving free films because the polymers remained adhered to the glass after curing. Another concern to address was the wrinkling of the polymer films which has been attributed to the creation of internal stress in the polymer, during the cure process. Therefore, a release agent was primarily trialled in attempt to achieve a free polymer thin film and hopefully reduce wrinkling. Marbocote 227 CEE (aliphatic hydrocarbon based) was employed as the release agent a since it is specifically designed to release epoxy-based thermosetting resins and can easily applied to the substrate by brush or cloth application directly to the glass substrate, according to the manufacturers guidance.[228] However, upon draw-down attempts, an even film could not be attained as the polymer would coagulate into a non-uniform shape, thicker than the original draw-down thickness. This was in response to the extreme non-stick surface achieved via the Marbocote addition but due to the lack of uniformity of the resulting polymer film, the desired dimensions required for tensile testing could not be cut.

The next substrate tested was a silicone baking matt. The polymers would stick to the substrate just enough to maintain its shape but could still be easily removed when solidified, by removal with a thin spatula. This worked well to achieve free polymer films after a room temperature cure for 24 hours, as shown in Figure 135. However, some warping of the material occurred in places as the polymer cures. This was attributed to the tendency of the silicone matt to move with the polymer still attached, in response to polymer shrinkage, or if the matt had been bent in storage, the polymer would respond to the shape of the bend in the substrate. Furthermore, the resulting polymer networks appeared to become slightly opaque, which was likely due to the polymer taking on the texture of the substrate it was attached to. This was also evident when a non-stick PTFE baking sheet was used as a substrate. This material had an obvious texture to it and the resulting polymers also maintained the texture once removed in the glassy state as well as being more prone to warping as the polymer cured due to it being a thin paper-like material.
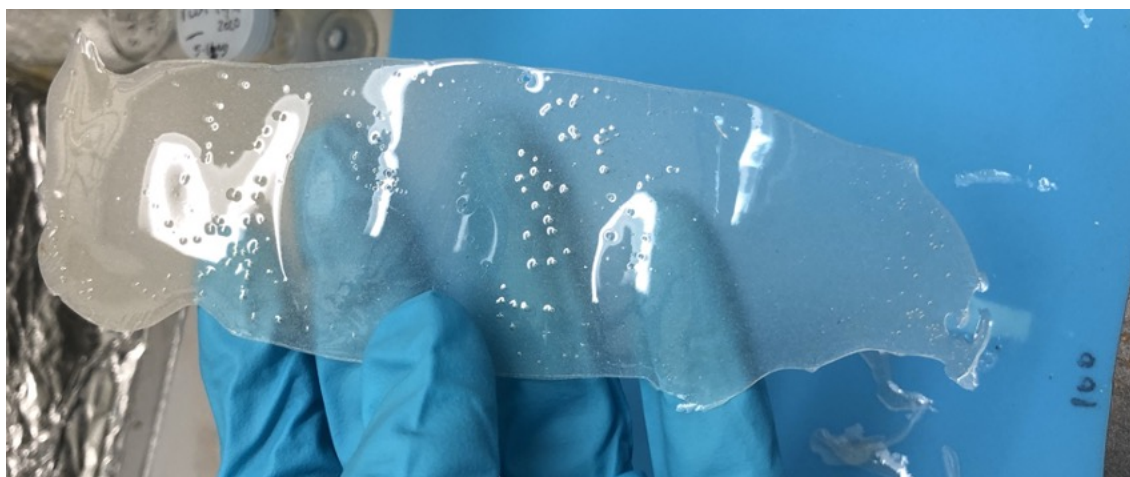
Figure 135: Polymer HA-E2(DEA-5)-D-100 after room temperature cure for 24 hours under the N_2 flow through the funnel.

To develop the polymers into more uniform samples, it was hypothesised that a non-moveable solid, non-stick substrate would be ideal. Thus, utilisation of a large glass plate with a non-stick PTFE tape adhered was trialled, as the non-stick surface could not move

during curing, due to the adhesion strength of the tape to the glass being more than the grip of the polymer on the PTFE substrate. Upon comparison to the polymers removed from the silicone sheet, the polymers from the PTFE taped glass substrate was more transparent, which is shown in Figure 136. Polymers also appeared to be more uniform in thickness on the PTFE taped glass as this was the most uniform substrate and could remain level on the lab bench without the need for a tray for movement between the fume-hood and oven. This impacted the silicone materials due to the fact the trays were not always level and thus, liquid polymer pooled to a side more due to gravity.
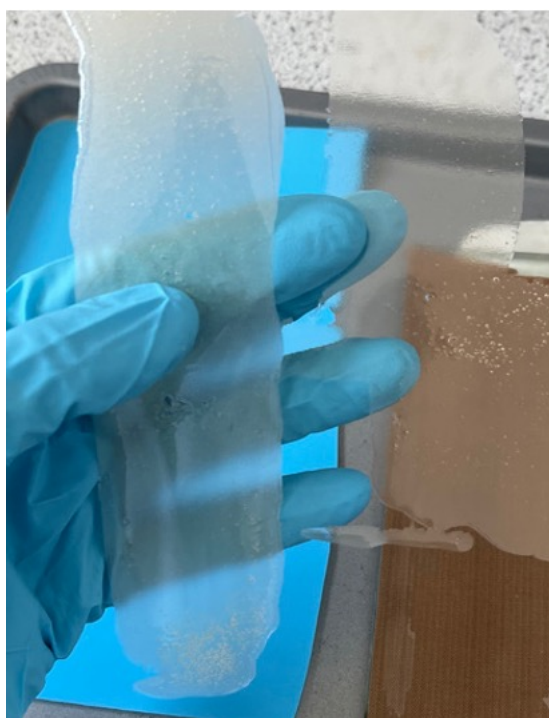
Figure 136: Picture of HA-E2(DEA-5)-D-100 after release from silicone (left) and PTFE (right).

4.6 Linear Epoxy Modified n-Hexylamine-based Polymer Networks (HA-E2)

As discussed previously, an improvement to the polymer formulation was required to overcome the brittle polymer concern arising in the earlier polymeric materials. It was hypothesised that inclusion of a di-functional, linear aliphatic epoxy monomer, instead of an aromatic epoxy, would produce less rigid and less brittle materials due to having

increase degrees of freedom and molecular motion along the polymer backbone. It would also be likely to decrease any secondary molecular interactions such as pi-pi stacking between aromatic rings of different polymer segments. Furthermore, it was hoped that reducing the chain rigidity would lower the materials T_g.

On another note, it was previously observed that the n-hexylamine-epoxy-boronic polymerisation reactions appeared to proceed relatively fast with the inclusion of catalyst, as was observed by the film produced in Figure 115 compared to the viscous liquid without catalyst. This was therefore removed from the polymer formulation, to allow sufficient time to prepare draw-downs, whilst the polymer was still a liquid and try to prevent a skin forming before the draw-down was completed. The DMP-30 catalyst was also deemed unnecessary due to adopting a cure schedule with a thermal post-cure. The removal of catalyst would also reduce the risk of epoxy homopolymerisation reactions occurring and ensure that all of the epoxy functional groups would react with the amine group twice to form the desired DEA functional groups, for subsequent reactions with the boronic ester (**6**).

Moreover, the inclusion of a monofunctional epoxy (phenyl glycidyl ether – PGE) was maintained in the formulations to limit the epoxy-amine polymer chain growth and provide a variable that can control the average molecular weight of the chains. As PGE controls the degree of polymerisation, it also has some control over the average functionality of the polymer chains. In this project, they were still designed to have a number average functionality of 5 DEA functional groups and the intended structure is shown in Figure 137, with a target number average molecular weight of 1615 g mol^{-1}.
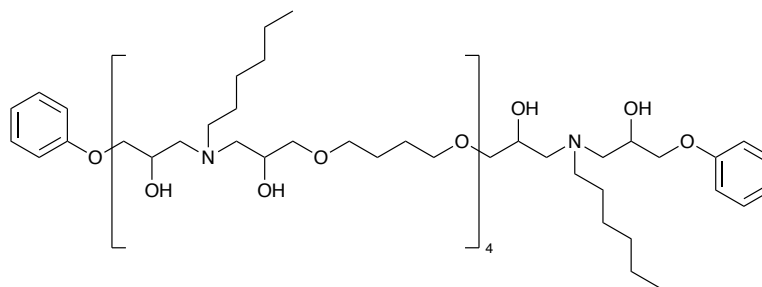
Figure 137: HA-E2 polymer formulated to have 5 DEA functionalities per chain.

PGE controls the average functionality of the polymer in this case since it controls polymer chain growth. Therefore, controlling the functionality can provide a route for controlling the desired properties of the material. For example, one can adjust the crosslink density to obtain a material as a glassy, network or as a rubbery thermoplastic by manipulating the formulations to result in a P_{gel} value < 1 (network) or > 1 (thermoplastic), which represents the reaction extent needed to meet the critical gel point (P_{gel}). In the case of the linear polymer depicted in Figure 137, the P_{gel} value is 1.22 based on an average epoxy functionality of 1.67 and average amine functionality of 2. The calculations of this value can be found in the appendix, Section 10.2. As a result, this formulation will never achieve gelation as it would require a 122% reaction extent.

Additionally, the control material so far throughout this research programme has been based on the linear thermoplastic polymer. However, in order to compare the effects of boronic ester crosslinks on the structure-property relationship of the material, a complimentary control material was required to deliver a similar representation of a standard epoxy-amine polymer network. Therefore, the control material used throughout the remainder of this research would utilise a diamine with a functionality of 4 to incorporate crosslinks concomitantly with the 2 functional n-hexylamine. This would ensure the number of crosslinked junctions in the control material would equal the number of crosslinks in the boronic ester network, where the DEA is consumed. As the amine is what forms the DEA groups in the material and hence, is a point of crosslinking

for both comparative materials. This was deemed to be the fairest comparison of evaluating the performance of the novel epoxy-amine-dioxazaborocane material and how it may differ from a standard material of the same class of polymer.

It is predicted that the dioxazaborocane material should behave as a covalent adaptive network, as discussed in Section 1.4.2.6.1. This means that the materials are expected to be able to relax stresses or self-heal in response to stimuli known to affect boronic esters, such as heat or pH. Consequently, it was anticipated that in order to achieve a covalent adaptive network, the boronic ester material would likely require unoccupied DEA sites to allow boronic transesterification to occur. Therefore, varying the percentage of crosslinks (occupied DEA sites) may alter the recycling behaviour of the material as well as the material properties such as ultimate tensile strength (UTS) and Youngs modulus (YM), providing another controllable variable.

A series of materials were fabricated, both the comparable epoxy-amine crosslinked polymers (A series) and dioxazaborocane crosslinked polymers (D series), with a systematic range of varying crosslink densities, ranging from 0% to 100% (A/D0 – A/D100). The structures of the polymers under investigation are shown in Figure 138 and would represent a material with 20% crosslink density (occupied sites). In the A series polymer, the corresponding unoccupied sites were designed to arise from n-hexylamine in order to obtain materials with a consistent polymer backbone to allow maximum molecular synergy between the A-series control polymer and the novel D-series polymer.
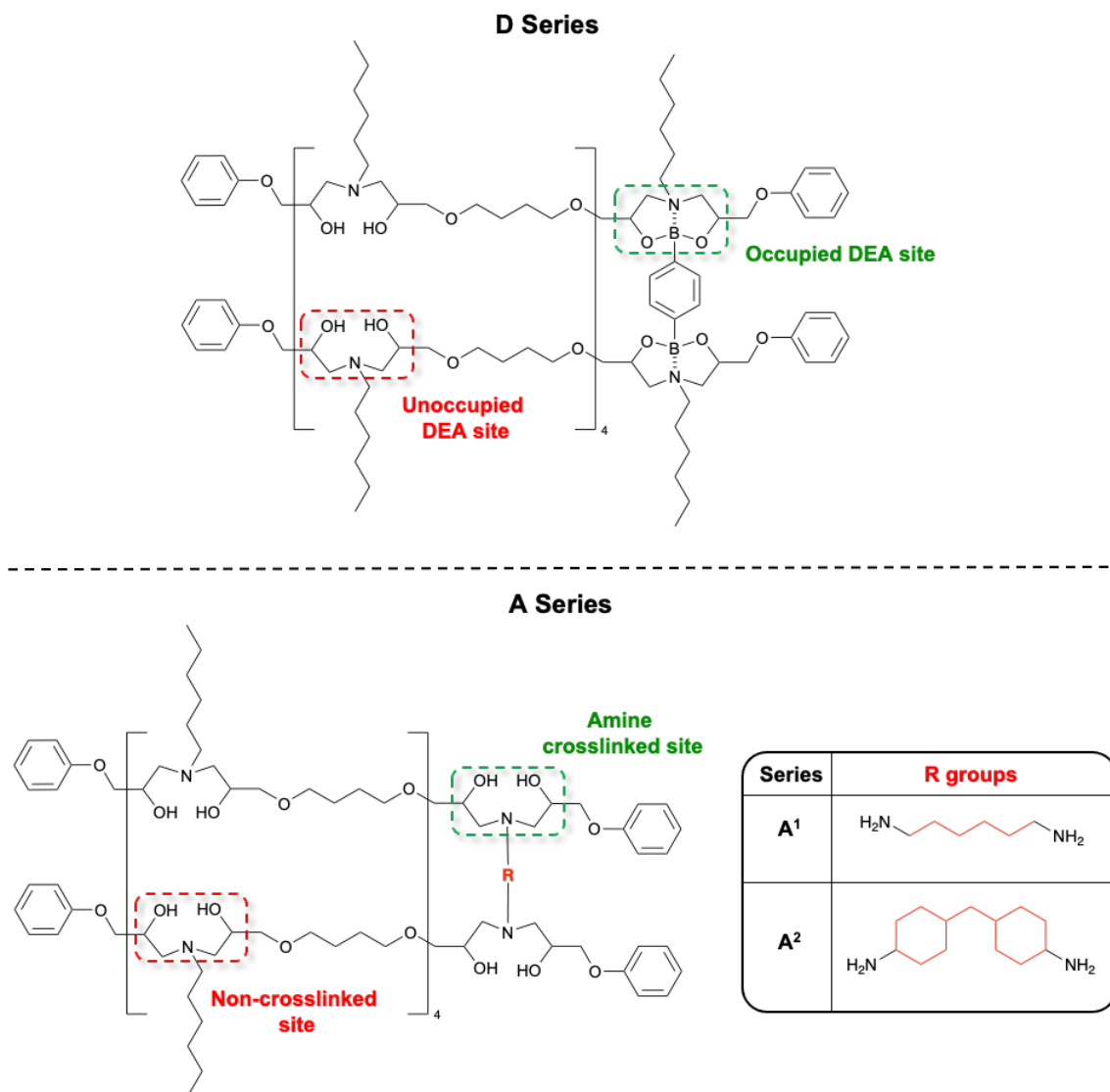
Figure 138: HA-E2 based dioxazaborocane and amine polymers prepared in this research, where the percentage of unoccupied and non-crosslinked sites vary. The R groups responsible for crosslinking in the A-series arise from 4-functional amines - dihexylamine (A[1]) and PACM (A[2]). The red sections of the diamine structures shown correspond to the red R group in the polymer structure.

The one-pot synthesis strategy, incorporating the N_2 funnel cure environment, followed by a thermal cure, was retained for the remainder of this research. Table 15 shows the percentage crosslink density of the polymer backbone based on the number of occupied sites, which could be calculated as a percentage of the total moles of amine groups in the reaction, as these were the reactive functionalities that facilitated crosslinking in the D-series materials. For the equivalent A-series polymer, the ratio of diamine to n-

hexylamine was calculated as a percentage of the total moles of epoxy in the reaction based on the required crosslink density.

Table 15: HA-E2(DEA-5) type polymers prepared in this research.

Series	Occupied Sites / % (dioxazaborocane (D) / diamine (A))	n-Hexylamine / %
Linear thermoplastic Polymer (A/D)	0	100
D	20	100
	40	100
	60	100
	80	100
	100	100
A	20	80
	40	60
	60	40
	80	20
	100	0

The main difference in the synthetic procedure of HA-E2(DEA-5) polymers, compared to previous methods, is that the reaction mixture was heated in the flask before drawdown. The reaction was heated at 55 °C until there was a clear increase in viscosity, which was evident upon the appearance of air bubbles forming during stirring. Heating the mixture promotes high conversion and eliminated the need for a catalyst to reduce reaction time. It was found that 1 hour and 30 minutes at 55 °C was ideal to ensure a smooth draw-down on a non-stick substrate (Silicone or PTFE plates) which did not coagulate if a network material was fabricated. Materials with a crosslink density below 40%

188

coagulated after drawdown for both the A and D-series. This is likely due to the formulation not meeting the required stoichiometry to achieve P_{gel}. This method produced polymers with a range physical states. A/D-0 were liquid and did not vitrify upon thermal cure. D20 and D40 were low viscosity polymers at room temperature which is likely due to not achieving P_{gel}. D-60 to D-100 were solid, brittle materials. The A-series material followed a similar trend upon increasing crosslink density. However, the resultant materials were not brittle and offered a good degree of flexibility in the resultant films. The dihexylamine crosslinked materials (A[1]) were observed to be more flexible than the PACM (A[2]) materials.

4.6.1 Aromatic HA-E1(DEA-5) A[3]-X System

Upon thermal and mechanical testing, it was apparent that the A[1] and A[2] polymer series were in the rubbery state with T_g's mostly below room temperature, therefore an aromatic epoxy monomer was utilised in the formulations as a representative high-performance epoxy-amine (non-adaptable) comparison, which will be discussed in Chapter 5.

4.6.2 P_{gel} Estimations of HA-E2(DEA-5) Polymers

In order to determine whether the materials were a network or thermoplastic, P_{gel} values could be obtained from Equation 3 in Section 1.1, and the results are shown below in Table 16. The calculations of these values can be found in the appendix chapter, Section 10.2.

Table 16: P_{gel} value calculations for HA-E2(DEA-5) polymers.

Occupied sites / %	P_{gel} value
0	1.22
20	1.04
40	0.91
60	0.83
80	0.76
100	0.71

For calculating the P_{gel} values across both the A and D series, the route of polymerisation was expected to be equal, with regards to crosslinking. This is due to the dioxazaborocane networks being designed to have the same number of crosslinks per polymer chain that are also designed to have an average of 5 amine groups per chain. The P_{gel} values, at various crosslink densities (0%-100%) of the traditional amine polymers (A-Series) were calculated with a constant stoichiometry value (r) of 1, as the stoichiometry of amine to epoxy remained constant and the variability in the P_{gel} calculations was the average functionality of the amines (F_b). However, when applying P_{gel} to the dioxazaborocane D-Series, the stoichiometry of crosslinks are designed to equal that of the amine, therefore, for the P_{gel} calculations the boronic ester is treated as a 4-functional amine with regards to the Flory-Stockmayer theory. The boronic ester is treated as such because there would need to be 4 amine epoxy reactions in order for the boronic ester to form a crosslink, meaning a functionality of 4. This method was chosen as the best representation of the critical gel point and has been visualised in Figure 139. In order for a network to theoretically be formed the percentage of crosslinking must be at least 25%, and based on the assumptions in this theory, which were discussed in Section 1.1.
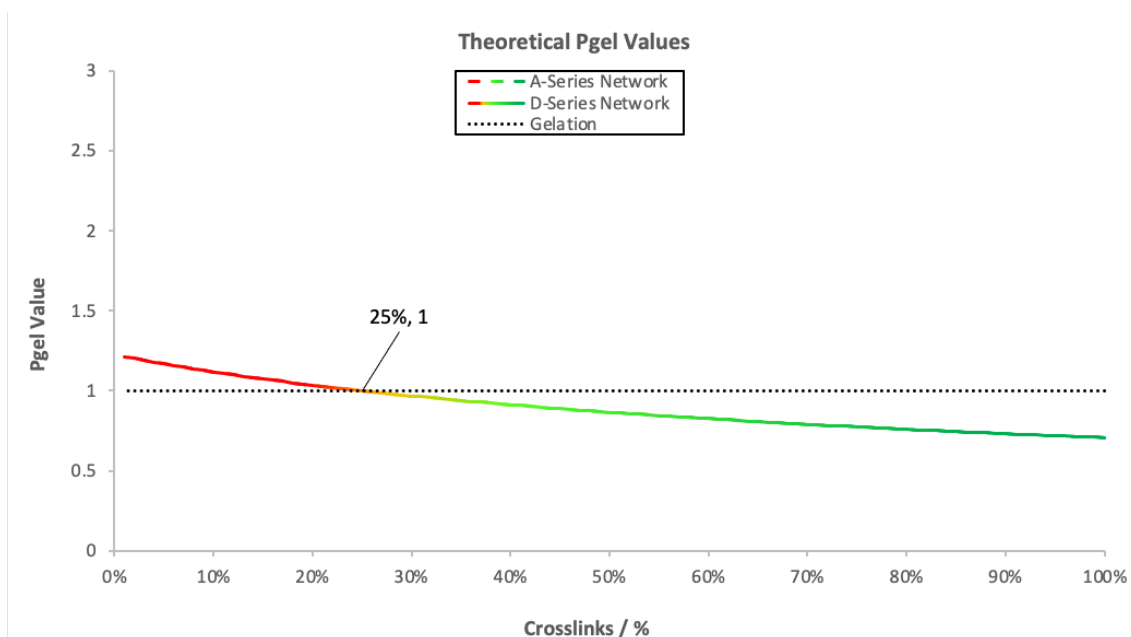
Figure 139: P_{gel} estimations from Flory-Stockmayer theory (Equation 3)

Observations of the polymers fabricated are supported by the determined P_{gel} calculations as the linear (thermoplastic) polymer was a viscous liquid after curing. Furthermore, the viscosity of the polymer materials appeared to increase gradually as the crosslink density increased, from 0% to 40% crosslinks where 40% was observed to be a soft, tacky solid. As 40% was likely to have surpassed the critical gel point, the T_g of the material is likely to be below room temperature and therefore causes this to be a network in the rubbery physical state. Between 40% and 60% crosslinks is where the physical state of the material changes from a rubbery state that can flow to glassy state that cannot flow. This is a likely result of the glass transition temperature (T_g) of the material increasing due to the increasing crosslink density restricting the segmental motion of the polymer chains. Therefore, determination of the T_g is vital to understand the relationship between the crosslink density and the material behaviour. The T_g of the materials will be discussed further in Section 5.1.1.

4.6.3 Thermally Accelerated Polymer Degradation

Another noteworthy observation of these materials was that, upon increasing boronic ester content, the materials are considerably more colourless, which is shown in Figure 140. The linear (thermoplastic) polymer is considerably more discoloured (yellowing) after a thermal cure compared to the highly crosslinked D-series, whereas the A-series polymers remained similarly discoloured regardless off the number of crosslinks. A well-known cause of discolouration in epoxy-amine polymers is through irreversible degradation mechanisms, such as radical oxidation in the presence of air.[229–232]
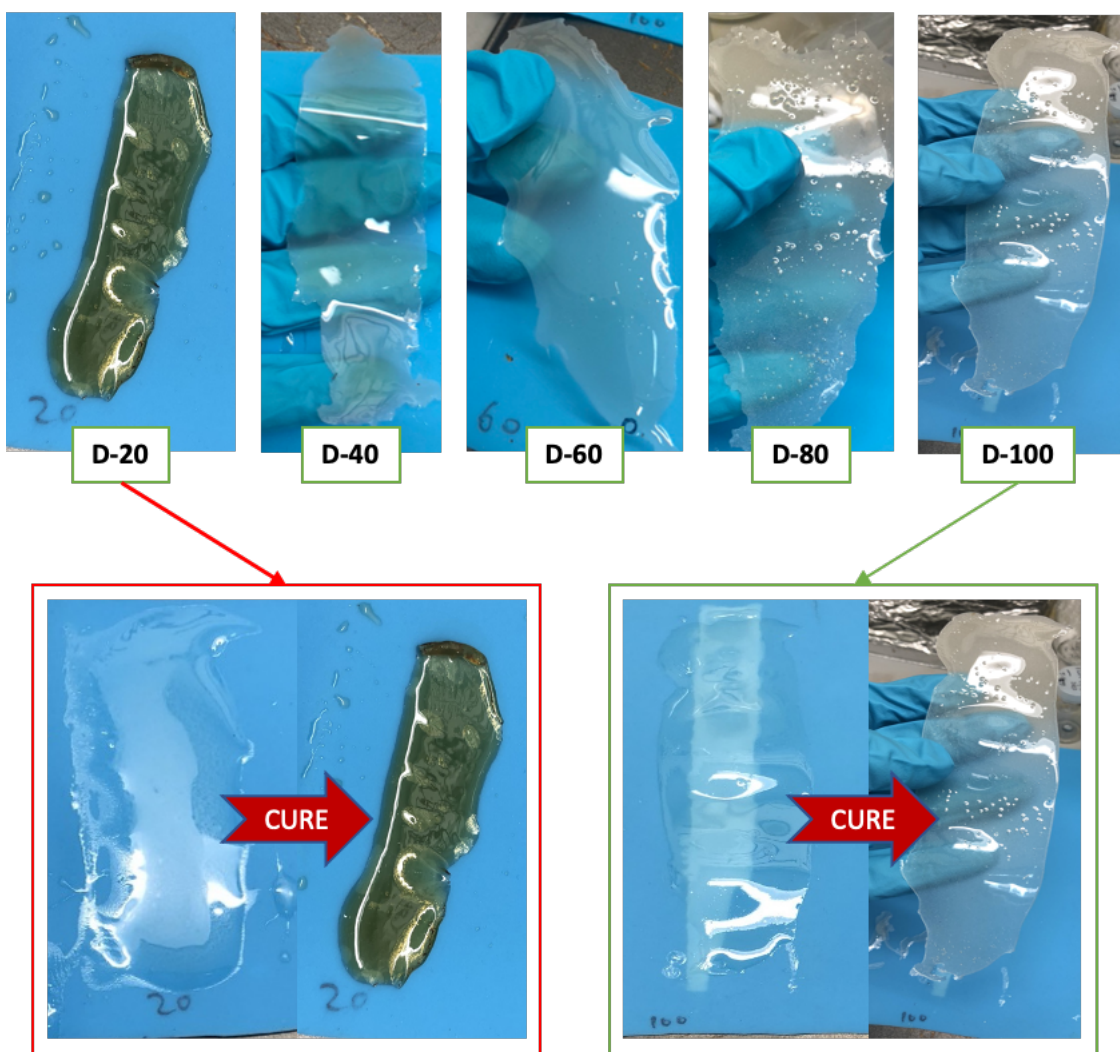
Figure 140: Thermally induced yellowing in the HA-E2(DEA-5) D-series after a thermal post-cure at 80 °C.

In the case of the polymers investigated in this research, discolouration is hypothesised to be accelerated by heat, since the discolouration did not occur until the thermal post-cure. Thus, a thermally accelerated amine oxidation mechanism is considered to be the origin of the colour change. The exact mechanism behind the cause has not been investigated further in this research since all the fabricated polymers have been treated with the same thermal post-cure. However, it is hypothesised that the reduction in the discolouration, upon increasing crosslinks, in the D-series polymers has been attributed to the increased consumption of the DEA functional groups by the boronic ester.

4.7 Conclusions

In the pursuit of polymer network films suitable for mechanical testing, chemical manipulation at the molecular level and polymer fabrication methods have been developed that 1) minimise boronic ester hydrolysis by utilising inert curing environments, 2) procure hard network films, free from substrates, which do not suffer from extreme brittle properties and finally 3) minimise defects (bubbling) in the material that arises from expelled butanol during the dioxazaborocane crosslinking reaction.

Chapter 5

Characterisation and Material

Performance

5   Chapter 5 – Characterisation and material performance

This chapter is dedicated to characterising the thermal and molecular aspects of the dioxazaborocane thermoset polymers (D-series) and subsequently comparing these to equivalently crosslinked epoxy-amine thermoset polymers, which have been chosen to be the best representation of a covalent (non-adaptable) network in this work. The tensile properties are assessed to determine the ultimate performance of the material as this is indicative of potential high-performance end-use applications, such as those utilised in wind turbine blades.

5.1   Thermal Characterisation

5.1.1 T_g Determination by DSC

5.1.1.1   Introduction

Dynamic scanning calorimetry (DSC) is a technique utilised in polymer chemistry for the thermal analysis of polymers. DSC measures the heat flow to or from a sample as a function of time in response to a programme of controlled heat changes. The results reveal important phase changes, by analysis of the thermogram produced. As a thermoset does not melt, DSC also reveals 2nd order transitions such as the glass-transition temperature (T_g), which is a subject of investigation for the polymer networks fabricated throughout this research. Measuring the T_g provides insights into possible end-use safe service temperatures and the limitations associated with this. It also provides valuable information about the morphology of the network and supports the performance evaluation in Section 5.4.1.3.

5.1.1.2   Instrumentation and Sample Preparation

The instrument employed in this work is a power compensation DSC, which utilises two aluminium sample pans, one of which remains empty as a reference the other containing a small amount of sample (around 2 mg - 20 mg). Both pans are heated in separate cells

within two separate furnaces and kept at the same temperatures, by varying the power input to the furnaces in response to exothermic or endothermic changes. The differential heat input required to maintain the temperatures is measured as the specific heat capacity or enthalpy change in the sample cell relative to the reference cell. The specific heat capacity of a material is defined as the heat capacity divided by the mass, with the heat capacity being defined as the amount of heat required to induce a single unit change in temperature. A material in the glassy state has a lower heat capacity than when in the rubbery state, therefore this difference in heat capacity induces a visible gradient step change (Figure 141) during the temperature range where these transitions occur. In addition, the rate of heating can enhance small transitions in the material. For example, in polymers where the T_g is barely observable at a standard heating rate of 20 °C per minute, hyper-DSC (heating rate of 100 °C - 300 °C per minute) can be employed to enhance the transition step on the thermogram. However, the faster rate results in higher measured T_g values in comparison to the former (slower) heating rate. A typical thermogram is shown in Figure 141, indicating the glass transition. The T_g is typically be taken as the midpoint between the two tangents of the traces before and after the step change. DSC traces for polymers in this work can be found in the appendix in Section 10.1.6.
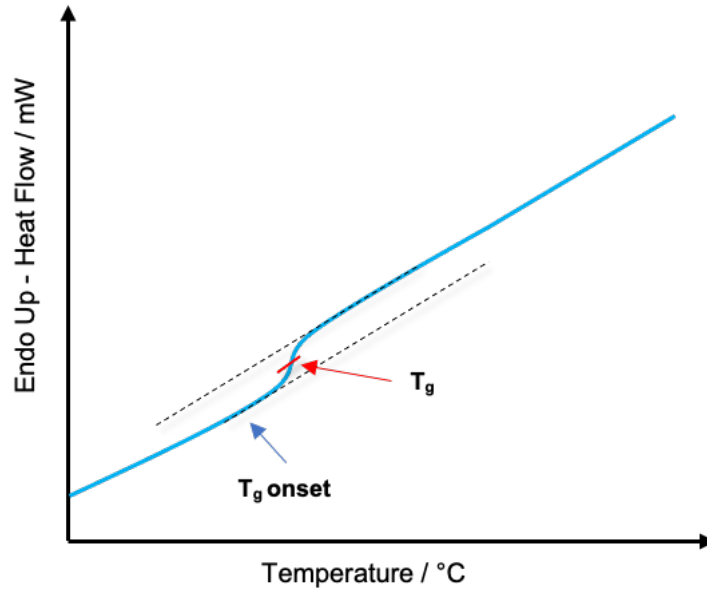
Figure 141: Typical DSC thermogram showing a T_g step.
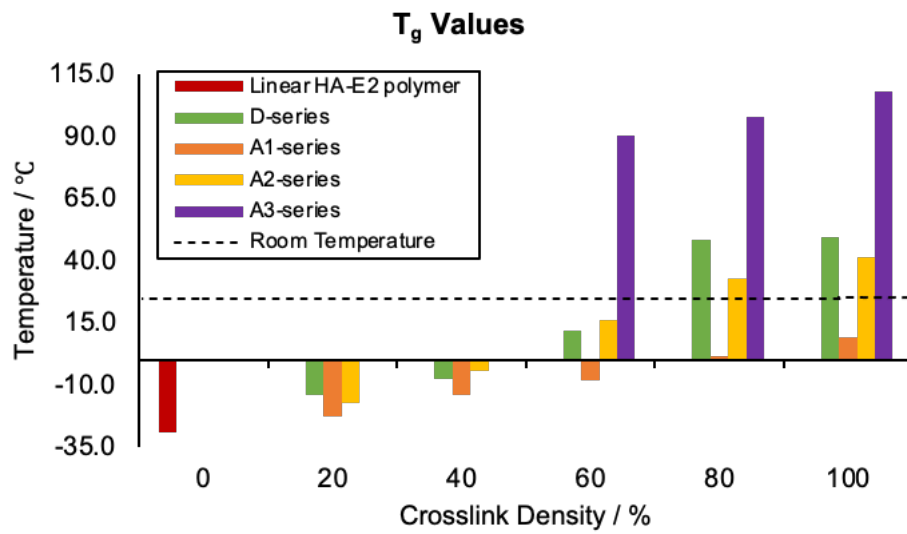
5.1.1.3 T_g Results

Figure 142: T_g temperatures for each polymer series studied in this research. A3-series is discussed later in Section 5.4.1.3. The black dashed line represents room temperature at 25 °C.

Table 17: T_g values of polymers studied in this research.

Polymer	% Occupied Sites	T_g / °C
Linear HA-E2	0	-29.2
D-20	20	-13.9
D-40	40	-7.7
D-60	60	11.7
D-80	80	48.3
D-100	100	49.7
A^1-20	20	-22.5
A^1-40	40	-14.1
A^1-60	60	-8.1
A^1-80	80	1.4
A^1-100	100	9.1
A^2-20	20	-17.2
A^2-40	40	-4.5
A^2-60	60	16.4
A^2-80	80	32.9
A^2-100	100	41.5
A^3-60	60	90.7
A^3-80	80	97.9
A^3-100	100	108.2

The T_g values obtained by DSC show increasing trends across all polymer series as the concentration/density of crosslinks increase. This evidence suggests that the T_g can be manipulated by crosslinking which adds a controllable variable to the polymer formulations. All of the polymer series were designed to have the maximum molecular synergy possible. From Figure 142 and the values in Table 17, it can be hypothesised that the A^1-series suffers from low T_g values as a direct result of the flexible 1,6-diaminohexane crosslinker as the values are significantly lower than that of the equivalent A^2-series, which utilised a cycloaliphatic crosslinking diamine (PACM). The A^3-series utilised the aromatic bisphenol A based diepoxy DER 332 (E1) and a cycloaliphatic amine (cyclohexylamine - CHA) for the unoccupied amine sites along with the cycloaliphatic diamine crosslinker (PACM). The results obtained show a large increase in T_g compared to all other equivalently crosslinked polymers in this research, which is attributed to the rigidity of the amine and aromatic epoxy monomers, resulting

in restriction of molecular motions and resulting decreased free volume. All of these factor then result in a material with higher T_g. The D-series materials were found to have slightly higher T_g values to the A^2- series at 80% and 100% crosslink densities, which is a likely result of the increased content of rigid 5,5-fused rings in the dioxazaborocane crosslinks. In contrast, the D-series could not meet the same level of T_g as in the A^3 series, which is due to the significantly increased rigidity designed into the polymer backbones via aromatic rings and cyclic amines. Furthermore, it is expected that the aromatic polymers may partake in other interactions, such as intermolecular bonding through pi-stacking, which would likely reduce chain mobility and influence the T_g.
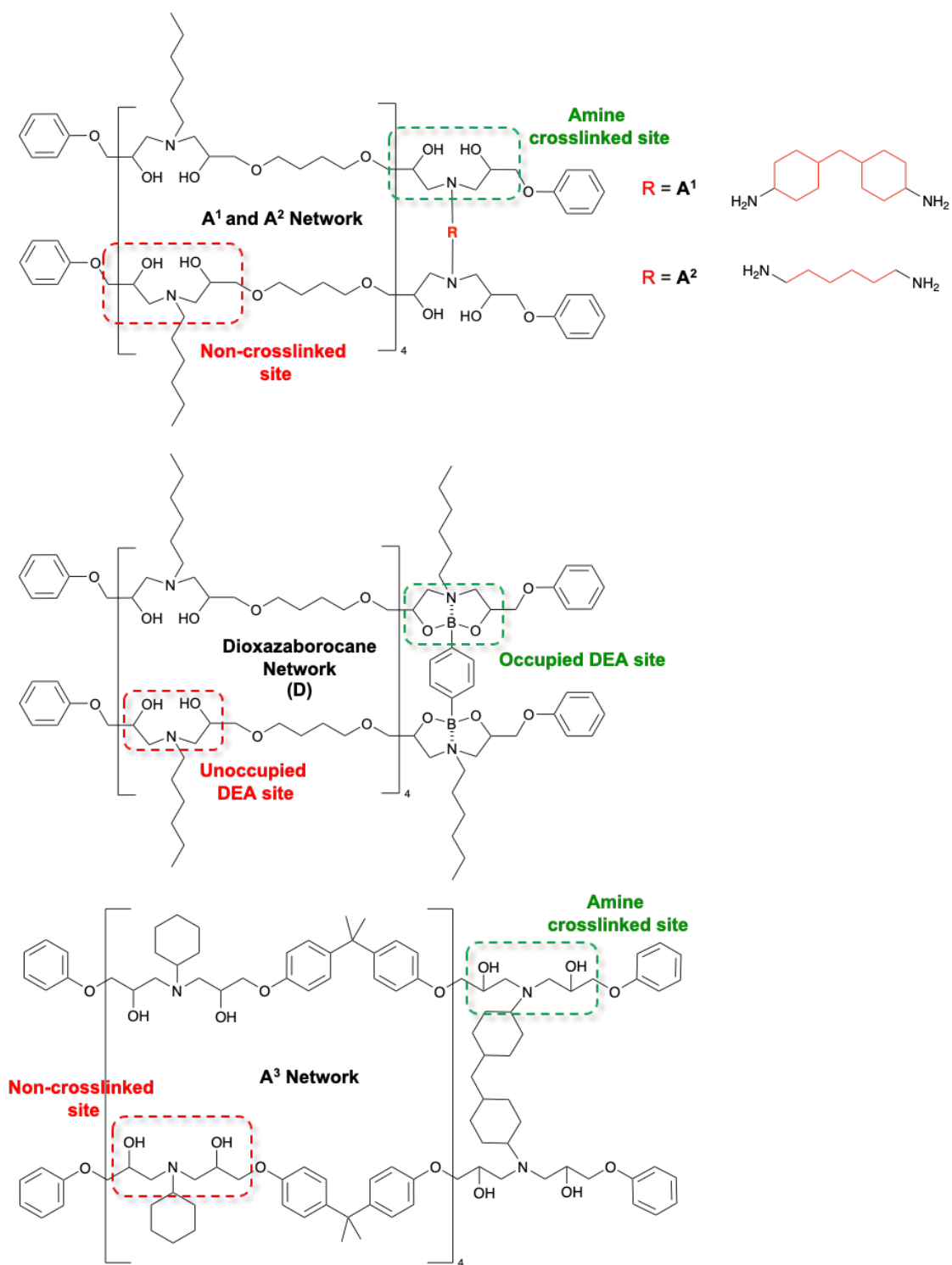
Figure 143: Network polymers characterised in this work using traditional amine crosslinkers and dynamic boronic crosslinkers in both aromatic and non-aromatic epoxy amine polymers. .

5.1.1.4 Factors Affecting the T_g

There are numerous factors that can influence the T_g of a polymer. One factor is the nature of the molecular motion in of the monomers.[233] As discussed briefly in the polymer development chapter, this research sought to utilise an aromatic epoxy as these are well known polymers with high T_g values, since the aromatic diepoxy monomers have restricted molecular motion, which increases the T_g. However, the high T_g came at the expense of brittle mechanical properties. The introduction of a flexible crosslinking monomer (A^1 - 1,6-diaminohexane) with increased molecular motion translated to increased segmental motion in the polymer chains, which enabled more flexibility in the materials and was evidenced by the lower T_g value. This evidence suggested that the final properties of the resulting polymeric material could be controlled at the molecular level. Another factor that can affect the T_g is the free volume in the polymer. The free volume of a polymer is the space in the polymer sample that is not occupied by the molecules of the polymer.[233] Polymers with increased degrees of freedom/increased molecular motion results in an increase in free volume within the material. This is seen in the resulting lower Tg value.

It is well known that properties such as polymer molar weight distribution, degree of branching and degree of crosslinking all affect T_g.[233] In amorphous polymers, increasing the molar mass of the polymer increases the T_g. For polymers with the same number average molecular weights (M_n), the polymer with more branching in the chain will have a reduced T_g. This is in relation to the free volume concept. With more branching resulting in a larger free volume. When an amorphous polymer is cured by crosslinking reactions, the free volume in the polymer drastically reduces and thus, an increase in T_g is observed. It is known that film thickness can reduce the T_g, when compared to the value of the bulk polymer, as there is thought to be more polymer mobility at the surface.[233] The surface of a thin film makes up a larger proportion of the polymer compared to the bulk and hence, can be seen by a fall in the T_g value.

For the polymers investigated in this research, the molecular architecture develops from a linear (thermoplastic) polymer with a controlled M_n value to a highly crosslinked (network) polymer. Therefore, significant changes to the T_g, throughout each polymer series, have been observed as a direct result of the changing free volume designed into the polymers. Furthermore, as the film thickness is intended to be the consistent for all polymers, this is unlikely to have a significant effect on the T_g results presented but is worth considering that the T_g observed in this research will most likely be lower than in the end-use material.

5.1.2 T_g Determination by Dynamic Mechanical Thermal Analysis (DMTA)

Another method of determining a material's T_g is by utilising dynamic mechanical thermal analysis. This technique applies a small sinusoidal deformation to the material and measures the response to stress, temperature, frequency or strain. Figure 144 shows the sinusoidal waves of the applied force (stress) vs the displacement (strain) indicating the phase angle (δ).
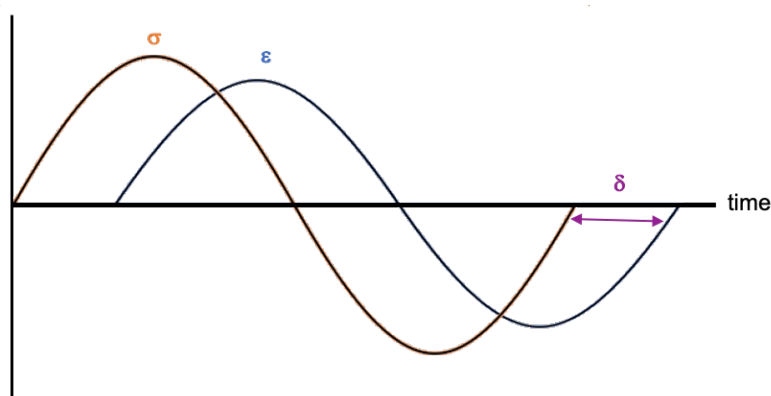

Figure 144: Sinusoidal wave relationship between stress (σ) and strain (ε) in DMTA analysis.

The main measurements taken from DMTA are the storage modulus (**E'**), Loss modulus (**E''**) and the tan delta *(tan δ)*. Storage modulus is a measure of the material's elastic behaviour, to store energy, and is defined by Equation 6 below.

$$E' = \frac{\sigma}{\varepsilon} \cos \delta \qquad (6)$$

The loss modulus is the material's ability to dissipate energy as heat. And is defined in DMTA by Equation 7 below.

$$E'' = \frac{\sigma}{\varepsilon} \sin \delta \qquad (7)$$

The loss factor or tan delta (**tan δ**) is the ratio between storage and loss modulus and provides a damping measurement. Damping is the dissipation of energy in the material in response to a cyclic load. This usually results in a peak that is often reported as the T_g of the material.

$$\tan \delta = \frac{E''}{E'} \qquad (8)$$

The model applied in DMTA is the crankshaft model, which treats the material as mobile segments that have some degree of motion, in terms of free volume, where the larger free volume coincides with increased mobility in the polymer chains. The movements are classified as α, β and γ transitions, by type of motion, an example of the α transition is the T_g (Figure 145) and β and γ are secondary transitions in the solid, glassy physical state.[234] These arise due to localised movements that do not disperse energy effectively, such as bending, stretching and rotation. The storage modulus curve can show these several phase transitions, as shown in Figure 145 for an idealised material.
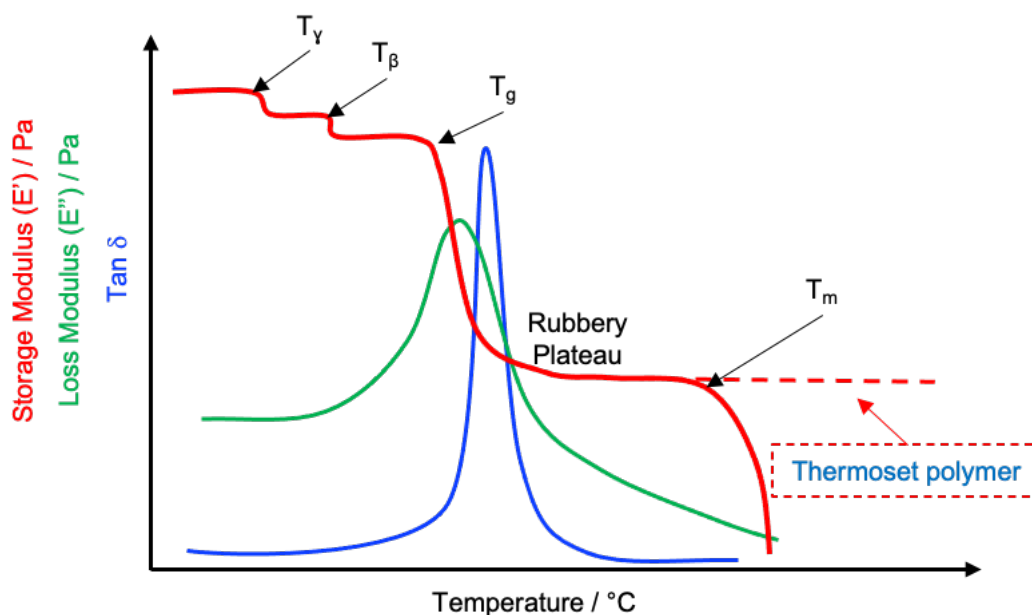
Figure 145: Example DMTA curves, for a typical amorphous polymer and thermoset polymer (dashed line). The storage modulus is shown in red, the loss modulus is shown in green and the tan delta is shown in blue.

The T_g onset of the material can be taken from the onset of the storage modulus curve before the sudden drop indicated on the graph in Figure 145, which induces mechanical failure of a material around this temperature. T_g can also be taken as the peak of the loss modulus, which is related to physical property changes and reflects molecular behaviour, such as the onset of segmental motion. From the Tan delta peak, the T_g midpoint reflects the temperature at which the material is at the midpoint of the glassy and rubber state.

5.1.2.1 DMTA Results

The T_g interpretation was quite difficult whilst utilising DSC as the method for the D-Series materials, due to the scarcely visible step in the curve this may occur as T_g onset may coincide with the onset of bond and topological rearrangements ($T_v < T_g$), as a result of this, T_g transition may be lost in the base line. DMTA analysis can often give clearer

T_g transitions, particularly T_g onset or tan delta peaks, which are both commonly referenced in literature. The A^1-series polymers with 60-100% crosslink densities were compared to the D-series with equivalent crosslinks in these experiments.

Temperature scans were performed on 30 mm x 5 mm x 0.3 mm rectangular samples and were analysed in tension geometry with a fixed length of 11.52 mm, a frequency of 1 Hz and a constant temperature ramp of 3 °C per minute from -80 °C to 170 °C . The results of these experiments are shown in Figure 146.

The results of DMTA analysis are in apparent agreement with the DSC trends, which show the dioxazaborocane crosslinked polymers having larger T_g values than their diamine equivalents. This trend was evident by all means of DMTA T_g characterisation. However, it became apparent, upon completion of the temperature programme, that the dioxazaborocane crosslinked materials were behaving unusually, both from the modulus results and upon physical inspection of the material. Figure 147 shows a material sagging as a result of either the oscillations or gravity (or perhaps a combination) in response to heat.
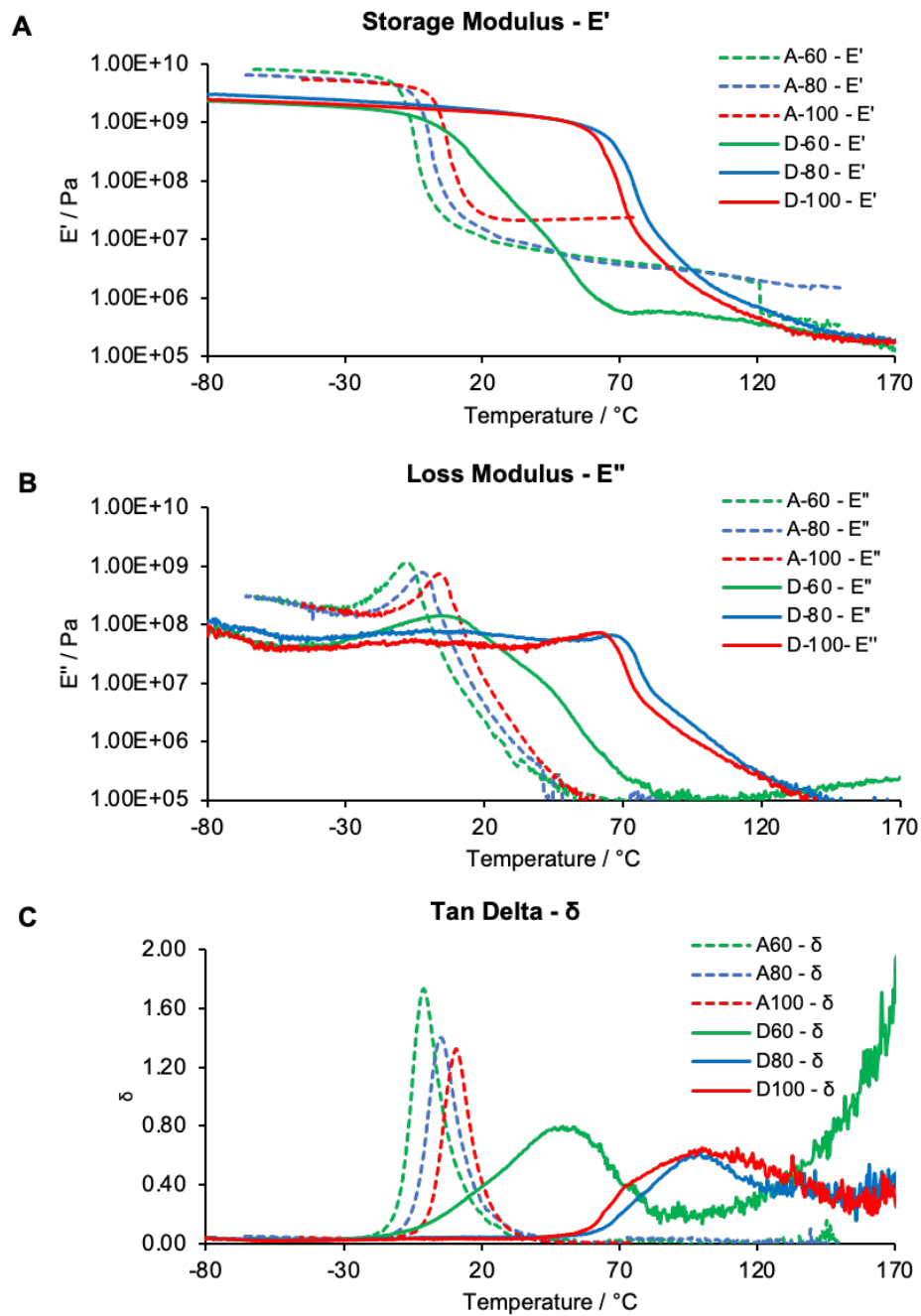
Figure 146: DMTA results of A[1]-series and D-series network polymers.
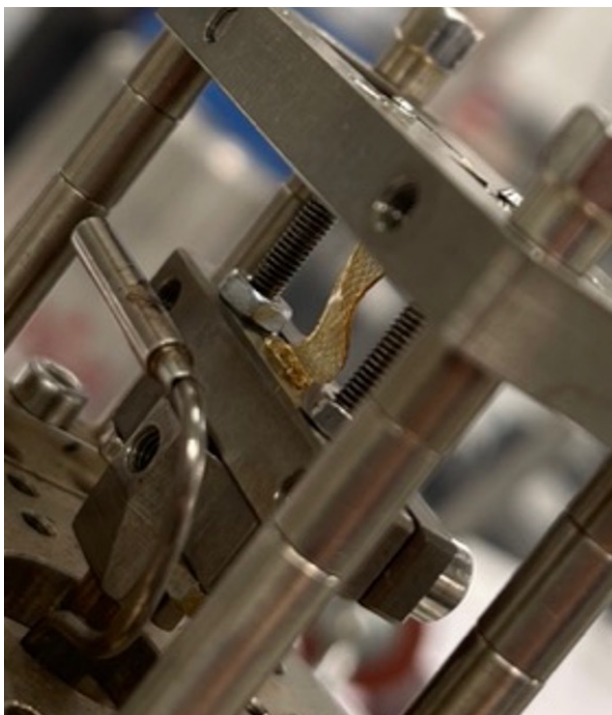
Figure 147: Picture of D-series material after completion of a DMTA analysis temperature programme showing sagging after exposure to heat under external force.

In this characterisation method, T_g onset (from storage modulus of from the beginning of the $\tan\delta$ peak) would be a useful measurement to use for analysis of the thermal behaviour of the polymer networks. As these materials are glassy at room temperature, the sagging phenomenon is expected to arise due to the temperature increasing above T_g. The sagging has been hypothesised to occur due to bond rearrangement resulting from the well-established exchange reaction of boronic esters with diols.[39,40,201,210,235–238] This is likely to cause fast topological exchange rearrangements by boronic transesterification. Ultimately, temperatures above T_g are hypothesised to cause mechanical failure, Thus, for this research, DMTA should provide useful insights of the upper service temperatures of the dioxazaborocane networks, since the sagging phenomenon is likely to render DMTA analysis of dioxazaborocane samples invalid for tan delta T_g assignment due deforming samples.

Upon inspection of the storage and loss modulus curves (Figure 146 - A and B), there appears to be a non-smooth decline after $T_{g\,onset}$, which indicates additional transitions. This is hypothesised to occur due to the boronic transesterification reactions rearranging rapidly between occupied (dioxazaborocane) and unoccupied (DEA) reactive sites in the polymer chains, as this non-smooth decline is not observed in the diamine crosslinked comparative samples. In addition, there does not appear to be any T_{β} or T_{γ} transitions visible before the sharp decline (T_g) of the storage modulus curves. This evidence suggests that the D-series behaves similar to the A^1-series materials below T_g and are both frozen in the glassy physical state. However, upon closer inspection of the loss modulus (Figure 148), there appears to be secondary transitions occurring around 0 °C, which may be indicative of the secondary transitions not visible in the storage modulus curve.
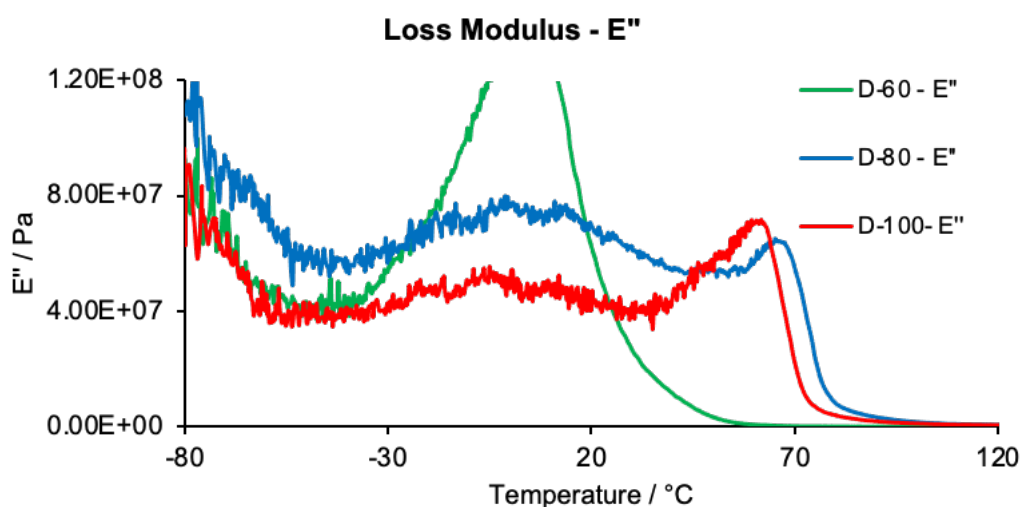
Figure 148: Zoom of the D-series loss modulus results in the temperature range below T_g.

It has been proposed, and discussed in Section 1.4.2, that the existence of a topology freezing temperature (T_v) for vitrimer materials, which would explain the unusual behaviour after T_g.[22,57,59,61] The T_v is the temperature at which the dynamic exchange reactions are 'frozen' and therefore topological changes in the molecular structure do not

occur within a visible timescale below this temperature. It is defined as temperature at which the material reaches a viscosity of 10^{12} Pa.[57,117,239] Thus, it is hypothesised that the boronic transesterification reactions is likely to have a lower T_v temperature than the material's T_g temperature and therefore, upon surpassing T_g onset, proceed to engage in fast bond exchange reactions. This could either result in a sharp decrease in viscosity (in a non-Arrhenius fashion) or result in energy dissipation process that are captured by the DMA. This is rarely seen in literature, as most vitrimer materials have an apparent T_v above the T_g, but it has been shown to occur by Nishimura et al. for silyl ether vitrimers, using the currently accepted method of calculating T_v from viscosity measurements.[239] Although, the viscosity of the material has not been investigated in this research, due to time constraints and equipment access throughout this project, but remains an interesting area of research to investigate in the future.

The tan delta curves (Figure 146 – C) show a broad peak for the D-series materials, in contrast to the A^3-series. This indicates the $T_v<T_g$ is therefore likely to be responsible for the unusual DMA curves. Also, since topological rearrangements after the onset of the T_g result in flow of the sample, the sample is no longer under tension in the DMA so measurements after this point are not able to be reliably analysed. The sagging of the material, in response to heat and stresses, suggests that the material may be in a viscous region, although thermosets do not typically experience this region. This hypothesis suggests that the D-series materials, behaving as a thermoset below T_g but as a viscous material after T_g, have the potential for thermal mechanical recycling, which will be discussed in Chapter 6. This would present an exciting progression in the field of high performing epoxy-amine thermoset materials which cannot currently be recycled.

5.1.2.2 Stress Relaxation by DMTA

Within the topic of vitrimer chemistry, activation energies of the dynamic exchange are often quoted. It is hypothesised that lower bond exchange activation energy's (E_a) correspond to a reduced energy barrier to rearrangement and hence, a lower temperature dependence, for the thermally activated system, and enhanced rates of exchange. These results are most commonly achieved by stress relaxation experiments, where the materials are subjected to a constant strain at specific temperatures, and the force response to maintain that strain is measured over time. A material with exchangeable bonds is expected to alleviate the stress in material caused by displacement, more than traditional thermoset polymers, where the bonds are essentially locked, and thus, the force required to hold the applied strain will decrease over time as the sample "relaxes". Stress relaxation experiments of vitrimers are usually conducted at elevated temperatures to avoid interference from the glassy state, and hence diffusion control, below and around T_g.

As the temperature is increased over a series of stress relaxation tests, the force required to hold the strain decreases, and it follows an Arrhenius temperature dependence relating to the kinetics of the dynamic exchange reactions. For example, at higher temperatures the dynamic reaction kinetics will have a faster rate and hence a faster relaxation time. Relaxation times are calculated following a Maxwell model, which defines relaxation time (τ) as the time required for the elastic modulus (G') to relax to $\frac{1}{e}$ or 37%, where Equation 9 defines G' values at specific times when the modulus has relaxed. [240]

$$G_{(t)}/G_0 \; = \; \frac{1}{e} \; . \tag{9}$$

The results are usually normalised and therefore, at a defined percentage of normalised stress relaxation ($\frac{1}{e} = 0.37$) on the relaxation curve, the activation energy of the dynamic

exchange mechanism can be extrapolated, by fitting the relaxation time by a straight line Arrhenius plot using Equation 10 below which gives Equation 11 as a linear Arrhenius equation, where τ is the time at $\frac{1}{e}$ and R is the gas constant.[117]

$$\tau = \tau_0 e^{-\frac{E_a}{RT}} \tag{10}$$

$$\ln \tau = \frac{E_a}{RT} + \ln(\tau_0) \tag{11}$$

The plot will show ln τ on the y-axis plotted against $\frac{1000}{T}$ (K^{-1}) on the x-axis and the slope of the tangent till give $\frac{E_a}{RT}$ from Equation 11 above and therefore an E_a value, expressed in kJ mol^{-1}, can be assigned.

In this research, attempts at stress relaxation experiments were attempted on a dynamic mechanical analyser in tensile mode (DMA 8000 – PerkinElmer). However, due to the sagging problem discussed in the previous section, above T_g experiments were unreliable for the D-series and attempts to collect this data would not produce meaningful results. Therefore, it was deduced that a rheometer utilising shear mode would better suit the dioxazaborocane materials at elevated temperatures. Due to time constraints of this project and gaining access to a rheometer limited this section of research. Stress relaxation data will be the main goal of future work, regarding the materials fabricated in this research. This will permit activation energies of the dynamic exchange reaction to be established and thus, will allow meaningful comparison to other covalent adaptable networks (CANs). This area of research will also provide valuable insights by investigating the effect of the network structure on the relaxation properties, as it is understood that materials with larger amounts of crosslinking extends relaxation times at the same temperatures, when compared to the same material with less crosslinks.[241]

Furthermore, creep is another phenomenon suffered by covalent adaptable networks. This often comes hand in hand with stress relaxation as the principles are similar but on the basis of creep experiments is application of a constant force and the strain is measured to hold the force on the sample. From the observational evidence presented by DMTA, these experiments will be vital towards the properties of the end-use polymers as creep is detrimental to product performance, where structural integrity is desirable. Future work will involve capturing creep data, for the dioxazaborocane materials in this research, to assess the performance compared to other classes of CANs.

5.1.3 Thermogravimetric Analysis (TGA)

5.1.3.1 Introduction

Thermogravimetric analysis (TGA) is an analytical technique that measures the mass of a sample in response to temperature or time, utilising a controlled temperature programme. The thermogravimetric analyser consists of a sample pan (crucible) which is supported on a precision balance. This is contained within a furnace for heating and cooling the sample. A purge gas controls the environment and the mass is measured over a controlled time-dependant temperature range. This technique offers valuable insights about the thermal stability of the sample. During the heating ramp mass losses are observed due to chemical changes in the material. With regards to thermoset polymers, TGA can reveal if thermal decomposition reactions can occur due to the thermal post-cure. It also provides upper use temperatures during the service life of the material.

In this research, the TGA is conducted under an inert atmosphere (N_2), to prevent combustion and ensure the mass loss is due to the thermal decomposition of organic matter, which leaves behind a small mass fraction that consists of the inorganic matter in the material. All polymers were tested using the same heating ramp of 20 $^\circ$C per

minute, from 25 °C to 650 °C, to remain comparable, as the rate off heating can vary the decomposition temperature. The percentage mass loss was calculated from Equation 12 below, where W_0 is the initial sample weight and W_t is the weight at a specified temperature.

$$Weight\ Fraction\ (\%) = \frac{W_t}{W_0} x\ 100 \qquad (12)$$

Utilising this method, the thermal decomposition temperature could be ascertained for D-series polymers and A-series polymers. Knowing the thermal decomposition temperature was important, for the polymers fabricated in this research, as the thermal-post cure was subjected to temperatures up to 170 °C and thus, determining whether the polymers undergo decomposition during post-cure, or recycling, was vital. This post-cure temperature was required to ensure that no residual polymerisation reactions would occur due to the mechanical recycling temperatures reached during heat pressing, which will be discussed separately in Chapter 6.

5.1.3.2 TGA Results

Firstly, the residual masses at 600 °C were recorded in Table 18, as a percentage of the original mass, and displayed as a bar chart in Figure 149. Observation of the trend of increasing residual mass across the D-series (1.5-14%) was hypothesised to arise due to increasing inorganic boron content, as a result of the boronic ester content. This was proportional to the increasing mass of boronic ester (0% - 100%) used in the polymer series. The equivalent A-series materials showed significantly less residual mass percentages (1.5-5.4%), which suggests that the increased mass was likely a result of boronic inorganic matter. This was likely to be thermally stable boron-oxide structures such as boroxines.
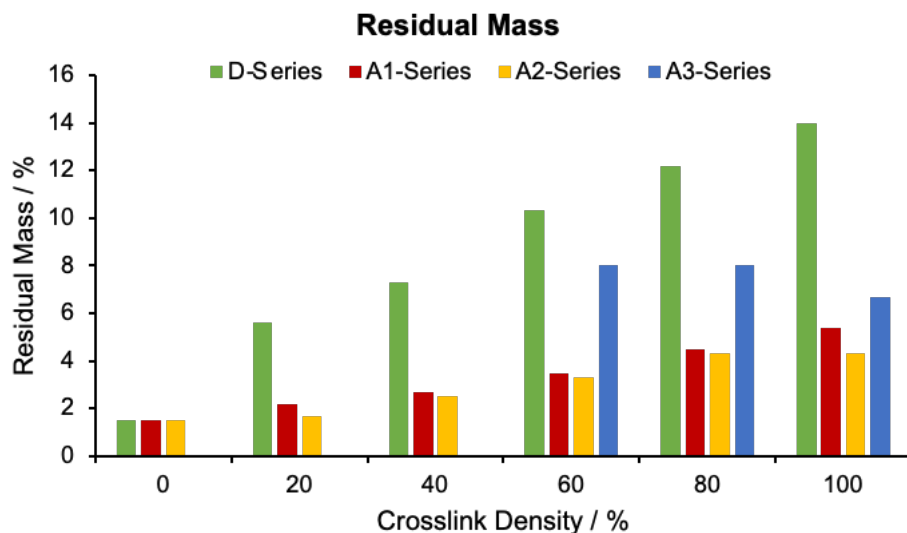
Figure 149: Bar chart showing residual masses of all A-series and D-Series polymers.

Table 18: Residual masses of A-series and D-series polymers

Polymer	% Occupied Sites	Residual Mass / %
Linear HA-E2	0	1.5
D-20	20	5.6
D-40	40	7.3
D-60	60	10.3
D-80	80	12.2
D-100	100	14.0
A^1-20	20	2.2
A^1-40	40	2.7
A^1-60	60	3.5
A^1-80	80	4.5
A^1-100	100	5.4
A^2-20	20	1.7
A^2-40	40	2.5
A^2-60	60	3.3
A^2-80	80	4.3
A^2-100	100	4.3
A^3-60	60	8.0
A^3-80	80	8.0
A^3-100	100	6.7

The thermograms produced from the data, reveal the temperature at which thermal decomposition occurs, which is shown in Figure 150.
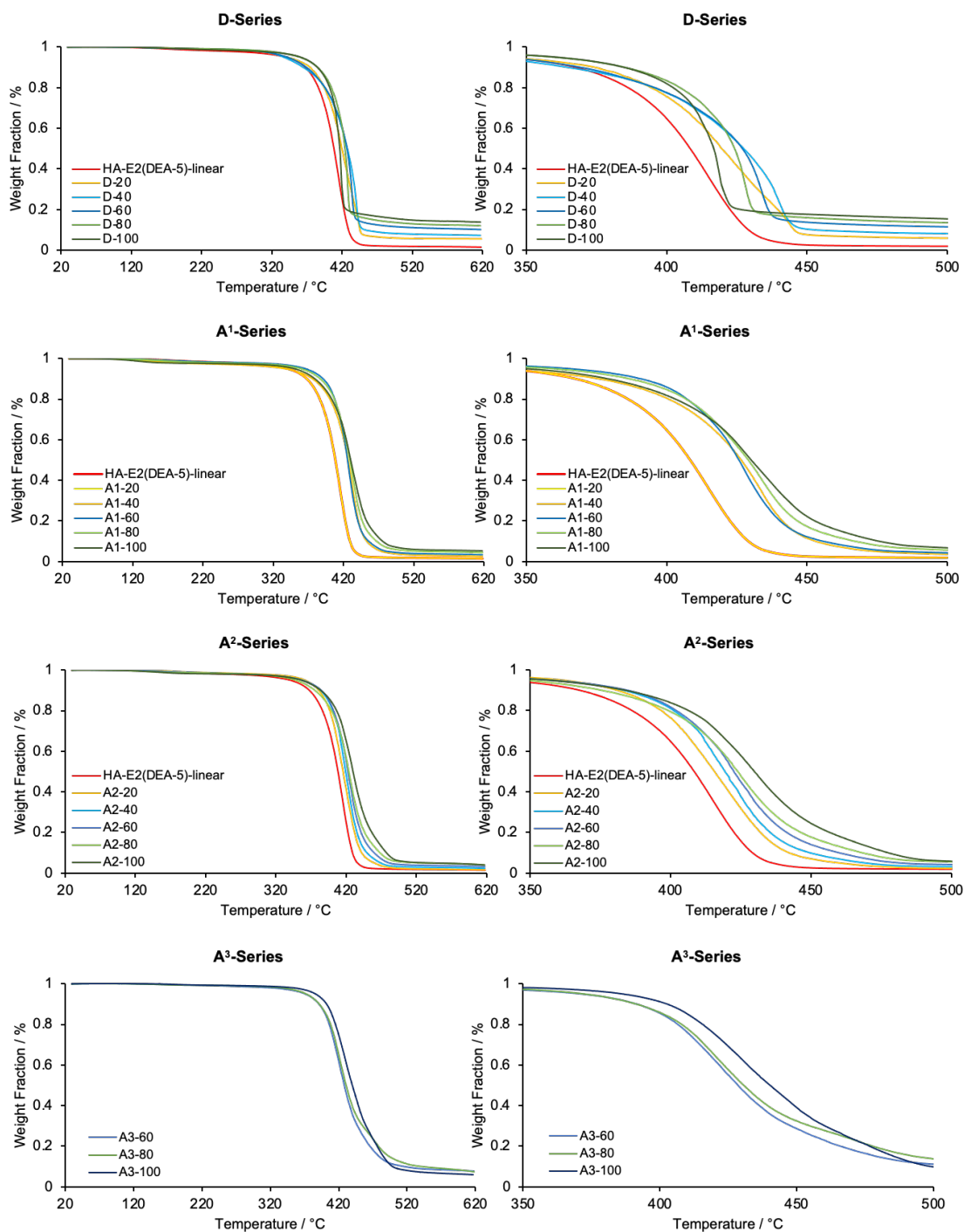

Figure 150: TGA thermogram of all polymer series in this research, showing the full temperature response (left) and a zoomed graph showing the thermal decomposition event (right).

The onset of thermal decomposition begins at around 320 °C for all A-series and D-series polymers. This suggests that dioxazaborocane materials can withstand similar service temperatures to the equivalent epoxy-amine networks prior to decomposition.

Upon closer inspection of the decomposition temperature range, with respect to the number of crosslinks, the graphs on the right-hand side of Figure 150 show a trend across the A-series, where materials with more crosslinks are thermally more stable. However, the trend was different for the D-series as crosslinks increased. The decomposition appears to occur over a much narrower temperature range as the number of crosslinks increased, with the full decomposition temperature of the material reducing as the network crosslink density increased. This phenomenon has not been studied further in this research but is a noteworthy observation, nonetheless. It is hypothesised that boronic or boric acids that are formed from thermal decomposition of the dioxazaborocane network may catalyse the thermal degradation of the organic polymer network, but further work in this area would be required to support this hypothesis.[242]

Figure 151 shows the TGA curves for the fully crosslinked polymer networks overlayed for comparison of thermal decomposition temperatures to the linear thermoplastic polymer, shown by the red dashed curve. As anticipated, the aromatic-epoxy based (E1) network (A^3) was more thermally stable than the linear-epoxy based (E2) networks (A^1 and A^2). The higher residue content for the aromatic-epoxy (A^3) at 600°C from Table 18, compared to the linear epoxy polymers is hypothesised to arise from the carbonisation of the aromatic rings of bisphenol A repeating units.[97]

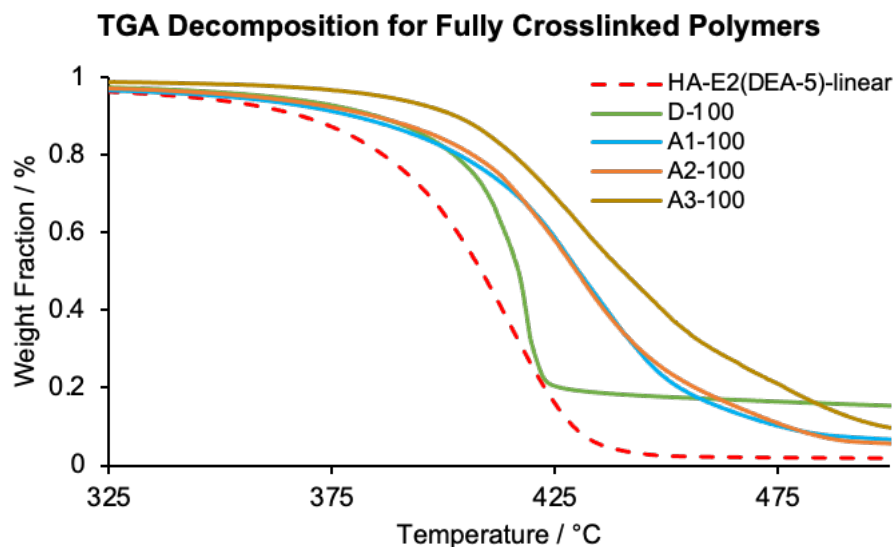**TGA Decomposition for Fully Crosslinked Polymers**

Figure 151: TGA curves for all fully crosslinked materials in this research.

5.2 Molecular Weight Characterisation

5.2.1 GPC

5.2.1.1 Introduction

A ubiquitous method for determining the molecular weight distributions of a polymer is by a technique called gel permeation chromatography (GPC). This method separates polymers based on their hydrodynamic size in solution by filtration through columns packed with unreactive porous beads such as crosslinked polystyrene.[2] The retention times of the polymers in the column corresponds to the size of the polymer chains, as smaller chains take longer to elute, as they get trapped in the porous beads for longer. A visualisation of this is shown in Figure 152. The molecular weights are calibrated to a low polydispersity polymer such as polystyrene over a range of molecular weights. However, although use of a universal calibration standard presents advantages such as repeatability and ease of setup, this method of calibration also presents disadvantages since the molecular weights are only truly accurate for the same polymer type. Using the equation generated by the software for the calibration curve, molecular weights can be

generated from retention times. As polystyrene is known to be a linear polymer it is difficult to determine exact molecular weights where branching is present.
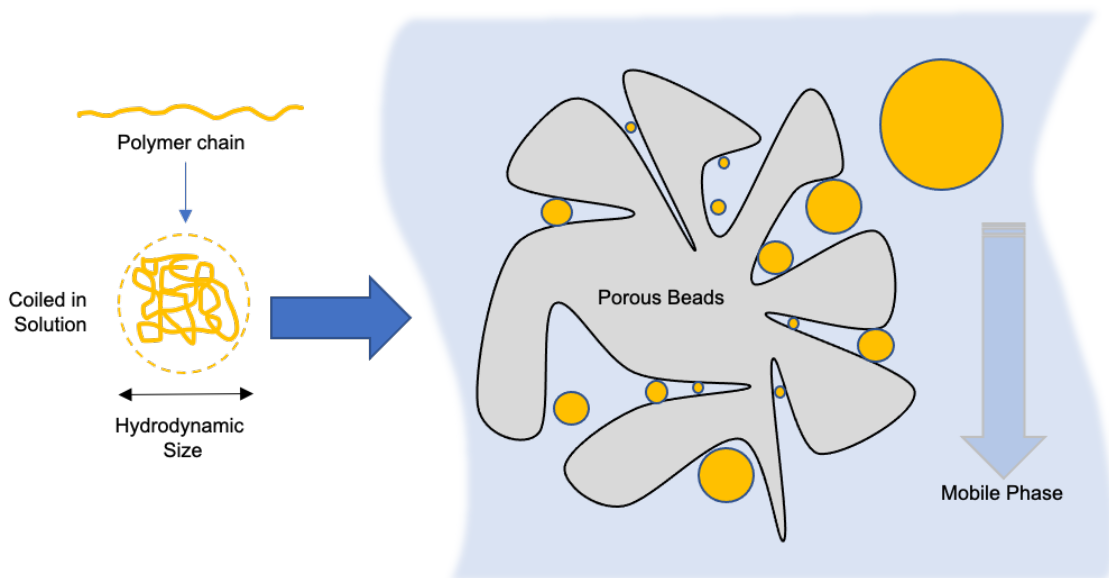

Figure 152: GPC diagram of polymer retention in the porous beads packed in the column, as the mobile phase travels through.

This technique has recently been utilised, with regards to polymers with dynamic enamine bonds, by Fulton's group to assess the collapse of intramolecular crosslinking in single chain polymer nanoparticles in response to pH.[112] The hydrodynamic size reduced with crosslinking and was increased upon de-crosslinking, which could be seen in the GPC distributions. This was possible as the nanoparticles were soluble in the mobile phase, which is most commonly THF solvent. GPC does not show network polymers as the key quality of these materials is insolubility.

The main type of detector utilised in GPC analysis is a refractive index (RI) detector. This provides concentrations of the polymers in solution based on the refractive index difference between the pure solvent and the mobile phase. The detector response is proportional to the concentration of the polymer in solution.

5.2.1.2 GPC results

GPC samples prepared by dissolving the polymer samples in THF at a concentration of 2 mg/mL and filtered through 0.2 μm nylon filters.

In this research, the crosslinking density is gradually increased for each polymer in the A-series and D-series, of which both are based on the same linear chain (thermoplastic) polymer (with the exception of A^3). At this point of the research project, molecular weight analysis would only be suitable for the linear (thermoplastic) polymer as the network critical gel point calculated by P_{gel} to have formed at a 25% crosslink density. This would give support to the polymer design strategy by providing an experimental molecular weight value to compare to the target molecular weight and provide insights on the molecular weight distribution. Therefore, an assessment of the 0% linear HA-E2(DEA-5) polymer with a targeted molecular weight of 1615 g mol^{-1} on average was conducted and the molecular weight distribution is shown in Figure 153. GPC analysis will a key component and be discussed further in the recycling section of this research, in Chapter 6.
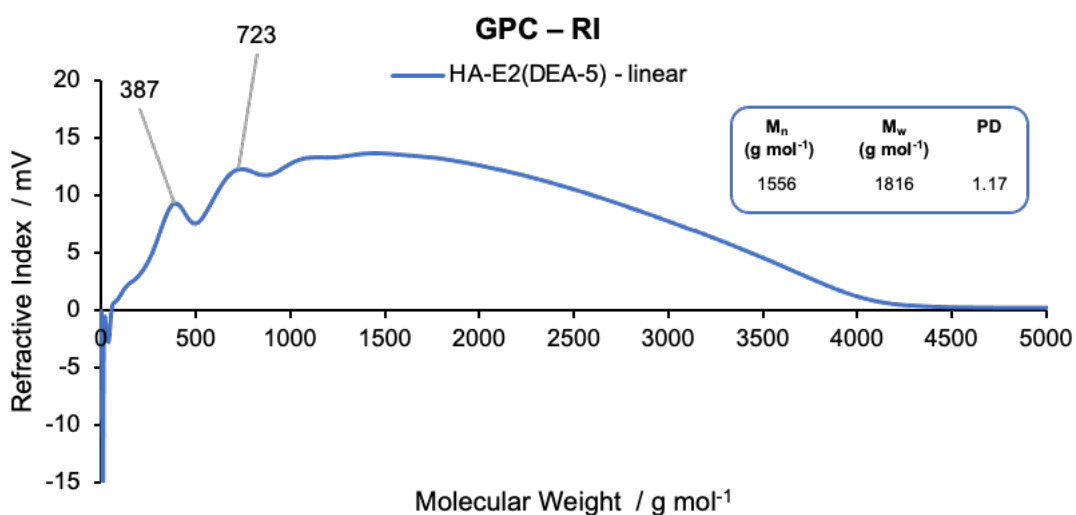

Figure 153: GPC molecular weight plot for the linear (thermoplastic) polymer in this research.

The distribution of the linear (thermoplastic) polymer HA-E2(DEA-5) shows good accordance with the targeted average molecular weight by molecular design. The more defined peaks in the low molecular weight section of the GPC trace is expected due to the nature of stepwise polymerisations and have been highlighted in Figure 154. The structures indicated are a likely cause of peaks in this region due to the possibilities of the mono functional epoxy (PGE) to react with the same amine group twice or with polymer chains in the early stages.
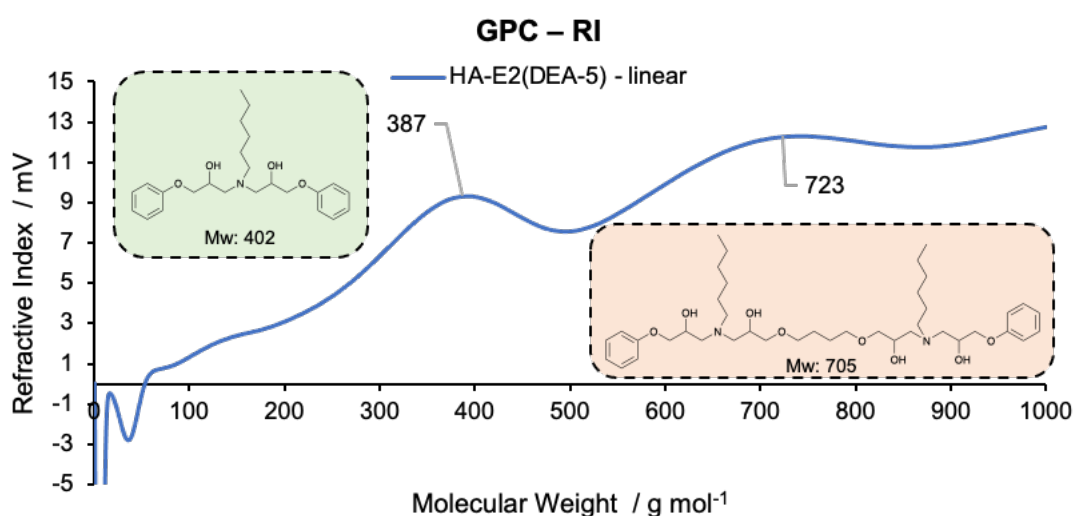

Figure 154: Low molecular weight GPC peaks for HA-E2(DEA-5)-linear (thermoplastic) polymer.

In contrast, the fully crosslinked D-series and A^2-series (D-100 and A^2-100), when the sol content was extracted with THF, showed no evidence of high molecular weight chains present in the GPC sample, the results of which are shown as an overlayed molecular weight distribution in Figure 155. This is expected due to the 3-dimensional network structure of the material which renders it insoluble in organic solvents. Therefore, the GPC distributions support the formation of network polymers in both polymer classes (A^2 and D). The small peaks at low molecular weight are also likely a result of formation of the small oligomeric molecules indicated in Figure 154, since these molecules are low in

functionality, it is more probably that such species are not attached to the polymer network and can therefore be extracted on immersion in THF (known as 'sol').
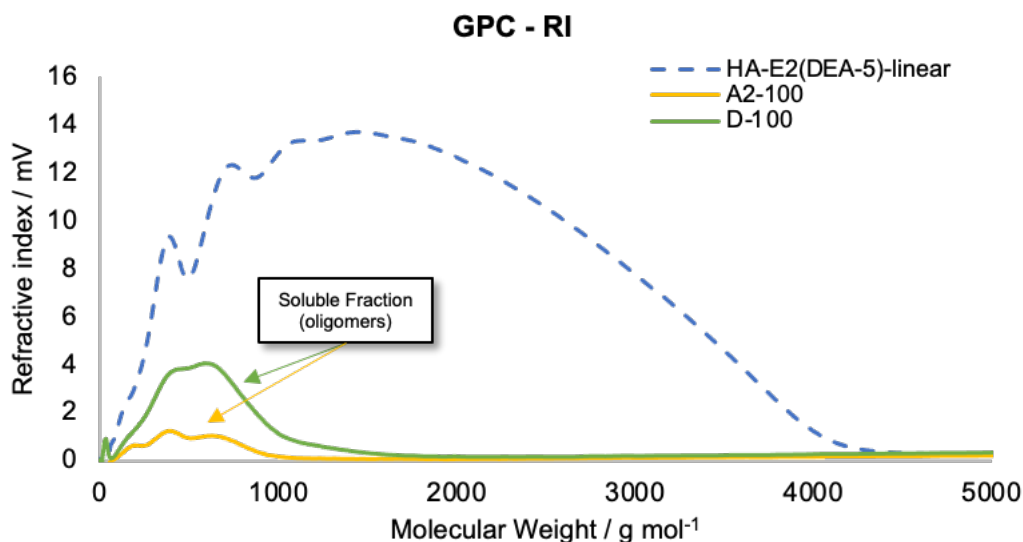

Figure 155: Molecular weight distribution of 100% crosslinked A^2 and D-series polymers. The blue dashed line represents a the linear (thermoplastic) HA-E2(DEA-5) polymer as the reference control polymer since these should form the main chain polymer backbones.

In addition, there is a broader distribution in the molecular weight distribution in the low molecular weight peak of the sol extract for the D-100 and A^2-100 polymer networks when directly compared to the more well defined low molecular weight peaks epoxy-amine linear polymer (HA-E2(DEA-5)). This is hypothesised to arise as a result of the diboronic esters ability to link two of the small oligomer molecules together, through the DEA groups present in the D-series, or the diamine directly reacting with only PGE molecules in the A^2-series. The structures of these are shown in Figure 156 below and represents the lowest possible molecular weight dioxazaborocane crosslinked molecule, that cannot participate in the polymer network. These structures may account for the higher concentration, of the low molecular weight distribution, at slightly higher molecular weights in the D-100 material compared to the A^2-100 material accounting on the

molecular weight discrepancies of the small molecule structures hypothesised to populate the soluble fraction.
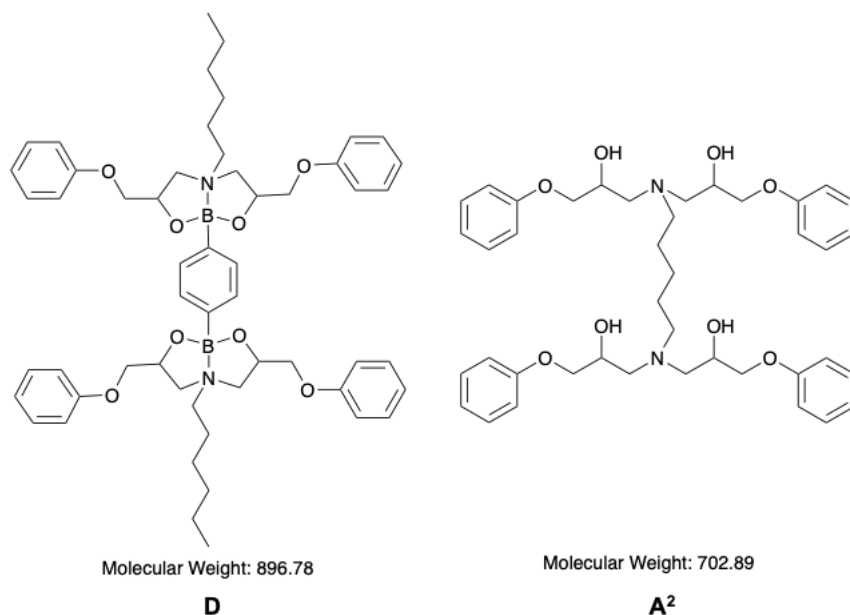

Figure 156: Smallest possible molecules formed with dioxazaborocane crosslinking in the D-series or a diamine crosslinking only PGE molecules at all four reactive centres polymers in the A^2-series.

5.3   Chemical Characterisation

5.3.1   Functional Group Analysis by FTIR

5.3.1.1   Introduction to FTIR

Fourier transform Infrared Spectroscopy (FTIR) is a commonly employed diagnostic tool in most chemistry laboratories due to its simplicity, reliability and rapid analysis of an organic molecule providing a structural fingerprint. With regards to polymers, FTIR can provide a method of analysing the functional groups present in the structure based on the characteristic peaks present in the resultant spectrum.

5.3.1.1.1 Principles of FTIR spectroscopy

FTIR involves the absorption of electromagnetic radiation in the infrared region (Figure 157). During absorption, energy is transferred from the radiation to the molecule and a transition occurs between two vibrational energy levels. The energy (**E**) is related to the frequency (***v***) by Equation 13 below, where ***h*** is the Planck constant (6.624 x 10^{-34} J s).

$$E = h\nu \tag{13}$$

In a standard FTIR spectra the frequency is reported as a wavenumber ($\bar{v}$) which is a reciprocal of the wavelength (λ) and related to frequency or wavelength by Equation 14 below, where ***c*** is the speed of light in m per second (3 x 10^8).

$$\bar{\nu} = \frac{1}{\lambda} = \frac{\nu}{c} \tag{14}$$

FTIR provides a molecular fingerprint of the molecule with absorption bands that correspond to the vibrational frequency (Figure 157). Polar bonds with dipole moments produce stronger peaks in the IR spectrum and are known to be IR active whereas symmetrical bonds, without a dipole moment, absorb very little infrared radiation. In addition, the position of the bands in spectrum depend on bond lengths, bond strengths and whether the atom is bonded to a heavier atom. For example, short and strong bonds will have a higher frequency or shorter wavelength as well as atoms bonded to hydrogen are also observed at a higher frequencies, as opposed to the same atom bonded to a heavier oxygen or nitrogen atom.[243]
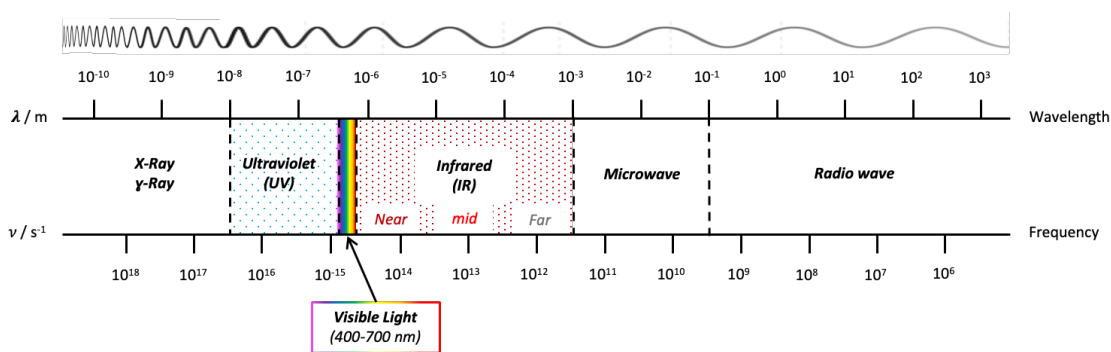
Figure 157: Electromagnetic radiation diagram

The most commonly utilised FTIR spectrometers use infrared radiation in the mid infrared section and observe a spectrum with wavenumbers from 4000 cm^{-1} to 450 cm^{-1}. The transmittance that is usually reported is the ratio of the transmitted intensity (I) and the incident intensity (I_0) of the radiation and shown in Equation 15 below.

$$T = \frac{I}{I_0} \qquad (15)$$

FTIR relies on a Michelson interferometer (Figure 158), which produces an interferogram in the time domain. The Michelson interferometer works by the IR source being split into two paths (A and B) by the beam splitter and then reflected by a fixed mirror and a moveable mirror ultimately recombining causing an interference pattern known as the interferogram. This is then Fourier transformed mathematically into the more familiar spectrum in a frequency domain.
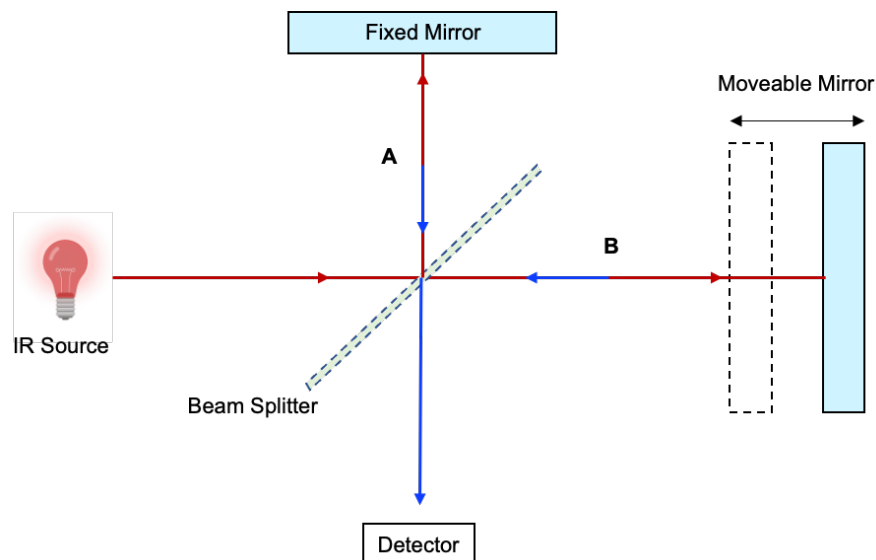
Figure 158: Diagram of a Michelson interferometer

Attenuated total reflectance (ATR), which is depicted in Figure 159) is the most widespread method of infrared spectroscopy due to the fact it requires little sample preparation or expertise to operate, affording reliable results. This method involves the incident infrared source being refracted through a crystal, such as diamond, and subsequently reflected at the crystal-sample interface. During this internal reflection, some of the IR radiation penetrates the sample by a few μm and is absorbed into the sample. This is known as the evanescent field. This gathers information of the structure before being reflected back out multiple times towards the detector.
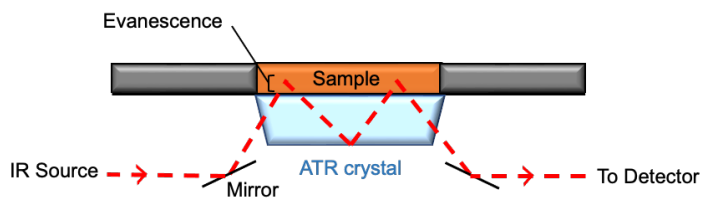

Figure 159: ATR-FTIR diagram.

5.3.1.2 FTIR Results

With regards to the polymers fabricated in this research the most chemically comparable amine-crosslinked polymer was the A^2-series which was crosslinked with PACM (structure R in Figure 160). Therefore, FTIR analyses were conducted to provide an insight into the structural differences between the two series of polymers. This also allows a comparison of how the functional groups change, with increasing crosslink density, and the subsequent deduction whether the boronic ester was actually crosslinking and not remaining unreacted and trapped in the polymer matrix. The full spectrum can be seen for all polymers in Sections 10.1.4.10 and 10.1.4.11 of the appendix.

It was anticipated that the D-series would differ by the amounts of OH functional groups present as these should be consumed by the boronic ester if the crosslinking reaction had occurred. Hence, the FTIR spectra overlayed in Figure 160 shows a decreasing trend in the broad OH band, at a wavenumber of around 3380 cm^{-1}.
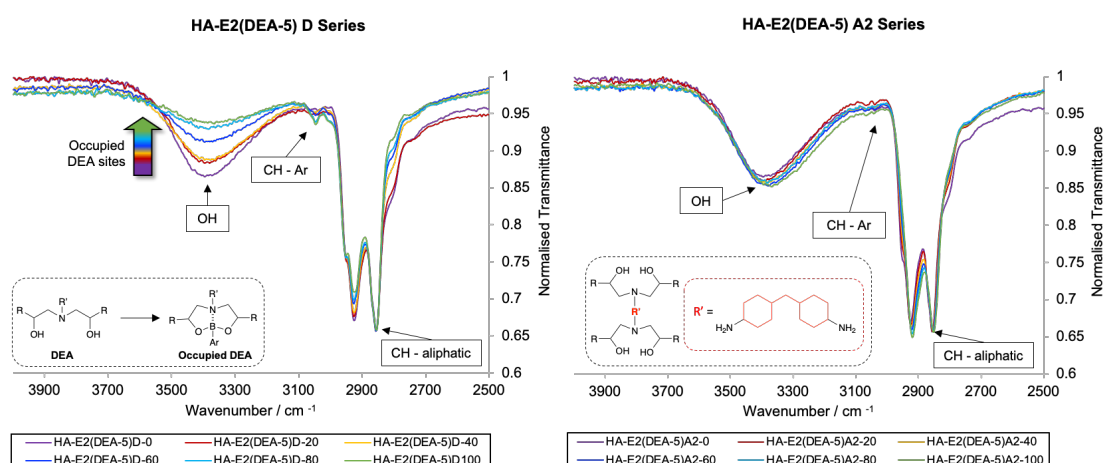

Figure 160: FTIR zoom of OH and CH region of D-series (left) and A2-series (right) in the 2700 cm^{-1} to 4000 cm^{-1} region.

226

This is proportional to increasing levels of boronic ester, which is supported by the increasing trend of the weak aromatic CH-stretching vibration at 3044 cm $^{-1}$ (shown in Figure 161). The trend is supported by the linear trend in the graphs shown in Figure 162, which compares the transmittance of the normalised CH-aliphatic bands to the OH and the CH-aromatic bands shows a proportional difference in transmittance between these two sets of bands that are representative of the increasing boronic ester content.
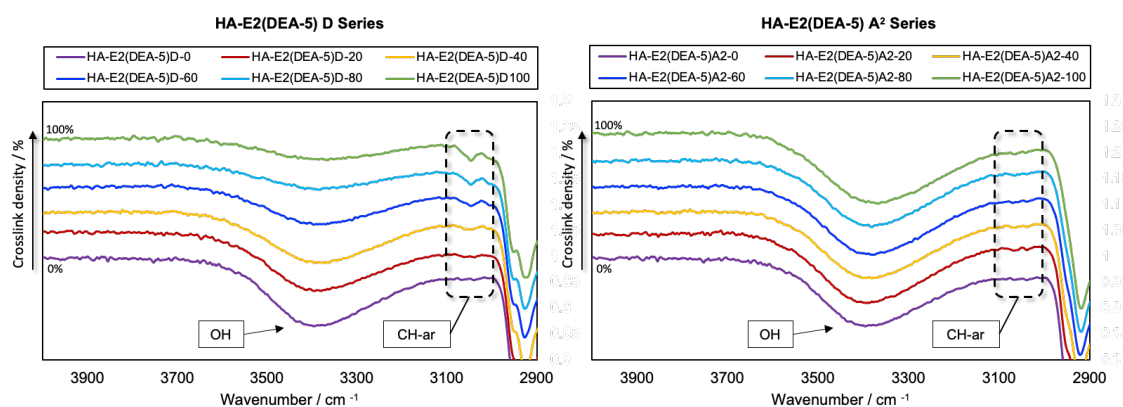

Figure 161: FTIR offset data of zoomed in 2900 cm^{-1} to 4000 cm^{-1} region.

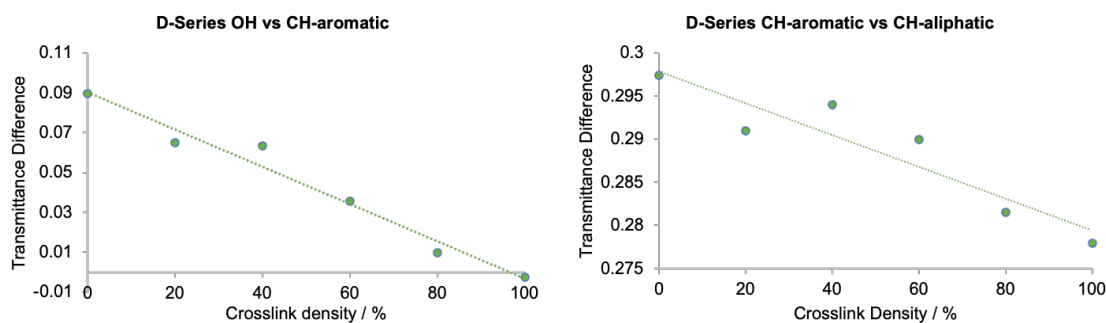*Figure 162: FTIR trends in D-series from 2700 cm^{-1} to 4000 cm^{-1}*

This evidence suggests that the boronic ester is reacting with the DEA groups as intended and is successful at crosslinking epoxy-amine polymer chains. This trend is not observed in the A^2-series as expected and the lack of any observable aromatic CH bands

is likely due to the small amount of PGE in the formulation being at constant level throughout the series.

On another note, the polymer degradation due to thermal oxidation mechanisms, previously mentioned as a probable cause of discolouration in Section 4.6.3, is supported by the FTIR bands presented in Figure 163.
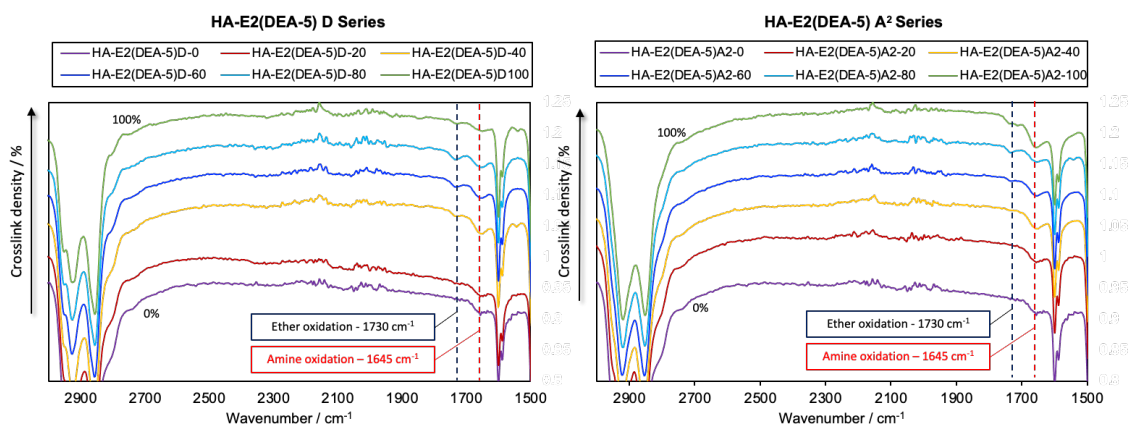

Figure 163: FTIR spectra highlighting the epoxy-amine oxidation vibrations observed in the D and A2-series where the wavenumbers are known from the literature.[229]

The literature suggests that bands at 1645 cm^{-1} are responsible for yellowing in epoxy-amine systems.[229–232] This is evident by the weak bands present in the FTIR spectra for the polymers synthesised in this research and is proportional to amine content which is equal in all polymer formulations and crosslink densities as they have all been subjected to the same thermal cure. The thermal oxidation of amines is believed to undergo a general radical autooxidation mechanism with peroxides in an oxygen rich environment. Oxidation can result in the formation of carbonyls, amides or double bonds as well as chain scissions, which can lead to degradation of the polymers and thus, reduced mechanical properties and reduction in T_g.[230] The effects of degradation due to oxidation in this research is studied further in Chapter 6. The mechanistic detail is debated in

literature and is beyond the scope of this research and therefore will not be probed further.

Upon analysis of the fingerprint region, the D-series showed a promising trend in the B-O/B-N stretching region at around 1380 cm $^{-1}$ and in the 1244 cm^{-1} and 1219 cm^{-1}regions, as shown in Figure 164.[244] The B-O or B-N 1380 cm $^{-1}$ band at appears to increase upon increasing crosslinking density which is expected. The emerging peak at 1219 cm^{-1} was proportional to the disappearance of the peak at 1244 cm^{-1}, which is evident by the trend observed from the difference between the transmittance of both peaks of the same spectra.

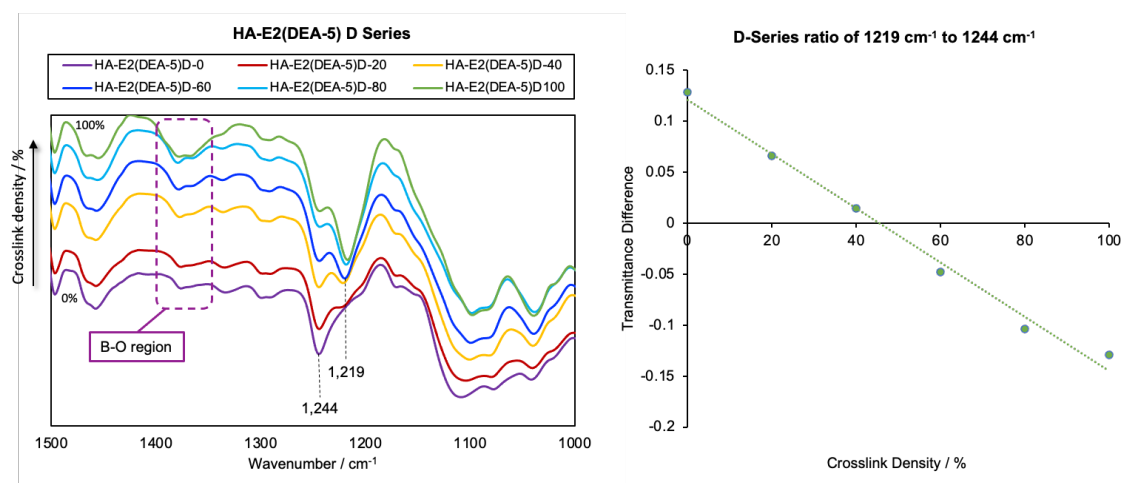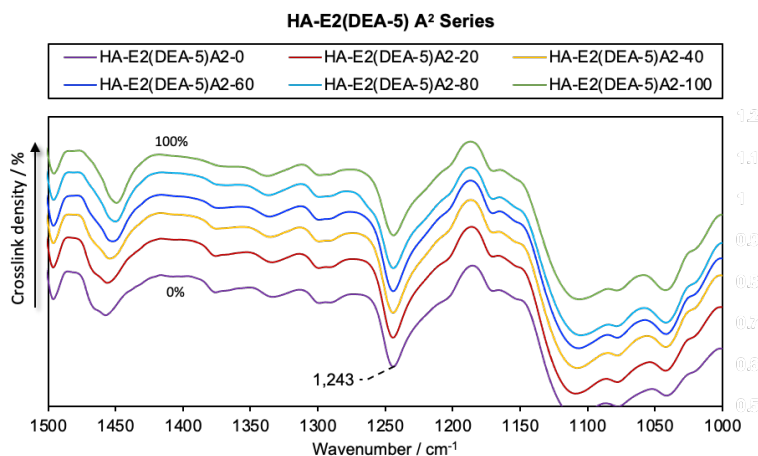*Figure 164: FTIR of D-series fingerprint region*

Figure 165: FTIR of A^2 series fingerprint region.

This was not observed in the A^{2-}series spectra, shown in Figure 165, as this peak remained constant upon increasing crosslinking. However, due to this region having a vast population of bands corresponding to different functional groups, assignment of a functional group to these bands remain a speculative assumption. With that said, and knowledge of the polymer structures, a likely functional group at 1244 cm^{-1}, that would be present in both A-series and D-series material and also susceptible to change upon increasing boronic ester crosslinks, is the C-N-C stretching vibrations. It is clear from the evidence that the band appearing at 1219 cm^{-1} increases as a result of boronic ester incorporation. Therefore, assignment of a C-N-C stretch vibration may be a reasonable suggestion, using Equations 13 and 14, due to a reducing wavenumber. This may arise as the boron coordinates to the nitrogen, which likely weakens the N-C bonds and reduces the frequency of the vibrations and increases wavelength, which reduces the resultant wavenumber observed.

In this research, FTIR has been used as a method to evaluate successful crosslinking reactions by functional group conversion to support physical observations of network formation beyond insolubility. The absolute assignment of bands in complex regions is beyond the scope of this project, as the focus is attaining network materials capable of

230

recycling. However, probing this subject further may be of interest in the future, as a means of monitoring the crosslinking reaction.

5.4 Material Performance

Due to the critical gel point estimations in Section 4.6.2, polymers with a crosslink density of 60%, 80% and 100% were selected for further testing of material performance as these were likely to provide the appropriate high-performance materials in a glassy physical state.

5.4.1 Tensile Testing

In order to assess the material performance and thus, suitability for use as a high-performance thermoset material. Tensile testing was undertaken to provide valuable insights on tensile strength and Young's modulus, which are key indicators of a material's overall strength. The aim behind tensile testing the materials in this research was to compare how the structural changes to the networks affected the material properties. As the polymers were designed to be structurally comparable (on a molecular level), differing only by the crosslinking chemicals, the changes in behaviour are expected to be a result of this change or as a result of the crosslink density.

5.4.1.1 Introduction to Tensile Testing

Tensile testing is a mechanical testing process which examines the force required to break a sample. The samples are usually in dog-bone shapes with known dimensions, preferably to an ASTM or ISO standard requirements. These standards ensure consistency across material tests and are shaped as such to ensure the best replication of results during testing. The dog-bone shape has been designed so that the test specimen consistently ruptures in the centre, which is intended to be the weakest spot. The test itself produces information of the materials response to the force (N) applied.

The preliminary results are then converted to stress (σ) and strain (ε) as the equations required for conversion are specific to the sample dimensions. Thus, this is a universally comparable method of reporting strengths of materials and is independent of the class of material studied. The equation for converting force to stress is shown in Equation 16 where **F** is the force and **A** is the cross-sectional area.

$$\sigma = \frac{F\,(N)}{A\,(mm^2)} \tag{16}$$

Tensile strain is defined by Equation 17 and is the fractional change in length in response to tensile stress, where **L** is the change in length and **L_0** is the original length of the narrow section indicated in the standard dog-bone diagram shown in Figure 166. The other features of the dog-bone used in these calculations are also shown in Figure 166.

$$\varepsilon = \frac{L}{L_0} \tag{17}$$

During experimental testing, the cross-sectional area was measured in triplicate and the average value was used as **A** in any stress calculations.

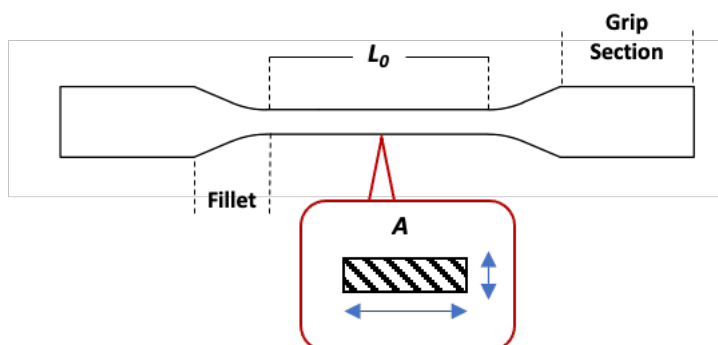*Figure 166: Dog-bone diagram indicating L_0 (length of narrow section) and cross-sectional area of the narrow section (A).*

The material specimens are commonly moulded to the required shape (Figure 167) or physically cut to the dimensions required.
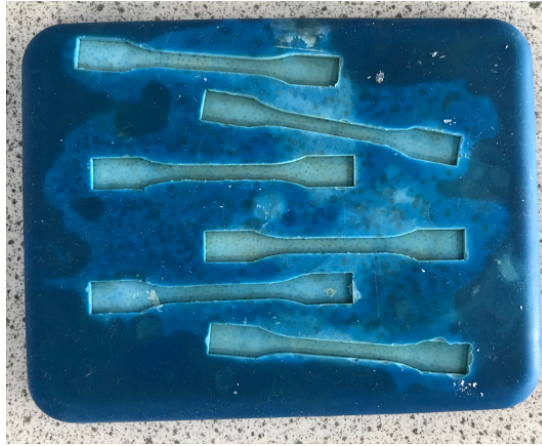

Figure 167: Picture of a dog-bone mould.

After the test graph has been plotted, Young's modulus (***E***) values can be obtained by Equation 18 below. Since the value comes from the ratio of tensile stress to tensile strain, the Young's modulus value can be obtained from the gradient of the linear-elastic region of the stress-strain graph (indicated on Figure 168), which is when the material still obeys Hooke's law.

$$\mathbf{E} = \frac{\sigma}{\varepsilon} \qquad \qquad (\mathbf{18})$$

The Young's modulus reveals how easily the material can deform and is useful at predicting the behaviour of the material. For example, a brittle polymer will have a high Young's modulus and be a strong material. However, this type of material will fracture immediately at failure. A ductile material will display several behaviours whilst experiencing a tensile force. These types of materials will first have a relatively strong elastic region before yielding into the plastic deformation region where it will undergo strain hardening to its ultimate strength then finally necking before fracture. Plastic

materials will have much lower Young's modulus value but will undergo a large amount of strain before failure.
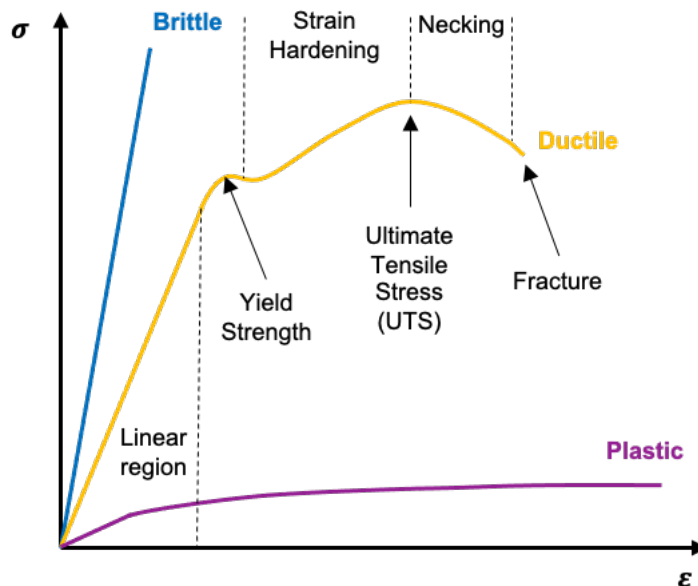

Figure 168: Idealised examples of tensile results of materials with differing properties, with indication of deformation behaviours highlighted for the ductile material.

The information yielded by the test delivers insights on the conditions the material can withstand during its service life. Often, high-performance polymers are required to withstand huge amounts of force and is vital, from a safety perspective, that they can continually deliver their performance without material failure.

5.4.1.2   Sample preparation

During this research the polymers fabricated were unsuitable for mould-casting, due to the formation of air bubbles, and were also too brittle to cut. Therefore, the thin films that were free of bubbles were laser-cut to the desired sample dimensions, which can be found in the appendix - Section 10.3. The advantage associated with laser cutting is that the samples are uniformly cut to identical sizes offering good reproducibility in testing,

compared to mechanically cut samples or moulded samples that may cure differently due to external stresses from the moulded environment.

As a laser produces large temperatures at the contact point with the sample, it could cause some thermal degradation to the polymer, which may weaken the material to a certain degree. However, the material tested in this work had all undergone a high temperature post-cure process, so the impact of further thermal (laser) treatment was anticipated to be minimal. Also, all specimens were prepared via the same laser cutting method, therefore experiencing the same environment and conditions so could be compared in a fair and consistent way. An interesting observation during laser cutting, was that the boronic ester crosslinked polymers exhibited a stringing phenomenon in the ventilated chamber it was cut in, which is shown in Figure 169.
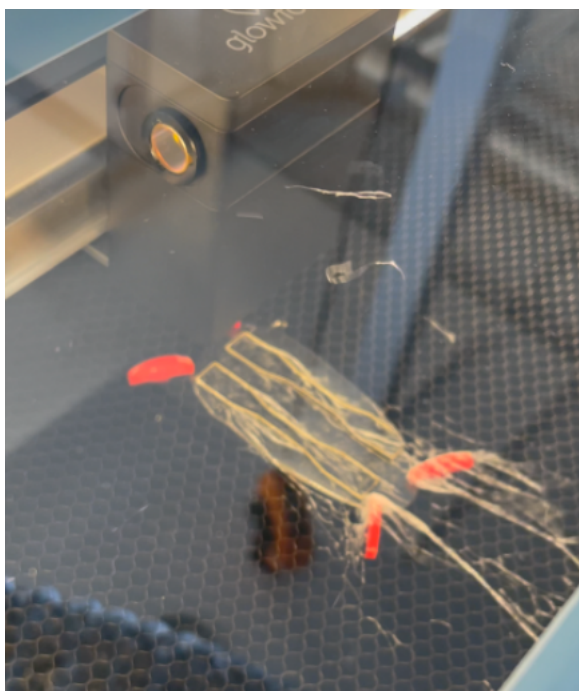
Figure 169: Stringing phenomenon during laser cutting for D-series polymers.

This phenomenon was hypothesised to occur due to the dioxazaborocane network behaving like a covalent adaptable network (thermoplastic-like) above its T_g, which is often observed in thermally activated CAN materials.[245] As the polymer was freely flowing above T_g, the air exhaust ventilating the chamber applied a force to stretch the material. This indicated that heating the material whilst applying some force may be a viable method of mechanical recycling the dioxazaborocane networks presented in this research. This hypothesis will be investigated further in Chapter 6.

5.4.1.3 Tensile Results

The materials selected for testing were the 60%-100% dioxazaborocane crosslinked polymers as these were calculated to have exceeded the critical extent of reaction required for gelation (P_{gel}) and should therefore all be a network polymers/thermosets.[2] Due to the low T_g associated with the 1,6-diaminohexane crosslinker in the A^1-series (and therefore in the rubbery state at room temperature), only the A^2-series and D-series were utilised for tensile experiments, as these had similar T_g values and were thought to be more comparable during tensile testing at room temperature. However, it became immediately apparent that the A^2-series exhibited a lower Youngs modulus and higher strain in comparison to the D series, as shown in Figure 170.
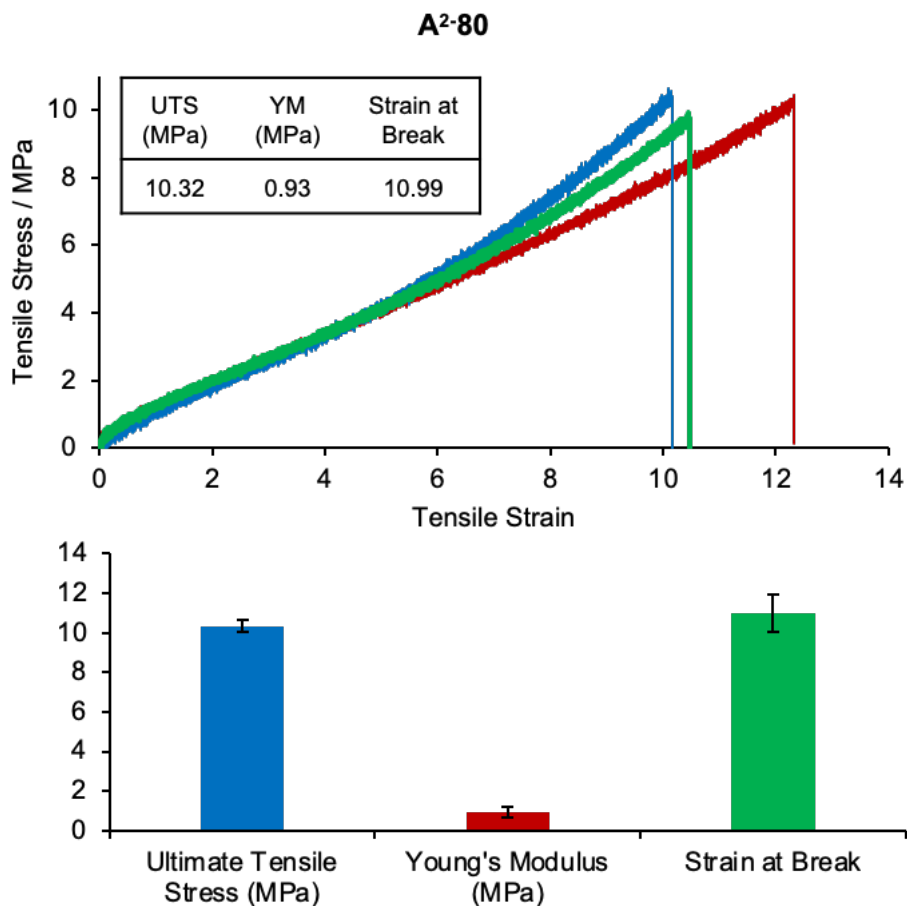
Figure 170: Tensile data for A²-80 showing the tensile profiles and calculated mechanical properties from the dimensions of the narrow section of the dog-bones.

In comparison to the equivalent dioxazaborocane polymer D80, which was significantly more brittle in nature from the results shown in Table 19 (UTS – 33.13 MPa, YM - 119.13 MPa, strain at break - 0.37). It was therefore deemed that the butyl epoxy monomer was much weaker in a traditional epoxy-amine system than when compared to the same dioxazaborocane network system. The significant difference in behaviour can be attributed to the T_g of the traditional A²-80 system being close to room temperature, whereas the D-80 materials T_g was significantly higher than room temperature. This evidence suggested that the D-series would out-perform the A series with equivalent amounts of crosslinking. Figure 171 and Figure 172 show the main findings of the tensile tests for the D-series polymers from 60%-100% crosslinked.
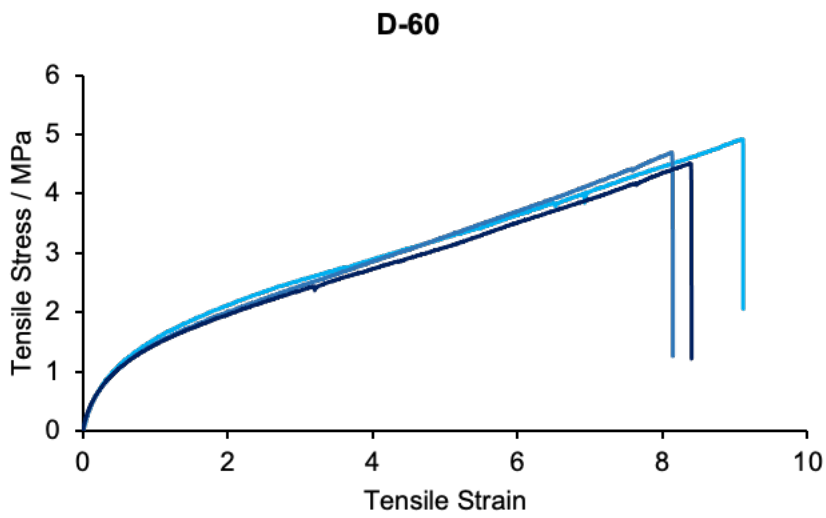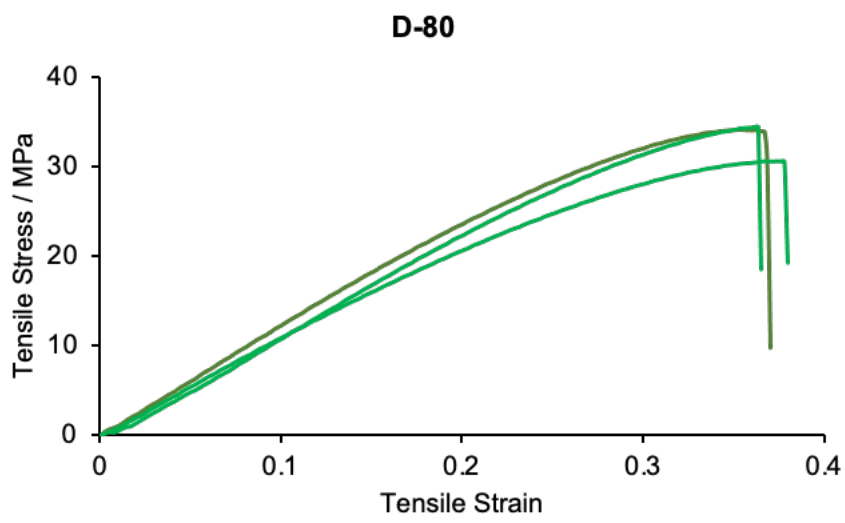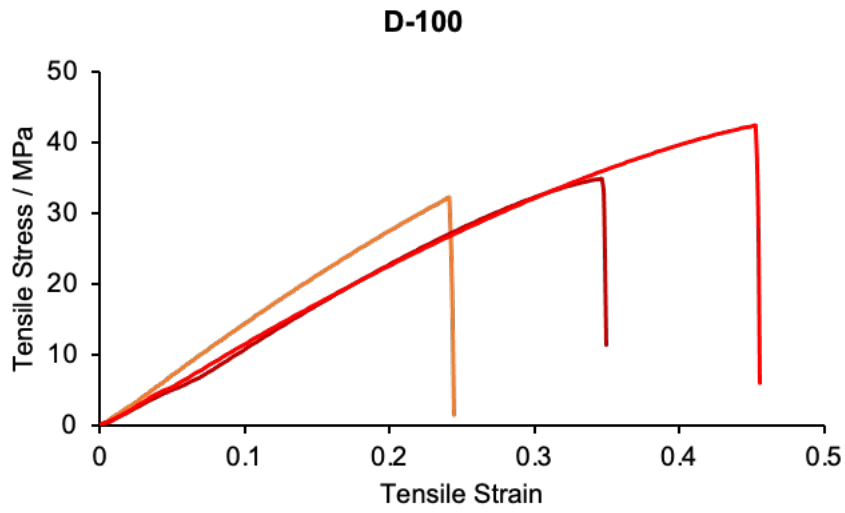
Figure 171: Tensile test results of D-series polymer networks.
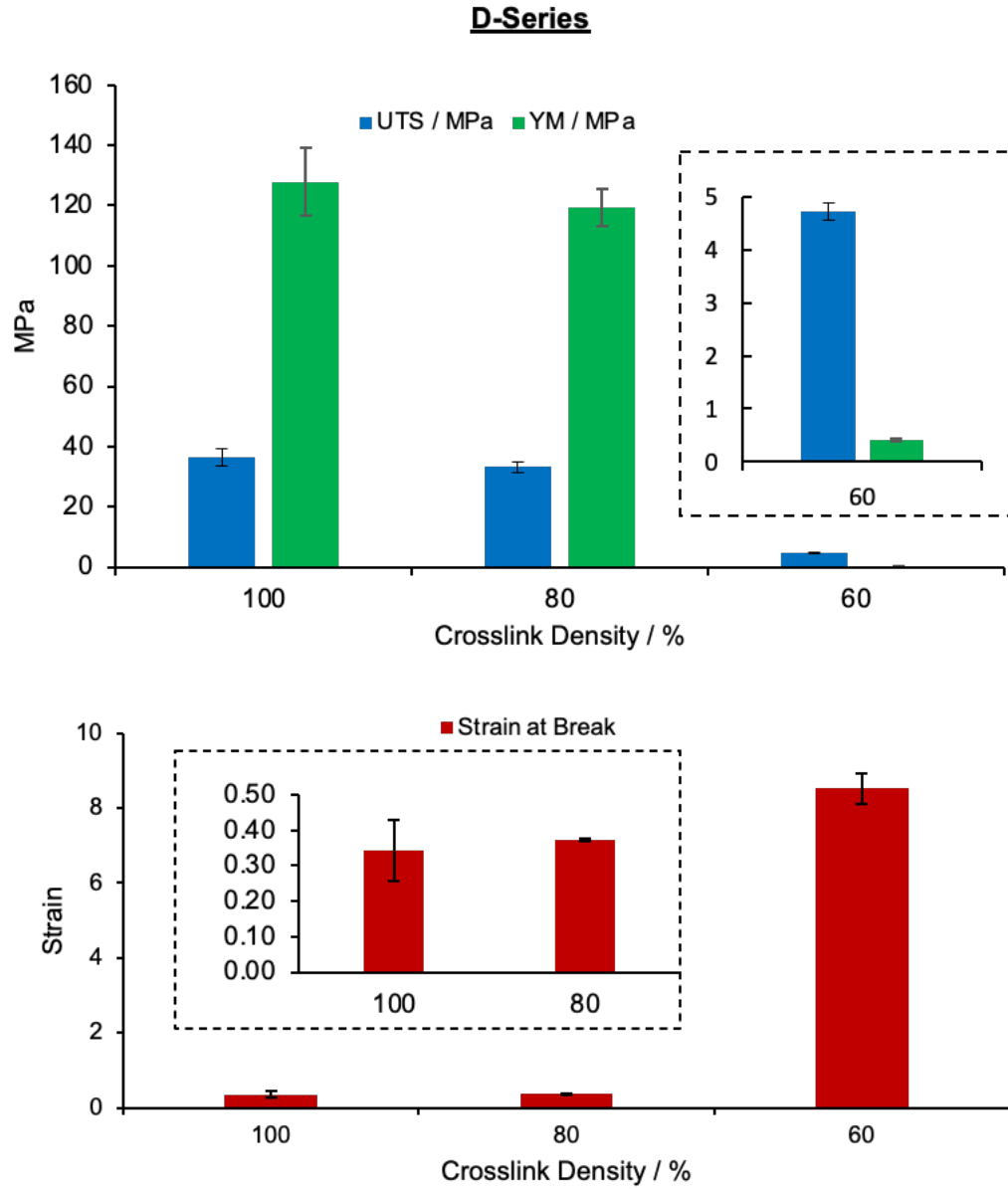
Figure 172: Key mechanical measurements demonstrating the performance of D-series network polymers.

Table 19: D-series tensile results table.

D-Series

Crosslinks	Ultimate Tensile Stress (MPa)	+/-	Young's Modulus (MPa)	+/-	Strain at Break	+/-
100%	36.48	2.99	127.86	11.28	0.34	0.09
80%	33.13	1.76	119.13	6.18	0.37	0.00
60%	4.71	0.17	0.42	0.02	8.53	0.41

The results show that the 80% and 60% are brittle polymers with high Young's modulus values, whereas the 60% crosslinked polymer was significantly more plastic in behaviour, with a low Young's modulus, as it could withstand significantly more strain than the more densely crosslinked material. This evidence showed that the material properties of the resultant polymer could be manipulated by the amount of crosslinking present, with less crosslinks in a material decreasing strength and the brittle behaviour.

The change in behaviour could also be attributed to the T_g of this polymer being below room temperature and in a rubbery physical state during testing. For polymers with a T_g above room temperature, they will be in the glassy physical state. Since the scope of the project was to attain high-performance thermosets, it was hypothesised that the epoxy-amine reference polymer should have a higher T_g for comparison to the D series materials. As a result, a new A-series polymer network (Figure 173) was fabricated, using the E1 bisphenol A based diepoxy DER 332™ (A^3-series) and cyclohexylamine (CHA), which was previously discussed in the polymer development chapter – Section 4.3.1, to combat the effects of low T_g physical parameters.

The average functionality was maintained at 5 DEA groups on the polymer chains, with the only alteration being the diepoxy monomer and a cycloaliphatic amine. The A^3 polymers fabricated in this research were a closer representation to a standard composite material utilised in high-performance industrial applications and hence, would endow a high-performing standard benchmark to aim to achieve with the dioxazaborocane materials.
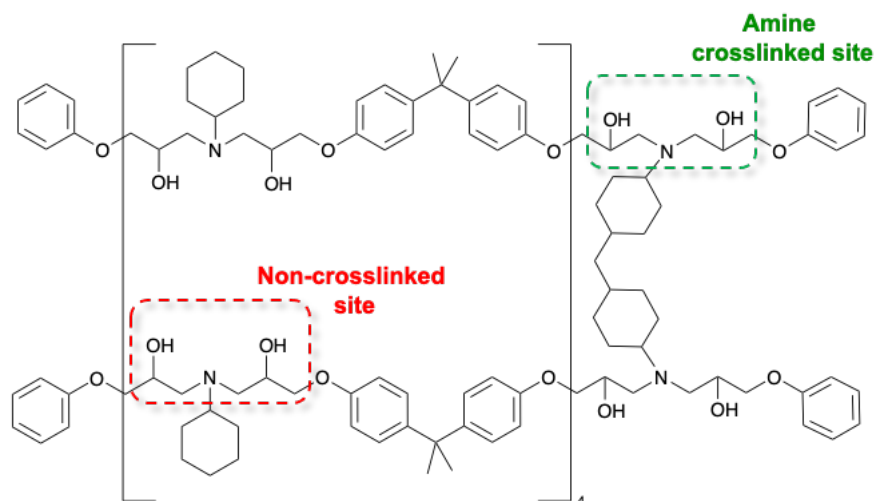
Figure 173: CHA-E1(DEA-5)A3 epoxy-amine polymer networks.

The tensile results of the A^3 Polymer with 60%-100% crosslinks, shown in Table 20 , Figure 174 and Figure 173, showed a brittle mechanical behaviour with a high Young's modulus and a low strain resistance. This was similar to the dioxazaborocane materials with 80 and 100% crosslinks. However, the trend in strain across the series was not the same as the dioxazaborocane. The A^3 polymer could withstand increased levels of strain before fracture with a larger crosslinked network, which is the opposite of the dioxazaborocane material. This evidence indicates a stronger or more ductile material, which is likely related to the molecular structure. In addition, the D80 and D100 are in the same order of magnitude as the A^3-80 and A^3-100. So even though the D-series are slightly less 'high-performance' they show great promise and can be optimised further to match the performance or the standard epoxy-amine materials. Ultimately the overall tensile stress the material could withstand, before fracture, increased with increasing crosslinks.

Table 20: A³ series tensile result table

A³ Series

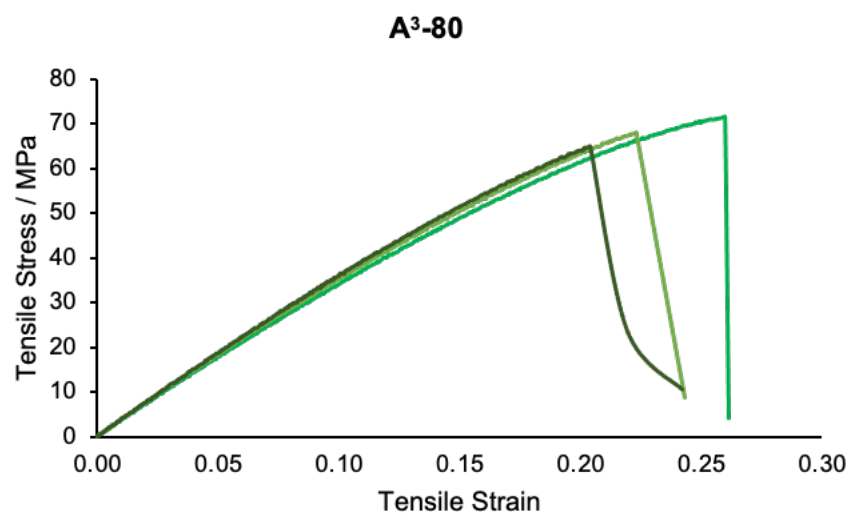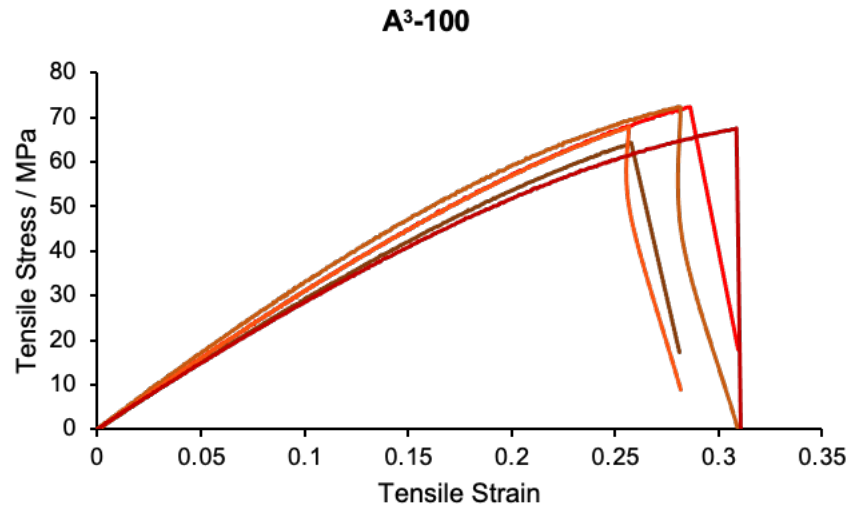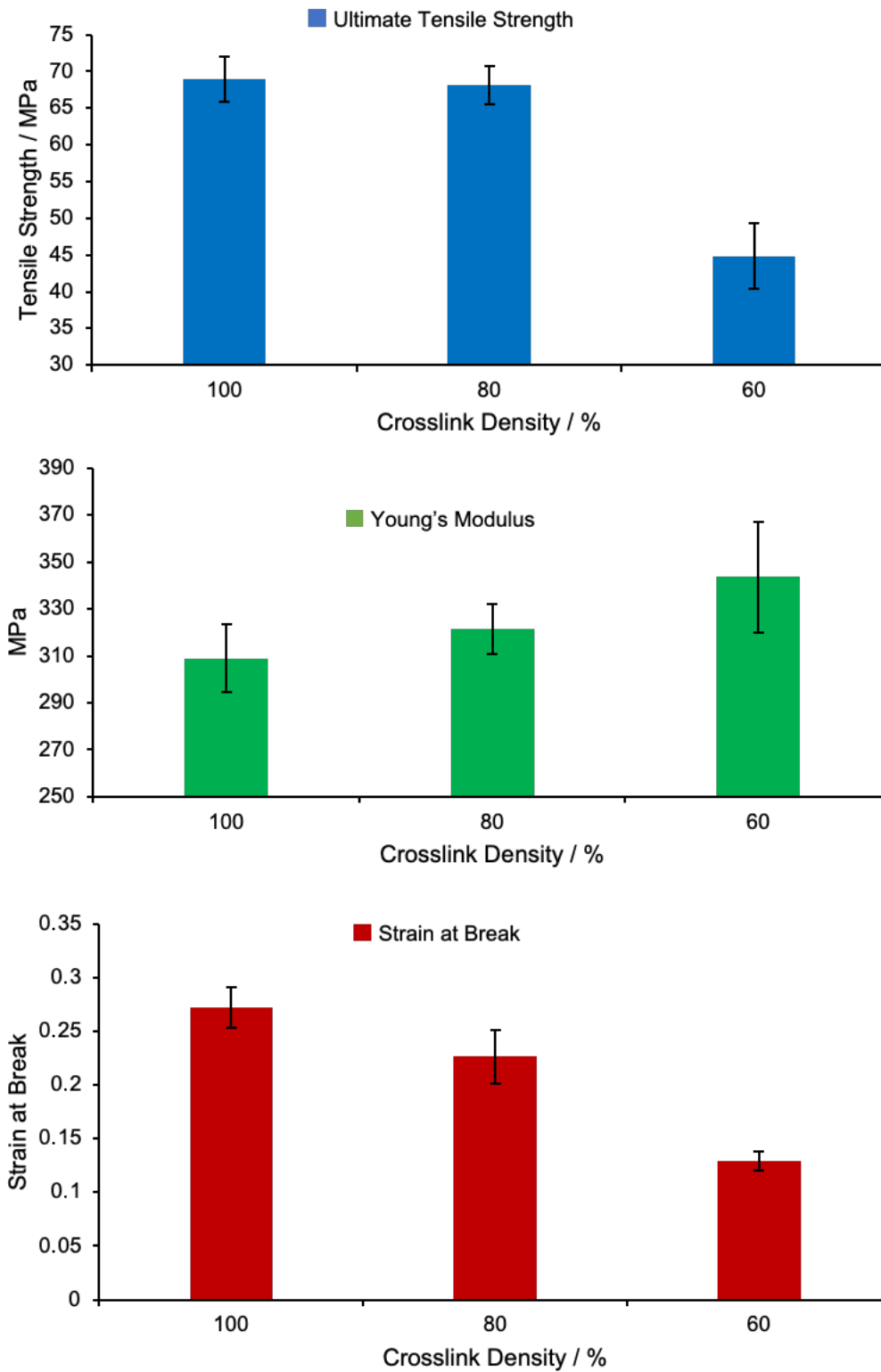| Crosslinks	Ultimate Tensile Stress (MPa)	+/-	Young's Modulus (MPa)	+/-	Strain at Break	+/-
100	68.88	3.06	308.98	14.42	0.27	0.02
80	68.12	2.65	321.49	10.77	0.23	0.02
60	44.81	4.47	343.67	23.47	0.13	0.01
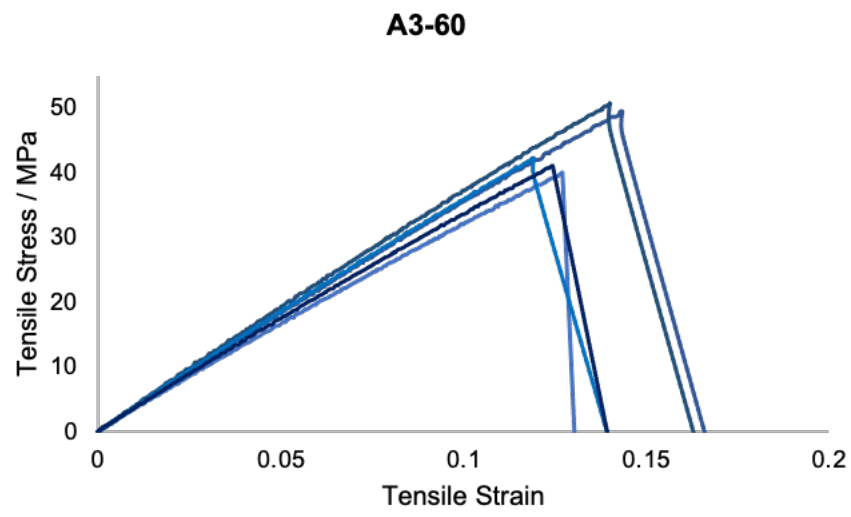
Figure 174: A³ network tensile graphs.

Figure 175: A³ series tensile properties

The bar charts in Figure 176 show the differences between the materials. In comparison with the dioxazaborocane series, the A^3-series was a significantly stronger material, which was expected due to the aromatic DER 332 (E1) polymer chain. However, the dioxazaborocane did appear to be a promising candidate as a high-performing thermoset.
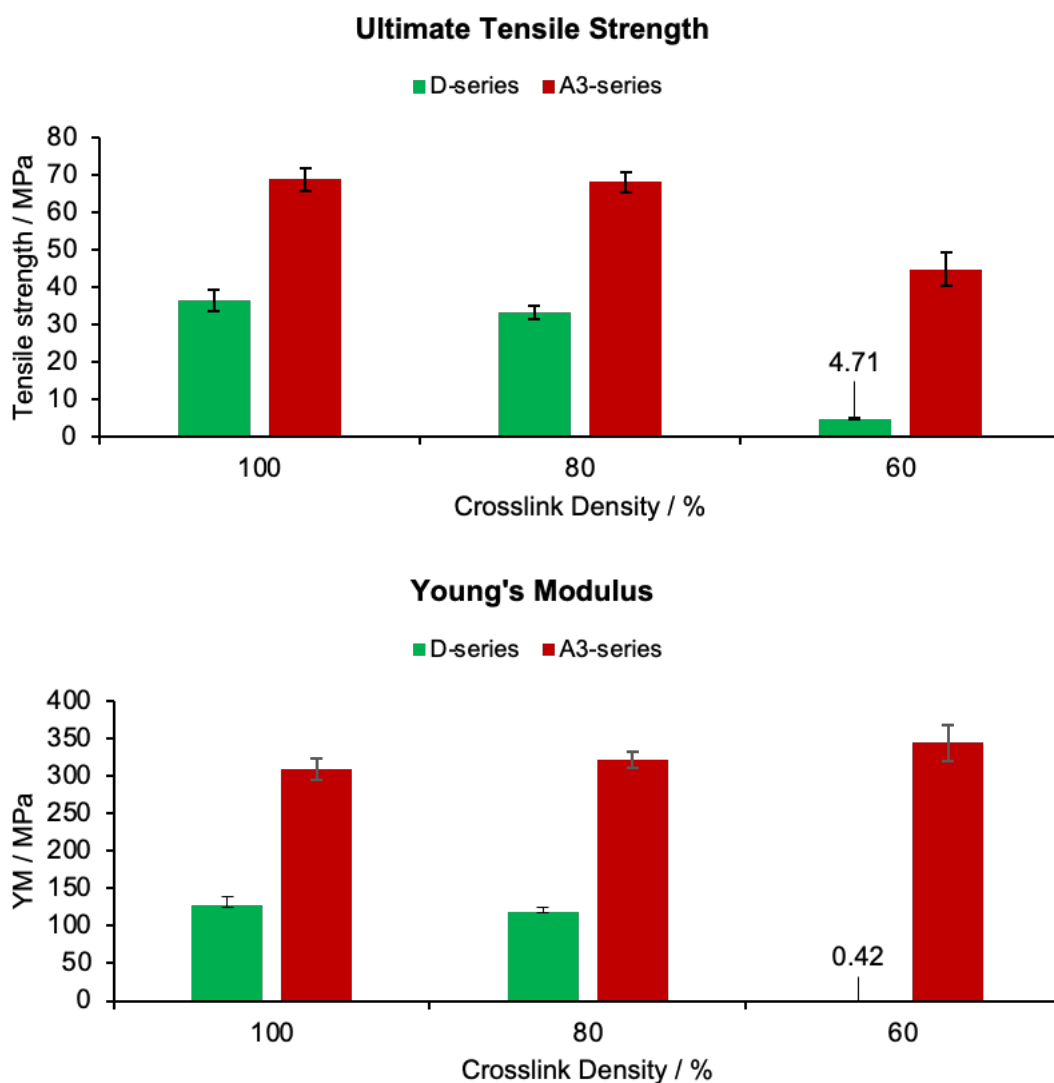

Ultimate Tensile Strength

Young's Modulus

Figure 176: Comparative tensile properties of D-series versus A^3-series.

The ratios of the A^3-series versus the D-series is shown in Table 21 and highlights the percentage of the ultimate tensile stress and Young's Modulus that the D-series could achieve. For ultimate tensile strength, D-100 and D-80 were the best performing and the

closest match to the A^3 polymer compared to D-60, achieving 53% (D-100) and 49% (D-80) of the strength shown by A^3 polymers with the same number of crosslinks per chain. The Young's modulus values in the D-series remained insignificant in comparison to the A^3 polymers, with an equivalent number of crosslinks, as a result of the differences in strain behaviour between the two series, however they were in the same order of magnitude for the D80 and D100 materials which shows great promise as a high-performance material.

Table 21: Comparison of strength properties between the A^3-series and the D-series of polymers.

Ratio of strength properties of A^3-series to D-series

Crosslinks / %	Ultimate Tensile Stress Ratio	Percentage of A^3 / %	Young's Modulus Ratio	Percentage of A^3 / %
100	1.89	53	27.39	41
80	2.06	49	52.02	37
60	9.51	11	17183.50	<1

5.5 Conclusions

To conclude this chapter, several characterisation techniques have been utilised to understand the impact on thermal behaviour (characterised by DSC, DMA and TGA) and material properties (characterised by tensile testing) based on the chemical structure of the polymer networks, which was controlled by the chain limiting PGE monomer, and was characterised by FTIR and GPC. Tensile testing showed good mechanical properties, for the novel dioxazaborocane covalent adaptable network (CAN), which was in the same order of magnitude as a traditional high-performance non-adaptable epoxy-amine polymer network with an ultimate tensile strength of 36 MPa and a Young's Modulus value of 128 MPa compared to 69 MPa and 309 MPa respectively for the highest performing aromatic amine series of the same formulation (A^3).

Chapter 6

Dioxazaborocane Thermoset Polymer

Recycling

6 Chapter 6 – Dioxazaborocane Thermoset Polymer Recycling

6.1 Introduction

So far, this research has been dedicated to preparing dioxazaborocane crosslinked polymer networks via simple, single-stage mixing and casting process, from readily available commodity epoxy resins, amines and boronic acid esters. This research presented several obstacles to achieve free polymer films suitable for characterisation and testing material mechanical performance, which was required to assess the viability for the high-performance applications behind the overall scope of the project.

After successful design at the molecular level, the HA-E2(DEA-5)-D-series materials were obtained and showed great promise as a novel CAN material with excellent mechanical properties. As these polymers have recyclability designed into their structures, so the next logical step, in line with the scope of the research, was to begin recycling the materials via mechanical upcycling methods or molecular disassembly methods. The dynamic nature of the dioxazaborocane crosslinks should allow for facile topological rearrangement at temperatures above T_g, which presents obvious mechanical heat pressing advantages. The dynamic nature also provides recycling routes by exploiting the dynamic bond and chemically manipulating the polymer network structure. Either of these methods can likely provide efficient and novel routes of incorporating thermoset epoxy-amines into a circular economy, which has been visually aided by the idealised scheme in Figure 177.
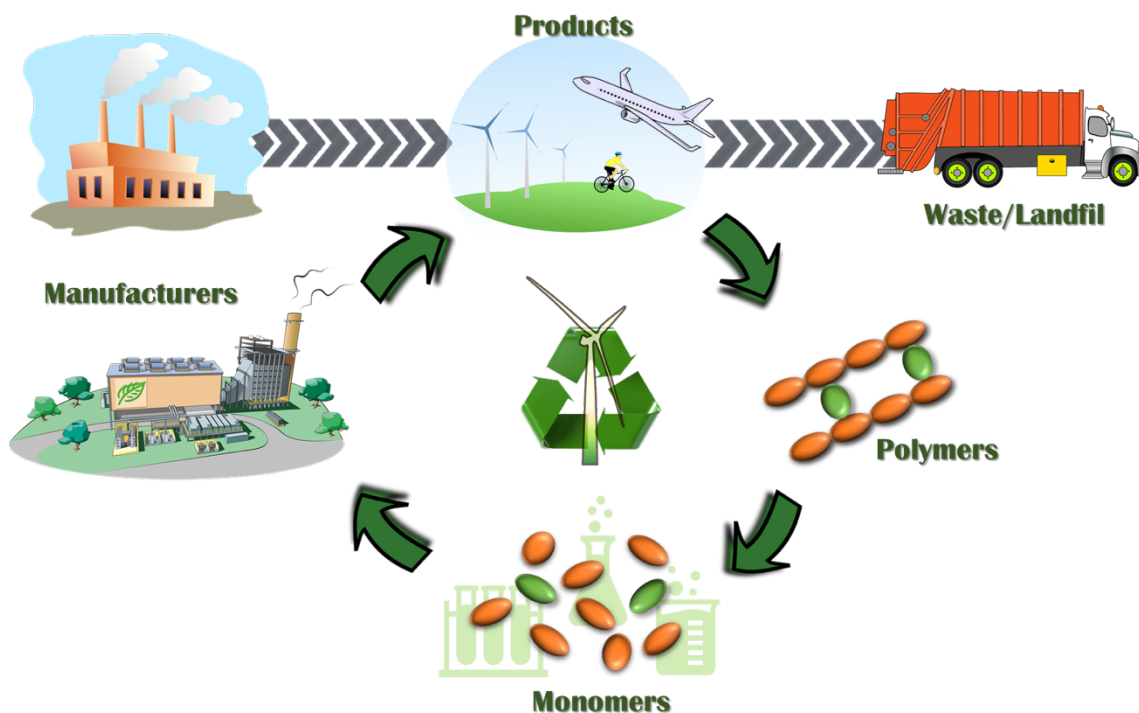
Figure 177: Idealised chemical recycling route for a thermoset polymer partaking in a circular economy recycling process, bypassing its destiny to go to landfill at the end of its service life.

The work presented in this section is the beginning of a long but prosperous journey towards the sustainable future of epoxy-amine thermosets, and where time constraints have somewhat limited the progress (chemical recycling), this work provides a proof of concept.

6.2 Mechanical Recycling

6.2.1 Introduction

Mechanical recycling is the process of turning waste plastics into a secondary raw material without significantly altering the materials chemical structure. This is the most common method in industry and is universally used to recycle thermoplastics as these can all be theoretically recycled by this method with limited impact on material quality.[246,247] Thermosets however cannot undergo this process as they do not melt and therefore cannot flow in response to heat, due to the densely crosslinked structure,

essentially locking polymer segments in place. Figure 178 shows the steps during mechanical processing of currently recycled thermoplastics.
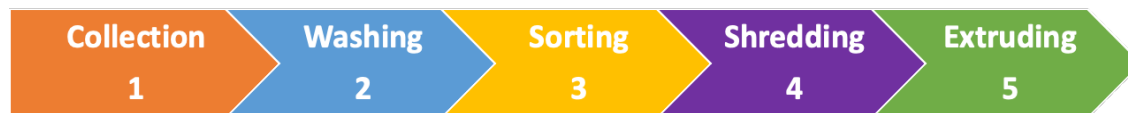

Figure 178: Several steps during a mechanical recycling process

The first three steps of the mechanical recycling process is for the waste to be collected, washed and sorted by type. Washing is an important step as this will remove dust, dirt and impurities from the waste, such as food debris, as impurities can detrimentally affect the integrity of the reprocessed polymers. They are then sorted by colour and thickness before moving on to the shredding stage where they are shredded into smaller pieces ready for reuse. This stage reduces the volume, for easy transportation of waste, as well as ensuring homogeneity in the reprocessed material is maintained.[248] The final step of extrusion is where the shredded plastic can be fabricated into new products by an extruder. The extruder works by using heat to melt the previously separated and shredded polymer as a feedstock, which is fed into and forced through a heated temperature controlled chamber, with rotating screws to soften the material, and is eventually forced out the end as a fixed cross-section extrudate. [249]

In this research so far in Chapter 5, there were observational indications during thermal characterisation techniques and sample preparation techniques that led to the hypothesis that the dioxazaborocane crosslinked materials would flow above T_g temperatures due to the proposed topological rearrangement induced by the dynamic boronic ester bonds. Therefore, rendering these materials viable for thermal recycling methods.

6.2.2 Mechanical Recycling Results

For the mechanical recycling in this work, the D-series materials were ground into smaller particles and heated under compression (170 °C, 30 minutes) using a simple bench-top hot press. The samples were allowed to cool slowly to room temperature overnight in the hot-pressing mould until equilibrated to room temperature (annealing). For all the materials, a cohesive polymer sheet was produced from the ground particles.

6.2.3 Evolution of Mechanical Heat Pressing

During preliminary testing for heat pressing the D-80 material, shown in Figure 179, the ground polymer became a cohesive sheet of recycled polymer, thus proving that mechanical recycling was possible.
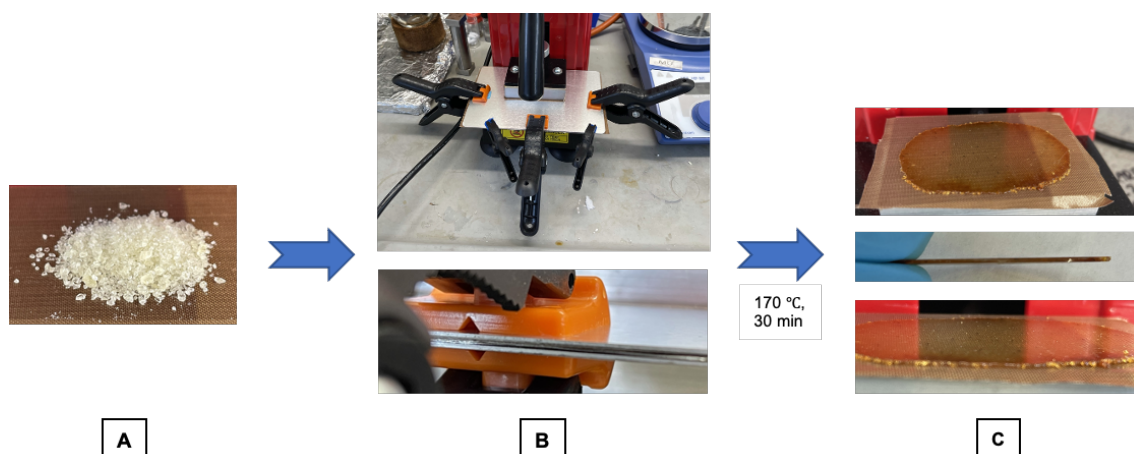

Figure 179: Initial mechanical heat press technique for D-80 materials where A) ground polymer sample is placed on an aluminium plate coated in a non-stick PTFE tape. B) the second aluminium plate is pressed on top and locked in place by bulldog clips the sample is compressed by the pressing block providing pressure. C) shows the resultant polymer sheet.

When the equivalent A^3-80 polymer was subjected to the same conditions for mechanical recycling (Figure 180), the resultant product remained in the same state apart from some degree of yellowing, which is expected for thermoset polymers. This meant that no cohesive sheet was formed and the polymer remained unusable waste, which is the overall obstacle that drives this research.
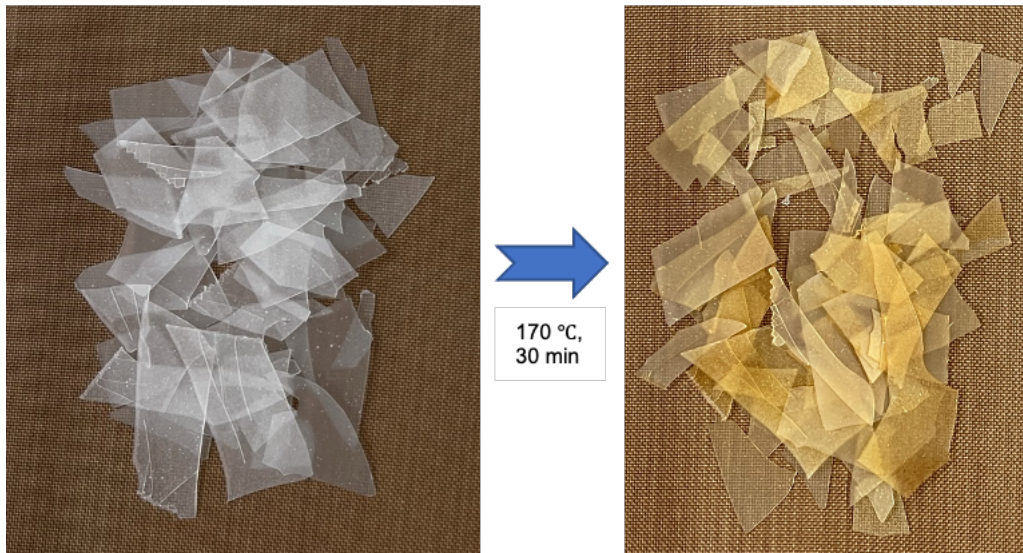
Figure 180: A^3-80 subjected to mechanical recycling conditions.

It is also evident from Figure 179-C that there is clear discolouration, which was previously discussed and hypothesised to be induced by thermal degradation. This will be investigated in Section 6.4. At this point in the research materials had previously only experienced temperatures of 80 °C in the thermal post-cure, which is often the temperature recommended by resin suppliers. Thus, heat pressing at 170 °C produced further yellowing in the polymer as a direct result of the heat press. Therefore, it was decided going forward that the polymers would have a thermal post-cure schedule that reached 170 °C to eliminate any residual polymerisations occurring as result of the mechanical recycling, as this may alter the polymer structure. Furthermore, the edges of the D-80 polymer appeared to be significantly discoloured compared to the centre (Figure 179-C). This was hypothesised to arise due to the exposure to air, caused by the gap between the aluminium plates that can be seen in Figure 179-B. This would result

in increased thermal oxidation at the edges with no contact to the plates or protection from the external environment. This also suggests that measures may be taken to minimise this effect by hot-pressing in an oxygen free atmosphere.

As a result, an aluminium mould was fabricated to alleviate this problem and also provide a means to control the thickness of the polymer sheets produced, which is shown in Figure 181. This appeared to reduce the imperfections at the edges of the recycled sheets. This enabled materials to be recycled and suitable for laser cutting fresh tensile dogbones to assess the key physical parameters to be retained by the recycled polymers, such as Young's modulus and tensile strength.
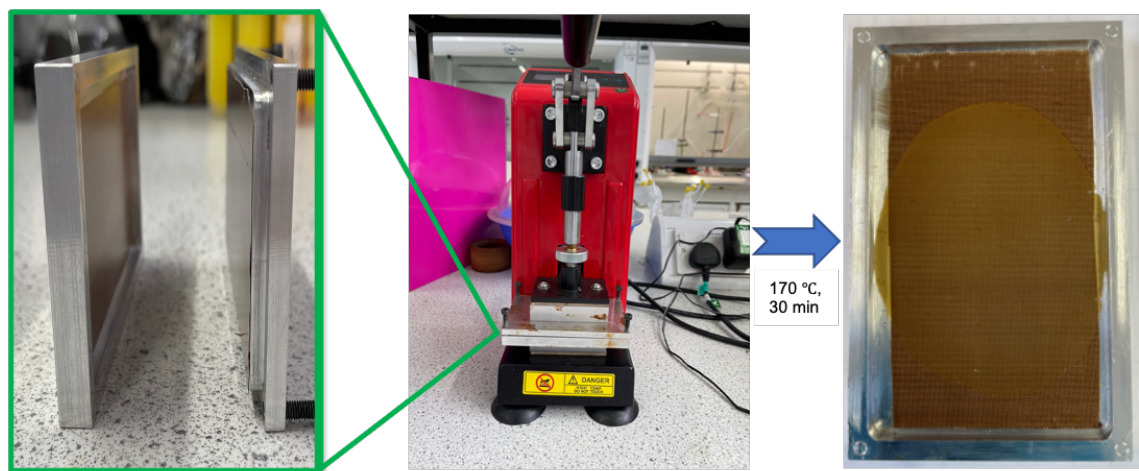

Figure 181: D-80 recycled polymer sheet produced in an aluminium mould (highlighted in green).

It was hypothesised that the D-100 materials may be less able to achieve facile topological rearrangement due to the lack of free diethanolamine (DEA) groups to exchange with.[40] However, it was apparent, from the evidence in Figure 182, that the D-100 materials could form cohesive sheets effectively. Theories regarding the effects of free DEA groups on mechanical recycling have not been probed further due to time constraints on this project but remain an area to focus research efforts on in the future. This may also be complimented with studies on the effects of increasing

dioxazaborocane content on the thermal degradation of the D-series polymers as it is hypothesised that the coordination of the nitrogen lone pair to boron may protect the nitrogen from oxidation.
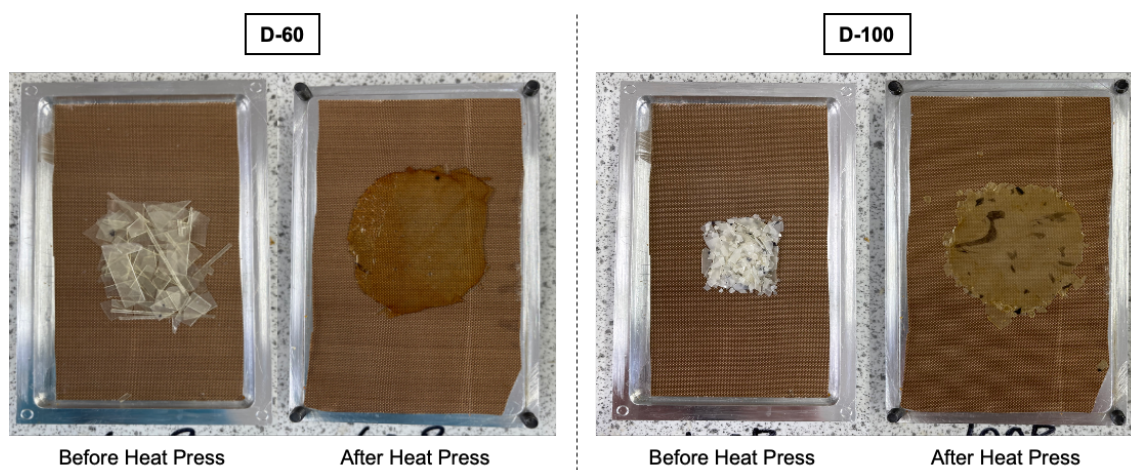

Figure 182: Broken test samples of D-60 and D-100 materials before and after heat pressing in the aluminium mould.

6.2.4 Tensile Evaluation of Mechanically Recycled Material

As it was previously established in the characterisation chapter, the D-60 polymers had a T_g temperature below room temperature and hence, were in the rubbery state at room temperature, so exhibited relatively high strain values (at low stress) compared to the D-80 and D-100 materials. The glassy dioxazaborocane crosslinked polymers (D80-D100) demonstrate similar high Young's Moduli and are better suited for high-performance applications.

D-60 parent materials were mechanically recycled and fresh dog-bone specimens were laser-cut for tensile testing. The results are displayed below in Figure 183 and Figure 184. With this material there is a significant difference in the ultimate tensile stress (UTS) between the parent (D-60) material and the mechanically recycled (D^R-60) material, with the recycled material only retaining an average of 38% of the original UTS properties.

However, the strain remained statistically unchanged for this material, retaining 97% of the original strain of the parent material. This resulted in a net reduction in Young's modulus for this material undergoing a mechanical recycling process, where the recycled material only had a Young's modulus value that was only 43% of the original parent material and thus, was outside the error of the original significantly.
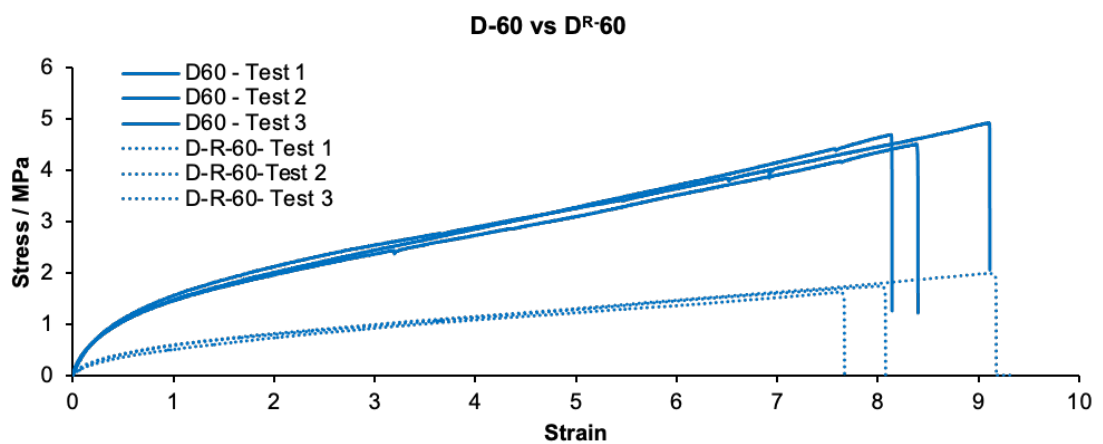

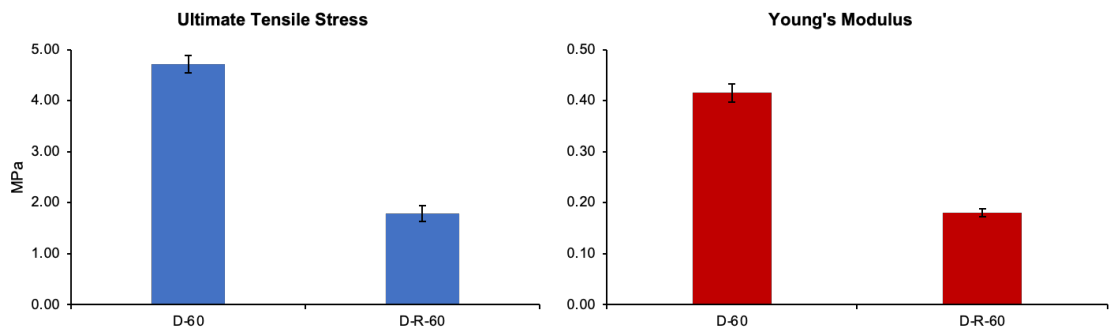Figure 183: Tensile results for D-60 (parent) vs D^R-60 (recycled).

Figure 184: D-60 vs D^R-60 bar graph showing UTS and Young's modulus results.

Table 22: Average D-60 vs D^R-60 key physical parameters measured by tensile tests with standard deviations.

Polymer	Ultimate Tensile Stress / MPa	+/-	Young's Modulus /MPa	+/-	Strain at Break	+/-
D-60	4.71	0.17	0.42	0.02	8.53	0.41
D-R-60	1.79	0.15	0.18	0.01	8.28	0.65

The results of the 80-100% crosslinked material tests are shown in Figure 185 and Table 23. For the D-80 and D-100 materials, the key physical parameter of UTS in the recycled materials remained relatively similar, in comparison to the parent material, which is in contrast to the D-60 materials. The UTS for the D^R-80 material was 91% of the original and the D^R-100 material had a slight increase of 4% of the original parent material, which were both within the error of the original samples. The Young's modulus of the D^R-80 material retained 81% of the original parent material. This lies outside the error range of the original due to the large difference in strain (40%) but is less significant than the 60% crosslinked samples. The D^R-100 samples showed a 7% increase in the Young's modulus value, within the reported error, compared to the original. The increase in these material properties after annealing in the D^R-100 materials is hypothesised to arise due to new crosslinks forming as a result of minor residual unreacted boronic crosslinker, which may occur due to the material flowing under pressure and heat to a preferable alignment or may simply be due to the annealing process. Some residual boronic ester content is likely, since the critical gel point (P_{gel}) is reached with less conversion of the polymerisation reaction when the stoichiometry is increased and thus, some boronic esters may not be in close enough proximity to the complimentary reactivity of a DEA group to react before the topology is frozen in a glassy physical state. Therefore, it would be an interesting development to further investigate the annealing process as part of the post-cure treatment of the original materials as future work. The strain at break in the recycled 80% and 100% crosslinked materials increased by 40% and 17% respectively.

Furthermore, for the D-80 materials there was a noticeable change in the ductile behaviour of the recycled materials, in the stress-strain curves, which exhibited an increase in strain and some degree of yielding compared to the parent material. Although the D^R-100 materials were statistically unchanged in their strain at break they did also experience increased yielding compared to the parent material. This was hypothesised to be a result of the annealing process during mechanical recycling, which may reduce stresses imparted in the material from the original cure process and allow the polymer segments to arrange themselves in a preferable formation since they can flow at the high temperature.
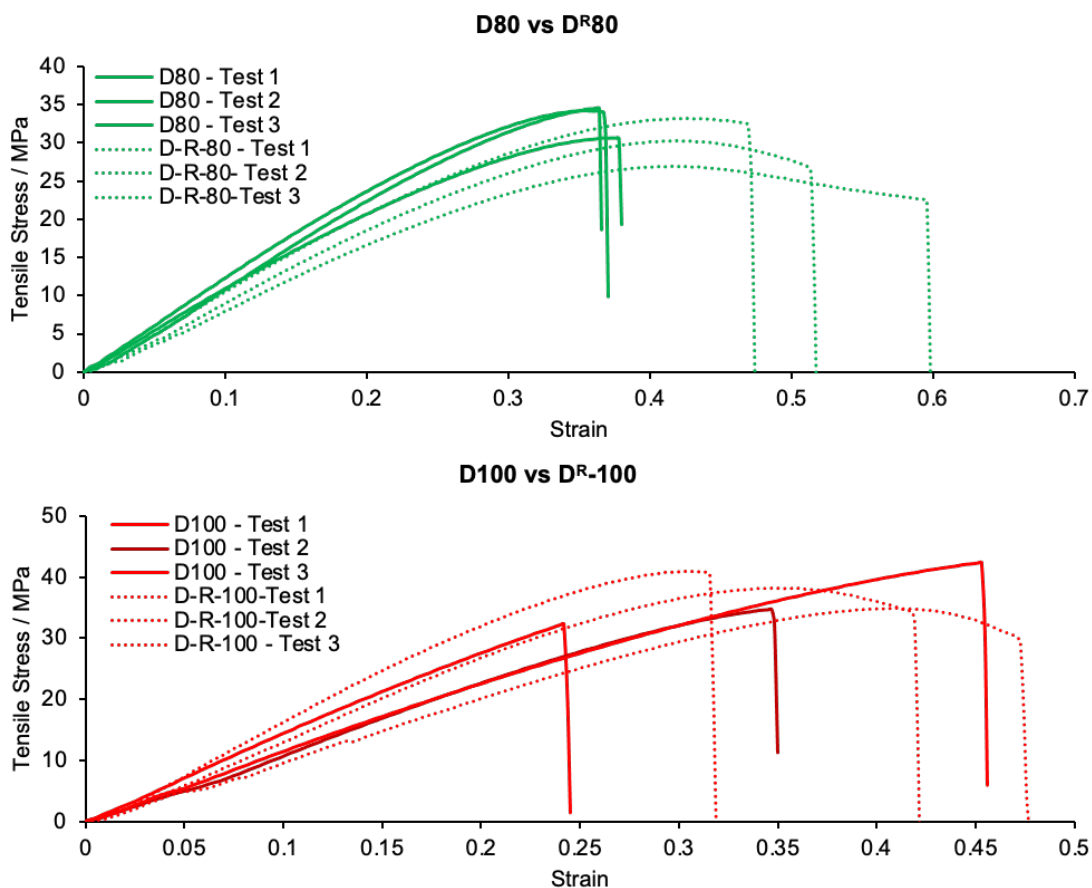

Figure 185: Tensile results for D-80 and D-100 (parent) materials vs D^R-80 and D^R-100 (recycled) materials.

257

Table 23: Key physical parameters, from tensile testing, for D-80 and D-100 (parent) materials vs D^R-80 and D^R-100 (recycled) materials.

Polymer	Ultimate Tensile Stress / MPa	+/-	Young's Modulus / MPa	+/-	Strain at Break	+/-
D-80	33.132	1.758	119.130	6.177	0.373	0.005
D-R-80	30.106	2.517	96.212	7.736	0.522	0.056
D-100	36.480	2.992	127.857	11.281	0.343	0.086
D-R-100	37.965	2.461	136.457	25.031	0.402	0.065

In comparison with the A^3-series materials, the results previously described with regards to the parent D-series (Chapter 5 - Section 5.4.1.3) remain the same (within error) for the recycled materials and comparative bar graphs have been shown in Figure 186 below.
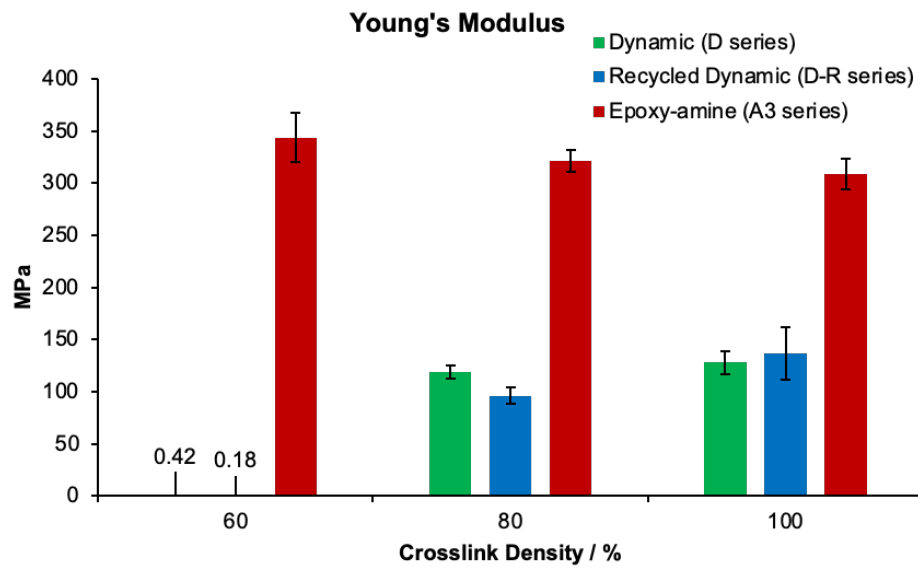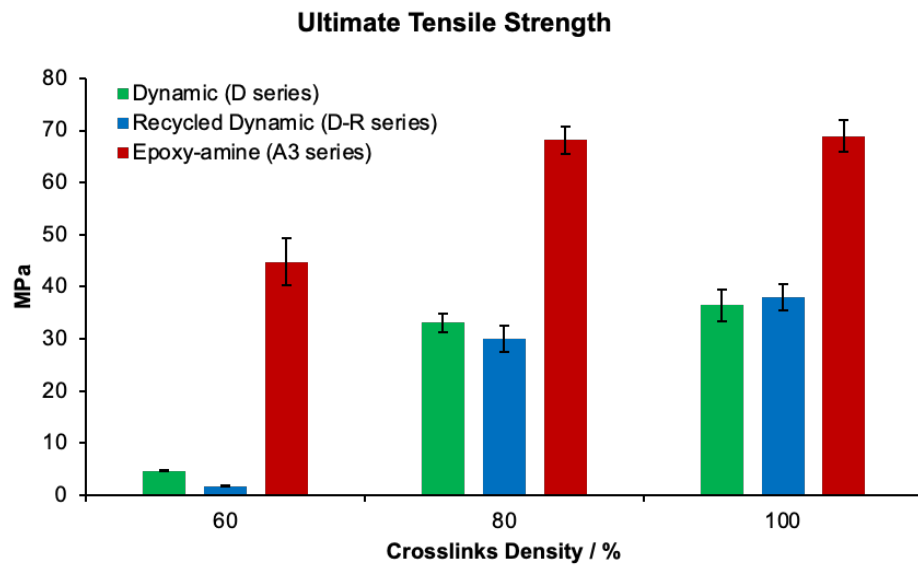
Figure 186: Bar chart showing comparative tensile properties of the D-series, recycled D-series and A^3-series materials with 60-100% crosslinking.

The trend observed with increasing crosslink density is that the more crosslinks in a material the more the properties of the original/parent material are retained in the recycled material, as visualised in Figure 187.
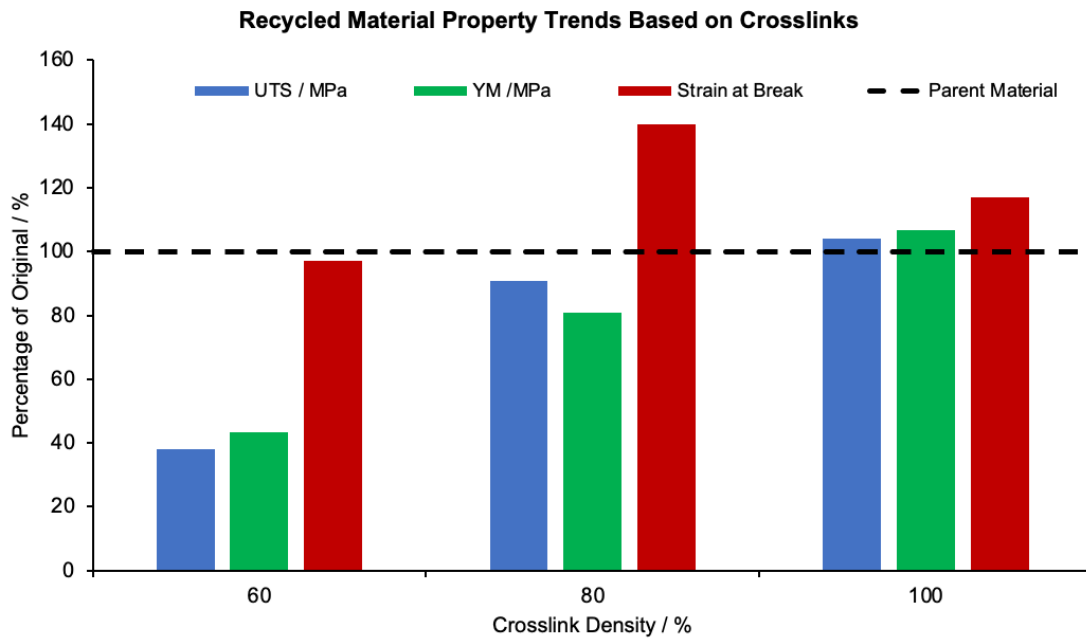
Figure 187: Material property retention in recycled materials

On another note, the mechanical recycling/annealing process was also effective at removing bubbles formed during curing in some of the thicker polymer films. This is shown in Figure 188 below, where a bubbled polymer film of D-80 material was snapped in two pieces and one piece was annealed to show the effect. After the annealing process the bubbled defects were not present in the same material. This would present an attractive opportunity to develop the polymer curing process in the future, particularly to increase the ductility of the polymers for their end-use, as this will provide more reliable products. However, only materials without bubbles in their original cure were studied in this research.
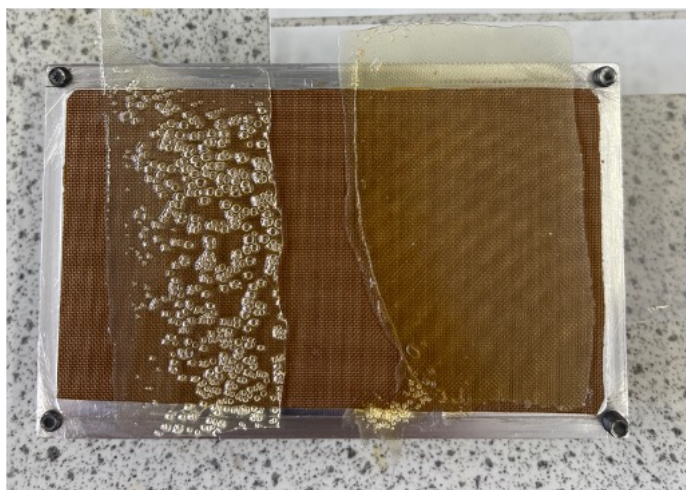
Figure 188: D-80 polymer which had bubbles prior to annealing at 170 °C (left) and after annealing (right.

In conclusion, Whilst the A^3-series exhibit a higher ultimate tensile strength and Young's modulus than the D-series as well as the recycled D-series, the dioxazaborocane networks show great promise as a new class of high-performing materials, especially since these can be recycled whilst retaining most of the material integrity for the more densely crosslinked materials. A full table of material properties can be found in Section 10.3.1 of the appendix.

6.3   Chemical Recycling

Whilst mechanical recycling presents excellent opportunities for upcycling, and re-use. This requires the secondary use of the material to require the same polymeric structure as the original and therefore cannot be molecularly fine-tuned for the next envisioned purpose. Ultimately, this method is limited due to degradation inducing recycling process and relies heavily on uncontaminated waste streams, which is hard to avoid in a post-consumer market as mixed material composites cannot be mechanically recycled due to the inability to separate the different materials.

To circumvent this problem another route to recycling is to deconstruct the thermoset polymeric materials to its molecular building block state, which can then be separated from mixed materials and potentially fabricated into new materials or composites. A chemical process which allows the selective disassembly of the dioxazaborocane network was designed by exploiting the equilibrium of the boronic esters, that form the crosslinks, to deconstruct the polymer network. This would allow dissolution of the resulting linear (thermoplastic) polymer chain and separate boronic ester crosslinkers in solution, when exposed to specific conditions that unlock the network structure. Theoretically, the soluble components can then be separated.

One of the key attributes of high-performance thermoset networks is that they are resistant to a wide range of aggressive chemicals and should remain undamaged and insoluble upon exposure.[250–252] Therefore, the D-100 polymer network was immersed in a range of solvents including ethanol, DMSO, toluene, acetone, THF, distilled water and 1M NaOH, which all showed no material integrity loss after 72 hours of immersion, which is expected in traditional epoxy-amine thermosets. Interestingly the D-100 material did not degrade upon exposure to water which is renowned for hydrolysing boronic esters back to the boronic acid.[187,203] The enhanced stability of the dioxazaborocane network, through the N-B coordination, is attributed as the main factor preventing hydrolysis of the crosslinked esters, thus increasing the materials hydrolytic stability.[220,253]

In the work presented in this research, it was envisioned that an excess of monoboronic acid or an excess of diol would force the boronic ester equilibrium to entropically favour the monoboronic ester rather than the diboronic ester crosslinked state. This is sometimes referred to in literature as diolysis.[194] The two chemical disassembly routes are shown in Figure 189. Method A utilises a monoboronic ester to displace the diboronic ester. However, this would inherently return an altered linear polymer containing non-crosslinking dioxazaborocane groups and thus, method B was proposed as a route that

would be better for a circular economy, as this returns a simple epoxy-amine linear polymer ready for re-use, and not just those requiring dioxazaborocane crosslinked polymers.
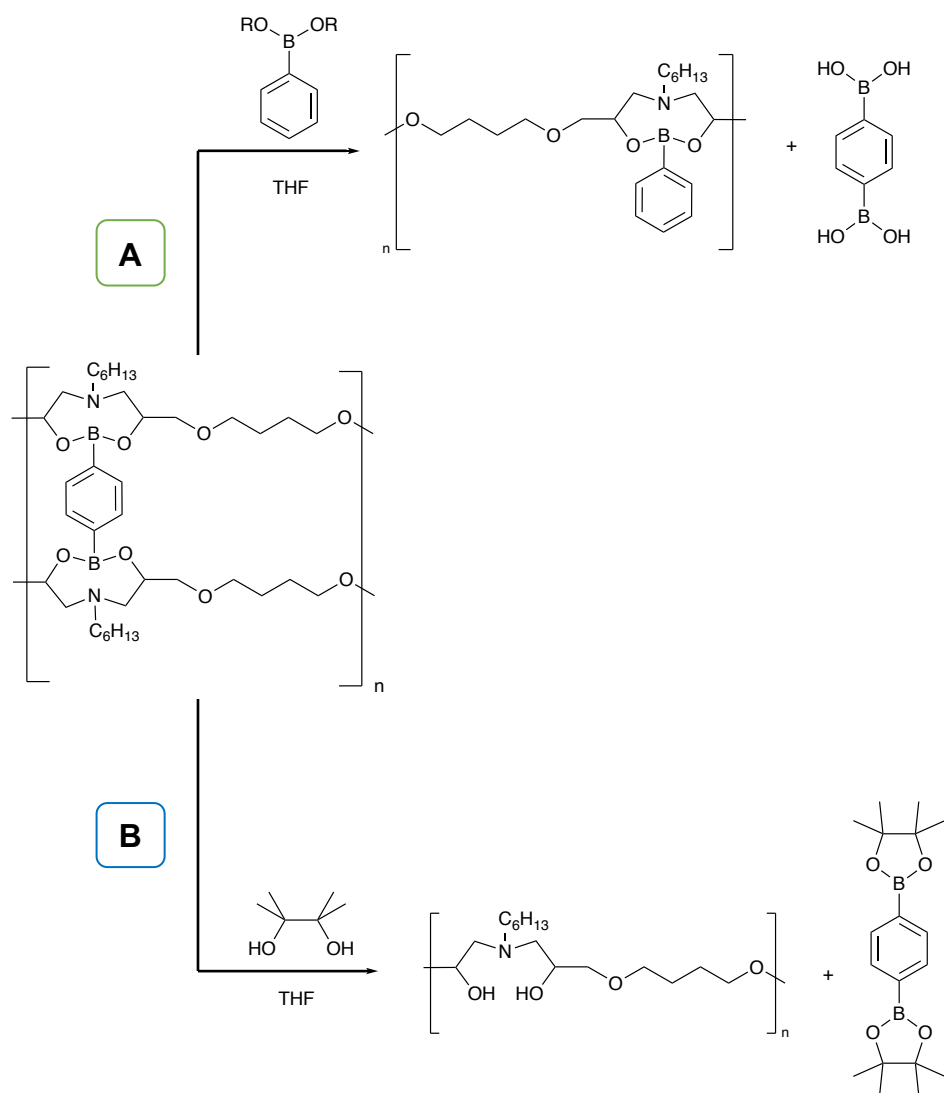

Figure 189: Chemical disassembly pathways. A) utilises monoboronic ester 1d and (B) utilises commercially available pinacol.

6.3.1 Method A – Monoboronic Ester Recycling

In this method of chemical recycling, the D-100 and A^2-100 polymer networks were investigated and compared. The proof of concept behind this route was realised by successful solubility in THF. THF was chosen as the solvent for GPC analysis to be

conducted if successful. The GPC results of these were also compared to the pinacol recycling method (method B).

Preliminary solubility of the D-100 material was tested to predict the viability of this recycling method. Samples of a set size (10mm x 5 mm x 0.3mm) of D-100 and A^2-100 materials were immersed in THF solvent as a control and solution of THF with a 5% (w/v) of monoboronic ester (1d) mixed as the recycling solution. This resulted in no dissolution of the control THF samples and no dissolution of the A^2-100 sample in the recycling solution. The D-100 material did dissolve in the recycling solution, which indicated that the monoboronic ester addition was responsible for dissolution and thus, supported the hypothesis. The dissolution is shown in Figure 190. It is worth noting that dissolution was apparent after 24 hours but the samples were left up to 72 hours to ensure maximum dissolution and to give the control solutions more time, in the case the D-100 may dissolve. The lack of dissolution suggested the D-100 materials had good chemical resistance, which is expected of thermoset epoxy-amine polymers.
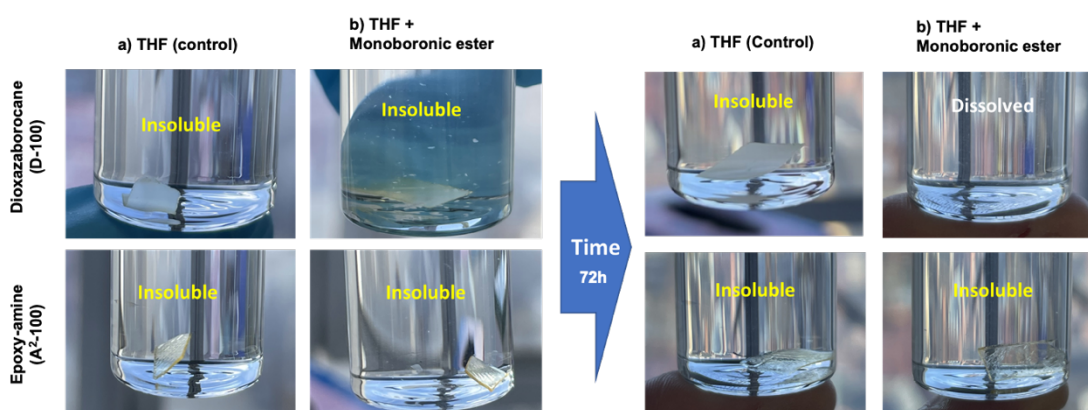

Figure 190: Dissolution of dioxazaborocane material (D-100) after 72 hours in a solution of monoboronic ester -1d (b) compared to A.

6.3.2 Method B – Pinacol Diolysis

Method B, of Figure 189, was investigated since it proposed a more scalable and low-cost route for returning the original linear polymer and hence, a better option for a circular economy in the future. Pinacol has recently been successfully employed by Tajbakhsh et al. to de-crosslink self-healable, boronic acid functional methacrylate linear polymers, that were originally crosslinked with the complementary reactive 1,2-diol functional polymers of the same type of methacrylate polymer chain.[254,255] However, it has not been achieved with dioxazaborocane crosslinked materials to the best of my knowledge.

A more controlled evaluation method was required so GPC evaluations would be effective at comparing both recycling systems, as the large excess of monoboronic ester or pinacol recycling agent would saturate the GPC graphs produced. Therefore, knowledge of the mass of the polymer allowed the calculation of moles of reactive groups in the polymer. Hence, limiting the excess to 5 equivalents per amine group in the polymer sample for all polymer types could be achieved.

The 100% crosslinked materials were selected for this investigation since the excess approach would theoretically occupy all of the reactive sites. The most highly crosslinked dioxazaborocane material was chosen for this study, which was established in Section 5.4.1.3 (~36 MPa for UTS), as this represented the most challenging to disassemble due to the high crosslink density and expected lower penetrability of small molecules (such as pinacol and THF).[208] The selected 100% crosslinked polymers were weighed (D-100 = 20 mg, A^2-100 = 20 mg) and were immersed in 10 mL of THF solvent as a control. This was to enable GPC analysis to be conducted without the need for serial dilutions. Sample sets were also immersed in 10 mL of THF containing monoboronic ester (**1d**) for dissolution route A, or pinacol for dissolution route B, in a 5:1 excess to DEA groups (amine) in the polymer, which is equal to the number of reactive groups used for

crosslinking the boronic ester. This excess was back-calculated from the overall mass of the original polymer formulation and hence, the amount of moles of amine in the total formulated polymer could be established and subsequently the fraction of amine present in the 20 mg sample. The number of moles of amine is equal to the monoboronic ester per functional group of diboronic ester therefore multiplying this by 5 would create a 5:1 excess. An example calculation has been shown in the appendix Section 10.5 for a D-80 polymer, which is to be discussed in Section 6.4 regarding the degradation.

As expected from the preliminary trial of the D-100 material in monoboronic ester the traditional epoxy-amine polymer (A^2-100) did not dissolve and the only peaks visible on the GPC chromatograms were the recycling agent peaks and small oligomeric chains previously discussed in Section 5.2.1.2. The D-100 samples dissolved in both pinacol and monoboronic ester solutions. This proved the hypothesis for the pinacol method - B. The GPC chromatograms of the D-100 material in the various conditions are overlayed and shown in Figure 191 along with the linear polymers (D0 control and D0 with 1d) as a reference. The molecular weight data retrieved from the GPC software is shown in Table 24.
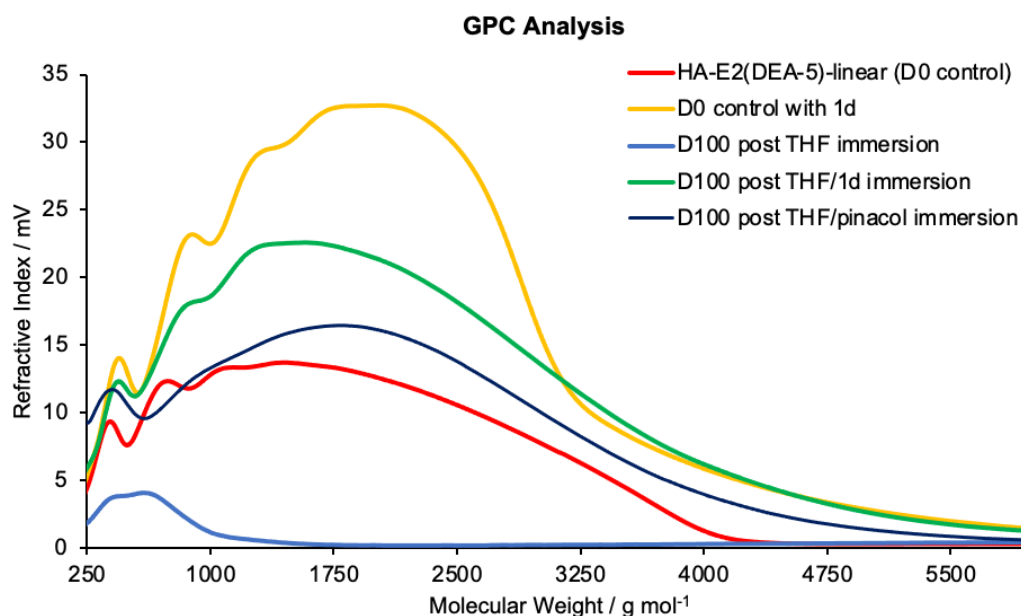
Figure 191: GPC chromatograms of the chemical recycling pathways of D-100 compared to the linear polymer and linear polymer in the presence of monoboronic ester (1d). The x-axis begins at 250 g mol^{-1} to omit the large peaks that arise due to the small recycling agent molecules (1d or pinacol).

Table 24: GPC molecular weight outputs for recycled D-100 materials with comparative control materials.

GPC Results

Polymer / Recycling Agent	M_n (g/mol)	M_w (g/mol)	PD
D0 control	1556	1816	1.17
D0 / MBE-1d	1845	2103	1.14
D100 / MBE-1d	1312	1751	1.33
D100 / Pinacol	1387	1812	1.31

Table 24 shows that the D-100 polymers have similar molecular weight (M_w) values as the linear polymer (D0). This suggests the dioxazaborocane network has been disassembled, as intended, to the linear (thermoplastic) polymer, which is soluble. The D0 material that was dissolved in the THF solution has a slightly high molecular weight

267

values as this linear polymer will have phenyl boronic ester groups complexed to the polymer chain that have reacted with the DEA groups, thus increasing the molecular mass. The number average molecular weight (M_n) of the recycled D-100 polymers is revealed to be slightly lower than the original thermoplastic D0 polymer. This evidence supports a hypothesis that the network polymers may be less efficient at chain growth as the viscosity of the rubbery increases to a glassy network during the polymerisation reaction, resulting in suppression of reaction at high conversion due to limited diffusion as the materials undergo vitrification.

The solvent resistance of D-100 is displayed by the D-100 post THF (light blue) line. This is evident as there is very little soluble oligomer content and almost no high molecular weight content, which is due to the insolubility of the network polymer/thermoset in THF. In comparison, the D-100 material immersed in a solution with 5 equivalents of recycling agent (pinacol = dark blue, 1d = green) shows a large concentration of soluble polymer content and both have a molecular weight distribution similar to the linear polymers (D0 in THF and D0 with monoboronic ester (1d)). It is noticed that the relative concentrations of the soluble polymers are slightly different, which is likely due to some measuring error as a result of the small masses of polymer samples (mg) and thus, concentrations naturally may vary slightly from 2 mg/ml.

Overall, the GPC analysis supports both mechanistic pathways for dioxazaborocane network disassembly. In order to support this evidence further, the pinacol recycled D-100 solution was subjected to evaporation, to remove the THF, and the residue was dissolved in $CDCl_3$ for ^1H NMR analyses. This results are shown in Figure 192. This evidence showed that the residue of the D-100 polymer recycled via method B was a mixture of 1,4-phenylenediboronic pinacol ester (**7**) and the linear polymer, which is evident from the identical spectra of **a** with **b** and **c** in Figure 192. This is acknowledged

as there are no discernible hydrogen environments to indicate dioxazaborocane complexation, which was previously established from the model tests in Chapter 3.
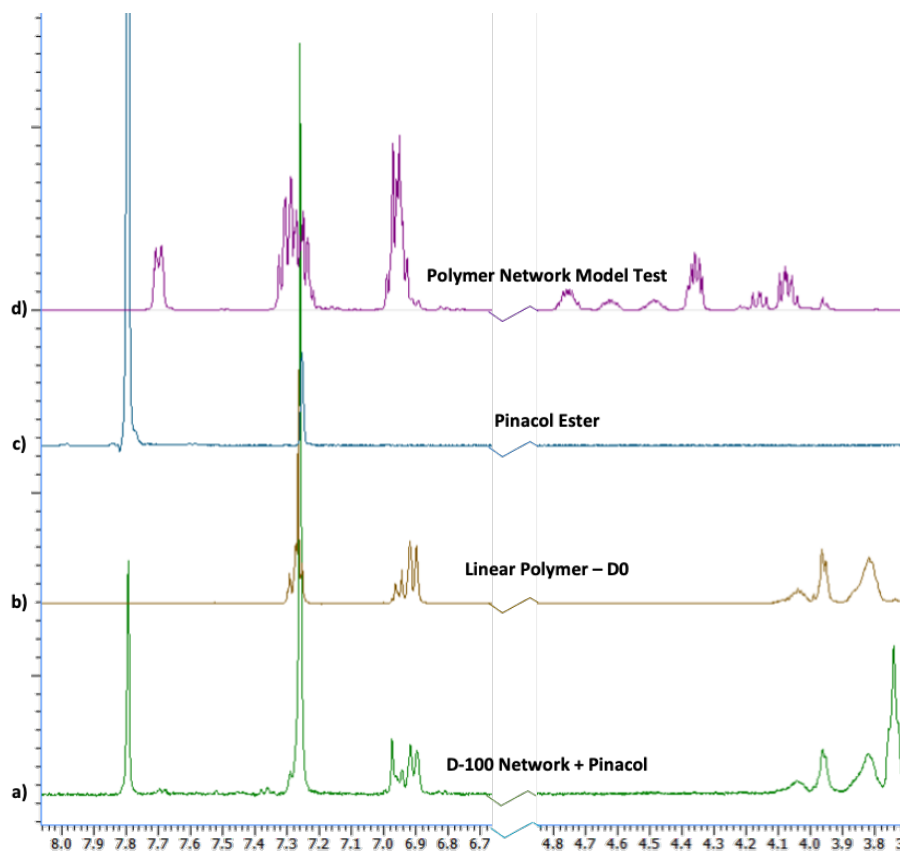

*Figure 192: ^{1}H NMR overlays of a) D-100 after dissolution in the THF/pinacol solution via method B (green), b) the linear polymer D0 (brown), c) 1,4-phenylenediboronic pinacol ester (**7**) (blue) and d) the model tests showing the successful dioxazaborocane complexation at 7.7 ppm and the diastereomer peaks between 4.3 ppm and 4.8 ppm (pink). The section between 4.8 ppm and 6.7 ppm has been omitted due to lack of any peaks for clarity.*

The evidence presented in the previous two sections supports the hypothesis that the dioxazaborocane network polymers can effectively be recycled back to the molecular building blocks via molecular manipulation by exploitation of the dynamic boronic ester bonds. Unfortunately, due to time constraints on this project, separation of the products from the recycling solutions has not been realised for the time being. Therefore, this research remains as a proof of concept and subject to future work in order to achieve its

full potential towards a circular economy. This chemical recycling method provides two promising routes of recycling: a) solubilising the polymer will enable recovery of high-performance fibres (carbon/glass) from the polymer matrix ready for re-use and b) potential collection of molecular building blocks to reform the network. This shows great promise towards a circular recycling economy for thermoset polymers, which is vital for the reduction of plastic waste.

6.4   Degradation of Mechanically Recycled D-80 Materials

The purpose of designing recyclability into the molecular structure of the polymer is to enable the repurposing of these indestructible materials, at the end of their service life, into new recycled products. It is expected that the materials will undergo several recycling cycles over the course of their existence. During mechanical recycling, the material is subjected to extreme heat for extended periods. Therefore, a more comprehensive evaluation of the impact of repeated mechanical recycling on the chemical, thermal and mechanical properties was required.

For this work, a virgin sample of D-80 was prepared and was subjected to 3 mechanical recycling processes, described in Section 6.2, with characterisation by infra-red spectroscopy, GPC (after chemical disassembly in THF/ pinacol), tensile testing and thermal analysis (T_g by DSC) at each stage of recycling, plus characterisation of the virgin D-80 polymer.

6.4.1   Oxidation by FTIR

Infrared spectroscopy revealed low levels of apparent thermal oxidation.[229] This is shown in Figure 193. This is characterised by the presence of weak absorption bands indicated on Figure 193 at 1658 cm^{-1}, which is associated with amine oxidation, and at 1738 cm^{-1}, which is characteristic of epoxy resin oxidation.

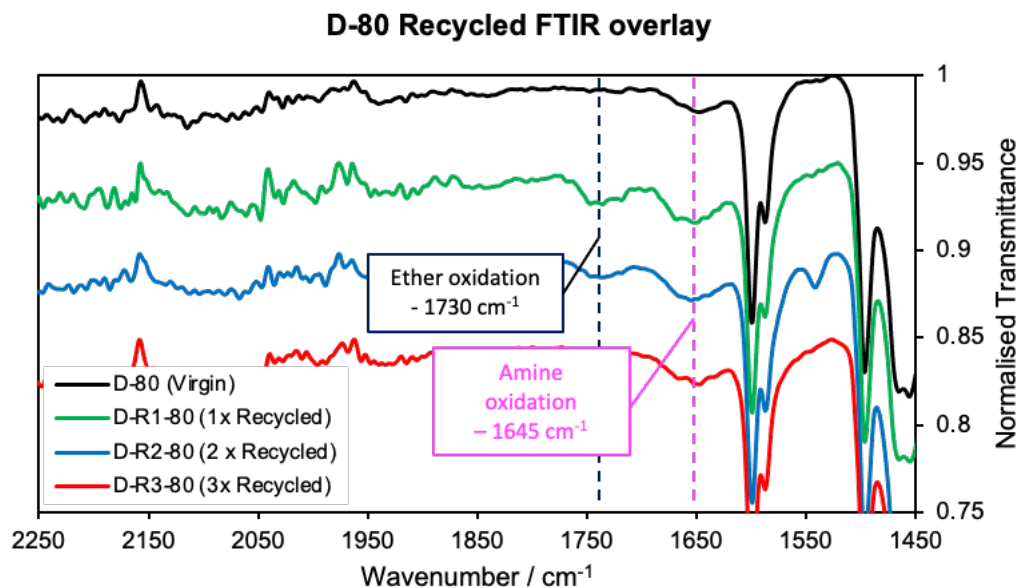*Figure 193: FTIR spectra of D-80 polymer through 3 mechanical recycling processes normalised to CH stretching peak at 2854 cm^{-1}.*

6.4.2 Molecular weight by GPC

Polymers exposed to extreme temperatures, are prone to degradative oxidation reactions as well as chain scission reactions in the polymer chains.[229,256] Therefore, to examine the possibility of both, the polymer was subjected to the pinacol chemical recycling method, after each mechanical recycling stage, and analysed by GPC. The results of this analysis are shown in Figure 194. The results here have been normalised to the maximum peak height above a molecular weight of 600 g mol^{-1}. This was to enable a better comparison of the molecular weight distribution of the polymeric material, at each mechanical recycling stage, and negate the effects of large recycling agent peaks at molecular weights below this value. The samples were run in triplicate and the averages of the molecular weight values are shown in Table 25.

A slight reduction in the molecular weight distribution was observed at the higher molecular weight upon mechanical recycling, which was proportional to the number of

recycling processes the material was subjected to. This evidence suggests a slightly larger proportion of shorter chains which is hypothesised to arise as a result of apparent degradative oxidation or chain scission reactions at elevated temperatures.
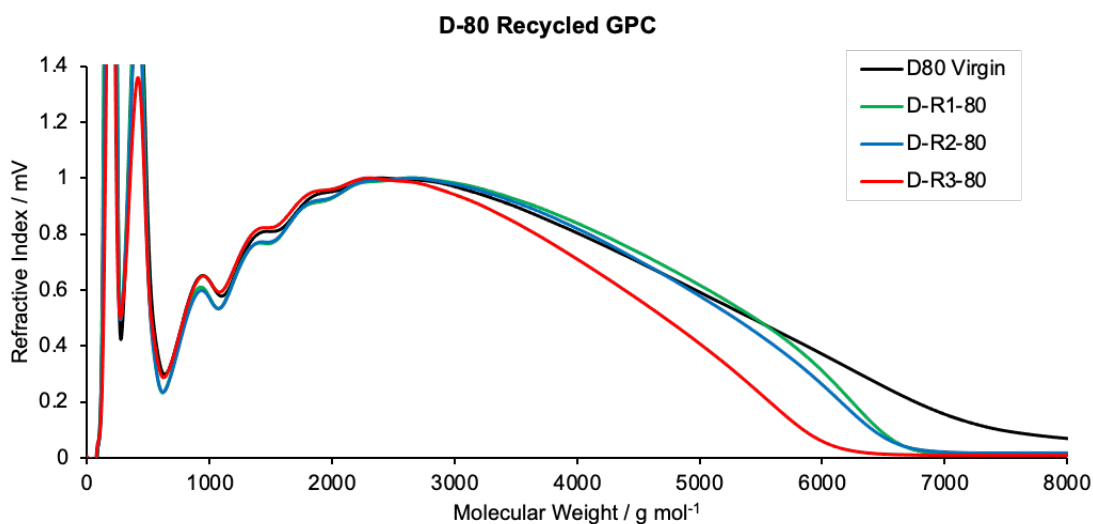

Figure 194: GPC graphs of a D-80 polymer, chemically recycled by method B, after each successive mechanical recycling step.

Table 25: Molecular weight values for D-80 polymers subjected to multiple mechanical recycling processes.

	M_n (g/mol)	Std Dev	M_w (g/mol)	Std Dev	PD	Std Dev
D-80 (virgin)	1780.667	4.028	2530.000	6.481	1.421	0.003
D-R1-80	1874.250	63.077	2665.000	126.890	1.421	0.021
D-R2-80	1821.250	35.770	2555.500	77.240	1.400	0.020
D-R3-80	1735.500	38.590	2351.250	64.590	1.350	0.010

6.4.3 Mechanical Properties

Furthermore, the mechanical properties were assessed after each successive mechanical recycling process by tensile testing. The results are shown in Figure 195 and Table 26. The ultimate tensile strengths of the recycled material were generally retained in the materials R1-R3, with a slight reduction from the virgin D-80 polymer after the initial recycling process. As discussed previously, the annealing process is hypothesised to

increase the ductility of the polymer network, reducing the brittle properties, as is evident from the increased strain at break and slight yielding.
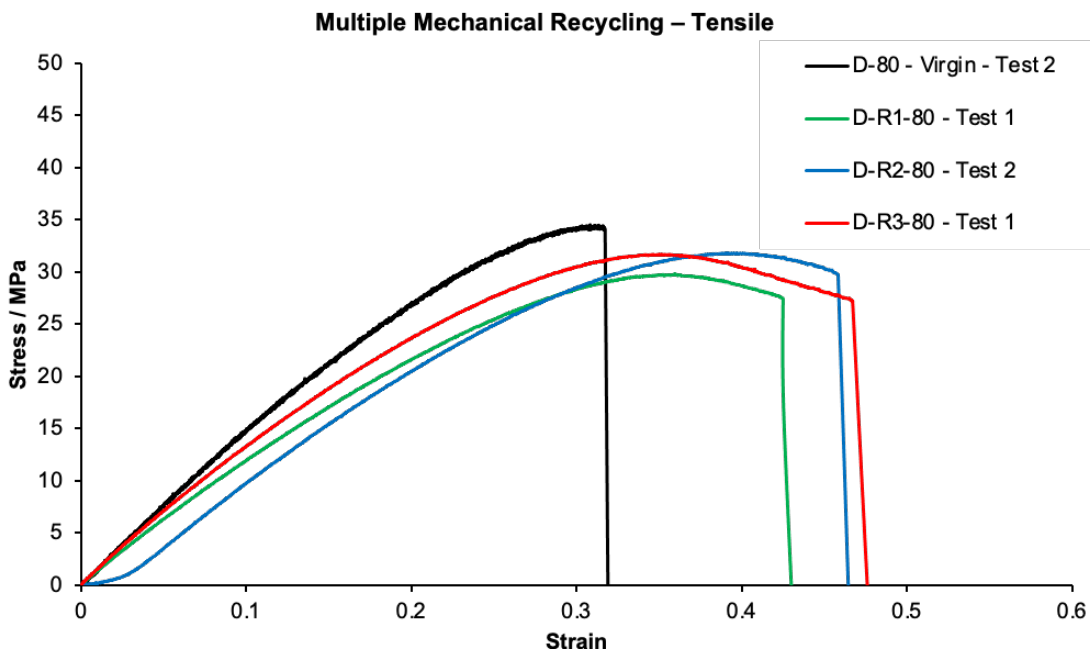

Figure 195: Selected representative tensile results of D-80 polymer after 3 mechanical recycling processes. All tests are overlayed in the appendix Section 10.6.2.

Table 26: Key tensile testing parameter values.

	Ultimate tensile strength / Mpa	Std Dev	Youngs Modulus / MPa	Std Dev	Strain at Break	Std Dev	Stress at break / MPa	Std Dev
D80 Virgin	33.77	1.47	114.52	3.29	0.32	0.02	33.41	1.09
D80 - 1x Recycled	29.81	0.16	95.16	1.91	0.43	0.01	27.59	0.07
D80 - 2x Recycled	30.91	0.77	101.59	1.66	0.49	0.03	27.27	2.44
D80 - 3x Recycled	31.65	-	112.23	-	0.47	-	27.21	-

The tensile strength decreased, from an average of 33.77 MPa to between 29.81-31.65 MPa for recycled materials, after the first mechanical recycling process but remained statistically similar between subsequent recycling processes. Thus, indicating minimal

degradation through repeated recycling processes which is promising for the intended end-use.

6.4.4 Thermal Properties by DSC

Degradative thermal oxidation processes are known to result in lowering of the T_g values of polymers as a result of chain scissions.[257] Therefore, thermal analysis of the D-80 materials by DSC, after each successive mechanical recycling process, was conducted to determine the T_g temperatures of the material. The temperature runs were performed at 100 °C per minute, as the lower 20 °C per minute runs showed little T_g response. The results of the first temperature run at 100 °C per minute (as these had the strongest response) for each recycled material are shown on a comparative graph below in Figure 196.
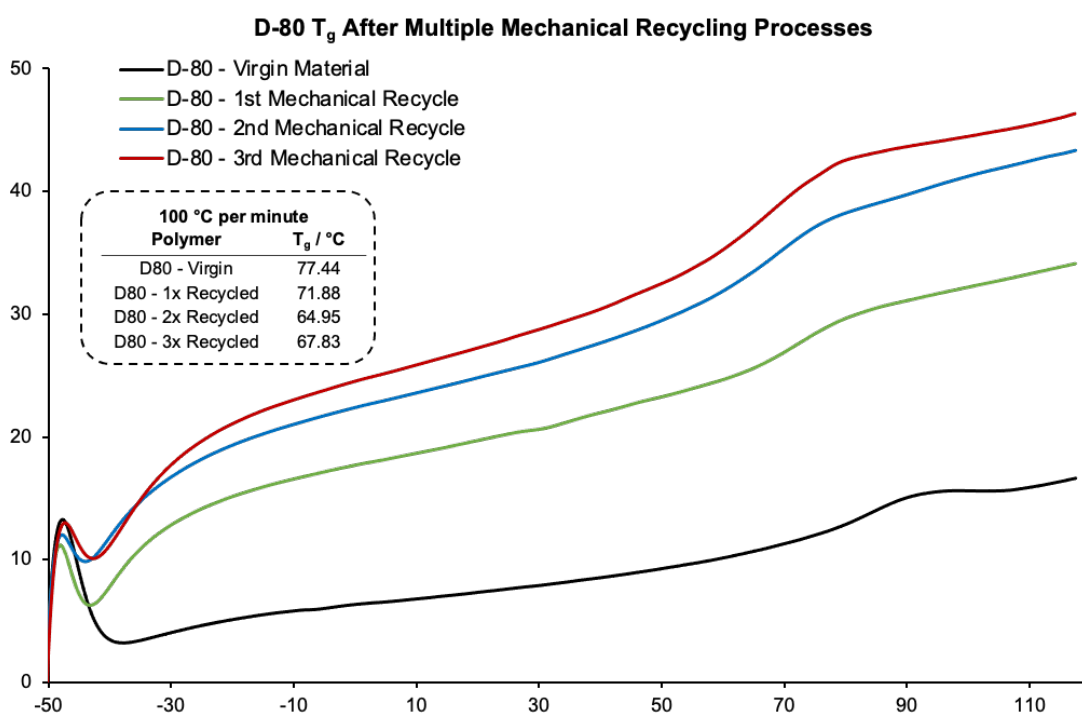
Figure 196: Mechanically recycled D-80 DSC thermograms after multiple cycles, indicating the T_g temperatures calculated from the 100 °C per minute temperature ramp. Full DSC Output can be seen in the appendix Section 10.6.3.

The thermal analysis, by DSC, of the samples subjected to repeated mechanical recycling cycles revealed a slight depression in T_g from 77.4 °C to 67.8 °C. This is likely linked to the reduction in the molecular weight distribution observed by GPC,[258,259] which is likely due to associated polymer oxidation.[229–232]

In conclusion, the ability of the materials to undergo several mechanical recycling processes, with minimal degradation, confirms the robustness of the dioxazaborocane network. Since oxidation is a well-known route to polymer degradation and is likely to be accelerated by the heat and shredding during the recycling process, it is reasonable to assume that this is the main cause of degradation in the polymers in this research.[229–232] This hypothesis is supported by FTIR analyses revealing small amounts of well-known oxidation peaks, modest reductions in molecular weight and T_g by GPC and DSC analyses respectively as well as a slight reduction to the ultimate tensile strengths and Young's modulus of the networks. However, tensile tests reveal an increasingly ductile behaviour upon mechanical recycling which is attractive from an end-use safety outlook.

Chapter 7

Optimization of HA-E1-

Dioxazaborocane Materials

7 Chapter 7 – Optimization of HA-E1-dioxazaborocane materials

The work in this chapter focuses on the development of network films to enhance the mechanical performance properties of the dynamic polymers discussed so far in this work. The motivation behind this effort was to produce recyclable polymers with a similar mechanical strength to those applied in high performance applications such as wind turbines, aerospace, or sports equipment. Also, Chapter 4 previously relayed the difficulties of achieving free polymer films with DER 332™ as the formulated epoxy. However, DER 332™ is a standard and widely used bisphenol A based epoxy resin commercially employed for high performance composite polymers.[260] Thus, manipulation of the epoxy-amine polymer formulations previously investigated in this work, to allow incorporation of DER 332™, is deemed a critical component to achieve network polymers with comparable mechanical performance standards to those of industrial applications.

The aim of this short chapter was to apply the established 'one-pot' polymer fabrication method, to the aromatic-based polymer formulations, as a route to achieve smooth films with better material performance than the linear butyl epoxy-based materials, and to establish as basis for future work in this area. However, this was not achievable with the current formulation of 5 DEA groups on average in the polymer backbone. Therefore, it was hypothesised that the reduction of phenyl glycidyl ether (PGE) in the formulation would result in high degrees of polymerisation in the epoxy-amine polymer back bones, which may result in an improvement in material properties including reduced brittle behaviour and increased flexibility and ductility. This is generally due to increased entanglement and increased intermolecular forces. Thus, the extreme bubbling and brittle behaviour observed in these films during polymer development (Section 4) is hypothesised to reduce and hence be less hindering for the dioxazaborocane crosslinked

polymers function as a free film. This work was limited due to time constraints and will also be discussed for future work.

7.1 Aromatic Polymer Development

For this research a range of polymer networks were fabricated with strategic reduction of the amounts of PGE in the formulation, to increase to degree of epoxy-amine polymerisation. The amounts of PGE was calculated based on the original number of moles in the formulation, to give an average of 5 DEA functional groups in the polymer backbone, being the 100% PGE content. This amount was strategically reduced to 0%, producing sets of polymers with a PGE content of 100%, 50%, 25%, 12.5% and 0%. The non-crosslinked linear (thermoplastic) polymers were fabricated as control samples for comparative molecular weight analysis by GPC. Whilst GPC analysis investigated molecular weight increase upon reducing PGE content, for tensile analysis only networks with only 0% or 50% PGE content were fabricated and the resultant materials are shown in Figure 197. The corresponding stoichiometric (infinite) networks crosslinked with PACM (A^4-series) were also fabricated. The current method utilised for polymer synthesis was adopted here with a slight adaption during the thermal post cure, where a second PTFE-tape coated glass plate was placed on top of the room temperature cured films to prevent material from curling due to internal stress. The dioxazaborocane networks were only successfully made into free films with minimal defects for the 0% PGE content networks via this method. Dioxazaborocane networks with 50% PGE content were inundated with bubbles throughout. Therefore, tensile analysis could not be compared for these materials as the extreme bubbling rendered them unsuitable for tensile testing. Of those that had minimal bubbling in the films (0% PGE- D60-D100 crosslinked), only the D80 could provide defect free dog-bones (Figure 198), as the small bubbles in 60% and 100% crosslinked samples were randomly distributed throughout the film and thus, defect free areas in the dog-bone dimensions could not be attained.

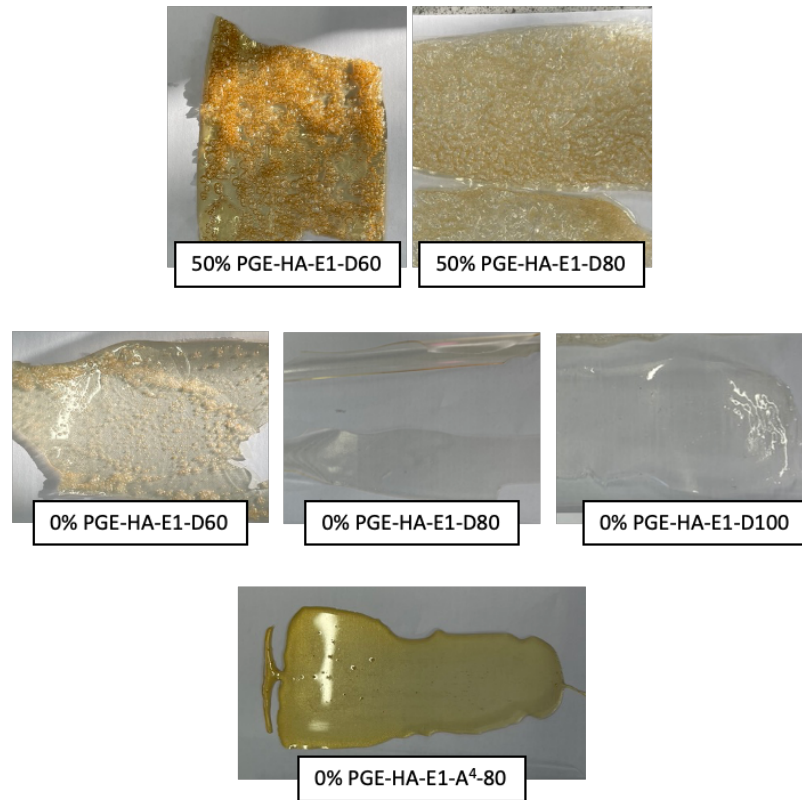Therefore, further testing of the material properties was conducted on the 80% crosslinked polymer networks.

Figure 197: 0% and 50% PGE content polymer networks discussed in this research showing bubbles at in the 50% PGE content polymers.
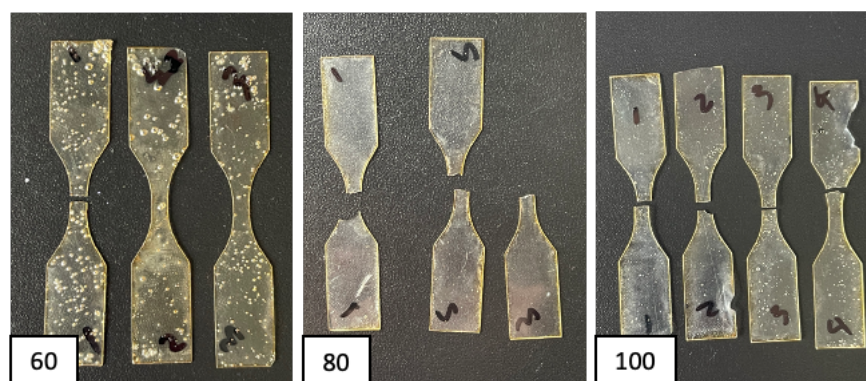

Figure 198: 0% PGE-HA-E1-dioxazaborocane (D) infinite polymer networks showing bubbles in the D60 and D80 dog-bone specimens.

7.2 Molecular Weight Analysis of Polymer Backbones

To determine the molecular weight distribution of the polymer backbones with reducing PGE content, the linear polymers of both the linear epoxy and aromatic epoxy polymers (HA-E2 and HA-E1 respectively) were fabricated with strategic reduction of PGE in the formulations (as described in the previous section) and dissolved into THF at a concentration of 2 mg/mL for GPC analysis. The refractive index response was normalised to compare the molecular weight distributions across the series and is shown overlayed below in Figure 199.
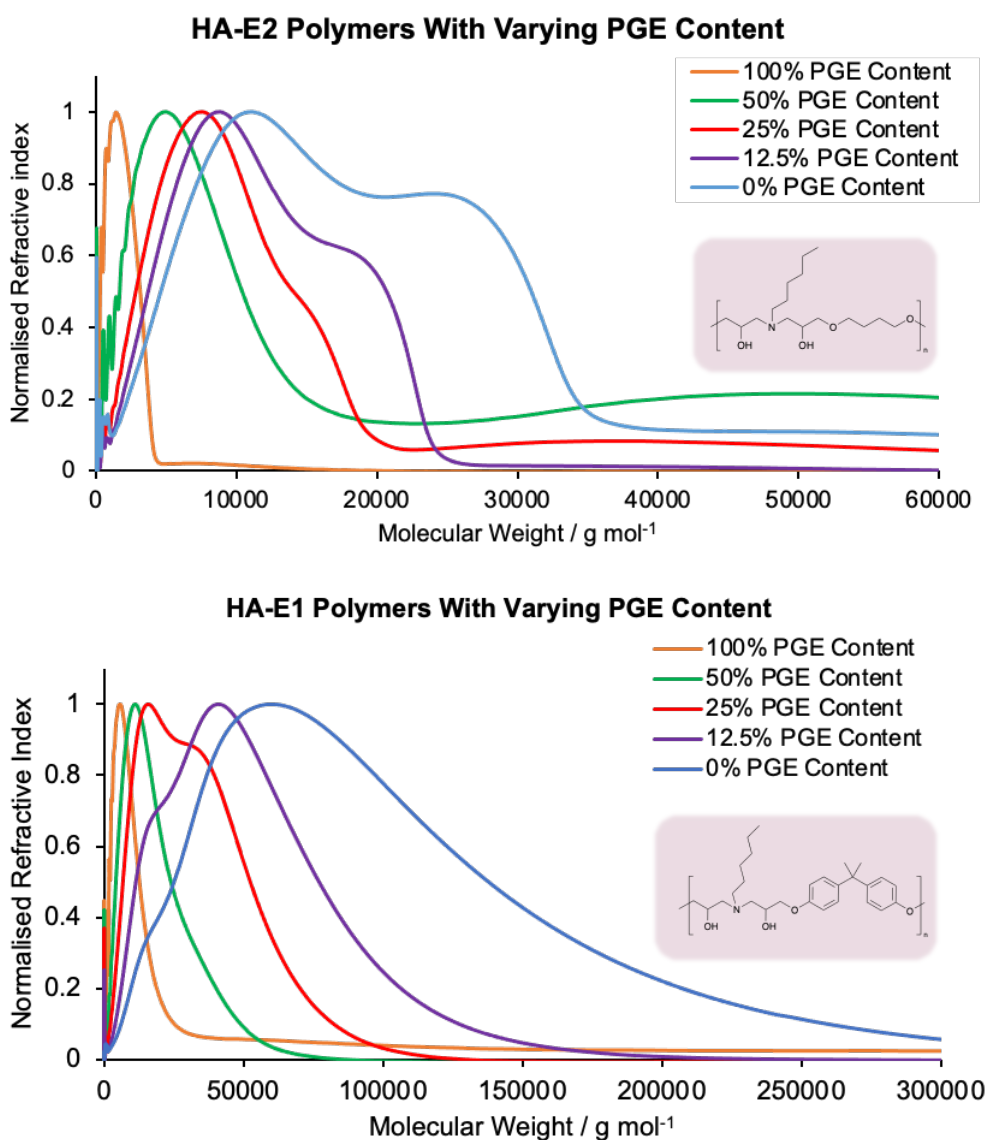
Figure 199: GPC overlays of reducing PGE content in aromatic and Linear epoxy-based polymers.

The results of the GPC analysis for both aromatic (DER) and linear epoxy-based polymers are shown in Table 27 and visualised in Figure 200.

Table 27: GPC analysis results for the reduction of PGE in the aromatic (DER) and linear (BGE) epoxy-based polymers.

PGE Content / %	Polymer	M_n	M_w	M_p	PD
0	BGE	2234	11862	11111	5.31
	DER	8241	56464	61077	6.85
12.5	BGE	3199	7919	8853	2.48
	DER	7698	31222	41409	4.06
25	BGE	2810	7452	7536	2.65
	DER	5705	19211	16050	3.37
50	BGE	2184	8115	4933	3.71
	DER	3892	10946	11248	2.81
100	BGE	733	1311	1459	1.79
	DER	2240	5943	5721	2.65
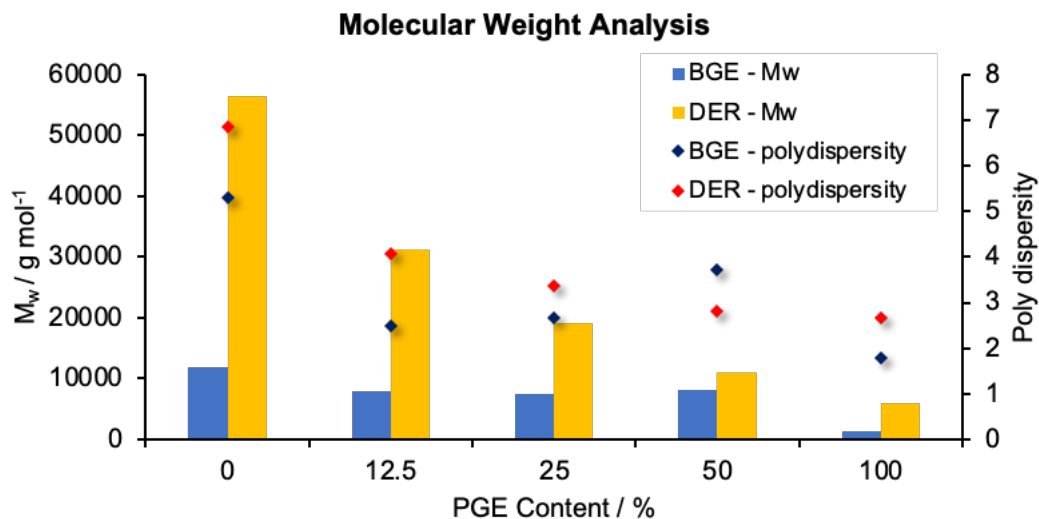
Figure 200: Molecular weight comparison of reducing PGE content in aromatic (DER) and Linear (BGE) epoxy-based polymers with the polydispersity's also indicated.

The evidence shows that upon reducing the amount of PGE in the formulation the molecular weights are increased. This shows that the one-pot synthesis method can successfully fabricate longer chain polymers which can be applied to the network formulations to increase the molecular weights of the polymer chains to be crosslinked. This is hypothesised to increase the flexibility in the materials and help to reduce defects and thus, provide a means of attaining aromatic epoxy-based polymer networks, which in turn is likely to increase the mechanical properties of the films produced. There is also a noticeable trend of increasing polydispersity within the polymers as the PGE is reduced, which can be seen in the GPC chromatograms as the appearance of a high molecular weight shoulder increases as the molecular weights are increased.

7.3 Tensile analysis of 80% crosslinked materials without PGE

HA-E2(DEA-5)-D80

HA-E1(DEA-infinite)-D80

CHA-E1(DEA-5)-A³-80

HA-E1(DEA-infinite)-A⁴-80
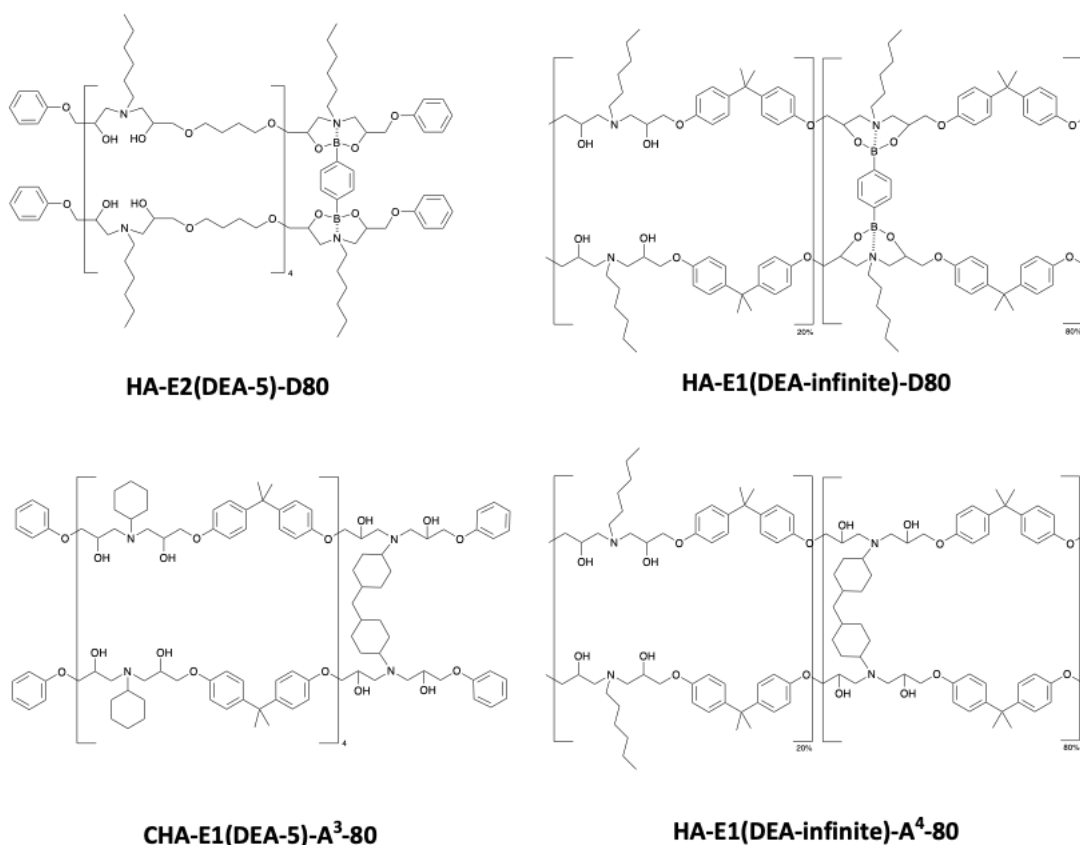
Figure 201: Structures of polymer networks where crosslinked sites consume 80% of the DEA sites in the polymer.

The stoichiometrically balanced (theoretical infinite epoxy amine molecular weight) polymer structures shown in Figure 201 were fabricated and tensile tested for comparative purposes against polymers previous investigated. The DEA-5 materials were the original networks that was previously assessed by tensile testing (Section 5.4.1). The results of which were used as a reference for the newly fabricated DEA-infinite networks, which are without PGE in the formulations that end-cap polymer chains. The comparative tensile data is shown in Figure 202, Table 28 and Figure 203 below.
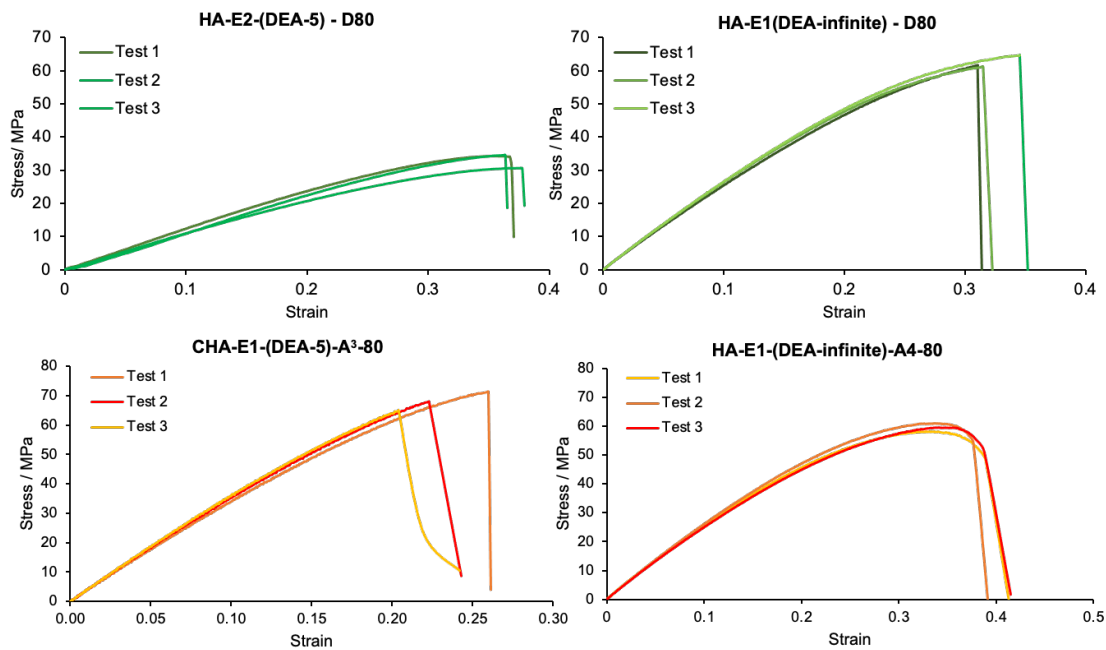
Figure 202: Tensile stress-strain graphs of the original comparative materials (left) and new infinite chain length materials (right).

Table 28: Comparative key tensile results for 80% crosslinked materials.

Entry	Polymer	Crosslink Density / %	PGE content	Ultimate Tensile Stress / MPa	+/-	Young's Modulus / Mpa	+/-	Strain at Break	+/-
1	HA-E2(DEA-5)-D80	80	100%	33.13	1.76	119.13	6.18	0.37	0.01
2	HA-E1(DEA-infinite)-D80	80	0%	62.56	1.48	261.12	4.80	0.33	0.02
3	CHA-E1-(DEA-5)-A3-80	80	100%	68.12	2.65	321.49	10.77	0.23	0.02
4	HA-E1(DEA-infinite)-A4-80	80	0%	59.57	1.25	257.76	5.41	0.41	0.01
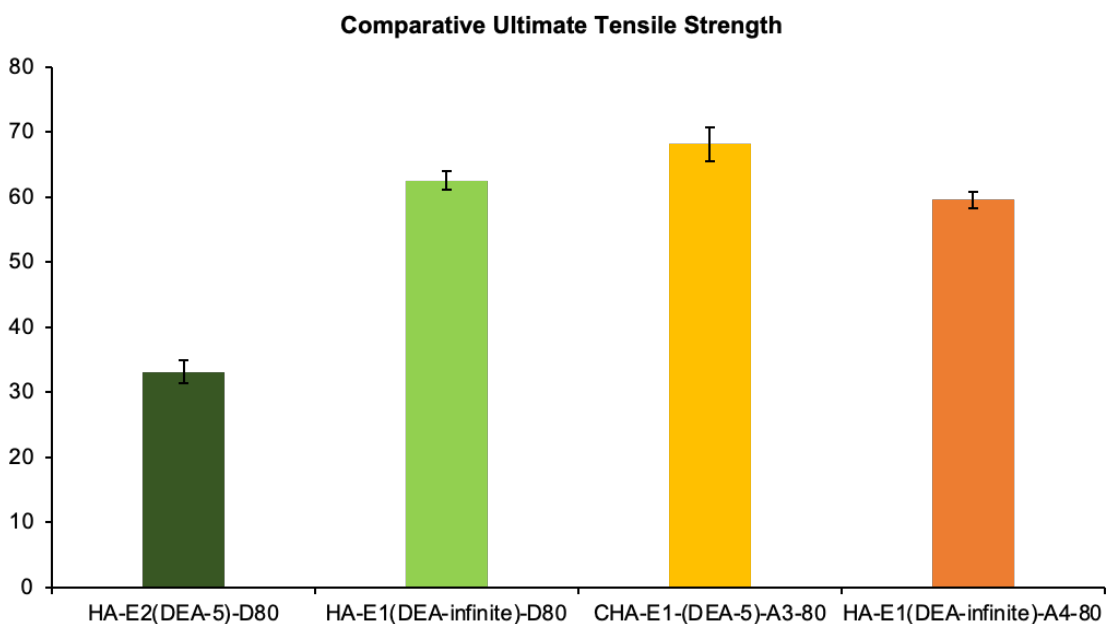
Figure 203: Tensile strength data for 80% crosslinked materials with reduced PGE content.

From the stress-strain graphs in Figure 202, it is evident that the DEA-infinite dioxazaborocane materials that contain an aromatic epoxy chain have significantly larger ultimate tensile strengths than the previously investigated shorter chain DEA-5 dioxazaborocane materials that utilise a linear epoxy chain. This is supported by the ultimate tensile strength data from Table 28, which is visualised in Figure 203 (Dark green = DEA-5, Light green = DEA infinite). However, this cannot directly be attributed to the longer chain length or the aromatic epoxy chain separately but rather as a combination of the two. Moreover, the stress strain graphs show that the amine crosslinked infinite network (A^4-DEA-infinite) network experienced less brittle behaviour than the A^3-DEA-5 network. This is hypothesised to be due to the longer polymer backbones which likely provide more flexibility in the material. Furthermore, upon comparison of the dioxazaborocane DEA-infinite network (light green) with equivalent amine crosslinked infinite network (dark orange = A^4 DEA- infinite) in Figure 203, the dioxazaborocane materials were statistically similar in ultimate tensile strength (~60-63 MPa) as well as strain at break, which also results in similar Youngs modulus values. This evidence suggests that the dioxazaborocane networks can match the material

performance of the same class of polymer with traditional amine crosslinks. Thus, this shows great promise as a high-performance material that can also be recycled by the methods previously proposed in this research, but due to time constraints the fabrication method requires more research to achieve defect free materials and maximise the performance integrity during service-life.

7.4 T_g Analysis

The T_g temperatures of the dioxazaborocane crosslinked materials with reduced PGE content were not visible by DSC. The output of the DSC data shows no discernible T_g steps, at either a slow ramp rate of 20 °C per minute or a faster ramp rate at 100 °C per minute and is shown for both ramp rates below (Figure 204) for the D-100 materials with no PGE content. To evaluate the T_g temperatures, further method development is needed regarding the DSC temperature ramp rates and sample preparation. Due to time constraints regarding this research this was not possible in this research.
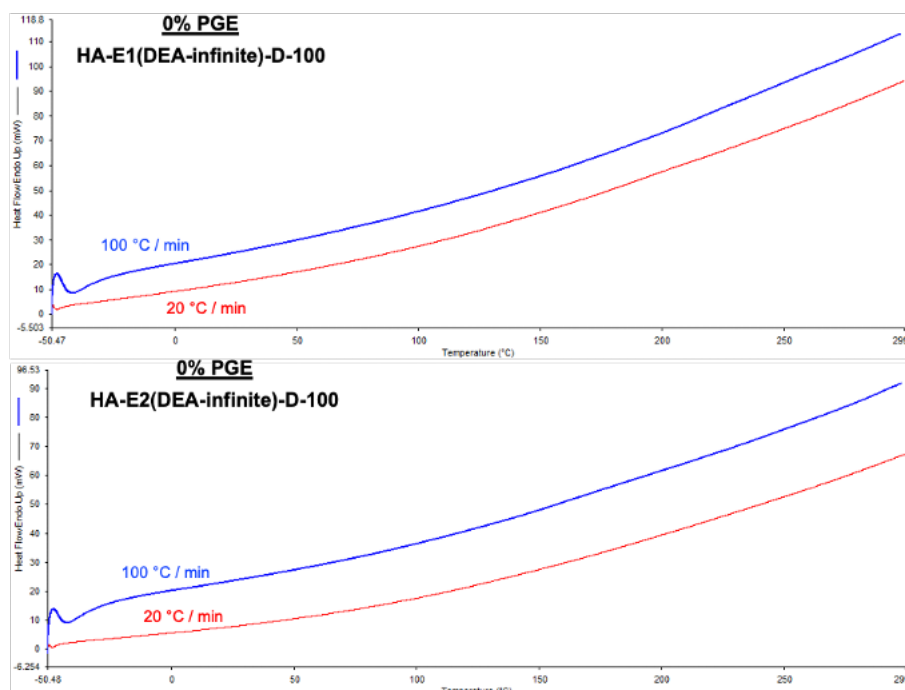
Figure 204: DSC thermograms of D-100 polymers with no PGE content for aromatic (E1) and Linear (E2) epoxy-based polymers.

7.5   TGA Analysis

The TGA plots, shown in Figure 205, revealed that reducing the PGE content (from 50% to 0%) in the polymer backbone formulation has no negative effects regarding the onset of degradation, since the onset nears 350 °C in both classes of epoxy (aromatic and linear) materials. This evidence suggests that increasing the polymer chain lengths will not likely cause a change to the service temperatures of the end use-materials. Thus, allowing molecular manipulation of polymer formulations to suit the desired material properties. For the crosslinked dioxazaborocane materials, The TGA results shown in Figure 206, indicate that utilisation of an aromatic epoxy backbone will likely result in materials with better thermal stability. This is promising in the pursuit to fabricate high-performance thermosets, as the aromatic (DER 332™) based epoxy-amine polymer with dioxazaborocane crosslinks is likely to enhance the thermal stability of the end-use material.
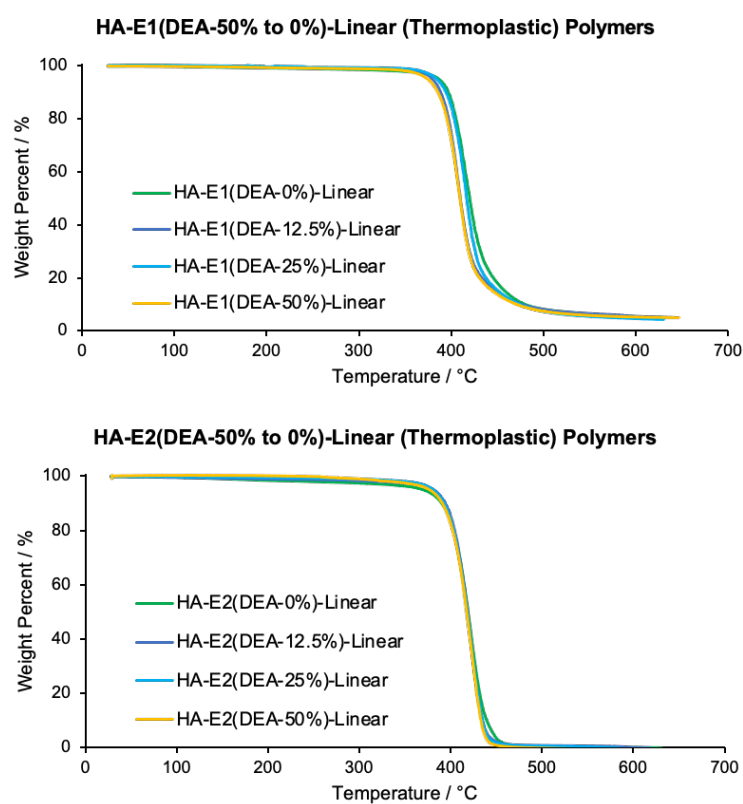
Figure 205: Overlayed TGA temperature response for aromatic (E1) vs Linear (E2) epoxy-based polymer backbone chains, reducing from 50% of the original PGE content in the D/A^2-0 linear polymer formulations.

TGA Results of D100 Dioxazaborocane Networks

Legend:
- HA-E2(DEA-100%)-D100 (green dashed)
- HA-E2(DEA-0%)-D100 (red solid)
- HA-E1(DEA-0%)-D100 (blue solid)
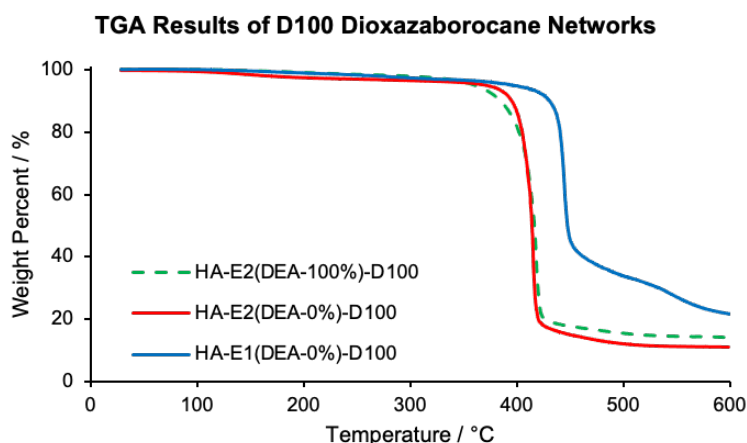
Figure 206: Comparison of fully crosslinked dioxazaborocane (D100) network polymers with the originally fabricated dioxazaborocane material that utilised PGE to limit chain growth.

The residual masses are similar for the same class thermoplastic polymers with differing levels of PGE, which is shown in Figure 207. However, the dioxazaborocane polymers have a significantly a larger residual mass, compared to the traditional diamine crosslinked polymers, as shown in Figure 208. This was previously hypothesised to be due to residual boron-oxide material discussed previously in Section 5.1.3.2.

Linear (Thermoplastic) Polymers

Legend: ■ Linear Epoxy (E2) ■ Aromatic Epoxy (E1)

Polymer	Residual Mass / %
HA-E2(DEA-100%)-linear	1.50
HA-E2(DEA-50%)-linear	0.14
HA-E2(DEA-25%)-linear	0.66
HA-E2(DEA-12.5%)-linear	0.85
HA-E2(DEA-0%)-linear	0.53
HA-E1(DEA-100%)-linear	5.193
HA-E1(DEA-50%)-linear	5.134
HA-E1(DEA-25%)-linear	4.585
HA-E1(DEA-12.5%)-linear	5.294
HA-E1(DEA-0%)-linear	5.19
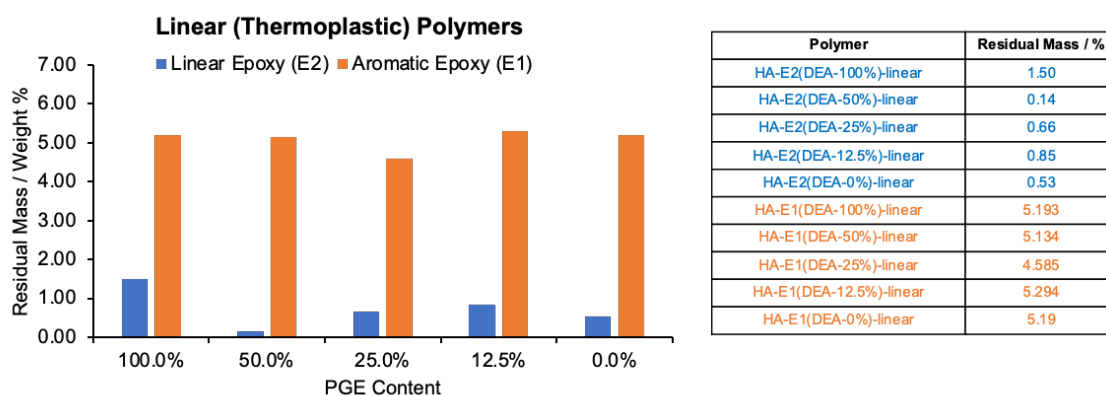
Figure 207: Bar chart overlay of the residual mass of the linear chain (thermoplastic) epoxy-amine polymers after TGA analysis, indicating the percentage weight in the table to the right, where blue represents the linear epoxy (E2 = butyl glycidyl ether - BGE) and orange represents the aromatic epoxy (E1 = DER 332).

Linear Epoxy - BGE	
Polymer	Residual Mass
HA-E2(DEA-0%)-A4-100	1.228
HA-E2(DEA-0%)-A4-80	0.277
HA-E2(DEA-0%)-A4-60	0.228
HA-E2(DEA-0%)-D-100	11.23
HA-E2(DEA-0%)-D-80	8.976
HA-E2(DEA-0%)-D-60	7.877

Aromatic Epoxy - DER 332	
Polymer	Residual Mass
HA-E1(DEA-0%)-A4-100	0.674
HA-E1(DEA-0%)-A4-80	0.197
HA-E1(DEA-0%)-A4-60	0.725
HA-E1(DEA-0%)-D-100	21.696
HA-E1(DEA-0%)-D-80	22.323
HA-E1(DEA-0%)-D-60	16.797
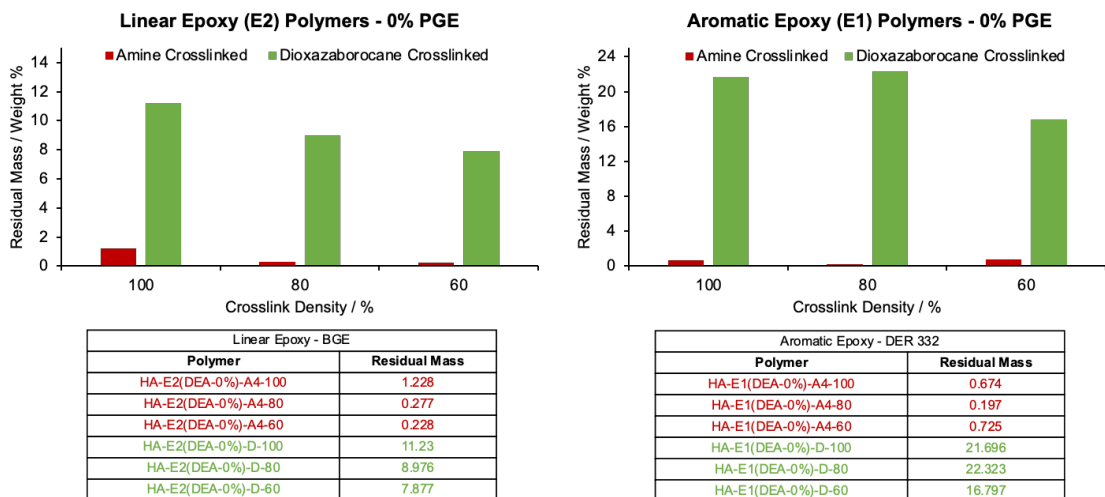
Figure 208: TGA residual mass results of 60-100% crosslinked networks with no PGE in the formulations.

In conclusion, the evidence in this section of research suggests that fabricating defect free epoxy-amine polymers by based on the aromatic epoxy monomers, such as DER 332™ resin, with dioxazaborocane crosslinks can produce materials with improved performance compared to the previous dioxazaborocane network polymers in this research. This is supported by improved ultimate tensile strengths that match that of traditionally crosslinked epoxy-amine materials (A^4), improved thermal stability from TGA analysis. The GPC analysis in this research shows that manipulation of molecular weight of the polymer chains is controlled by the amount of PGE in the formulations. Therefore, future research efforts should be dedicated to developing a method to reduce bubbling in the aromatic-based epoxy-amine materials, whilst maintaining a polymer network. The consequence of bubbling is hypothesised to arise due to the expelled butanol in the crosslinking reaction. Hence, investigations tailored towards lowering the amount of boronic ester, whilst maintaining network integrity, will assist in the pursuit of useable, high-performing aromatic-based epoxy-amine materials that can be recycled. This is possible that this could be achieved by manipulating the stoichiometry of crosslinks, such that the critical gel point (P_{gel}) value closer to 1 (but without exceeding 1), so the required extent of reaction to reach the critical gel point will be higher before gelation occurs. This may allow the liberated butanol, and other trapped gasses, adequate time to diffuse

through the polymer, whilst it is still a viscous liquid, reducing solidified bubbles throughout the final gelled polymer.

Chapter 8

Conclusions and Future Work

8 Conclusions and Future work

8.1 Conclusions

The work presented in this research has investigated a novel dioxazaborocane crosslinked epoxy-amine thermoset network polymer designed to be adaptable at the molecular level by use of dynamic covalent bonds (boronic esters). A new methodology has been developed, which overcomes the practical limitations associated with the material properties of the polymer network material based on manipulation of the epoxy-amine polymer backbone. Limitations associated with the boronic ester crosslinking monomers, such as miscibility in the epoxy resin and reactivity with the diethanolamine (DEA) reactive functional group (formed in epoxy-amine polymerisation reactions) have been overcome to allow preparation of novel covalent adaptable networks (CANs) by a simple, single-stage film casting process.

Comparative 'traditional' epoxy-amine materials have been prepared, which enabled an assessment on the performance of the novel CAN material presented in this research, compared to materials generally utilised in industrial wind turbine applications (bisphenol A type epoxy resin-based thermosets). The thermal, chemical and mechanical characterisation of the polymer network properties have been analysed.

Two methodologies have been presented for the recycling of the dioxazaborocane materials. Method 1 exploits the dynamic nature of epoxy-amine-dioxazaborocane thermosets that allows for facile topological rearrangement and flow when heated above T_g. Thus, delivering an effective mechanism for thermal mechanical reprocessing of the materials. Method 2 exploits the reactivity of the dioxazaborocane crosslink sites. This process uses simple and readily available reagents (pinacol or a monoboronic ester) and highlights a potential route to recycling and separation and recovery of molecular building blocks. The proof of concept for recovery of the polymer building blocks was evident from

dissolution of the polymer network and was further evidenced by ^{1}H NMR analysis of the dissolved polymer solution.

Overall, the dioxazaborocane materials presented in this research show great potential for industrial applications with material properties, such as ultimate tensile strength (UTS) and Young's modulus, with results in same order of magnitude as a commodity epoxy-amine thermoset materials (between 60-70 MPa for UTS and 260-322 for YM). Therefore, this research presents the opportunity to fabricate high-performance thermoset materials with mechanical and chemical recyclability designed into the molecular structure via a simple, single-stage casting process suitable for industrial scale up. Furthermore, the dynamic bond exchange capability of the dioxazaborocane networks provides the opportunity to design polymers for smart, responsive materials for uses in self-healing, or 3D printing applications.

8.2 Future work

8.2.1 Mechanical property optimisation

Chapter 7 presented developed the methodology of fabricating free polymer films with aromatic-based epoxy monomers which increased mechanical properties such as ultimate tensile strength and Young's modulus. This was achieved by manipulating the polymer the chain length to allow more flexibility in the polymer films fabricated from DER 332 ™ epoxy resin and, which increased the performance of the material by restricting the molecular motion of the polymer backbone and increasing chain entanglement. However, it was apparent that this method was not optimal due to bubbling in the resultant materials. Therefore, future work should focus on achieving free films of this aromatic class of epoxy-amine thermosets without defects. This could theoretically be achieved by the reduction of boronic acid in the network formulations whilst maintaining an 'infinitely' long polymer chain length. Complementing this with the recycling studies

probed in this research will likely provide a means to attain CAN with better performance that can still be recycled. Furthermore, the effects of the annealing on mechanical properties were evident in the mechanical recycling procedure. Therefore, further investigation into utilising this as a post cure method may prove valuable.

8.3 Recycling

Due to the time constraints imposed on this research project, the ultimate recovery of the separated polymer building blocks, after chemical dissolution, was not achieved. Since the scope behind this project is to achieve recyclable thermosets by chemical design, the recovery of individual chemical building blocks should be realised. This will involve subsequent work up methods to separate the individual chemical components.

However, the ultimate dissolution of polymer network will likely allow the recovery of embedded carbon/glass fibres in composite applications. Therefore, fabrication of these types of material followed my subsequent characterisation and chemical dissolution recovery of the carbon fibres will prove valuable for future materials of this type, as the recovery of intact carbon fibres (whilst maintaining their original mechanical properties) will reduce the expensive and energy intensive processes of making carbon fibres as well as waste destined for landfill.

9 References

1   R. J. Young and P. A. Lovell, in *Introduction to Polymers*, CRC Press, Boca Raton, 3rd edn., 2011, pp. 3–14.

2   G. Odian, in *Principles of Polymerization*, John Wilery and Sons, Inc, Hoboken, 4th edn., 2004, pp. 103–114.

3   R. J. Young and P. A. Lovell, in *Introduction to Polymers*, CRC Press, Boca Raton, 3rd edn., 2011, pp. 21–60.

4   W. H. Carothers, *Trans. Faraday Soc.*, 1936, **32**, 39.

5   P. J. Flory, *J. Am. Chem. Soc.*, 1941, **63**, 3083–3090.

6   W. H. Stockmayer, *J. Chem. Phys.*, 1944, **12**, 125–131.

7   J.-E. Ehlers, N. G. Rondan, L. K. Huynh, H. Pham, M. Marks and T. N. Truong, *Macromolecules*, 2007, **40**, 4370–4377.

8   T. Vidil, F. Tournilhac, S. Musso, A. Robisson and L. Leibler, *Prog. Polym. Sci.*, 2016, **62**, 126–179.

9   B. Ellis, in *Chemistry and Technology of Epoxy Resins*, Springer Netherlands, Dordrecht, 1st edn., 1993, pp. 1–36.

10   United Nations, Sustainable Development Goals, https://www.un.org/sustainabledevelopment/sustainable-consumption-production/, (accessed 24 February 2023).

11   Y. Yang, R. Boom, B. Irion, D.-J. van Heerden, P. Kuiper and H. de Wit, *Chem. Eng. Process. Process Intensif.*, 2012, **51**, 53–68.

12   A. J. Timmis, A. Hodzic, L. Koh, M. Bonner, C. Soutis, A. W. Schäfer and L. Dray, *Int. J. Life Cycle Assess.*, 2015, **20**, 233–243.

13   Department for Business Energy & Industrial Strategy, Renewable Energy Planning Database: quarterly extract, https://www.gov.uk/government/publications/renewable-energy-planning-database-monthly-extract, (accessed 28 February 2023).

14   Epoxy Resin Committee (ERC) and E. R. Committee, 2015, 2–3.

15   K. Gupta, D. K. Paliwal and P. Bajaj, *Polym. Rev.*, 1991, **31**, 1–89.

16   Easy Composites, Prepreg Reinforcements, https://www.easycomposites.co.uk/xc130-300g-unidirectional-prepreg-carbon-fibre, (accessed 25 February 2023).

17   B. A. Newcomb, *Compos. Part A Appl. Sci. Manuf.*, 2016, **91**, 262–282.

18   Z. Fu, B. Liu, Y. Liu, B. Li and H. Zhang, *Ind. Eng. Chem. Res.*, 2018, **57**, 8348–8359.

19   Epoxy Resin Committee (ERC) and E. R. Committee, *The Socio-Economic Value of Epoxy Resins - Main Findings*, 2017.

20   Epoxy Resin Committee (ERC), *Epoxy Resins in Wind Energy Applications Assessment of Potential Bpa Emissions*, 2015.

21   Epoxy Resin Committee (ERC), *Recycling of Epoxy: Challenges and options*, 2020.

22   P. Chakma and D. Konkolewicz, *Angew. Chemie Int. Ed.*, 2019, **58**, 9682–9695.

23   Y. Jin, C. Yu, R. J. Denman and W. Zhang, *Chem. Soc. Rev.*, 2013, **42**, 6634–6654.

24   L. M. De Espinosa, G. L. Fiore, C. Weder, E. Johan Foster and Y. C. Simon, *Prog. Polym. Sci.*, 2015, **49**–**50**, 60–78.

25   W. P. J. Appel, G. Portale, E. Wisse, P. Y. W. Dankers and E. W. Meijer, *Macromolecules*, 2011, **44**, 6776–6784.

26   B. J. B. Folmer, R. P. Sijbesma, R. M. Versteegen, J. A. J. Van Der Rijt and E. W. Meijer, *Adv. Mater.*, 2000, **12**, 874–878.

27   R. Agnaou, M. Capelot, S. Tencé-Girault, F. Tournilhac and L. Leibler, *J. Am. Chem. Soc.*, 2014, **136**, 11268–11271.

28   L. Fang, M. A. Olson, D. Benítez, E. Tkatchouk, W. A. Goddard and J. F. Stoddart, *Chem. Soc. Rev.*, 2010, **39**, 17–29.

29   X. Huang, S. Nakagawa, H. Houjou and N. Yoshie, *Macromolecules*, 2021, **54**,

4070–4080.

30   G. N. Lewis, *J. Am. Chem. Soc.*, 1916, **38**, 762–785.

31   N. J. Van Zee and R. Nicolaÿ, *Prog. Polym. Sci.*, 2020, **104**, 101233.

32   M. M. Perera and N. Ayres, *Polym. Chem.*, 2020, **11**, 1410–1423.

33   S. Zhao and M. M. Abu-Omar, *Macromolecules*, 2018, **51**, 9816–9824.

34   L. Lu, J. Pan and G. Li, *J. Mater. Chem. A*, 2017, **5**, 21505–21513.

35   L. Lu, J. Fan and G. Li, *Polymer (Guildf).*, 2016, **105**, 10–18.

36   Z. P. Zhang, M. Z. Rong and M. Q. Zhang, *Prog. Polym. Sci.*, 2018, **80**, 39–93.

37   A. P. Bapat, B. S. Sumerlin and A. Sutti, *Mater. Horizons*, 2020, **7**, 694–714.

38   F. Altuna, C. Hoppe and R. Williams, *Polymers (Basel).*, 2018, **10**, 43.

39   J. J. Cash, T. Kubo, A. P. Bapat and B. S. Sumerlin, *Macromolecules*, 2015, **48**, 2098–2106.

40   J. J. Cash, T. Kubo, D. J. Dobbins and B. S. Sumerlin, *Polym. Chem.*, 2018, **9**, 2011–2020.

41   J. N. Cambre and B. S. Sumerlin, *Polymer (Guildf).*, 2011, **52**, 4631–4643.

42   L. He, D. E. Fullenkamp, J. G. Rivera and P. B. Messersmith, *Chem. Commun.*, 2011, **47**, 7497–7499.

43   S. Ma and D. C. Webster, *Prog. Polym. Sci.*, 2018, **76**, 65–110.

44   C. J. Kloxin and C. N. Bowman, *Chem. Soc. Rev.*, 2013, **42**, 7161–7173.

45   W. L. A. Brooks and B. S. Sumerlin, *Chem. Rev.*, 2016, **116**, 1375–1397.

46   M. K. McBride, B. T. Worrell, T. Brown, L. M. Cox, N. Sowan, C. Wang, M. Podgorski, A. M. Martinez and C. N. Bowman, *Annu. Rev. Chem. Biomol. Eng.*, 2019, **10**, 175–198.

47   M. Podgórski, B. D. Fairbanks, B. E. Kirkpatrick, M. McBride, A. Martinez, A. Dobson, N. J. Bongiardina and C. N. Bowman, *Adv. Mater.*, 2020, **32**, 1–26.

48   T. Maeda, H. Otsuka and A. Takahara, *Prog. Polym. Sci.*, 2009, **34**, 581–604.

49   A. J. R. Amaral and G. Pasparakis, *Polym. Chem.*, 2017, **8**, 6464–6484.

50   N. Kuhl, S. Bode, R. K. Bose, J. Vitz, A. Seifert, S. Hoeppener, S. J. Garcia, S.

Spange, S. Van Der Zwaag, M. D. Hager and U. S. Schubert, *Adv. Funct. Mater.*, 2015, **25**, 3295–3301.

51   Y. Jin, Z. Lei, P. Taynton, S. Huang and W. Zhang, *Matter*, 2019, **1**, 1456–1493.

52   R. Baruah, A. Kumar, R. R. Ujjwal, S. Kedia, A. Ranjan and U. Ojha, *Macromolecules*, 2016, **49**, 7814–7824.

53   D. J. Fortman, J. P. Brutman, G. X. De Hoe, R. L. Snyder, W. R. Dichtel and M. A. Hillmyer, *ACS Sustain. Chem. Eng.*, 2018, **6**, 11145–11159.

54   Clarivate, Web of Science, https://www.webofscience.com/wos/woscc/summary/5b1b77cc-237a-41cc-bb10-2460b4331701-6458c7dd/relevance/1, (accessed 8 December 2022).

55   C. J. Kloxin, T. F. Scott, B. J. Adzima and C. N. Bowman, *Macromolecules*, 2010, **43**, 2643–2653.

56   B. J. Adzima, H. A. Aguirre, C. J. Kloxin, T. F. Scott and C. N. Bowman, *Macromolecules*, 2008, **41**, 9112–9117.

57   D. Montarnal, M. Capelot, F. Tournilhac and L. Leibler, *Science (80-.).*, 2011, **334**, 965–968.

58   M. Capelot, D. Montarnal, F. Tournilhac and L. Leibler, *J. Am. Chem. Soc.*, 2012, **134**, 7664–7667.

59   W. Denissen, J. M. Winne and F. E. Du Prez, *Chem. Sci.*, 2016, **7**, 30–38.

60   M. Guerre, C. Taplan, J. M. Winne and F. E. Du Prez, *Chem. Sci.*, 2020, **11**, 4855–4870.

61   B. Krishnakumar, R. V. S. P. Sanka, W. H. Binder, V. Parthasarthy, S. Rana and N. Karak, *Chem. Eng. J.*, 2020, **385**, 123820.

62   F. Van Lijsebetten, T. Debsharma, J. M. Winne and F. E. Du Prez, *Angew. Chemie Int. Ed.*, 2022, **61**, 1–14.

63   J. Zheng, Z. M. Png, S. H. Ng, G. X. Tham, E. Ye, S. S. Goh, X. J. Loh and Z. Li, *Mater. Today*, 2021, **51**, 586–625.

64   K. Yu, A. Xin and Q. Wang, *J. Mech. Phys. Solids*, 2018, **121**, 409–431.

65   J. Clayden, N. Greeves and S. Warren, *Organic Chemistry*, Oxford University Press, 2nd edn., 2012.

66   Clarivate, Web of Science (DA), https://www.webofscience.com/wos/woscc/summary/a762df68-75d2-423e-a86a-e22753c43ae3-6526bd83/relevance/1, (accessed 12 December 2022).

67   Y. Zhang, L. Zhang, G. Yang, Y. Yao, X. Wei, T. Pan, J. Wu, M. Tian and P. Yin, *J. Mater. Sci. Technol.*, 2021, **92**, 75–87.

68   G. M. Scheutz, J. J. Lessard, M. B. Sims and B. S. Sumerlin, *J. Am. Chem. Soc.*, 2019, **141**, 16181–16196.

69   K. K. Oehlenschlaeger, J. O. Mueller, J. Brandt, S. Hilf, A. Lederer, M. Wilhelm, R. Graf, M. L. Coote, F. G. Schmidt and C. Barner-Kowollik, *Adv. Mater.*, 2014, **26**, 3561–3566.

70   G. Zhang, Q. Zhao, L. Yang, W. Zou, X. Xi and T. Xie, *ACS Macro Lett.*, 2016, **5**, 805–808.

71   X. Chen, M. A. Dam, K. Ono, A. Mal, H. Shen, S. R. Nutt, K. Sheran and F. Wudl, *Science (80-.).*, 2002, **295**, 1698–1702.

72   A. Lendlein, M. Behl, B. Hiebl and C. Wischke, *Expert Rev. Med. Devices*, 2010, **7**, 357–379.

73   S. Yu, R. Zhang, Q. Wu, T. Chen and P. Sun, *Adv. Mater.*, 2013, **25**, 4912–4917.

74   D. J. Dobbins, G. M. Scheutz, H. Sun, C. A. Crouse and B. S. Sumerlin, *J. Polym. Sci. Part A Polym. Chem.*, 2019, 193–203.

75   N. Kuhl, S. Bode, M. D. Hager and U. S. Schubert, in *Self-Healing Polymers Based on Reversible Covalent Bonds*, Springer, 2015, vol. 32, pp. 1–58.

76   N. Yoshie, S. Saito and N. Oya, *Polymer (Guildf).*, 2011, **52**, 6074–6079.

77   E. B. Murphy, E. Bolanos, C. Schaffner-Hamann, F. Wudl, S. R. Nutt and M. L. Auad, *Macromolecules*, 2008, **41**, 5203–5209.

78   P. T. Corbett, J. Leclaire, L. Vial, K. R. West, J.-L. Wietor, J. K. M. Sanders and S. Otto, *Chem. Rev.*, 2006, **106**, 3652–3711.

79   P. Schwab, M. B. France, J. W. Ziller and R. H. Grubbs, *Angew. Chemie Int. Ed. English*, 1995, **34**, 2039–2041.

80   M. Scholl, S. Ding, C. W. Lee and R. H. Grubbs, *Org. Lett.*, 1999, **1**, 953–956.

81   Y. X. Lu, F. Tournilhac, L. Leibler and Z. Guan, *J. Am. Chem. Soc.*, 2012, **134**, 8424–8427.

82   Y. Lu and Z. Guan, *J. Am. Chem. Soc.*, 2012, **134**, 14226–14231.

83   J. R. GRIFFITH, 1979, pp. 259–262.

84   H. Schiff, *Ann. der Chemie und Pharm.*, 1864, **131**, 118–119.

85   J. Collins, Z. Xiao, M. Müllner and L. A. Connal, *Polym. Chem.*, 2016, **7**, 3812–3826.

86   M. Ciaccia and S. Di Stefano, *Org. Biomol. Chem.*, 2015, **13**, 646–654.

87   Y. Xin and J. Yuan, *Polym. Chem.*, 2012, **3**, 3045–3055.

88   M. Ciaccia, S. Pilati, R. Cacciapaglia, L. Mandolini and S. Di Stefano, *Org. Biomol. Chem.*, 2014, **12**, 3282–3287.

89   M. E. Belowich and J. F. Stoddart, *Chem. Soc. Rev.*, 2012, **41**, 2003–2024.

90   J. Wu, K. C. F. Leung and J. F. Stoddart, *Proc. Natl. Acad. Sci. U. S. A.*, 2007, **104**, 17266–17271.

91   NobelPrize.org, The Nobel Prize in Chemistry 2016, https://www.nobelprize.org/prizes/chemistry/2016/summary/, (accessed 19 December 2022).

92   J. Strätz, A. Liedmann, M. L. Trutschel, K. Mäder, T. Groth and S. Fischer, *Cellulose*, 2019, **26**, 7371–7382.

93   P. Taynton, K. Yu, R. K. Shoemaker, Y. Jin, H. J. Qi and W. Zhang, *Adv. Mater.*, 2014, **26**, 3938–3942.

94   P. Taynton, H. Ni, C. Zhu, K. Yu, S. Loob, Y. Jin, H. J. Qi and W. Zhang, *Adv. Mater.*, 2016, **28**, 2904–2909.

95   A. W. Jackson and D. A. Fulton, *Macromolecules*, 2012, **45**, 2699–2708.

96   H. Liu, H. Zhang, H. Wang, X. Huang, G. Huang and J. Wu, *Chem. Eng. J.*, 2019,

368, 61–70.

97   S. Wang, S. Ma, Q. Li, W. Yuan, B. Wang and J. Zhu, *Macromolecules*, 2018, **51**, 8001–8012.

98   H. Memon, H. Liu, M. A. Rashid, L. Chen, Q. Jiang, L. Zhang, Y. Wei, W. Liu and Y. Qiu, *Macromolecules*, 2020, **53**, 621–630.

99   S. Mukherjee, W. L. A. Brooks, Y. Dai and B. S. Sumerlin, *Polym. Chem.*, 2016, **7**, 1971–1978.

100   C. He, S. Shi, D. Wang, B. A. Helms and T. P. Russell, *J. Am. Chem. Soc.*, 2019, **141**, 13753–13757.

101   S. Mukherjee, M. R. Hill and B. S. Sumerlin, *Soft Matter*, 2015, **11**, 6152–6161.

102   A. Dirksen, S. Dirksen, T. M. Hackeng and P. E. Dawson, *J. Am. Chem. Soc.*, 2006, **128**, 15602–15603.

103   W. G. Skene and J. M. P. Lehn, *Proc. Natl. Acad. Sci. U. S. A.*, 2004, **101**, 8270–8275.

104   G. Deng, C. Tang, F. Li, H. Jiang and Y. Chen, *Macromolecules*, 2010, **43**, 1191–1194.

105   M. B. Sims, K. Y. Patel, M. Bhatta, S. Mukherjee and B. S. Sumerlin, *Macromolecules*, 2018, **51**, 356–363.

106   S. Mukherjee, A. P. Bapat, M. R. Hill and B. S. Sumerlin, *Polym. Chem.*, 2014, **5**, 6923–6931.

107   N. Boehnke, C. Cam, E. Bat, T. Segura and H. D. Maynard, *Biomacromolecules*, 2015, **16**, 2101–2108.

108   P. Haida, G. Signorato and V. Abetz, *Polym. Chem.*, 2022, **13**, 946–958.

109   P. Haida and V. Abetz, *Macromol. Rapid Commun.*, 2020, **41**, 2000273.

110   W. Denissen, G. Rivero, R. Nicolaÿ, L. Leibler, J. M. Winne and F. E. Du Prez, *Adv. Funct. Mater.*, 2015, **25**, 2451–2457.

111   W. Post, A. Susa, R. Blaauw, K. Molenveld and R. J. I. Knoop, *Polym. Rev.*, 2020, **60**, 359–388.

112   A. Sanchez-Sanchez, D. A. Fulton and J. A. Pomposo, *Chem. Commun.*, 2014, **50**, 1871–1874.

113   W. Denissen, M. Droesbeke, R. Nicolaÿ, L. Leibler, J. M. Winne and F. E. Du Prez, *Nat. Commun.*, 2017, **8**, 14857.

114   W. Denissen, I. De Baere, W. Van Paepegem, L. Leibler, J. Winne and F. E. Du Prez, *Macromolecules*, 2018, **51**, 2054–2064.

115   Y. Spiesschaert, M. Guerre, I. De Baere, W. Van Paepegem, J. M. Winne and F. E. Du Prez, *Macromolecules*, 2020, **53**, 2485–2495.

116   F. Van Lijsebetten, S. Engelen, E. Bauters, W. Van Vooren, M. M. J. Smulders and F. E. Du Prez, *Eur. Polym. J.*, 2022, **176**, 111426.

117   J. J. Lessard, L. F. Garcia, C. P. Easterling, M. B. Sims, K. C. Bentz, S. Arencibia, D. A. Savin and B. S. Sumerlin, *Macromolecules*, 2019, **52**, 2105–2111.

118   C. Taplan, M. Guerre, J. M. Winne and F. E. Du Prez, *Mater. Horizons*, 2020, **7**, 104–110.

119   J. Tellers, R. Pinalli, M. Soliman, J. Vachon and E. Dalcanale, *Polym. Chem.*, 2019, **10**, 5534–5542.

120   J. Otera, *Chem. Rev.*, 1993, **93**, 1449–1470.

121   M. Giebler, C. Sperling, S. Kaiser, I. Duretek and S. Schlögl, *Polymers (Basel).*, 2020, **12**, 1–14.

122   M. Capelot, M. M. Unterlass, F. Tournilhac and L. Leibler, *ACS Macro Lett.*, 2012, **1**, 789–792.

123   D. Montarnal, F. Tournilhac, M. Hidalgo and L. Leibler, *J. Polym. Sci. Part A Polym. Chem.*, 2010, **48**, 1133–1141.

124   W. J. Blank, Z. A. He and M. Picci, *J. Coatings Technol.*, 2002, **74**, 33–41.

125   A. Demongeot, R. Groote, H. Goossens, T. Hoeks, F. Tournilhac and L. Leibler, *Macromolecules*, 2017, **50**, 6117–6127.

126   A. Demongeot, S. J. Mougnier, S. Okada, C. Soulié-Ziakovic and F. Tournilhac, *Polym. Chem.*, 2016, **7**, 4486–4493.

127 Y. Zhang, Y. Qi, S. Ulrich, M. Barboiu and O. Ramström, *Mater. Chem. Front.*, 2020, **4**, 489–506.

128 M. Hong and E. Y. X. Chen, *Green Chem.*, 2017, **19**, 3692–3706.

129 G. Yang, B. J. Rohde, H. Tesefay and M. L. Robertson, *ACS Sustain. Chem. Eng.*, 2016, **4**, 6524–6533.

130 J. Michałowicz, *Environ. Toxicol. Pharmacol.*, 2014, **37**, 738–758.

131 T. Liu, C. Hao, S. Zhang, X. Yang, L. Wang, J. Han, Y. Li, J. Xin and J. Zhang, *Macromolecules*, 2018, **51**, 5577–5585.

132 T. Liu, B. Zhao and J. Zhang, *Polymer (Guildf).*, 2020, **194**, 122392.

133 S. Debnath, S. Kaushal and U. Ojha, *ACS Appl. Polym. Mater.*, 2020, **2**, 1006–1013.

134 M. C. Hennessy and T. P. O'Sullivan, *RSC Adv.*, 2021, **11**, 22859–22920.

135 G. B. Dharma Rao, B. N. Acharya and M. P. Kaushik, *Tetrahedron Lett.*, 2013, **54**, 6644–6647.

136 N. B. Cramer, S. K. Reddy, A. K. O'Brien and C. N. Bowman, *Macromolecules*, 2003, **36**, 7964–7969.

137 C. E. Hoyle, T. Y. Lee and T. Roper, *J. Polym. Sci. Part A Polym. Chem.*, 2004, **42**, 5301–5338.

138 B. D. Fairbanks, D. M. Love and C. N. Bowman, *Macromol. Chem. Phys.*, 2017, **218**, 1–11.

139 K. F. Long, H. Wang, T. T. Dimos and C. N. Bowman, *Macromolecules*, 2021, **54**, 3093–3100.

140 S. Chatani, D. P. Nair and C. N. Bowman, *Polym. Chem.*, 2013, **4**, 1048–1055.

141 D. P. Nair, M. Podgórski, S. Chatani, T. Gong, W. Xi, C. R. Fenoli and C. N. Bowman, *Chem. Mater.*, 2014, **26**, 724–744.

142 G. B. Lyon, L. M. Cox, J. T. Goodrich, A. D. Baranek, Y. Ding and C. N. Bowman, *Macromolecules*, 2016, **49**, 8905–8913.

143 C. F. H. Allen, J. O. Fournier and W. J. Humphlett, *Can. J. Chem.*, 1964, **42**, 2616–

2620.

144   C. J. Stubbs, A. L. Khalfa, V. Chiaradia, J. C. Worch and A. P. Dove, *J. Am. Chem. Soc.*, 2022, **144**, 11729–11735.

145   N. Kuhl, R. Geitner, R. K. Bose, S. Bode, B. Dietzek, M. Schmitt, J. Popp, S. J. Garcia, S. van der Zwaag, U. S. Schubert and M. D. Hager, *Macromol. Chem. Phys.*, 2016, **217**, 2541–2550.

146   P. Chakma, L. H. Rodrigues Possarle, Z. A. Digby, B. Zhang, J. L. Sparks and D. Konkolewicz, *Polym. Chem.*, 2017, **8**, 6534–6543.

147   B. Zhang, Z. A. Digby, J. A. Flum, P. Chakma, J. M. Saul, J. L. Sparks and D. Konkolewicz, *Macromolecules*, 2016, **49**, 6871–6878.

148   J. M. Winne, L. Leibler and F. E. Du Prez, *Polym. Chem.*, 2019, **10**, 6091–6108.

149   D. Berne, V. Ladmiral, E. Leclerc and S. Caillol, *Polymers (Basel).*, , DOI:10.3390/polym14204457.

150   S. P. Daymon and K. M. Miller, *Polymer (Guildf).*, 2018, **145**, 286–293.

151   N. J. Bongiardina, K. F. Long, M. Podgórski and C. N. Bowman, *Macromolecules*, 2021, **54**, 8341–8351.

152   M. Liras, E. Peinado, P. Cañamero, I. Quijada-Garrido and O. García, *J. Polym. Sci. Part A Polym. Chem.*, 2014, **52**, 3087–3095.

153   S. Aksakal, R. Aksakal and C. R. Becer, *Polym. Chem.*, 2018, **9**, 4507–4516.

154   C. Wang, T. M. Goldman, B. T. Worrell, M. K. McBride, M. D. Alim and C. N. Bowman, *Mater. Horizons*, 2018, **5**, 1042–1046.

155   US Pat., US20210292482-A1, 2021.

156   A. V. Bordoni, M. V. Lombardo and A. Wolosiuk, *RSC Adv.*, 2016, **6**, 77410–77426.

157   C. Ghobril, K. Charoen, E. K. Rodriguez, A. Nazarian and M. W. Grinstaff, *Angew. Chemie - Int. Ed.*, 2013, **52**, 14070–14074.

158   M. D. Konieczynska, J. C. Villa-Camacho, C. Ghobril, M. Perez-Viloria, K. M. Tevis, W. A. Blessing, A. Nazarian, E. K. Rodriguez and M. W. Grinstaff, *Angew.*

Chemie - Int. Ed., 2016, **55**, 9984–9987.

159   R. Winters, W. Heinen, M. A. L. Verbruggen, J. Lugtenburg, M. van Duin and H. J. M. de Groot, *Macromolecules*, 2002, **35**, 1958–1966.

160   A. Y. Coran, *J. Appl. Polym. Sci.*, 2003, **87**, 24–30.

161   D. M. Beaupre and R. G. Weiss, *Molecules*, 2021, **26**, 3332.

162   B. Gyarmati, Á. Némethy and A. Szilágyi, *Eur. Polym. J.*, 2013, **49**, 1268–1286.

163   J. M. Matxain, J. M. Asua and F. Ruipérez, *Phys. Chem. Chem. Phys.*, 2016, **18**, 1758–1770.

164   I. Azcune and I. Odriozola, *Eur. Polym. J.*, 2016, **84**, 147–160.

165   J. Canadell, H. Goossens and B. Klumperman, *Macromolecules*, 2011, **44**, 2536–2541.

166   Y. Zhang, L. Yuan, G. Liang and A. Gu, *Ind. Eng. Chem. Res.*, 2018, **57**, 12397–12406.

167   R. Caraballo, M. Rahm, P. Vongvilai, T. Brinck and O. Ramström, *Chem. Commun.*, 2008, 6603.

168   A. Ruiz De Luzuriaga, R. Martin, N. Markaide, A. Rekondo, G. Cabañero, J. Rodríguez and I. Odriozola, *Mater. Horizons*, 2016, **3**, 241–247.

169   A. Rekondo, R. Martin, A. Ruiz De Luzuriaga, G. Cabañero, H. J. Grande and I. Odriozola, *Mater. Horizons*, 2014, **1**, 237–240.

170   T. Ohishi, Y. Iki, K. Imato, Y. Higaki, A. Takahara and H. Otsuka, *Chem. Lett.*, 2013, **42**, 1346–1348.

171   H. Otsuka, S. Nagano, Y. Kobashi, T. Maeda and A. Takahara, *Chem. Commun.*, 2010, **46**, 1150–1152.

172   S. S. Rahman, M. Arshad, A. Qureshi and A. Ullah, *ACS Appl. Mater. Interfaces*, 2020, **12**, 51927–51939.

173   Z. Xu, S. Liu, Y. Kang and M. Wang, *ACS Biomater. Sci. Eng.*, 2015, **1**, 585–592.

174   M. A. Alraddadi, V. Chiaradia, C. J. Stubbs, J. C. Worch and A. P. Dove, *Polym. Chem.*, 2021, **12**, 5796–5802.

175 N. Tratnik, N. R. Tanguy and N. Yan, *Chem. Eng. J.*, 2023, **451**, 138610.

176 Z. Guo, B. Liu, L. Zhou, L. Wang, K. Majeed, B. Zhang, F. Zhou and Q. Zhang, *Polymer (Guildf).*, 2020, **197**, 122483.

177 X. Guo, F. Liu, M. Lv, F. Chen, F. Gao, Z. Xiong, X. Chen, L. Shen, F. Lin and X. Gao, *Polymers (Basel).*, 2022, **14**, 3953.

178 S. Majumdar, H. Zhang, M. Soleimani, R. A. T. M. Van Benthem, J. P. A. Heuts and R. P. Sijbesma, *ACS Macro Lett.*, 2020, **9**, 1753–1758.

179 S. C. L. Kamerlin, P. K. Sharma, R. B. Prasad and A. Warshel, *Q. Rev. Biophys.*, 2013, **46**, 1–132.

180 X. Feng and G. Li, *Chem. Eng. J.*, 2021, **417**, 129132.

181 W. Schmolke, N. Perner and S. Seiffert, *Macromolecules*, 2015, **48**, 8781–8788.

182 T. Debsharma, V. Amfilochiou, A. A. Wróblewska, I. De Baere, W. Van Paepegem and F. E. Du Prez, *J. Am. Chem. Soc.*, 2022, **144**, 12280–12289.

183 P. Zheng and T. J. McCarthy, *J. Am. Chem. Soc.*, 2012, **134**, 2024–2027.

184 M. O. Saed and E. M. Terentjev, *ACS Macro Lett.*, 2020, **9**, 749–755.

185 R. C. Osthoff, A. M. Bueche and W. T. Grubb, *J. Am. Chem. Soc.*, 1954, **76**, 4659–4663.

186 E. Frankland, *J. Chem. Soc.*, 1862, **15**, 363–381.

187 D. G. Hall, in *Boronic Acids*, Wiley-VCH Verlag GmbH & Co. KGaA, Weinheim, Germany, 2011, pp. 1–133.

188 D. G. Hall, *Chem. Soc. Rev.*, 2019, **48**, 3475–3496.

189 B. Rohrig, *ChemMatters*, 2004, 13–16.

190 J. S. Hansen, J. B. Christensen, J. F. Petersen, T. Hoeg-Jensen and J. C. Norrild, *Sensors Actuators B Chem.*, 2012, **161**, 45–79.

191 Y. Guan and Y. Zhang, *Chem. Soc. Rev.*, 2013, **42**, 8106–8121.

192 V. V. Karnati, X. Gao, S. Gao, W. Yang, W. Ni, S. Sankar and B. Wang, *Bioorg. Med. Chem. Lett.*, 2002, **12**, 3373–3377.

193 M. Mortellaro and A. DeHennis, *Biosens. Bioelectron.*, 2014, **61**, 227–231.

194   M. Röttger, T. Domenech, R. Van Der Weegen, A. Breuillac, R. Nicolaÿ and L. Leibler, *Science (80-.).*, 2017, **356**, 62–65.

195   W. A. Ogden and Z. Guan, *J. Am. Chem. Soc.*, 2018, **140**, 6217–6220.

196   Y. Chen, Z. Tang, X. Zhang, Y. Liu, S. Wu and B. Guo, *ACS Appl. Mater. Interfaces*, 2018, **10**, 24224–24231.

197   A. Stubelius, S. Lee and A. Almutairi, *Acc. Chem. Res.*, 2019, **52**, 3108–3119.

198   D. Roy, J. N. Cambre and B. S. Sumerlin, *Chem. Commun.*, 2009, **7345**, 2106.

199   W. L. A. Brooks, C. C. Deng and B. S. Sumerlin, *ACS Omega*, 2018, **3**, 17863–17870.

200   S. Wang, X. Xing, X. Zhang, X. Wang and X. Jing, *J. Mater. Chem. A*, 2018, **6**, 10868–10878.

201   A. P. Bapat, D. Roy, J. G. Ray, D. A. Savin and B. S. Sumerlin, *J. Am. Chem. Soc.*, 2011, **133**, 19832–19838.

202   R. L. Snyder, D. J. Fortman, G. X. De Hoe, M. A. Hillmyer and W. R. Dichtel, *Macromolecules*, 2018, **51**, 389–397.

203   C. D. Roy and H. C. Brown, *J. Organomet. Chem.*, 2007, **692**, 784–790.

204   H. Bonin, T. Delacroix and E. Gras, *Org. Biomol. Chem.*, 2011, **9**, 4714–4724.

205   H. C. Brown and J. V. N. V. Prasad, *J. Org. Chem.*, 1986, **51**, 4526–4530.

206   WO2015/165808A1, 2015.

207   WO2017/068015A1, 2017.

208   M. G. Unthank, C. Cameron, A. Wright, D. Hughes, M. A. Alam and M. R. Probert, *Polym. Chem.*, 2019, **10**, 4920–4929.

209   V. Stepanenko, M. de Jesús, C. Garcia, C. L. Barnes and M. Ortiz-Marciales, *Tet. Lett.*, 2012, **53**, 910–913.

210   Y. Ito, J. Kida, D. Aoki and H. Otsuka, *Chem. Commun.*, 2018, **54**, 12930–12933.

211   Y. Ito, D. Aoki and H. Otsuka, *Polym. Chem.*, 2020, **11**, 5356–5364.

212   R. J. Friary, V. Seidl, J. H. Schwerdt, M. P. Cohen, D. Hou and M. Nafissi, *Tetrahedron*, 1993, **49**, 7169–7178.

213   Y. Min, S. Huang, Y. Wang, Z. Zhang, B. Du, X. Zhang and Z. Fan, *Macromolecules*, 2015, **48**, 316–322.

214   Z. Feng, B. Yu, J. Hu, H. Zuo, J. Li, H. Sun, N. Ning, M. Tian and L. Zhang, *Ind. Eng. Chem. Res.*, 2019, **58**, 1212–1221.

215   Z. Wang, X. Zhang, R. Wang, H. Kang, B. Qiao, J. Ma, L. Zhang and H. Wang, *Macromolecules*, 2012, **45**, 9010–9019.

216   Y. Li, T. Liu, S. Zhang, L. Shao, M. Fei, H. Yu and J. Zhang, *Green Chem.*, 2020, **22**, 870–881.

217   C. Hao, T. Liu, S. Zhang, W. Liu, Y. Shan and J. Zhang, *Macromolecules*, , DOI:10.1021/acs.macromol.9b02243.

218   G. Wesela-Bauman, M. Urban, S. Luliński, J. Serwatowski and K. Woźniak, *Org. Biomol. Chem.*, 2015, **13**, 3268–3279.

219   C. D. Roy and H. C. Brown, *Monatshefte fur Chemie*, 2007, **138**, 879–887.

220   H. Steinberg and D. L. Hunter, *Ind. Eng. Chem.*, 1957, **49**, 174–181.

221   P. B. Hodgson and F. H. Salingue, *Tetrahedron Lett.*, 2004, **45**, 685–687.

222   M. Tiecco, L. Testaferri, L. Bagnoli, C. Scarponi, V. Purgatorio, A. Temperini, F. Marini and C. Santi, *Tetrahedron: Asymmetry*, 2005, **16**, 2429–2435.

223   E. K. Lermontova, M. M. Huang, S. S. Karlov, M. V. Zabalov, A. V. Churakov, B. Neumüller and G. S. Zaitseva, *Russ. Chem. Bull.*, 2008, **57**, 1920–1930.

224   J. Clayden, N. Greeves, S. Warren and P. Wothers, in *Organic Chemistry*, Oxford University Press, Oxford, 1st edn., 2001, pp. 864–70.

225   T. Caron, P. Palmas, C. Frénois, C. Méthivier, E. Pasquinet, C.-M. Pradier, F. Serein-Spirau, L. Hairault and P. Montméat, *New J. Chem.*, 2020, **44**, 4114–4121.

226   W. Zhao, L. An and S. Wang, *Polymers (Basel).*, 2021, **13**, 296.

227   C.-M. Chen and S. Yang, *Polym. Int.*, 2012, **61**, 1041–1047.

228   Marbocote ltd, Mould Release Agents for Composite, https://www.marbocote.co.uk/products/mould-release-agents-for-composite-components/, (accessed 9 April 2023).

229 S. Morsch, Y. Liu, S. B. Lyon, S. R. Gibbon, B. Gabriele, M. Malanin and K.-J. Eichhorn, *Polym. Degrad. Stab.*, 2020, **176**, 109147.

230 A. E. Krauklis and A. T. Echtermeyer, *Polymers (Basel).*, 2018, **10**, 1017–1032.

231 E. Ernault, E. Richaud and B. Fayolle, *Polym. Degrad. Stab.*, 2016, **134**, 76–86.

232 C. Galant, B. Fayolle, M. Kuntz and J. Verdu, *Prog. Org. Coatings*, 2010, **69**, 322–329.

233 R. J. Young and P. A. Lovell, in *Introduction to polymers*, CRC Press, Boca Raton, 3rd edn., 2011, pp. 381–465.

234 J. Heijboer, *Int. J. Polym. Mater. Polym. Biomater.*, 1977, **6**, 11–37.

235 M. Chen, Y. Wu, B. Chen, A. M. Tucker, A. Jagota and S. Yang, *Proc. Natl. Acad. Sci. U. S. A.*, 2022, **119**, 1–9.

236 Z. Wang, Y. Gu, M. Ma and M. Chen, *Macromolecules*, 2020, **53**, 956–964.

237 C. Zhang, Z. Yang, N. T. Duong, X. Li, Y. Nishiyama, Q. Wu, R. Zhang and P. Sun, *Macromolecules*, 2019, **52**, 5014–5025.

238 C. C. Deng, W. L. A. Brooks, K. A. Abboud and B. S. Sumerlin, *ACS Macro Lett.*, 2015, **4**, 220–224.

239 Y. Nishimura, J. Chung, H. Muradyan and Z. Guan, *J. Am. Chem. Soc.*, 2017, **139**, 14881–14884.

240 A. Erice, A. Ruiz de Luzuriaga, I. Azcune, M. Fernandez, I. Calafel, H. J. Grande and A. Rekondo, *Polymer (Guildf).*, 2020, **196**, 122461.

241 X. Kuang, G. Liu, X. Dong and D. Wang, *Mater. Chem. Front.*, 2017, **1**, 111–118.

242 S. Ullah, F. Ahmad and P. S. M. M. Yusoff, *J. Appl. Polym. Sci.*, 2013, **128**, 2983–2993.

243 L. D. Field, H. L. Li and A. M. Magill, *Infrared (IR) Spectroscopy*, Wiley, Hoboken, 6th edn., 2020.

244 J. B. Lambert, S. Gronert, H. F. Shurvell and D. F. Lightner, *Organic Structural Spectroscopy*, Pearson, Upper Saddle River, 2nd edn., 2011.

245 Q. Shi, K. Yu, X. Kuang, X. Mu, C. K. Dunn, M. L. Dunn, T. Wang and H. Jerry Qi,

Mater. Horizons, 2017, **4**, 598–607.

246   Plastics   Europe,   Recycling   Technologies, https://plasticseurope.org/sustainability/circularity/recycling/recycling-technologies/#:~:text=Mechanical recycling refers to the,or no impact on quality., (accessed 25 April 2023).

247   J. Flizikowski, W. Kruszelnicka and M. Macko, *Polymers (Basel).*, 2021, **13**, 1–44.

248   N. Fomina, V. Khozin, A. Strakhov and A. Ismagilov, *E3S Web Conf.*, 2021, **263**, 01018.

249   Z. O. G. Schyns and M. P. Shaver, *Macromol. Rapid Commun.*, 2021, **42**, 1–27.

250   M. Jackson, M. Kaushik, S. Nazarenko, S. Ward, R. Maskell and J. Wiggins, *Polymer (Guildf).*, 2011, **52**, 4528–4535.

251   S. T. Knox, A. Wright, C. Cameron and J. P. A. Fairclough, *Macromolecules*, 2019, **52**, 6861–6867.

252   S. T. Knox, A. Wright, C. Cameron and J. P. A. Fairclough, *ACS Appl. Polym. Mater.*, 2021, **3**, 3438–3445.

253   S. Gulyuz, Y. Yagci and B. Kiskan, *Polym. Chem.*, 2022, **13**, 3631–3638.

254   S. Tajbakhsh, F. Hajiali, K. Guinan and M. Marić, *React. Funct. Polym.*, 2021, **158**, 104794.

255   S. Tajbakhsh, F. Hajiali and M. Marić, *ACS Appl. Polym. Mater.*, 2021, **3**, 3402–3415.

256   B. Gewert, M. M. Plassmann and M. Macleod, *Environ. Sci. Process. Impacts*, 2015, **17**, 1513–1521.

257   B. J. Anderson, *Polym. Degrad. Stab.*, 2013, **98**, 2375–2382.

258   T. G. Fox and P. J. Flory, *J. Polym. Sci.*, 1954, **14**, 315–319.

259   J. Hintermeyer, A. Herrmann, R. Kahlau, C. Goiceanu and E. A. Rössler, *Macromolecules*, 2008, **41**, 9335–9344.

260   Olin, Liquid Epoxy Resins, https://olinepoxy.com/products/liquid-epoxy-resins/, (accessed 8 May 2023).

10 Appendix

10.1 Spectra
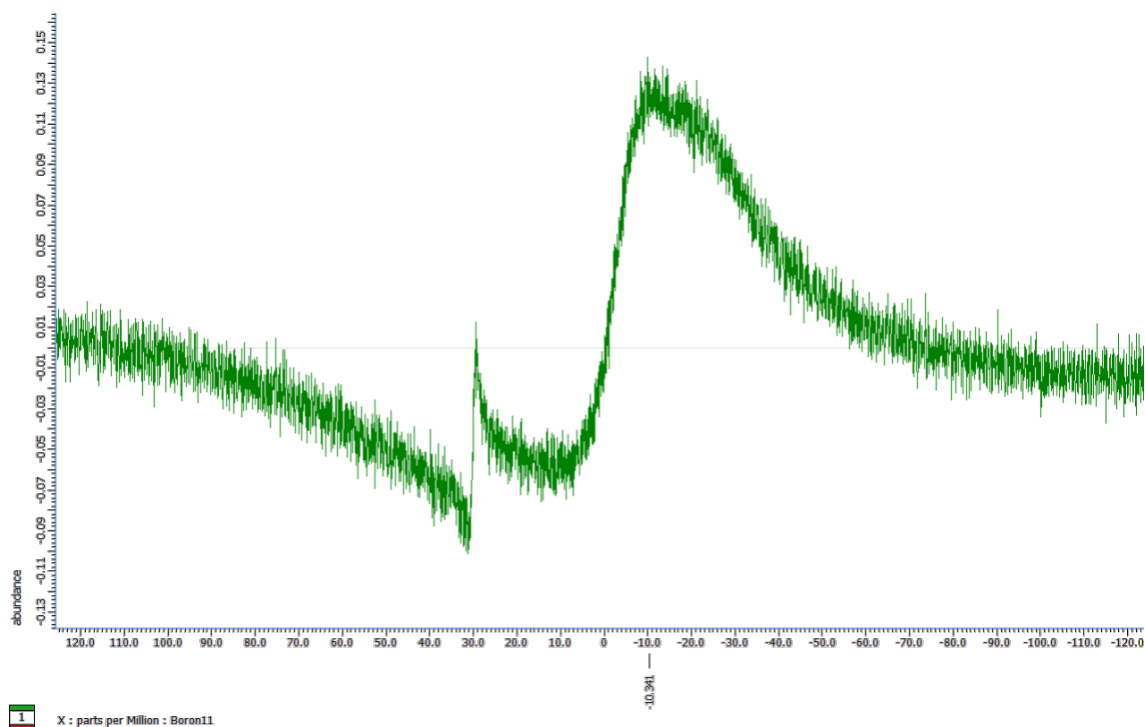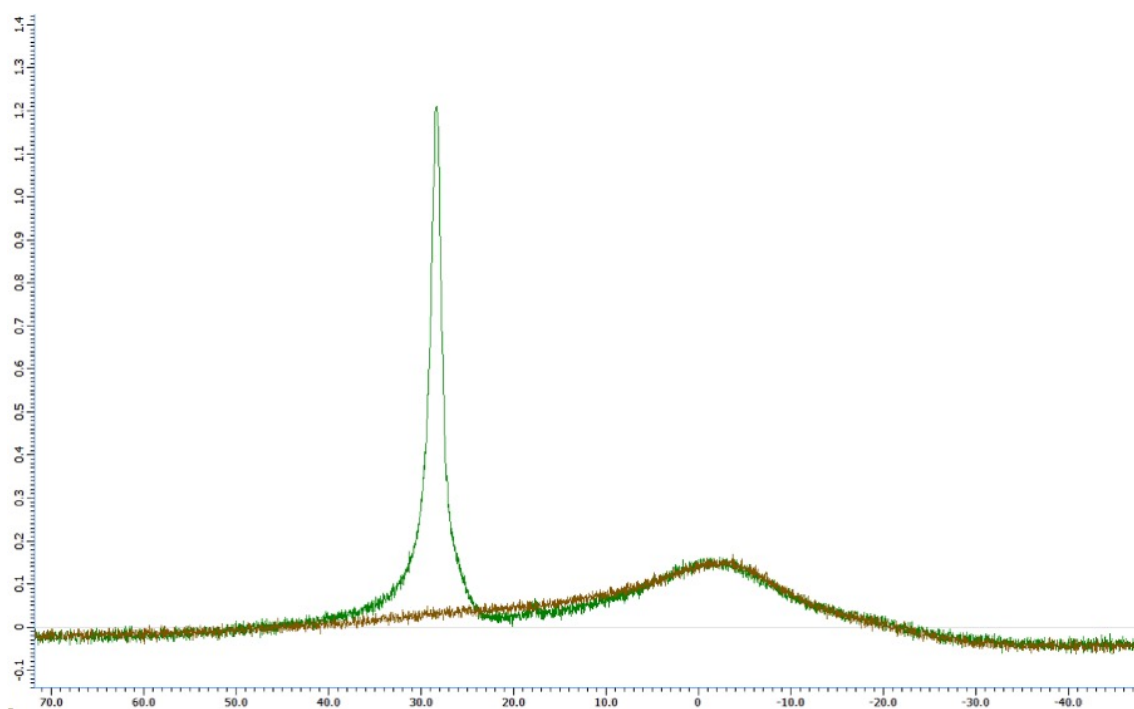
10.1.1 ^{1}H NMR

10.1.1.1 Phenylboronic acid 1,2-ethanediol ester (1a)
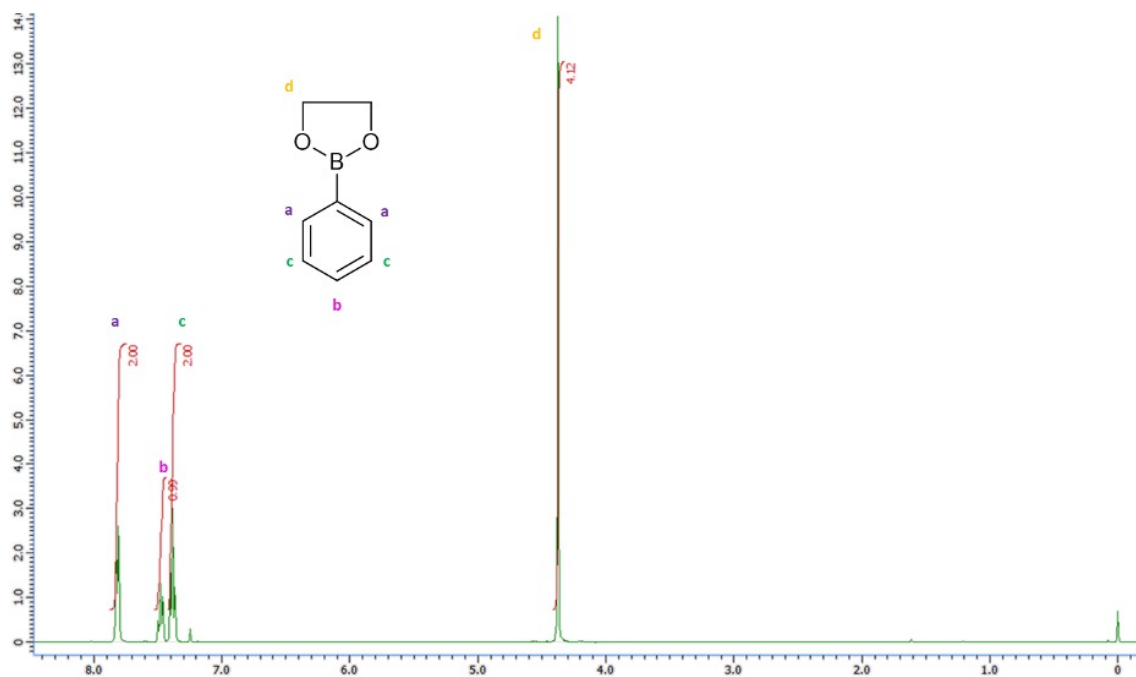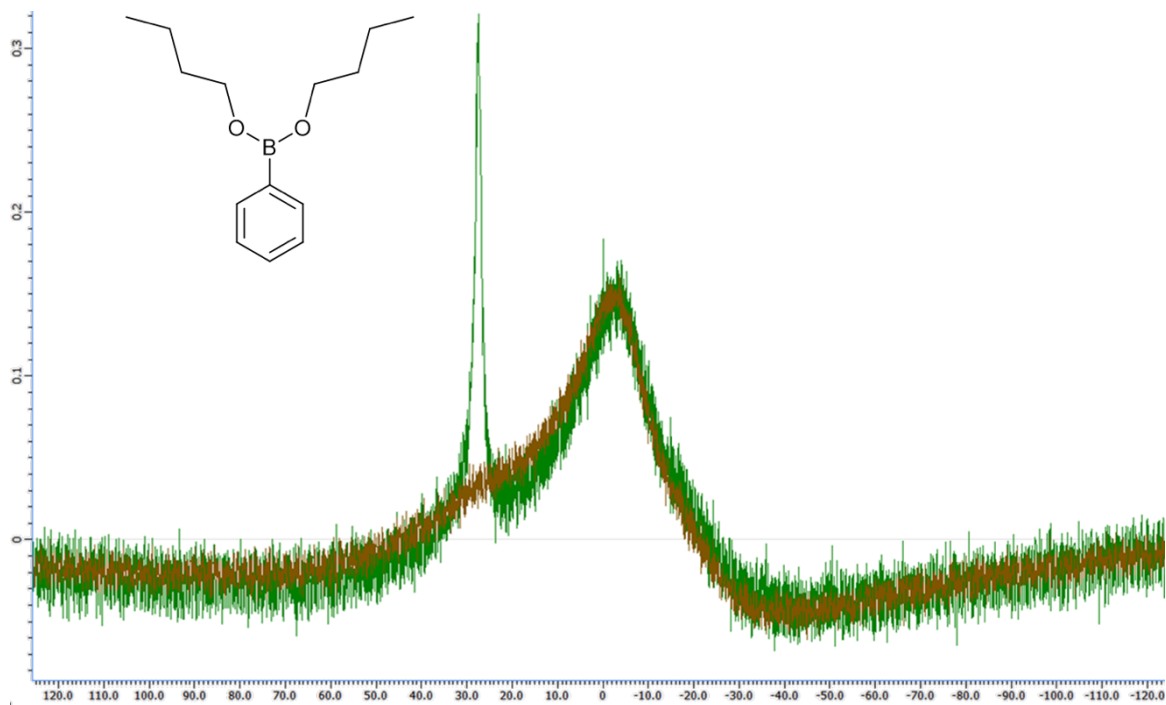

10.1.1.2 Phenylboronic acid pinacol ester (1b)
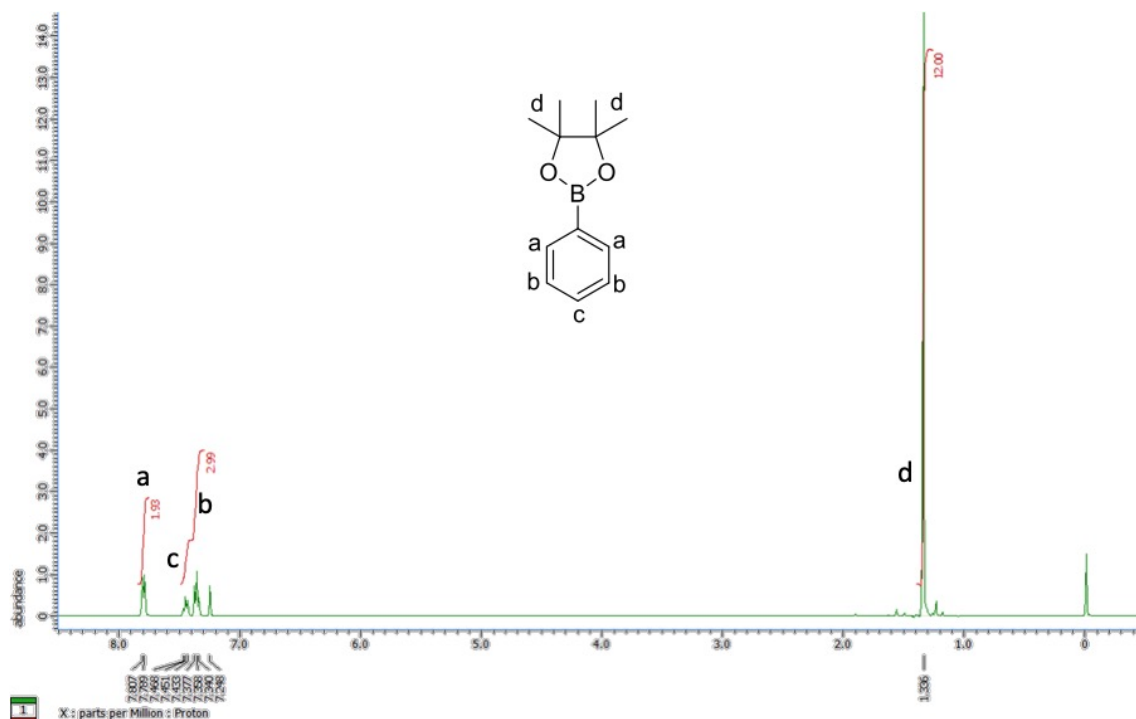
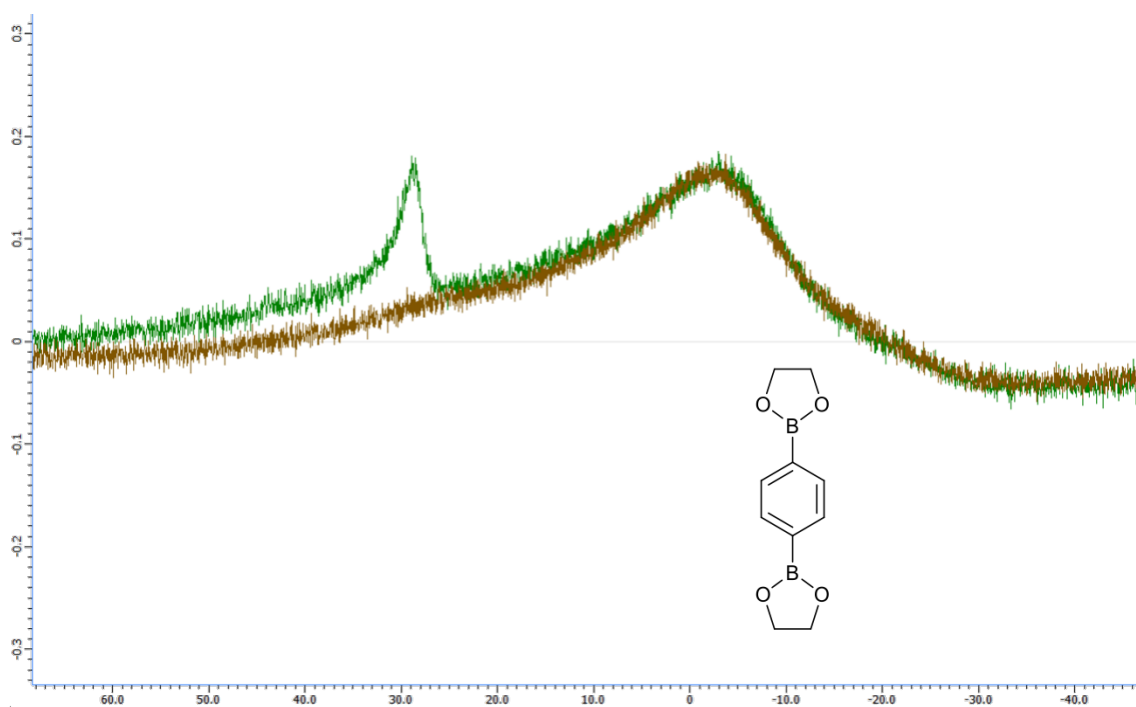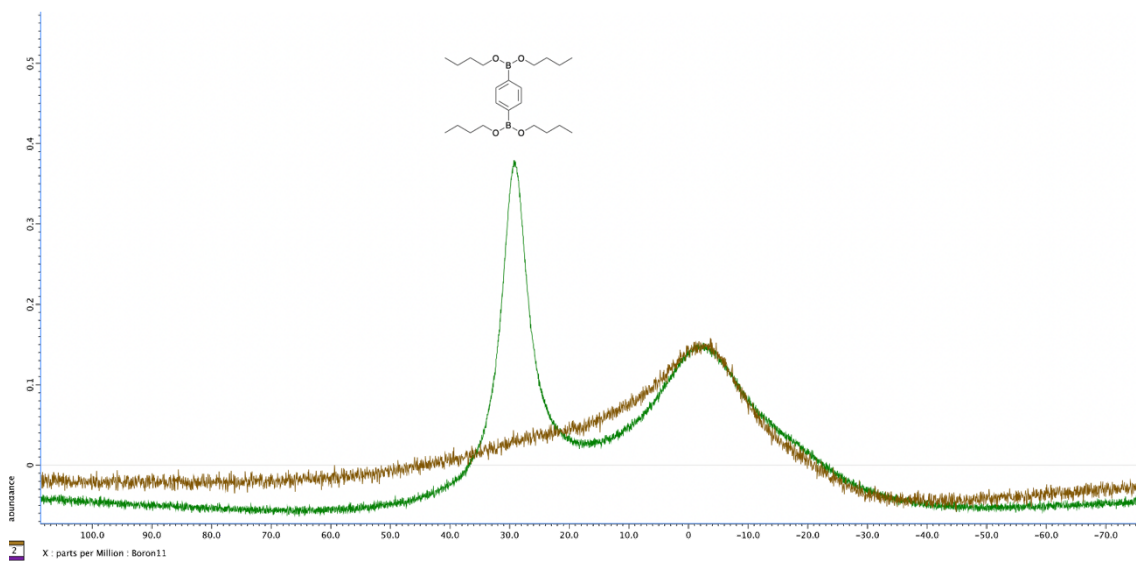### 10.1.1.3 Bis(propan-2-yl)phenylboronate (1c)
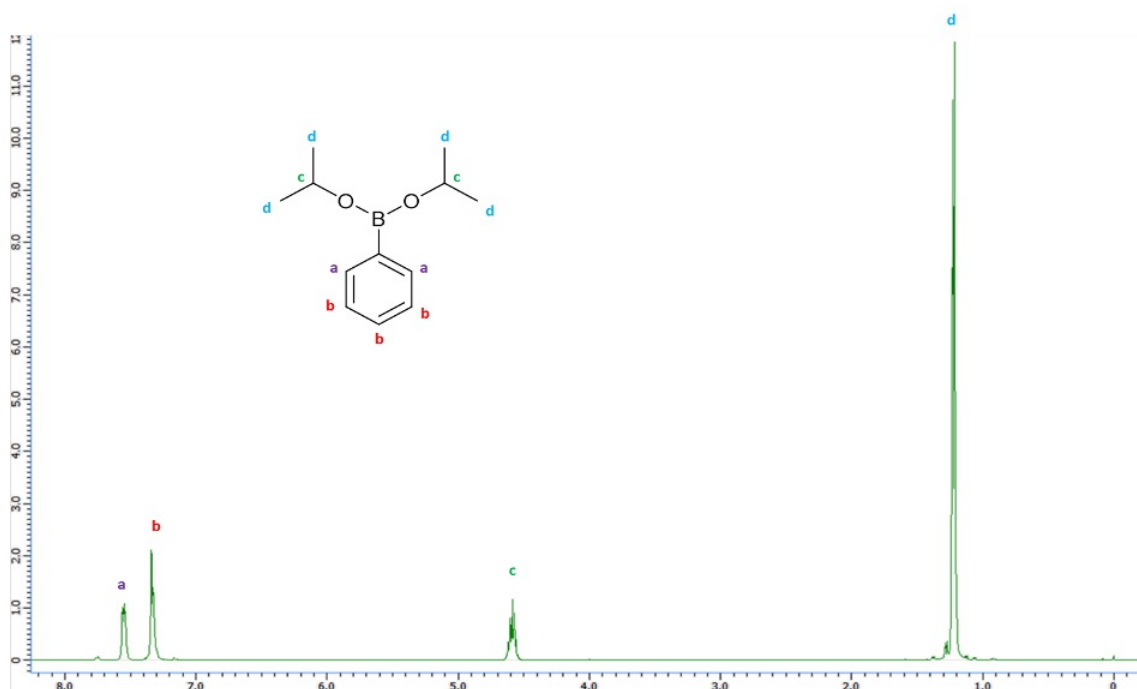
10.1.1.4 Bis(butyl)phenylboronate (1d)
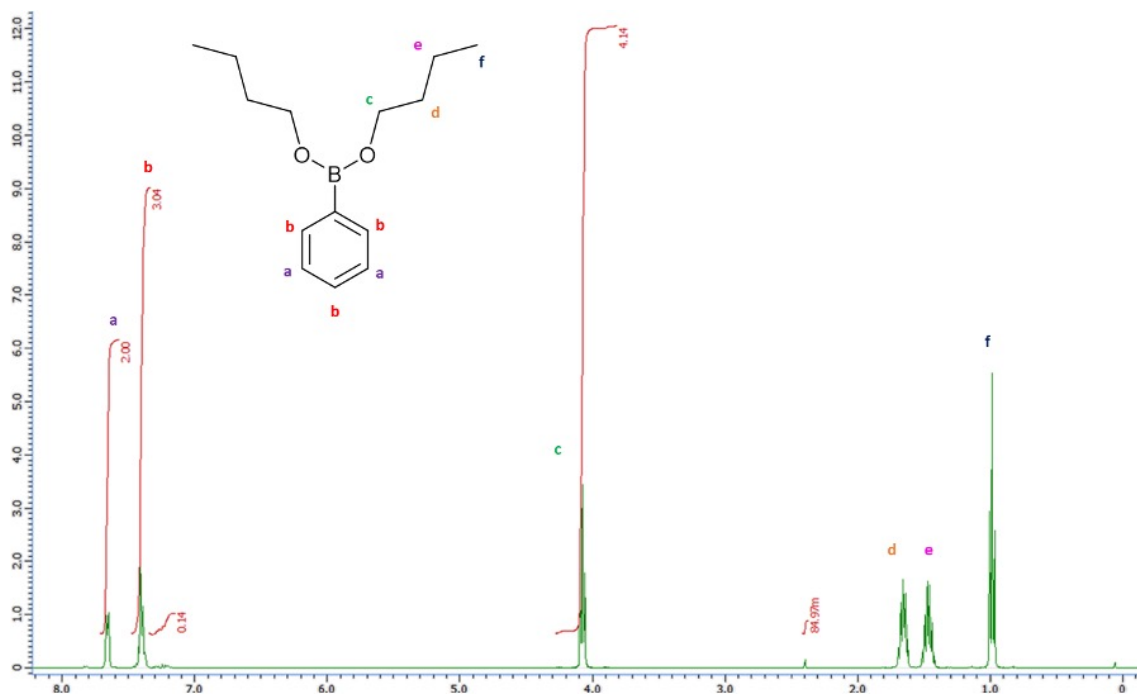
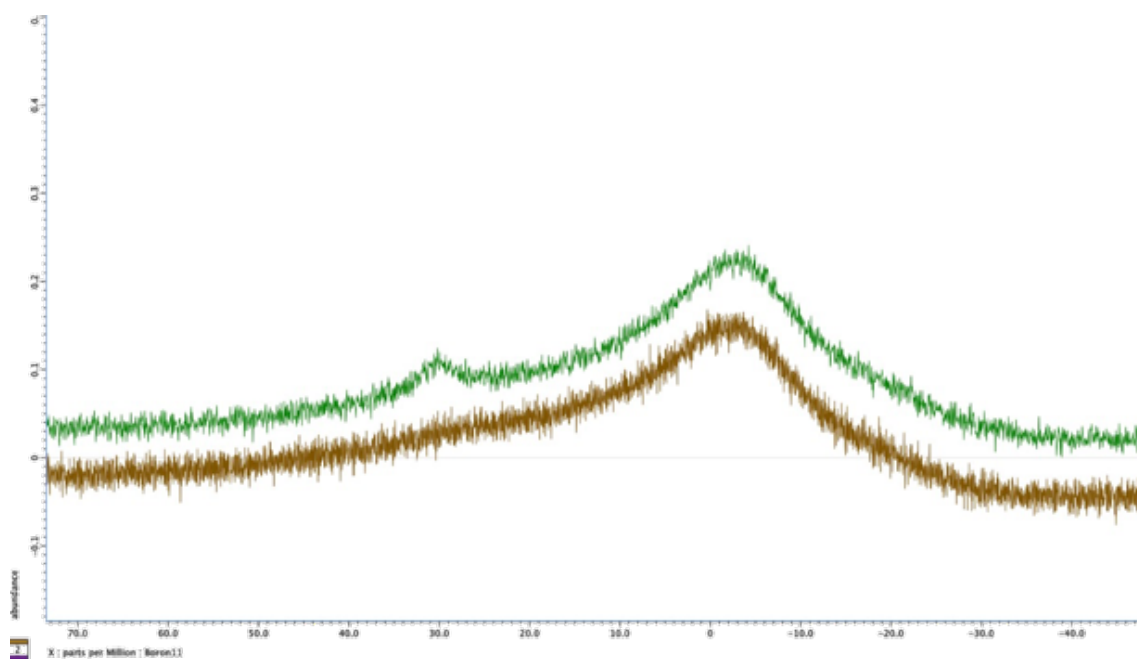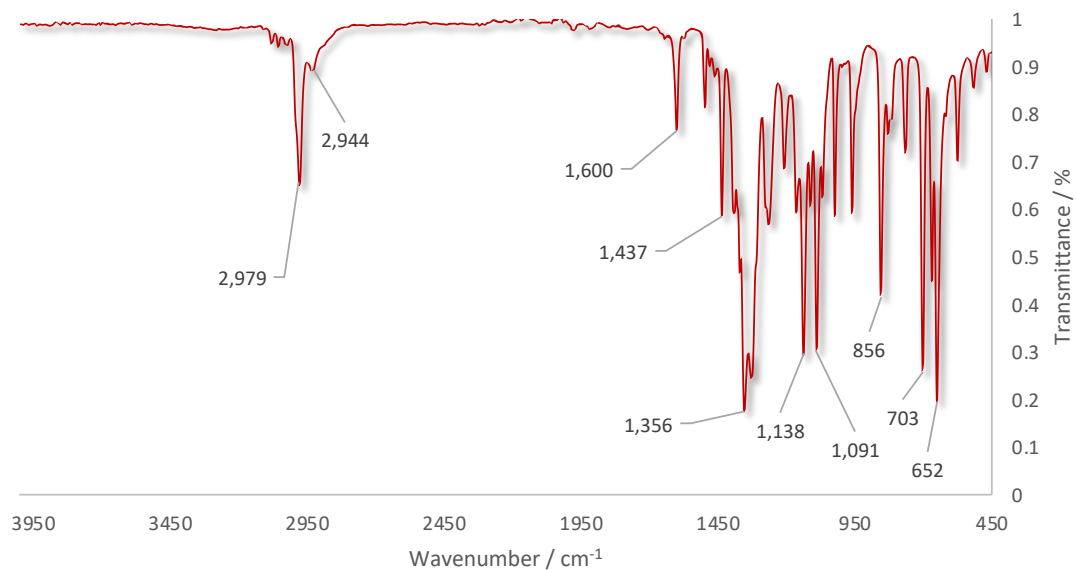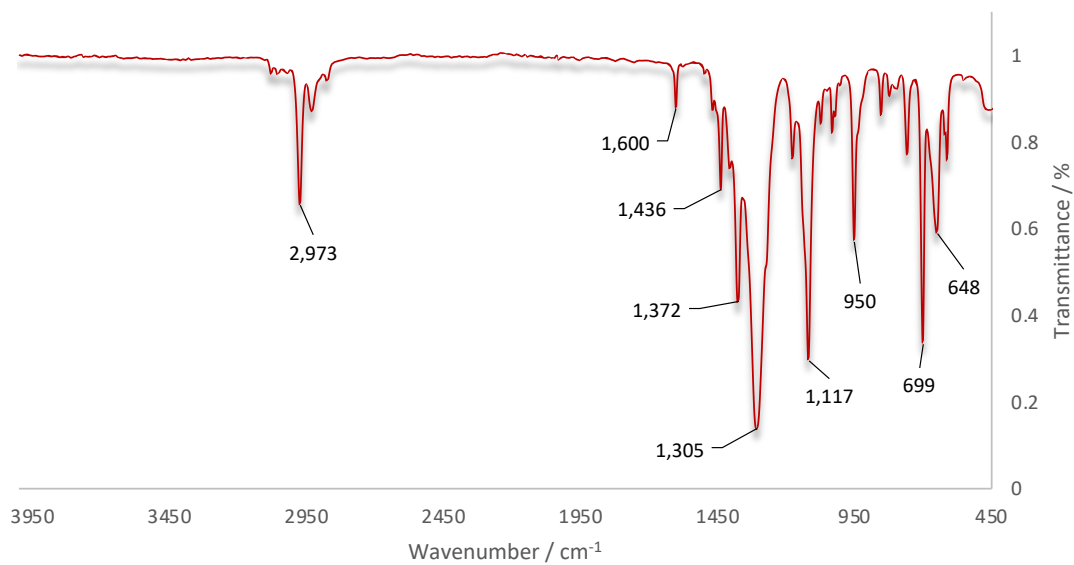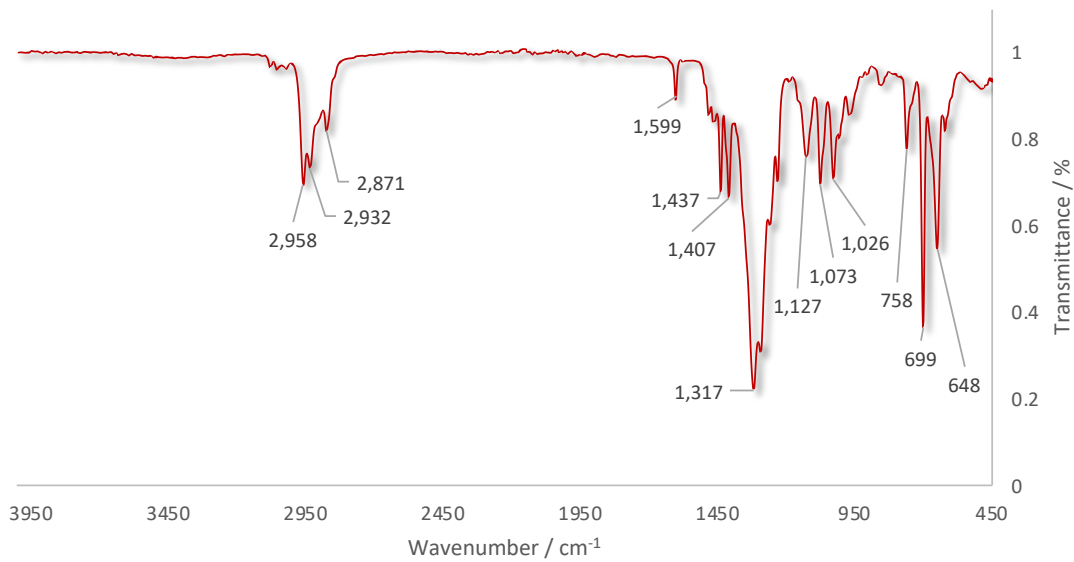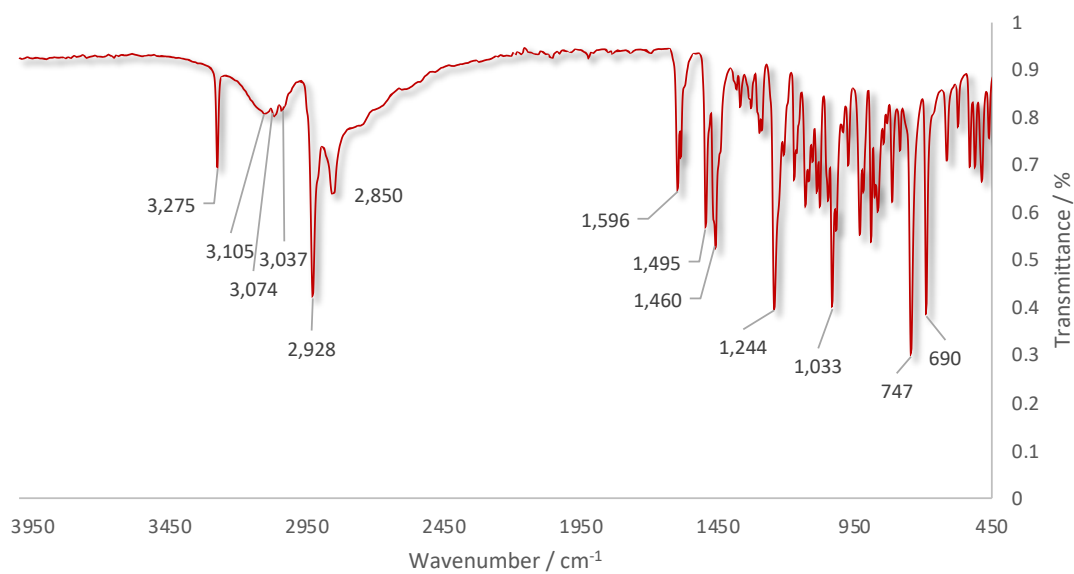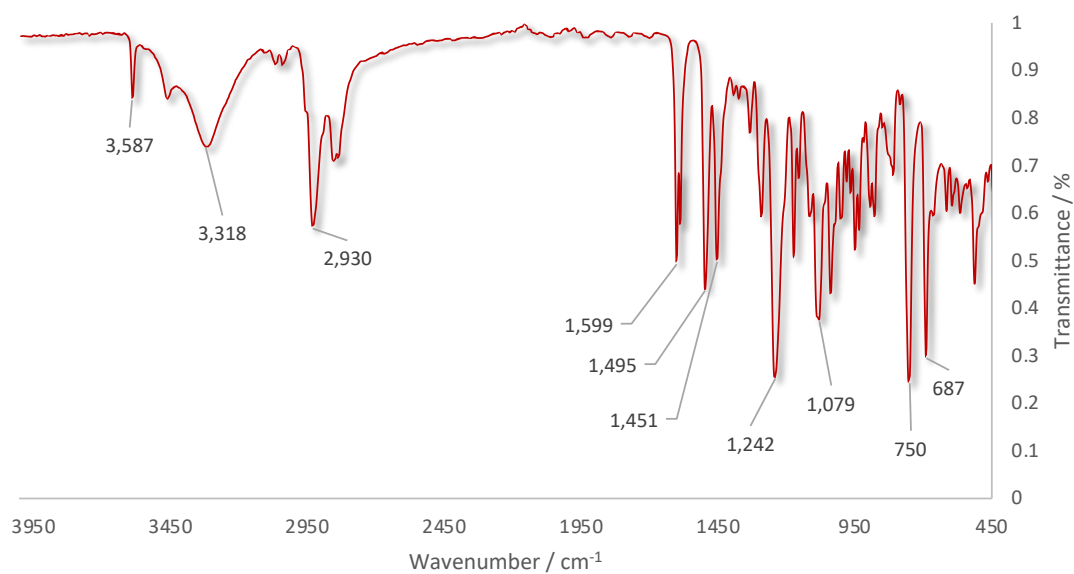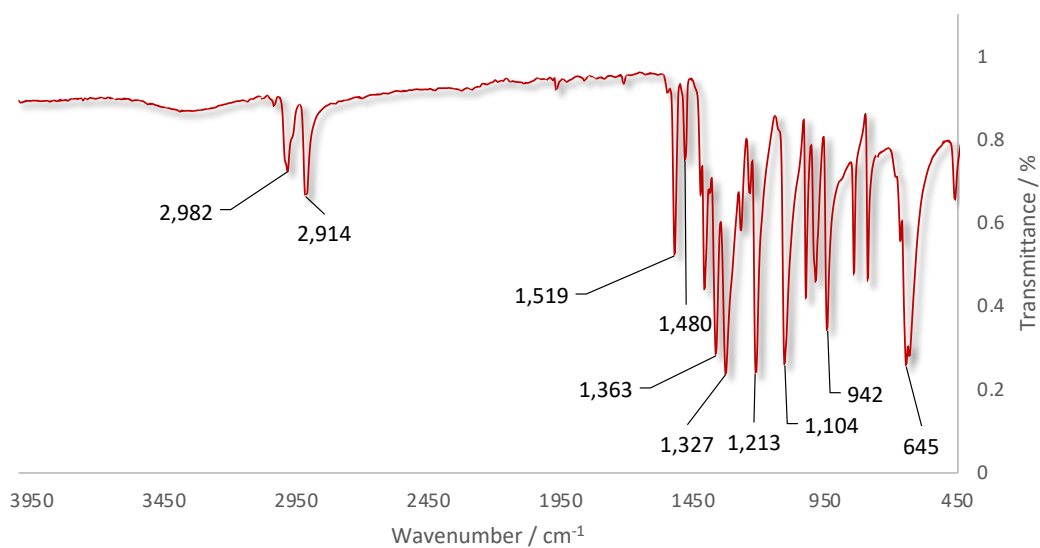## 10.1.1.5 *N*-(cyclohexylamino)-3-phenoxypropan-2-ol (2)
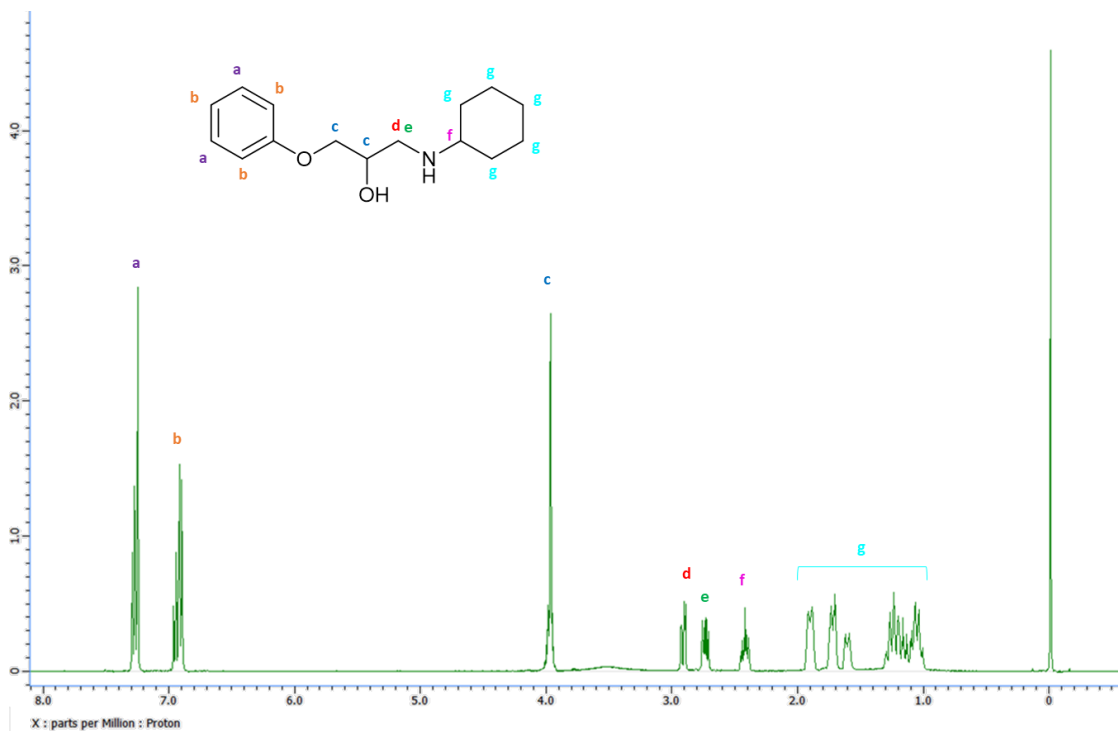
10.1.1.6 N,N-bis(2-hydroxy-3-phenoxy-propyl)-cyclohexanamine (β-amino diol (3))
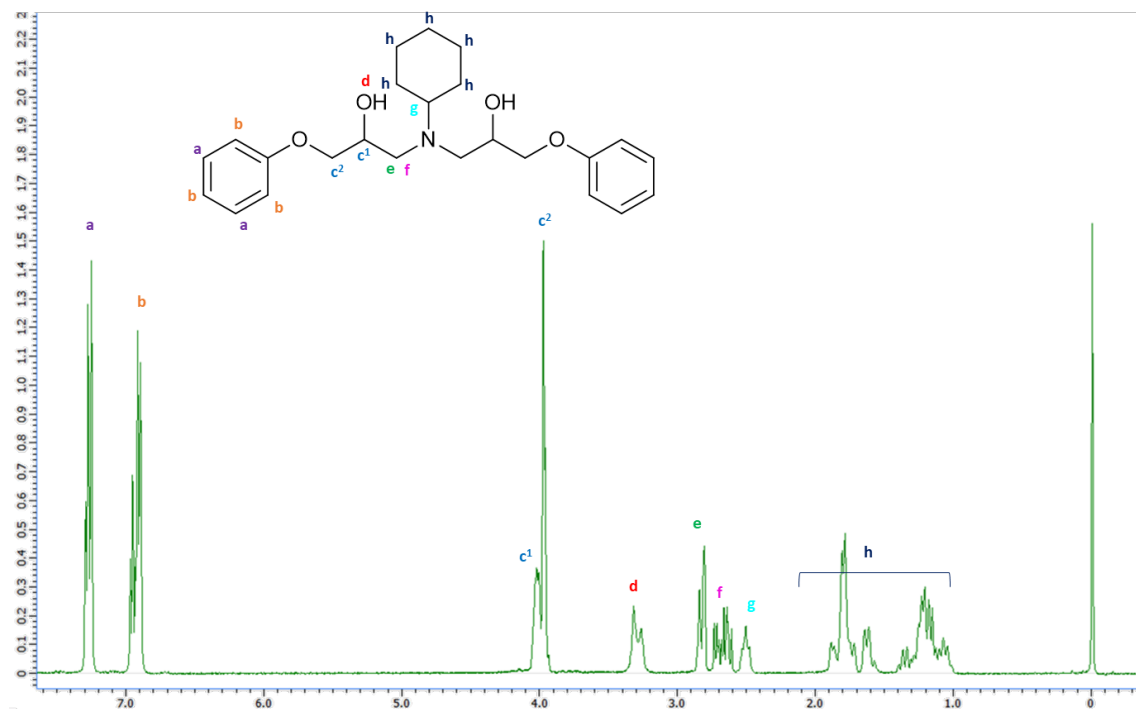
10.1.1.7 4-1a - Dioxazaborocane model test over time

Overlays

Dioxazaborcane **4-1a**

96 hours

45 mins

10 mins

1a

X : parts per Million : Proton
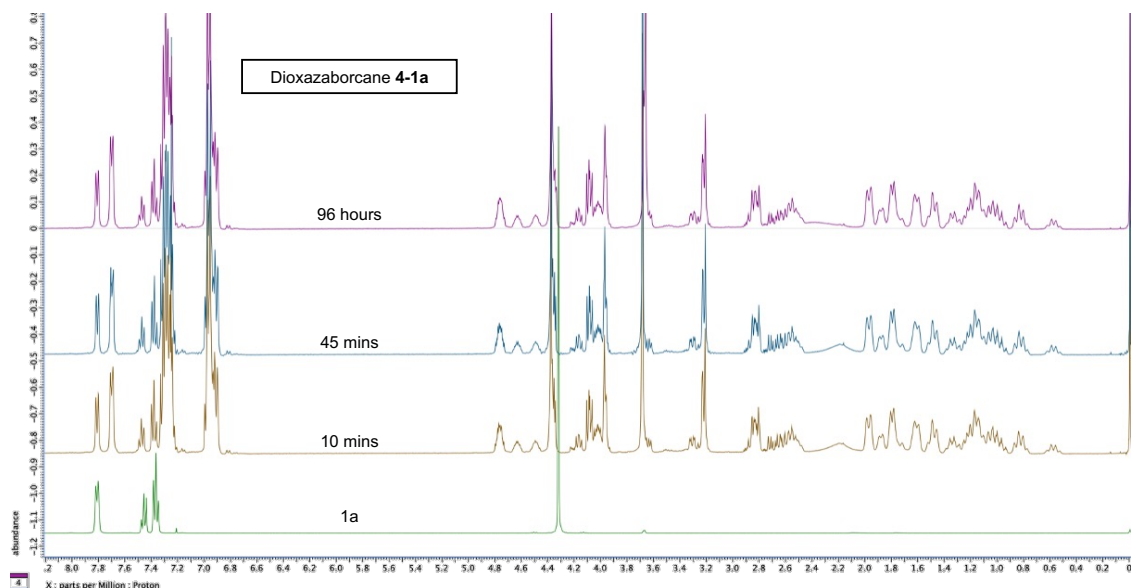
Integration of $H_{1\ (7.8\ ppm)}$ and $H_{2\ (7.7\ ppm)}$ peaks

The integrals of the starting material peak (H_1) have been compared to the product peak (H_2) for the same proton environment. A normalised integration for the product peak (H_2) was used to calculate a percentage using the following equation, when H_2 is equal to 2.00:

$$\frac{H_2}{H_2 + H_1} \ x \ 100 = \% \ Dioxazaborocane$$

Dioxazaborcane **4-1a**

Time	H_1	H_2	Dioxazaborocane 4-1b / %
10 minutes	1.10	2.00	64.52
45 mins	1.09	2.00	64.72
96 hours	1.03	2.00	66.00

iv
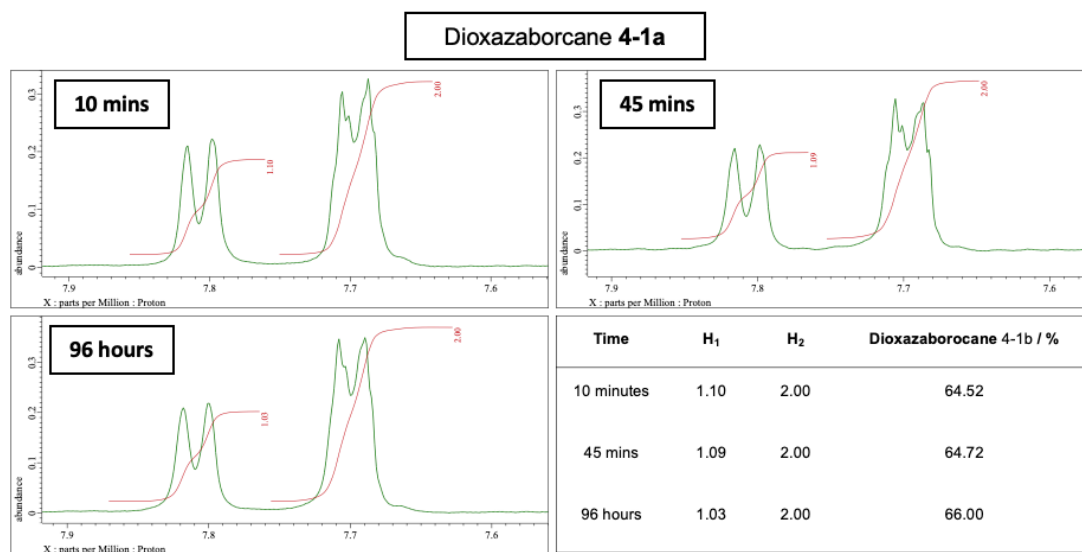
10.1.1.8 4-1b - Dioxazaborocane model test over time

Overlays

Dioxazaborcane **4-1b**
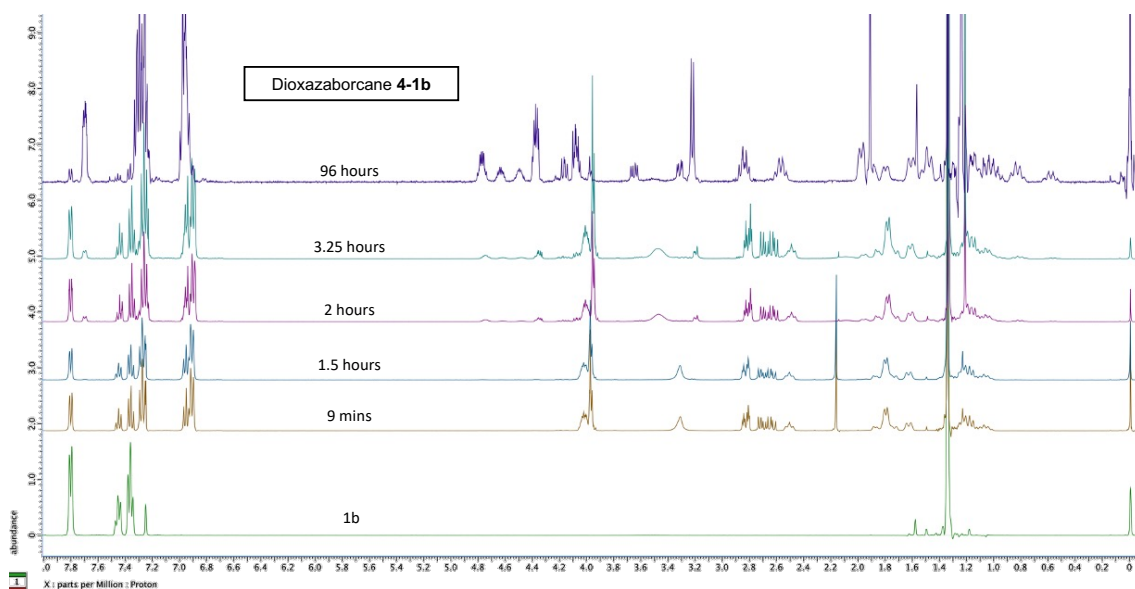
Integration of H$_1$ $_{(7.8\ ppm)}$ and H$_2$ $_{(7.7\ ppm)}$ peaks

Following the same method as the integration ratio of 4-1a, the pinacol ester (4-1b) gave the following results:

Dioxazaborcane **4-1b**

Time	H$_1$	H$_2$	Dioxazaborocane 4-1b / %
9 minutes	777.00	2.00	0.26
1.5 hours	152.12	2.00	1.30
2 hours	13.25	2.00	13.11
3.25 hours	10.87	2.00	15.54
96 hours	0.16	2.00	92.59
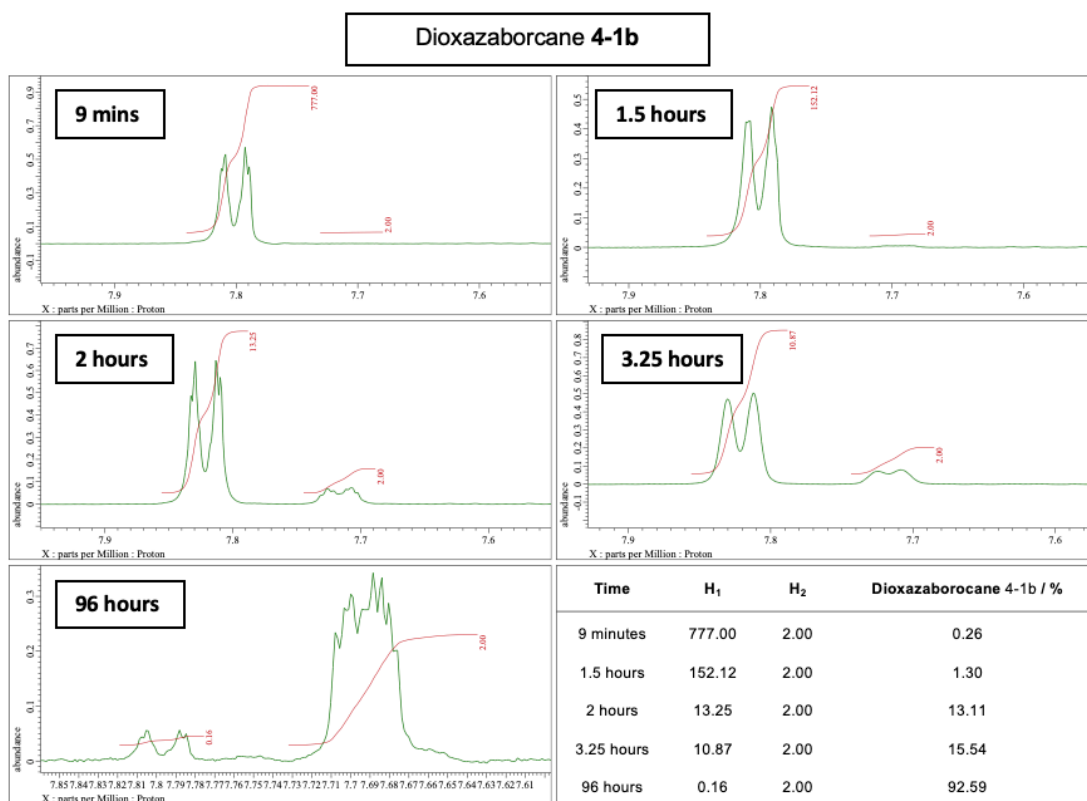
10.1.1.9 4-1c - Dioxazaborocane model test over time
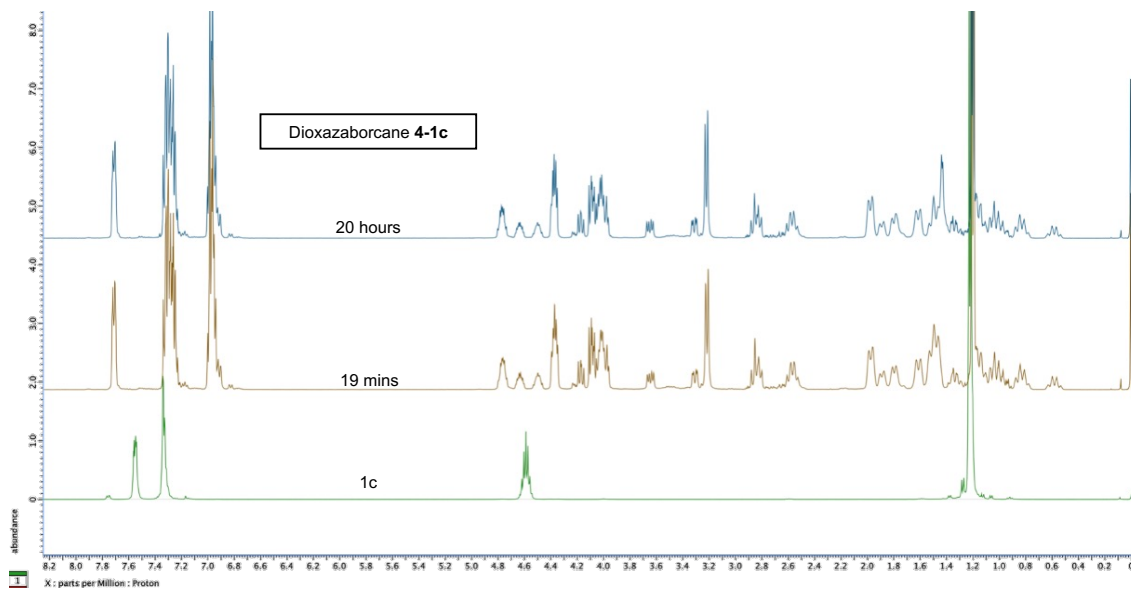
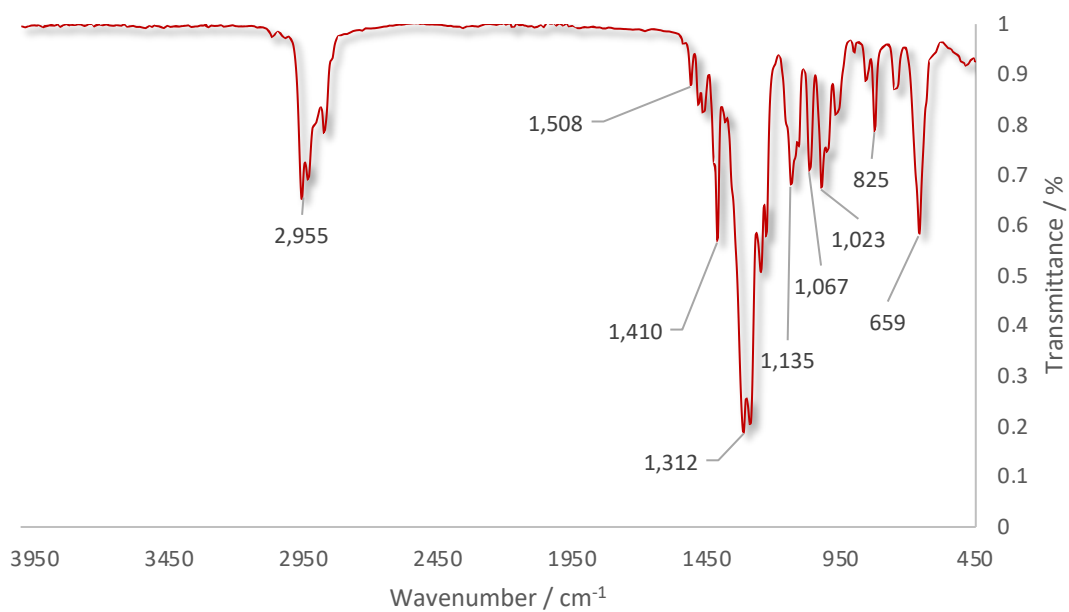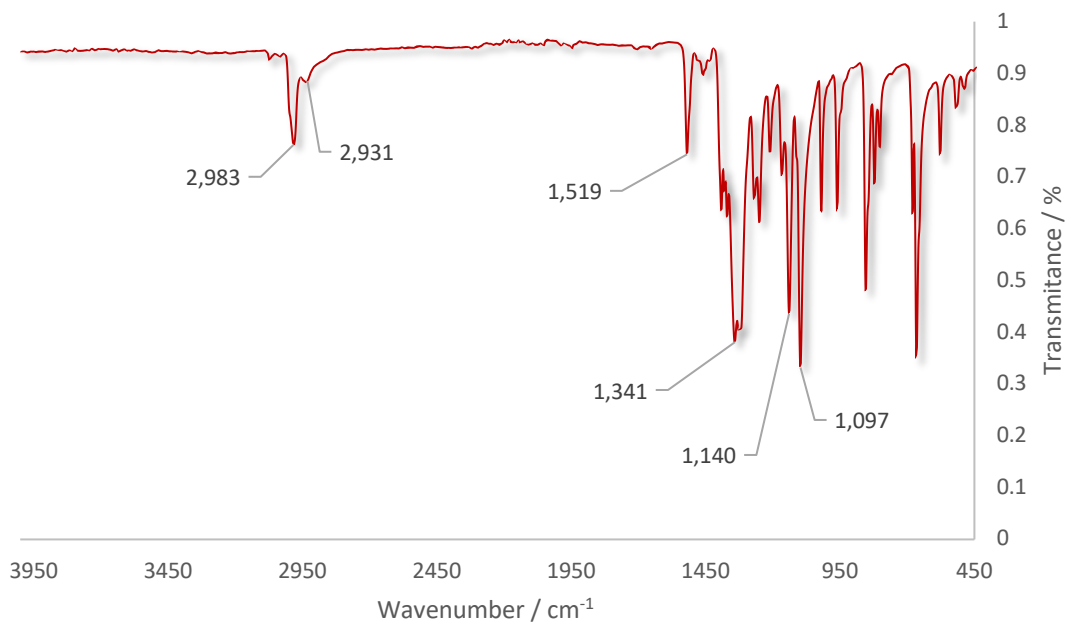
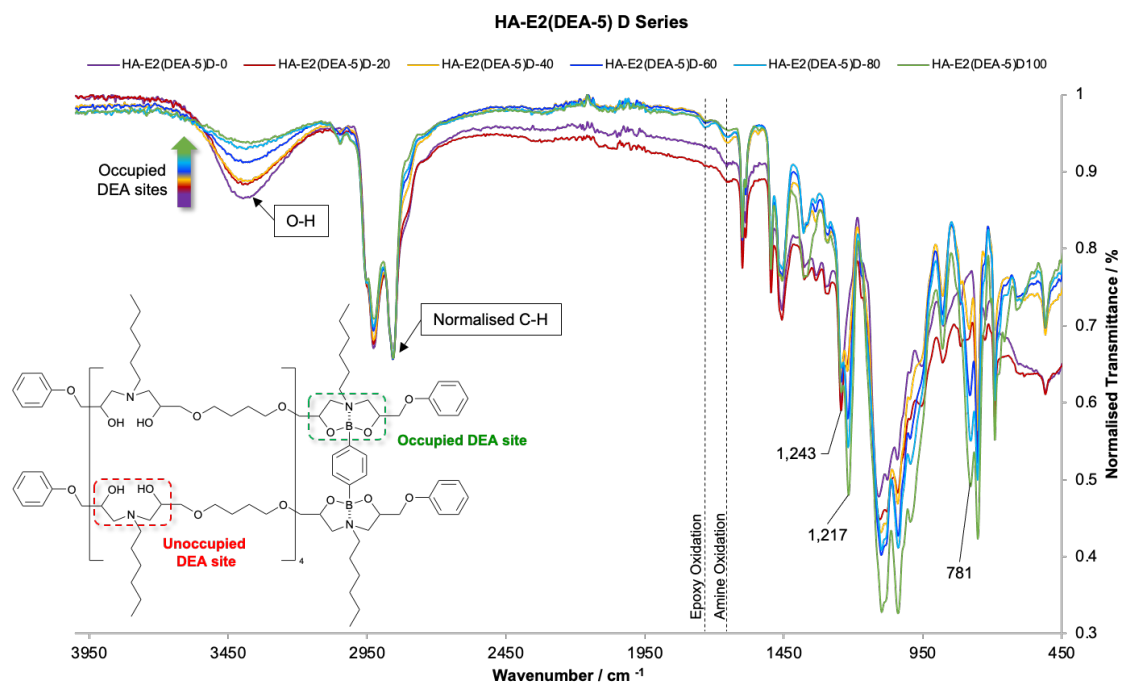## 10.1.1.10   1,4-Phenylenediboronic bis(1,2-diol) ester (5)
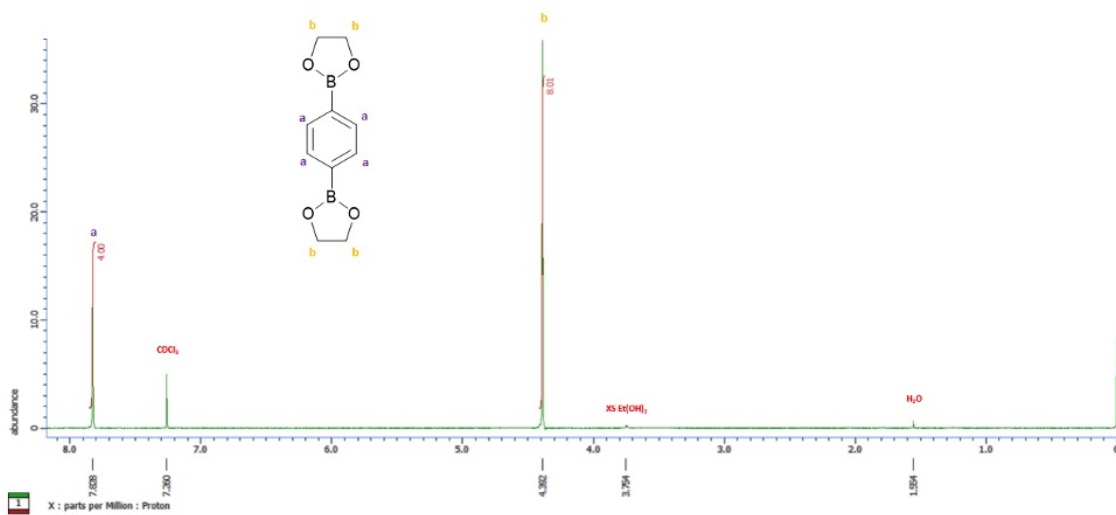
10.1.1.11   1,4-Phenylenediboronic acid tetrabutyl ester (6)
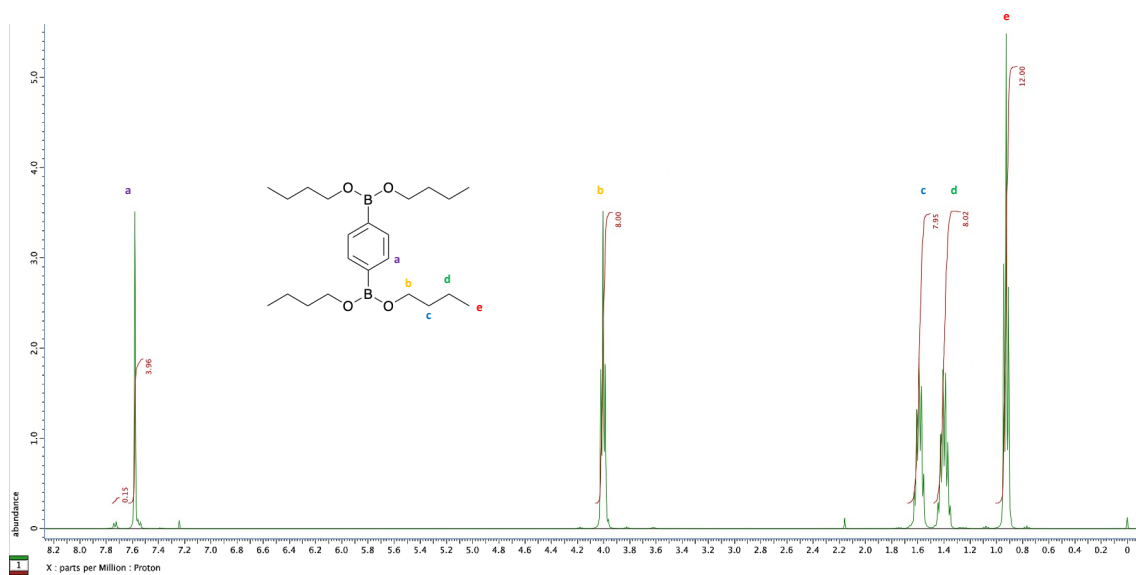
COSY
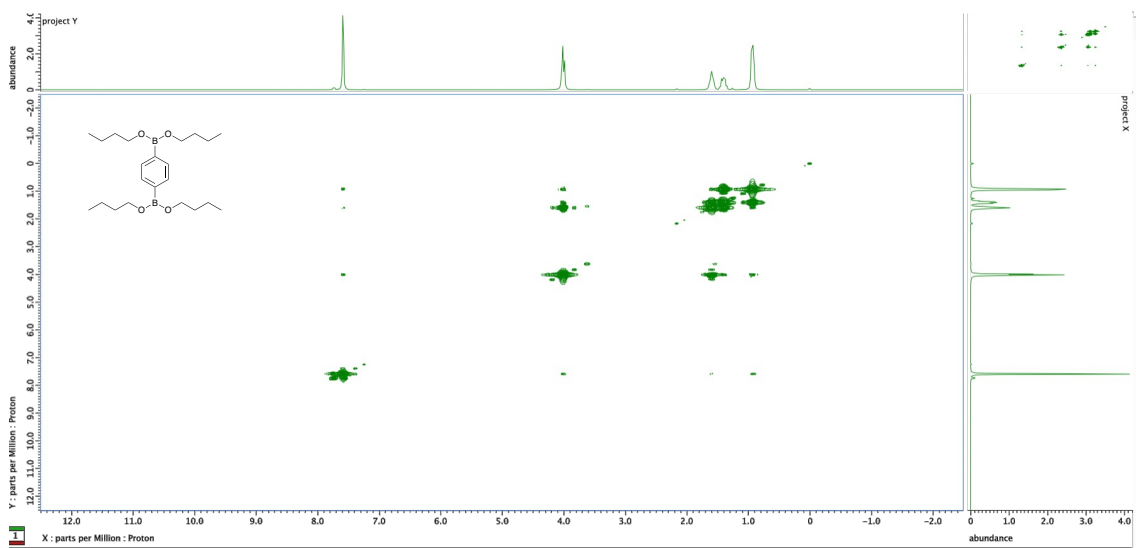
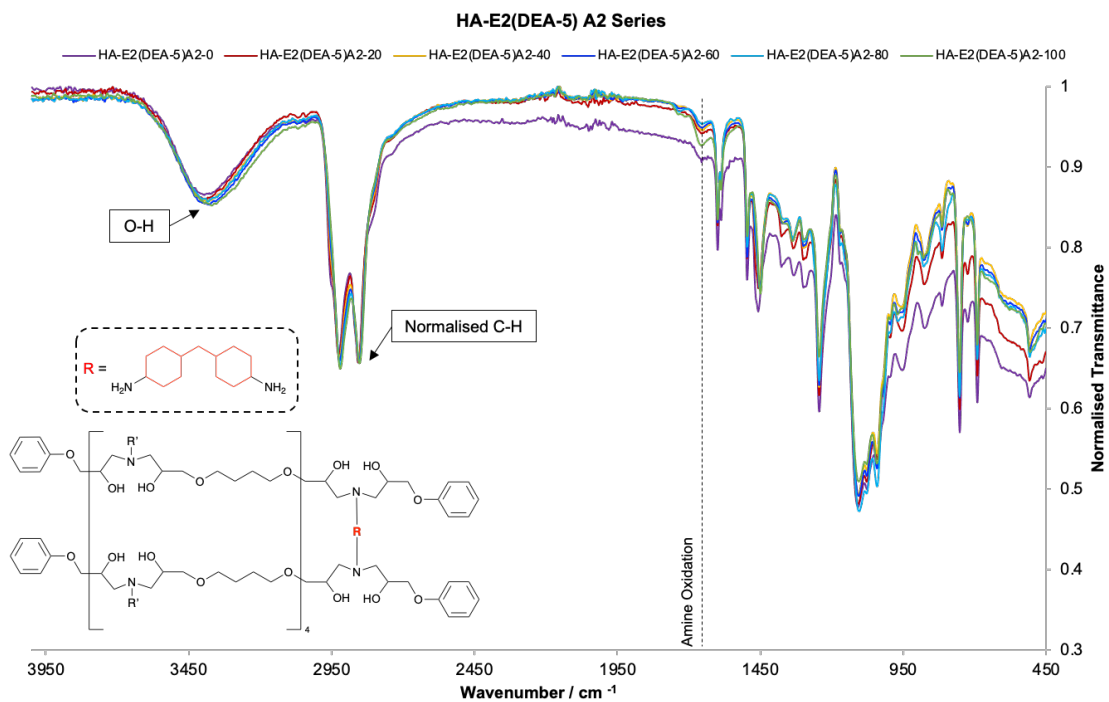## 10.1.1.12 1,4-Phenylenediboronic acid pinacol ester (7)
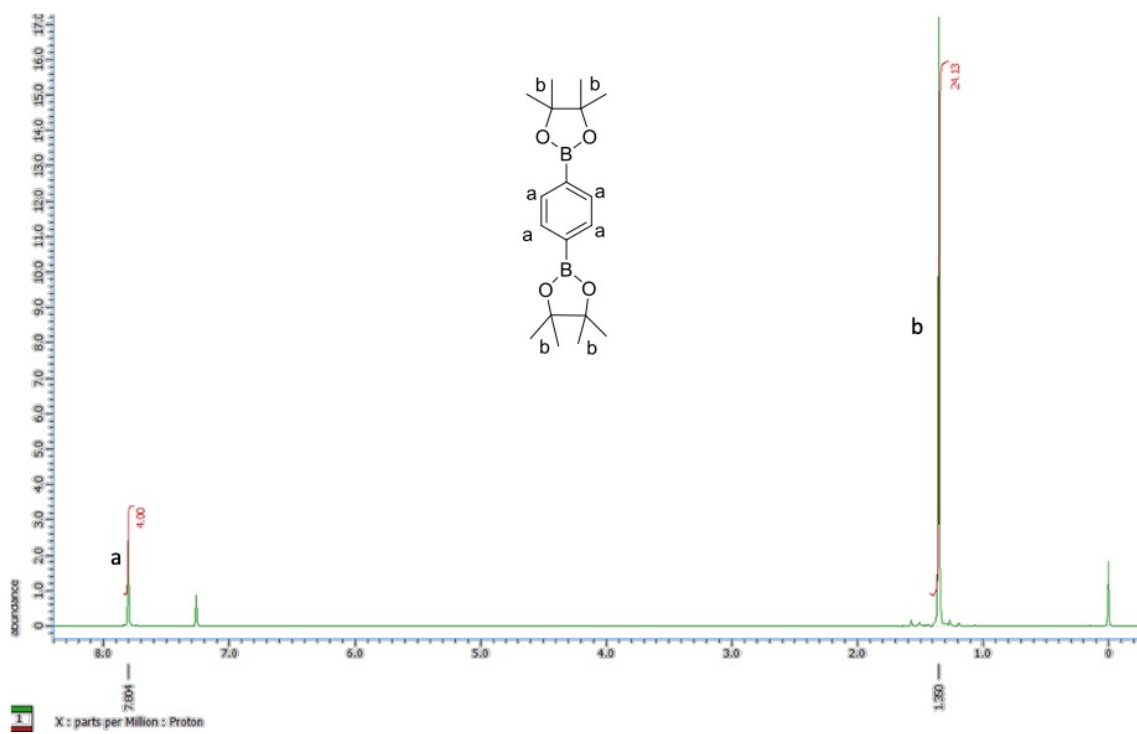
10.1.2 ¹³C NMR

10.1.2.1 Phenylboronic acid 1,2-ethanediol ester (1a)
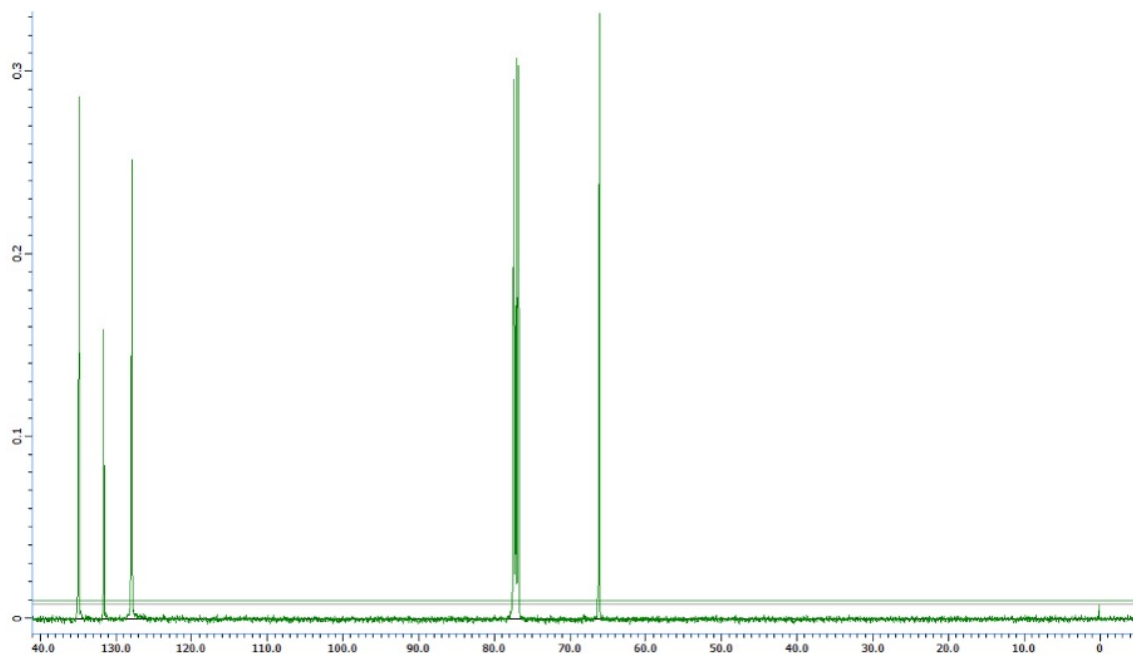
DEPT
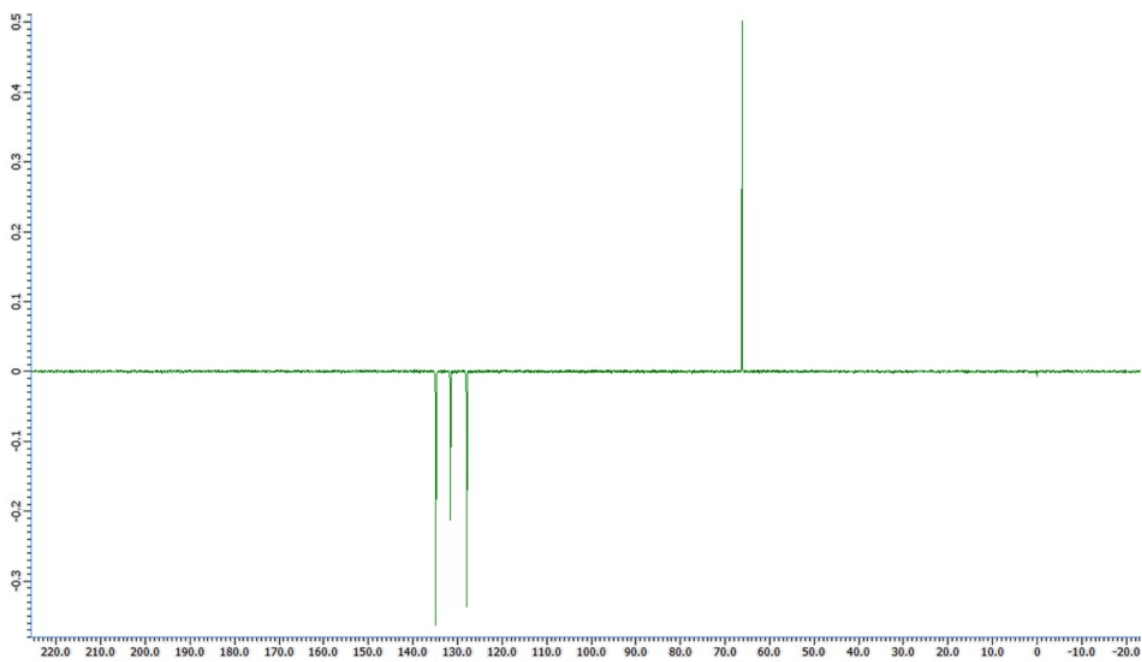
10.1.2.2 Phenylboronic acid pinacol ester (1b)

X : parts per Million : Carbon13

10.1.2.3 Bis(propan-2-yl)phenylboronate (1c)

X : parts per Million : Carbon13

x
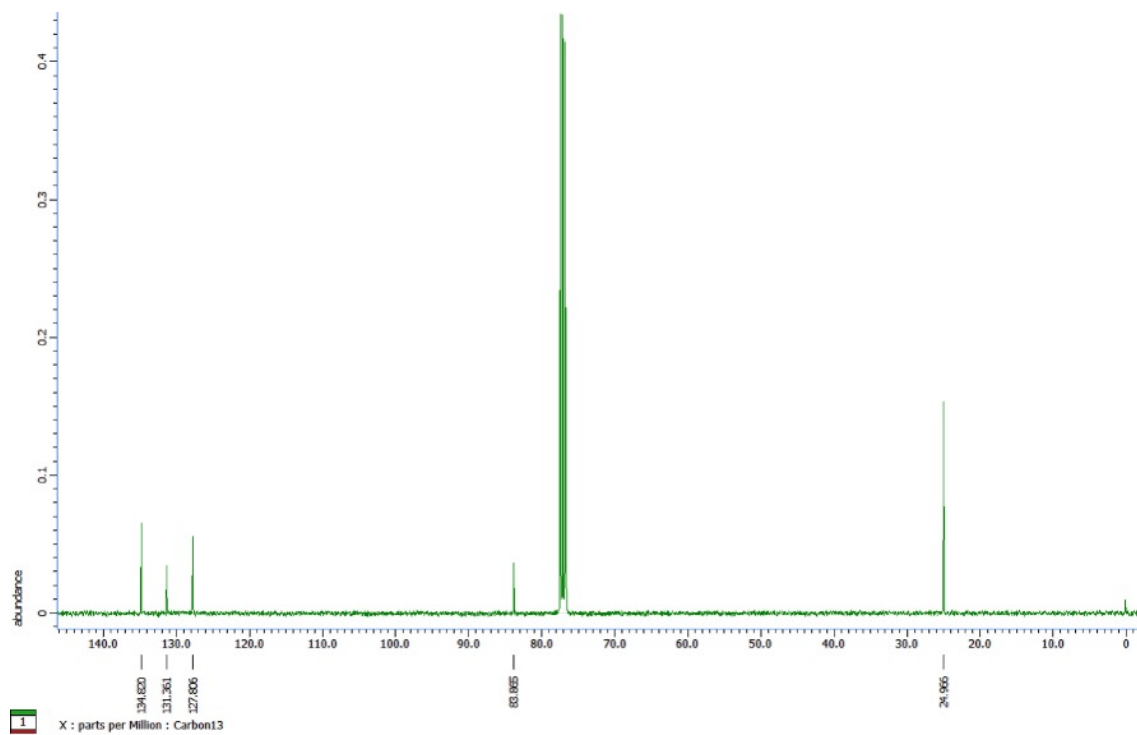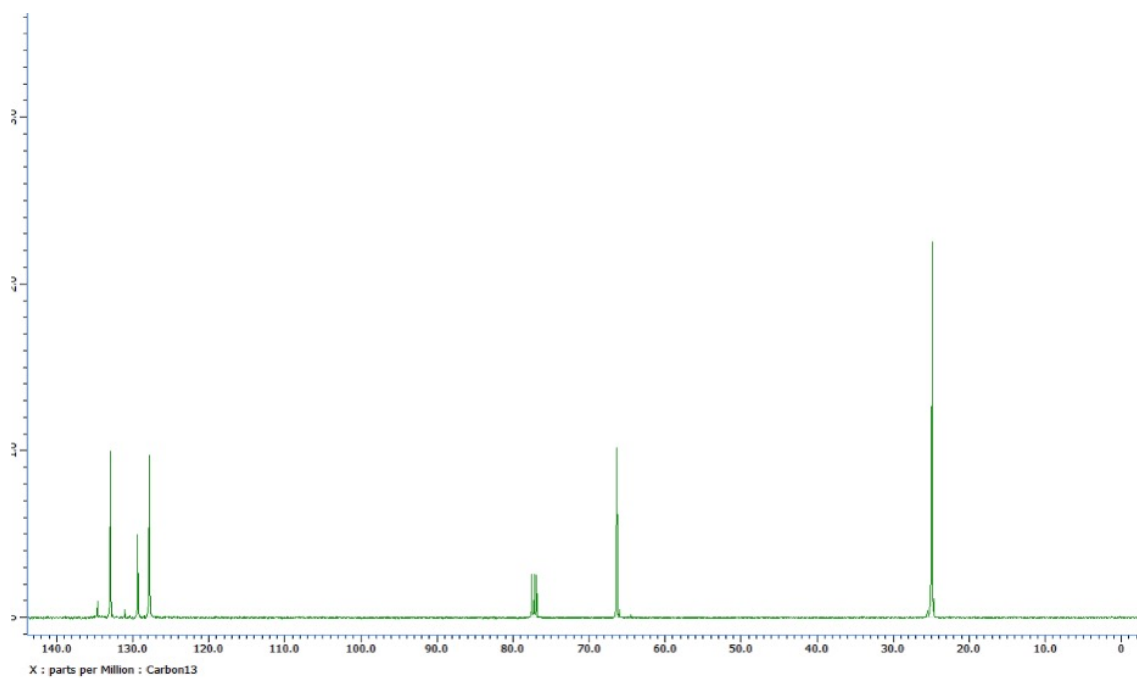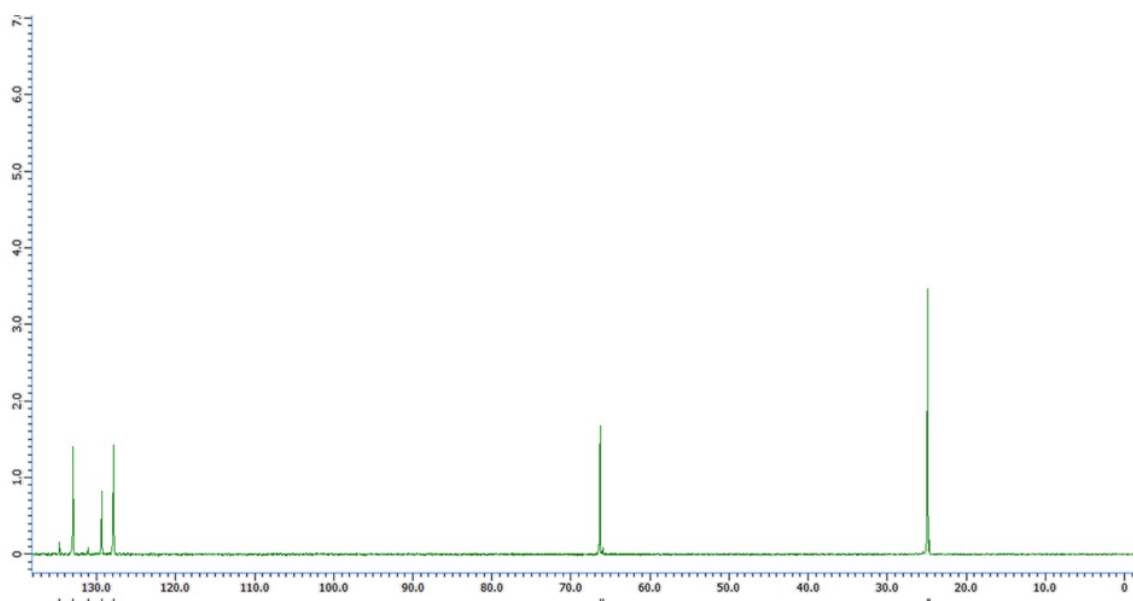
DEPT

10.1.2.4 Bis(butyl)phenylboronate (1d)
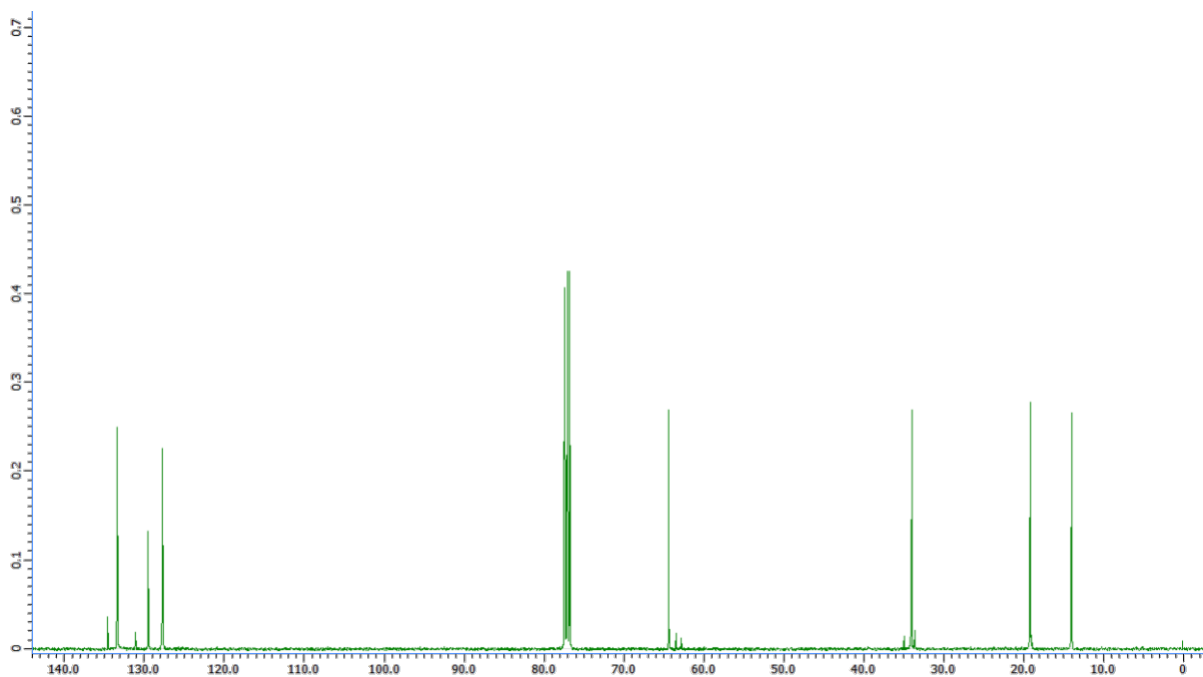
DEPT
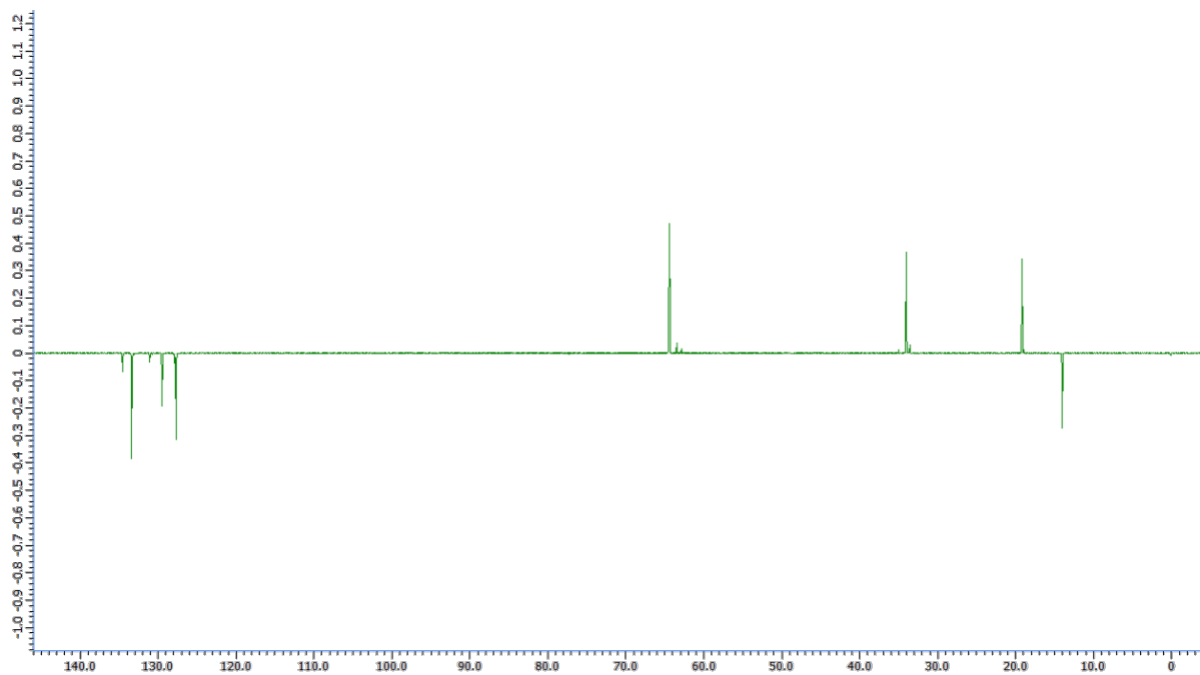
10.1.2.5 *N*-(cyclohexylamino)-3-phenoxypropan-2-ol (2)
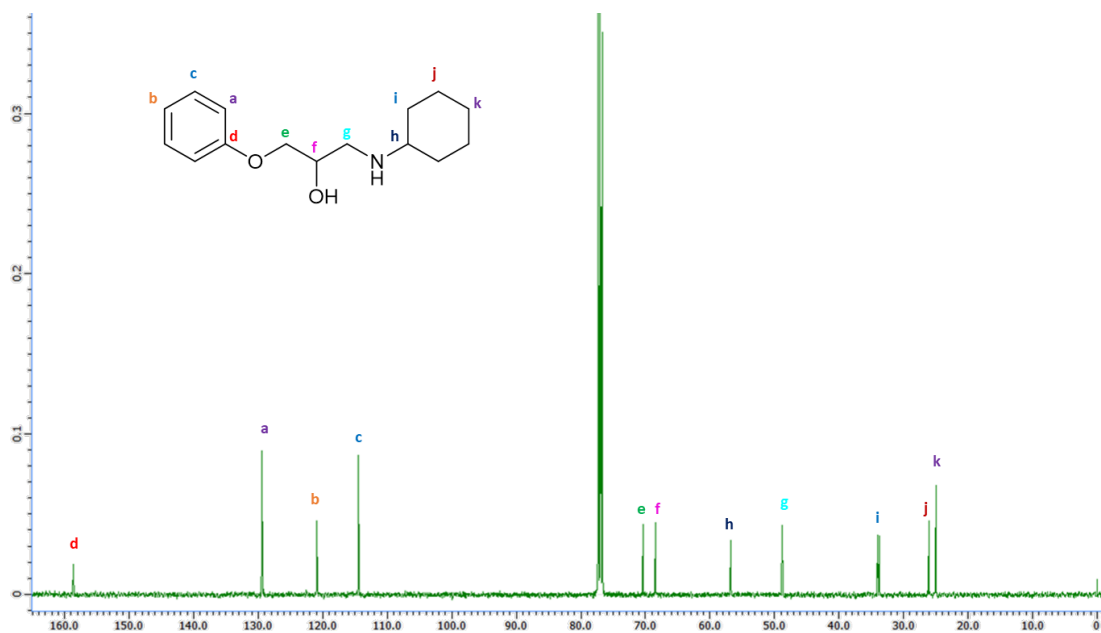
DEPT
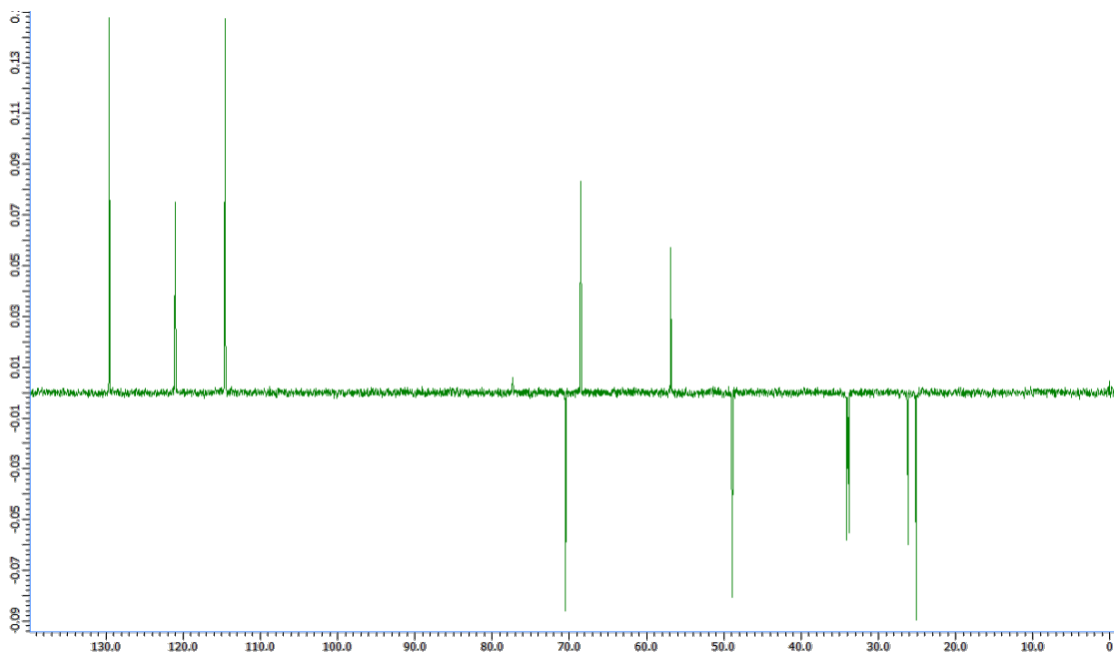
10.1.2.6 N,N-bis(2-hydroxy-3-phenoxy-propyl)-cyclohexanamine (β-amino diol (3))
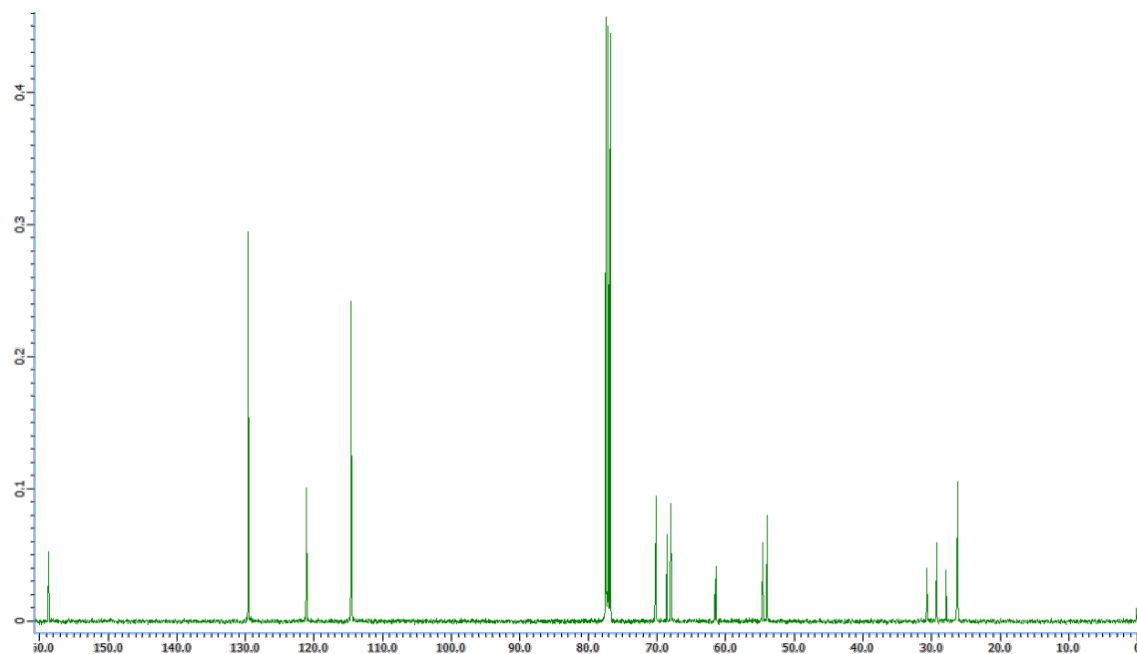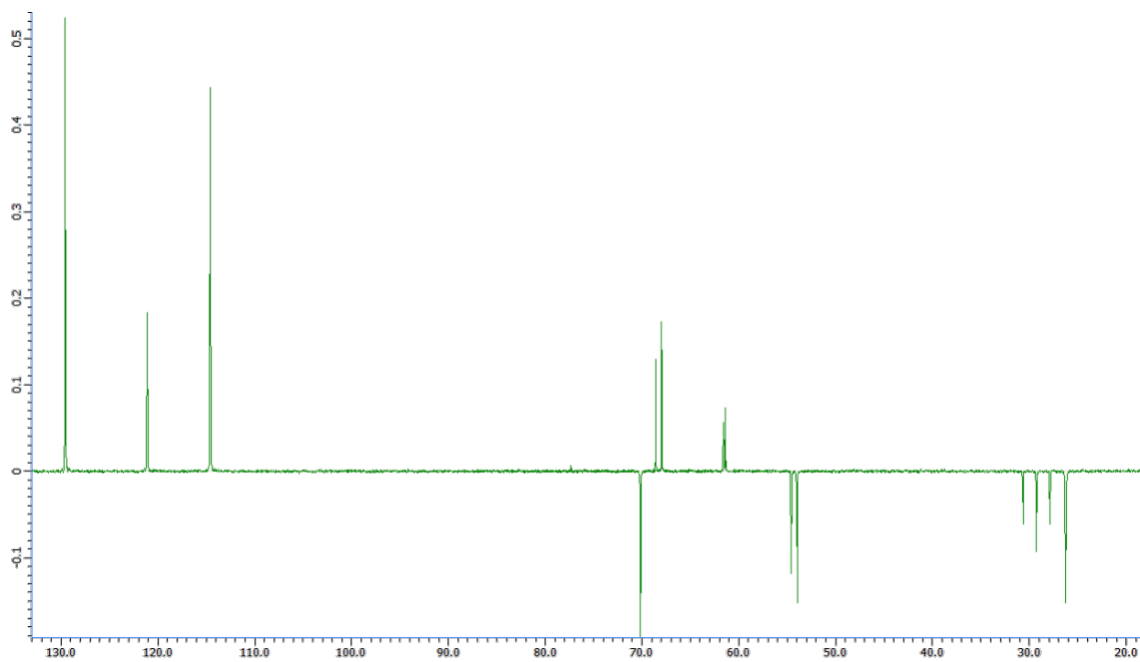

DEPT

10.1.2.7 1,4-Phenylenediboronic bis(1,2-diol) ester (5)
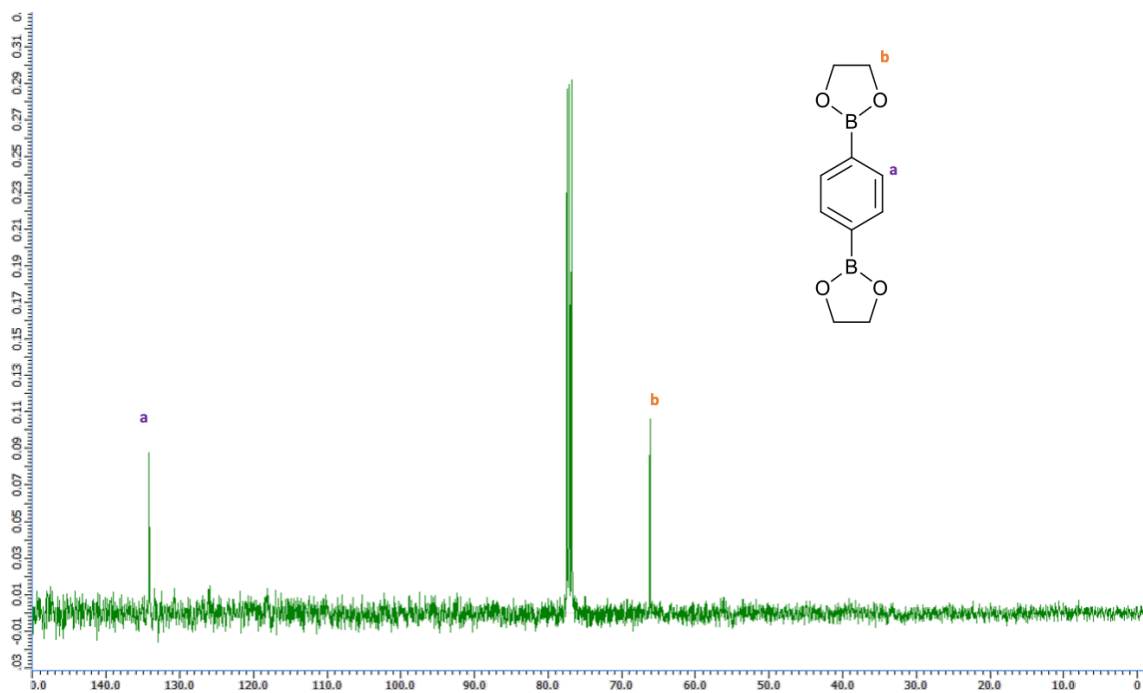
DEPT

10.1.2.8 1,4-Phenylenediboronic acid tetrabutyl ester (6)

X : parts per Million : Carbon13
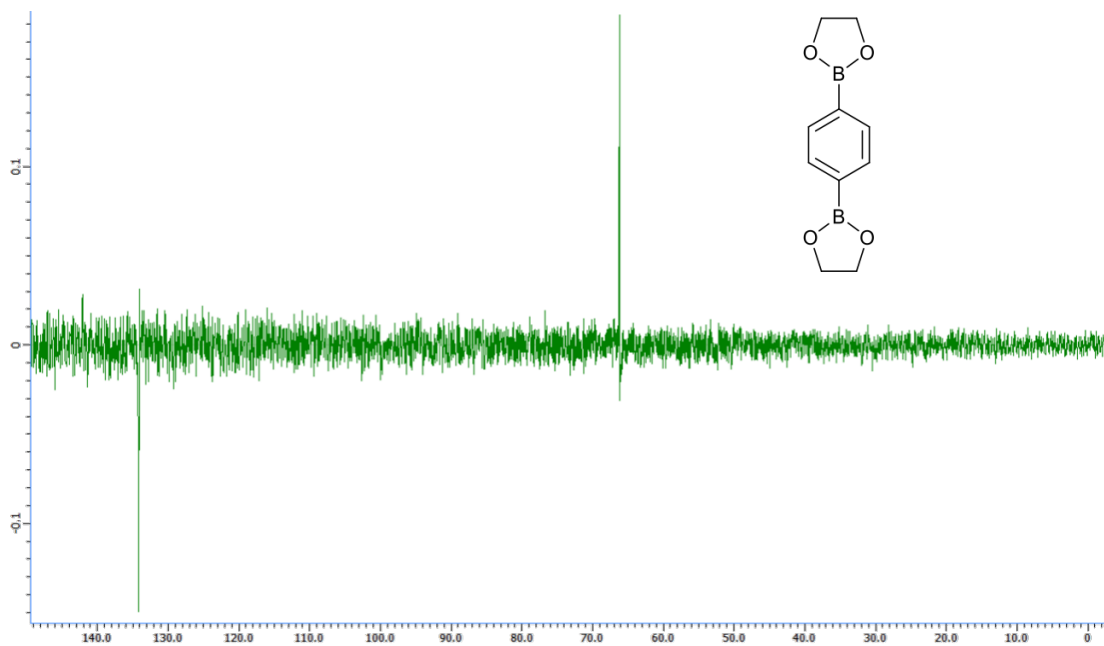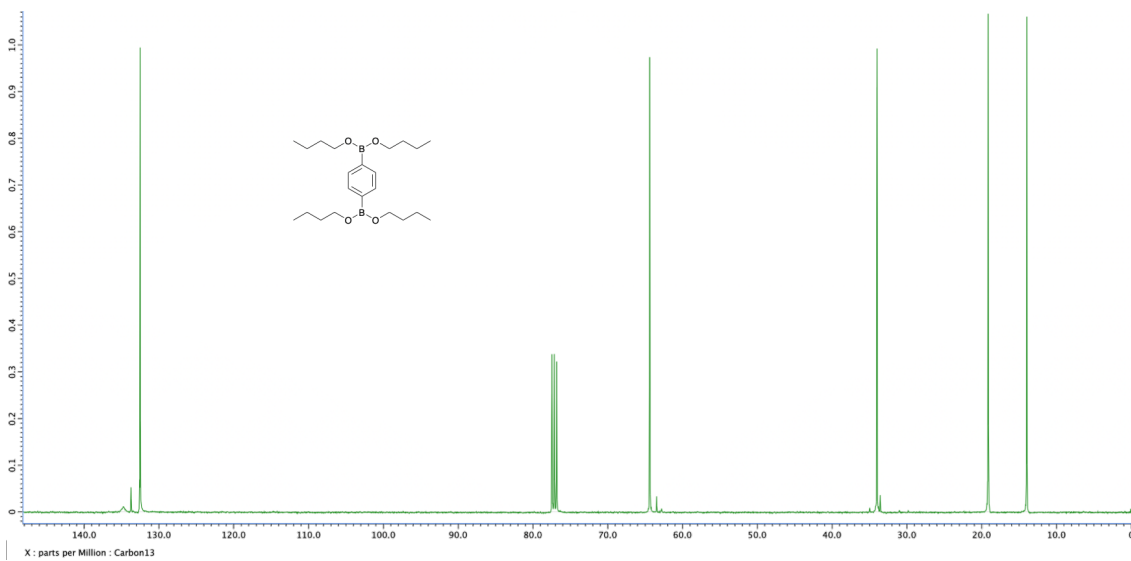
DEPT
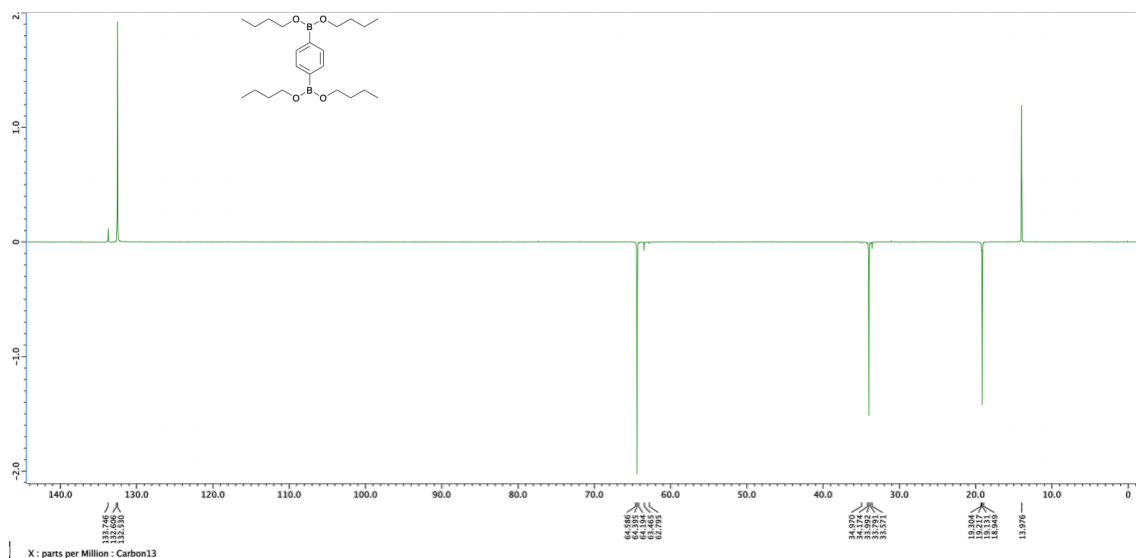
10.1.2.9 1,4-Phenylenediboronic acid pinacol ester (7)
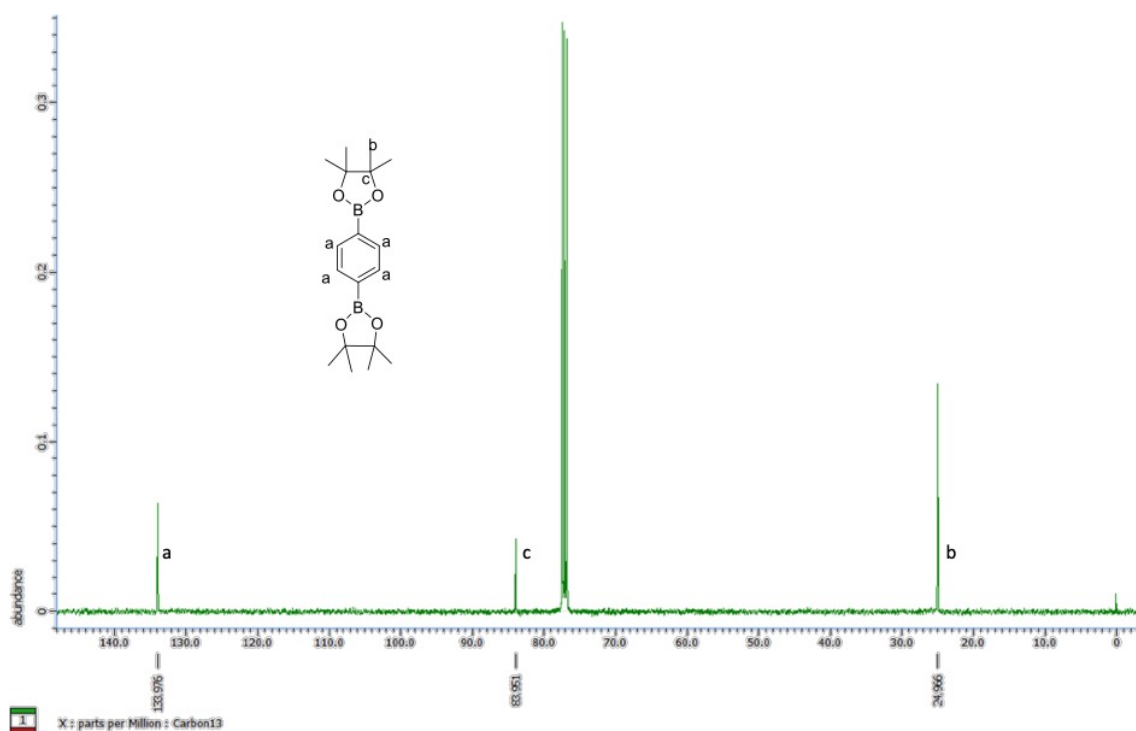
10.1.3 ^{11}B NMR

10.1.3.1 Phenylboronic acid 1,2-ethanediol ester (1a)

10.1.3.2 Phenylboronic acid pinacol ester (1b)

X : parts per Million : Boron11
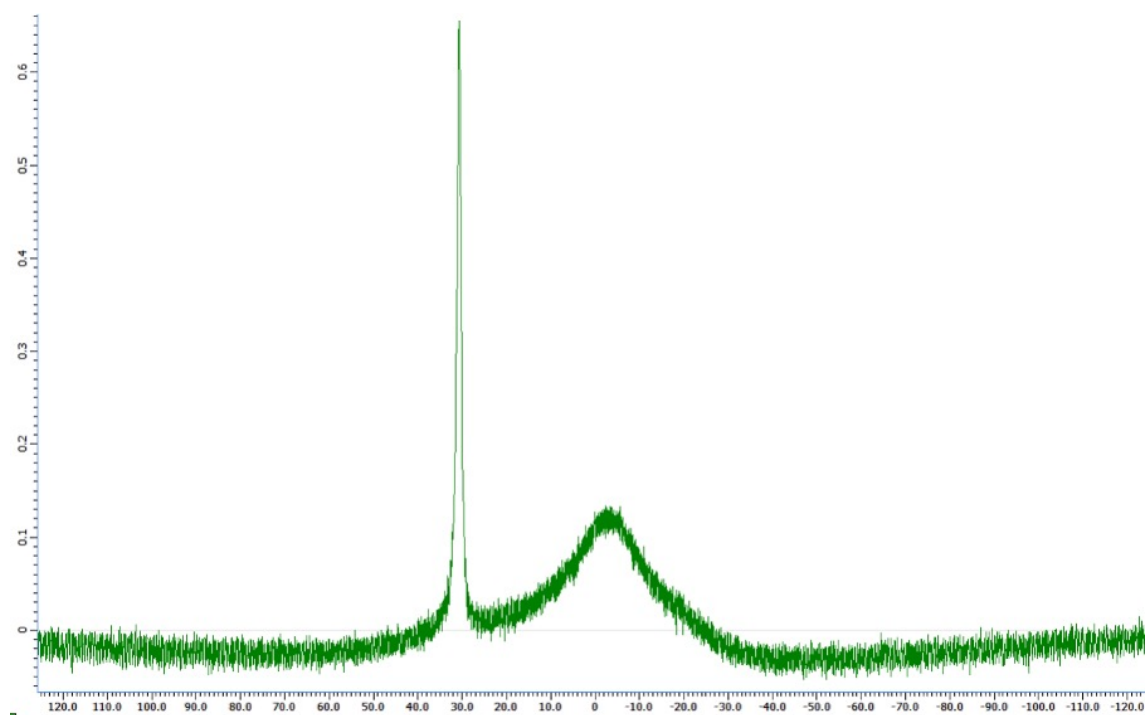
10.1.3.3 Bis(propan-2-yl)phenylboronate (1c)

10.1.3.4 Bis(butyl)phenylboronate (1d)

10.1.3.5 1,4-Phenylenediboronic bis(1,2-diol) ester (5)

10.1.3.6 1,4-Phenylenediboronic acid tetrabutyl ester (6)

10.1.3.7 1,4-Phenylenediboronic acid pinacol ester (7)

10.1.4 FTIR

10.1.4.1 Phenylboronic acid 1,2-ethanediol ester (1a)
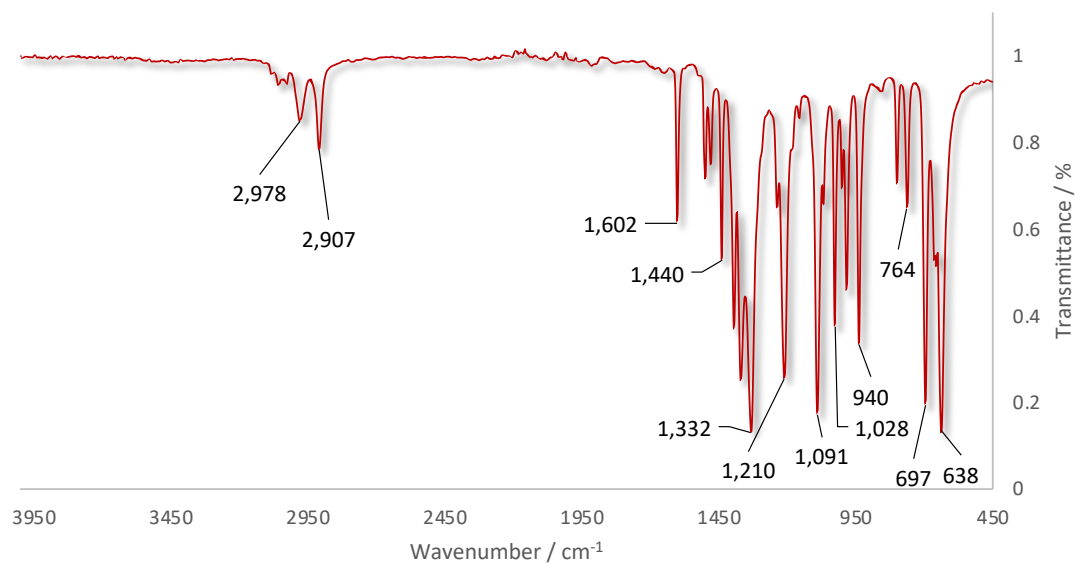
10.1.4.2 Phenylboronic acid pinacol ester (1b)

10.1.4.3 Bis(propan-2-yl)phenylboronate (1c)

10.1.4.4 Bis(butyl)phenylboronate (1d)

10.1.4.5 *N*-(cyclohexylamino)-3-phenoxypropan-2-ol (2)

10.1.4.6 N,N-bis(2-hydroxy-3-phenoxy-propyl)-cyclohexanamine (β-amino diol (3))

10.1.4.7 1,4-Phenylenediboronic bis(1,2-diol) ester (5)

10.1.4.8 1,4-Phenylenediboronic acid tetrabutyl ester (6)

10.1.4.9 1,4-Phenylenediboronic acid pinacol ester (7)

10.1.4.10   D-Series polymer networks

10.1.4.11   A²-Series polymer network

HA-E2(DEA-5) A2 Series

Legend: HA-E2(DEA-5)A2-0 — HA-E2(DEA-5)A2-20 — HA-E2(DEA-5)A2-40 — HA-E2(DEA-5)A2-60 — HA-E2(DEA-5)A2-80 — HA-E2(DEA-5)A2-100

O-H

Normalised C-H

Amine Oxidation

R =

Wavenumber / cm⁻¹

Normalised Transmittance

10.1.5 Mass Spectrometry

10.1.5.1 *N*-(cyclohexylamino)-3-phenoxypropan-2-ol (2)
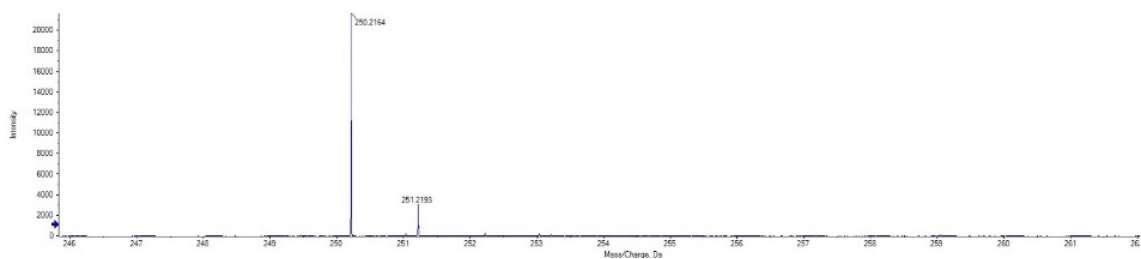
10.1.5.2 N,N-bis(2-hydroxy-3-phenoxy-propyl)-cyclohexanamine (β-amino diol (3))
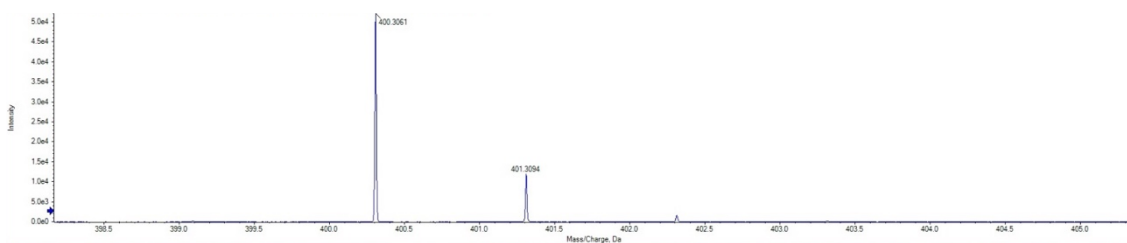
10.1.6 DSC

10.1.6.1 Small Molecule Melting Points

10.1.6.1.1 N-(cyclohexylamino)-3-phenoxypropan-2-ol (2)
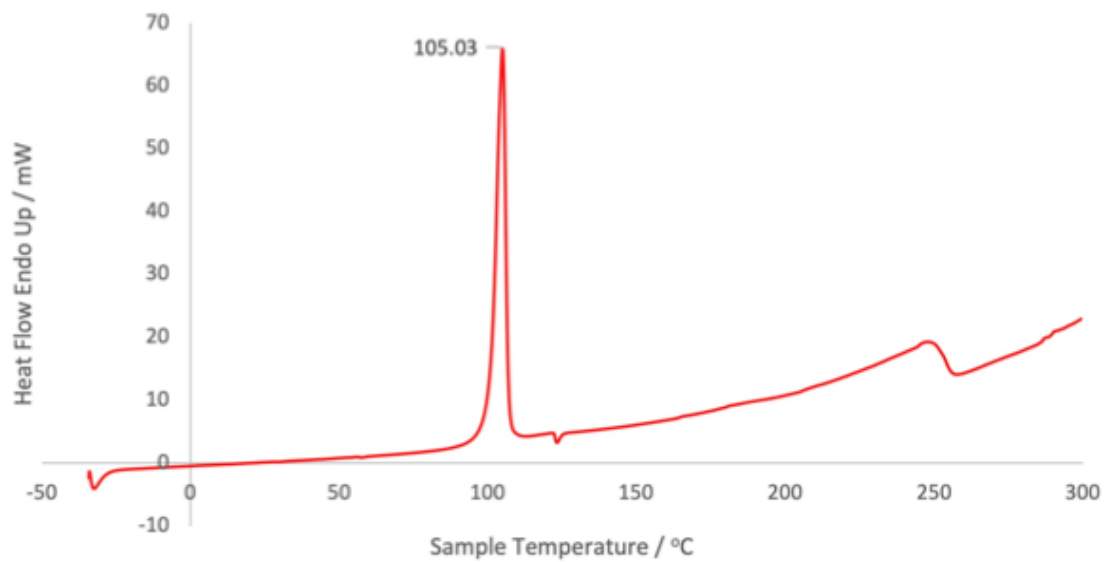
10.1.6.2 1,4-Phenylenediboronic bis(1,2-diol) ester (5)
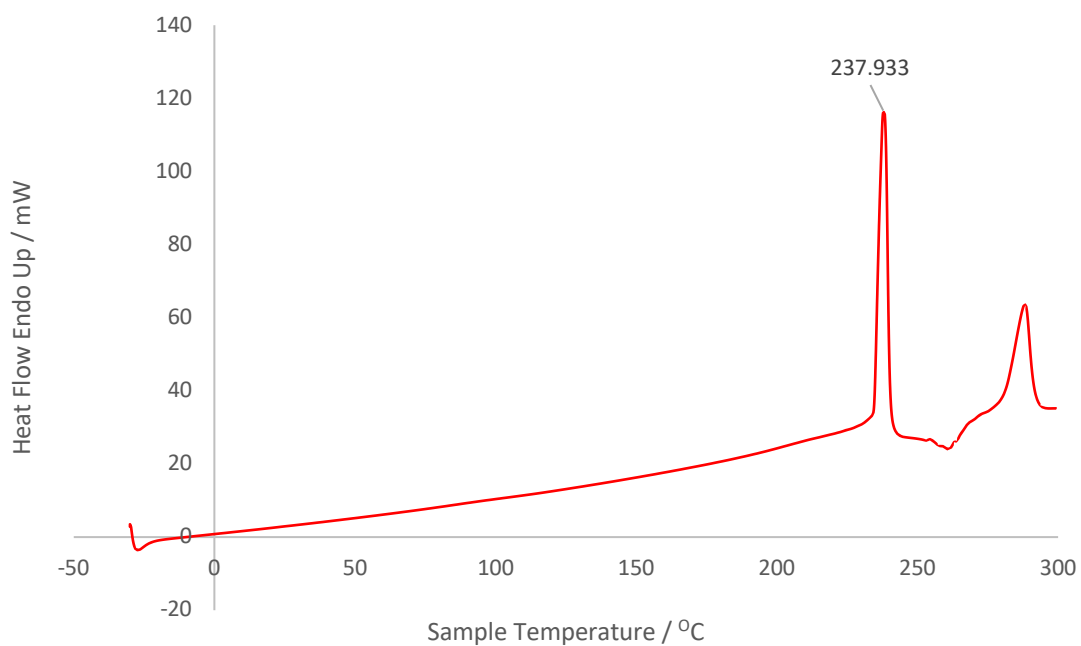
10.1.6.3 Polymer Thermograms

All polymer T_g values are recorded with a heating ramp of 20 °C per minute unless indicated otherwise.
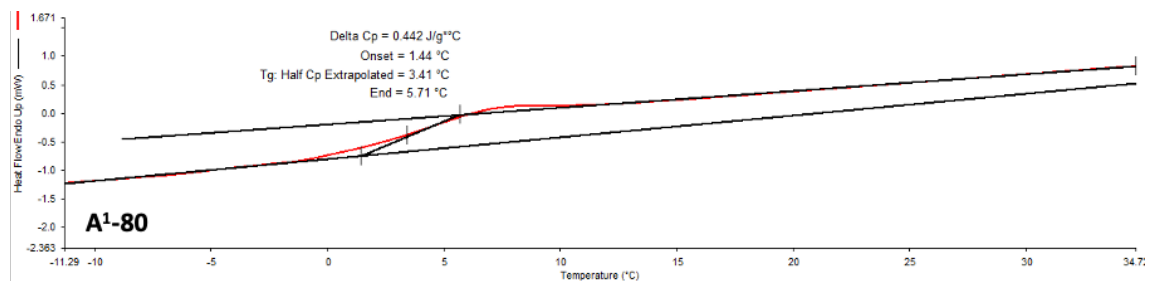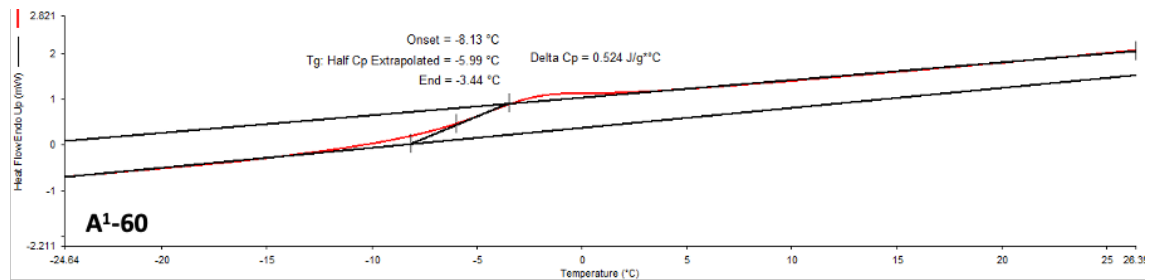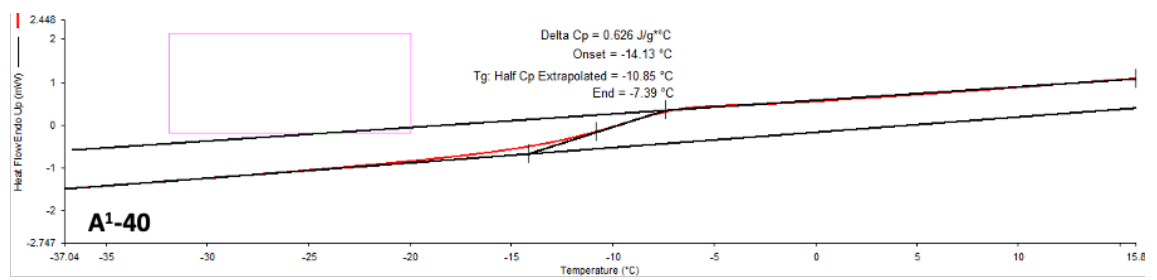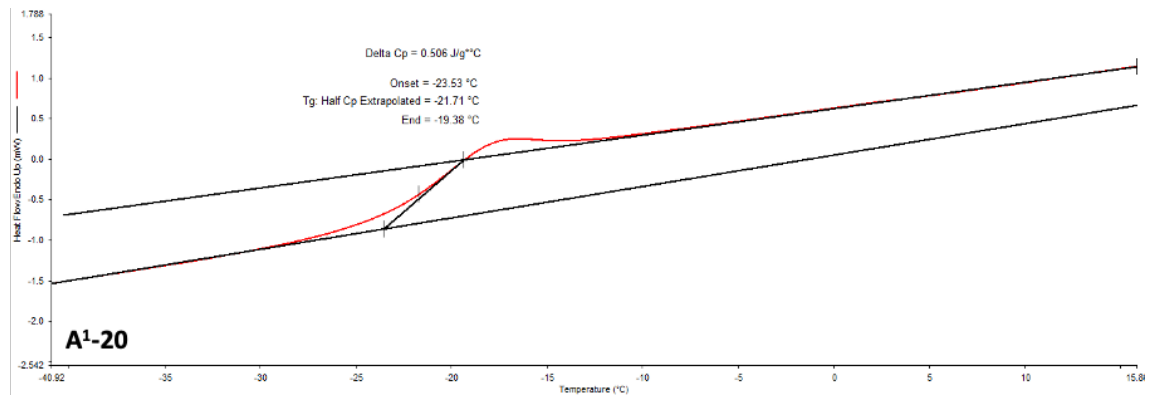
10.1.6.3.1 HA-E2(DEA-5) – linear polymer
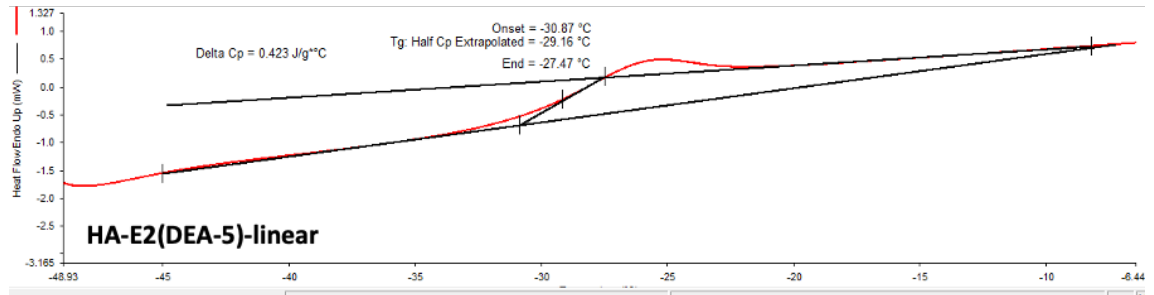
10.1.6.3.2 HA-E2(DEA-5)D-Series polymers

D-60

Delta Cp = 0.344 J/g*°C
Tg: Half Cp Extrapolated = 11.71 °C
End = 23.29 °C
0.57 °C   Onset = 13.61 °C
2.3804 mW

D-80

Delta Cp = 0.687 J/g*°C
Onset = 42.67 °C
Tg: Half Cp Extrapolated = 48.26 °C
End = 60.66 °C

D-100

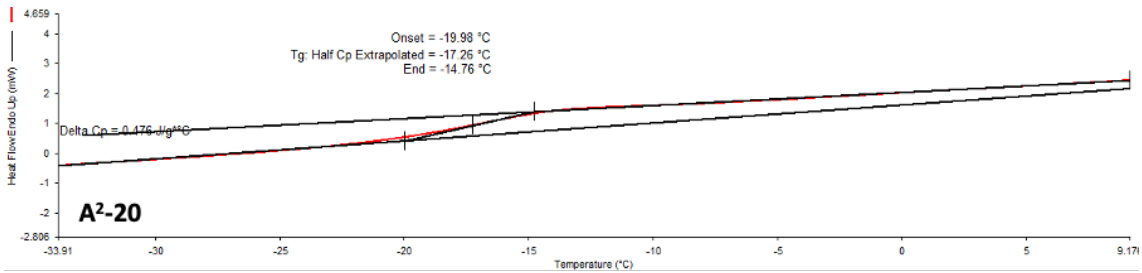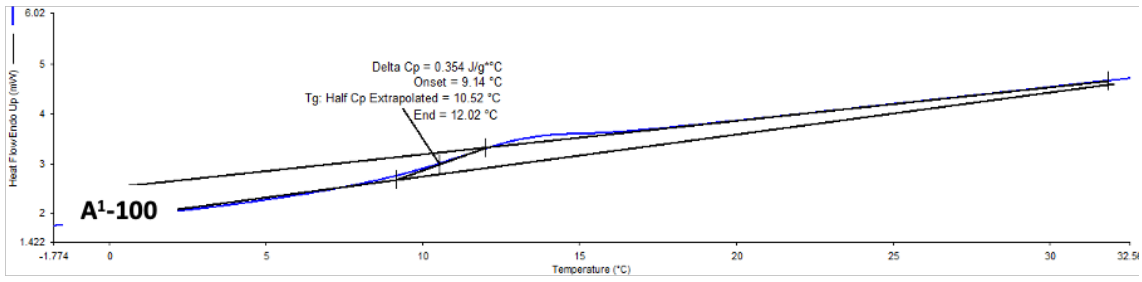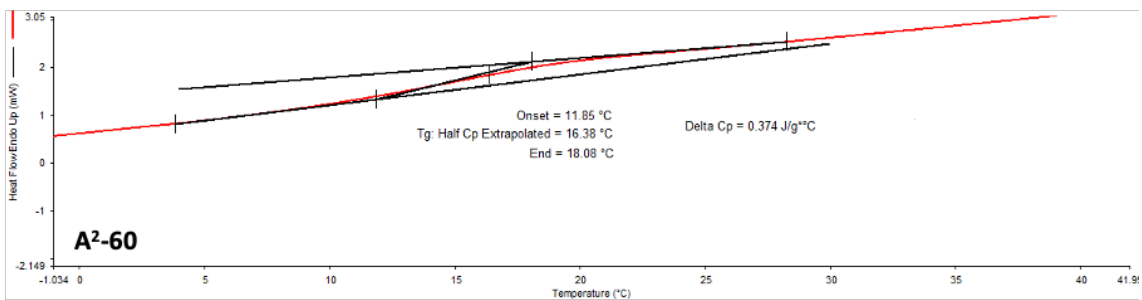Onset = 34.64 °C
Tg: Half Cp Extrapolated = 49.68 °C
End = 63.65 °C

Delta Cp = 0.365 J/g*°C

xxx
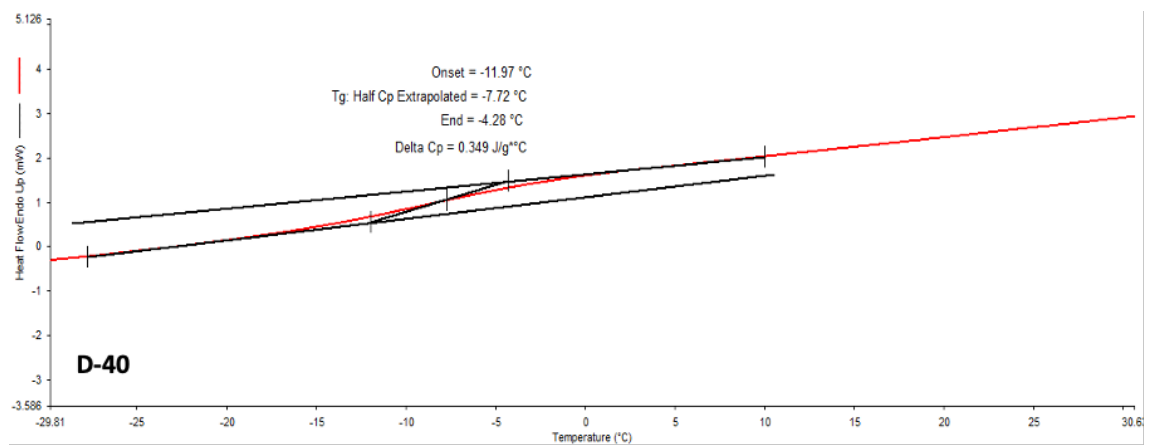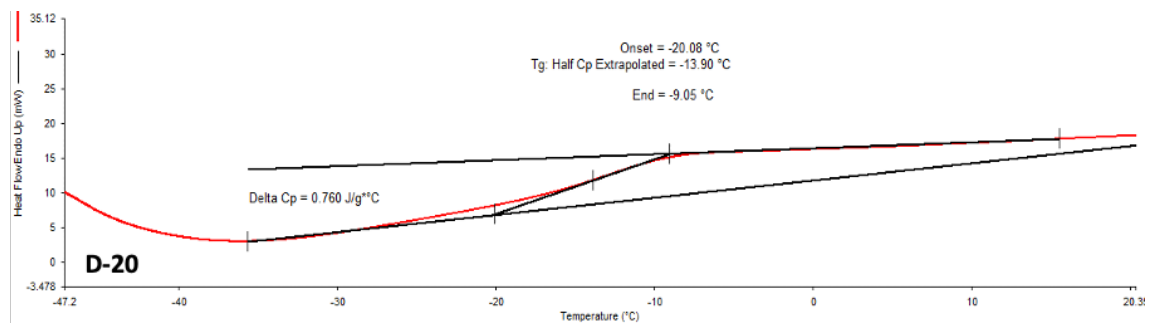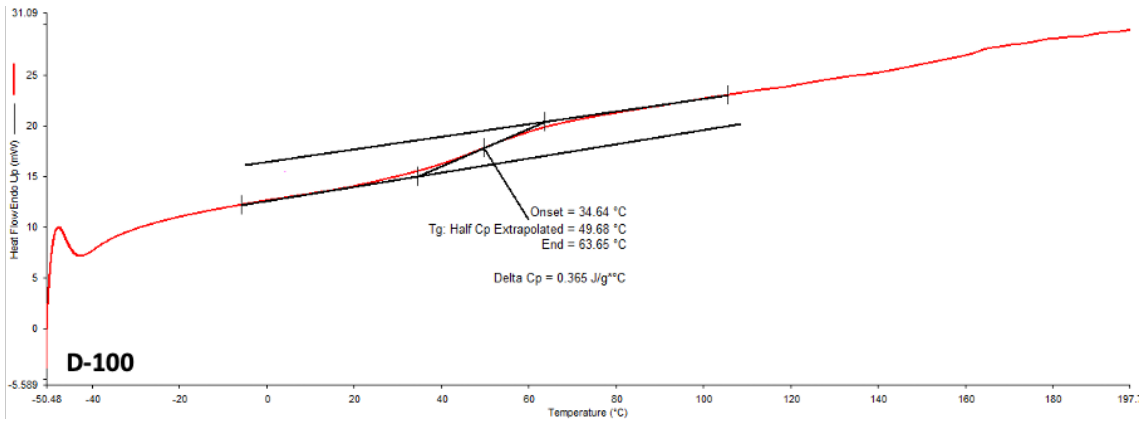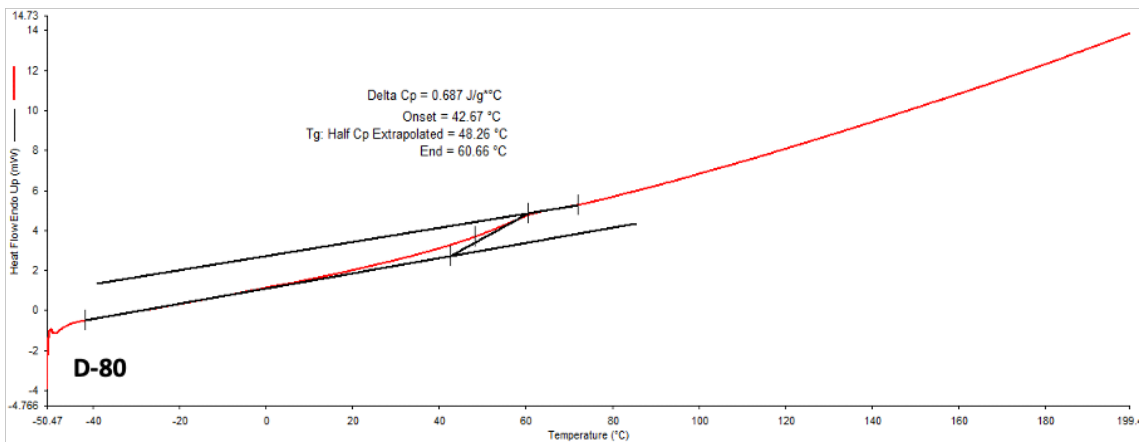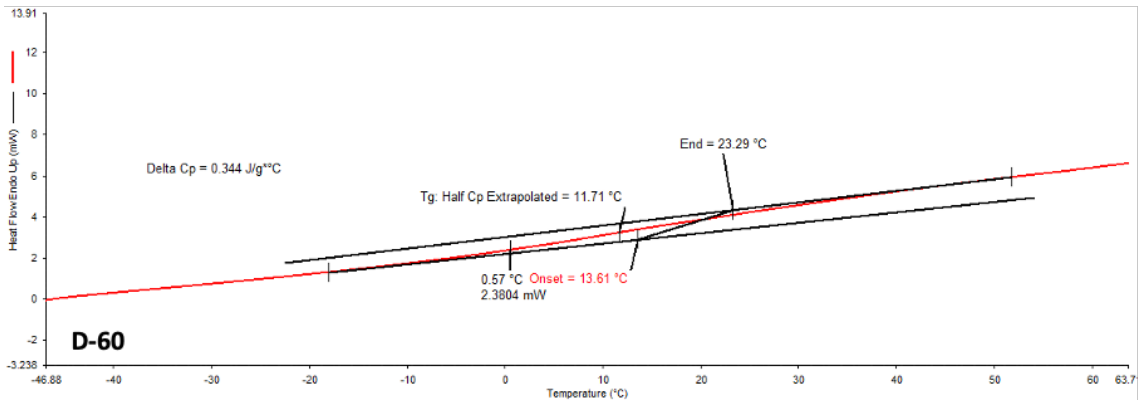
10.1.6.3.3 HA-E2(DEA-5)A¹-Series polymers

Delta Cp = 0.506 J/g·°C
Onset = -23.53 °C
Tg: Half Cp Extrapolated = -21.71 °C
End = -19.38 °C

A¹-20

Delta Cp = 0.626 J/g·°C
Onset = -14.13 °C
Tg: Half Cp Extrapolated = -10.85 °C
End = -7.39 °C

A¹-40

Onset = -8.13 °C
Tg: Half Cp Extrapolated = -5.99 °C   Delta Cp = 0.524 J/g·°C
End = -3.44 °C

A¹-60

Delta Cp = 0.442 J/g·°C
Onset = 1.44 °C
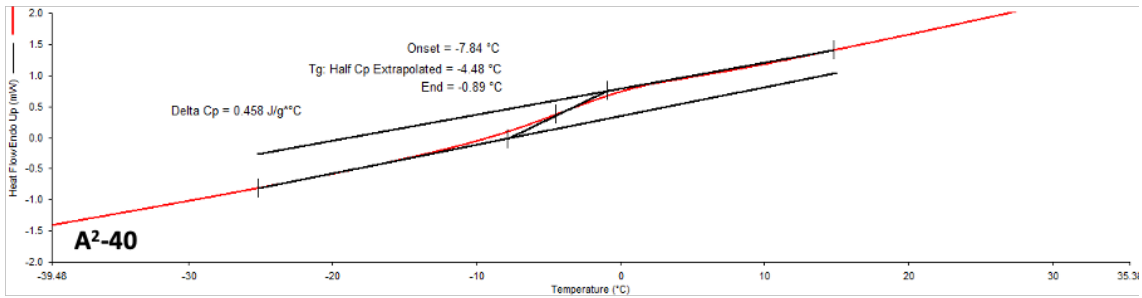Tg: Half Cp Extrapolated = 3.41 °C
End = 5.71 °C

A¹-80

A[1]-100

A[2]-20

10.1.6.3.4 HA-E2(DEA-5)A[2]-Series polymers

A[2]-40

A[2]-60

A²-80

Delta Cp = 0.340 J/g*°C

Onset = 29.74 °C
Tg: Half Cp Extrapolated = 32.84 °C
End = 35.12 °C

A²-100

Delta Cp = 0.308 J/g*°C

Onset = 37.51 °C
Tg: Half Cp Extrapolated = 41.63 °C
End = 47.13 °C
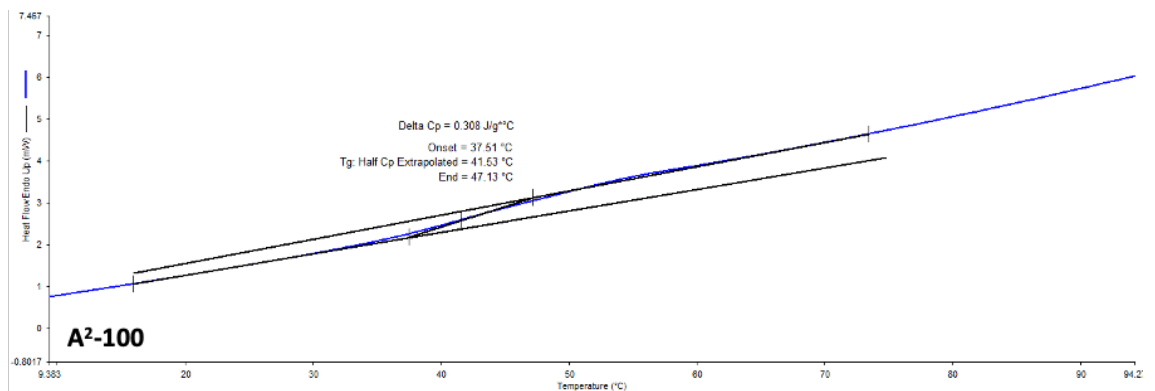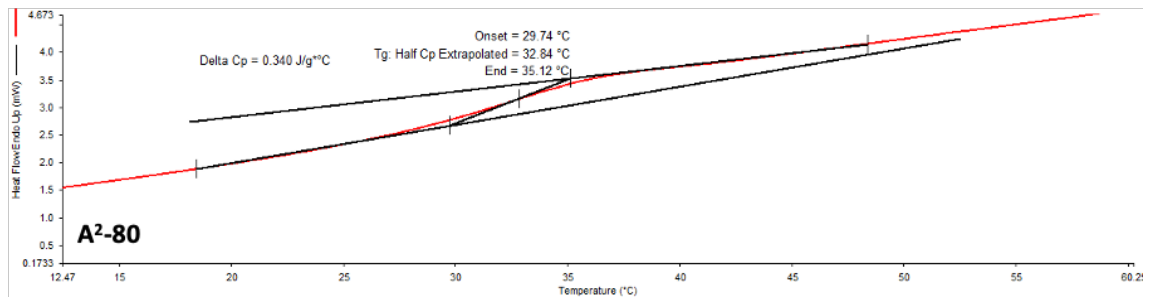
10.1.6.3.5 HA-E2(DEA-5)A³-Series polymers

A³-60

Delta Cp = 0.490 J/g*°C
Onset = 86.74 °C
Tg: Half Cp Extrapolated = 90.65 °C
End = 94.95 °C

A³-80

Delta Cp = 0.500 J/g*°C

Onset = 94.78 °C
Tg: Half Cp Extrapolated = 97.92 °C
End = 102.33 °C
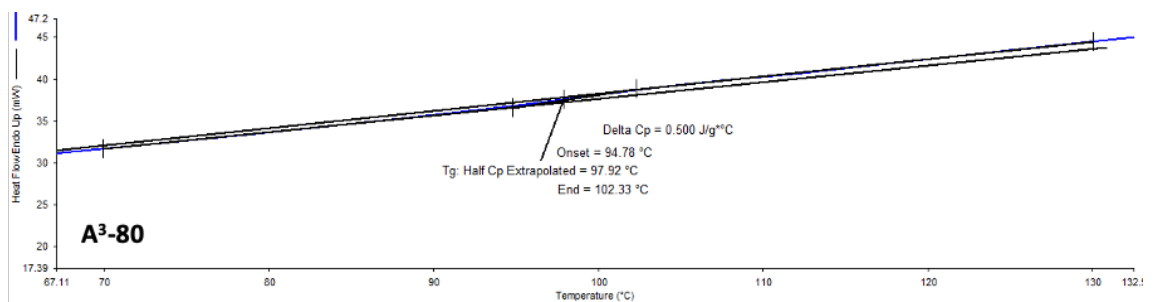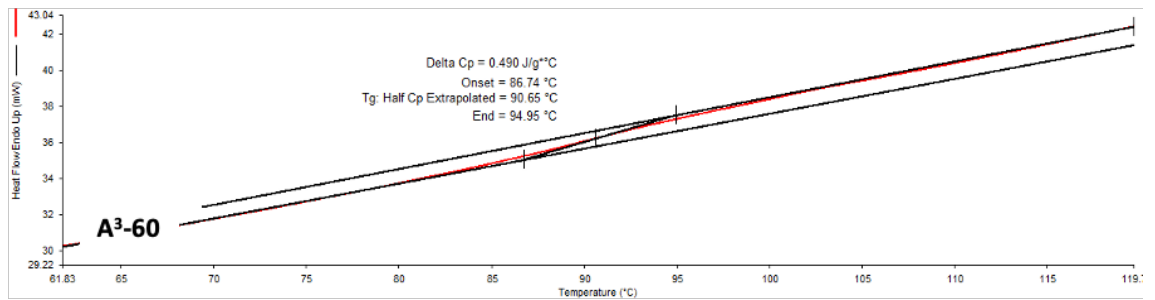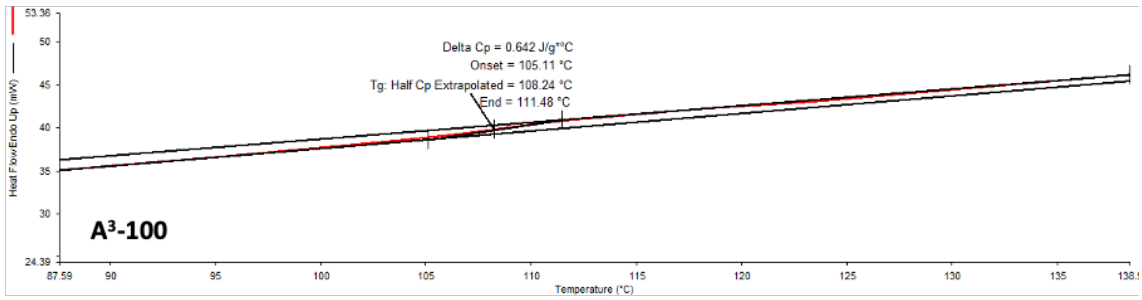
10.2 P_gel Calculations

The P_{gel} values were calculated in excel as shown below, where F_a was the average epoxy functionality and f_b was the average amine functionality.

| A Series									Pgel
Crosslinks	Fa	Fb	fa-1	fb-1	fa-1*fb-1	r	fa-1*fb-1*r	√fa-1*fb-1*r	1/√fa-1*fb-1*r
100%	1.666666667	4	0.6666667	3	2	1	2	1.414	0.707106781
80%	1.666666667	3.6	0.6666667	2.6	1.733333333	1	1.7333333	1.317	0.759554525
60%	1.666666667	3.2	0.6666667	2.2	1.466666667	1	1.4666667	1.211	0.825722824
40%	1.666666667	2.8	0.6666667	1.8	1.2	1	1.2	1.095	0.912870929
20%	1.666666667	2.4	0.6666667	1.4	0.933333333	1	0.9333333	0.966	1.035098339
0%	1.666666667	2	0.6666667	1	0.666666667	1	0.6666667	0.816	1.224744871

10.3 Tensile Testing

10.3.1 Tensile properties

All the measured calculated properties of the tensile testing are presented in the table below.

Polymer	Ultimate tensile strength / Mpa	std dev	Youngs Modulus / MPa	std dev	Strain at Break	std dev	Stress at break / MPa	std dev
D60	4.713	0.168	0.415	0.018	8.533	0.409	4.620	0.081
D80	33.132	1.758	119.130	6.177	0.373	0.005	33.056	1.731
D100	36.480	2.992	127.857	11.281	0.343	0.086	37.071	3.825
D-R-60	1.789	0.153	0.180	0.008	8.280	0.647	1.469	0.342
D-R-80	30.106	2.517	96.212	7.736	0.522	0.056	26.883	4.107
D-R-100	37.965	2.461	136.457	25.031	0.402	0.065	34.279	4.550
A-3-60	44.813	4.467	343.670	23.469	0.129	0.009	44.094	3.892
A-3-80	68.125	2.652	321.490	10.771	0.227	0.025	68.125	2.652
A-3-100	68.879	3.062	308.978	14.420	0.273	0.019	68.864	3.045

10.3.2 Dog-bone Dimensions

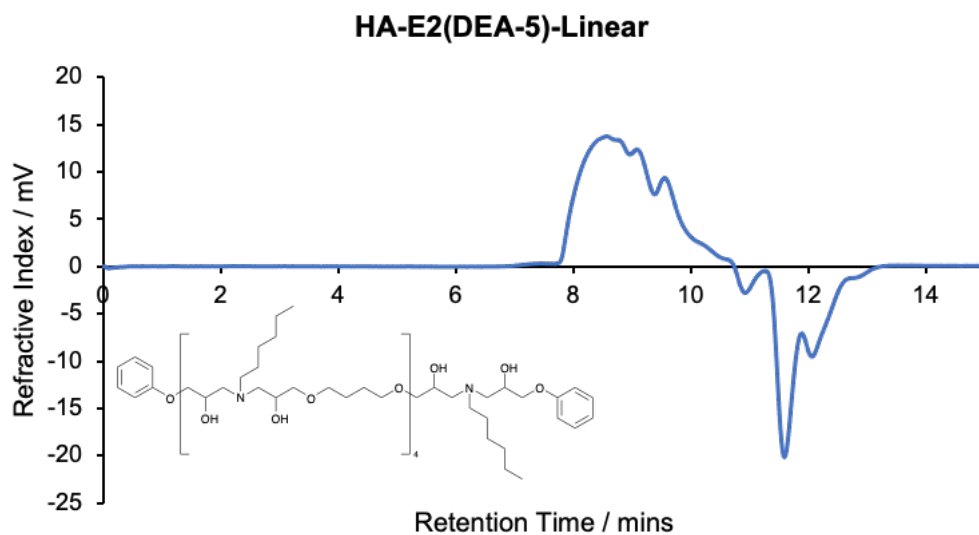The dimensions of the dogbones used in this research are shown below and are expressed in mm.
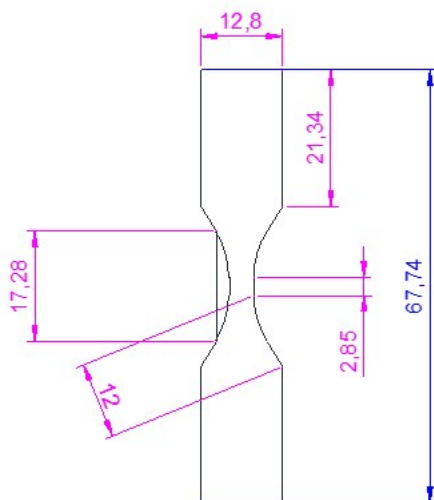
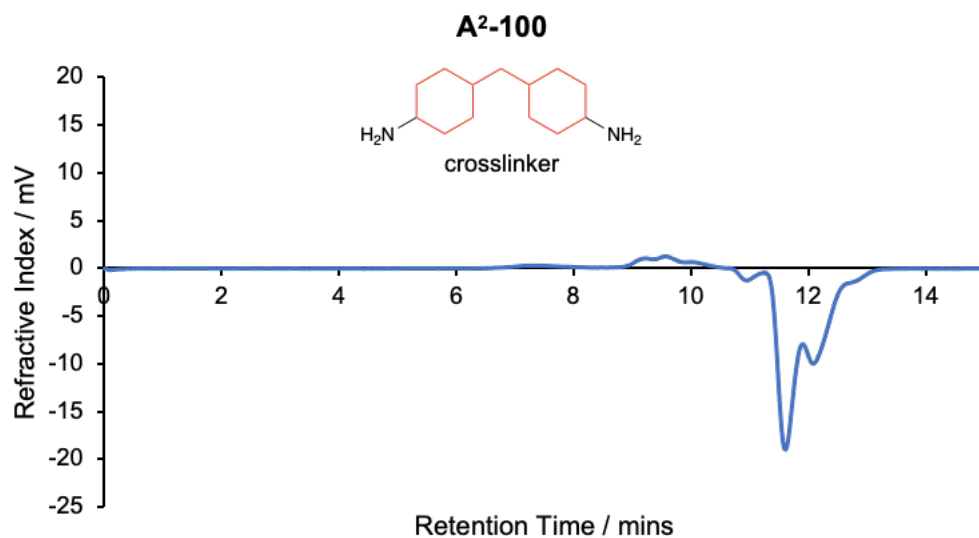## 10.4 GPC raw data graph (RI vs Retention Time)

Molecular weight graphs were calculated from retention times using the calibration equation below in Microsoft excel:

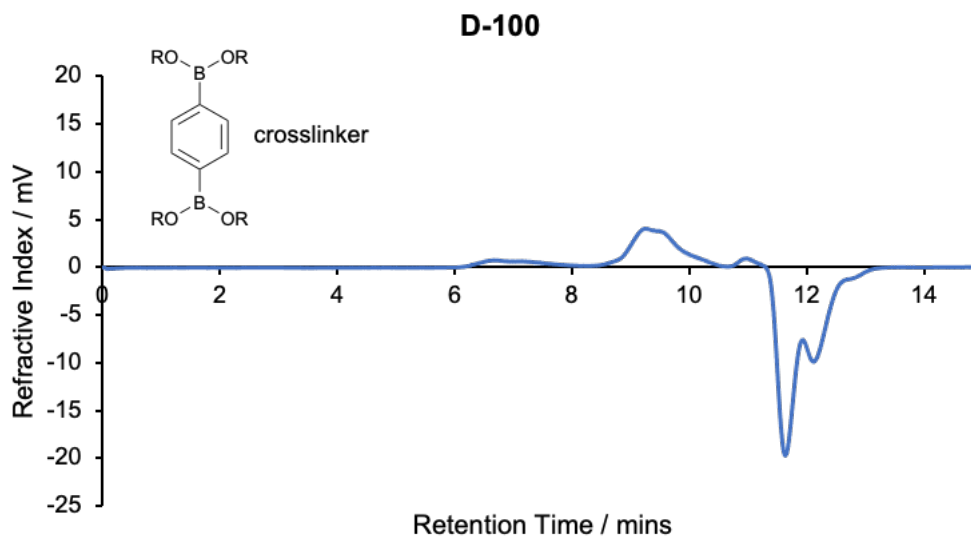$$y = -0.02775x^3 + 0.728x^2 - 6.926x + 26.52$$

10.4.1 HA-E2(DEA-5)-linear

HA-E2(DEA-5)-Linear

10.4.2 A²-100

A²-100

10.4.3 D-100

D-100

Refractive Index / mV vs Retention Time / mins. Structure labelled "crosslinker" showing RO–B(OR) groups on a benzene ring.

10.5 Chemical Recycling

10.5.1 GPC calculations

Example calculations of pinacol method B in a 5 times excess per DEA group. This example is taken from the mechanical recycling degradation studies of the D-80 polymer but is applicable for monoboronic ester and any other proposed recycling agent. Simple substitution of the pinacol molecular weight for the molecular weight of the recycling agent will enable 5 equivalents per amine to be calculated for the specific mass.

Based on D-80 polymer with 12g of butyl glycidyl ether

80% BDBE polymer	Chemical	MWt	EW	Functiona lity	eq Moles of function al group	NH group moles	epoxy group moles	actual moles	Mass
	1,4-Butyl glycidilether	202.25	101.125	2.0000	0.1187	-	0.118665019	0.0593	12
	PGE	150.18	150.18	1.0000	0.0297	-	0.029666255	0.0297	4.455278
	Hexylamine	101.19	50.595	2.0000	0.1483	0.1483	-	0.0742	7.504821
	BDBE	390.31	195.155	2.0000	0.0593	-	-	0.0297	11.57904
Totals									35.53913

Pinacol Recycling - method B
(to make 2 mg/mL samples)

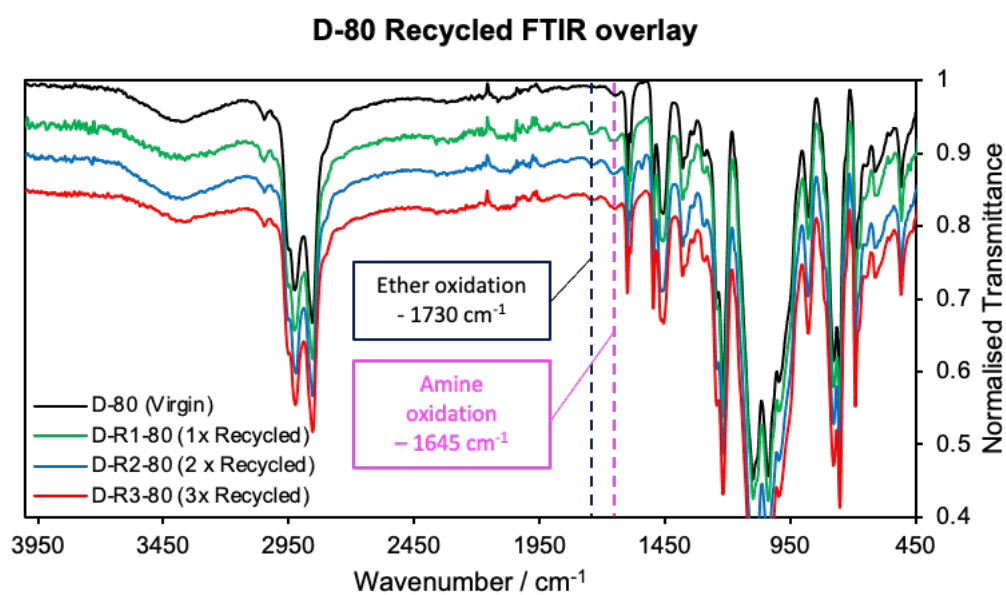|	
total polymer mass	35.53913473
mass of sample	0.02
factor	1776.956737
moles amine groups in full formulation	0.0742
moles of pinacol needed 1:1	4.17374E-05
5x excess of pinacol moles	0.000208687
g pinacol required for 5x excess	**0.02466057**

10.5.2 ^{1}H NMR overlay

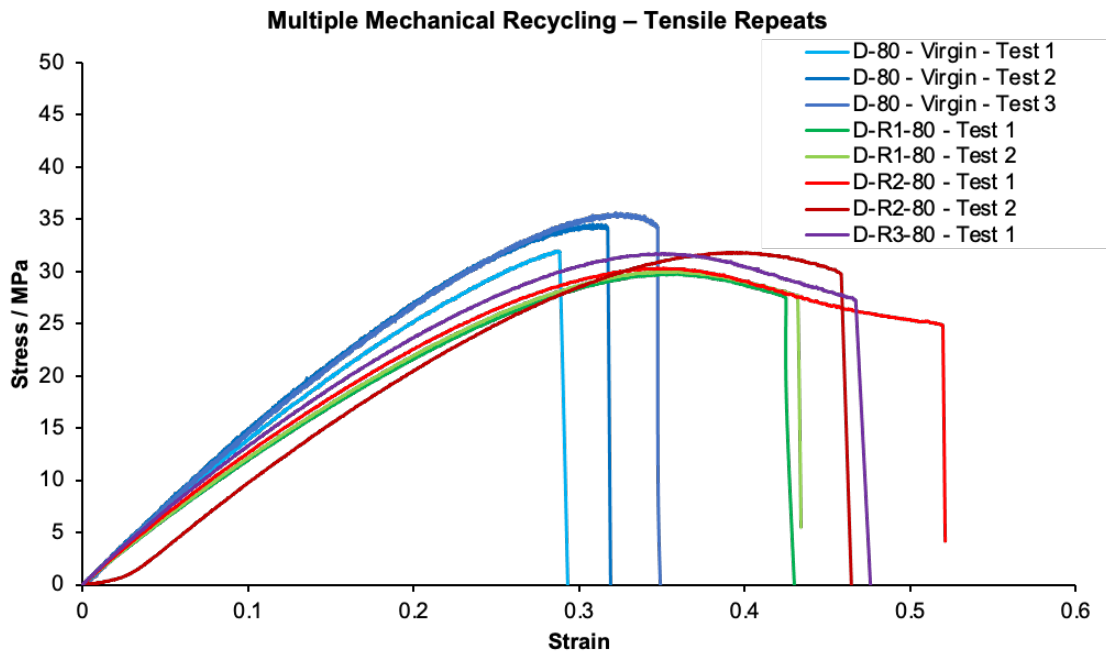The D-100 chemical recycling ^{1}H NMR overlays showing the region omitted in the main text.
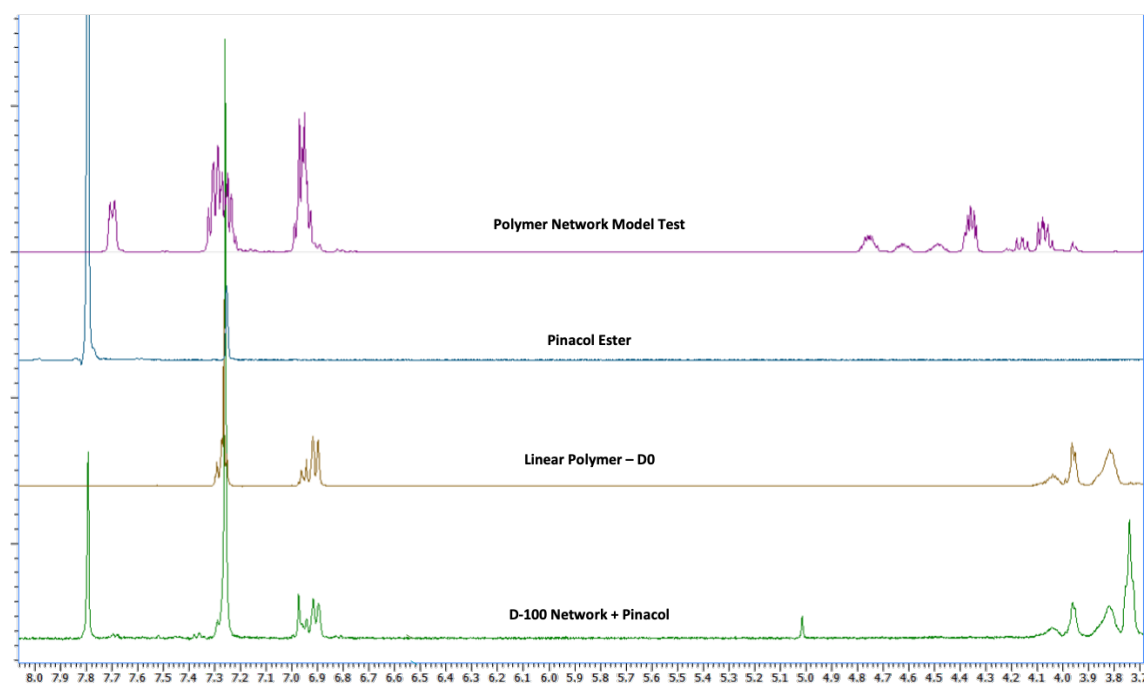
10.6 Mechanical Recycling Degradation Characterisation

10.6.1 FTIR overlay - full spectrum.

D-80 Recycled FTIR overlay

10.6.2 Tensile repeats and results

Multiple Mechanical Recycling – Tensile Repeats

Legend:
- D-80 - Virgin - Test 1
- D-80 - Virgin - Test 2
- D-80 - Virgin - Test 3
- D-R1-80 - Test 1
- D-R1-80 - Test 2
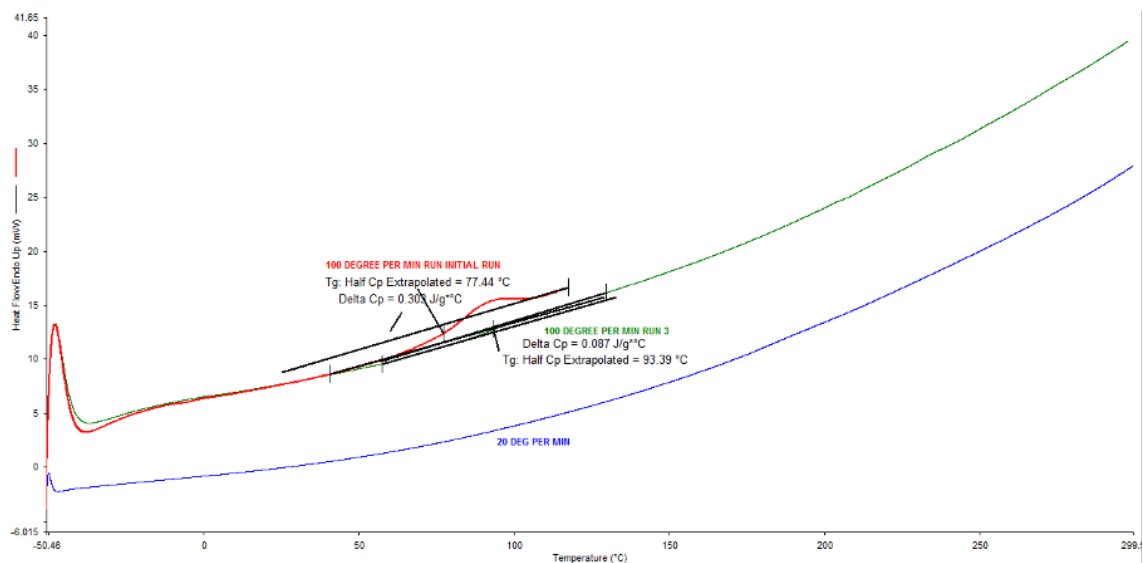- D-R2-80 - Test 1
- D-R2-80 - Test 2
- D-R3-80 - Test 1

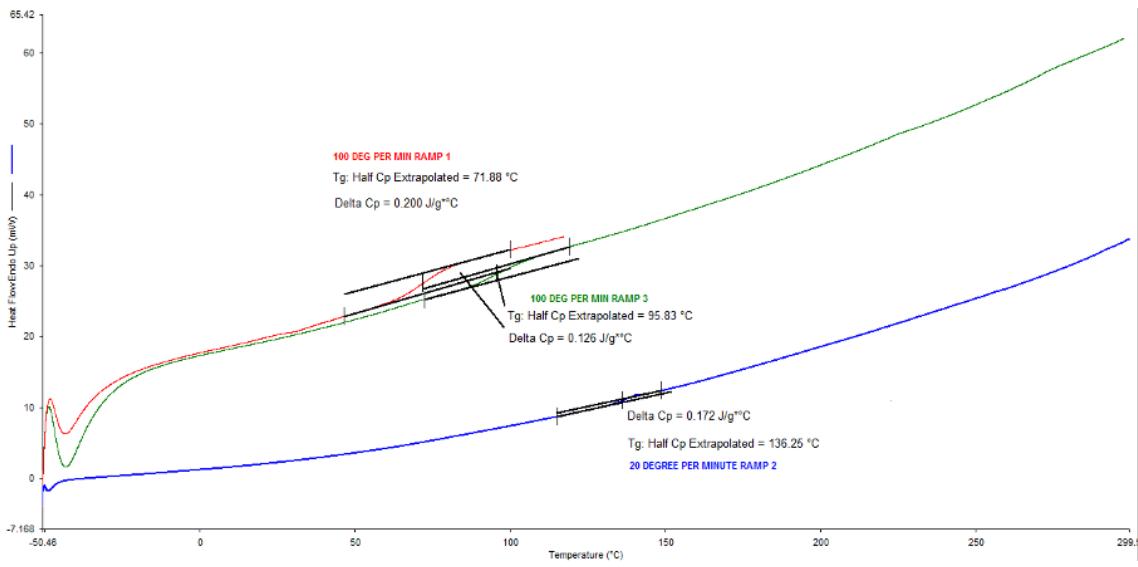|	Ultimate tensile strength / Mpa	Std Dev	Youngs Modulus / MPa	Std Dev	Strain at Break	Std Dev	Stress at break / MPa	Std Dev
D80 Virgin	33.77	1.473839	114.52	3.29443	0.316667	0.020548	33.41333	1.0873
D80 - 1x Recycled	29.81	0.16	95.155	1.905	0.425	0.005	27.59	0.07
D80 - 2x Recycled	30.905	0.765	101.59	1.66	0.485	0.025	27.265	2.435
D80 - 3x Recycled	31.65	-	112.23	-	0.47	-	27.21	-

10.6.3 T_g – DSC traces

Original output from DSC thermal scans using the temperature programme (left) and legend key (right) below.
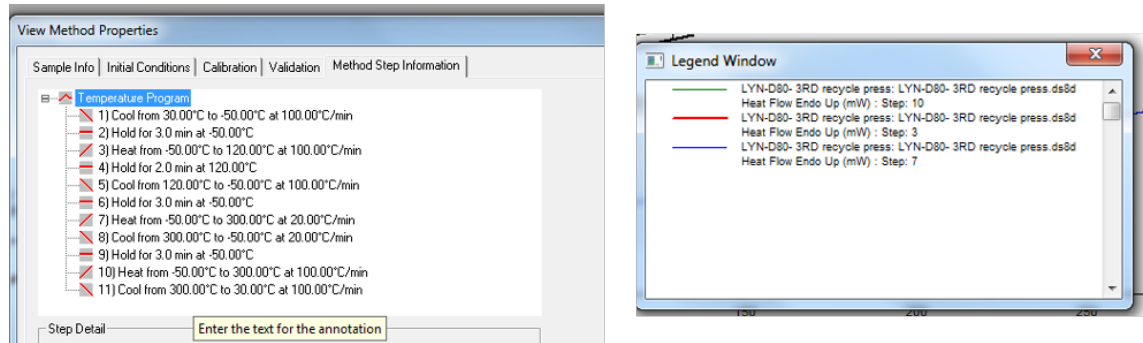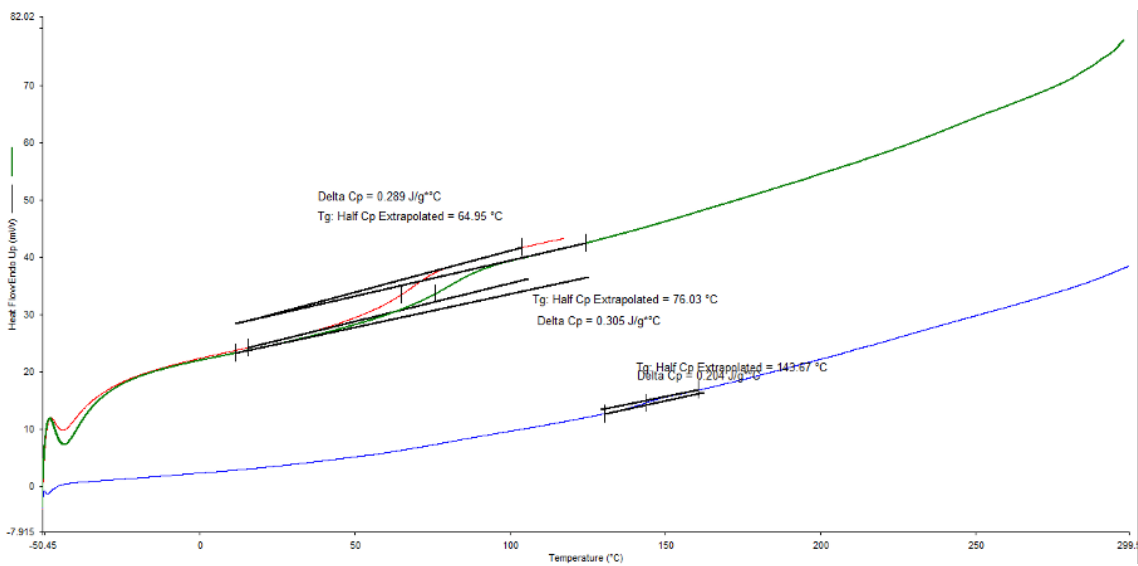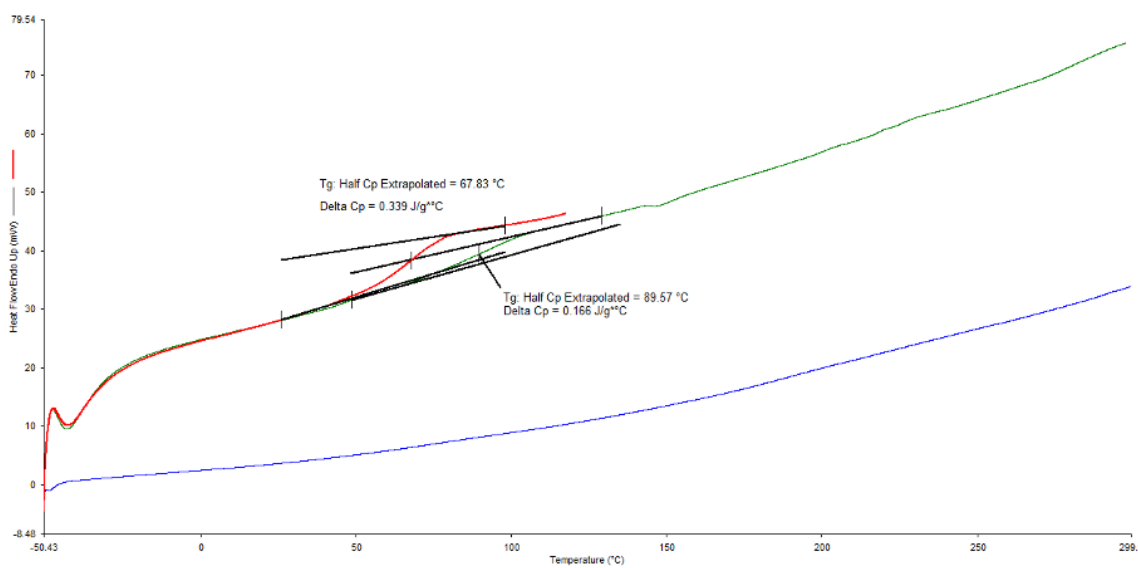

10.6.3.1 D-80 virgin material

10.6.3.2 D^{R1}-80 (1 x recycled)

10.6.3.3 D^{R2}-80 (2 x recycled)

10.6.3.4 D^{R3}-80 (3 x recycled)

Tg: Half Cp Extrapolated = 67.83 °C
Delta Cp = 0.339 J/g*°C

Tg: Half Cp Extrapolated = 89.57 °C
Delta Cp = 0.166 J/g*°C

10.7 DSC of D-100 dioxazaborocane materials with reduced PGE content

DSC thermograms of romatic (HA-E1) and linear (HA-E2) epoxy based polymers with reduced PGE content are shown below.

10.7 DSC of D-100 dioxazaborocane materials with reduced PGE content

DSC thermograms of romatic (HA-E1) and linear (HA-E2) epoxy based polymers with reduced PGE content are shown below.